

This electronic thesis or dissertation has been downloaded from the King's Research Portal at <https://kclpure.kcl.ac.uk/portal/>



The Construction of α,δ -Foldamer into a 13/11 Helix and its Application in Organocatalysis

Lin, Qi

Awarding institution:
King's College London

The copyright of this thesis rests with the author and no quotation from it or information derived from it may be published without proper acknowledgement.

END USER LICENCE AGREEMENT



Unless another licence is stated on the immediately following page this work is licensed

under a Creative Commons Attribution-NonCommercial-NoDerivatives 4.0 International

licence. <https://creativecommons.org/licenses/by-nc-nd/4.0/>

You are free to copy, distribute and transmit the work

Under the following conditions:

- Attribution: You must attribute the work in the manner specified by the author (but not in any way that suggests that they endorse you or your use of the work).
- Non Commercial: You may not use this work for commercial purposes.
- No Derivative Works - You may not alter, transform, or build upon this work.

Any of these conditions can be waived if you receive permission from the author. Your fair dealings and other rights are in no way affected by the above.

Take down policy

If you believe that this document breaches copyright please contact librarypure@kcl.ac.uk providing details, and we will remove access to the work immediately and investigate your claim.

The Construction of α,δ -Foldamer into a 13/11 Helix and its Application in Organocatalysis



Qi Lin

Supervisor: Dr. Andre Cobb

Dr. Manuel Müller

Department of Chemistry

King's College London

This dissertation is submitted for the degree of

Doctor of Philosophy

December 2023

Declaration

I hereby declare that except where specific reference is made to the work of others, the contents of this dissertation are original and have not been submitted in whole or in part for consideration for any other degree or qualification in this, or any other University. This dissertation is the result of my own work and includes nothing which is the outcome of work done in collaboration, except where specifically indicated in the text. This dissertation contains less than 100,000 words including appendices, bibliography, footnotes, tables and has less than 500 figures.

Qi Lin

December 2023

Acknowledgements

I would like to thank my first supervisor, Dr. Andre Cobb, for providing unwavering support in making this thesis possible, and for being a friendly and supportive supervisor, I am also thankful to my second supervisor, Dr. Manuel Muller, for all of their guidance and advice on the data, experiments, and the entire project.

A thanks to Callum Johnston, for being a kind and supportive team member who uplifted my spirits during my Ph.D., and to Ines Blanco, who has always been lovely and helpful. I extend my appreciation to Damien Dattler, Nicholas Lees, and Ryan Stendall for their valuable advice with the project. I'm grateful to Laszlo Kondacs, Wenjun Cai, Sofia Schoenbauer, Zongyao Zhang, and Yanjun Xu for being outstanding group members and for fostering a wonderful community.

I am thankful to CSC and K-CSC for funding my studies, as well as to the tech team and faculty at KCL for their kind support. My heartfelt thanks go to my friends Yujie Guo, for being a great flatmate, and to Xuemei Ma, Yue Yang for their friendship and companionship, to Fen Yu and Yuanyuan Liu for being wonderful friends, and to Shennan Gong for always being there to help me overcome difficulties.

Lastly, I want to express great thanks and love to my mum for her unconditional support and constant presence; to my beloved dad, my brother, and my entire family, who have always encouraged me to pursue knowledge and have been proud of me all the time.

Abstract

The study of peptides constructed with β , γ -amino acids has rapidly developed in recent years. In contrast, research on δ -amino acids is still in its infancy due to the difficulty in synthesizing enantiopure δ -amino acids. Regarding the mimicry of natural peptides, δ -amino acids are unique among artificial amino acids because the length of the δ -amino acid backbone is nearly equal to that of the α -dipeptide. Consequently, peptides constructed with δ -amino acids are more likely to adopt an H-bond pattern resembling the 13-helix that α -helices adopt.

In this thesis, we successfully synthesized an enantiopure δ -amino acid precursor and solved the lactam formation issue during the peptide synthesis. The XRD and refined solution state characterization of the 13/11 helix is presented in Chapter 2. Based on the structure we got, several features were discovered in this 13/11 helix: (i) the adjacent α -residues are relatively proximal, which is possible for the bifunctional catalyst design. (ii) The α -residue in the helix was embedded in the center of the helix circle, and the δ -residue is located at the outer circle of the helix, which builds up the environment for enantioselectivity. (iii) The ethyl of the δ -residue is pointing to the cyclohexane of the following δ -residue, which, on the one hand, might help stabilize the secondary structure, on the other hand, could be a candidate for the bifunctional catalyst design.

Chapter 3 explores the functionality of the bis-ornithine foldamer through retro-aldol cleavage. In chloroform, where the secondary structure was maintained, the bis-ornithine heptamer demonstrated the anticipated bifunctionality. Additionally, the crystal structure of the Boc-protected bis-ornithine foldamer confirmed the proximity of two side chains on adjacent α -residues. In aqueous solution, where the secondary structure might experience some degree of unfolding, the phase-transfer ability of the bis-ornithine foldamer was discovered.

Chapter 4 delves into the study of retro-aldol reactions catalyzed by foldamers with shorter amine side chains. Enantioselectivity was achieved, and it was found that reversible enantioselectivity of the foldamer is achievable by altering the position of the amine side chain. This investigation extended to photocatalysis in Chapter 5 by conjugating a flavin residue to the foldamer via reductive amination, revealing the foldamer's effectiveness in the decarboxylative cyanation of tyrosine.

The thesis primarily focuses on constructing the 13/11 helix structure and the catalytic functionalities derived from this secondary structure. Each chapter meticulously describes organic synthesis, kinetic studies, enantioselectivity, and photocatalysis. Major methods employed for characterizations and analyses included NMR, MS, XRD, Plate reader, MS, CD, and HPLC.

Contents

Contents	viii
List of Figures	xi
List of Tables	17
List of Abbreviation	18
Chapter 1 Introduction.....	22
1.1 A Brief Discussion of Secondary Structure and Foldamers	22
1.2 Foldamers.....	23
1.3 Homogeneous Peptidic Foldamer	23
1.3.1 Homogeneous β -Foldamers	23
1.3.2 Homogeneous γ - and δ -Foldamers	26
1.4 Heterogeneous Peptidic Foldamer	28
1.4.1 α,β -Foldamers.....	29
1.4.2 α,γ -Foldamers	31
1.4.3 α,δ -Foldamers.....	33
1.5 Other Foldamer Systems.....	34
1.5.1 Urea Oligomers.....	34
1.5.2 Oligoarylamide Foldamers.....	35
1.6 Foldamer Catalysis.....	37
1.6.1 Bifunctional Foldamer Catalyst	38
1.6.2 Other Enantioselective Helical Catalysis.....	44
1.6.1 Catalysis with Higher-Order Structure	49
Chapter 2 A Novel 13/11 Helix from 1:1 α - and δ -Amino Acids	55
2.1 Introduction.....	55
2.2 α,δ -Foldamer Synthesis.....	57
2.3 Results and Discussion	59
2.3.1 Synthesis of δ -Amino Acid.....	59
2.3.2 Synthesis of Building Block 28	60
2.3.3 Synthesis of δ -Building Block 53	65
2.3.4 Study on D-Alanine Constructed Peptides	66
2.3.5 Study on Aib Constructed Peptides	72
2.3.6 Study on L-Alanine Constructed Peptides.....	74
2.4 Conclusion	85

Chapter 3	Catalytic Retro-Aldol Cleavage by Bis-Amine α,δ -Foldamer.....	86
3.1	Introduction.....	86
3.2	Results and Discussion	90
3.2.1	Synthesis of Bis-Amine Foldamer	90
3.2.2	Catalytic Retro-aldol Reaction in Chloroform.....	98
3.2.3	Catalytic Retro-aldol Reaction in Aqueous Solution.....	106
3.2.4	CD Spectrum of Foldamer in Aqueous Solution	116
3.2.5	Mechanism of Retro-Aldol Catalysis in Buffer	116
3.3	Conclusion	119
Chapter 4	The Reversible Enantioselectivity of α,δ -Foldamer Catalyst	121
4.1	Introduction.....	121
4.2	Results and Discussion	125
4.2.1	Enantioselectivity of Bis-Dap Foldamer.....	125
4.2.2	Synthesis of Histidine-Containing Foldamer.....	138
4.2.3	Optimizing the Catalytic Condition of Foldamer 300	145
4.3	Conclusion	148
Chapter 5	Other Experiments	150
5.1	A Flavin Conjugated Foldamer for Decarboxylative Cyanation	150
5.1.1	Aims and Plans	150
5.1.2	Post-synthetic Modification Method for the Synthesis of Flavin-Foldamer.	158
5.2	Synthesis of Piperidine-Based δ -amino acid	162
5.2.1	Aims and Plans	162
5.2.2	Synthesis of Building Blocks.....	164
5.3	Synthesis of Tyrosine Containing Foldamer.....	175
5.4	Conclusion	178
Chapter 6	Experimental Section	181
6.1	Methods and Materials.....	181
6.2	Synthesis and Characterization for Chapter 2.....	182
6.2.1	Preparation of δ -amino Acid Precursor	182
6.2.2	General Procedure for Foldamer Synthesis	198
6.2.3	Synthesis of Foldamer 72.....	200
6.2.4	Synthesis of Foldamer 86.....	202
6.2.5	Synthesis of Foldamer 97.....	205
6.2.6	Synthesis of Foldamer 103.....	208
6.3	Synthesis and Characterization for Chapter 3.....	209

6.3.1	Synthesis of Methodol	209
6.3.2	Synthesis of Catalytic Foldamer 233	210
6.3.3	Synthesis of Foldamer 244.....	215
6.3.4	Synthesis of Tripeptide 250	218
6.4	Synthesis and Characterization for Chapter 4.....	220
6.4.1	Synthesis of 290.....	220
6.4.2	Synthesis of Foldamer 288.....	221
6.4.3	Synthesis of Foldamer 300.....	224
6.4.4	Synthesis of Foldamer 310.....	227
6.4.5	Characterization of Foldamer 350	230
6.5	Synthesis and Characterization for Chapter 5.....	233
6.5.1	Synthesis of Flavin-Conjugated Foldamer F34	233
6.5.2	Synthesis of Piperidine-Based δ -Amino Acid	240
6.5.3	Synthesis of Foldamer 707.....	246
6.6	Spectrum of Key Compounds.....	251
6.7	Kinetic Data of Plate Reader Reading	270
6.8	Fershtp 147 Equation	275
6.9	X-Ray Crystallography	276
6.9.1	XRD Methodology.....	278
Chapter 7	Conclusion and Outlook	281
References	283

List of Figures

Figure 1.1 (a) Structure of α -helix. ⁶ (b) Structure of anti-parallel β -sheet. ⁶ (c) Structure of β -strands. ⁷ (d) Structure of turns.....	23
Figure 1.2 The structure of β -peptides (a) Linear β -peptide. ⁹ (b) <i>trans</i> -ACHC constructed hexamer displays 14-helix. ¹⁰ (c) <i>trans</i> -ACPC constructed octamer displays 12-helix. ¹¹ (d) Crystal structure of <i>trans</i> -ACHC constructed 14-helix. ¹⁰ (e) Crystal structure of <i>trans</i> -ACPC constructed 12-helix. ¹¹	25
Figure 1.3 Switch of helical preference by changing a single atom on N-terminal residue. ...	26
Figure 1.4 Structures of γ -peptide	27
Figure 1.5 (a) Comparison between α -dipeptide and δ -amino acid. (b) Carbohydrate-derived δ -peptide by Gervay and co-workers. (c) Tetrahydrofuran-derived δ -peptide by George and co-workers.....	28
Figure 1.6 (a) The three building blocks of α - and β -amino acid and a library of α/β peptide. (b) The crystal structure of 11-helical α/β -7 (left); crystal structure of 14/15-helical α/β -10 (right)	30
Figure 1.7 Examples of α , β -peptides.....	31
Figure 1.8 Examples of γ -amino acid and α,γ -peptides	33
Figure 1.9 Examples of α , δ -peptide backbones.....	34
Figure 1.10 The sequences and structures of urea-bonded oligomers	35
Figure 1.11 (a) DNA double helical structure. (b) The chemical structure of aromatic foldamer and the illustration of its dimerization into a double helix.	36
Figure 1.12 Structure and crystal structure of quinoline foldamer.	37
Figure 1.13 (a) The structures of five building blocks, P (red), Q^F (grey), Q (blue), A^F (grey). (b) Crystal structure of the heterogeneous oligomer encapsulating 4-amino-1-butanol.....	37
Figure 1.14 The sketch diagram of the active sites of chymotrypsin facilitating the peptide cleavage.....	38
Figure 1.15 Illustration of bifunctional peptide catalyst	43
Figure 1.16 (a) Structure of building blocks. (b) Asymmetric hydrogenation induced by right-handed helix. (c) Remote asymmetric induction through achiral helices.	45
Figure 1.17 The structure of peptoid foldamers and their efficiency on alcohol oxidation....	47
Figure 1.18 The catalytic Machel addition reaction and the helical structure of thiazole peptide.....	48
Figure 1.19 The helical structure of urea foldamer and the catalytic reaction.....	49

Figure 1.20 Crystal structure of linalool dehydratase and the proposed mechanism of dehydration and isomerization.	51
Figure 1.21 The helix bundle of β -peptide and the structure of retro-aldol cleavage.....	52
Figure 1.22 The dimerization of the helical structure and the catalytic hydrolysis reaction. .	53
Figure 2.1 The helical structure of homo- δ -peptides	55
Figure 2.2 Representatives of different helical types.....	56
Figure 2.3 Top and side view of calculated 1:1 α,δ -peptides, green color represents α -amino acid, blue color represents δ -amino acid.....	56
Figure 2.4 The building blocks for synthesizing α,δ -peptide	60
Figure 2.5 ^1H NMR, C NMR and HMBC of lactam in CDCl_3	62
Figure 2.6 Cyclization process monitored by ^1H NMR: (400 MHz, CDCl_3). lactam is marked by “■”; dipeptide is marked by “▲”; α -residue is marked by “●”.	65
Figure 2.7 Stacked ^1H NMR (400 MHz, CDCl_3) of the amide protons of dimer, tetramer, hexamer, and octamer.	71
Figure 2.8 ^1H NMR (400 MHz, CDCl_3) of hexamer at 10, 5, 2, 1, 0.1 mM concentration. ...	72
Figure 2.9 Change of δ -value of individual amide proton under an accumulative volume of DMSO added into the CDCl_3 solution of 20mM of Hexamer, monitored by ^1H NMR (400 MHz, CDCl_3) at room temperature.	72
Figure 2.10 Stacked ^1H NMR (400 MHz, CDCl_3) of the amide protons of dimer 84 , tetramer 85 , hexamer 86	74
Figure 2.11 Stacked ^1H NMR (400 MHz, CDCl_3) of the amide protons of dimer, tetramer, hexamer, and octamer.	76
Figure 2.12 ^1H NMR (400 MHz, CDCl_3) of foldamer 96 at 8, 4, 2, 0.5, 0.1 mM concentration.....	77
Figure 2.13 δ -value of individual amide proton under an accumulative volume of DMSO added into the CDCl_3 solution of 20mM of foldamer 97 , monitored by ^1H NMR (400 MHz, CDCl_3) at room temperature.	78
Figure 2.14 The NOE-correlation observed on ROESY (400 MHz, CDCl_3) and the speculated H-bond pattern.	79
Figure 2.15 The XRD structure of foldamer 97 (CCDC 2252028), molecule on the left is the (<i>e,e</i>) conformer, molecule on the right is the (<i>a,a</i>) conformer.....	80
Figure 2.16 Partial ^1H NMR of tripeptide 101	83
Figure 2.17 The XRD structure of foldamer 103 (CCDC : 2251914), top view(left) and side view(right).....	83
Figure 2.18 (a) The absorbance of peptides from 205 nm to 270 nm in methanol. (b) Dependency of molar ellipticity on the number of amide bond.	84
Figure 3.1 Proposed mechanism for retro-aldol cleavage by artificial enzymes.	89
Figure 3.2 Schematic representation of a β -peptidic retroaldolase. Self-assembly of the peptide (right) further promotes activity. Reproduced from reference. ⁴³	90
Figure 3.3 Structure of bis-amine catalytic foldamer.	91
Figure 3.4 Synthetic breakdown of foldamer 202	91

Figure 3.5 Single crystal structure of foldamer 243 (CCDC : 2252029).....	97
Figure 3.6 Stacked ¹ H NMR of foldamer 232 , foldamer 243 tripeptide 241 (from top to bottom), ▲ represent the BocNH on the side chain, ■ represent the N-terminal Cbz-protected amide.....	98
Figure 3.7 Stacked ¹ H NMR (400 MHz, CDCl ₃) of different catalysts (1.5 mM free amine) mixed with 15 mM substrate after 72 h. The aldehyde proton at 10.2 ppm is marked by a blue square on the spectrum.....	100
Figure 3.8 Time-based product formation of blank contrast: 15 mM of methodol in CDCl ₃ . The data was monitored via NMR, which subjected to 5% error of NMR integration.	100
Figure 3.9 (a) Mechanism of catalytic reaction where E represent catalyst, S represent substrate. (b) Time-based aldehyde formation of different catalysts (at 1.5 mM) on [methodol] (15 mM) at 20 °C in CDCl ₃ using ¹ H NMR and the kinetic equation used for the catalysts. (c) the rate constant calculated from the Fershtp 147 ⁸⁴ equation.....	102
Figure 3.10 The structure of the intermediate and its calculated M/Z. Condition: 15 mM of methodol was reacted with 0.75 mM of foldamer 244 in 500 uL of CHCl ₃ for 2 hours, 1 mg of Na(CH ₃ COO) ₃ BH (10 mM) was added, the mixture was reacted overnight at room temperature, the reductive intermediates were analyzed by HRMS.....	103
Figure 3.11 At 20 °C, in CHCl ₃ , monitored by ¹ H NMR over 6 hours, methodol concentration [8-30 mM] (a) The amount of aldehyde produced using foldamer 244 under different concentrations of methodol. (b) Dependence of rate on [methodol] (2-30 mM)....	104
Figure 3.12 At 20 °C, in CHCl ₃ , monitored by HPLC over 6 hours, methodol concentration [2-30 mM] (a) The amount of aldehyde produced using foldamer 244 under different concentrations of methodol. (b) Background reaction without any catalyst. (c) Background-corrected dependence of rate on [methodol].....	105
Figure 3.13 The dependence of the reaction's rate on the concentration of butylamine. The reaction is monitored by a microplate reader using a black 96-well plate reader, reading from the top.....	107
Figure 3.14 The proceeded product formation with 50 μM of foldamer 244 and varying substrate concentration (0.125-1 mM), 30 °C, 10% CH ₃ CN in Tris buffer (50 mM Tris, pH=8, 150 mM NaCl), monitored by plater reader, black 96-well plate, read from top.	108
Figure 3.15 At 25 °C, in 10% CH ₃ CN in Tris buffer (50 mM Tris, pH=8, 150 mM NaCl), monitored by plate reader, (a) Product formation vs substrate concentration (0.25-2 mM). (b) Product formation using 200 μM of butylamine vs substrate concentration (0.25-2 mM). (c) Product formation using 100 μM of foldamer 244 vs substrate concentration (0.25-2 mM). (d) Rate comparison between blank contrast, 200 μM butylamine, and 100 μM foldamer 244 of catalyzed reactions at different methodol concentrations (0.25-2 mM).	109
Figure 3.16 At 30 °C, in 20% CH ₃ CN in Tris buffer (50 mM Tris, pH=8, 150 mM NaCl) monitored by plate reader, (a) Product formation vs substrate concentration (0.25-10 mM). (b) Product formation with 100 μM of foldamer 244 vs substrate concentrations (0.25-10 mM). (c) Rate comparison between blank contrast and the foldamer 244 -catalyzed reaction at different methodol concentrations (0.25-10 mM).....	110
Figure 3.17 Yield comparison of butylamine (2 mM) and foldamer 244 (1 mM) with methodol (10 mM) in 10% CD ₃ CN in Tris buffer, 20% CD ₃ CN in Tris buffer, 50% CD ₃ CN in D ₂ O, monitored by ¹ H NMR at 20°C.....	111

Figure 3.18 Reaction rate at varying substrate concentration over 20 hours at 25°C. (a) Comparison of rate with either 100 µM of foldamer 244 , 200 µM butylamine, or blank vs substrate concentration (0.25-2mM), in 5% CH ₃ CN in Tris buffer (50 mM Tris, pH=8, 150 mM NaCl) monitored by plate reader. (b) Comparison of rate with either 100 µM of foldamer 244 , 200 µM butylamine, 200 µM tripeptide 9 , or blank and varying substrate concentration (0.2-2.4 mM) in 5% CH ₃ CN in PBS (42.5 mM, pH=7.5) monitored by plate reader.	112
Figure 3.19 5% CH ₃ CN in PBS buffer (42.5 mM, pH=7.5), monitored by HPLC at 25°C (a) Product formation vs substrate concentration (0.25-2 mM). (b) Product formation with 200 µM of butylamine vs substrate concentration (0.25-2 mM). (c) Product formation with 100 µM of foldamer 244 vs substrate concentration (0.25-2 mM). (c) Rate comparison between blank contrast, 200 µM butylamine, and 100 µM foldamer 244 catalyzed reactions at different methodol concentrations (0.25-2 mM).	113
Figure 3.20 (a) Using 5% CH ₃ CN in PBS buffer (42.5 mM, pH=7.5) at 25°C, the amount of aldehyde formed with (i) 15 mM of substrate (in blue), 15 mM of substrate and 2 mM of butylamine (in purple), and 15 mM of substrate and 1 mM of foldamer 244 (in pink), as monitored by HPLC (see experimental). (b) The solubilising phenomenon of foldamer 244 within the vials. Without it, a clear precipitation is observable.	114
Figure 3.21 5% CH ₃ CN-PBS buffer, room temperature, 24 h reaction time, monitored by HPLC. 15 mM substrate and 1 mM foldamer or 2 mM monoamine, CTAC+Butylamine assay: 15 mM substrate, 2 mM CTAC, 2 mM butylamine. SDS+ Butylamine assay: 15 mM substrate, 2 mM SDS, 2 mM butylamine.	115
Figure 3.22 CD pectrum of foldamer 244 , foldamer 233 , and Tripeptide 250 in 20% CH ₃ CN in H ₂ O.	116
Figure 3.23 Founded M/Z of intermediates.	118
Figure 4.1 The structures of peptide catalysts for β-aminoalcohol resolution.....	125
Figure 4.2 Illustration and structure of the bis-ornithine foldamer and bis-dap foldamer....	126
Figure 4.3 ¹ H NMR (400 Mz, CDCl ₃), 20 ° C, stacked ¹ H NMR of aldehyde reference, 15 mM substrate mixed with 0.75 mM foldamer 244 (after 72 h), 15 mM substrate mixed with 0.75 mM foldamer 288 (after 72 h), alkene reference from top to bottom. The aldehyde proton was marked by ▲, and the alkene-double bond proton was marked by ■.	129
Figure 4.4 Time-based aldehyde and alkene formation under foldamer 244 and foldamer 288 (at 0.75 mM) on [methodol] (15 mM) at 20 °C in CDCl ₃ , monitored by ¹ H NMR.....	130
Figure 4.5 ¹ H NMR (400 Mz, CDCl ₃), room temperature, stacked ¹ H NMR of 15 mM substrate mixed with 0.75 mM foldamer 288 (after 72 h), 15 mM substrate mixed with 1.5 mM foldamer 310 (after 72 h), 15 mM substrate mixed with 1.5 mM foldamer 300 (after 72 h) from top to bottom. The aldehyde proton was marked by ▲. The alkene-double bond proton was marked by ■.	131
Figure 4.6 Time-based alkene-product formation under foldamer 300 (1.5 mM), foldamer 288 (0.75 mM), and foldamer 310 (1.5 mM) on [methodol] (15 mM) at 20 °C in CDCl ₃ , monitored by ¹ H NMR. (a) Scheme of the reaction. (b) In terms of aldehyde formation. (c) In terms of alkene formation.	133
Figure 4.7 The chiral HPLC results in the kinetic resolution of different catalysts.	134
Figure 4.8 Time-based aldehyde/alkene formation under foldamer 300 (1.5 mM), foldamer 288 (0.75 mM), and foldamer 310 (1.5 mM) on [methodol] (15 mM) at 20 °C in CDCl ₃ , monitored by ¹ H NMR.....	135

Figure 4.9 Time-based product formation under foldamer 288 (0.75 mM) on [methodol] (15 mM) at 20 °C in CDCl ₃ , yield is monitored by ¹ H NMR, ee is monitored by chiral HPLC .	136
Figure 4.10 Time-based product formation under foldamer 300 (1.5 mM) on [methodol] (15 mM) at 20 °C in CDCl ₃ , yield is monitored by ¹ H NMR, ee is monitored by chiral HPLC .	136
Figure 4.11 Time-based product formation under foldamer 310 (1.5 mM) on [methodol] (15 mM) at 20 °C in CDCl ₃ , yield is monitored by ¹ H NMR, ee is monitored by chiral HPLC .	137
Figure 4.12 The HPLC and HRMS of the mixture of foldamer 351 and 357 .	145
Figure 4.13 Time-based product formation at 20 °C in CDCl ₃ , yield is monitored by ¹ H NMR, ee is monitored by chiral HPLC. The comparison between foldamer 300 (1.5 mM) on [methodol] (15 mM) and foldamer 300 (15 mM) on [methodol] (150 mM).....	146
Figure 4.14 Time-based product formation under foldamer 300 (20 mM) on [methodol] (200 mM) at 20 °C in CDCl ₃ , yield is monitored by ¹ H NMR, ee is monitored by chiral HPLC .	146
Figure 4.15 ee of foldamer 300 (2 mM) on [methodol] (20 mM) at 20 °C in different solvents, monitored by chiral HPLC.....	147
Figure 4.16 Aldehyde formation of: 15 mM substrate and 1 mM foldamers 244 /1 mM foldamers 288 /2mM foldamer 300 /2mM unstructured amine were stirred in 100 μL of 5% CH ₃ CN-PBS buffer at room reacted for 24 h. The reaction was diluted with 200 μL of H ₂ O and 200 μL of CH ₃ CN, and the aldehyde product was monitored by HPLC.	148
Figure 5.1 Two approaches to synthesize flavin conjugated foldamer. (a) Synthesize the flavin-conjugated α-amino acid, then build this amino acid into a foldamer. (b) Build a foldamer with a reactive site reserved on the side chain, then bond the flavin onto the foldamer.	151
Figure 5.2 Synthesis of F31 and its ¹ H NMR in chloroform.	159
Figure 5.3 The catalytic decarboxylative cyanation and the LC-MS result.....	162
Figure 5.4 The crystal structure of foldamer 103 , the pink colour marked the two proximal positions.	163
Figure 5.5 Retrosynthesis of piperidine-based foldamer and the structure of the building block 500 , 501 , 503 , 504	164
Figure 5.6 The aldehyde formation of (a) In CDCl ₃ , foldamer 707 (1.5 mM) on [methodol] (15 mM) at 20 °C, monitored with ¹ H NMR every 6 h. (b) In 5% CH ₃ CN-PBS buffer, 15 mM substrate and 1 mM foldmaer 707 at room temperature, were monitored by HPLC after 48 hours of reaction time.	178
Figure 6.1 The molecular structure of foldamer 97 (CCDC 2252028). Thermal ellipsoids displayed at the 50% probability level. Hydrogen atoms are pictured as spheres of arbitrary radii (and most have been omitted for clarity).....	277
Figure 6.2 The molecular structure of foldamer 103 (CCDC : 2251914). Thermal ellipsoids displayed at the 50% probability level. Hydrogen atoms are pictured as spheres of arbitrary radii (and most have been omitted for clarity). The terminal – C(CH ₂ CH ₃)CH ₂ CONHC(CH ₃)COOCH ₃ group (C46, C47, C48, C49, C50, O8, N7 C51, C52, C53, O9, O10, C54) is disordered across two positions, and the position of highest relative occupancy (57%) is displayed. The water molecule (O11) is also disordered across three positions, and the position of highest relative occupancy (57%) is displayed.....	277

Figure 6.3 The molecular structure of bis-Boc-ornithine heptamer **243** (CCDC : 2252029). Thermal ellipsoids displayed at the 50% probability level. Hydrogen atoms are pictured as spheres of arbitrary radii (and most have been omitted for clarity). The terminal –OCH₂C₆H₅ group (O14, C62, C63, C64, C65, C66, C67, C68) is disordered across two positions, and the position of highest relative occupancy (85%) is displayed).278

List of Tables

Table 1-1 Isolated yield of catalytic reaction.	44
Table 2-1 The cyclohexyl δ -residue 19 was shown to comfortably adopt a conformation that would lead to the most stable 13/11-helix according to calculations	57
Table 3-1 The catalytic efficiency of foldamer 244 in different solvents	106
Table 3-2 Conditions for attempted enantioenrichment.....	119
Table 4-1 Yield and ee's of proline catalyzed aldol product.	122
Table 4-2 Yield and ee of foldamer 300 (1.5 mM), cocatalyst (1.5 mM) on [methodol] (15 mM) at 20 °C in CHCl ₃ after two days. Yield is monitored by HPLC, and ee is monitored by chiral HPLC.	138
Table 5-1 The result of 420 catalyzed decarboxylative reduction on four substrates.....	161
Table 5-2 Methods of bromination/chlorination reactions.....	166
Table 5-3 Methods of nitration reaction.....	167
Table 6-1 Crystallographic data for foldamer 97 , foldamer 103 , foldamer 243	280

List of Abbreviation

Aib	2-Aminoisobutyric acid
Ala	Alanine
Ar	Aryl
Bn	Benzyl
Boc	tert-Butyloxycarbonyl
BTA	Butylamine
Bu	Butyl
nBuLi	n-Butyllithium
CAN	Ceric ammonium nitrate
CBZ	Carbobenzyloxy
COSY	Correlated Spectroscopy
DAP	2,3-diaminopropionic acid
DCE	Dichloroethane
DIBAL-H	Diisobutylaluminum hydride
DIPEA	N,N-Diisopropylethylamine
DMF	N,N-Dimethylformamide
DMSO	Dimethyl sulfoxide
dr	Diastereomeric ratio
EDCI	1-Ethyl-3-(3-dimethylaminopropyl)carbodiimide

ee	Enantiomeric excess
eq.	Equivalent
er	Enantiomeric ratio
EtOAc	Ethyl Acetate
de	Diastereomeric excess
HOBt	1-Hydroxybenzotriazole hydrate
HRMS	High Resolution Mass Spectrometry
HSQC	Heteronuclear Single Quantum Coherence Spectroscopy
LDA	Lithium diisopropylamide
MHz	Megahertz
MS	Mass spectrometry
MW	Molecular weight
NaHMDS	Sodium bis(trimethylsilyl)amide
NOESY	Nuclear Overhauser Effect Spectroscopy
NMO	N-Methylmorpholine N-oxide
NMR	Nuclear Magnetic Resonance
PCC	Pyridinium chlorochromate
ppm	Parts per million
rt	Room temperature
R	Alkyl group
T	Temperature

TBAF	Tetra-n-butylammonium Fluoride
TEA	Triethylamine
TEMPO	(2,2,6,6-Tetramethylpiperidin-1-yl)oxyl
TFA	Trifluoroacetic acid
THF	Tetrahydrofuran
TLC	Thin Layer Chromatography
TMS	Tetramethylsilyl

Chapter 1 Introduction

Nature relies on enzymes to implement most of the metabolic and biochemical reactions that occur in organisms. Generally, more than 100 amino acids are required for proteins to adopt a higher-ordered structure which contains a specific binding pocket for substrate binding. Over the past few decades, scientists have designed smaller molecules with their own innate folding abilities, denoted as “Foldamers”.¹ Compared with natural enzymes, artificial peptidomimetic foldamers usually compose less than 20 building blocks, and their secondary structures are readily predictable. Furthermore, the foldamers are more resistant to harsher conditions than native biological systems, such as greater temperature variation, or greater resistance to a broader pH range. Foldamer research has burgeoned from simply accessing well-defined secondary structures, to their application in catalysis, substrate recognition, and drug delivery.

2-5

1.1 A Brief Discussion of Secondary Structure and Foldamers

Typical secondary structures within proteins include helices (Figure 1.1a), sheets (Figure 1.1b), strands (Figure 1.1c) and turns (Figure 1.1d). Of these, the helical structure is one of the most prevalent secondary structures in proteins and is stabilized by intramolecular hydrogen bonds between non-adjacent peptide group. These non-covalent bonds are individually weak, but collectively can stabilize the resultant helical structure.

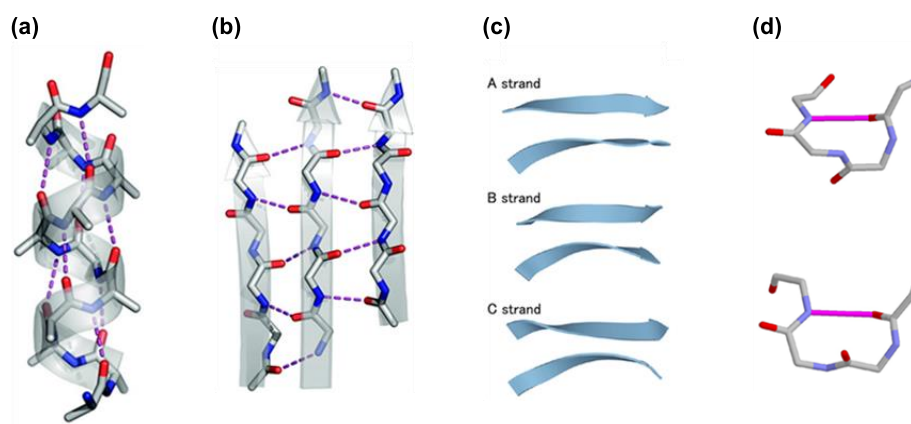


Figure 1.1 (a) Structure of α -helix. ⁶ (b) Structure of anti-parallel β -sheet. ⁶ (c) Structure of β -strands. ⁷ (d) Structure of turns.

1.2 Foldamers

Foldamers are any non-natural compound - normally oligomers or polymers - that can fold into a well-defined structure. A primary objective of designing these systems is to gain access to higher order structures that have the ability to mimic natural peptides and indeed - protein protein interactions. Yet their applications cover far broader disciplines, catalysis to drug delivery, molecular information to antimicrobial effects. ⁸

1.3 Homogeneous Peptidic Foldamer

1.3.1 Homogeneous β -Foldamers

The study of non-canonical β , γ , δ -amino acids has significantly enlarged the number of foldamer structures in recent years. In particular, β -peptides have been extensively reported - particularly in the early years of foldamer studies due to their relatively easier synthetic accessibility. In 1996, Seebach's group reported a linear β -amino acid-constructed peptide that adopted a helical structure (Figure 1.2a). ⁹ In the same year, Gellman's group reported a cyclically constrained β -peptide (*trans*-ACHC) that adopted a 14-helix (14 atoms between consecutive intramolecular hydrogen bond) (Figure 1.2b, Figure 1.2d), ¹⁰ and later, in 1997,

the first 12-helix structure constructed from *trans*-ACPC (Figure 1.2c, Figure 1.2e).¹¹ In both cases, the helical conformations were initially predicted *via* computational calculation which then proved correct by XRD structure of the designed foldamers. The cyclic constraints in the five- and six-membered rings help stabilize the helical conformation by restricting the freedom of the bond rotation, thereby limiting the number of possible helix alternatives. In contrast, the different ring size changes the torsional angles within the backbone, and this leads to a different helix type being formed.

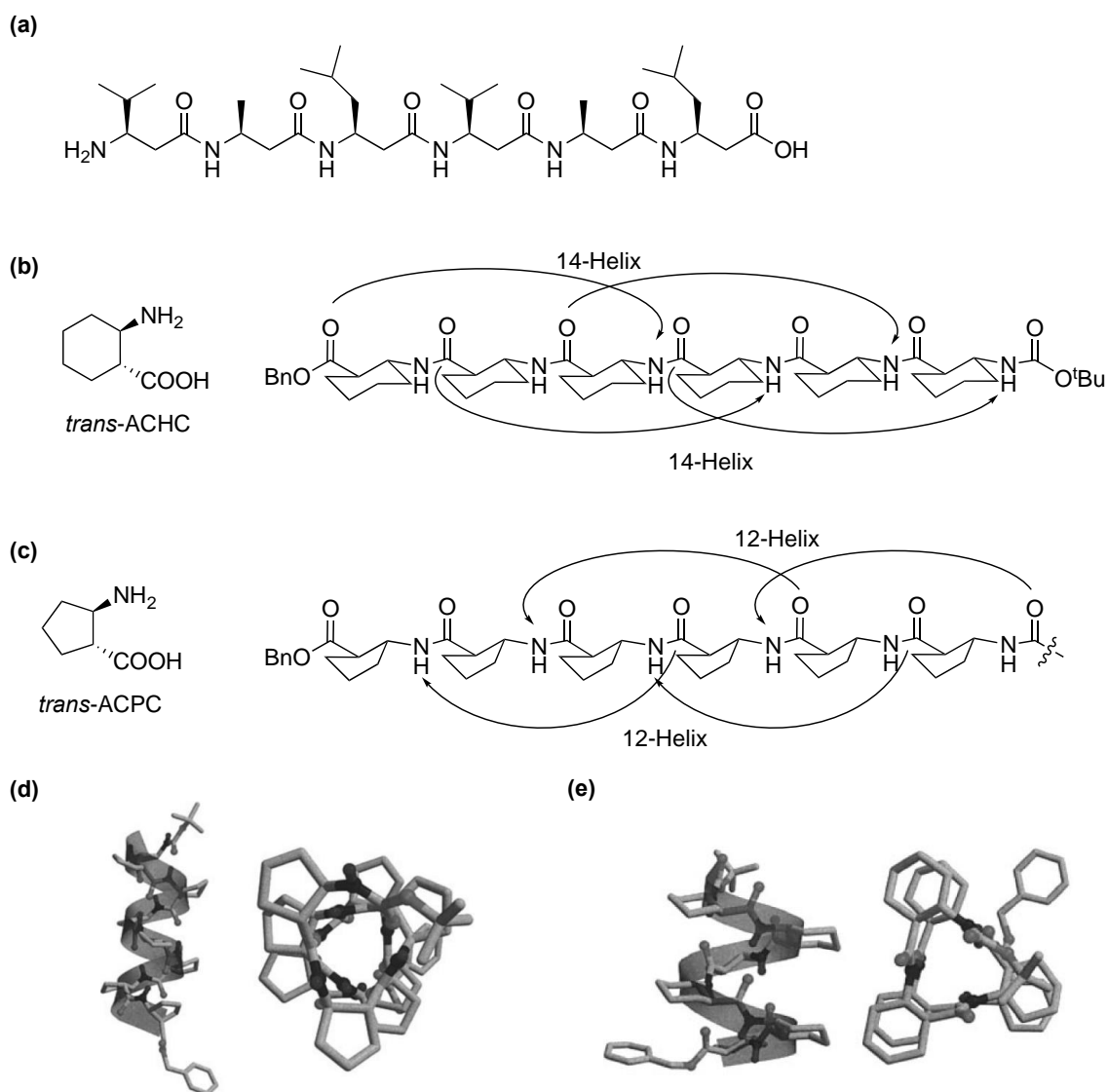


Figure 1.2 The structure of β -peptides (a) Linear β -peptide.⁹ (b) *trans*-ACHC constructed hexamer displays 14-helix.¹⁰ (c) *trans*-ACPC constructed octamer displays 12-helix.¹¹ (d) Crystal structure of *trans*-ACHC constructed 14-helix.¹⁰ (e) Crystal structure of *trans*-ACPC constructed 12-helix.¹¹

Aitken's group developed a β -amino acid (*t*ACBC) composed of a cyclobutane, which, upon incorporation into a pentamer, adopted a 12-helix structure, despite the preferred conformation of its dipeptide and tetrapeptide being an 8-helix.¹² As the nitrogen atom has a different covalent bond angle from the carbon atom, changing the cyclobutane ring to an azetidine ring produced another β -amino acid (AAzC) with a strong tendency to adopt an 8-helical conformation. Using AAzC as an 8-helix primer at the N-terminus of the *t*ACBC tetramer, the helical structure altered to 8-helix. However, the induction of the 8-helix primer is limited to a

certain length of the oligomer, the transformation effect would fade when the peptide length of the *t*ACBC oligomer reaches above eight residues, and the 12-helix was resumed with this peptide length.¹³ These results indicated that a subtle change of one atom on the peptide backbone might induce the alteration of the helical pattern of the oligomer structure (Figure 1.3).

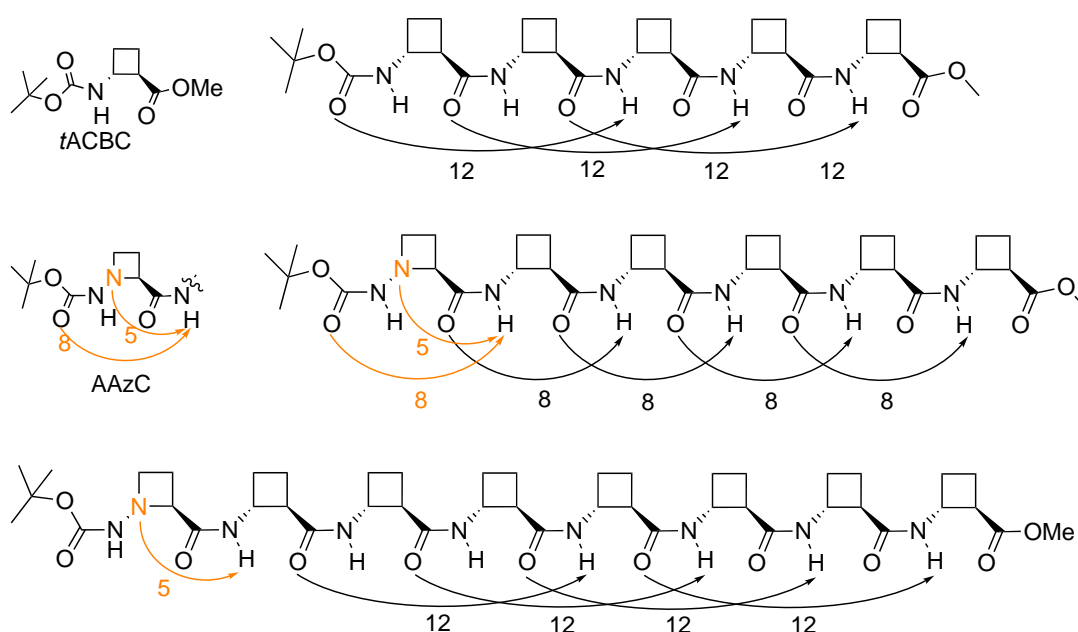


Figure 1.3 Switch of helical preference by changing a single atom on N-terminal residue.

1.3.2 Homogeneous γ - and δ -Foldamers

Similarly to β -helices, the use of γ -amino acids has led to even more variation of helix types. For example, Seebach and co-workers reported a γ -peptide built from (*R*)-4-amino-5-methylhexanoic acid, (*S*)-4-aminopentanoic acid and (*R*)-4-amino-6-methylheptanoic acid in 1998 (Figure 1.4a),¹⁴ this γ -hexapeptide adopted a right-handed 14-helix that is more stable than corresponding α -peptide. In the same year, Michnick and co-workers reported a linear γ -peptide synthesized from simple homologation of α -amino acids, the resulting tetramer and hexamer showed stable right-handed 14-helix.¹⁵ Maillard and co-workers discovered a thiazole-based γ -amino acid and constructed it into γ -peptide (Figure 1.4b).¹⁶ The thiazole ring confers a torsion restraint, forcing the peptide to adopt a 9-helix. Royo's and co-workers

designed a library of cyclically constrained γ -peptides constructed from the cyclic *cis*- γ -amino-L-proline (Figure 1.4c).¹⁷

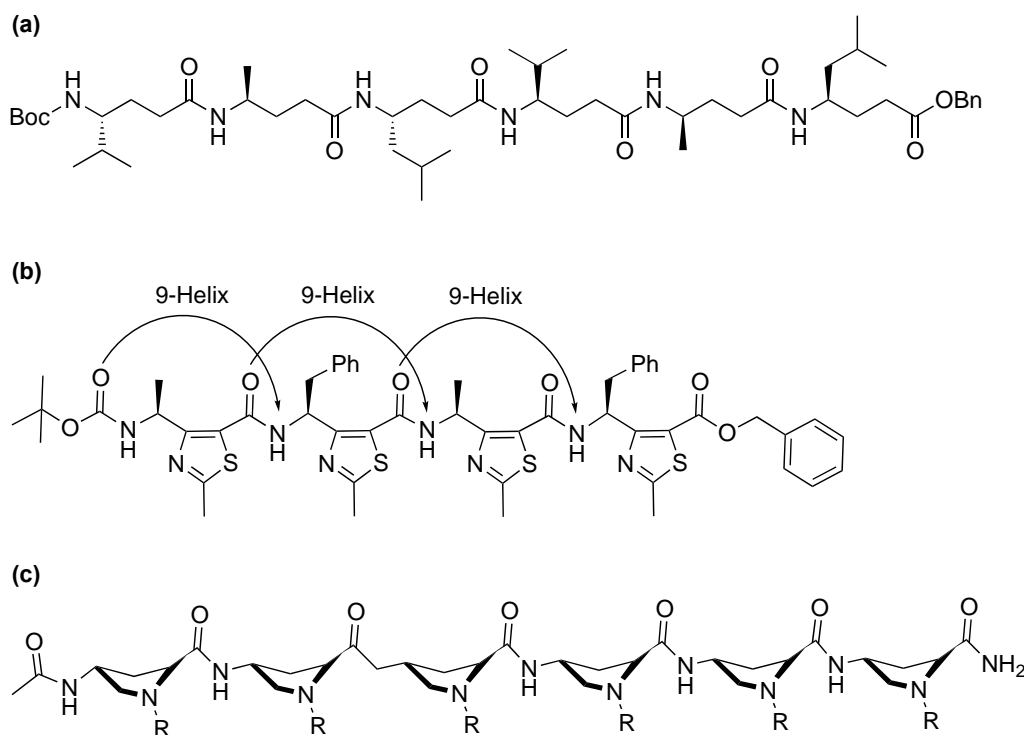


Figure 1.4 Structures of γ -peptide

Homogeneous δ -helices are in contrast extremely rare, which is interesting given that δ -residue is essentially a α -dipeptide mimic (Figure 1.5a). Gervay and co-workers have synthesized a constrained carbohydrate-derived δ -peptide based upon an N-acetylneuraminic acid scaffold (Figure 1.5b), although the conformation of the oligomers was not confirmed, the results showed that the oligomer adopted a secondary structure.¹⁸ George and co-workers have also investigated the secondary structure of carbohydrate-derived δ -peptides.¹⁹ The use of cyclically constrained tetrahydrofuran amino acids as frameworks allows for both *cis*- and *trans*- conformations with respect to the 2- and 5-positions (Figure 1.5c). Interestingly, the *cis*-foldamer of both the tetramer and hexamer adopt the β -turn structure whereas the conformation of the *trans*-foldamers is dependent on the substituent side chain of its δ -residue. When the diol of the *trans*-foldamers was protected with two *trans*-acyl groups, its tetramer did not have any conformational preference, in contrast, its octamer exhibits a well-defined left-handed helix.

Other examples of tetrahydrofuran constructed peptides were also studied by Tushar and co-workers.^{20,21}

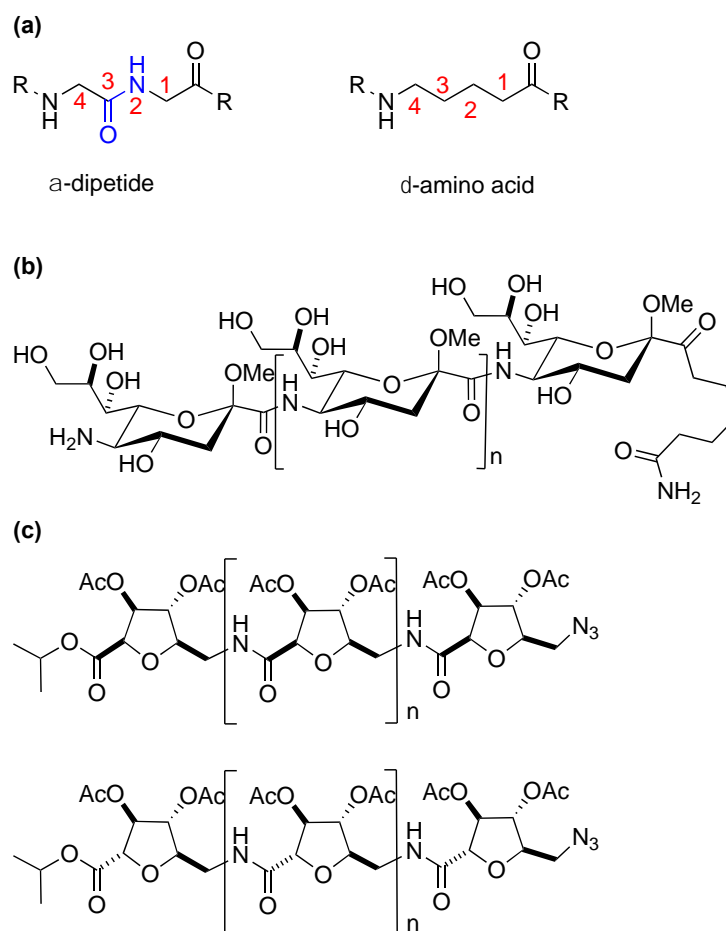


Figure 1.5 (a) Comparison between α -dipeptide and δ -amino acid. (b) Carbohydrate-derived δ -peptide by Gervay and co-workers. (c) Tetrahydrofuran-derived δ -peptide by George and co-workers.

1.4 Heterogeneous Peptidic Foldamer

In addition to the homogeneous foldamers, combinations of $\alpha,\beta,\gamma,\delta$ -residues have bloomed peptidomimetic foldamer research by yet again increasing the diversity of secondary structures available. A diverse foldamer toolkit is critical in uncovering impactful applications such as in catalysis, therapeutics, and materials and systems that incorporate α -amino acids have the added advantage that they already have great side chain diversity that can be exploited towards these potential applications.

1.4.1 α,β -Foldamers

Gellman and co-workers designed hybrid peptides with $\alpha\beta$ repeat sequence where β -residue is ACPC ((*S,S*)-trans-2-aminocyclopentanecarboxylic acid), α -residues are α -aminoisobutyric acid (Aib) or L-alanine. The previously research on the cyclically constrained ACPC constructed peptides has proposed that ACPC could promote two types of helical structure: the 11-helix that contains a *i,i+3* hydrogen bond pattern, the 14/15-helix that contains a *i,i+4* hydrogen bond pattern.^{22, 23} The crystal structure and 2D NMR of a library of 1:1 alternating α/β peptides as listed in Figure 1.6a has confirmed the existence of either 11-helix or 14/15-helix as shown in Figure 1.6b. The shorter peptide, $\alpha/\beta\cdot\mathbf{6}$, $\alpha/\beta\cdot\mathbf{7}$, and $\alpha/\beta\cdot\mathbf{8}$ display a 11-helix. The longer peptide $\alpha/\beta\cdot\mathbf{9}$, and $\alpha/\beta\cdot\mathbf{10}$ prefer a 14/15-helix.²⁴

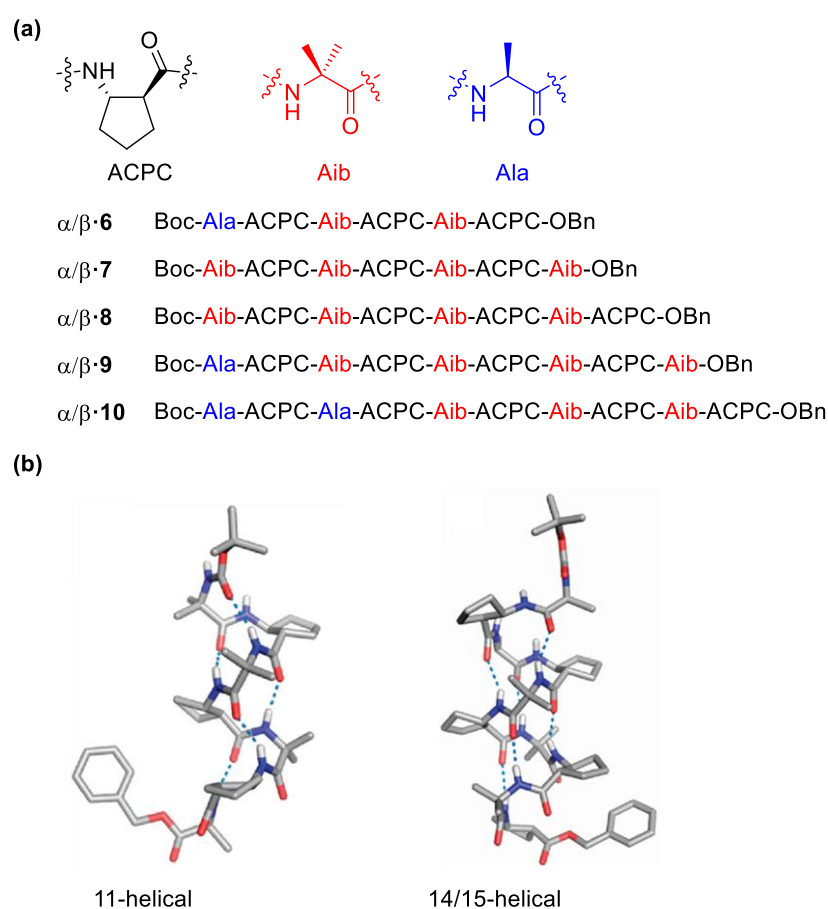


Figure 1.6 (a) The three building blocks of α - and β -amino acid and a library of α/β peptide. (b) The crystal structure of 11-helical $\alpha/\beta\cdot 7$ (left); crystal structure of 14/15-helical $\alpha/\beta\cdot 10$ (right)

Reiser and co-workers developed a structurally defined α,β -peptide consisting of *cis*- β -aminocyclopropanecarboxylic acids and (*S*)-alanine, both the hexamer and heptamer of these alternating α,β -peptides displayed defined helical structures (Figure 1.7a).²⁵ Hyuk Choi and co-workers designed an alternating α,β -peptide constructed from an α -amino acid and *cis*-2-amino-*cis*-4-methylcyclohexanecarboxylic acid.²⁶ Its pentamer was found to adopt an 11/9-helix. Although most of the reported α,β -peptides consisting of cyclically constrained β -residues stabilized the helix propensity in terms of their secondary structure, some linear β -amino acids with a variety of side chains have also contributed greatly to the study of hybrid foldamers.^{27, 28} Sharma and co-workers reported an α, β -peptide synthesized from L-alanine and the *S*-epimer of carbo- β^3 -amino acid (Figure 1.7b), in this research, the pentamer and hexamer adopt 9/11 helices.²⁹ Furthermore, even the tripeptide with L-ala-Caa β^3 -L-ala

sequence was found to adopt a robust helical structure. Moretto and co-workers exploited the photo-switchable foldamer by incorporating four continuously unsaturated β -amino acids into the peptide backbone and incorporated α -amino acids at both the N terminus and C terminus of the oligomer (Figure 1.7c), this peptide-based foldamer was proposed applicable in designing optical materials and devices.³⁰

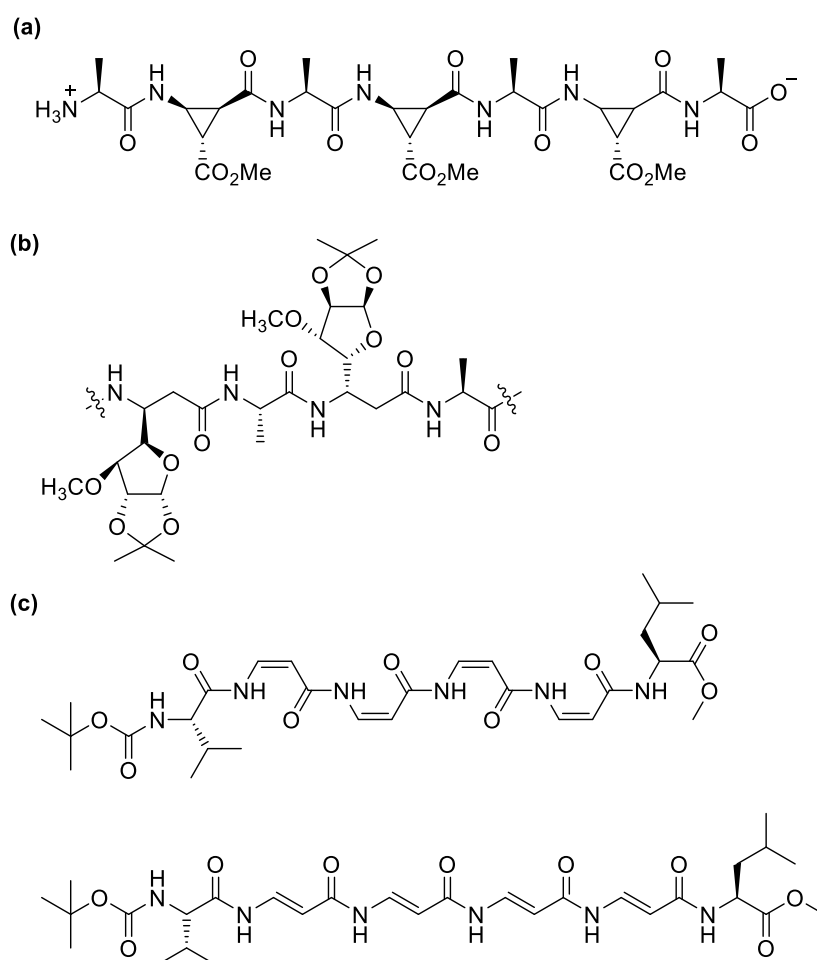


Figure 1.7 Examples of α , β -peptides.

1.4.2 α,γ -Foldamers

Although the insertion of more methylene groups into the backbone of the peptide may introduce additional degrees of torsional freedom, the richer landscape of possibilities among γ -amino acid have garnered great interest from foldamer scientists. The side chain of γ -amino acid can be placed on one position that is adjacent to carbonyl group (γ^2 residue), in the middle

(γ^3 residue), adjacent to nitrogen (γ^4 residue), or occupied two or three positions ($\gamma^{2,3}$ residue, $\gamma^{2,3,4}$ residue) (Figure 1.8a). Balaram and co-workers synthesized an γ^4 -amino acid from homologation of the corresponding proteinogenic α -amino acid (Figure 1.8b),³¹ the resulted α,γ -peptide dodecamer was found to adopt a right-handed 12-helix which is stabilized by six intramolecular hydrogen bond. This long α,γ -peptide composed entirely of unconstrained residues was remarkably able to adopt a stable helix structure. Later, Balaram and co-workers designed a foldamer constructed from the γ^3 residue gabapentin (1-aminomethylcyclohexaneacetic acid) (Figure 1.8c).³² The cyclic constraint is not placed within the backbone of the target foldamer but attached on the C^β carbon atom as a side chain. Incorporation of different numbers of this γ -amino acid into α -peptide leads to a different secondary structure. When one gabapentin was inserted at the middle of the α -peptide (Boc-Leu-Phe-Val-Aib-Gpn-Leu-Phe-Val-OMe), the resulted α,γ -peptide adopt a β -hairpin structure that is supported by the β -turn derived from the centrally positioned Gpn residue. In contrast, the alternating α,γ -peptide (Boc-Gpn-Aib-Gpn-Aib-Gpn-Aib-Gpn-Aib-OMe) was proved to adopt a stable 12-helix (Figure 1.8c). Gellman and co-workers have extensively studied the impact of cyclic constraints on the secondary structure of γ -amino acid-contained foldamers. They designed cyclohexane substituted $\gamma^{2,3}$ -amino acid with different stereocenters at the substitution sites, the *trans*-foldamer of the 1:1 α,γ -peptide adopted an unexpected 12/10-helix (Figure 1.8d),³³ while the corresponding *cis*-foldamer adopted a stable 12-helix.³⁴

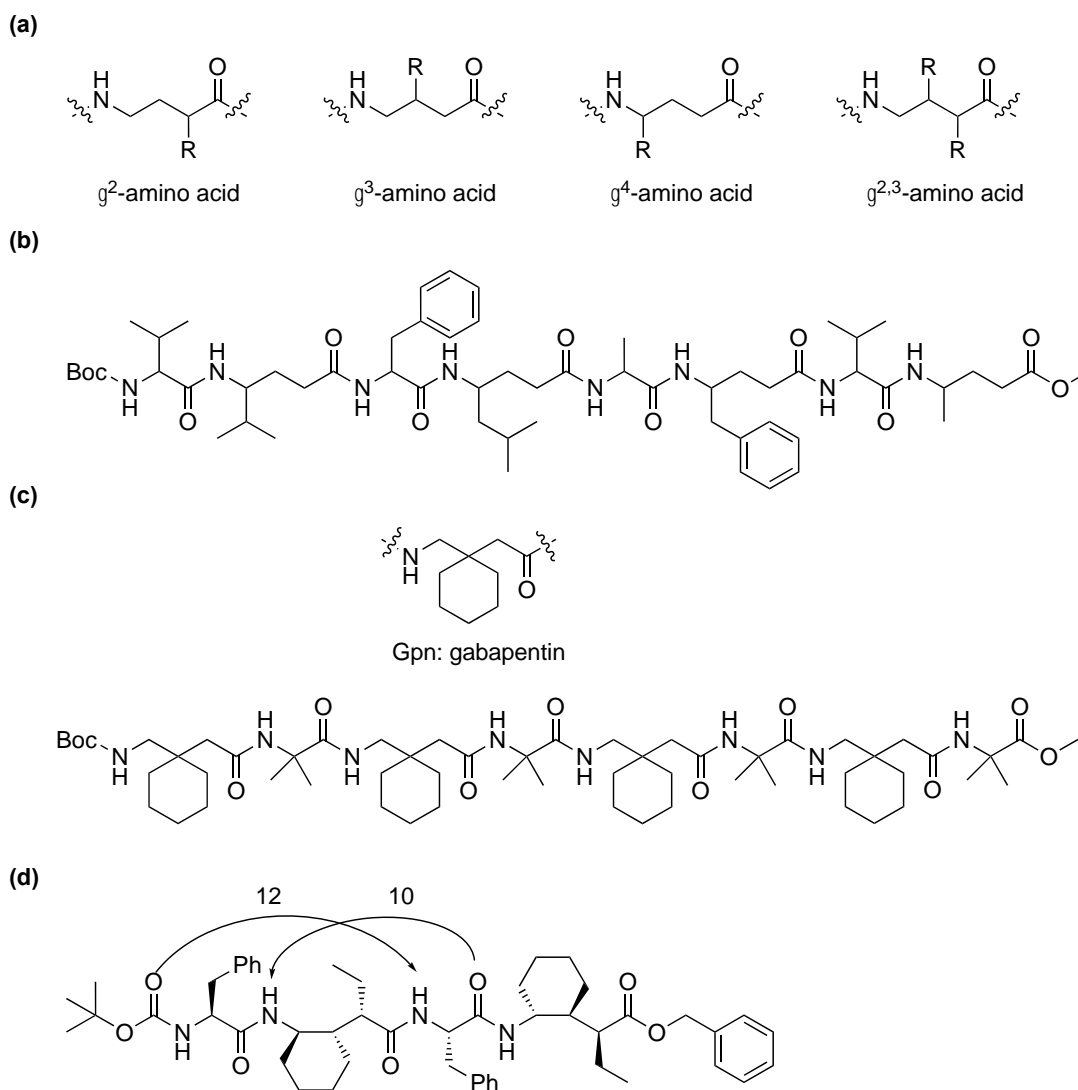


Figure 1.8 Examples of γ -amino acid and α,γ -peptides

1.4.3 α,δ -Foldamers

As they had with the α,β - and α,γ -1:1 foldamers, Hofmann and co-workers also predicted the ideal δ -residue conformations that would lead to a range of folded 1:1 α,δ -hybrid peptides.³⁵ One of these - a proposed 13/11-mixed helix led to their design of a δ -constituent where 5-aminopentanoic acid is appended with a δ -xylose side chain at its δ^5 position (Figure 1.19a). In a similar way to cyclically constrained homologated systems, this side-chain provides sufficient rigidity to the foldamer to allow it to adopt the proposed 13/11-mixed helical pattern.

Hosahudya and co-workers designed another linear δ -amino acid where the new δ -residue was also incorporated into α,δ -hybrid peptides (Figure 1.9b).³⁶ Again, this adopted a 13/10-membered hydrogen bond.

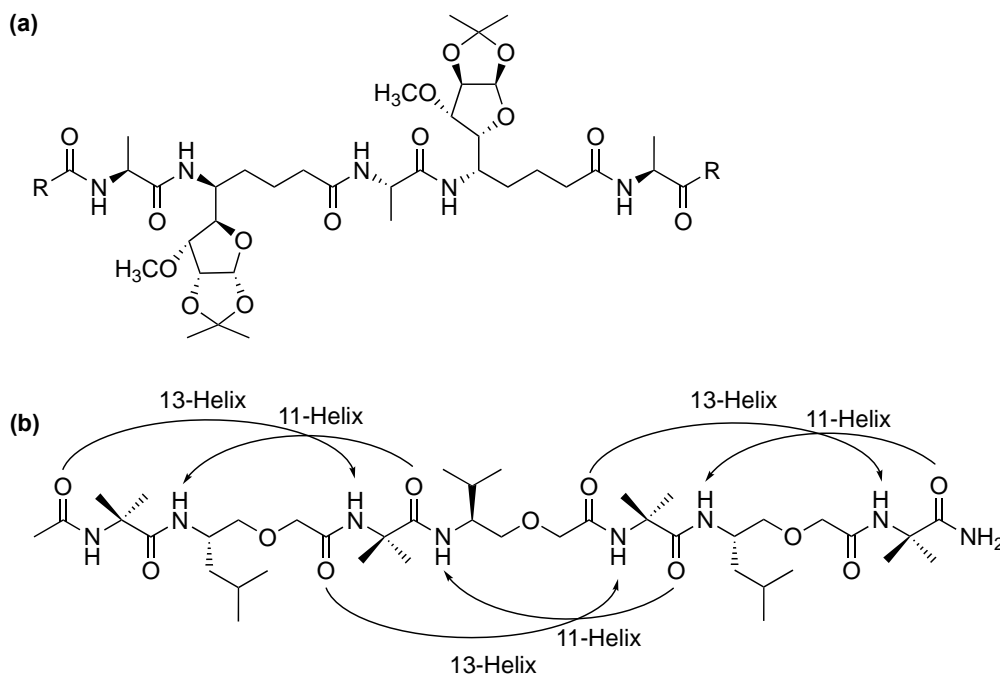


Figure 1.9 Examples of α , δ -peptide backbones.

1.5 Other Foldamer Systems

1.5.1 Urea Oligomers

Gurchard's group reported another type of peptidomimetic foldamer constructed from urea backbones.^{37, 38} Unlike canonical γ -peptide oligomers, where amide bonds link the amino acids, the oligoureas foldamers' subunits were bonded through urea groups, which stabilize its structure by extra backbone rotation restriction and by providing an additional H-bond donor. In 2009, Guichard's group reported the first crystal structure of enantiopure N,N' -linked oligourea structure, which adopted a right-handed 2.5 helical fold that matches the previous structure calculations.³⁹ They also employed hybrid urea (U), amide (A) and carbamate (C) linkages to build the heterogeneous γ -peptide sequences,⁴⁰ the crystal structure of uAUUAU,

cUCUCU, cUUAUU sequences showed helical structures with different folding propensities, by varying the constituent of U in the sequence, the folding was found to be heavily dependent on the U units, whose strong folding tendency could compensate the relatively lower folding ability of A and C units (Figure 1.10).

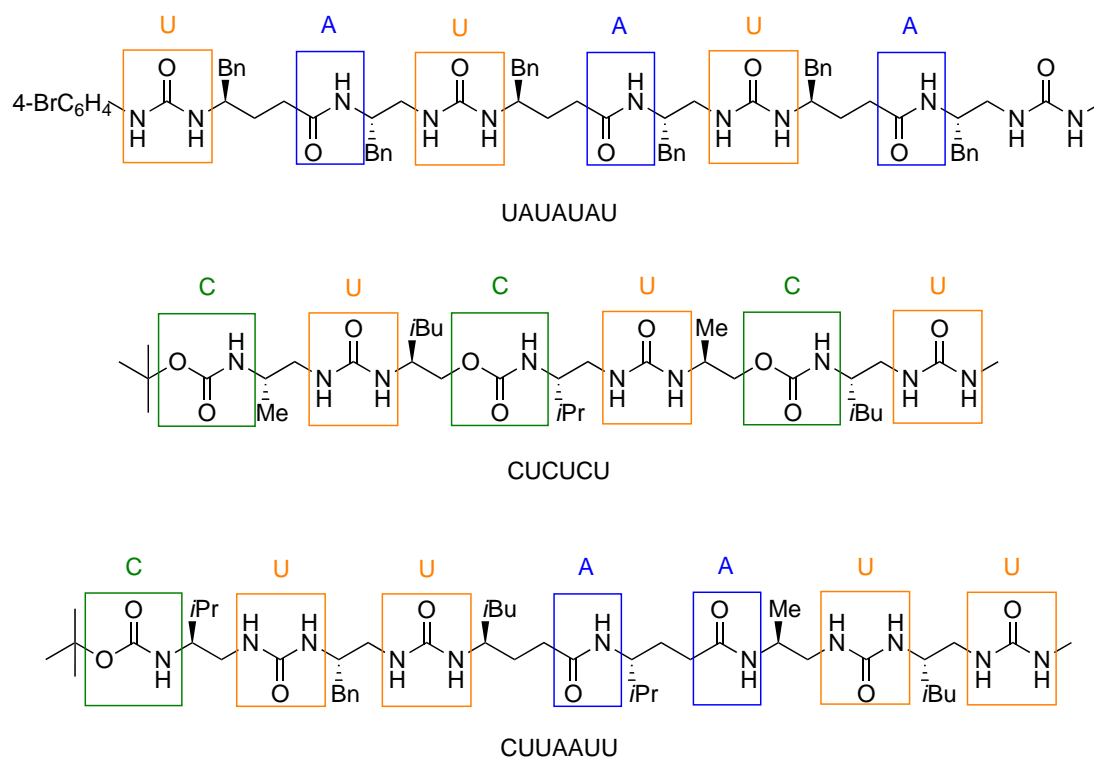


Figure 1.10 The sequences and structures of urea-bonded oligomers

1.5.2 Oligoarylamide Foldamers

In addition to peptidic foldamers, there is a great deal of interest in abiotic (not based on peptidic or nucleic acid) foldamer research. Unlike the peptidic foldamers, abiotic foldamers are composed of non-natural, synthetic building blocks, these components are not typically found in biological system. The arrangement of the subunit in the sequence, the linkage between the monomers, and electrostatic interactions (π - π stacking) are the driving forces for the folding of aromatic foldamers. Huc and co-workers have reported a series of helical structures with aromatic backbones: the pyridine dicarboxamide oligomers, which assembled into a double helix through extensive π - π stacking is reminiscent of DNA double-helix (Figure 1.11),⁴¹ whereas, in nature, the double strand structure is stabilized by the complementary H-

bonds of Watson and Crick, this not the case for the double-helix conformation of the foldamers. Fascinatingly, the perimeter of the helix structure in aromatic foldamers can be modified by changing the aromatic ring of the monomers. Also described by Huc and co-workers, the quinoline monomer (another type of δ -amino acid), forms a stable helical structure with different helical diameters from the pyridine oligomers (Figure 1.12).⁴² The structural variation that these different monomers lead to can be exploited to achieve even more complex secondary structures by mixing them into heterogeneous oligomers. For example, an oval-shaped helical structure has been achieved, where the helix has a narrow diameter at two ends and wide diameter in the middle (Figure 1.13). In this system, quinoline trimers, previously demonstrated to adopt a narrow helical structure, are positioned at each end of the hybrid oligomer to function as a cap of the oval shape.⁴³ The anthracene residues are placed in the middle of the sequence to guarantee the maximum diameter of the oval shape, and this special structure displayed an ability to bind various guests.

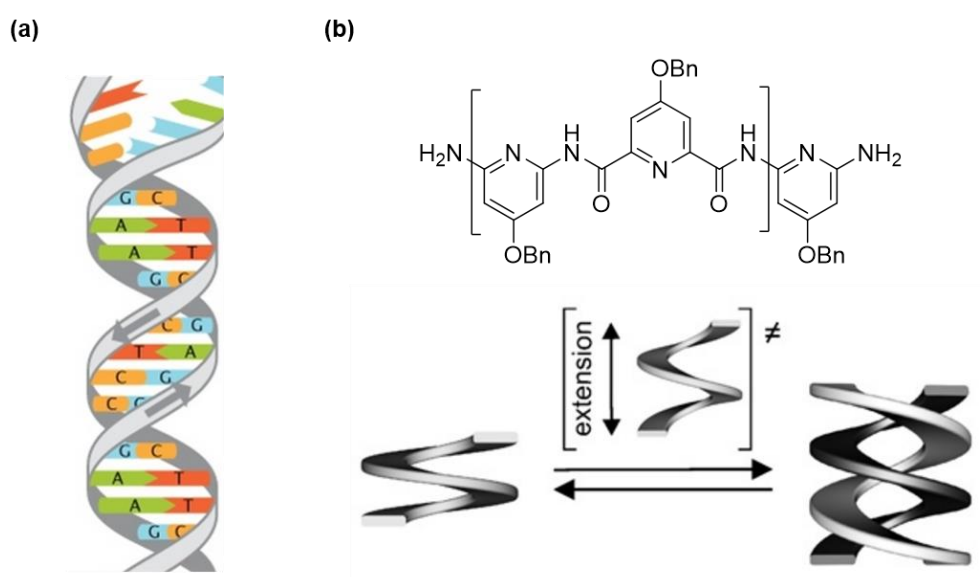


Figure 1.11 (a) DNA double helical structure. (b) The chemical structure of aromatic foldamer and the illustration of its dimerization into a double helix.

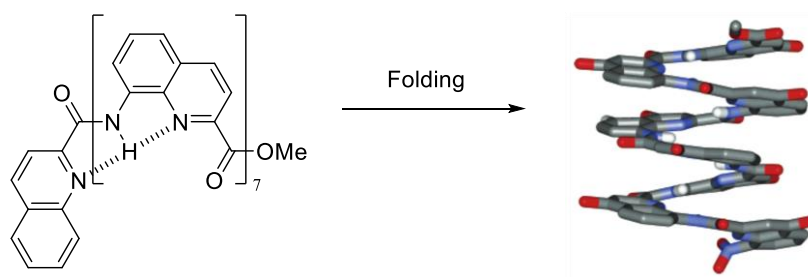


Figure 1.12 Structure and crystal structure of quinoline foldamer.

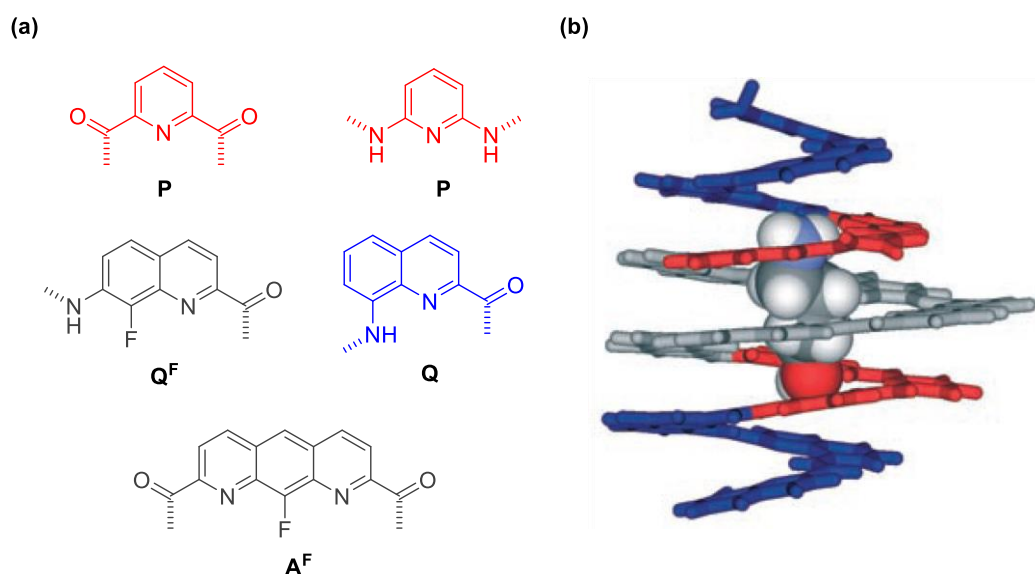


Figure 1.13 (a) The structures of five building blocks, **P** (red), **Q^F** (grey), **Q** (blue), **A^F** (grey). (b) Crystal structure of the heterogeneous oligomer encapsulating 4-amino-1-butanol.

In conclusion, the research into foldamer structure is not limited specific types of monomers. A variety of molecules can be incorporated into their design, and a diversity of building blocks brings an enrichment of secondary structure and - ultimately - functionality, which - pertinent to this thesis - includes catalysis.

1.6 Foldamer Catalysis

Unnatural peptides that fold into a helix will lead to a highly defined molecule which has a specific inner cavity, a helical chirality, and - importantly - a particular arrangement of the side

chains in three-dimensional space. Whilst the first of these is a potentially useful quality in host-guest recognition, as in Huc's systems described in the previous chapter, the latter two are potentially exploitable for asymmetric catalysis.

1.6.1 Bifunctional Foldamer Catalyst

Natural enzymes carry out their catalysis in a binding pocket where several functional groups are positioned to bind with the substrate, form the intermediate, and facilitate the product's release. Chymotrypsin is a well-understood example of this and facilitates peptide cleavage. Its catalysis is realized through what is described as the "catalytic triad" of serine, histidine, and asparagine. Despite being distant in the primary structure, the serine, imidazole, and asparagine side chains are close enough to form a hydrogen bond via the higher order structure that is adopted by the enzyme which brings these functionalities into close proximity.^{44, 45} During a peptide cleavage process, the serine functions as a nucleophile, and the histidine and asparagine assist with the proton transfer which ultimately precipitate the cleavage of the target peptide (Figure 1.14).

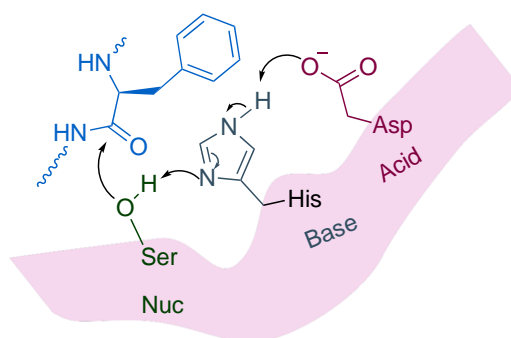
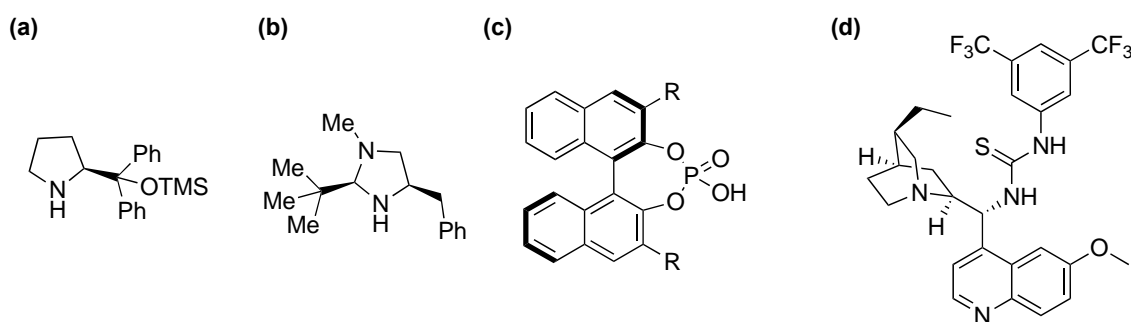


Figure 1.14 The sketch diagram of the active sites of chymotrypsin facilitating the peptide cleavage.

This multifunctional catalysis has inspired chemists to adopt the same approach but with much smaller and more simplified systems. In particular, organocatalysts are small molecules that catalyze reactions ranging from redox processes to C-C bond-forming and C-X bond-forming processes.⁴⁶⁻⁴⁸ They have the added advantage that they can be more durable under harsh conditions than proteins, and are less toxic than their metal catalysts counterparts. The Nobel Prize in 2021 was awarded to Benjamin List and David Macmillan for their seminal contributions to organocatalysis during the early 2000s, but the original inspiration came from

the proline catalysed Hajos-Parrish-Eder-Sauer-Wiechert domino process.⁴⁹ Whilst a small system in itself, proline is a bifunctional catalyst with its secondary amine and carboxylic acid functionality, which are both critical to its mode of action.

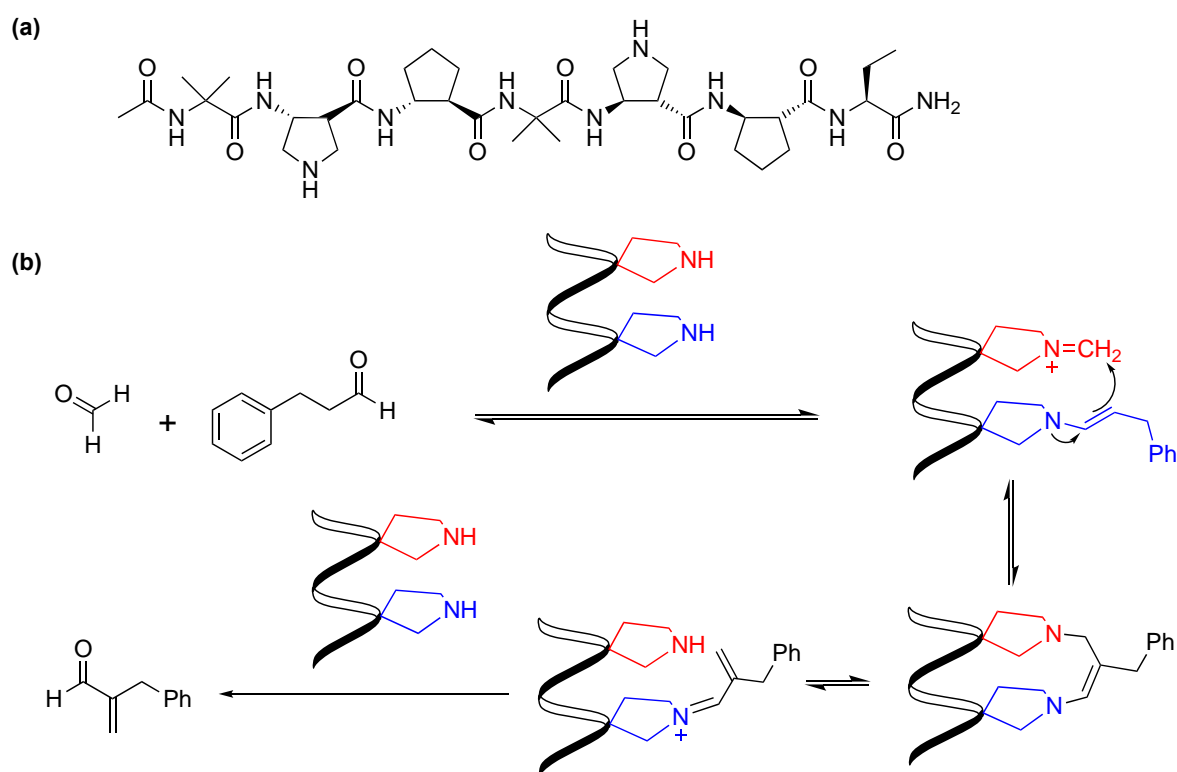
As shown in Scheme 1-1, a variety of common organocatalysts have been discovered over the years, all of which are capable of catalysing a diverse range of different processes to varying degrees of success, including proline derivative catalysts such as the Jørgensen system (Scheme 1-1a),⁵⁰ the imidazolidinones of MacMillan (Scheme 1-1b),^{51, 52} chiral phosphoric acids - commonly in the form of the BINOL systems (Scheme 1-1c),⁵³ and the bifunctional thiourea catalysts (Scheme 1-1d).^{54, 55} This review does not intend to be a comprehensive assessment of these modes of catalysis, but shows that with the right selection and placement of functionality on any scaffold (such as a helix), a catalytic framework can be produced.



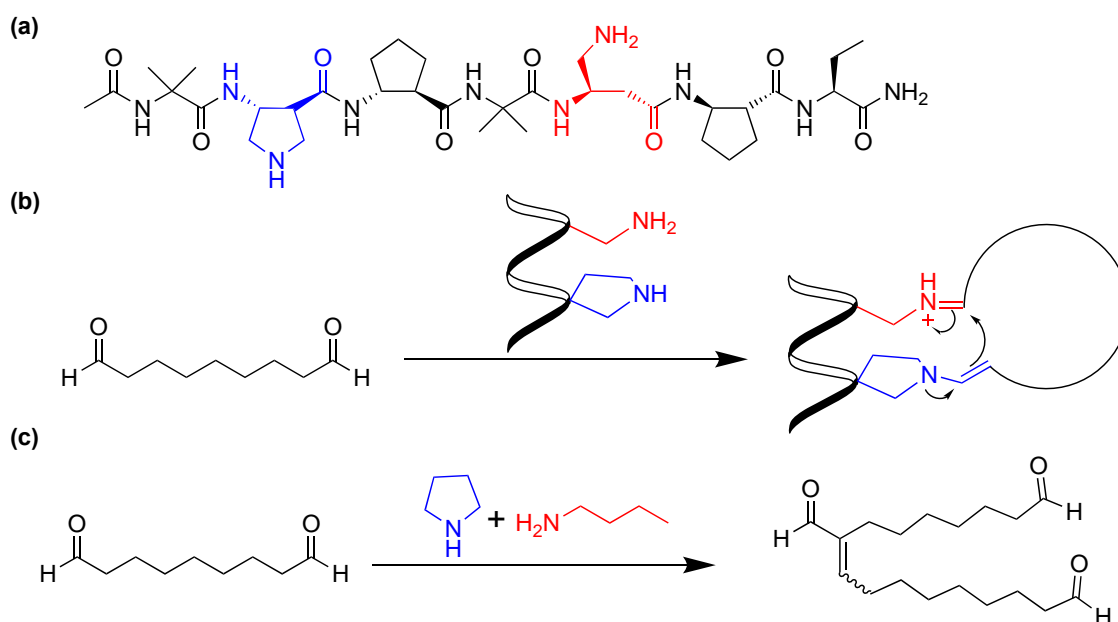
Scheme 1-1 Structures of organocatalysts of proline, imidazolidinone, phosphoric acid, thiourea derivatives.

Foldamers are good candidates for bifunctional catalyst design, as their folding propensity can bring functional group partners into useful proximity. A recent example of this was reported by Gellman and co-workers,⁵⁶ using a bifunctional foldamer constructed from α -amino acid and β -amino acids as described in section 1.4.1 The secondary structure of these scaffolds can be altered by alternating the ratio and arrangement of α - and β -residues, allowing for an easily adjustable catalytic foldamer structure that can be tailored towards a given model reaction. In this report, the aldol reaction was chosen as an assessment of activity using this library of β -peptides, 1:1 α,β -peptides, and 1:2 α,β -peptides.⁵⁶ The most successful catalysts of the library were those which folded to bring two amines together at a specific distance within the secondary structure. Initially, these were both pyrrolidines (i.e., secondary amines), where an electrophilic formaldehyde would condense with one of these (Scheme 1-2a, red part of

structure) to form an iminium ion, and the second pyrrolidine in blue would form the enamine with hydrocinnamaldehyde to generate the enamine. This then attacks the iminium, which is proximal enough thanks to the folding of the system, and thus form a new C-C bond. The relative rate was significantly improved using the combination of a secondary amine and a primary amine (Scheme 1-3). Furthermore, the aforementioned folding that brings the necessary bifunctionality together is critical for this reaction, as without it only a self-aldol reaction happens, as demonstrated when only butylamine and pyrrolidine were used without attachment to a preorganised scaffold (Scheme 1-3c).⁵⁷



Scheme 1-2 (a) Structure of α,β -foldamer catalyst. (b) Proposed mechanism of foldamer catalyzing aldol condensation.



Scheme 1-3 (a) Structure of foldamer catalyst. (b) Enamine and iminium intermediates-mechanism of peptide catalyzed ring-closing reaction. (c) Intermolecular aldol condensation catalyzed by butylamine and pyrrolidine.

Michaelis and Price and co-workers reported a further example of a bifunctional organocatalytic helix (Figure 1.15).⁵⁸ In this study, they used a 11-residue α -peptide where i and $i+3$ positions incorporated lysine and azidolysine respectively. As with Gellman's system, these residues became proximal in space by folding into a helix. These functionalities were well set up to attach catalytic functionality by click chemistry, first between the azidolysine residue and an alkyne-linked MacMillan imidazolidinone, and second through the reaction of the lysine residue with arylisothiocyanate. This generated a helix which contained a thiourea and a secondary amine in close proximity - common bifunctional partners in organocatalysis. As described in Figure 1.15, the catalytic Diels-Alder reaction is particularly well-served by the MacMillan catalyst and consequently, this was the reaction of choice for these catalyst systems. As might be expected, the CbzNH-diene substrate could interact via a hydrogen bonding between the carbamate and the thiourea, and the but-2-enal substrate could be activated via the iminium intermediate through interaction with the imidazolidinone. The first generation MacMillan catalyst **1** was chosen to contrast the reactivity of proximity-induced reactivity by foldamer **2**. The dienes CbzNH-diene **7** and cyclopenta-1,3-diene **8** were therefore used together in a competition study - the rationale being that the bifunctional foldamer catalyst would prefer reaction with the diene **1** (having been activated by the lysine residue), whereas

the MacMillan catalyst would prefer to accelerate the reaction of cyclopentadiene. Indeed in this study, this was shown to be the case where imidazolidinone **1** catalyzed the formation of product **6** in 27% yield and product **4** in 19% yield, whereas, the foldamer catalyst **2** catalyzed mainly the formation of product **4** in 48% yield and product **6** in 3% yield - remarkably with only 1 mol% loading (Scheme 1-4a, Table 1-1). The bifunctional catalyst **2** was also found effective in the indole alkylation reaction between Cbz-protected N-methyltryptamine **10** and acrolein **9** in 76% yield and 42% ee compared to 21% yield and 8% ee catalyzed by **1** (Scheme 1-4a, Table 1-1). However, it is unclear whether any enantioinduction comes from the helix or the local environment of the imidazolidinone.

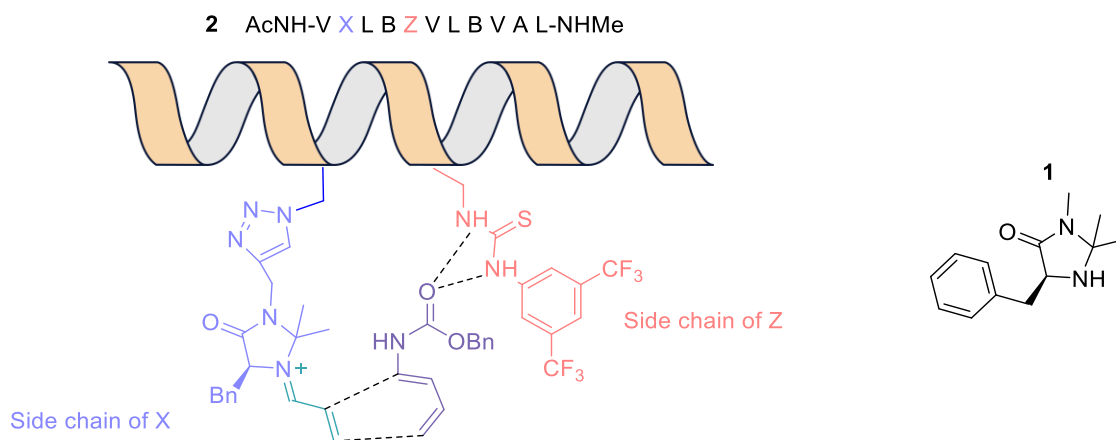
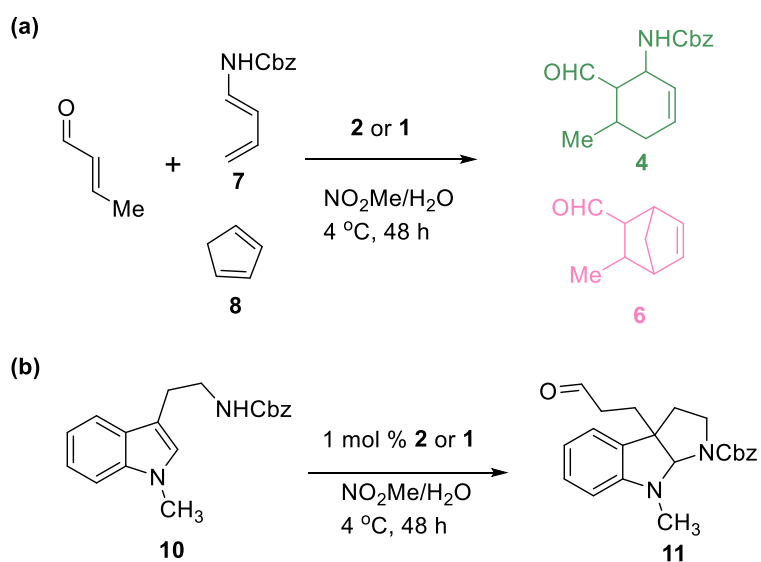


Figure 1.15 Illustration of bifunctional peptide catalyst



Scheme 1-4 (a) Diels-Alder reaction catalyzed by peptide **2** and MacMillan catalyst **1**. (b) alkylation of Cbz-containing indole derivatives catalyzed by peptide **2** and MacMillan catalyst **1**.

Table 1-1 Isolated yield of catalytic reaction.

	1 mol% 2	10 mol% 1	1 mol% 1
4	48	19	
6	3	27	
11	76 (42% ee)		21 (8% ee)

1.6.2 Other Enantioselective Helical Catalysis

The helical structure is the major secondary structure among foldamer research and can be either left-handed helix (*M*) or right-handed (*P*). This chiral folding pattern, therefore, has the potential to allow the transfer of chiral information.

Jonathan Clayden and co-workers has reported a foldamer helix where most of the constituent parts are actually achiral, but the terminal residue contains a stereocentre. This leads to a chirally selective induction over a distance up to 4 nm (Figure 1.16).^{59 58} The initial foldamer without this chirality-influencing terminal residue was constructed solely with the *gem*-dimethyl amino acid aminoisobutyric acid (Aib), where the resulting oligomer adopts a 3₁₀ helical racemic mixture of left-handed and right-handed structures which can interconvert rapidly in solution. By introducing one or two L- α -methylvaline residues at the N-terminus, the resulting structure preferred right-handed structure in MeOH and THF. In THF, the oligomer with two L- α -methylvaline ligated at the N-terminus adopted a quantitative amount of just the right-handed structure. The ligation of three L- α -methylvaline shows no improvement in the oligomer's chiral preference, indicating that two chiral residues are sufficient for the induction of foldamer chirality. The property was then applied to the asymmetric induction of a prochiral alkene reduction reaction on the oligomer side chain. By replacing the middle Aib residue with Phenylethene-residue, after treating the metal reductive reagent, the hydrogenated product preferred the L-conformation, with 95:5 selectivity in

dichloromethane and 89:11 selectivity in ethanol (Figure 1.16b). Furthermore, the asymmetric induction was demonstrated to transfer from one end of the helix to the other, leading to control of an asymmetric C-C bond forming reaction over 60-bonds away with 88:12 selectivity (Figure 1.16c).

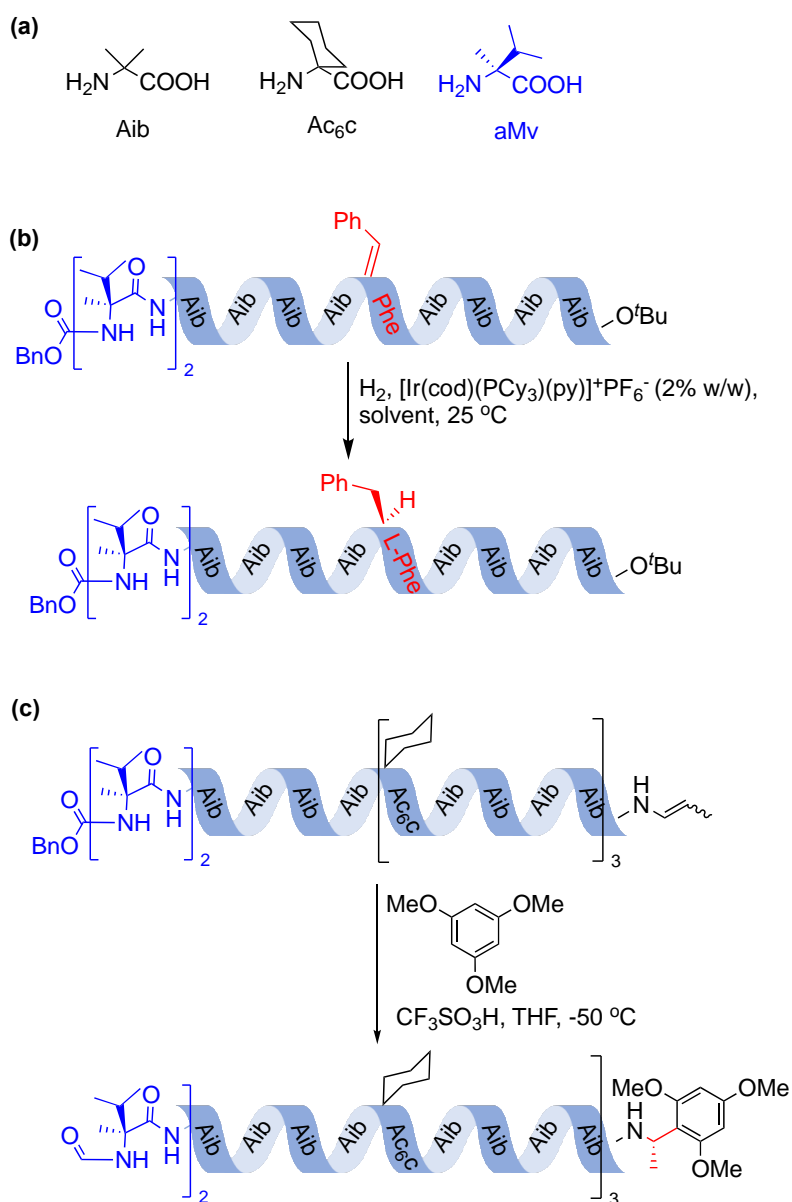
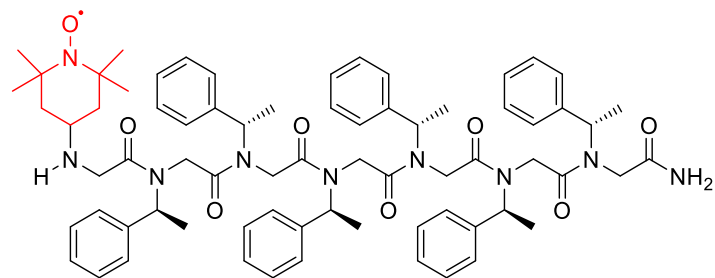
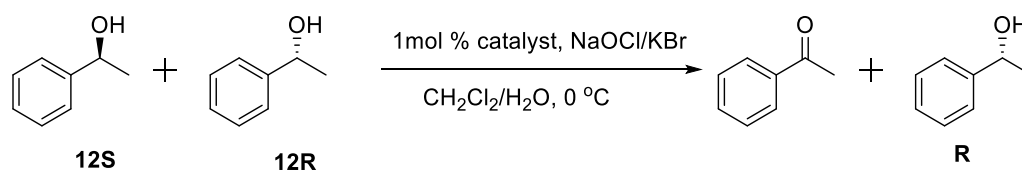


Figure 1.16 (a) Structure of building blocks. (b) Asymmetric hydrogenation induced by right-handed helix. (c) Remote asymmetric induction through achiral helices.

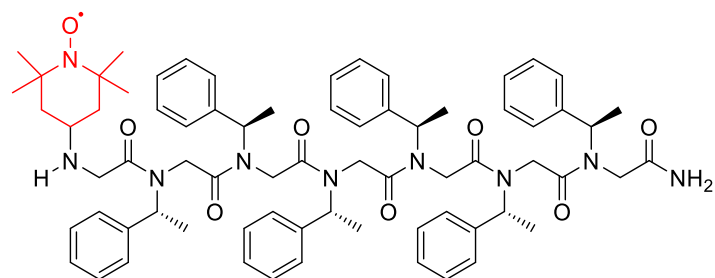
Kent Kirshenbaum and co-workers has reported a series of peptoid oligomers that catalyse an asymmetric resolution of secondary alcohols by oxidation. The peptoid foldamers were

constructed with a glycine-derived backbone, where side chains at the nitrogen atoms on the backbone introduced chirality. The catalytic site of the foldamer catalyst was introduced by covalently bonding TEMPO at specific N-positions of the backbone.⁶⁰ (Figure 1.17). The CD spectrum shows the peptoid oligomer adopts an ordered secondary structure, where the spectra of **1S** and **1R** show inverted CD profiles suggesting that they have mirror-imaged secondary structures. The oxidation resolution of 1-phenylethylamine **12** was chosen as a model reaction, where in addition to the catalytic peptoids, the combination of TEMPO and phenylethylamine were tested as a non-structural controls. As expected, **1S** and **1R** facilitated the oxidation of one enantiomer of **12** over the other at the same rate of conversion but with opposite enantioselectivities. However, catalysts with TEMPO at the non-terminal positions of the backbone, as shown in **2S** and **3S**, were slightly active but no enantioselectivity was observed - presumably caused by lack of interaction between the substrate and any significant chiral environment. This work exhibits a way of synthesizing a new type of peptoid oligomer and introduces a way of installing chirality onto the non-chiral backbone. The activity and enantioselectivity of peptoid catalysts also demonstrated that chiral information could be transferred to the achiral catalytic site via side-chain modification, bringing up a new method for asymmetric catalyst design.

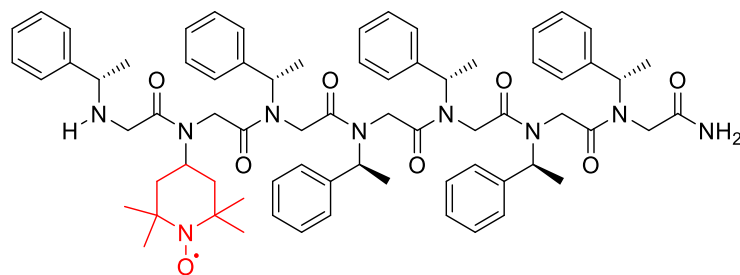
Maillard and co-workers have reported a thiazole-based γ -peptide being used as an enantioselective catalyst for Michael addition reaction (Figure 1.18).⁶¹ The thiazole based γ -amino acid was demonstrated to have a high helical propensity both in solid state and in organic solvents, and even in water. The substitution on the side chains shows little effect on the secondary structure of the helix. Hence the carboxylic acid and proline were installed on one residue to functionalize as a catalyst for the enantioselective Michael addition reaction. Compared with the monomer catalyst **17** which gave just 45% ee of Michael adduct, the tripeptide with a secondary structure enhanced the ee to 74%. Extending the peptide length to pentamer shows no further improvement in the enantioselectivity. Likewise, shortening the carboxylic acid side chain did not affect enantioselectivity either, but the yield of the reaction was decreased, implying a necessary cooperative role of the carboxylic acid group in the process.



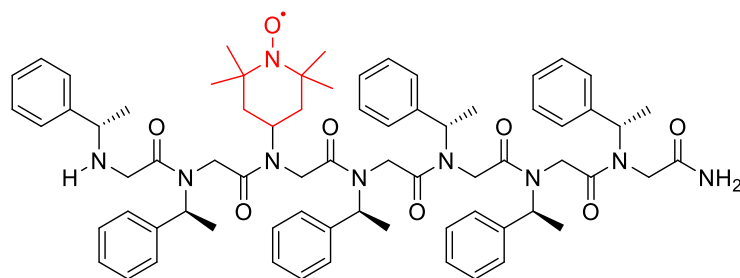
1S 84 % conversion, >99 % (R) ee



1R 85 % conversion, >99 % (S) ee



2S 26 % conversion, None ee



3S 25 % conversion, None ee

Figure 1.17 The structure of peptoid foldamers and their efficiency on alcohol oxidation.

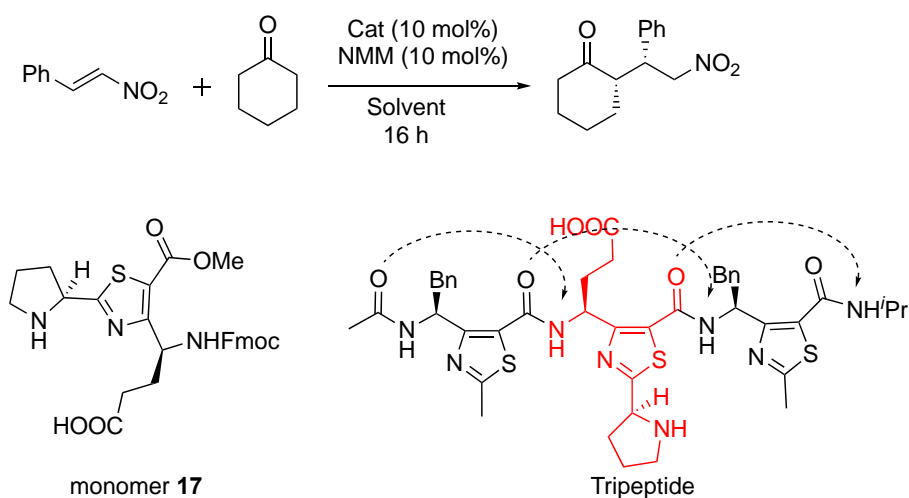


Figure 1.18 The catalytic Michael addition reaction and the helical structure of thiazole peptide.

Guichard and co-workers have reported an oligoureia-based peptide and demonstrated its highly effective asymmetric catalysis on the Michael addition reaction with exceptionally low catalyst loading (0.01 mol%) (Figure 1.19).⁶² The result shows 99% ee was realized with only 0.1 mol% of oligoureia catalyst loading. Remarkably, the ee% could be still reasonably high - 74% - even at 0.001% loading. The thiourea foldamer analogue showed similar reactivity but slightly lower ee (93%) under the same conditions (compared with unfolded short oligomers where the monomer showed less than 8% ee - again indicating the importance of secondary structure on catalytic efficiency).

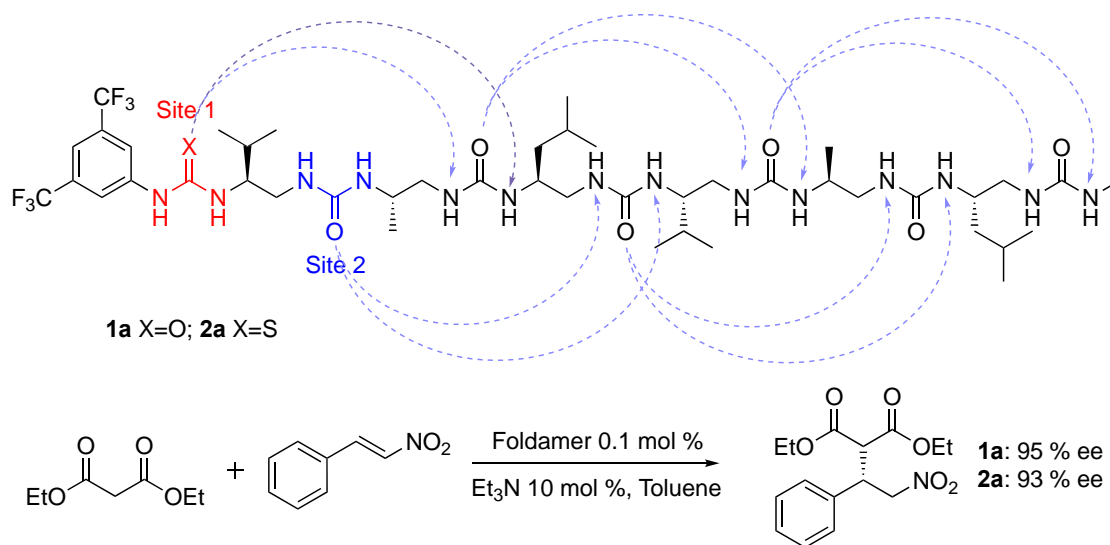


Figure 1.19 The helical structure of urea foldamer and the catalytic reaction.

1.6.1 Catalysis with Higher-Order Structure

In nature, some proteins implement functionality that is dictated by the quaternary structure adopted. Such quaternary structure is constructed by the precise arrangement of subunit domains to form dimers or larger homo-oligomers. Hence enzymatic catalysis happens not only within a protein monomer, but sometimes, the substrate might be encapsulated at the interface of several monomer conjunction sites. Linalool dehydratase (LinD) is an enzyme that catalyzes the dehydration of linalool to form the myrcene product and, in the absence of oxygen, can catalyze its isomerization to geraniol.⁶³ Whilst an accurate mechanism has not yet been confirmed for these processes, research has proposed that its quaternary structure is critical, a high resolution structure of it indicates a pentamer format, where the active site might be the interface of two adjacent monomers. Regardless, there are two possible mechanisms. In the first, the thiol of Cys-171 protonates the allylic alcohol of linalool **14**, thereby promoting either an E₁ elimination by Tyr-45 to give myrcene **15**, or an S_N1' attack by water, facilitated by Cys-180 to give geraniol **16** (Figure 1.20).

Similarly, foldamers could also be self-assembled into a higher-ordered structure to catalyse chemical reactions. In recent years, several groups have reported the formation of foldamer

bundles to enhance foldamer-driven catalysis. Donald Hilvert and co-workers reported a β -peptide, constituted with ACHC residues that assemble into a helix bundle that was utilized for the catalysis of a retro-aldol cleavage (Figure 1.21). The retro-aldol cleavage of β -hydroxyketone was chosen as a model reaction.⁶⁴ As is typical in aminocatalysis, the ketone on the oxalyl substrate forms an iminium ion intermediate with the catalyst. This tautomerises to the enamine, which then facilitates bond cleavage via retro-aldol and eventual recycling of the catalyst. The ACHC β -residue was demonstrated to adopt a stable 14-helix structure, with the side chain of i , $i+3$, and $i+6$ residue aligned along the same side of the helix. In aqueous solution, the cyclic constraint, and the electrostatic interactions between the lysine side chains stabilize the helicity of the peptide, and thus place all the amine side chains adjacent to each other on one side of the helix. The concentration of non-protonated amines is improved by the existence of adjacent cations, thus improving the nucleophilicity of the amine catalyst. This was confirmed when comparing the retro-aldol cleavage activity of self-assembled peptide and a non-bundled peptide, where the former has significantly improved retro-aldol efficiency.

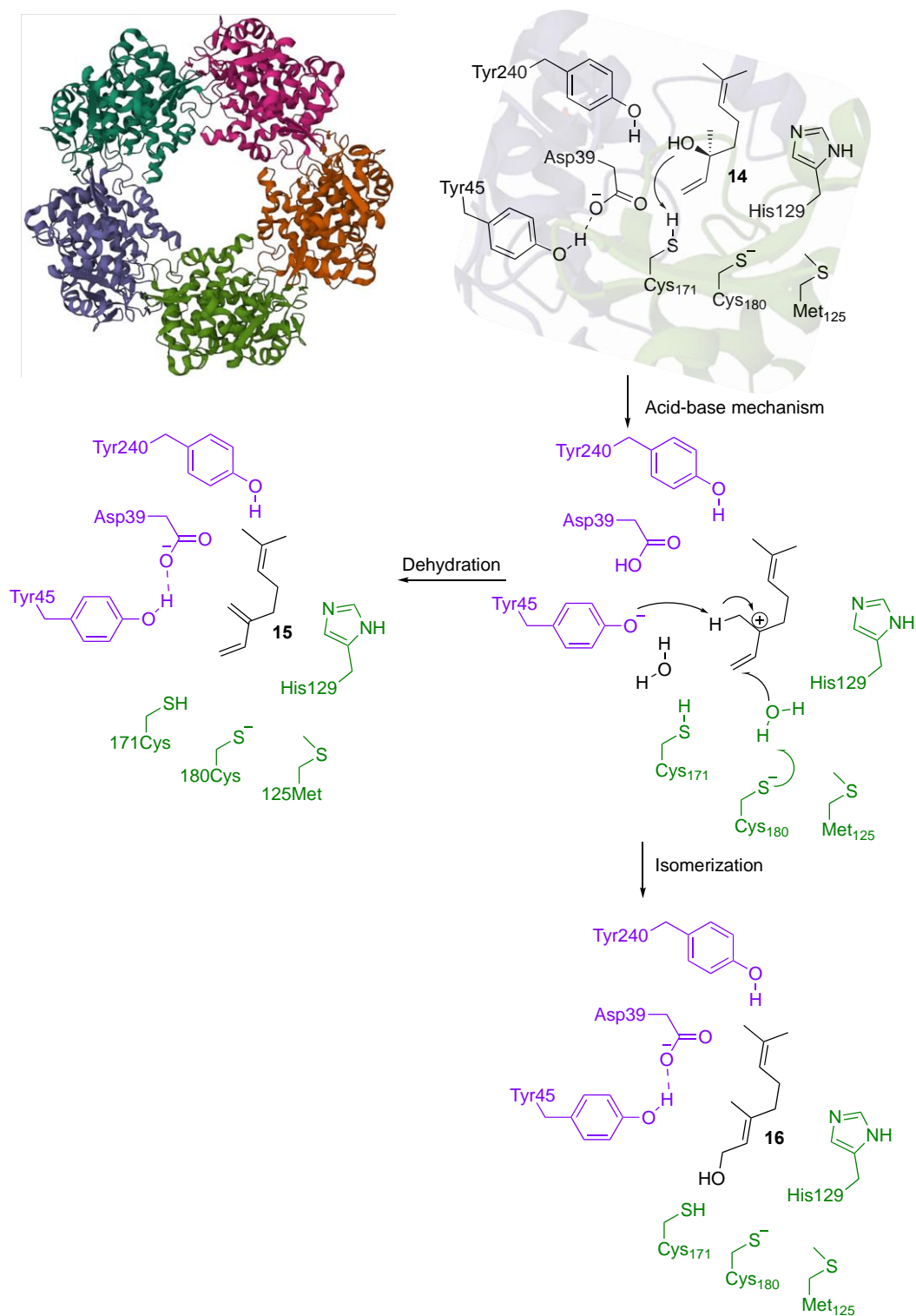


Figure 1.20 Crystal structure of linalool dehydratase and the proposed mechanism of dehydration and isomerization.

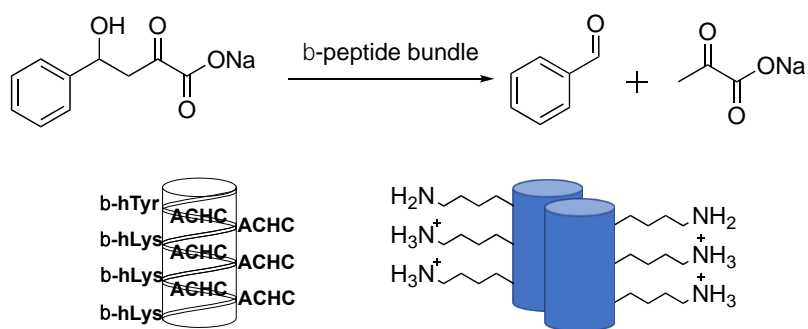


Figure 1.21 The helix bundle of β -peptide and the structure of retro-aldol cleavage.

Alanna Schepartz and co-workers have reported a protein-like helix bundle which possesses both thermostability and catalytic functionality. The β^3 amino acids constructed foldamer was demonstrated to form a helix which self-assembles into the structure of Zwit-EYYK (**12-mer**), which was demonstrated to be a kinetically stable bundle (Figure 1.22).⁶⁵ The hydrolysis of 8-acetoxypyrene-1,3,6-trisulfonate was chosen as the substrate to evaluate the esterase activity of the bundle structure. The guanidine side chain of the arginine is introduced to interact with the sulfonate groups on the substrate and the histidine function as an electrophile or acid/base catalyst. With the reasonably positioned arginine and histidine in the peptide sequence, the bundle structure could be minimally perturbed at high concentrations. However, some sequences were primarily monomeric below 25 μM . To maintain bundle stability, they designed a dimer by the covalent linkage of two monomers with a tetra- β -homoglycine linker (**28-mer**). The dimerization of the helical structure stabilized the bundle structure to >80% formation at 25 μM . The crystal structure of the helix bundle shows that the foldamer adopts a quaternary structure with tetramer-tetramer interaction to form an octameric structure. This resulting complex has an increased catalytic efficiency of almost 100-fold, which benefited from the higher order structure and accumulation of multiple catalytic sites in the appropriate positions.

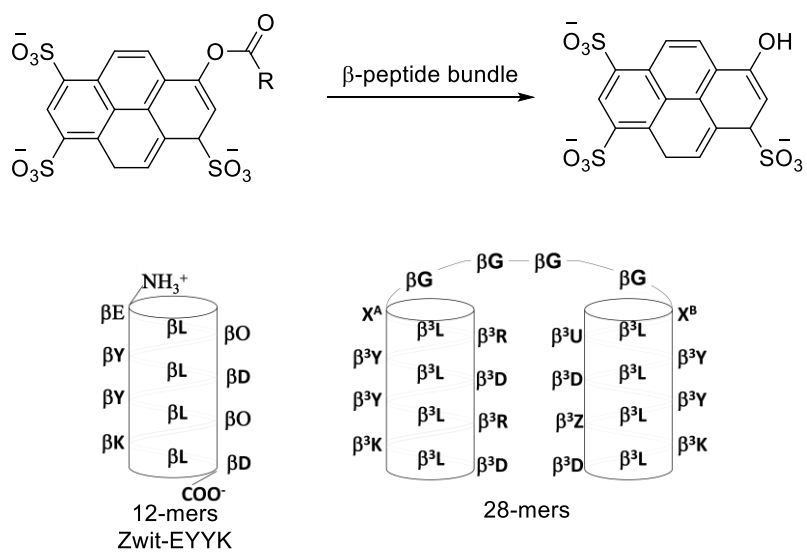


Figure 1.22 The dimerization of the helical structure and the catalytic hydrolysis reaction.

Chapter 2 A Novel 13/11 Helix from 1:1 α - and δ -Amino Acids

2.1 Introduction

As described in Chapter 1, foldamers are versatile structures with the potential to display functionality such that it can be exploited for catalysis. Nevertheless, the study of δ -foldamers in this respect, is still in its infancy - primarily because of the difficulties in synthesizing the required enantiopure δ -residues. The uniqueness of δ -amino acids amongst other unnatural amino acids is that there are the same number of atoms between the C- and N-termini as in one α -dipeptide, endowing δ -amino acids with the possibility of adopting a 13-helix structure as seen in a natural α -helix. Both Hofmann³⁵ and Hosahudya³⁶ have reported examples of aliphatic linear α,δ -peptide that adopt a 13/11-helix. Very recently Shuto and co-workers reported a cyclically constrained homo- δ -peptides which adopted a 14-helix, which was verified by crystal structure and NMR based calculation (Figure 2.1).⁶⁶

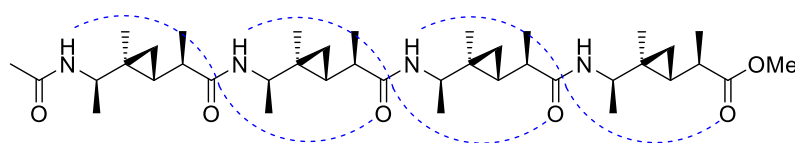


Figure 2.1 The helical structure of homo- δ -peptides

Hoffman and co-workers have calculated the possible folding pattern of α/δ peptides with a 1:1 alternating backbone. Figure 2.2 shows most stable helix types of α/δ hybrid peptides.³⁵

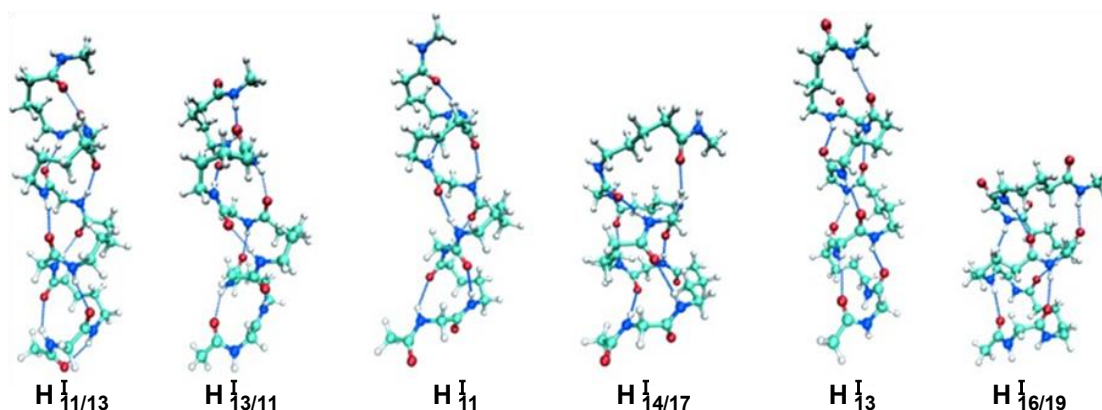


Figure 2.2 Representatives of different helical types.

Of all the structures predicted by Hoffman's calculations for these 1:1 α,δ -peptides, we were particularly drawn to the ones that might have a unique 13/11-helix, as we believed this structure would exhibit some very useful features for catalyst design. As shown in Figure 2.3, the α -residues (in yellow) appear within the helical centre and the δ -residues (in blue) occupy the perimeter of the helix. If the catalytic functionality is positioned on the α -residue, this would be embedded within the helix, with the neighbouring δ -residues furnishing the exterior. Together this would represent a potential designer binding site. The cyclohexyl δ -residue **19** (Table 2-1) was predicted to ideally adopt a conformation that would lead to the most stable 13/11-helix according to Hofmann's calculations.

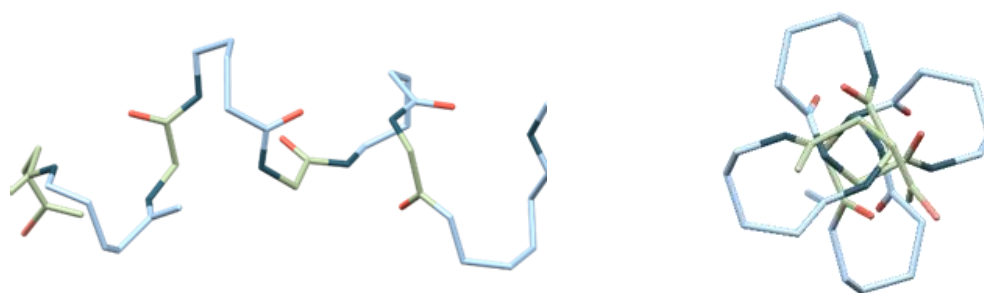
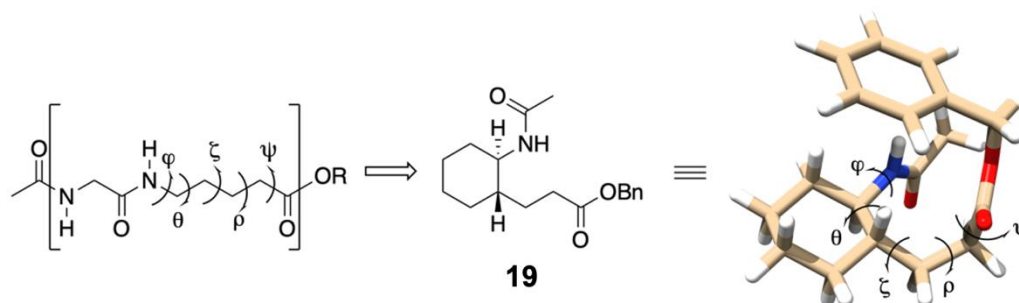


Figure 2.3 Top and side view of calculated 1:1 α,δ -peptides, green color represents α -amino acid, blue color represents δ -amino acid.

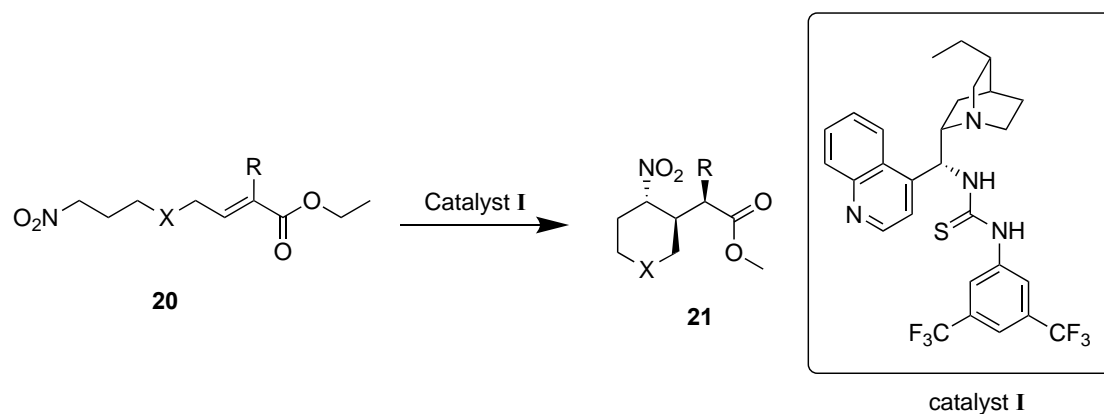
Table 2-1 The cyclohexyl δ -residue **19** was shown to comfortably adopt a conformation that would lead to the most stable 13/11-helix according to calculations



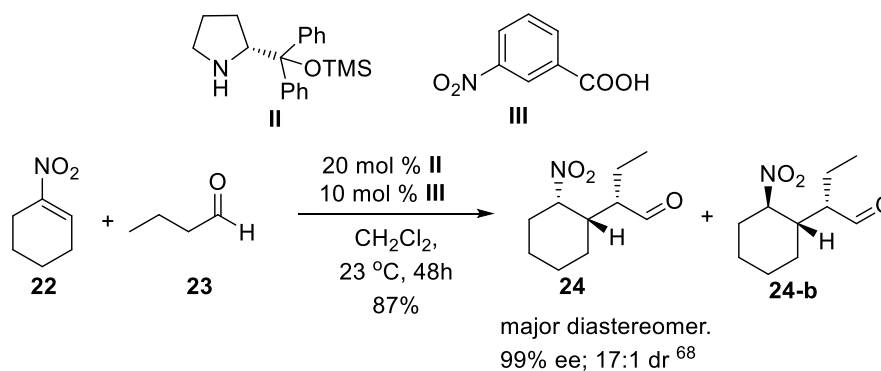
	φ	θ	ζ	ρ	ψ
Proposed angles for a 13,11-helix	-135.6	-72.4	66.9	54.9	-139.3
Low energy conformation of monomer 19	111.1	-63.6	73.2	48.5	-125.0

2.2 α,δ -Foldamer Synthesis

The cyclically constrained δ -residue could potentially be made by one of two methods, both involving the homologation of the related γ -amino acid precursor systems. The first, devised by Cobb and co-workers in 2009, involves catalysis by a thiourea catalyst **I** of intramolecular Michael addition of a nitronate onto a conjugated ester (Scheme 2-1).⁶⁷ Gellman and co-workers reported a different method of synthesizing a very similar γ -amino acid **24** (Scheme 2-2) by using pyrrolidine-catalyst **II**, which facilitated the Michael addition between butanal and nitro cyclohexene in high enantioselectivity.⁶⁸ Gellman and co-workers found that adding 10% cocatalyst **III** improved the product's yield and diastereoselectivity, as the benzoic acid might play an important role in the hydrolysis of the iminium intermediate. Due to both its scalability, and the easier homologation of the aldehyde compared to the ester, this method was chosen as a protocol for synthesizing γ -amino acids.



Scheme 2-1 The synthesis of γ -amino acid precursor proposed by Cobb's Group



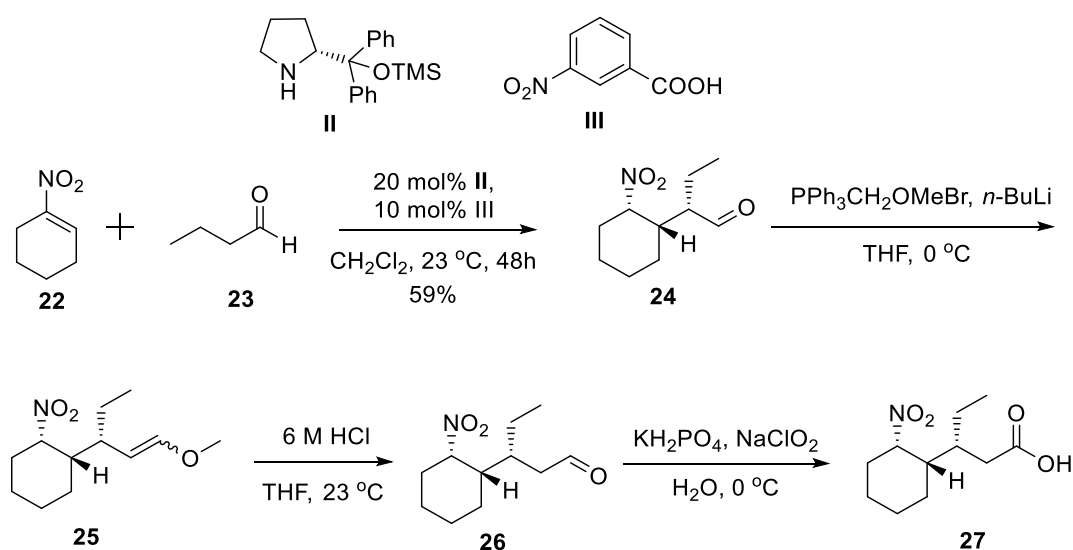
Scheme 2-2 The synthesis of γ -amino acid precursor proposed by Gellman's Group

The plan for constructing the α,δ -peptide is to access the desired δ -amino acid after homology and to combine it with the appropriate α -amino acid in a short oligomer sequence. In terms of the α -amino acid, alanine with its single methyl side-chain is a good choice to start with, as firstly, it improves solubility in organic solvent over glycine, also has the ability to adopt more conformations than glycine, and excludes potential side-chain interactions during any potential folding.

2.3 Results and Discussion

2.3.1 Synthesis of δ -Amino Acid

As shown in Scheme 2-3, the homologation of γ -amino acid precursor **24** through the Wittig reaction produced both the *Z* and *E*-configurations of the olefin **25**. The purification of these two stereoisomers is unnecessary, as the following hydrolysis will convert both configurations into a single aldehyde. Some epimerization occurs at the nitro-position at this stage, which presumably arises from reaction with any unreacted *n*-BuLi from the Wittig reaction. This mixture of **25** isomers were hydrolyzed to form the aldehyde **26** which was then oxidized to the carboxylic acid **27**. Again, during this process, some amount of the *trans*-adduct was discovered, but as the target δ -residue is the *trans*-conformer, which would be formed from epimerisation anyway, all material was taken through.



Scheme 2-3 Synthesis of δ -amino acid precursor

To study the structural preference of the α,δ -peptide, we planned to make an octamer with alternating 1:1 α,δ residues whose length would be sufficient to observe peptide folding properties. The 1:1 α,δ -peptide could be arranged with either α -residue at the N-terminus and δ -residue at the C-terminus or vice versa. For $\alpha\delta\alpha\delta\alpha\delta$ -sequence synthesizing, the building blocks are compounds **28** and **30** (Figure 2.4). For $\delta\alpha\delta\alpha\delta\alpha$ -sequence synthesizing, the

building blocks are compounds **29** and **31**. The α -alanine compounds are commercially available, whereas the δ -building blocks **28** and **29** must be synthesized from δ -residue precursor **27**.

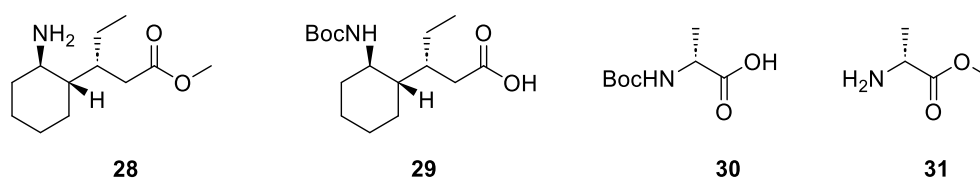
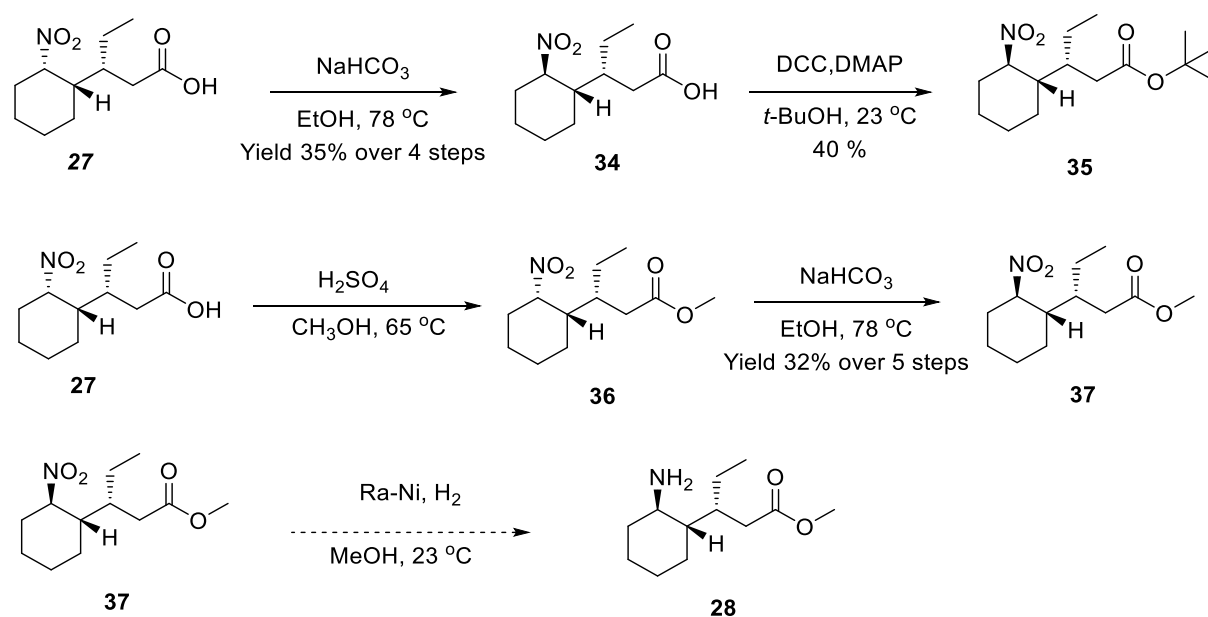


Figure 2.4 The building blocks for synthesizing α,δ -peptide

2.3.2 Synthesis of Building Block 28



Scheme 2-4 Synthesis of ester-protected δ -residue

We first tried to epimerize the *cis*-cyclohexane **27** to *trans*-conformer **34** at the carboxylic acid stage before adding the ester group, but unfortunately *tert*-butyl ester protection on carboxylic acid **34** using DCC-coupling gave only a 40% yield (Scheme 2-4). To improve this, we decided to have the C-terminus protected with a methyl ester, which was achieved a high yield by heating carboxylic acid **27** in methanol at reflux with a few drops of H_2SO_4 . The epimerization of *cis*-isomer **36** to *trans*-isomer **37** then proceeded smoothly using sodium bicarbonate in methanol (Scheme 2-4). However, on reduction of the nitro-group using Raney-Nickel

hydrogenation to generate building block **28**, we found an unexpected lactam formation. The possible mechanism behind this is that after the nitro was reduced to an amine, because of the geometry of the molecule and the stability of the six-membered ring, the amine would then attack the C-terminus of the δ -residue and form lactam within a few hours. The product was characterized by NMR which verified the formation of the lactam (Figure 2.5). The ^1H NMR showed a singlet at 6.9 ppm which is the amide bond of the lactam compound, and the C NMR confirmed a carbonyl carbon at 172.65 ppm, both verified the formation of lactam at room temperature. The 2D NMR correlation also proved the ring formation with the structure.

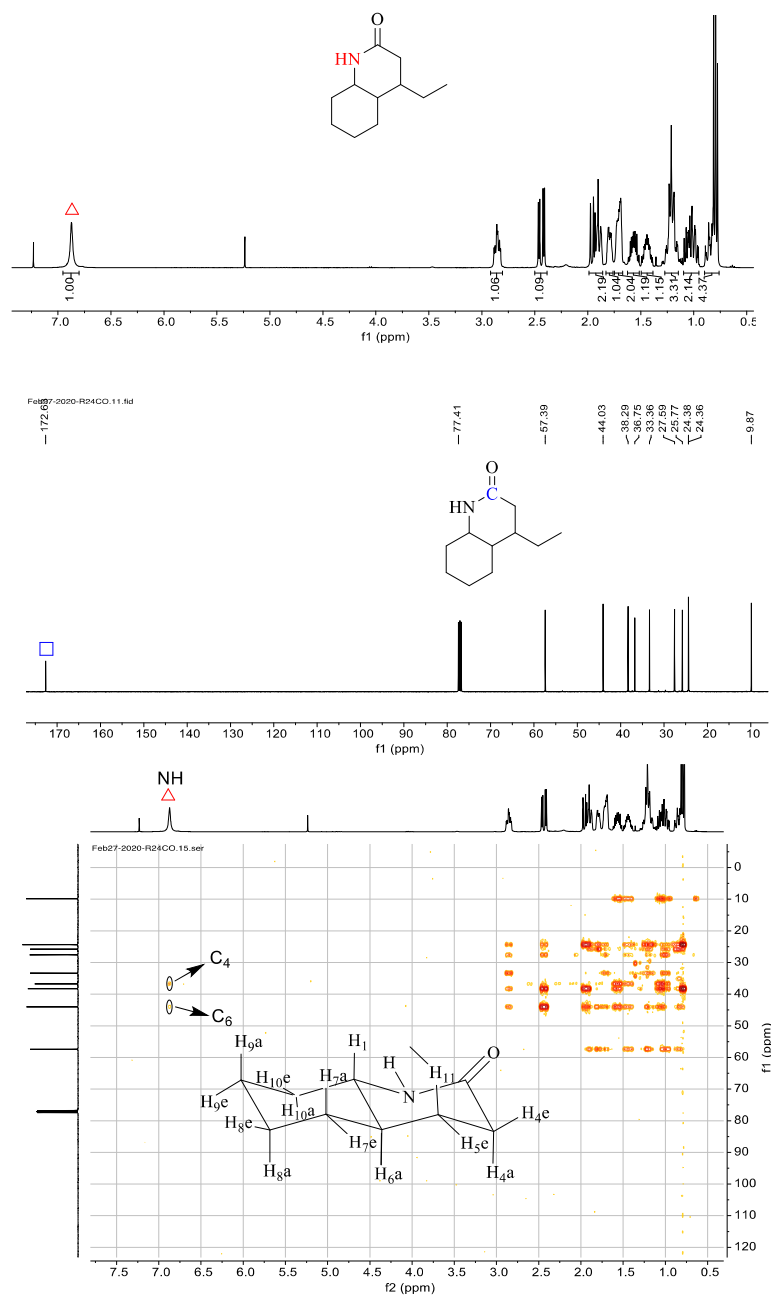
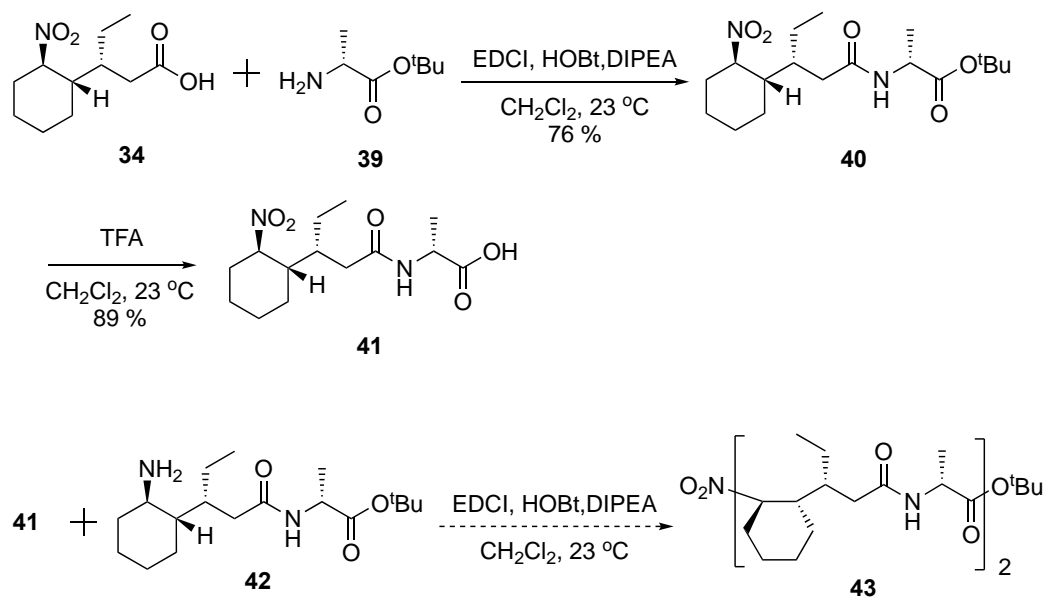


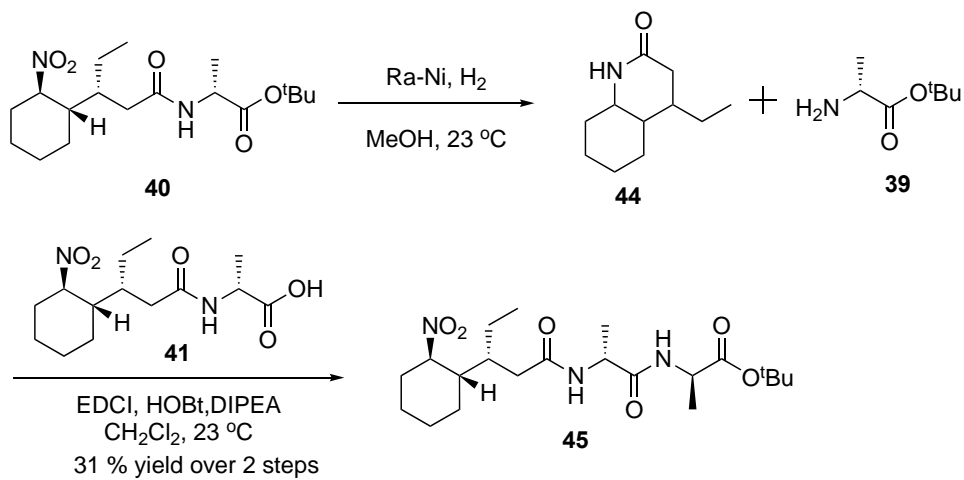
Figure 2.5 ¹H NMR, ¹³C NMR and HMBC of lactam in CDCl₃

To avoid lactam formation, we plan to synthesize the peptide with $\delta\alpha\delta\alpha\delta\alpha$ -sequence, using $\delta\alpha$ -dipeptide **40** as the building blocks where the δ - and α -residue are bonded with an amide bond (Scheme 2-5). As the amide is less reactive than an ester towards nucleophilic attack, there is less chance of lactam formation after the nitro is reduced to an amine. With the dipeptide **40** successfully synthesized in a high yield, the plan was to deprotect the C-terminus

to get **41**, reduce the nitro group to get **42**, and couple the two dipeptides to get a $\delta\alpha\delta\alpha$ -tetramer **43**. The Raney-Nickel hydrogenated crude product of **40** was brought directly into the next step without purification. However, instead of forming the tetramer, the coupling reaction between compound **41** and the hydrogenated product of **40** gave a product that was analysed to be **45** (Scheme 2-5), showing that δ -lactam formation is unavoidable even with the amide bond present. We then monitored the speed of spontaneous self-cyclization of **42** by NMR in CDCl_3 (Figure 2.6). After two hours of the hydrogenation reaction, 50% lactam was formed from the crude, and the total conversion was completed after 6 h.

Proposed scheme of synthesizing $\delta\alpha\delta\alpha$ tetramer

Actual products because of lactam formation

Scheme 2-5 Strategy of synthesizing $\delta\alpha\delta\alpha$ -tetramer

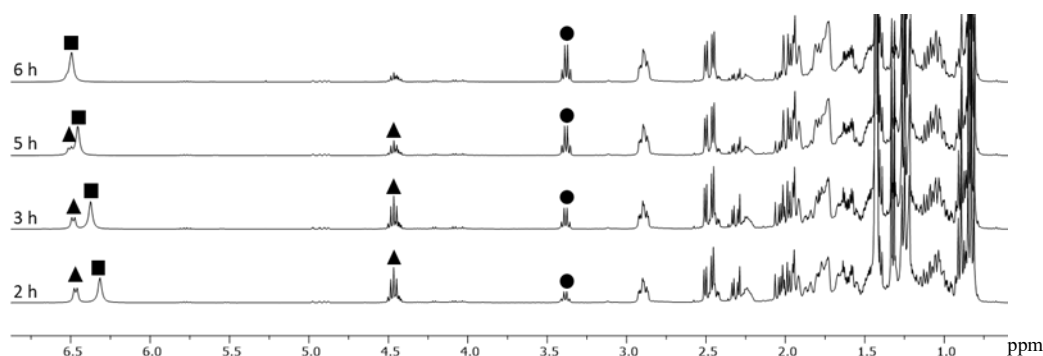
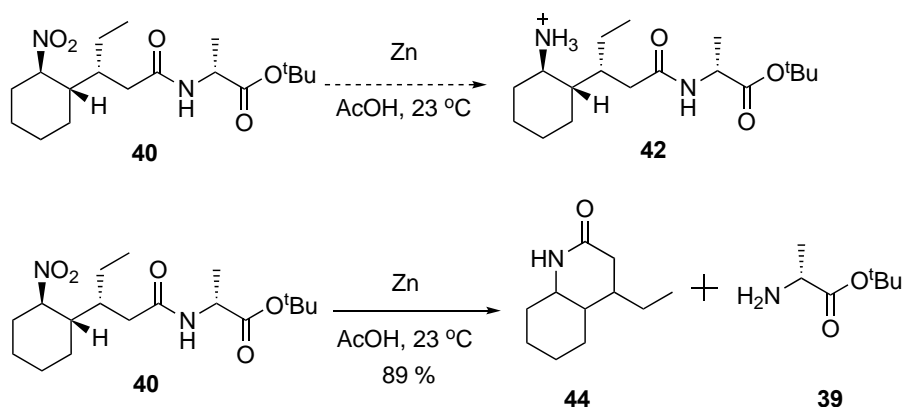


Figure 2.6 Cyclization process monitored by ^1H NMR: (400 MHz, CDCl_3). lactam is marked by “■”; dipeptide is marked by “▲”; α -residue is marked by “●”.

To circumvent this outcome, we decided to modify the conditions of the hydrogenation process in the hope that we could control the rate of cyclization. The hydrogenation of the nitro-group by Raney-Nickel is performed under neutral conditions, where the amine is unprotonated and whose nucleophilicity is stronger than the protonated amine. Therefore, we proposed to undertake the reduction in acidic conditions. Unfortunately, under the acidic conditions shown in Scheme 2-6, the product was fully transferred to lactam after 2 h of reaction.

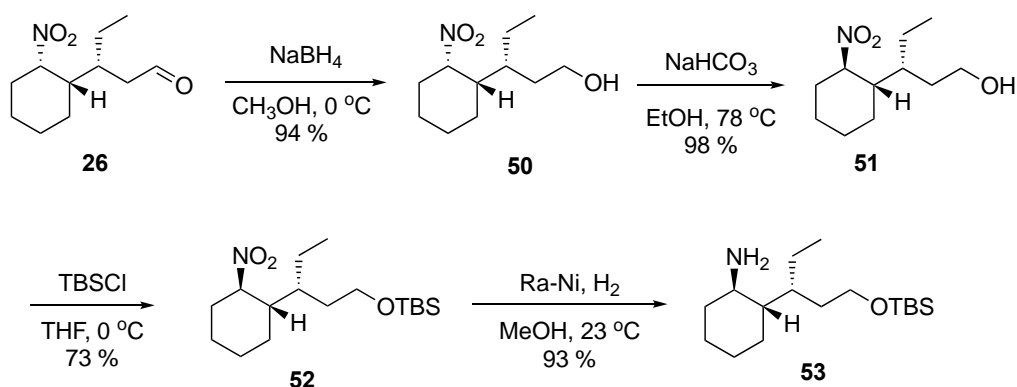


Scheme 2-6 Hydrogenation of the nitro group in acid condition.

2.3.3 Synthesis of δ -Building Block 53

After various trials with the hydrogenation process, we found that the amino- δ -residue has a high tendency to form lactam regardless of whether the carbonyl group is present as a carboxylic acid, ester, or amide, so the new strategy was to adopt the hydroxyl group at the C-terminus of the δ -residue. In this protocol, the primary alcohol needs to be protected to avoid

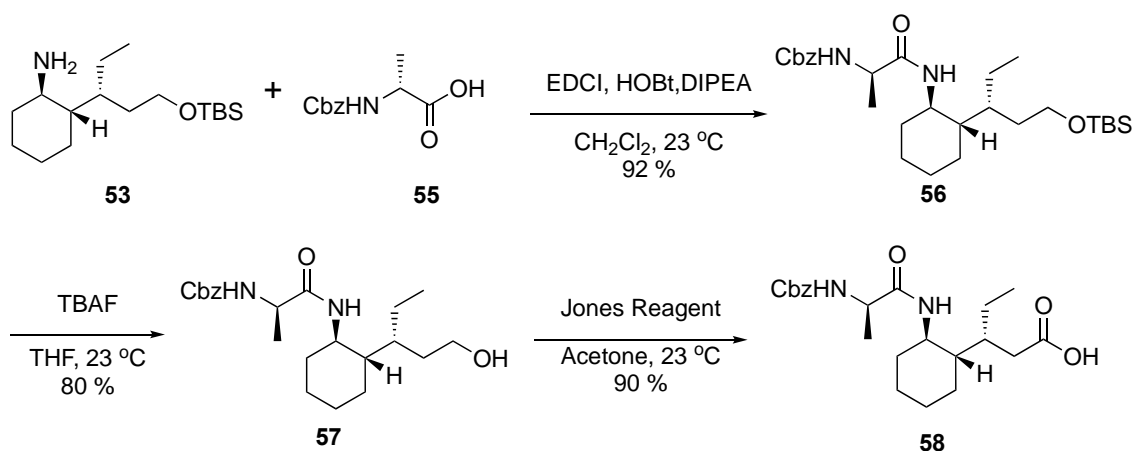
the coupling reaction between alcohol and the carboxylic acid used for N-terminus derivation. The reduction reaction from aldehyde **26** to primary alcohol **50** gave 94% yield, and the epimerization of **50** to *trans*-conformer **51** by refluxing in ethanol with NaHCO₃ gave a quantitative yield. Subsequent TBS protection gave **52** in a decent yield of 73%. The nitro group was then reduced to amine **53** which was used the subsequent coupling reactions (Scheme 2-7).



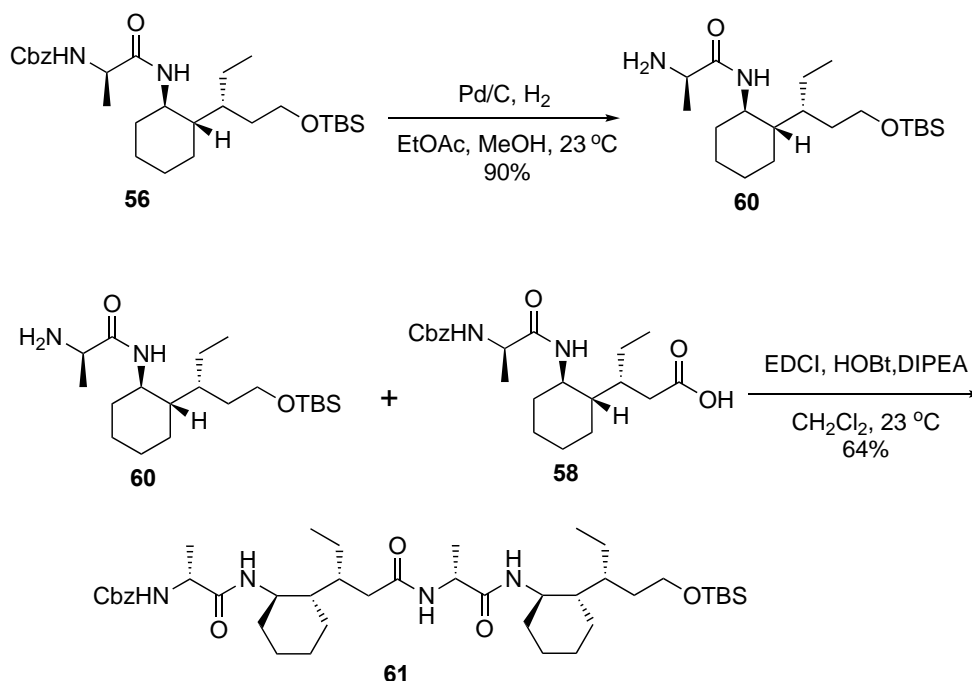
Scheme 2-7 Synthetic route for δ -amino acid precursor

2.3.4 Study on D-Alanine Constructed Peptides

Using EDCI, HOBT and DIPEA as coupling reagents produced 92% yield of α,δ -dipeptide **56** (Scheme 2-8), as the deprotection by hydrogenation of the N-terminus was performed under neutral conditions, the amine presented as a free amine, and the coupling reaction without DIPEA still gave around 78% yield. To get the $\alpha\delta\alpha\delta$ -tetramer, we need two substrates. One - **58** - where we have generated the C-terminus (cyclisation with the amide is of course not possible) and the second where we have unmasked the N-terminus of **56**. To achieve the former, removal of the TBS-protecting group produced **57** in 80% yield. Oxidation of the alcohol was attempted under a variety of conditions, including PCC and H₅IO₆ in anhydrous acetonitrile (0% yield),⁶⁹ oxone oxidation in DMF (30% yield),⁷⁰ and NMO/TPAP oxidation in acetonitrile (40%).⁷¹ However, Jones reaction produced carboxylic acid **58** in 72% over the two steps of deprotection and oxidation.⁷²

Scheme 2-8 Synthetic route for α,δ -dipeptide

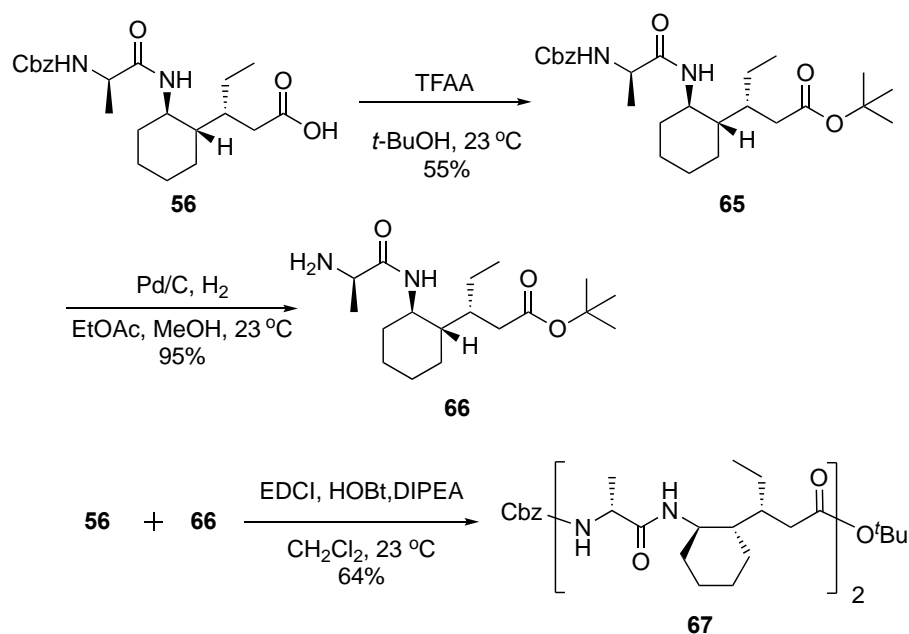
To get the amine coupling partner, we simply removed the Cbz-protection group of **56** to get the amino-dipeptide **60**. Given the amount of **56** we had in hand, we kept the C-terminus as TBS-alcohol to avoid the mass loss and then coupled **56** and **60** through the same coupling method to get the $\alpha\delta\alpha\delta$ -tetramer **61**, in 64% yield after purification.

Scheme 2-9 Synthetic route for tetramer **61**

Pleasingly, the NMR indicated that we had successfully synthesized the $\alpha\delta\alpha\delta$ -tetramer **61**, confirming that our strategy introducing an alcohol on the C-terminus of δ -residue to avoid

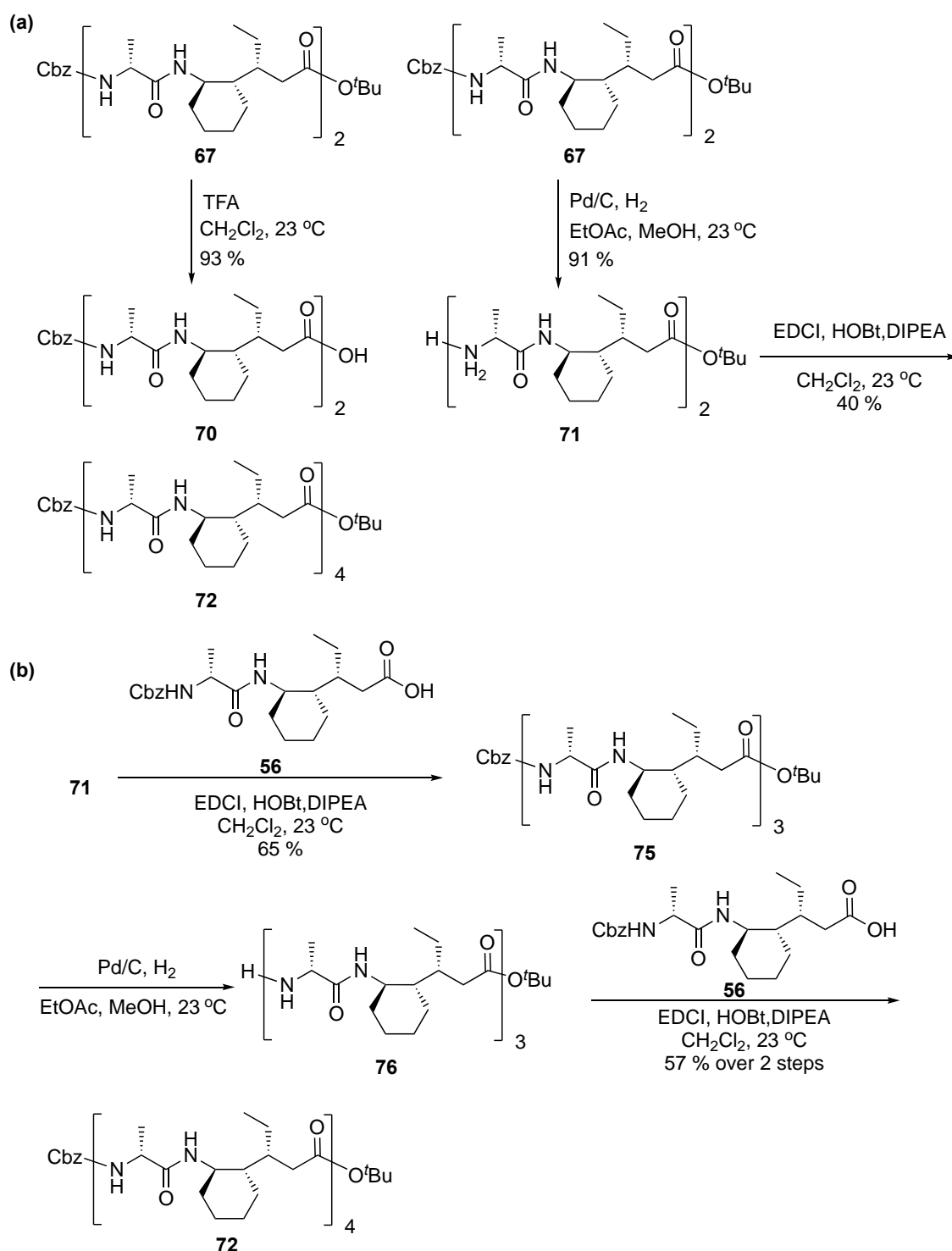
cyclization is feasible. Extensions of this oligomer could be synthesized via a similar procedure. However, the chemical shifts of the amide protons did not show a noticeable downfield shift which is a typical signal of intramolecular hydrogen bonding. In order to further encourage this peptide to fold in solution, we hypothesized that the C-terminus needed to be a carbonyl group rather than the protected alcohol, so that it could act as a hydrogen bond acceptor for the helix folding.

The new procedure required us to prepare the α,δ -dipeptide as a building block, orthogonally protected at both ends. With the Cbz protecting group at the N-terminus, the protecting group on the C-terminus could not be the benzyl ester which would be removed under the same condition. A *tert*-butyl ester was thought to be a good option here, as it is generally removed by treating with TFA and unaffected under Pd/C hydrogenation conditions. The *tert*-butyl esterification reaction on carboxylic acid **56** was therefore attempted under different conditions. First, the use of EDCI and HOBt gave no product and resulted only in unreacted starting material. The use of Boc-anhydride, DMP, and *tert*-butyl alcohol gave only 10% yield, with most of the starting material unreacted. Esterification with *tert*-butyl alcohol using trifluoroacetic anhydride gave an acceptable 55% yield (Scheme 2-10). With dipeptide **66** successfully synthesized, we then exposed the N-terminus of the dipeptide **65** to get the amine **66** in 95% yield, coupling **56** and **66** through EDCI and HOBt produced the $\alpha\delta\alpha\delta$ -tetramer **67** in 64% yield.



Scheme 2-10 Synthetic route for tetramer **67**

To obtain the target $\alpha\delta\alpha\delta\alpha\delta\alpha\delta$ octamer, we can either couple the two tetramers (Scheme 2-11a) or couple the tetramer with the dimer twice (Scheme 2-11b). Both methods were conducted to compare their yields and to elicit a general procedure. As the deprotection almost always gives a quantitative yield, the yield difference between these two approaches majorly depends on the coupling ability of the substrates. The coupling reaction of the two tetramers (**70** and **71**) gave 40% yield using EDCI in dichloromethane after 24 hours. In comparison, the yields of coupling the tetramer twice with dimer were 65% yield for the first tetramer-dimer coupling (**71** and **56**), and 57% yield for hexamer-dimer coupling (**76** and **56**), thus giving an overall yield of 37% yield. Whilst these are quite similar, the 4+4 procedure is clearly more direct, although the 4+2+2 procedure, give us one more peptide (the hexamer) to examine. Therefore, either method are good options depending on the data requirements.

Scheme 2-11 Synthetic route for peptide **72**

Using ^1H NMR, ^{13}C NMR and HRMS, we confirmed the successful synthesis of **72** (Bz-a-X-a-X-a-X-OtBu **72**). Unfortunately, the octamer does not show obvious H-bond forming on

the ^1H NMR (Figure 2.7). The δ value of amide protons increased by 0.9 ppm under the increase of peptide length from dimer to octamer, indicating some degree of secondary structure, but the interaction is not strong enough to adopt a high helical propensity.

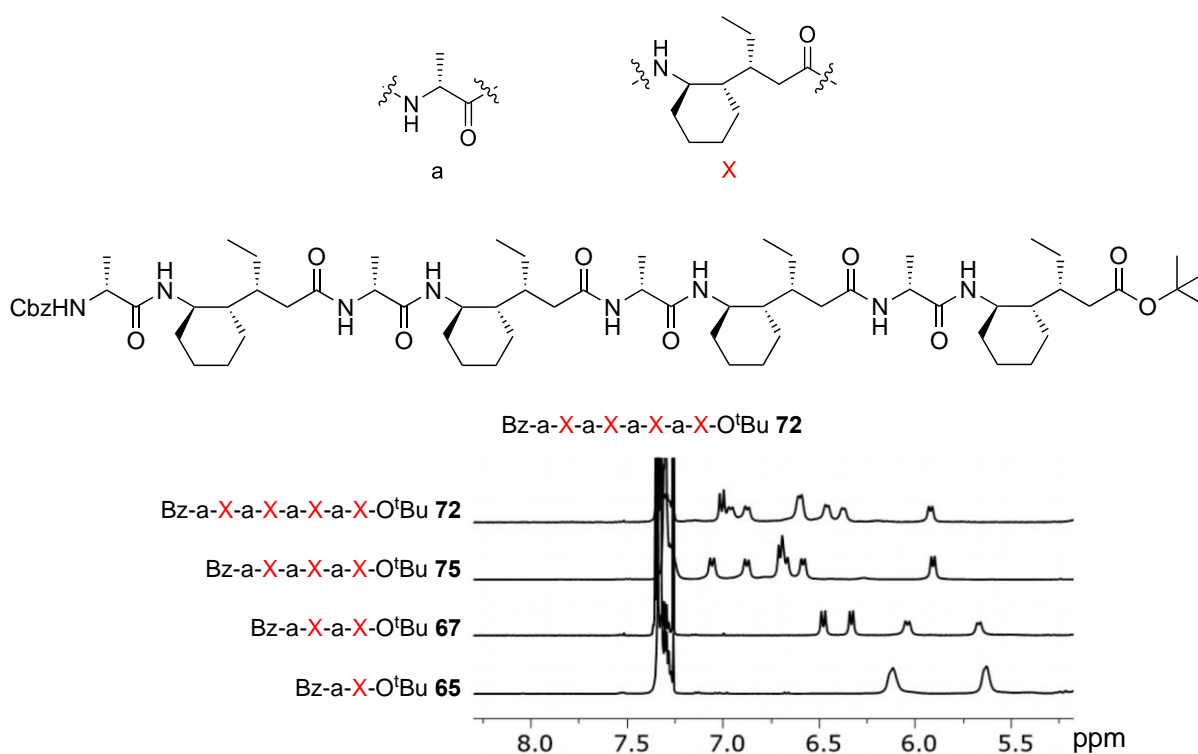


Figure 2.7 Stacked ^1H NMR (400 MHz, CDCl_3) of the amide protons of dimer, tetramer, hexamer, and octamer.

To understand whether the aggregation happened in the solution, the hexamer **75** was chosen to monitor the chemical shift change under different concentrations. The experiment started from a 10 mM peptide concentration and was sequentially diluted to 0.1 mM, over this concentration range, the δ value of amide protons barely changed, which indicated the hexamer did not aggregate under 10 mM (Figure 2.8).

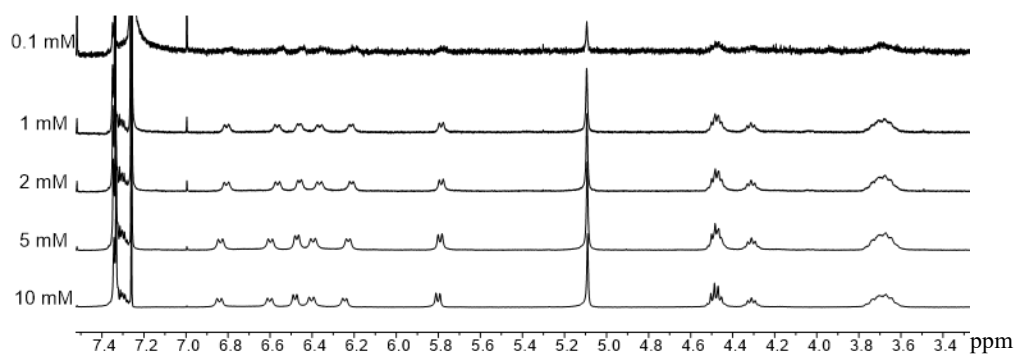


Figure 2.8 ^1H NMR (400 MHz, CDCl_3) of hexamer at 10, 5, 2, 1, 0.1 mM concentration.

To further investigate the H-bond formation properties of the D-alanine and δ -amino acid constructed oligomers, a DMSO titration experiment was performed at 20 mM oligomer concentration. All the amide protons of the hexamer **75** shifted downfield over the addition of DMSO into the solution (3, 5, 10, 15, 20, 40 μL). This indicates that this hexamer is unlikely to form intramolecular H-bonds, and thus the D-alanine constructed hexamer does not adopt a helical structure in CDCl_3 (Figure 2.9).

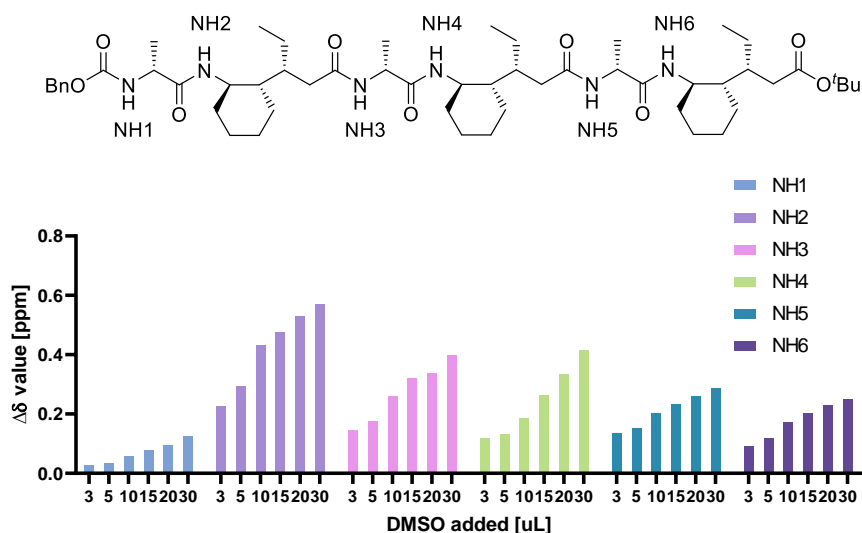
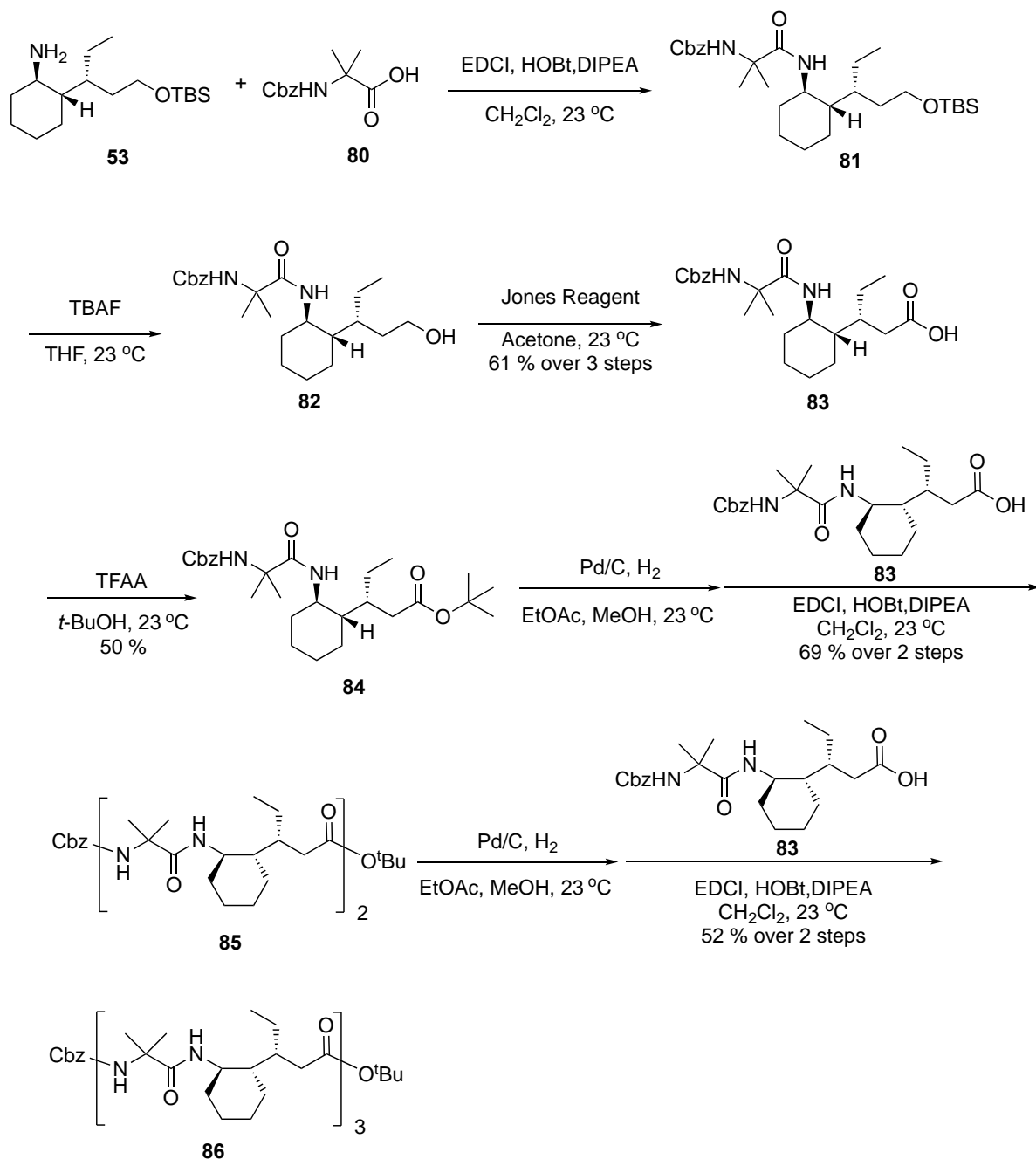


Figure 2.9 Change of δ -value of individual amide proton under an accumulative volume of DMSO added into the CDCl_3 solution of 20mM of Hexamer, monitored by ^1H NMR (400 MHz, CDCl_3) at room temperature.

2.3.5 Study on Aib Constructed Peptides

As has been reported in some publications, Aib-constructed oligomers can adopt a helical structure, and so this monomer was chosen for oligomer synthesis with the δ -residue. The construction of a helical structure can normally be observed once one helical pitch is formed, and so it was felt that the hexamer **86** would be of adequate length (Scheme 2-12). The ^1H NMR of this Aib-constructed oligomer showed that the δ value of amide NH remains below 7

ppm at the hexamer stage (Figure 2.10), once again indicating this α , δ -alternating sequence was unable to fold.



Scheme 2-12 Synthetic route for foldamer **86**

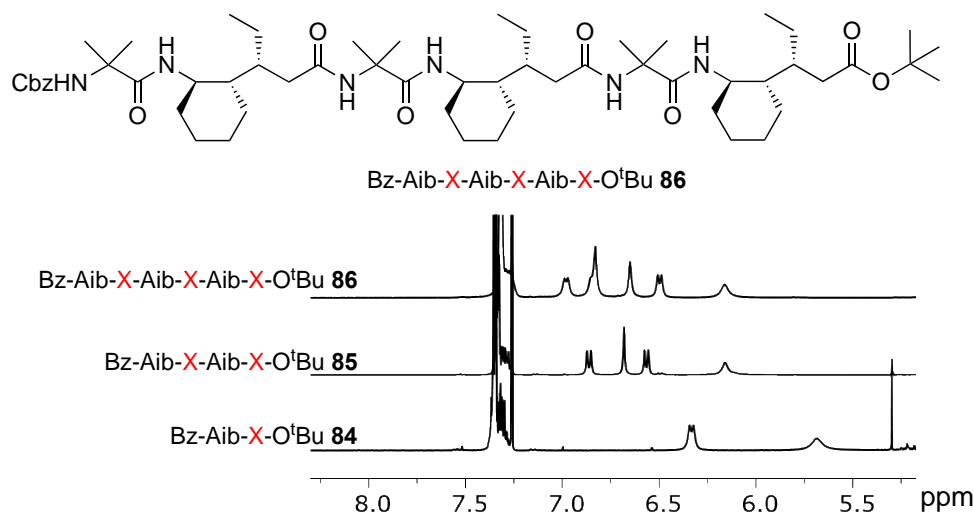
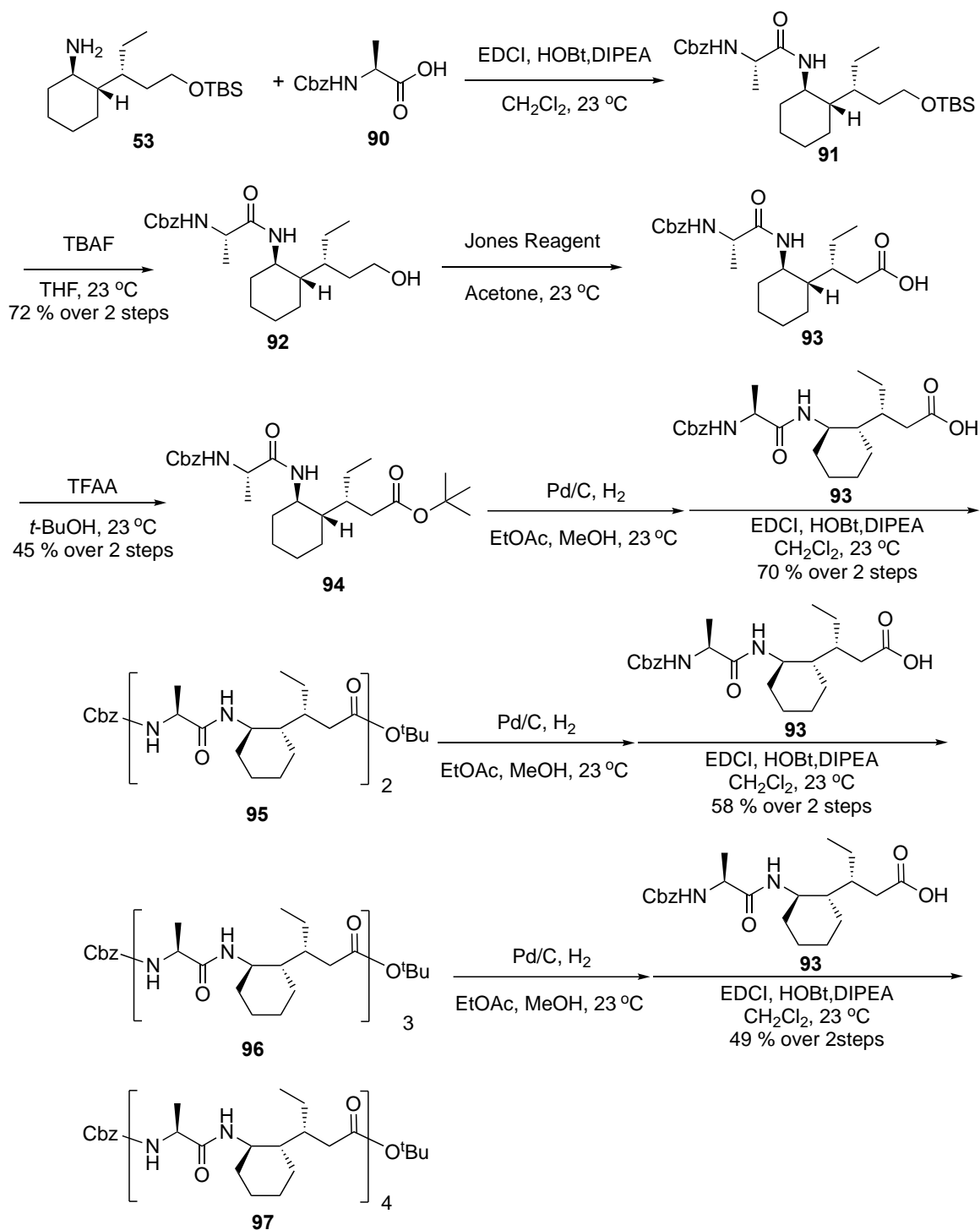


Figure 2.10 Stacked ¹H NMR (400 MHz, CDCl₃) of the amide protons of dimer **84**, tetramer **85**, hexamer **86**.

2.3.6 Study on L-Alanine Constructed Peptides

It was surmised that a possible reason why the D-alanine/Aib constructed α,δ -oligomer does not fold into a helix might be that the side-chain methyl group's orientation of D-alanine/Aib is incompatible with the cyclohexyl- δ -amino acid isomer for this to occur. We therefore synthesize the $\alpha\delta\alpha\delta\alpha\delta$ -octamer constructed from L-alanine and the same δ -residue through the above mentioned procedure (Scheme 2-13).



Scheme 2-13 Synthetic route for foldamer 97

In contrast to D-alanine constructed oligomers, L-alanine constructed oligomers showed intramolecular H-bond forming from the length of $\alpha\delta\alpha\delta$ -tetramer, the δ value of amide protons

of this shifted to 7.5 ppm from 6.4 ppm for the dipeptide (Figure 2.11), and then to 8.1 ppm for both the hexamer and the octamer. This change in chemical shift of the amide protons is a strong indicator of intramolecular hydrogen bonding, meaning that the oligomer might be adopting a stable secondary structure.

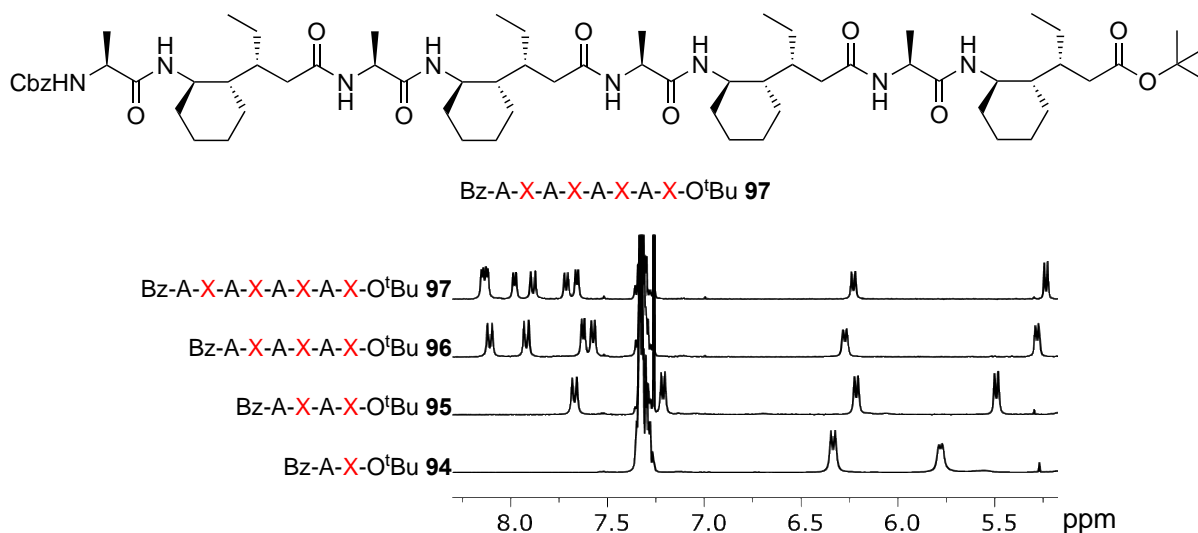


Figure 2.11 Stacked ¹H NMR (400 MHz, CDCl₃) of the amide protons of dimer, tetramer, hexamer, and octamer.

The self-aggregation experiment of foldamer **97** was conducted in the same way as for hexamer **75**. The chemical shift of amide bonds did not show a significant change of δ value and the peaks on the spectrum did not show any change in splitting, so the foldamer **97** is unlikely to aggregate in CDCl₃ under this concentration range (Figure 2.12).

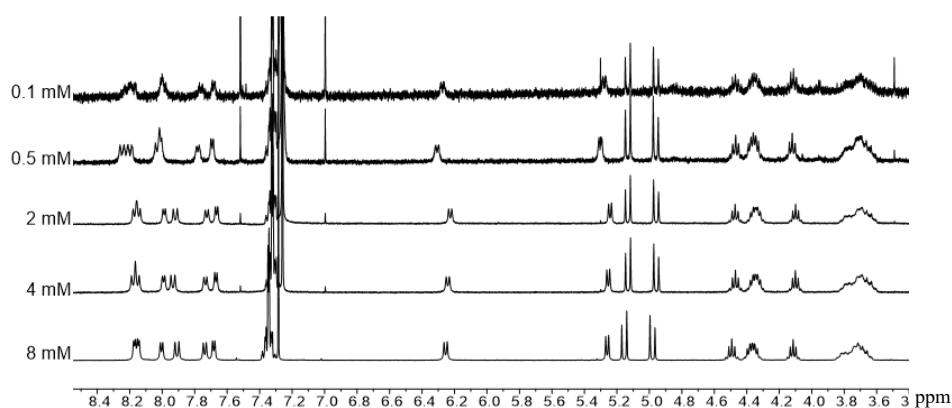


Figure 2.12 ^1H NMR (400 MHz, CDCl_3) of foldamer **96** at 8, 4, 2, 0.5, 0.1 mM concentration.

The DMSO titration experiment was conducted on 4 mM of foldamer **97** to confirm the intramolecular H-bonds within the L-alanine derived oligomers. The results showed that apart from the first and last amide proton, all the other amide proton shifted up-field along with the titration of DMSO, fitting the pattern of intramolecular H-bond forming, and that only the first

amide bond of N-terminal α -residue and the last amide bond of C-terminal δ -residue are not involved in H-bond formation (Figure 2.13).

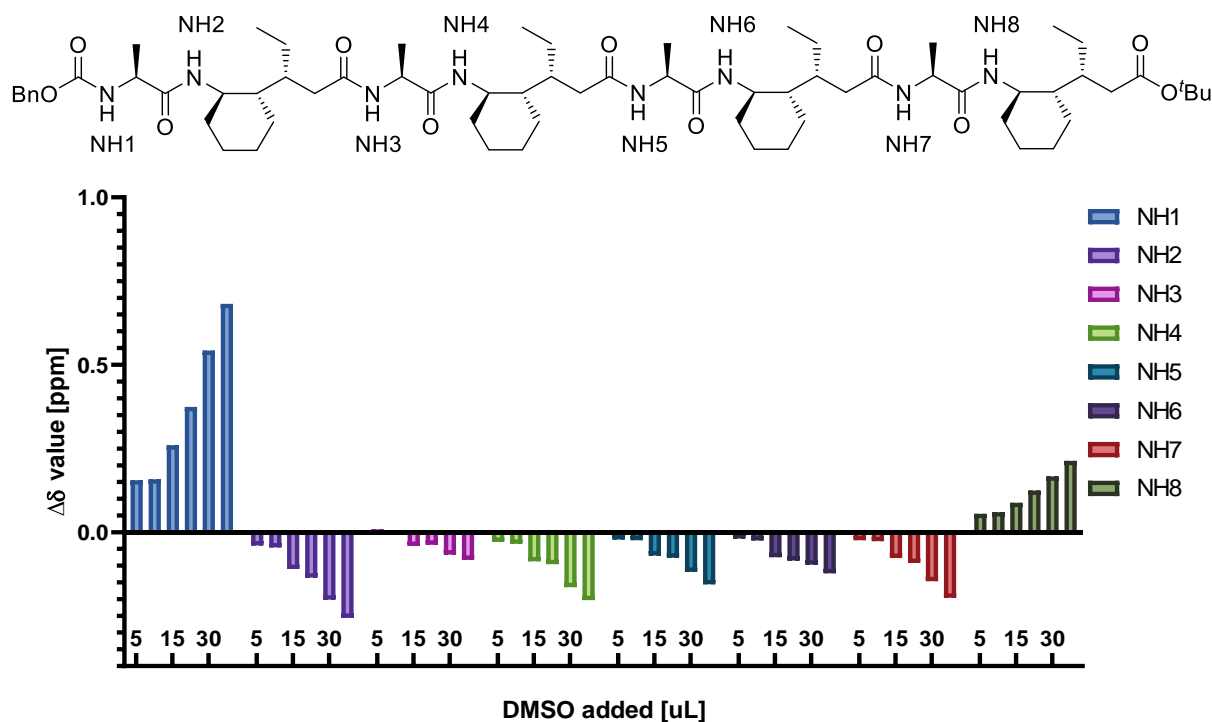


Figure 2.13 δ -value of individual amide proton under an accumulative volume of DMSO added into the CDCl_3 solution of 20mM of foldamer **97**, monitored by ^1H NMR (400 MHz, CDCl_3) at room temperature.

We then ran the 2D-NMR of both tetramer **95** and octamer **97** to get preliminary structural information. In addition to the observation that the first and last amide NH do not participate in hydrogen bond-forming, the NOESY spectrum suggested that it is likely foldamer **97** adopt

a 13/11-helix which is in accordance with Hoffman's calculation on the α,δ -foldamers (Figure 2.14).

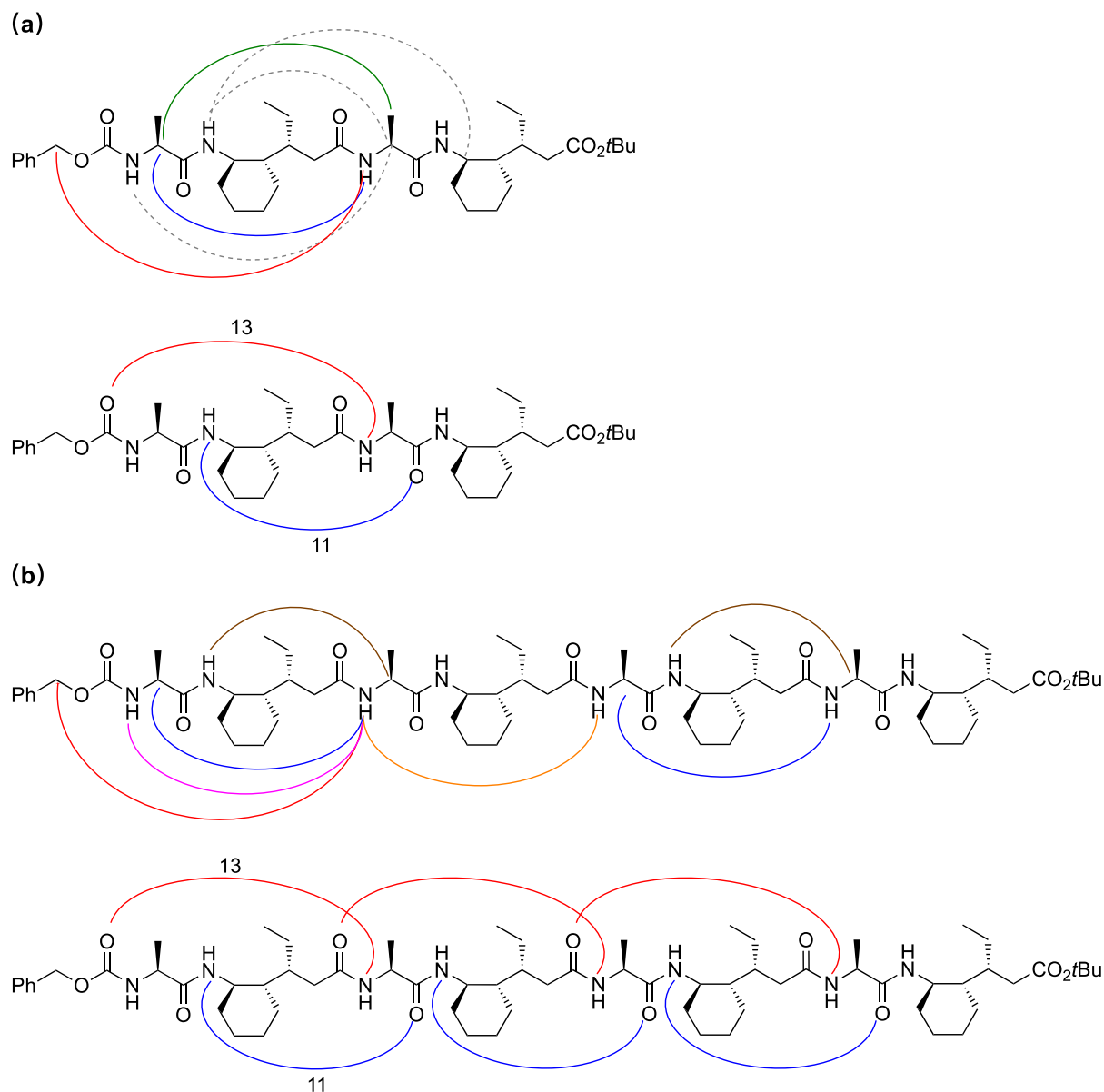


Figure 2.14 The NOE-correlation observed on ROESY (400 MHz, CDCl₃) and the speculated H-bond pattern.

The single crystal of foldamer **97** was obtained via slow diffusion of acetonitrile into chloroform. The refined XRD structure displays a 13/11 helix as we speculated (Figure 2.15). An interesting interaction was found on the structure whereby the ethyl-side chain on the δ -residue would point towards the cyclohexane of the next δ -residue, indicative of an apolar

interaction. Furthermore, two conformations exist in the minimum unit cell of the crystal structure. The main reason for this is that the last δ -residue lacks a hydrogen bonding partner and so is free to adopt two different conformations - the diaxial (a,a) or the diequatorial (e,e) due to the lack of this constraint. Whilst (e,e) is clearly a preferred conformation, the (a,a) is thought to be stabilised by the aforementioned apolar interactions.

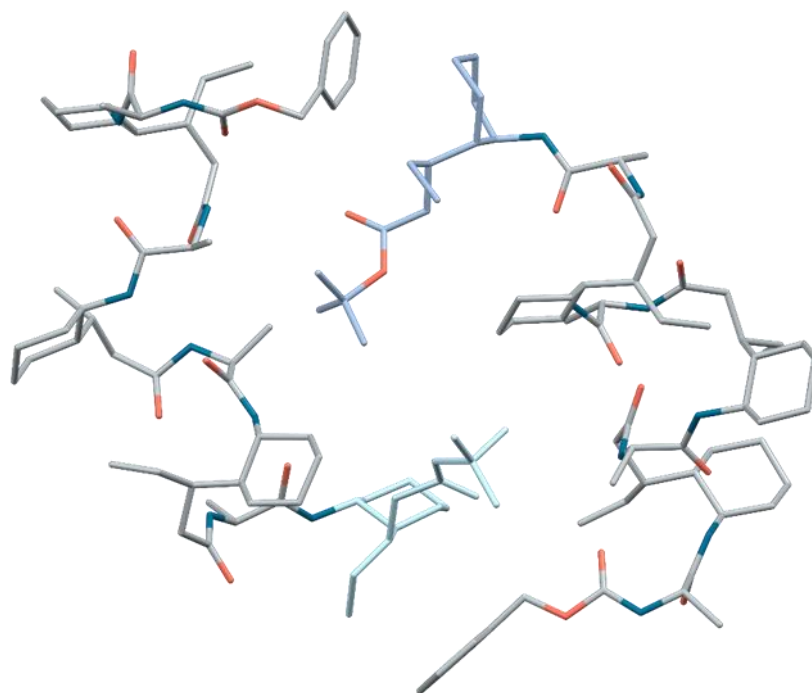
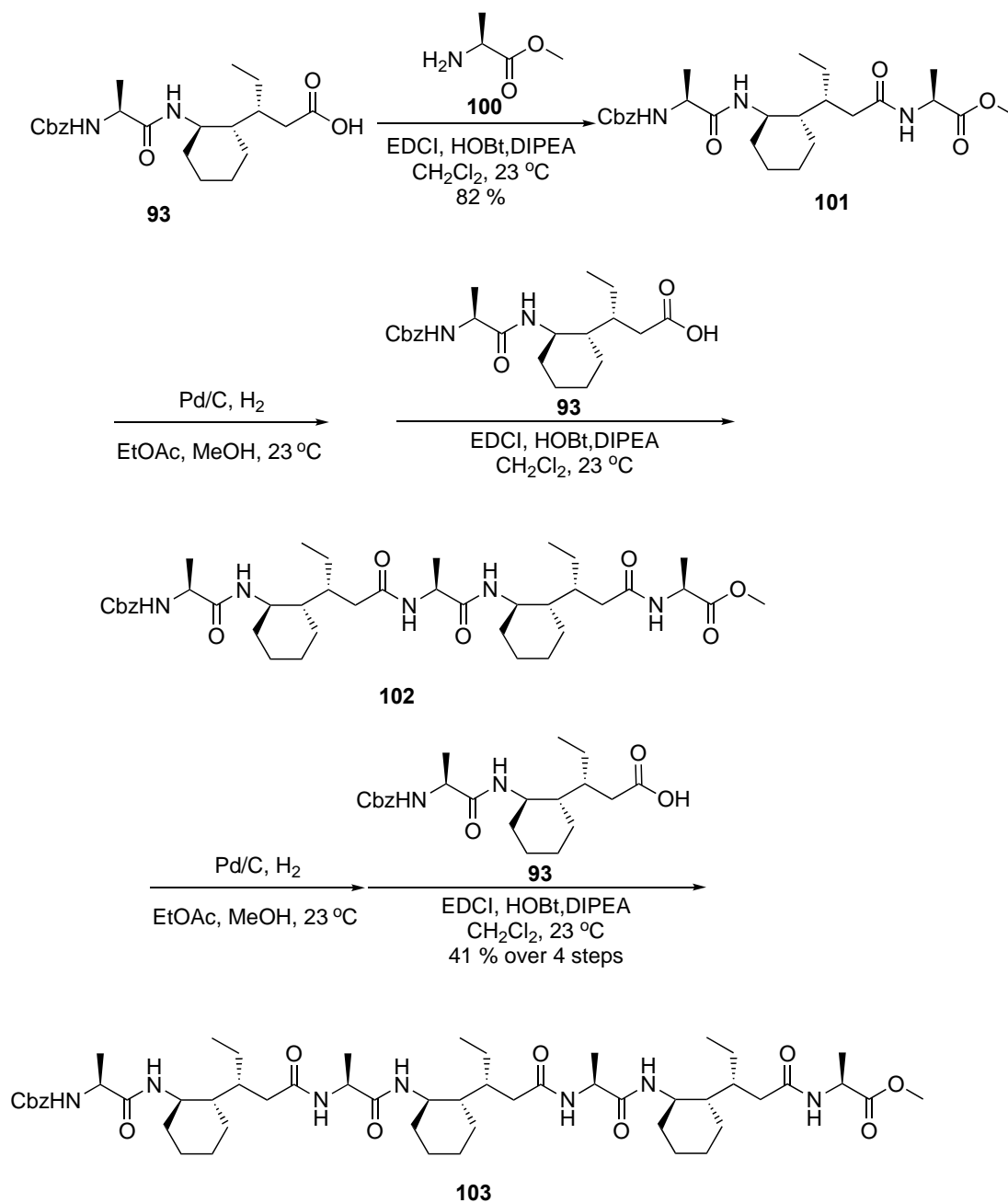


Figure 2.15 The XRD structure of foldamer **97** (CCDC 2252028), molecule on the left is the (e,e) conformer, molecule on the right is the (a,a) conformer

Our collaborators at Bristol University helped us to characterize the secondary structure in the solution state.⁷³ The conformation calculated from the NOESY overlays well with the XRD structure and both clearly explain why helix formation is disfavoured with D-alanine and Aib. The methyl group at this epimeric position will point into the helix centre, thus destabilising the helical structure. The NMR also showed that whilst the last δ -residue does not participate in the H-bond pattern of the helix, in solution it prefers the (e,e) conformation. Owing to the uncertainty that this terminal residue brings, we felt that we had one of two options. To either clip it completely or to turn the C-terminal into an amide, to give the final H-bond partner. For synthetic ease, we decided to adopt the former approach and access the heptamer.

To get the heptamer, we can either go through the 3+4 approach or the 3+2+2 approach. In the 3+4 approach, a Cbz- $\alpha\delta\alpha\delta$ -COOH tetramer and an NH₂- $\alpha\delta\alpha$ -OMe trimer are needed. In the 3+2+2 approach, an H₂N- $\alpha\delta\alpha$ -OMe trimer and a Cbz- $\alpha\delta$ -COOH are needed. Both approaches require a tripeptide building block, and as has been demonstrated in the octamer synthesis, the yield of the coupling between two long oligomers is close to the yield of the one-by-one addition of the dimer onto the longer oligomer. The yield-limiting step during the foldamer synthesis is the *tert*-butyl ester addition on the carboxylic acid dipeptide **93** which gives only 55% yield, whereas the coupling reaction between shorter peptide is relatively efficient and normally goes above 80% yield. We therefore decided to use the 3+2+2 approach by first adding an α -amino acid **100** onto the carboxylic acid dipeptide **93** to get tripeptide **101**, and to then couple the Cbz- $\alpha\delta$ -COOH onto this to get to pentamer **102** (Scheme 2-14). The tripeptide **101** was obtained with 82% yield, and the ¹H NMR shows probable intramolecular H-bond formation (Figure 2.16), which is promising, as it suggest that without the last δ -residue the heptamer might still adopt the same H-bond pattern required for the desired helix.

Scheme 2-14 Synthetic route for foldamer **103**

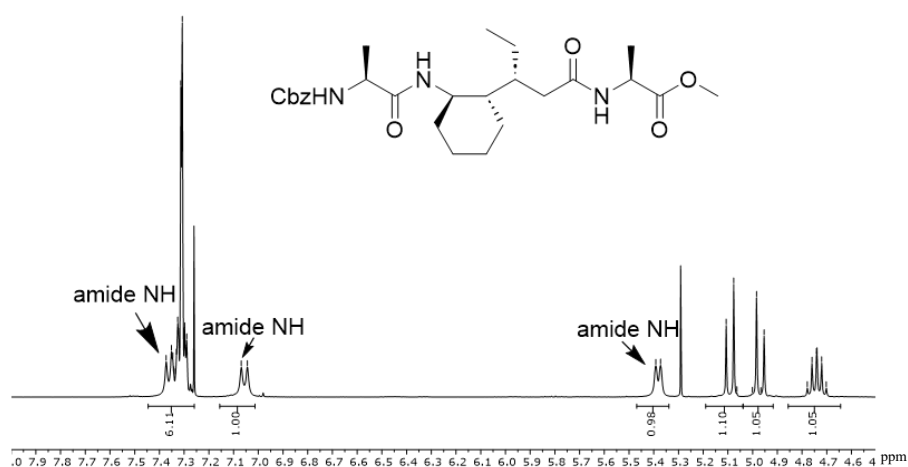


Figure 2.16 Partial ^1H NMR of tripeptide **101**

We then followed the deprotection-coupling protocols to get the final heptamer which was also characterized by NMR and HRMS. The ^1H NMR of foldamer **103** now only has one amide proton with a δ value below 7 ppm, which belongs to the first amide of N terminal α -amino acid. The crystal structure of foldamer **103** confirmed the unchanged 13/11 helix structure and the backbone of the heptamer overlaid perfectly with the 7 residues of octamer **97** (Figure 2.17).

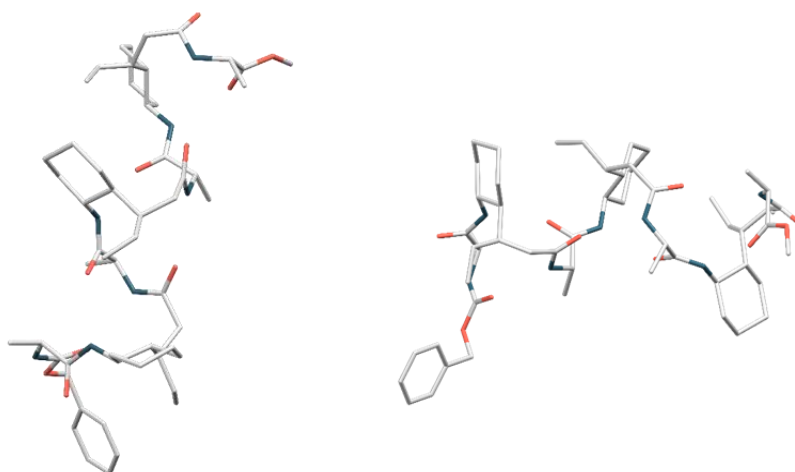


Figure 2.17 The XRD structure of foldamer **103** (CCDC : 2251914), top view(left) and side view(right).

The CD spectrum of all the foldamers and peptides synthesized were characterized in methanol because of the strong absorbance of chloroform between 200-240 nm which would interrupt

and cover the absorbance of the peptide. Methanol is both an H-bond donor and H-bond acceptor which might decrease the folding propensity of foldamer in a certain degree but maybe not completely. The results observed from the CD spectrum show that the foldamers appear to remain helical in methanol (Figure 2.18a). For the D-alanine or Aib-constructed peptides that were deduced not adopting a helical structure in chloroform, these did not show any increase in absorbance at 220 nm with increasing oligomer length, whereas the L-alanine constructed foldamer showed an increase of absorbance when the peptide was elongated from dimer through to the octamer (Figure 2.18b).

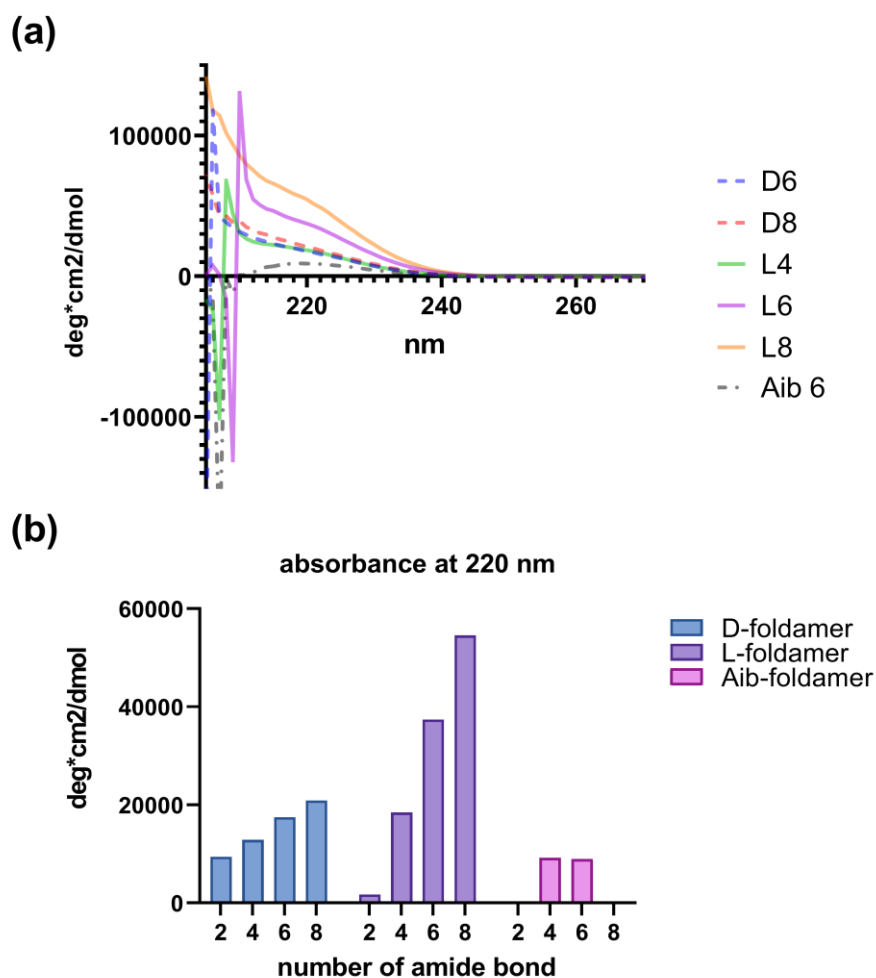


Figure 2.18 (a) The absorbance of peptides from 205 nm to 270 nm in methanol. (b) Dependency of molar ellipticity on the number of amide bond.

2.4 Conclusion

In summary, we used homologation chemistry to successfully synthesize an enantiopure δ -amino acid via the γ -amino acid precursor reported by Gellman. We have discovered and overcome the lactam formation tendency of δ -oligomer synthesis and consequently have proposed an effective procedure for the α,δ -peptide synthesis in solution phase. Using the general procedure we discovered, we successfully obtained D-alanine, L-alanine, and Aib-constructed peptides. Among these three peptides, only the L-alanine is compatible with the δ -amino acid and folds into a helix. The NMR, NOESY, self-aggregation experiment, DMSO titration experiment, and XRD consistently conclude that the L-alanine derived systems construct a stable 13/11 helix structure.

The XRD crystal structure displays a unique ethyl-cyclohexane interaction and two conformations adopted by the peptides in the solid state. We believe this is caused by the lack of constraint on the last δ -residue, and the cleavage of the last δ -residue from the octamer was proven not to change the secondary structure of the peptide backbone. The secondary structure of this 1:1 alternating α,δ -foldamer provides many unique structural features for catalyst design.

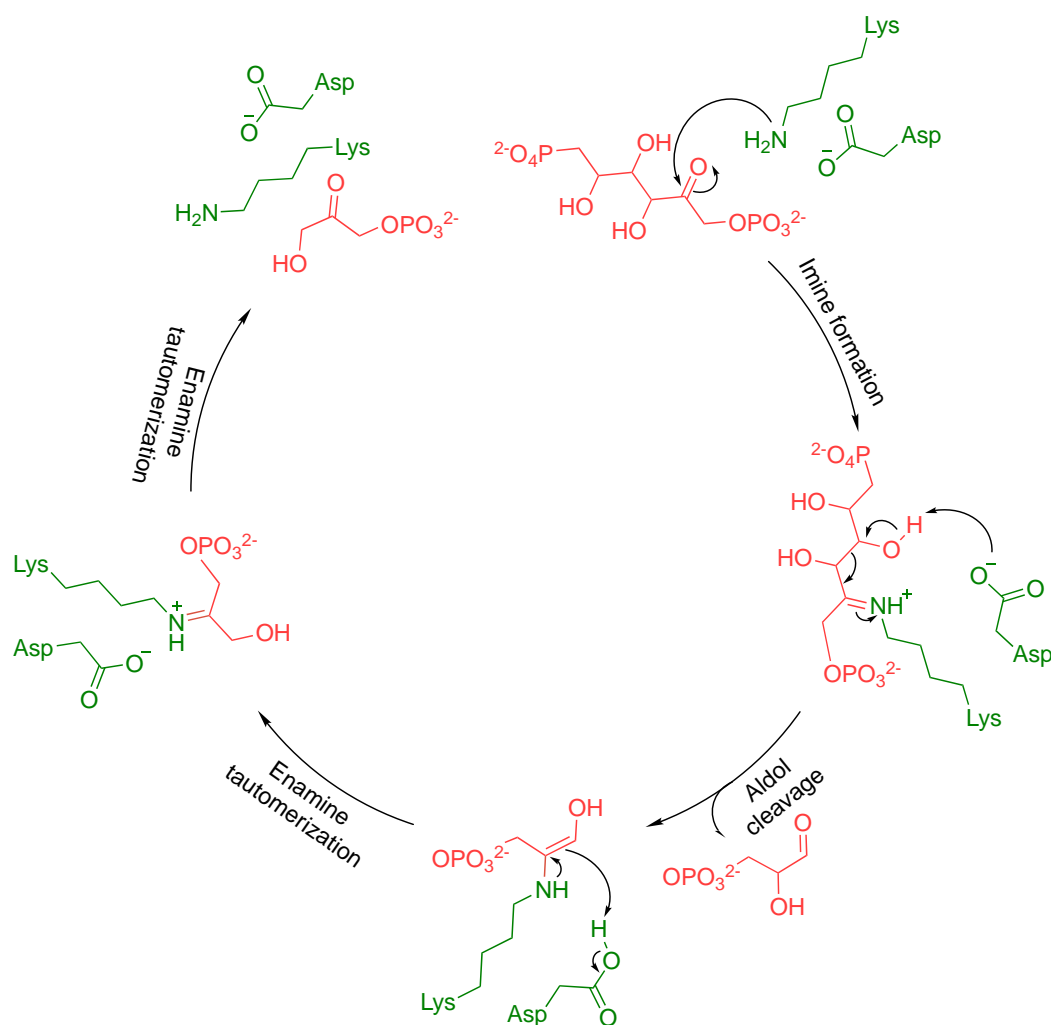
Chapter 3 Catalytic Retro-Aldol Cleavage by Bis-Amine α,δ -Foldamer

3.1 Introduction

There are two features on our α,δ -foldamer that could be exploited for catalyst design. One of these is that - although not aligned on the same side of the helix - the adjacent α -residues are still fairly proximal, which provides the possibility of bifunctional catalyst design. The other feature is that the α -residues are embedded within the helix, thus if the catalytic site is appended on an α -residue, the catalytic reaction could potentially occur closer to the helix center. At the same time, the δ -residues that occupy the helical perimeter could induce enantioselectivity through their steric presence. In this chapter, we described the design and application of the bifunctionality of the α, δ -foldamer structure. Retro-aldol cleavage was chosen as a model reaction to verify the bifunctionality of the constructed catalysts.

Retro-aldol cleavage catalysis *in vivo* is realized by a aldolases. Aldolase I is also known as fructose-bisphosphate aldolase and breaks down sugar to produce energy. There are three isoenzymes of aldolase I: Aldolase A, Aldolase B, and Aldolase C. Aldolase A is mainly found in developing embryos and adult muscles. The key amino acids responsible for its retro-aldol cleavage are tyrosine, lysine, and glutamic acid.^{74, 75} Tyrosine functions as the acid-base catalyst, lysine acts as a nucleophile which forms a Schiff base, and glutamic acid participates in acid-base catalysis during substrate binding, dehydration, and bond cleavage. Aldolase B is mainly expressed in the liver, it helps with the cleavage of fructose sugar, and the key amino acids for this isozyme are lysine and aspartic acid (Scheme 3-1).^{76, 77} Mechanistically, lysine forms a Schiff base with the substrate, and the aspartic acid deprotonates the hydroxyl group of the fructose to facilitate bond cleavage. Aldolase C is expressed in the brain, smooth muscle,

and neuronal tissue and is one of the key glycolysis enzymes. Although encoded by different genes and expressed in other organisms, the residues Asp33, Arg42, Lys107, Lys146, Glu187, Ser271, Arg303, and Lys229 are all conserved in the active sites of the three isozymes.⁷⁸



Scheme 3-1 Aldolase B catalytic mechanism

Inspired by the proficiency of enzymes, many enzyme-like proteins and antibodies have been designed in an attempt to understand the mechanism of retro-aldol cleavage and to mimic the catalytic ability of aldolase. Hilvert and co-workers developed a highly active artificial enzyme via computational design and directed evolution. The enzyme catalyzes the reversible aldol reaction with high stereoselectivity.⁷⁹ As shown in Figure 3.1, the catalysis of the retro-aldol reaction occurs within the catalytic tetrad of the artificial enzyme. The lysine initiates the reaction by attacking the carbonyl of the substrate. The dehydration of the hemiaminal

generates the protonated Schiff base. During this process, the asparagine is positioned to stabilize the iminium intermediate, and the tyrosine, now deprotonated, functions as a catalytic base to facilitate the bond cleavage of the iminium intermediate, leading to a release of an aldehyde. The resulting enamine is protonated to generate an iminium intermediate, which is in turn hydrolysed through the participation of tyrosine to regenerate the enzyme. In conclusion, the catalytic tetrad is responsible for Schiff base formation, proton transfer, and stabilisation of multiple transition states.

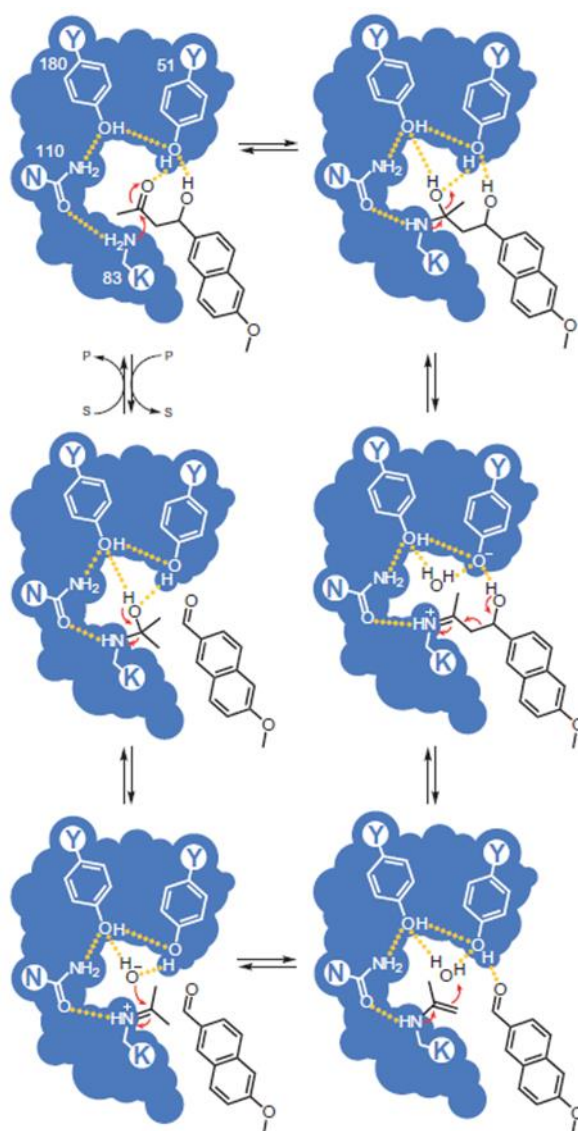


Figure 3.1 Proposed mechanism for retro-aldol cleavage by artificial enzymes.

Small peptides - even simpler mimics of the natural aldolase - could also accelerate the reaction significantly relative to the uncatalyzed reaction. In 2009, Hilvert and co-workers designed a β -peptide foldamer with several lysine side chains appended on the same side of the helical structure (Figure 3.2).⁴³ One of the amino groups could capture the substrate to form the enamine intermediate, whilst the other proximal amino could increase the nucleophilicity of the functional amine through coulombic interactions. Their optimal peptide gave a rate acceleration of $k_{\text{cat}}/k_{\text{uncat}} = 3\,000$.

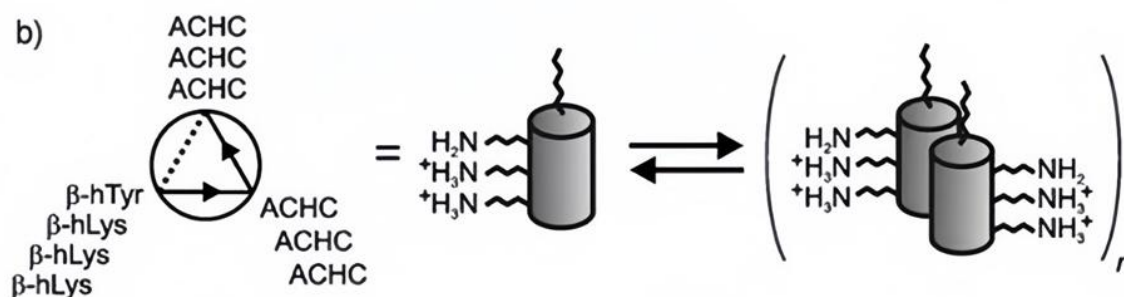


Figure 3.2 Schematic representation of a β -peptidic retroaldolase. Self-assembly of the peptide (right) further promotes activity. Reproduced from reference.⁴³

As described above, the mechanism of retro-aldol shows that the amine is important for forming the intermediate with the substrate to lower the energy barrier, and the base is important for facilitating the carbon-carbon bond cleavage of the intermediate, as well as the hydrolysis of the ketone-catalyst complex to regenerate the catalyst. By looking at the secondary structure of the non-catalytic foldamers we synthesized in Chapter 2, the two sequentially positioned α -residues (α^2 and α^3) are three-dimensionally proximal, and thus have the potential to be employed in bifunctional catalysis when converted to amine side chains. One of the amino groups could react with the substrate, and the other amino group could act as a base to accelerate the bond cleavage.

3.2 Results and Discussion

3.2.1 Synthesis of Bis-Amine Foldamer

The retro-aldol cleavage, a well-developed catalytic carbon-carbon cleavage reaction, was chosen to study the functionality of our foldamers. Enzymes and antibodies commonly implement the retro-aldol cleavage through a lysine residue and so, similarly, we decided to introduce a primary amine side chains onto the foldamer. Ornithine is a good option for our catalyst design whose side chain is not too far away from the helix and not too short to influence the secondary structure of the peptide (Figure 3.3).

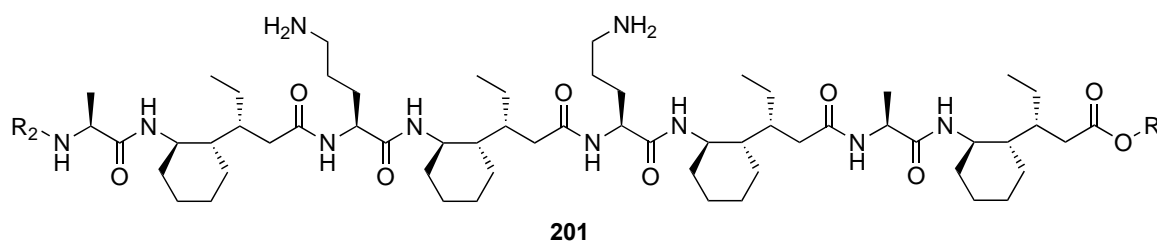


Figure 3.3 Structure of bis-amine catalytic foldamer.

As the introduced primary amine side chain needs to be protected during the peptide synthesis, the Boc-group was chosen for the side-chain amine protection. Therefore, a different protection group for the C-terminus needs to be introduced. Excluding the Boc, Cbz, and Fmoc protecting groups which were not useable in this synthesis owing to their non-orthogonality, few options remain for the C-terminus protection in the solution phase synthesis except for a methyl ester protection, which is tolerant of most of the conditions during the peptide synthesis.

To synthesize the catalytic octamer **202** consisting of δ -residue and two different α -residues, the 4+4 approaches mentioned before are no longer applied, as harsh conditions are required to deprotect the methyl ester. To avoid lactam formation, the smallest building block has to be a dipeptide, so the octamer is broken down into 3 dipeptides: dipeptide **97**, dipeptide **203** and dipeptide **204** (Figure 3.4), the synthetic technique would then be a 2+2+2+2 approach, starting from the C-terminus to the N-terminus which would avoid the deprotection of the C-terminus.

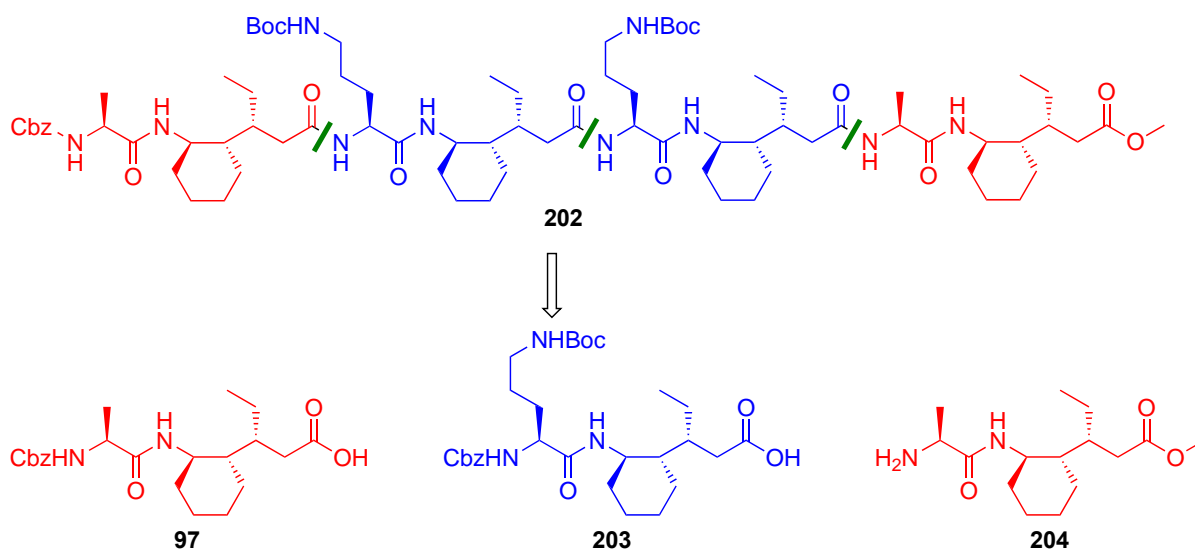
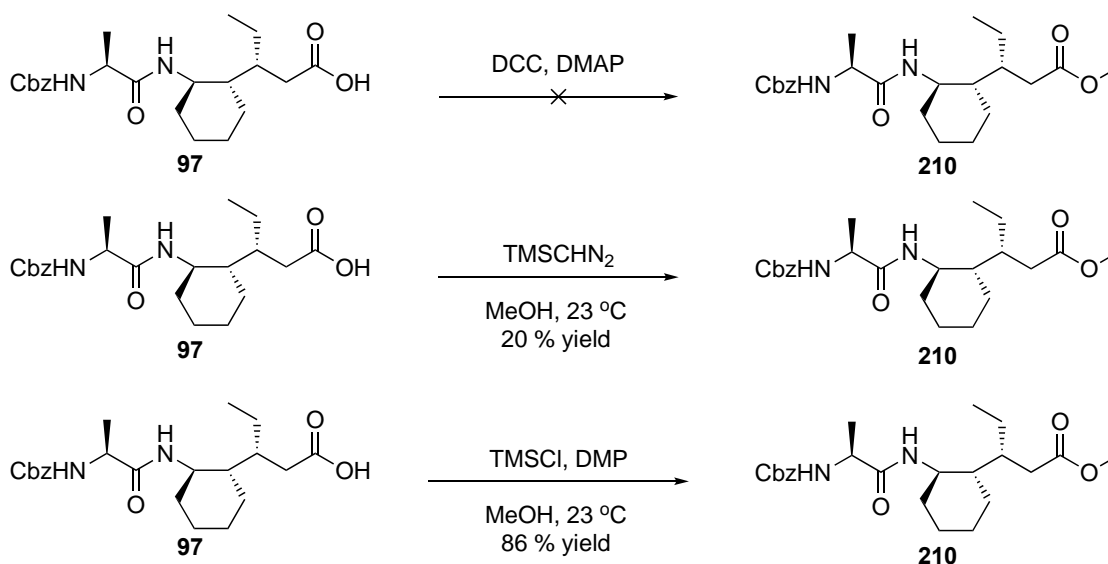


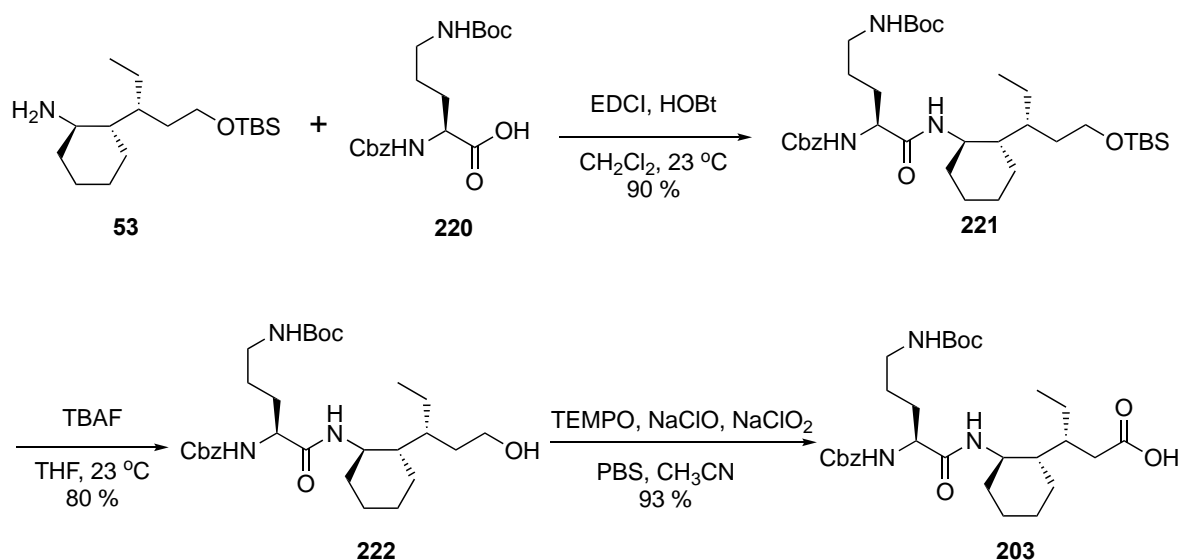
Figure 3.4 Synthetic breakdown of foldamer **202**

The Cbz-protected dipeptide **204** could be synthesized from the methylation of carboxylic acid dipeptide **97**. We tried several general approaches to methylate carboxylic acid **97**: The method of refluxing carboxylic acid in methanol with a few drops of H_2SO_4 usually has a high yield but might be a too harsh condition for the dipeptide substrate; The coupling of carboxylic acid with methanol through DCC gave nearly 0% yield with most of the substrate unreacted;⁸⁰ The methylation via TMSCHN_2 gave only a 20% yield but is a promising method.⁸¹ We then optimize the reaction by using another trimethylsilyl reagent-(trimethylsilyl)methyl chloride, which resulted in 86% yield (Scheme 3-2).⁸²



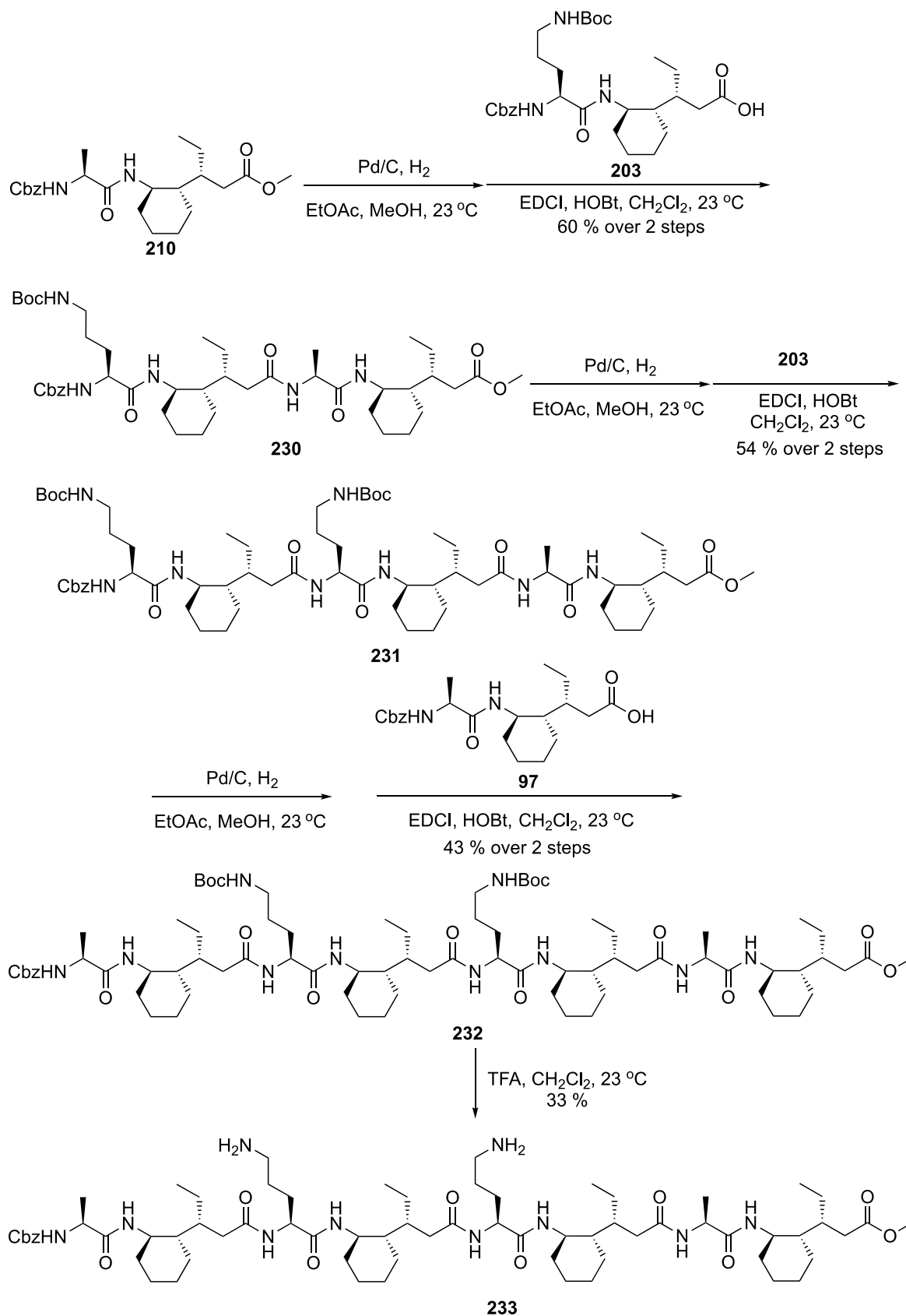
Scheme 3-2 Approaches for methylation on carboxylic acid.

To obtain dipeptide **203**, the δ -residue is still the same, the α -residue is Cbz-protected ornithine carboxylic acid. Using the general procedure for peptide coupling, we can easily synthesize the dipeptide alcohol **222**. With the Boc protecting group on the side chain, the subsequent Jones oxidation would be too acidic and so using TEMPO as a catalyst and sodium hypochlorite as an oxidation reagent in PBS buffer was applied to give the dipeptide **203** in over 90% yield (Scheme 3-3).⁸³



Scheme 3-3 Synthesis of dipeptide **203**

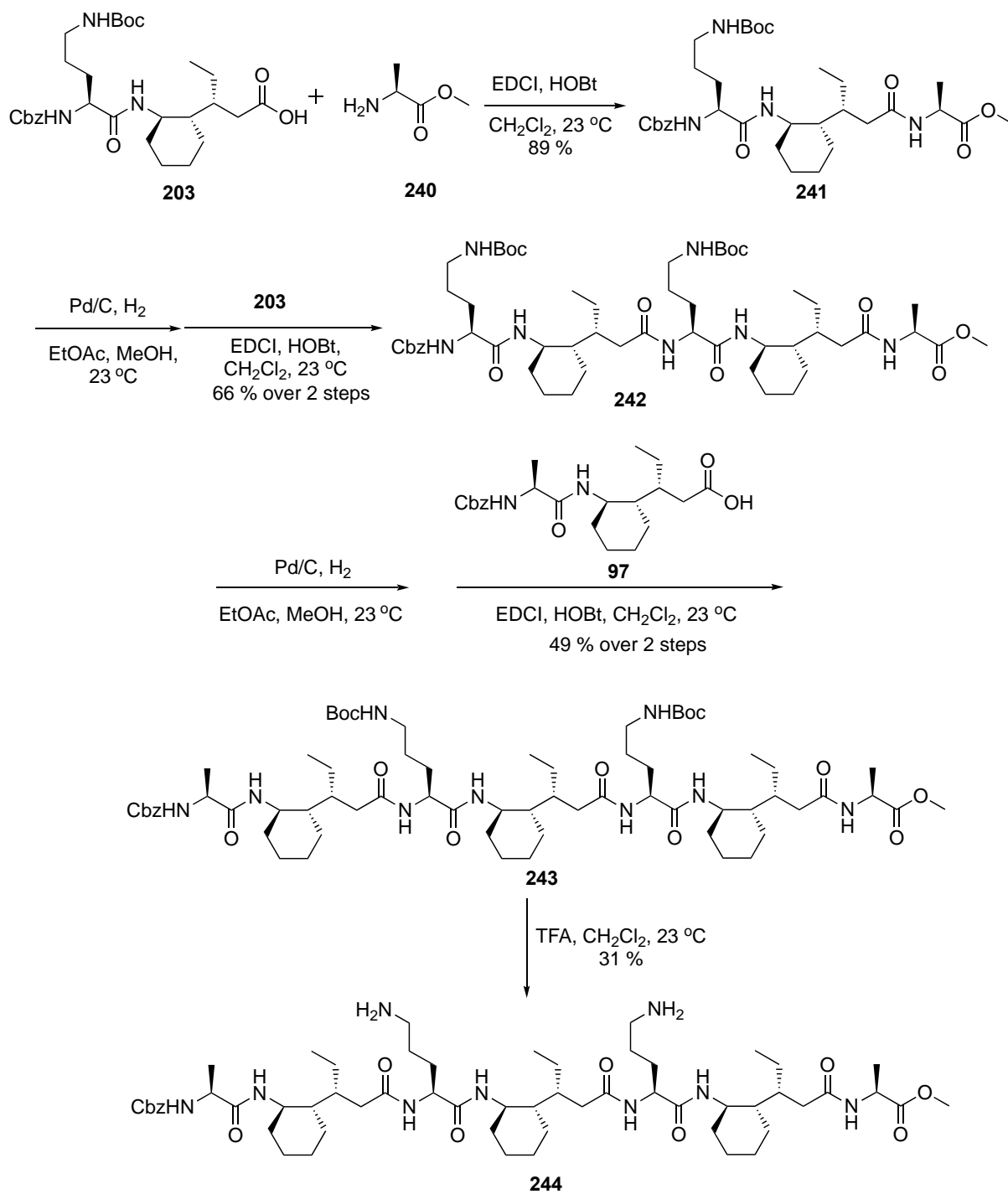
Following the general procedure developed for our first foldamer system, the Boc-protected bis-amine foldamer **232** was successfully synthesized (Scheme 3-4). Treating foldamer **232** with 50% of TFA in dichloromethane deprotected the Boc group and generated octameric catalyst **233** which could be accessed as either the free amine or the TFA salt; direct evaporation of the solvent after deprotection, followed by an ether wash will produce the TFA-salted ammonium catalyst **233**, and ethyl acetate extraction of this from aqueous NaHCO_3 generates amine foldamer as the free amine.



Scheme 3-4 Synthesis of bis-amine octamer **233**

Bis Boc-ornithine foldamer **232** was characterized by ^1H NMR, ^{13}C NMR, and HRMS, and catalyst **233** was characterized by ^1H NMR, HRMS, and HPLC to check the purity of the catalyst. The ^1H NMR of the bis-ornithine foldamers **232** and **233** clearly showed H-bond forming in chloroform where all the δ values of amide NH are above 7 ppm except for the amide protons of first α -residue at N-terminus and the last amide of δ -residue at C-terminus.

In the previous structural study, we found that the last δ -residue of the octamer is not required for the folding of the peptide, and the relatively conformationally-free residue might bring some unpredictability to the functionality. We therefore synthesized the heptamer catalyst where this terminal δ -residue was excluded. The synthesis of the catalytic heptamer **244** followed the same sequence as for heptamer **103**, and the deprotecting of the side chain amine followed the same TFA deprotection of foldamer **232** (Scheme 3-5). Similarly, the removal of that δ -residue did not change the H-bond pattern of the catalyst, and that the ^1H NMR shows only the first N-terminal amide of the α -amino acid lacks an H-bond partner. In addition, the single crystal of foldamer **243** was obtained, and the XRD structure fits the prediction of the heptamer catalyst, the introduction of the amine side chain wouldn't influence the secondary structure, and the heptamer is sufficient to adopt a stable 13/11-helix.

Scheme 3-5 Synthesis of bis-amine heptamer **244**

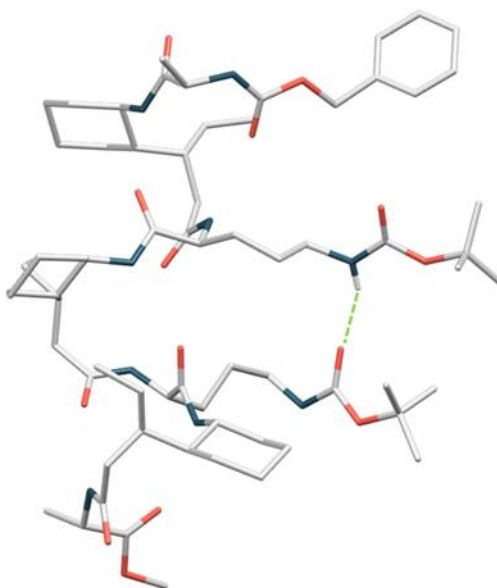


Figure 3.5 Single crystal structure of foldamer **243** (CCDC : 2252029)

Satisfyingly, the crystal structure of foldamer **243** (Figure 3.5), showed that a hydrogen bond was formed between two Boc protecting groups of the side chains, which also fits the chemical shifts we observed on the ^1H NMR in chloroform (Figure 3.6). With the tripeptide, where there is only one Boc-protected amine side chain, the chemical shift of that carbamate NH is around 4.6 ppm. However with the heptamer where there are now two Boc-protected side chains, one of the amide proton has shifts downfield to 5.4 ppm, verifying that the existence of this hydrogen bonding.

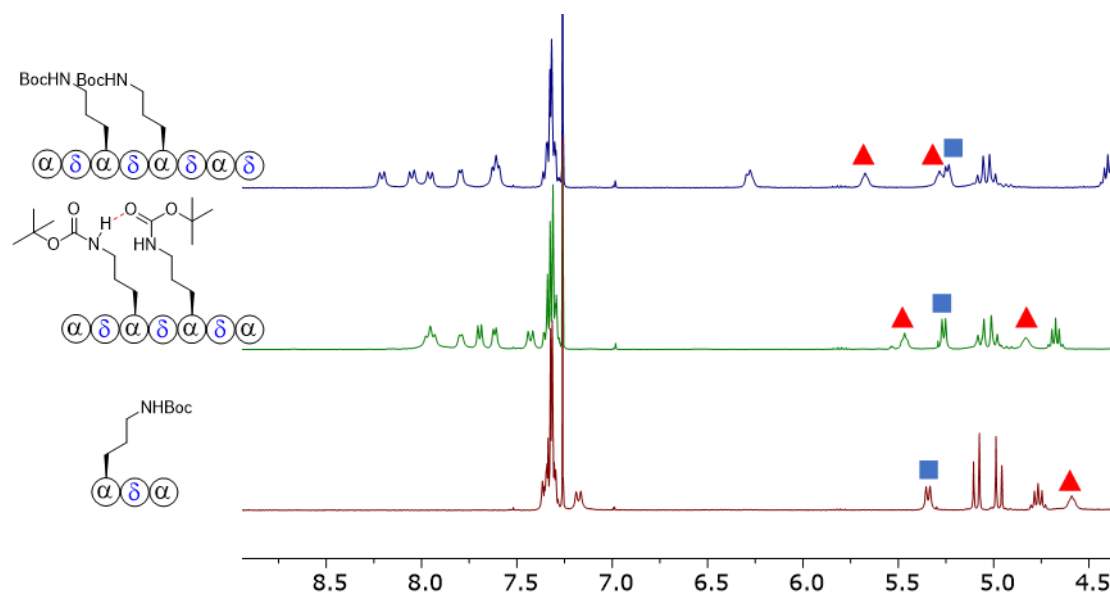


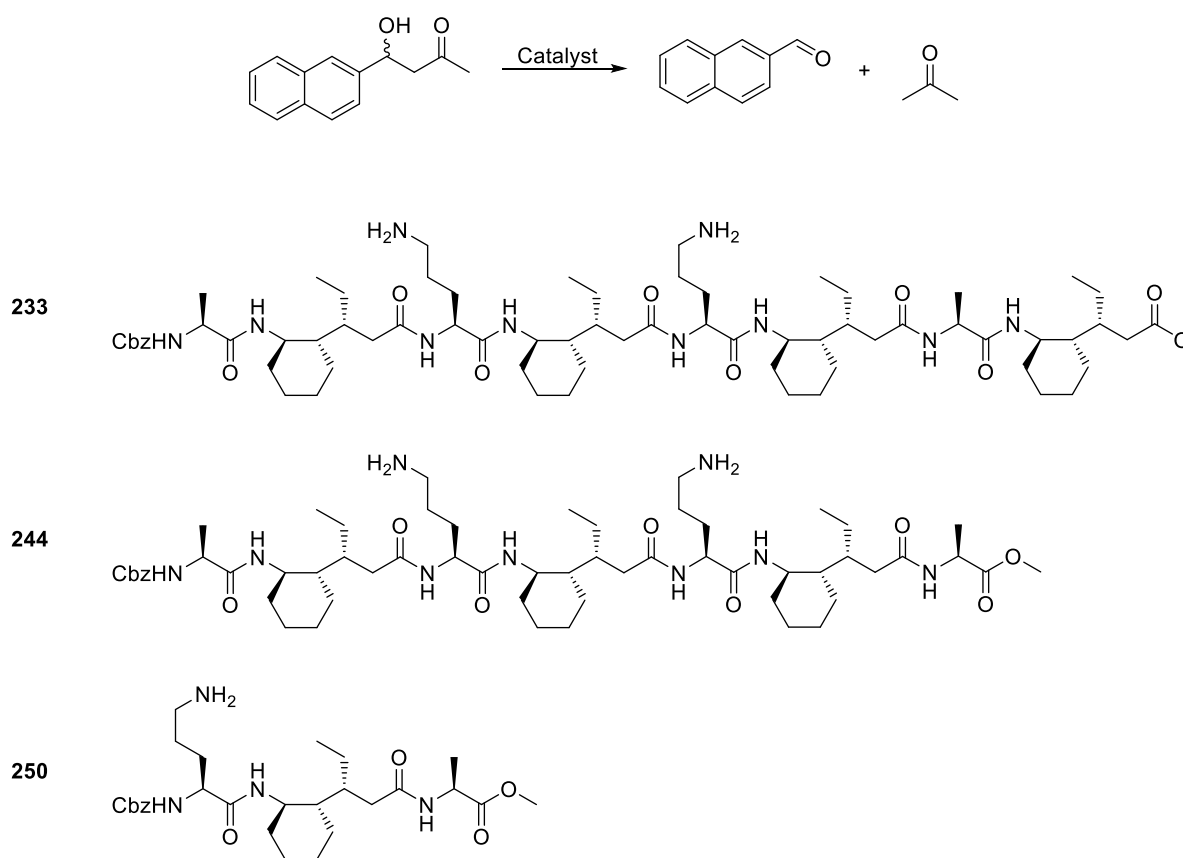
Figure 3.6 Stacked ¹H NMR of foldamer **232**, foldamer **243** tripeptide **241** (from top to bottom), ▲ represent the BocNH on the side chain, ■ represent the N-terminal Cbz-protected amide.

3.2.2 Catalytic Retro-aldol Reaction in Chloroform

As with the study by Hilvert and co-workers, 4-hydroxy-4-(6-methoxy-2-naphthyl)-2-butanone (“methodol”) was chosen as the aldol substrate, where the retro-aldol cleavage products are 6-methoxy-2-naphthaldehyde and acetone. This naphthaldehyde compound has a strong absorbance in the UV range, which is easily monitored by spectroscopy, and is thus an ideal substrate on which to obtain kinetic data, although ultimately, NMR proved best for monitoring catalytic effects in our studies.

As we had proven that both foldamer **232** and foldamer **243** have helical structures in chloroform, we decided to test the catalytic efficiency of the catalyst in that solvent. Butylamine was chosen as a control for simple amine unable to engage in bifunctional catalysis, triethyl amine was chosen as a base unable to catalyse retroaldolase reactions via an iminium mechanism, and finally the tripeptide as a good comparison to check for the importance of bifunctionality on the foldamer catalyst. The catalytic reaction was conducted with 15 mM of the substrate and 0.75 mM of bis-ornithine catalysts or 1.5 mM of mono-amine molecules, to provide equivalent concentrations of amino groups in the reaction. The reactions were monitored by ¹H NMR every 6 hours over 72 hours at room temperature.

After 72h, the amount of aldehyde produced with different catalysts was compared by $^1\text{H NMR}$ (Figure 3.7). In the blank control reaction, scarcely any aldehyde was produced after three days. To check the stability of the substrate and the rate of uncatalyzed reaction, the reaction monitoring was extended to 15 days, where still less than 1% of the product formed (Figure 3.8), proving that methodol is very stable in chloroform. The same lack of reactivity was shown using a catalytic amount of triethylamine, presumably because it cannot form an iminium intermediate with the substrate. For the peptide catalysts, the bis-ornithine catalyst **244** gave the best turnover amongst all the catalysts which producing 2.12 mM product, and tripeptide **250** catalysed 0.09 mM product formation confirming the anticipated synergy between the two amines. The bis-ornithine octamer **233**, which was synthesized to check if the last residue is redundant for the catalyst, was proved to have a catalytic efficiency lower than the heptamer where 1.1 mM product was formed, which may be because of the previously mentioned increased conformational freedom.



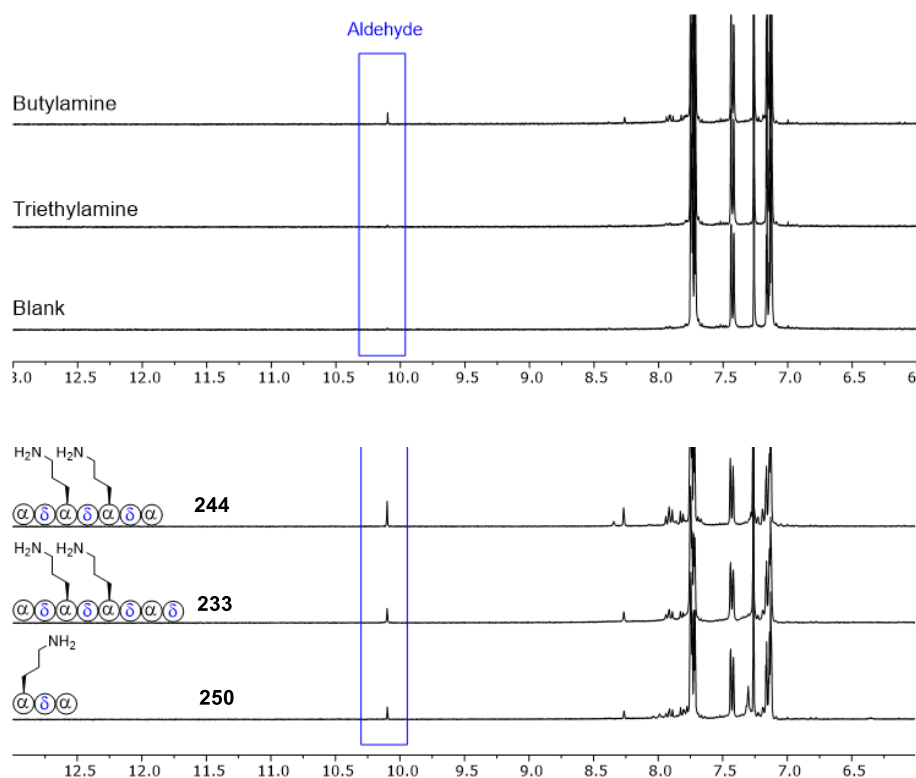


Figure 3.7 Stacked ^1H NMR (400 MHz, CDCl_3) of different catalysts (1.5 mM free amine) mixed with 15 mM substrate after 72 h. The aldehyde proton at 10.2 ppm is marked by a blue square on the spectrum.

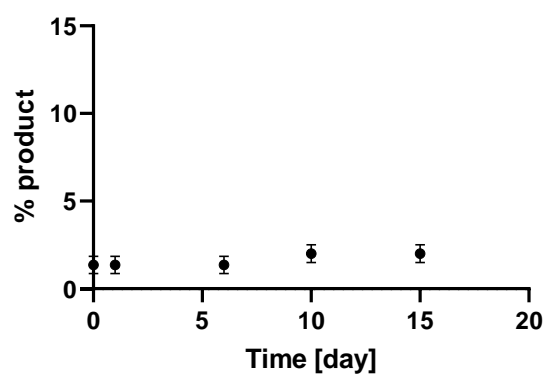
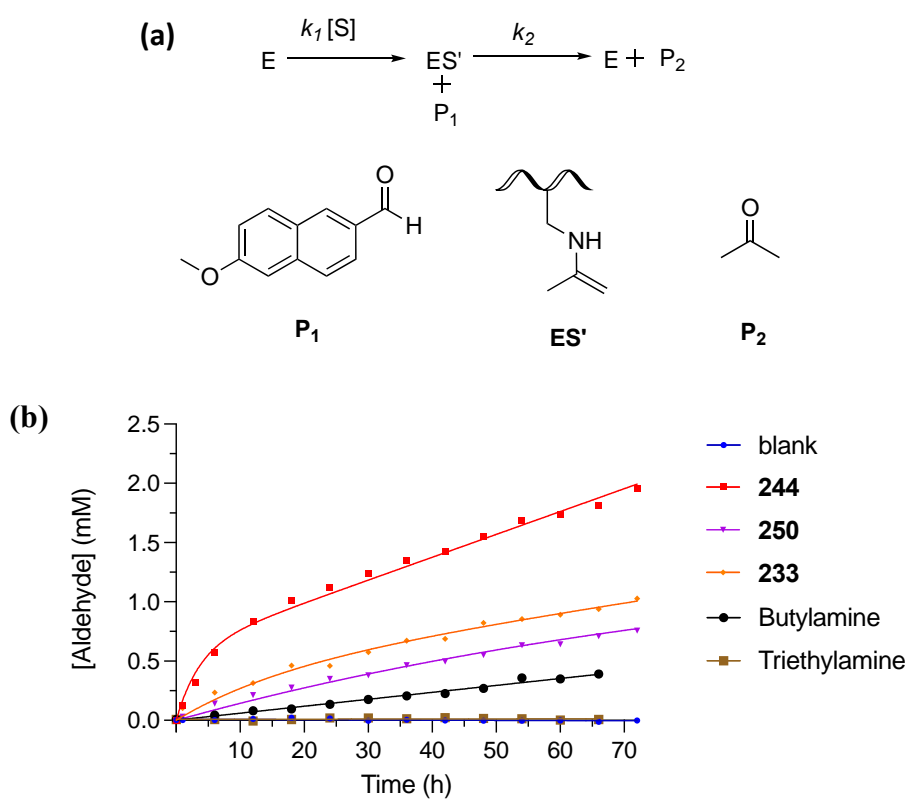


Figure 3.8 Time-based product formation of blank contrast: 15 mM of methodol in CDCl_3 . The data was monitored via NMR, which subjected to 5% error of NMR integration.

The time-based product formation was monitored by ^1H NMR, and the plotted graph shows that the kinetic varies between different catalysts (Figure 3.9). In the presence of butylamine,

a linear increase in product over 72 h is evident with a slope of $0.59 \pm 0.02 \times 10^{-2}$ mM/h. Dividing this rate by the concentration of butylamine in the reaction results in an apparent rate constant $k_{\text{butylamine}}$ of $3.9 \pm 0.2 \times 10^{-3}$ h⁻¹. The reaction progress for the bis-ornithine heptamer **244** the octamer **233** is biphasic. The heptamer **244** shows the highest rate acceleration with the burst-phase $k_{244} = 0.25 \pm 0.04$ h⁻¹, whereas the burst-phase rate constant of the octamer **233** is approx. 5-fold lower $k_{233} = 4.38 \pm 0.27 \times 10^{-2}$ h⁻¹. The structural tripeptide **250** shows the lowest rate acceleration where $k_{250} = 1.07 \pm 0.03 \times 10^{-2}$ h⁻¹.



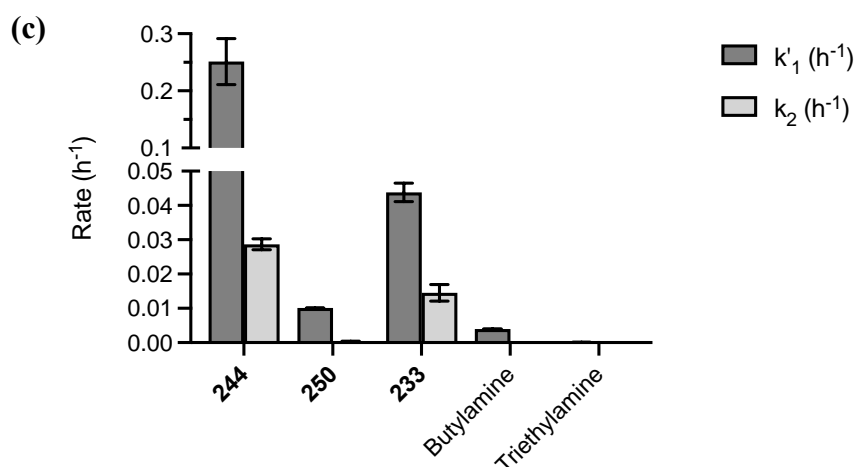


Figure 3.9 (a) Mechanism of catalytic reaction where E represent catalyst, S represent substrate. (b) Time-based aldehyde formation of different catalysts (at 1.5 mM) on [methodol] (15 mM) at 20 °C in CDCl_3 using ^1H NMR and the kinetic equation used for the catalysts. (c) the rate constant calculated from the Fershtp 147⁸⁴ equation.

The proposed mechanism for primary amine-catalyzed retro-aldol cleavage is that the catalyst amine forms an iminium ion intermediate with the substrate to facilitate the carbon-carbon bond cleavage. The kinetic results of both foldamer catalysts reveal a burst phase for the first few hours and a steady-state thereafter. The possible reason for this kinetic behaviour might be caused by the slow hydrolysis of the enamine or iminium intermediate ES' (as shown in Figure 3.9a). The burst rate represents the status when the 0.75 mM of catalyst initially interacts with the substrate to form the aldehyde as **P1**. The next step is the hydrolysis of the acetone-foldamer iminium to release the catalyst for the next round of catalysis. However, the hydrolysis of ES' is slower, and the average rate of the two processes displayed a steady state.

To confirm the possibility of enamine formation by foldamer **244**, the reductive reagent $\text{Na}(\text{CH}_3\text{COO})_3\text{BH}$ was used to trap the iminium as the corresponding amine (Figure 3.10). The enamine intermediate FMM and the condensation product-FMM- H_2O intermediate were found on the HRMS, which proved that an iminium ion between the catalyst and the substrate can form.

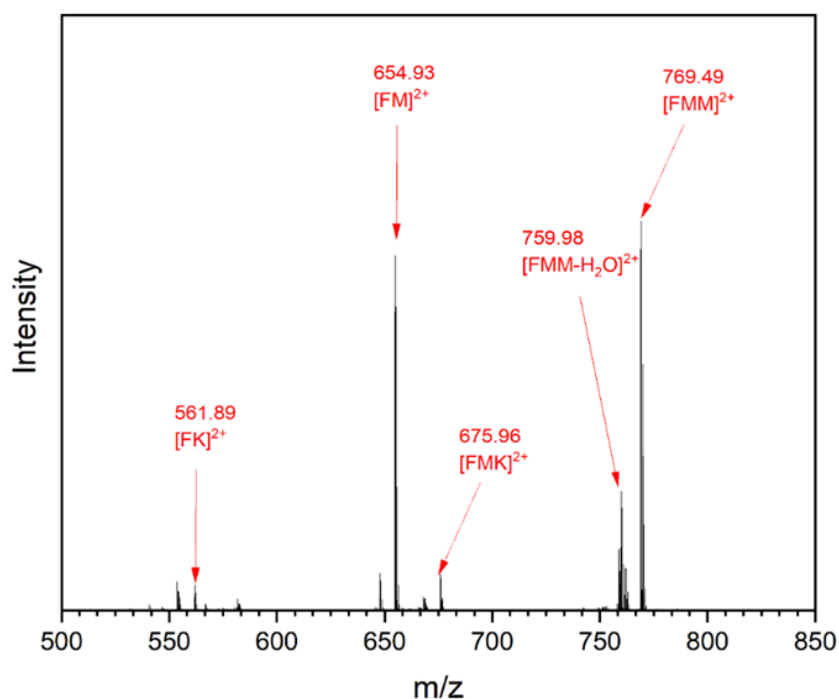
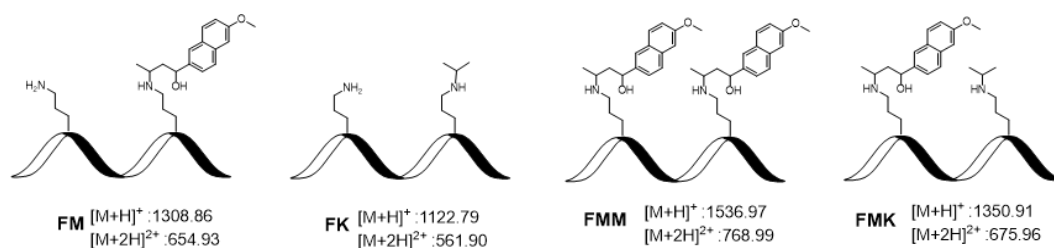


Figure 3.10 The structure of the intermediate and its calculated M/Z. Condition: 15 mM of methodol was reacted with 0.75 mM of foldamer **244** in 500 μ L of CHCl_3 for 2 hours, 1 mg of $\text{Na}(\text{CH}_3\text{COO})_3\text{BH}$ (10 mM) was added, the mixture was reacted overnight at room temperature, the reductive intermediates were analyzed by HRMS.

To understand the binding affinity of foldamer **244** to the substrate, the dependence of rate on the concentration of methodol was monitored via ¹H NMR (Figure 3.11a). The formation of aldehyde was monitored within the first 6 h (the burst state rate). On the rate vs. concentration graph (Figure 3.11b), the reaction proceeds at a linear rate which is dependent on the concentration of the substrate. This indicates that the reaction is first order when the methodol concentration is below 30 mM.

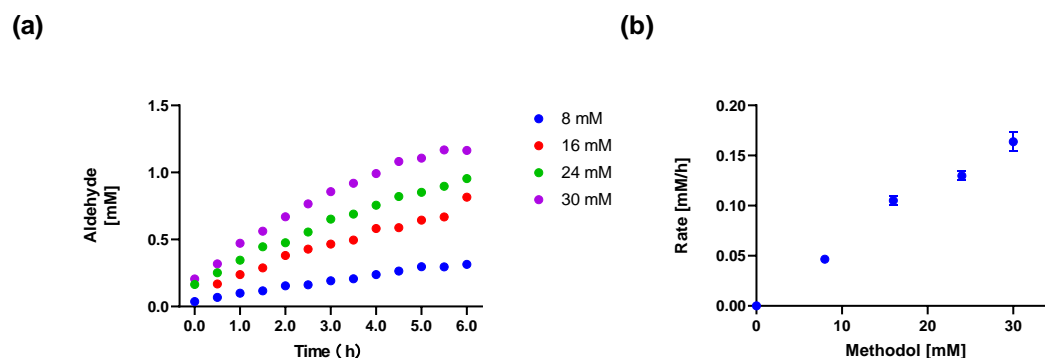


Figure 3.11 At 20 °C, in CHCl_3 , monitored by ^1H NMR over 6 hours, methodol concentration [8-30 mM] (a)

The amount of aldehyde produced using foldamer **244** under different concentrations of methodol. (b)

Dependence of rate on [methodol] (2-30 mM).

The kinetic data was also collected by HPLC monitoring (Figure 3.12). With these experiments, evaporation of the solvent leads to an increase in concentration and so the initial amount of the aldehyde in the starting material needs to be corrected. To achieve this, the blank control was subtracted from the catalytic assays. The data collected is then more uniform and agrees with the data collected from ^1H NMR, the rate linearly depends on the concentration where the $k_{\text{cat}}/K_{\text{m}} = 8.20 \pm 0.36 \times 10^{-3} \text{ mM}^{-1}\text{h}^{-1}$.

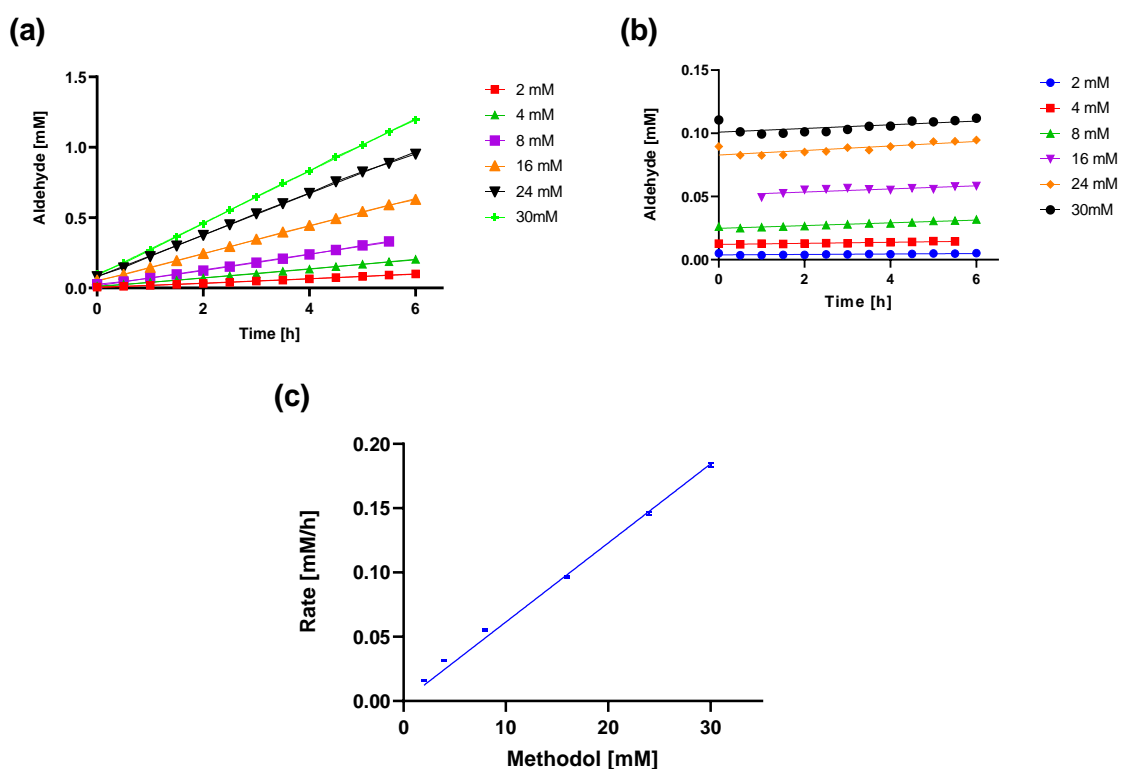


Figure 3.12 At 20 °C, in CHCl_3 , monitored by HPLC over 6 hours, methodol concentration [2-30 mM] (a) The amount of aldehyde produced using foldamer **244** under different concentrations of methodol. (b) Background reaction without any catalyst. (c) Background-corrected dependence of rate on [methodol].

In addition to chloroform, the retro-aldol efficiency of the foldamer catalysts was tested in other solvents (Table 3-1). As shown in the scheme below, neither different solvents nor addition of Lewis acids/bases improved the reaction rate. Given the shortage of material, only three sets of experiments were performed, with more condition screening planned for future work.

Table 3-1 The catalytic efficiency of foldamer **244** in different solvents

Catalyst	Solvent	Acid	Base	Temperature	Yield
10% mol 244	DMSO	2eq C ₇ H ₁₂ O ₂	2eq TEA	rt	1%/day
5% mol 244	MeOD	–	–	40 °C	6.31%/day
5% mol 244	CDCl ₃	–	–	rt	7.4 %/day

3.2.3 Catalytic Retro-aldol Reaction in Aqueous Solution

In nature, the retro-aldol cleavage is catalyzed by aldolase in water, and as such, most of the reported artificial enzymes and antibodies or detergents conduct the retro-aldol cleavage in aqueous solution. This is something we then attempted to do.

Butylamine was chosen as a reference to optimise suitable methods for the microplate reader assay. The kinetics were monitored by detecting the fluorescence of the aldehyde where the excitation is 320 nm, and emission is 460 nm. The second order rate constant of the butylamine catalyzed reaction was obtained by monitoring the rate of product formation with 300 μ M of methodol and varying concentrations of butylamine in in Tris buffer (50 mM Tris, pH=8, 150 mM NaCl) containing 10% CH₃CN at 30 °C, giving $k_{(\text{butylamine})} = 1.21 \pm 0.03 \times 10^{-3} \text{ mM}^{-1} \text{ h}^{-1}$ (Figure 3.13). The rate constant of butylamine fits the data in the literature,^{64, 85, 86} and so we deduced that the methods applied above are reasonable for monitoring the kinetics of this retro-aldol reaction.

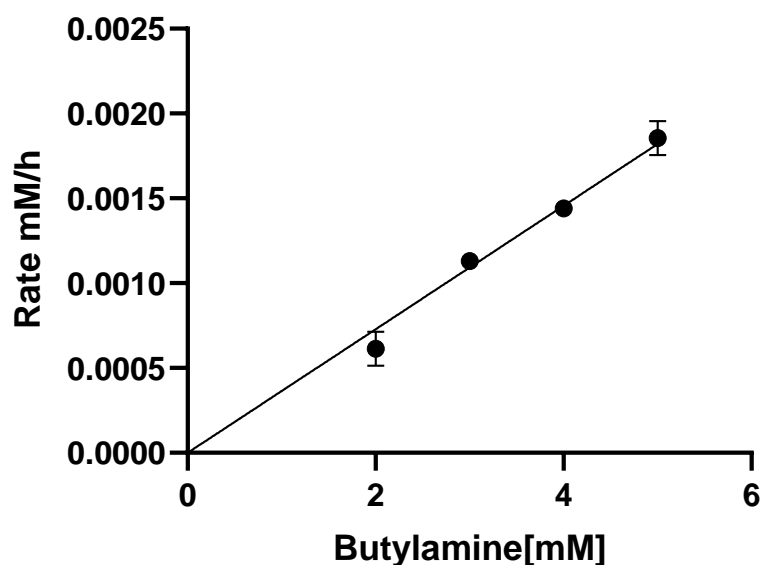


Figure 3.13 The dependence of the reaction's rate on the concentration of butylamine. The reaction is monitored by a microplate reader using a black 96-well plate reader, reading from the top.

We selected foldamer **244** to monitor the kinetic profile using 10% CH₃CN in Tris buffer because it was the most efficient catalyst in organic solvent. The data was collected in the same way as the butylamine assays to study the activity of the foldamer catalyst. However, the result did not show the expected trend of product formation. Instead, the data points became more scattered, particularly at higher concentrations (Figure 3.14). This was probably caused by the gradual evaporation of acetonitrile, causing the precipitation of the substrate or product from the buffer solution. We then replaced the all-black 96-well plate with a bottom-cleared black 96-well plate and applied an adhesive film on top of the 96-well plate, in an attempt to reduce evaporation and the data was collected from the bottom reading.

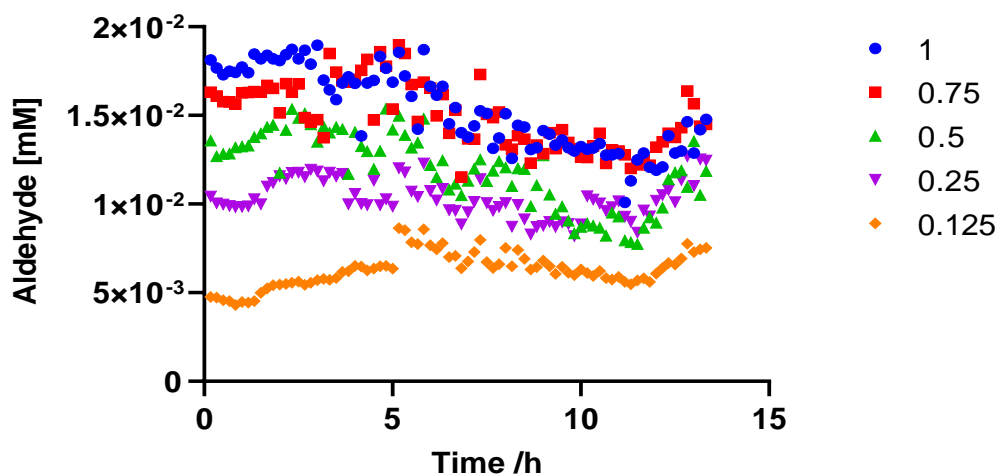


Figure 3.14 The proceeded product formation with 50 μM of foldamer **244** and varying substrate concentration (0.125-1 mM), 30 $^{\circ}\text{C}$, 10% CH_3CN in Tris buffer (50 mM Tris, pH=8, 150 mM NaCl), monitored by plater reader, black 96-well plate, read from top.

The repeat experiment in 10% CH_3CN in Tris Buffer using [bottom-cleared, black] 96-well plates gave more reasonable data (Figure 3.15). The $[\text{product}]/t$ looks more uniform when the substrate concentration is below 1 mM, however, when the methodol concentration increased to 2 mM, the data points in the blank assay became scattered, which might be because of the substrate being saturated at this concentration leading to precipitation. Remarkably, the data points in the foldamer **244**-containing assay look more uniform and surpass the blank at this concentration. The rate comparison between the blank assay and foldamer **244** assay below 1 mM of substrate concentration indicates that the foldamer starts to show extra rate acceleration when the substrate concentration reaches 1mM where the substrate is saturated. This observation indicates that - in water - the foldamer might act as a phase-transfer catalyst rather than a specific retro aldolase.

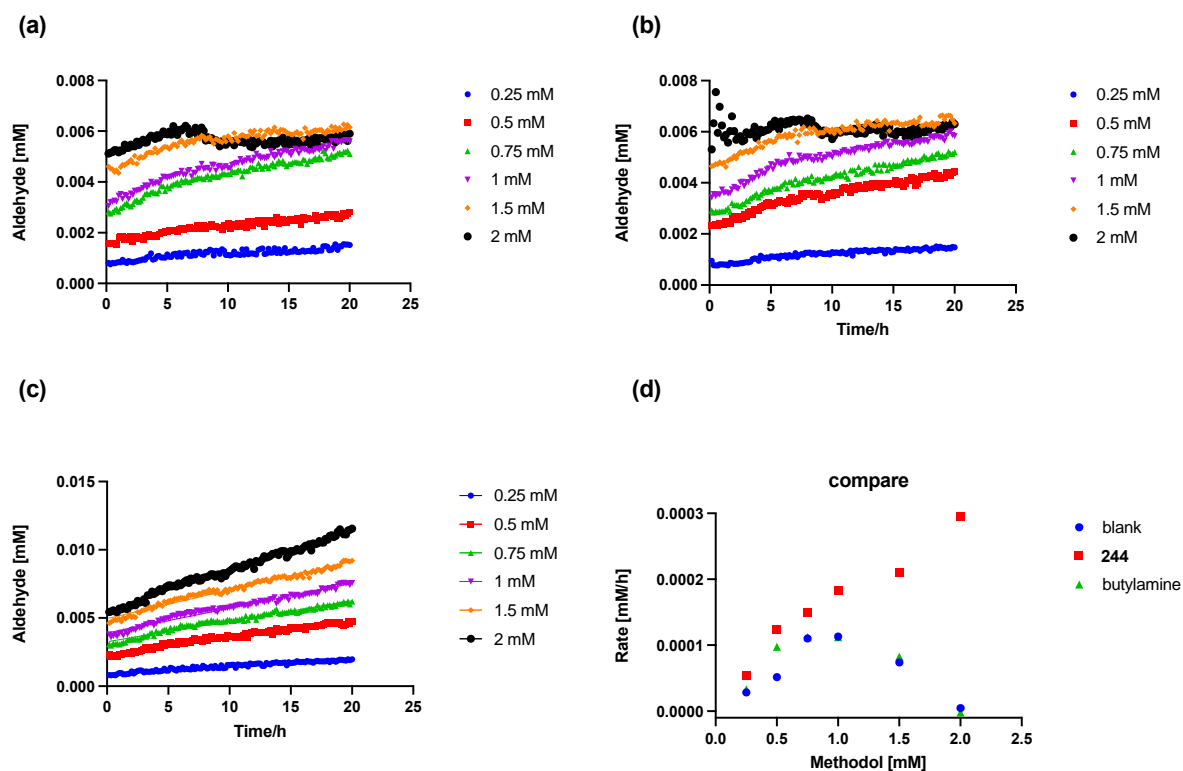


Figure 3.15 At 25 °C, in 10% CH₃CN in Tris buffer (50 mM Tris, pH=8, 150 mM NaCl), monitored by plate reader, (a) Product formation vs substrate concentration (0.25-2 mM). (b) Product formation using 200 μM of butylamine vs substrate concentration (0.25-2 mM). (c) Product formation using 100 μM of foldamer **244** vs substrate concentration (0.25-2 mM). (d) Rate comparison between blank contrast, 200 μM butylamine, and 100 μM foldamer **244** of catalyzed reactions at different methodol concentrations (0.25-2 mM).

To fully solubilize the substrate, the percentage of organic solvent was increased to 20% in Tris buffer, leading to a substrate concentration of 10 mM. In the blank assay, the data points started to become scattered when the substrate concentration reached above 10 mM (Figure 3.16a) for the reasons cited above, which indicates the saturated concentration of substrate was between 5 mM and 10 mM in 20% of CH₃CN in Tris buffer. In the foldamer **244** assay, the rate keeps increasing at 10 mM of substrate concentration (Figure 3.16b), and this result is similar to that in 10% CH₃CN in Tris buffer, where foldamer **244** starts to show higher efficiency when the substrate is saturated, whereas at lower concentrations, where the substrate is soluble in buffer, the catalyst barely surpasses the rate acceleration arising from the buffer. This unusual observation might be because the foldamer accelerates the reaction by helping *solubilize* the substrate in aqueous solution at the higher concentrations.

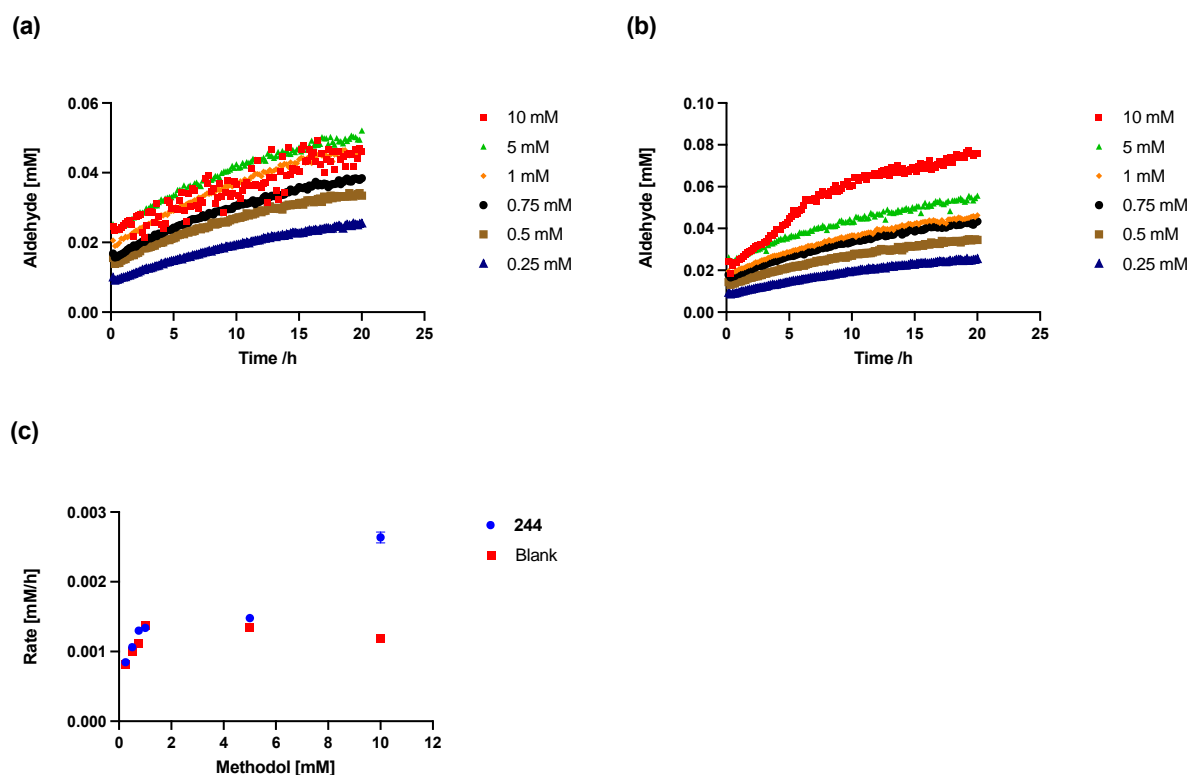


Figure 3.16 At 30 °C, in 20% CH₃CN in Tris buffer (50 mM Tris, pH=8, 150 mM NaCl) monitored by plate reader, (a) Product formation vs substrate concentration (0.25-10 mM). (b) Product formation with 100 μM of foldamer **244** vs substrate concentrations (0.25-10 mM). (c) Rate comparison between blank contrast and the foldamer **244**-catalyzed reaction at different methodol concentrations (0.25-10 mM).

As discussed above, we found that higher concentrations of organic solvent makes the data less scattered by fully dissolving the substrate, but also eliminates the privileges of foldamer catalyst over blank and butylamine. Furthermore, at the same substrate concentration, the increase of the organic solvent from 10% to 20% did not improve the rate of the reaction. To confirm the influence of organic solvent on the relative catalytic efficiency of the foldamer catalyst to the butylamine control. An NMR study was applied to monitor the exact reaction yield under different solvent systems by comparing the foldamer catalyst with butylamine. As shown in Figure 3.17, at 10% of CD₃CN in Tris, the foldamer produced 4.1% of aldehyde, which is 3.4-fold higher than butylamine. With 20% of CD₃CN in Tris, the yield of foldamer decreased to 2.3% which is only slightly higher than butylamine contrast. When the percentage of CD₃CN reached 50%, the activity of foldamer remains the same as in the 20% of CD₃CN, whilst the yield using butylamine under these conditions increased to 19.3%. This data

indicates that foldamer catalysis behaves more effectively at the lower percentage of organic solvent. Decreasing the percentage of organic solvent would improve the foldamer's efficiency on the retro-aldol cleavage.

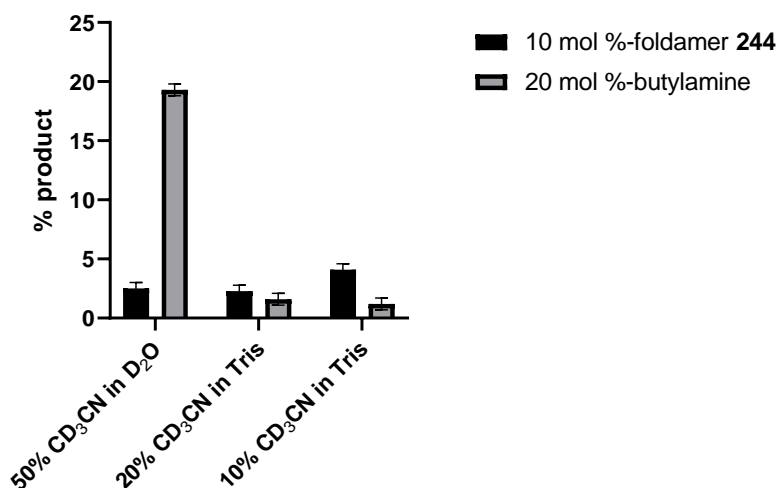


Figure 3.17 Yield comparison of butylamine (2 mM) and foldamer **244** (1 mM) with methodol (10 mM) in 10% CD₃CN in Tris buffer, 20% CD₃CN in Tris buffer, 50% CD₃CN in D₂O, monitored by ¹H NMR at 20°C.

We then investigated the best solvent system for displaying the optimal catalytic efficiency of the foldamer. As described previously, we believed that the greater volume of organic solvent eliminates the solubilizing effect originating from the foldamer catalyst. To check this, we investigated the reaction using 5% CH₃CN in buffer. By comparing the catalytic efficiency of foldamer **244** relative to the blank in PBS and Tris buffer, the 5% CH₃CN in PBS was demonstrated to be the best solvent for foldamer **244**. In 5% CH₃CN in Tris, the $V_{\text{foldamer}}/V_{\text{blank}}=1.7$ at 2 mM of the substrate (Figure 3.18a), whereas in PBS at the same concentration, $V_{\text{foldamer}}/V_{\text{blank}}=6.4$ (Figure 3.18b). To determine whether the solubilizing effect comes from the secondary structure of the foldamer, the kinetics of the non-structured tripeptide catalyst was tested as well. We found that the kinetics of tripeptide followed the same pattern as the butylamine catalyst, thus implying the positive effect of the ordered foldamer structure on the retro-aldol reaction in the aqueous phase.

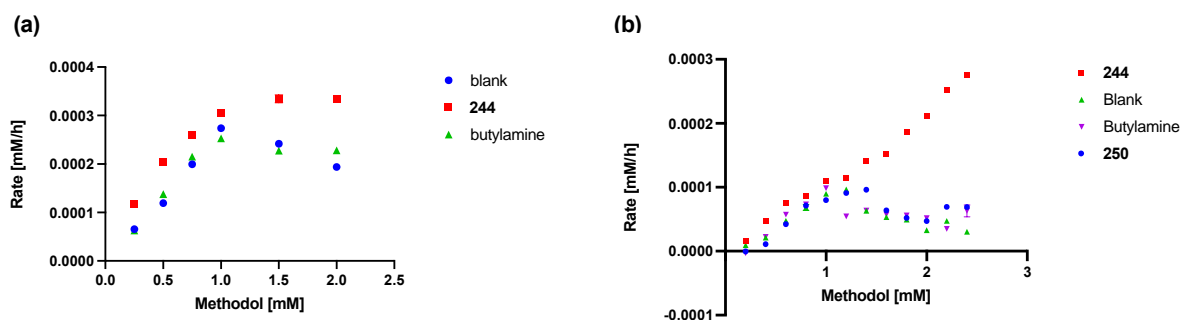


Figure 3.18 Reaction rate at varying substrate concentration over 20 hours at 25°C. (a) Comparison of rate with either 100 μ M of foldamer **244**, 200 μ M butylamine, or blank vs substrate concentration (0.25-2mM), in 5% CH_3CN in Tris buffer (50 mM Tris, pH=8, 150 mM NaCl) monitored by plate reader. (b) Comparison of rate with either 100 μ M of foldamer **244**, 200 μ M butylamine, 200 μ M tripeptide **9**, or blank and varying substrate concentration (0.2-2.4 mM) in 5% CH_3CN in PBS (42.5 mM, pH=7.5) monitored by plate reader.

To complement and solidify the results collected from the plate reader, the kinetics of 100 μ M of foldamer **244** in 5% CH_3CN in PBS was monitored by HPLC, as shown in Figure 3.19, to give data that is consistent with that collected from the plate reader. The substrate became saturated at 1 mM, and when the substrate concentration is below 1 mM, the foldamer **244** does not meaningfully surpass the blank and butylamine assays. When the substrate concentration is above 1 mM, foldamer **244** behaves as a phase-transfer catalyst to help solubilize the substrate and catalyze the reaction; as such the rate keeps improving as the concentration increases.

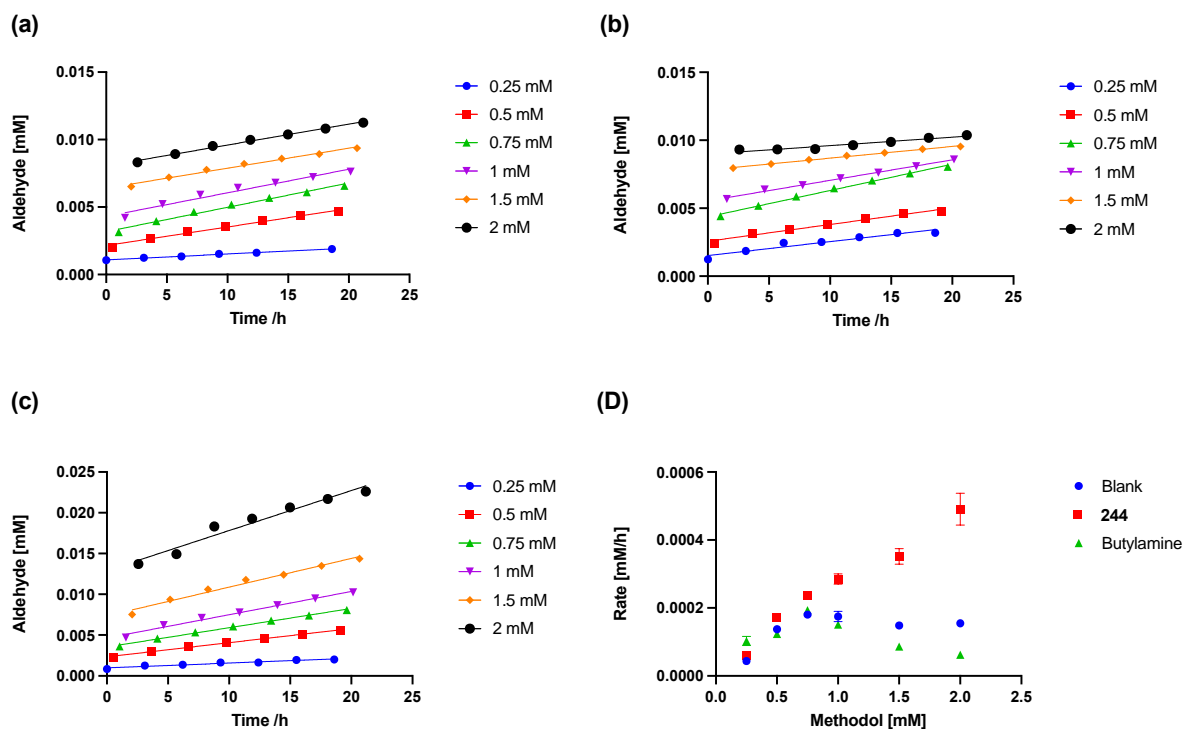


Figure 3.19 5% CH₃CN in PBS buffer (42.5 mM, pH=7.5), monitored by HPLC at 25°C (a) Product formation vs substrate concentration (0.25-2 mM). (b) Product formation with 200 μM of butylamine vs substrate concentration (0.25-2 mM). (c) Product formation with 100 μM of foldamer **244** vs substrate concentration (0.25-2 mM). (d) Rate comparison between blank contrast, 200 μM butylamine, and 100 μM foldamer **244** catalyzed reactions at different methodol concentrations (0.25-2 mM).

The substrate concentration was increased to 15 mM to further investigate the rate acceleration ability of foldamer **244** (Figure 3.20a). At this concentration, the substrate is not soluble in 5% CH₃CN in PBS buffer. For the initial rate, over the first 24 h, the blank corrected rate of the foldamer **244**-catalyzed reaction is 3.24×10^{-2} mM/h, and the blank corrected rate of the butylamine-catalyzed reaction is 0.08×10^{-2} mM/h, to give $v_{\text{foldamer}}/v_{\text{butylamine}}=38.4$. As shown in Figure 3.20b, in the blank and butylamine reaction vials, the precipitation is obvious, whereas in the foldamer **244** reaction vial, the precipitation was not observed. This is, perhaps, more straightforward evidence of the phenomenon of the solubilizing effect of the foldamer.

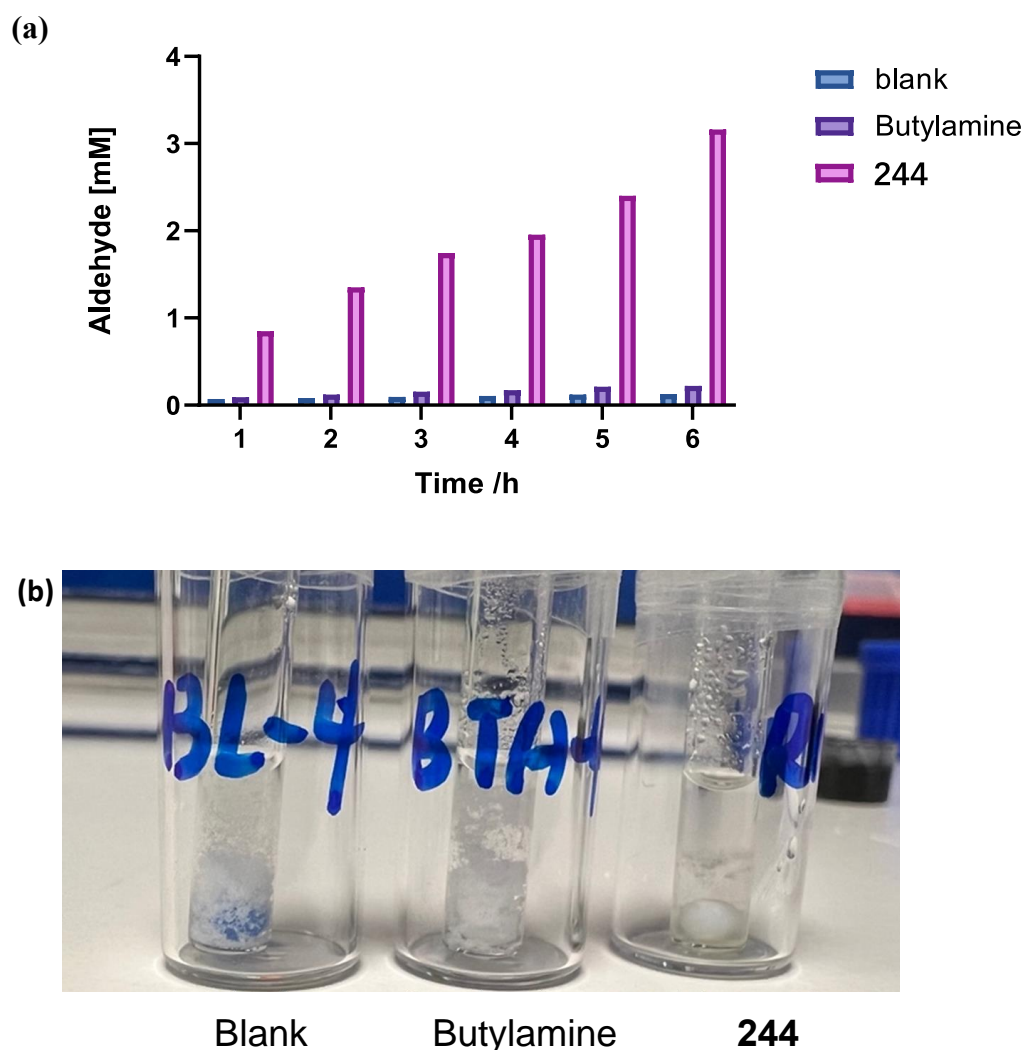


Figure 3.20 (a) Using 5% CH_3CN in PBS buffer (42.5 mM, pH=7.5) at 25°C, the amount of aldehyde formed with (i) 15 mM of substrate (in blue), 15 mM of substrate and 2 mM of butylamine (in purple), and 15 mM of substrate and 1 mM of foldamer **244** (in pink), as monitored by HPLC (see experimental). (b) The solubilising phenomenon of foldamer **244** within the vials. Without it, a clear precipitation is observable.

Foldamer is amphiphilic with a hydrophobic face and a small cationic region. Its quaternary structure in water isn't known, but will likely self-assemble. To investigate if amphiphilic detergents are similarly able to promote methodol solubility (and therefore its retroaldol cleavage), we used cetyltrimethylammonium chloride (CTAC, Figure 3.21) and sodium dodecyl sulfate (SDS, Figure 3.21) as a surfactant control to qualify the solubilizing effect of the foldamer. Over a 24 hour reaction time, with 15 mM substrate concentration and 2 mM of amino group (1 mM for bisornithine foldamer, 2mM for un-structured monoamine), the results

show that foldamer **244** is the best catalyst amongst all the tested systems (Figure 3.21) surpassing the CTAC-butylamine system that came out as second-best of all the test systems. The bis-ornithine octamer **233** which has that redundant terminal δ -residue is worse than CTAC-butylamine system, but still surpass the un-structural tripeptide and the butylamine system. In the SDS-butylamine mixture, the yield is similar to the blank, but lower than the butylamine control. This observation indicates that SDS might suppress the butylamine catalysis of the retro-aldol reaction by stabilising the unreactive butylammonium species. The efficiency order of all the catalysts in the aqueous phase is consistent with the order of all catalysts in chloroform.

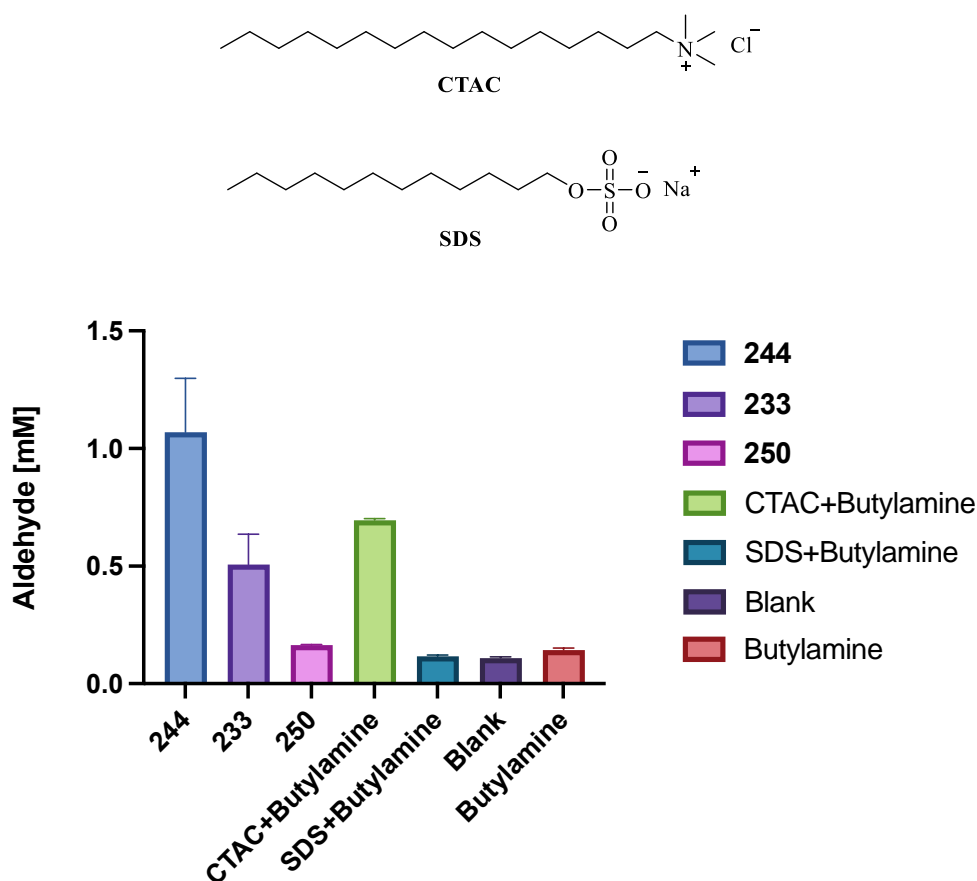


Figure 3.21 5% CH_3CN -PBS buffer, room temperature, 24 h reaction time, monitored by HPLC. 15 mM substrate and 1 mM foldamer or 2 mM monoamine, CTAC+Butylamine assay: 15 mM substrate, 2 mM CTAC, 2 mM butylamine. SDS+ Butylamine assay: 15 mM substrate, 2 mM SDS, 2 mM butylamine.

3.2.4 CD Spectrum of Foldamer in Aqueous Solution

The CD spectrum of tripeptide and foldamer catalysts was tested in 20% CH₃CN in water to determine the helical propensity of these peptides in the aqueous phase. By comparing the absorbance of foldamer **244** with tripeptide **250**, the foldamer seems to adopt some extent of helicity in aqueous solution (Figure 3.22).

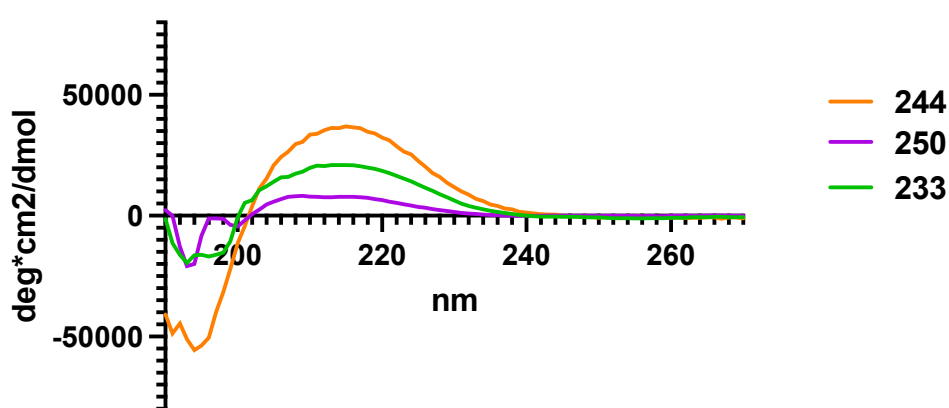
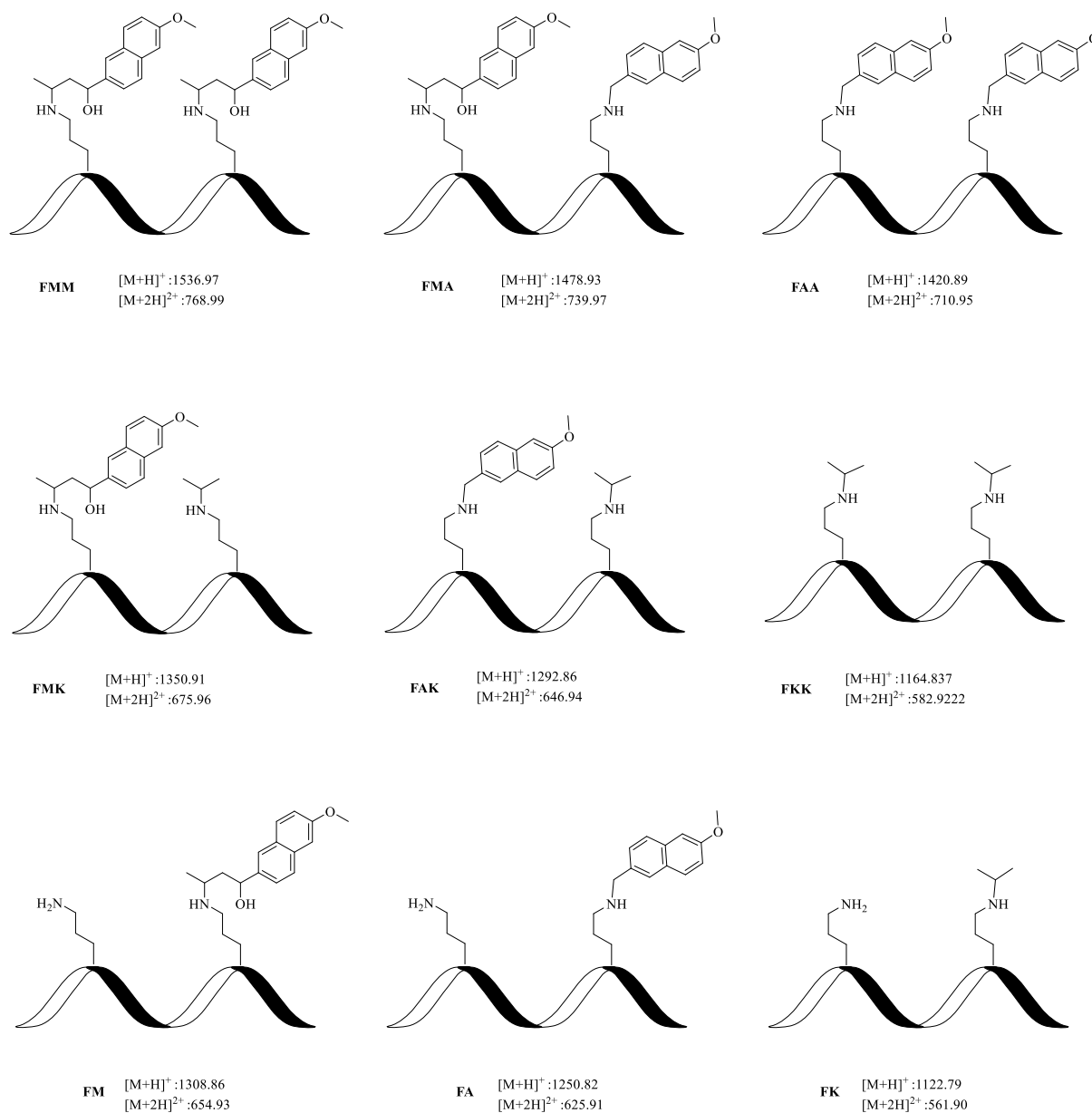


Figure 3.22 CD spectrum of foldamer **244**, foldamer **233**, and Tripeptide **250** in 20% CH₃CN in H₂O.

3.2.5 Mechanism of Retro-Aldol Catalysis in Buffer

The intermediate trapping experiment was also performed in an aqueous phase; 15 mM of methodol was reacted with 1mM of foldamer **244** in 100 μ L of 5% CH₃CN-PBS buffer for one day before sodium cyanoborohydride was subsequently added to give a final concentration of 20 mM. The mixture was incubated for eight hours then tested subjected HRMS, and the reduced adducts were identified (Figure 3.23). The results indicate that foldamer **244** is capable of forming iminium ion intermediates with ketones and aldehydes, which suggests that it can also catalyze the retro-aldol reaction in the aqueous phase via a standard enamine mechanism (Figure 3.23).



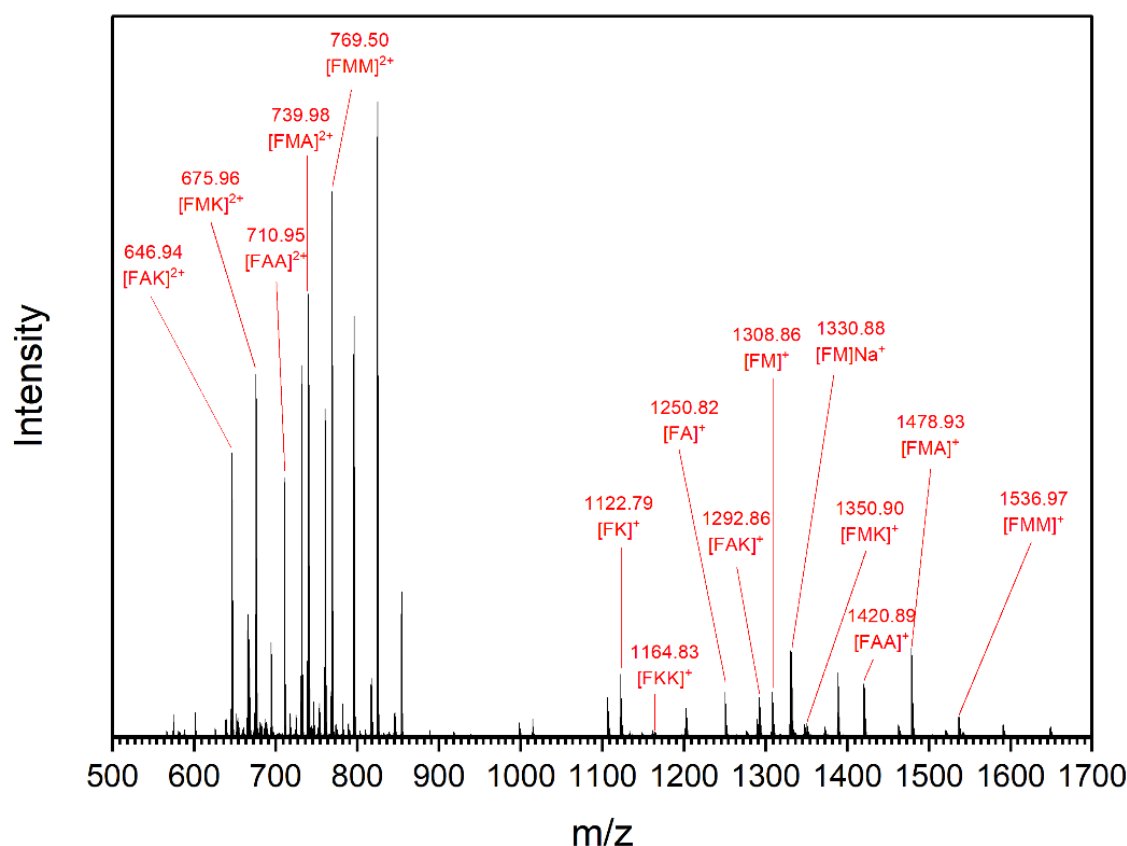


Figure 3.23 Founded M/Z of intermediates.

In addition to the rate acceleration of the foldamer catalyst, the enantioselectivity of foldamers was also tested (Table 3-2). The substrate is a racemic mixture with of (*R*)- and (*S*)-methodol. It is possible that the foldamer will discriminate the retroaldol cleavage of one enantiomer of the other owing to the single-handed helicity of the system. The ee was tested by chiral HPLC after the racemic mixture of methodol was incubated with foldamer **244** for 24 h. The unchanged ratio of two enantiomers indicates that the bis-ornithine catalysts did not reveal any discrimination over the two enantiomers either in chloroform or aqueous solution. The bis-ornithine side chains have three methylene between catalytic amine and foldamer backbone, making the catalytic reaction happen relatively far away from the chirality of the helix centre. The lack of interaction between the foldamer backbone and substrate is probably the reason for the non-selectivity of this system.

Table 3-2 Conditions for attempted enantioenrichment

Catalyst	Solvent	ee (%)	Temperature
20 mol% Triethylamine	10% CH ₃ CN in Tris buffer	—	40 °C
20 mol% Butylamine	10% CH ₃ CN in Tris buffer	—	40 °C
10 mol% foldamer 233	CDCl ₃	—	40 °C
10 mol% foldamer 233	10% CH ₃ CN in Tris buffer	—	40 °C
7.5 mol% foldamer 244	10% CH ₃ CN in Tris buffer	—	40 °C
7.5 mol% foldamer 244	10% CH ₃ CN in tris	—	30 °C

3.3 Conclusion

The work in this chapter focused on the kinetic study of the foldamer catalysts on a retroaldol cleavage. The synthesis of foldamer catalysts was guided by the structural information acquired from Chapter 2, and lead to the design of heptamer and octamer foldamer catalysts. These were compared to a tripeptide consisting of the same building blocks, and butylamine. The success of the foldamers over these controls demonstrated the structural advantages of the helix in chloroform. Although the efficiency of the foldamer catalysts is modest and far less than the natural enzyme or the antibody/peptides published before, the results still show an obvious increase in efficiency by placing two active sites that are proximal by virtue of the folding structure. This verifies the possibility of using simplified chemical structures to mimic the functionality of large and more complex biomacromolecules. The kinetics in chloroform showed that the terminal residue within the octamer had a detrimental side-effect on the catalytic efficiency.

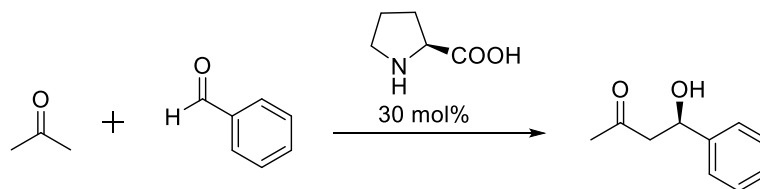
In an aqueous solution, water might compete with the foldamer's intramolecular hydrogen bonds, leading to a certain degree of unfolding of the helical structure. However, the hydrophobic interactions of the foldamer's backbone could partially contribute to maintaining the folding of its helical structure, allowing for some degree of helicity in aqueous solution. The mechanism of catalysis in the aqueous phase, although not confirmed yet, is interesting as it opens the possibility that the bis-ornithine foldamer is behaving as a phase-transfer catalyst to help solubilize substrate; this might arise from the orientation of the catalytic side chains and the foldamer backbone in aqueous solution. The intermediate trapping experiment also indicates that the foldamer can catalyse the reaction by an enamine mechanism.

Chapter 4 The Reversible Enantioselectivity of α,δ -Foldamer Catalyst

The helicity of foldamer structures make them potentially suitable candidates for asymmetric catalysis.^{87, 88} However, there are only a handful of examples of implementing the helical chirality of foldamers as asymmetric catalysts. Based on the described structural properties demonstrated in Chapter 2, our α,δ -peptide foldamer could be a promising structure for this application. Whilst the retro-aldol of the previous chapter showed no real enantioselection, bringing functionality closer to the helix would potentially imbue stereoselectivity upon the reaction.

4.1 Introduction

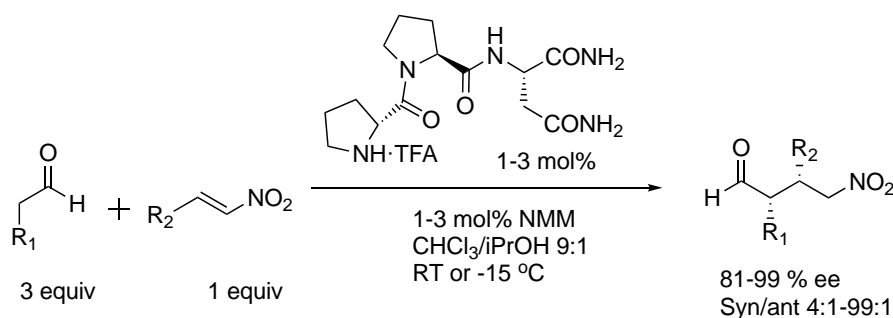
Over the past two decades, peptide or amino acid catalysts have contributed significantly to asymmetric catalysis. In 2000, List and coworkers discovered that proline could catalyze the asymmetric aldol reaction as a mimic of class I aldolase.⁸⁹ Proline has a nucleophilic amine group, that can interact with the ketone substrate and form the enamine/iminium intermediate, whilst the carboxylic acid on the proline acts as an acid co-catalyst to accelerate the rate of the catalytic aldol reaction. The enantioselectivity comes from the Zimmerman-Traxler transition state that favours the formation of one enantiomer over the other.⁹⁰ The yield and ee of the catalytic efficiency vary from the substrates. For the aromatic aldehyde substrates, the yields range from 54~94%, and the enantioselectivities are ranged from 60~77% (Table 4-1).

Table 4-1 Yield and ee's of proline catalyzed aldol product.

Product	Yield	ee
	68%	76%
	62%	60%
	74%	65%
	94%	69%
	54%	77%
	97	96%

Helma Wennemers and co-workers developed a short tripeptide catalyst for a highly enantioselective 1,4-addition reaction between nitro-olefin and aldehyde, with only 1~3 mol% catalyst loading (Scheme 4-1).⁹¹ As with the List system, the C-C bond-forming reaction relies on the presence of an amine group and a carboxylic acid group; the secondary amine on the tripeptide forms an enamine intermediate with the aldehyde substrate, and the carboxylic acid is responsible for the proton transfer, the conformation study of the tripeptide catalyst indicates

that the turn conformation of the tripeptide structure is crucial for realizing the high enantioselectivity. This research proved that peptide catalysts as concise enzyme mimics could be asymmetric catalysts with the help of a specific conformation adopted.



Scheme 4-1 Scheme of tripeptide catalyzed 1,4-addition reaction.

Scott Miller and co-workers have contributed significantly to developing peptide-based asymmetric catalysts too.⁹² The idea of using peptide structure for catalysis is to embed a nucleophile into the peptide and use the structural conformation of a peptide to position the active sites with a desired geometry to realize asymmetric catalysis. They designed the first-generation catalysts to contain an imidazole or 1-substituted imidazole group. The model reaction was the kinetic resolution of the acylation reaction on the *trans*-1,2-acetamidocyclohexanol. In the amino acid contrast, the histidine derivative-catalyst **272** has no enantioselective discrimination for the acylation of the alcohol substrate. When the histidine is constructed into a tripeptide catalyst **271**, which has a turn conformation, it shows a much higher ee where $k(S, S)/k(R, R)=17$. When the chirality of the proline changes, the catalyst **273** displays a different conformation with only one hydrogen bond adopted to stabilize the conformation, a moderate ee where $k(S, S)/k(R, R)=3$ was exhibited.^{93, 94} When the stereocentre on the proline was altered to D-proline, the resulting catalyst **274** adopted a more stable turn structure, and the imidazole group was positioned on the side of the turn structure, it showed a much higher ee where $k(S, S)/k(R, R)=28$. The difference between catalyst **273** and catalyst **274** is the stereo geometry of the proline residue, which demonstrates that the more refined structure resulted in a higher enantioselectivity. To further investigate the secondary structures' impact on the enantioselectivity of the catalyst, they designed several longer peptide sequences. Catalyst **276** contains a D-proline, which allows the peptide to adopt a beta-sheet structure that affords a high selectivity of up to $k(S, S)/k(R, R)=51$. The same sequence that contains L-proline

in the middle does not adopt a well-defined structure, thus showing a much lower selectivity of $k(S, S)/k(R, R)=7$ (Figure 4.11).⁹⁵ Apart from the asymmetric acyl transfer reaction catalyzed by peptide catalyst, Miller's and co-workers also found peptide catalysts efficient for the asymmetric phosphorylation reaction, asymmetric Morita-Baylis-Hillman reaction, and asymmetric conjugate addition.⁹⁶ The versatility and modularity of peptide catalysts have played an important role in their use in asymmetric catalysis.

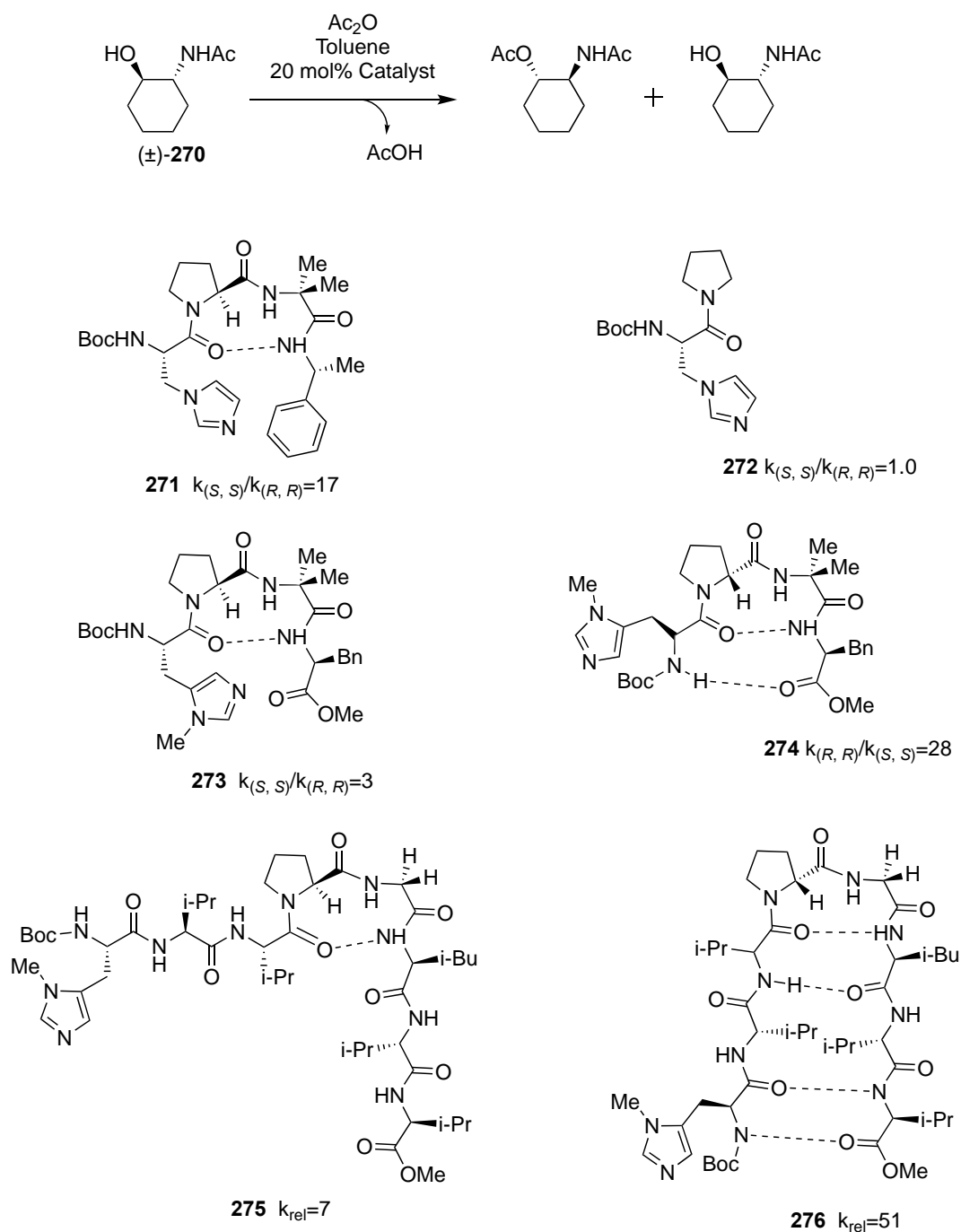


Figure 4.1 The structures of peptide catalysts for β -aminoalcohol resolution

4.2 Results and Discussion

4.2.1 Enantioselectivity of Bis-Dap Foldamer

Following up on the non-enantioselectivity of the bis-ornithine system, this chapter aims to realize the enantioselectivity of the α,δ -peptide. As we concluded from Chapter 2, this 1:1 α,δ -peptide scaffold would have its α -residue embedded more inside of the helix circle, and the result in Chapter 3 indicates that with the longer bis-ornithine side chain, the active sites are too far away from the helical backbone to induce any enantioselective discrimination of the aldol substrate. Hence, we decided to replace the ornithine on foldamer **244** with diamino propionic acid (Dap), which only has one methylene between the side-chain amine and peptide backbone (Figure 4.2). With the catalytic site closer to the helix center, the catalytic reaction would happen inside of the helical environment so that the substrate could interact with either the foldamer backbone or the outer circle of adjacent δ -residue, any interaction, or the steric hindrance between substrate and foldamer catalyst would be the origination of the kinetic resolution.

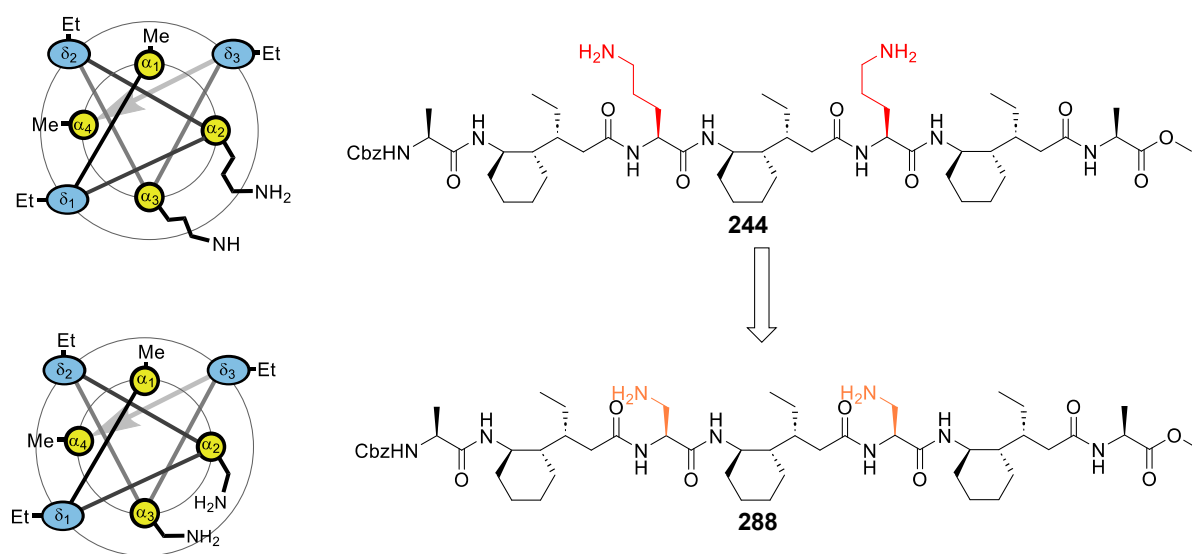
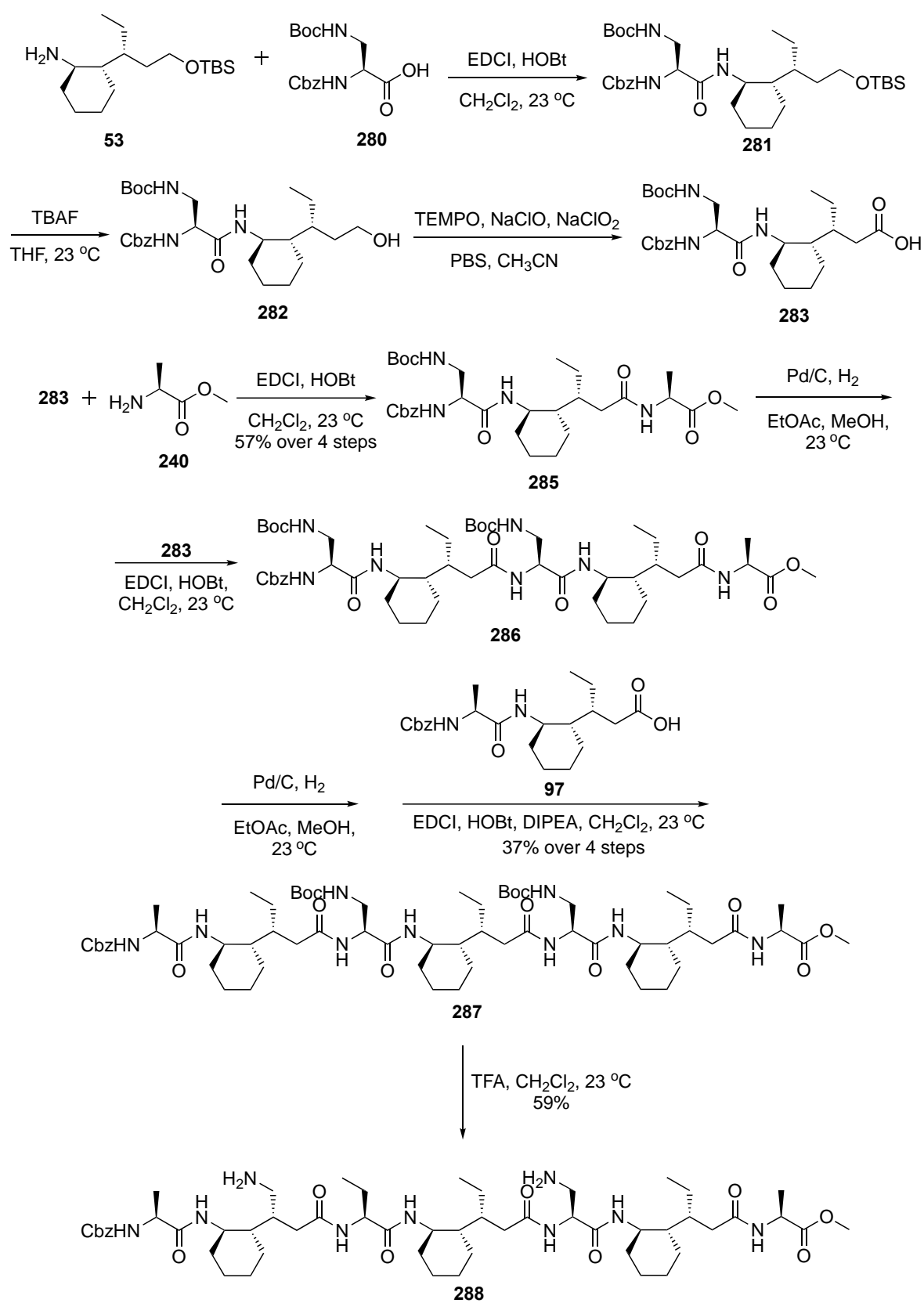


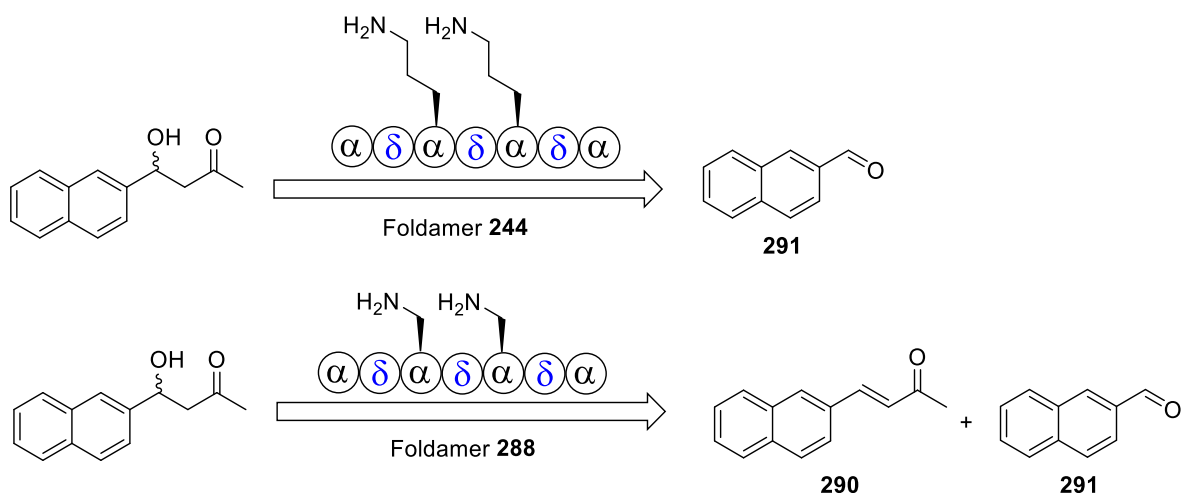
Figure 4.2 Illustration and structure of the bis-ornithine foldamer and bis-dap foldamer.

The synthesis of bis-Dap foldamer **288** follows the same procedure as the synthesis of foldamer **244** (Scheme 4-2). The bis-Dap foldamer was successfully synthesized and characterized by NMR, HRMS, and HPLC.



Scheme 4-2 Procedure for Synthesising Foldamer **288**

The catalytic efficiency of the bis-Dap catalyst on retro-aldol cleavage was tested under the same conditions as foldamer **244** assays. Unlike the bis-ornithine system, which only produced retro aldol cleavage product (6-methoxy-2-naphthaldehyde) **291**, the bis-Dap foldamer **288** produced aldol condensation product-alkene **290** (Scheme 4-3) together with aldehyde product **291**, indicative of a competing retro aldol. As shown in Figure 4.3, the bis-Dap-foldamer **288** produced around 1:1 amount of aldehyde (indicated with the blue triangle) and alkene (indicated with a red square), whereas the bis-ornithine foldamers and non-structural butylamine and tripeptide only produced the retro-aldol cleavage product. This that indicates bringing the catalytic site closer to the helical centre might induce some interaction that results in the formation of eliminated product.

**Scheme 4-3** Reactions catalyzed with different catalysts.

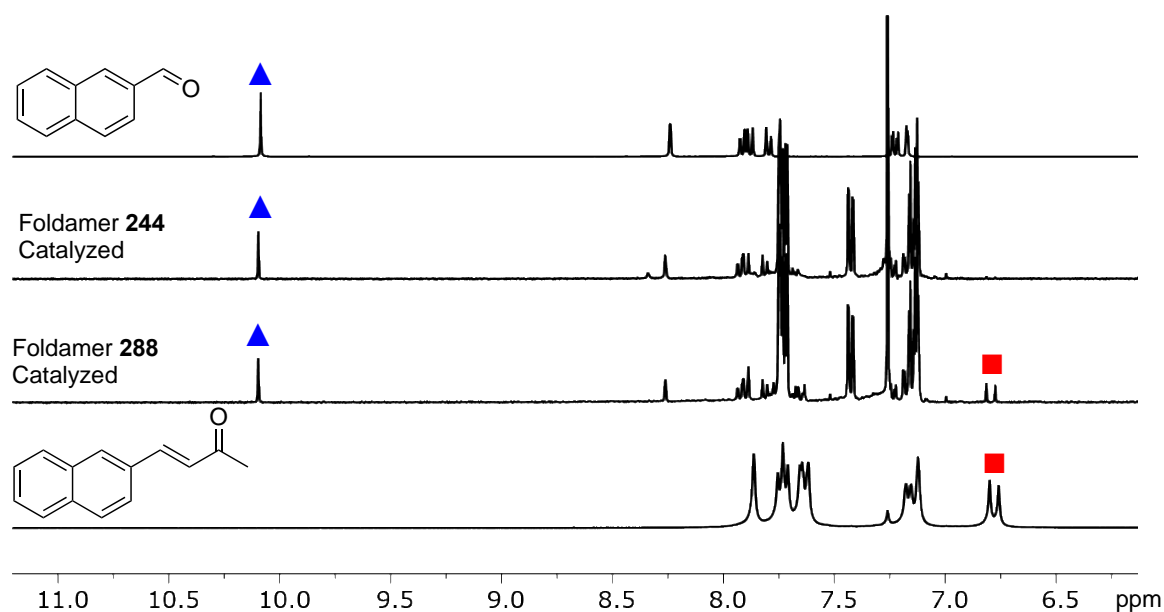


Figure 4.3 ^1H NMR (400 Mz, CDCl_3), 20 °C, stacked ^1H NMR of aldehyde reference, 15 mM substrate mixed with 0.75 mM foldamer **244** (after 72 h), 15 mM substrate mixed with 0.75 mM foldamer **288** (after 72 h), alkene reference from top to bottom. The aldehyde proton was marked by \blacktriangle , and the alkene-double bond proton was marked by \blacksquare .

The aldehyde and alkene formation rates under the catalysis of foldamer **288** and foldamer **244** were compared (Figure 4.4). With the same substrate concentration and same catalyst loading, foldamer **244** produced more aldehyde than foldamer **288**, which is reasonable as the two amines appended on the backbone of foldamer **288** are not proximal enough to adopt a high degree of bifunctionality as foldamer **244** does, the bifunctionality of retro-aldol cleavage that exists in foldamer **244** might decrease in foldamer **288**. For the foldamer **288** assay, the retro-aldol cleavage reaction is happening at a similar speed as the elimination reaction. It is unclear whether the retro-aldol cleavage and aldol elimination were catalyzed by each amine individually, we decided to synthesize two foldamers with either one amino group attached on the side chain. The first or second Dap residue on foldamer **288** was replaced with L-Ala to form the mono-amine foldamer **300** or mono-amine Foldamer **310**. The synthesis of mono-amine catalysts foldamer **300** and foldamer **310** followed the general protocol using the building blocks previously synthesized (Scheme 4-4).

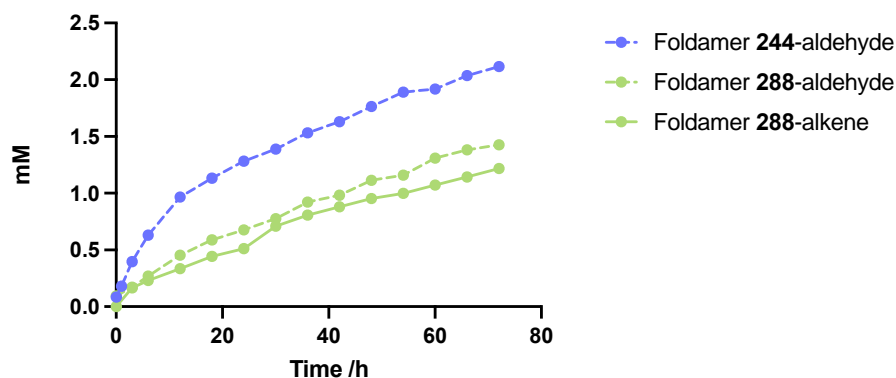
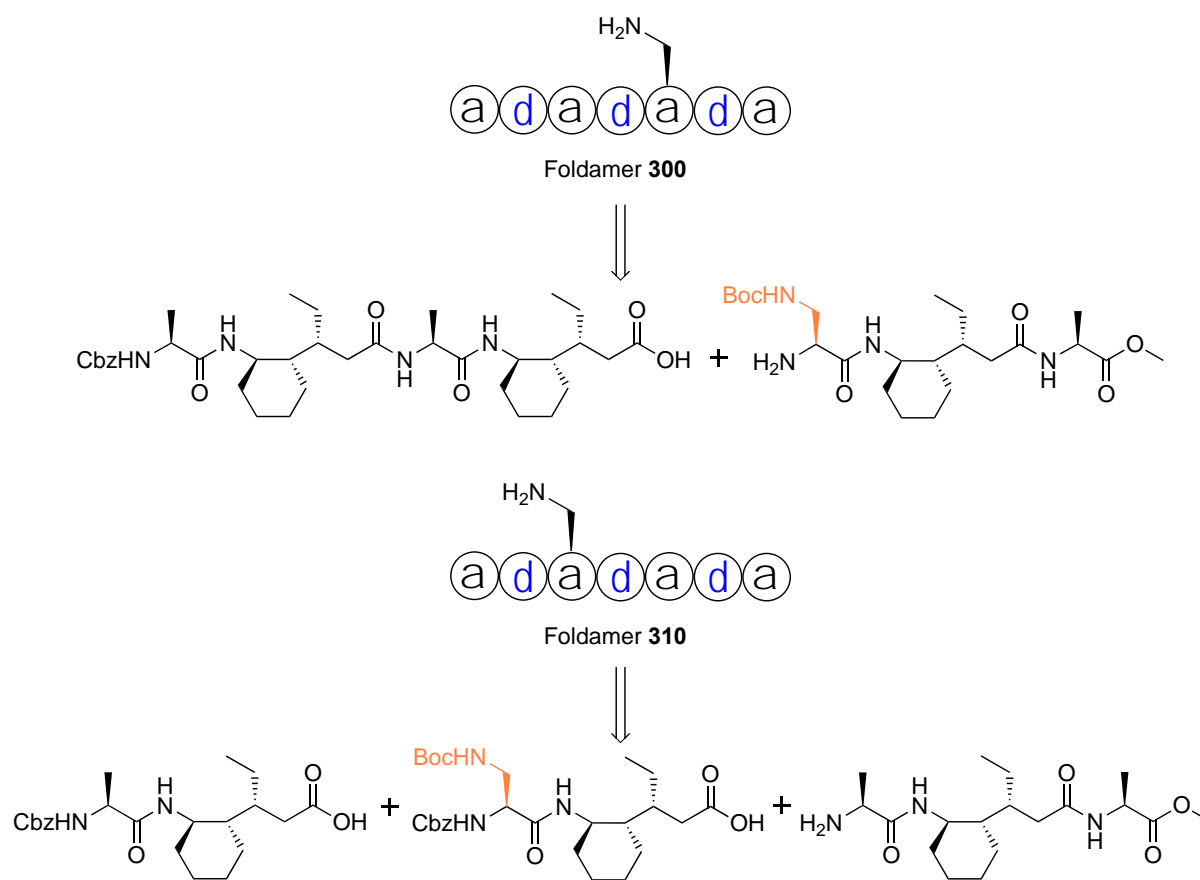
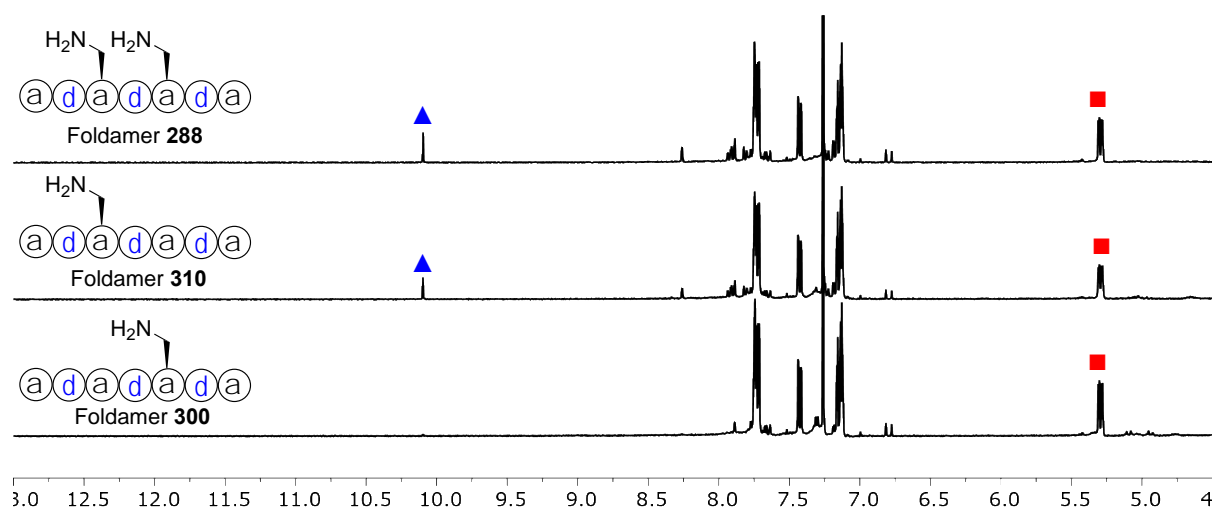


Figure 4.4 Time-based aldehyde and alkene formation under foldamer **244** and foldamer **288** (at 0.75 mM) on [methodol] (15 mM) at 20 °C in CDCl_3 , monitored by ^1H NMR.

The successfully synthesized foldamer **300** and **310** were applied to the catalytic study. The reactions were monitored by ^1H NMR spectroscopy using the same methods mentioned above (15 mM methodol, 1.5 mM free amine), as the mono-amine catalyst has one free amine on each backbone, 1.5 mM of mono-amine foldamer was added to equal the amount of free amine introduced into the reaction. When the Dap residue is at the α^3 position (foldamer **310**), the product formed from the methodol substrate is the same as bis-Dap foldamer **288**, both aldehyde and alkene products were observed. Whereas, when the Dap-residue is at the α^5 positions (foldamer **300**), only elimination product was observed (Figure 4.5)

**Scheme 4-4** Construction of foldamer 300 and foldamer 310**Figure 4.5** ¹H NMR (400 Mz, CDCl₃), room temperature, stacked ¹H NMR of 15 mM substrate mixed with 0.75 mM foldamer 288 (after 72 h), 15 mM substrate mixed with 1.5 mM foldamer 310 (after 72 h), 15 mM substrate

mixed with 1.5 mM foldamer **300** (after 72 h) from top to bottom. The aldehyde proton was marked by \blacktriangle . The alkene-double bond proton was marked by \blacksquare .

The kinetics of the two mono-amine catalysts were plotted and compared with bis-Dap foldamer **288** (Figure 4.6), as they were for the retro aldol cleavage. This showed that the bis-Dap foldamer **288** has the same scale of rate acceleration as mono-amine foldamer **310** where the $V_{\text{foldamer 288-aldehyde}} = 1.91 \pm 0.02 \times 10^{-2}$ mM/h and $V_{\text{foldamer 310-aldehyde}} = 1.49 \pm 0.06 \times 10^{-2}$ mM/h when the aldehyde concentration was plotted linearly vs time, the mono-amine foldamer **310** barely catalyze the retro aldol cleavage where the rate is $V_{\text{foldamer 300-aldehyde}} = 0.07 \pm 0.01 \times 10^{-2}$ mM/h. As for the elimination process, all three catalysts followed a similar pattern, the product formation is linearly dependent on the time, the $V_{\text{foldamer 288-alkene}} = 1.63 \pm 0.04 \times 10^{-2}$ mM/h and $V_{\text{foldamer 310-alkene}} = 1.40 \pm 0.04 \times 10^{-2}$ mM/h which is at the same scale of retro-aldol cleavage, and the $V_{\text{foldamer 300-alkene}} = 1.74 \pm 0.04 \times 10^{-2}$ mM/h. There are several factors extrapolated from this data as follows: (i) Calculated by the product formation, the α^3 position is more efficient than α^5 -position where 2.89 mM products were produced per hour, whereas α^5 -position displayed more selectivity where only alkene was formed at 1.74 mM per hours. (ii) There is still minimal bifunctionality exists in bis-Dap foldamer **288** for the retro-aldol cleavage and not for the aldol condensation. Counted by the aldehyde formation, foldamer **288** produced more aldehyde (1.27 per hour per amine) than the combination of foldamer **300** and foldamer **310** (0.52 per hour per amine). Counted by the alkene formation, the combination of foldamer **300** and **310** (1.05 per hour per amine) is nearly the same scale as foldamer **288** (1.09 per hour per amine). (iii) The different reactions under the catalysis of these three foldamer catalysts indicate a unique interaction of the foldamer with the substrate at each position, which is a promising phenomenon for realizing enantioselectivity.

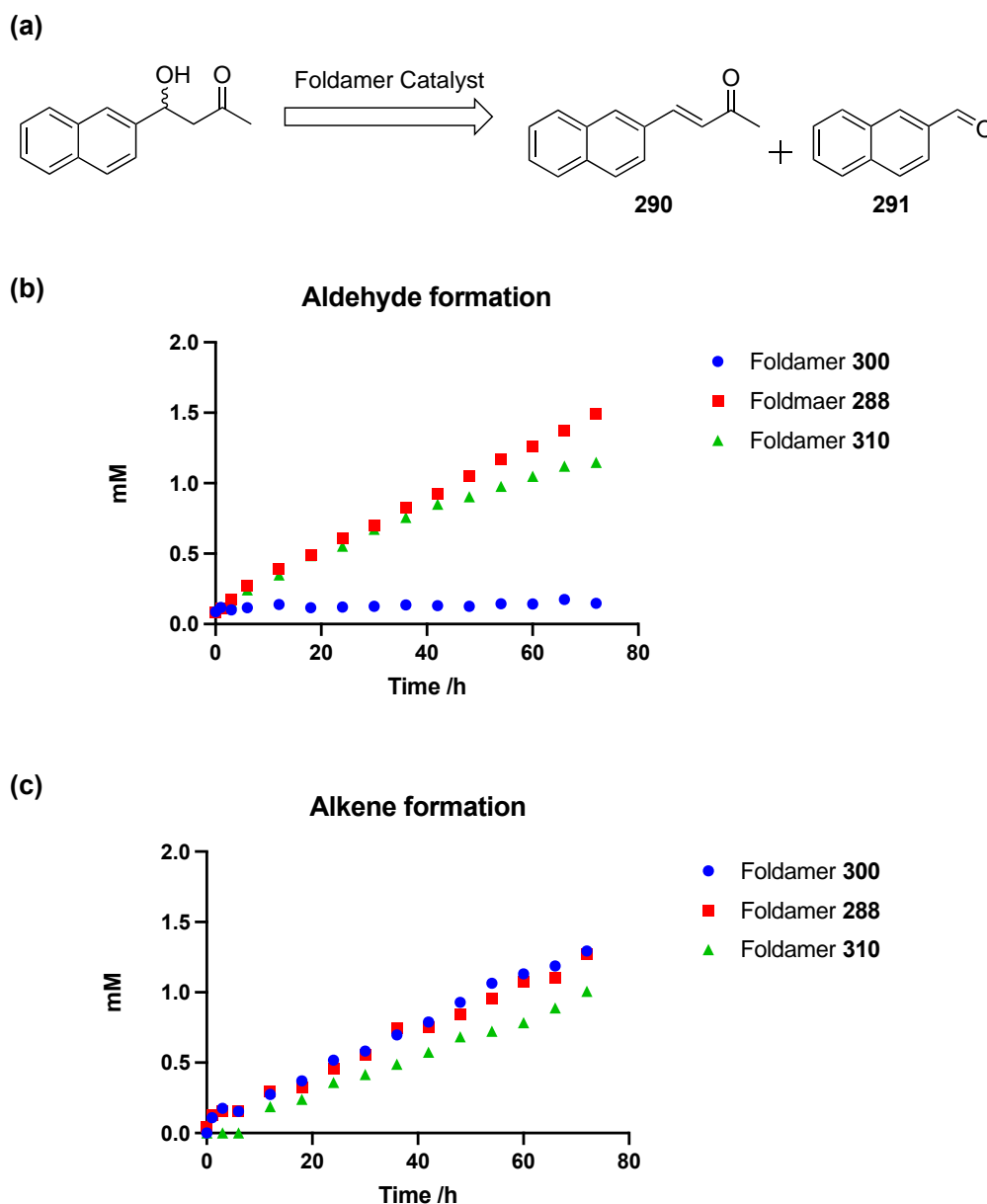


Figure 4.6 Time-based alkene-product formation under foldamer **300** (1.5 mM), foldamer **288** (0.75 mM), and foldamer **310** (1.5 mM) on [methodol] (15 mM) at 20 °C in CDCl₃, monitored by ¹H NMR. (a) Scheme of the reaction. (b) In terms of aldehyde formation. (c) In terms of alkene formation.

The enantioselectivity of the three foldamer catalysts was then analysed (Figure 4.7). The substrate is a racemic mixture of aldol compounds with 50% *R*-enantiomer and 50% *S*-enantiomer. The (*S*)-methodol was synthesized via D-proline catalysis and checked by chiral HPLC, demonstrating that the (*R*)-methodol eluted first under the method described in the SI. As we expected, the Dap-foldamer adopted the enantioselective discrimination over two

enantiomers. Surprisingly, the opposite ee was observed between foldamer **300** and **310**. Foldamer **300** preferred the (*R*)-methodol, whereas foldamer **310** preferred the (*S*)-methodol. And the bis-Dap foldamer **288** preferred the (*S*)-methodol. The result was inspiring as it suggests that the enantioselectivity does not come from the local environment (the stereochemistry is the same), but from the helical structure. Unlike in most of the cases where the opposite enantioselectivity should be realized by synthesizing a mirror-imaged catalyst, we could use the same scaffold to control the direction of ee by altering the position of the active site on the peptide backbone.

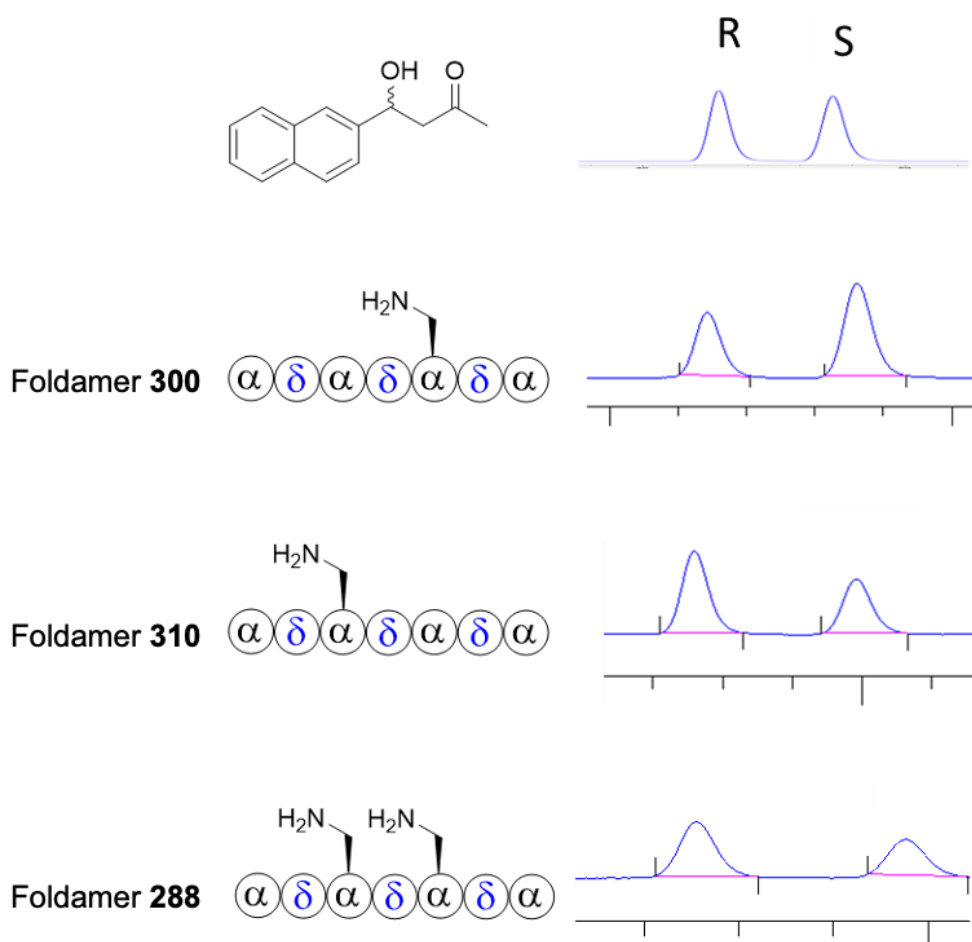


Figure 4.7 The chiral HPLC results in the kinetic resolution of different catalysts.

As the ee should theoretically increase with time (as more substrates is consumed), the enantioselective ability of the catalyst was monitored over 60 days, as shown in Figure 4.8. The time-dependent product formation of the three foldamer catalysts was checked by ¹H

NMR, the retro-aldol cleavage reaction would stop at a specific concentration which might be because the equilibrium of the reversible aldol-addition and retro-aldol cleavage when all the substrate and product are present in the same NMR tube. As no time spot is taken between 3 days and 14 days, the equilibrium for retro-aldol reaction should be reached around ten days, extrapolating from the saturated concentration and rate of the reaction. It is not clear why the elimination reaction catalyzed by foldamer **288** stopped along with the retro-aldol cleavage, whereas, in the assays of foldamer **300** and foldamer **310**, The elimination reaction keeps progressing. The time-based ee of different catalysts was monitored from the same aliquot taken from the yield monitoring. For foldamer **300** and foldamer **310**, the time was taken up to 61 days; foldamer **300** showed -39.2% ee (Figure 4.10), and foldamer **310** showed 15.5% ee (Figure 4.11). For foldamer **310**, the time was monitored up to 14 days, and the ee was 28.7% at a yield of 45.9%. The opposite ee of foldamer **300** and foldamer **310** indicates that the α^5 position and α^3 position on the foldamer provided an opposite chiral environment, whereas, in the bis-Dap foldamer **288** (Figure 4.9), the opposite ee was not cancelled out, which indicates that the bis-Dap foldamer **288** might have a different mechanism for the catalytic reaction, which agree with the possible certain-degree of bifunctionality on the Bis-Dap foldamer **288**. The property of the reversible enantioselectivity of the foldamer catalyst is promising. However, the efficiency of the catalysis is low, and the reaction takes a month to reach a 75% yield using foldamer **300** as the catalyst. The efficiency of the catalytic reaction needs to be improved, and the simplest way is to use a cocatalyst without altering the structure of the foldamer catalyst.

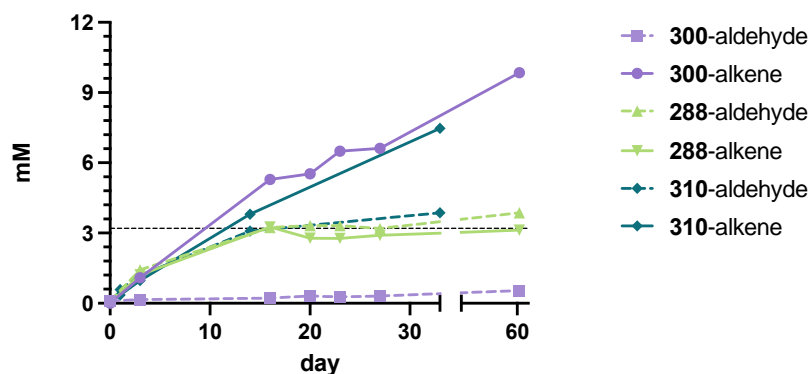


Figure 4.8 Time-based aldehyde/alkene formation under foldamer **300** (1.5 mM), foldamer **288** (0.75 mM), and foldamer **310** (1.5 mM) on [methodol] (15 mM) at 20 °C in CDCl₃, monitored by ¹H NMR.

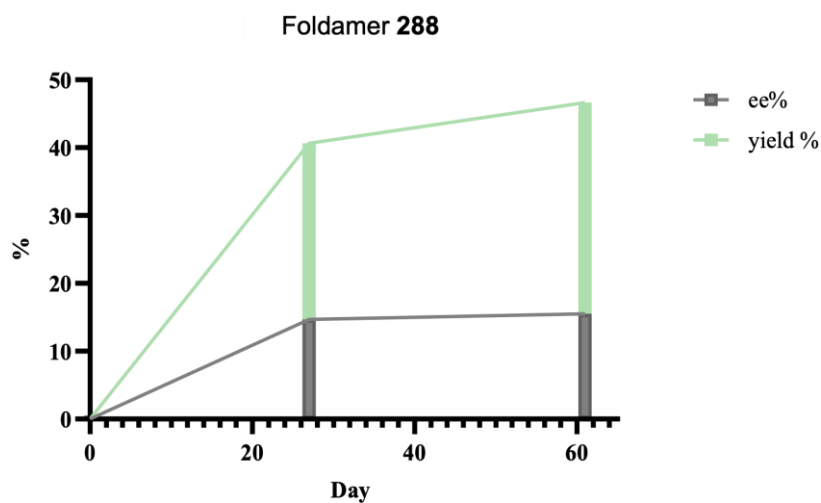


Figure 4.9 Time-based product formation under foldamer **288** (0.75 mM) on [methodol] (15 mM) at 20 °C in CDCl_3 , yield is monitored by ^1H NMR, ee is monitored by chiral HPLC

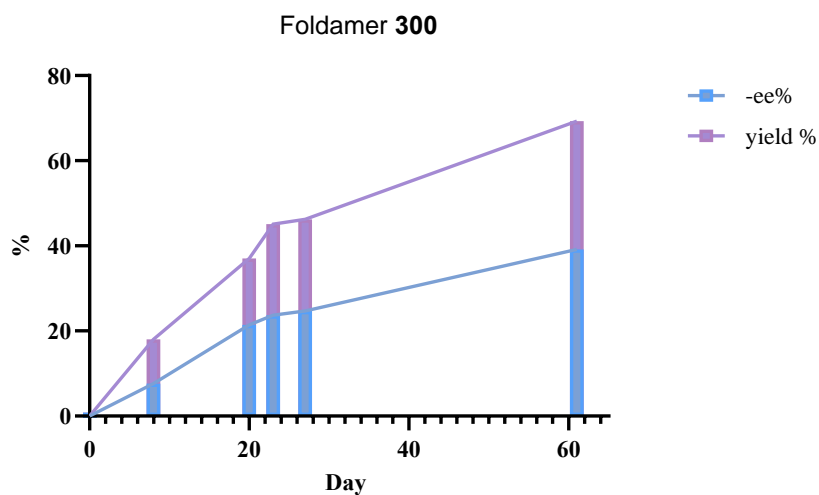


Figure 4.10 Time-based product formation under foldamer **300** (1.5 mM) on [methodol] (15 mM) at 20 °C in CDCl_3 , yield is monitored by ^1H NMR, ee is monitored by chiral HPLC

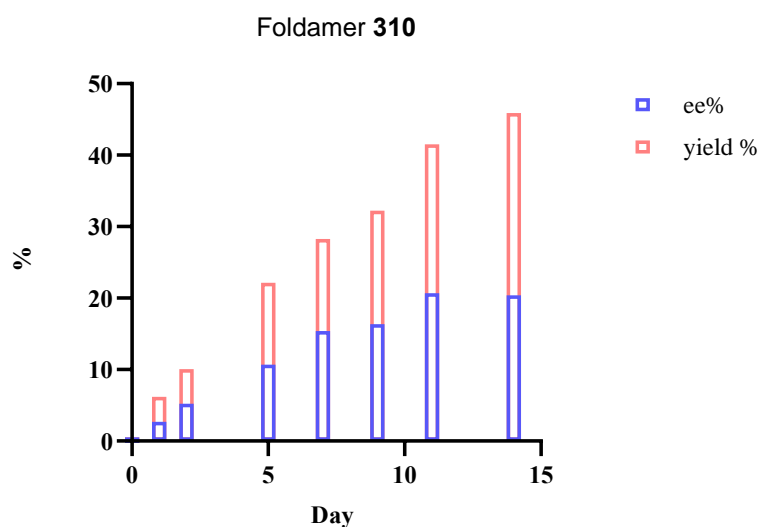


Figure 4.11 Time-based product formation under foldamer **310** (1.5 mM) on [methodol] (15 mM) at 20 °C in CDCl₃, yield is monitored by ¹H NMR, ee is monitored by chiral HPLC.

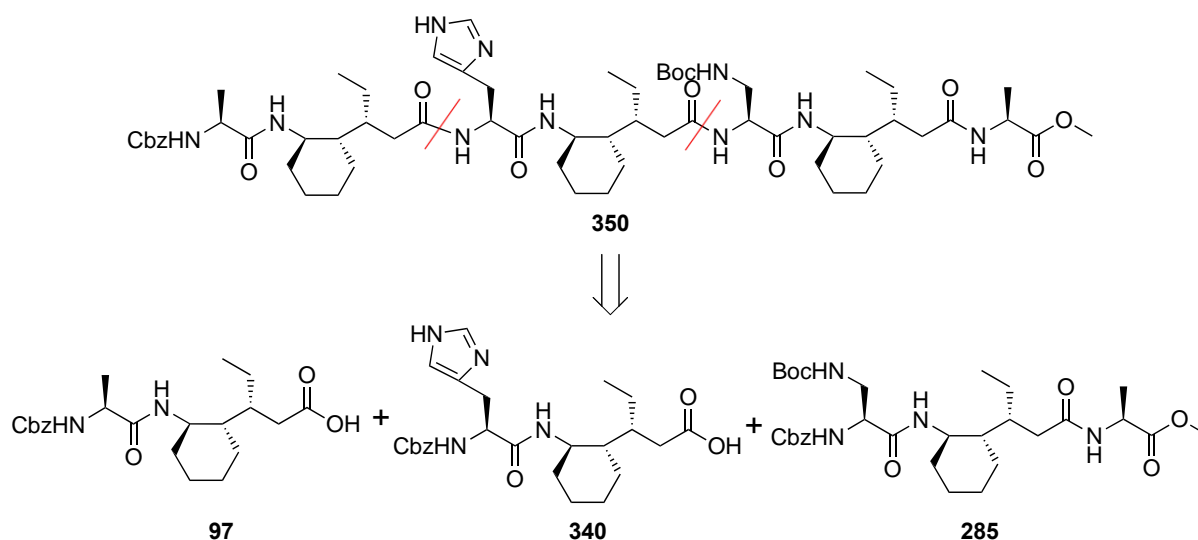
We then screened several acid/base cocatalysts using foldamer **300** as a standard catalyst. As shown in Table 4-2, the ee and yield were monitored after two days of catalysis. The benzoic acid, imidazole, and piperidine increased the reaction rate, but the benzoic acid and piperidine did not maintain enantioselectivity. The imidazole is a suitable candidate, as the imidazole could catalyze the reaction (and hopefully conserve some enantioselectivity). This can be easily achieved if histidine substitutes one of the Dap monomers on the foldamer structure to increase the reaction rate while maintaining the enantioselectivity.

Table 4-2 Yield and ee of foldamer **300** (1.5 mM), cocatalyst (1.5 mM) on [methodol] (15 mM) at 20 °C in CHCl₃ after two days. Yield is monitored by HPLC, and ee is monitored by chiral HPLC.

Cocatalyst	Alkene -2day	Aldehyde -2day	ee (%)
Benzoic acid	18.9%	5.3%	–
Nitrobenzoic acid	9.1%	6.25%	–
Nitrophenol	1.4%	3.1%	-3.2
TEA	0%	3.8%	–
Imidazole	29.1%	4.3%	-4.5
Piperidine	16.8%	4.0%	–

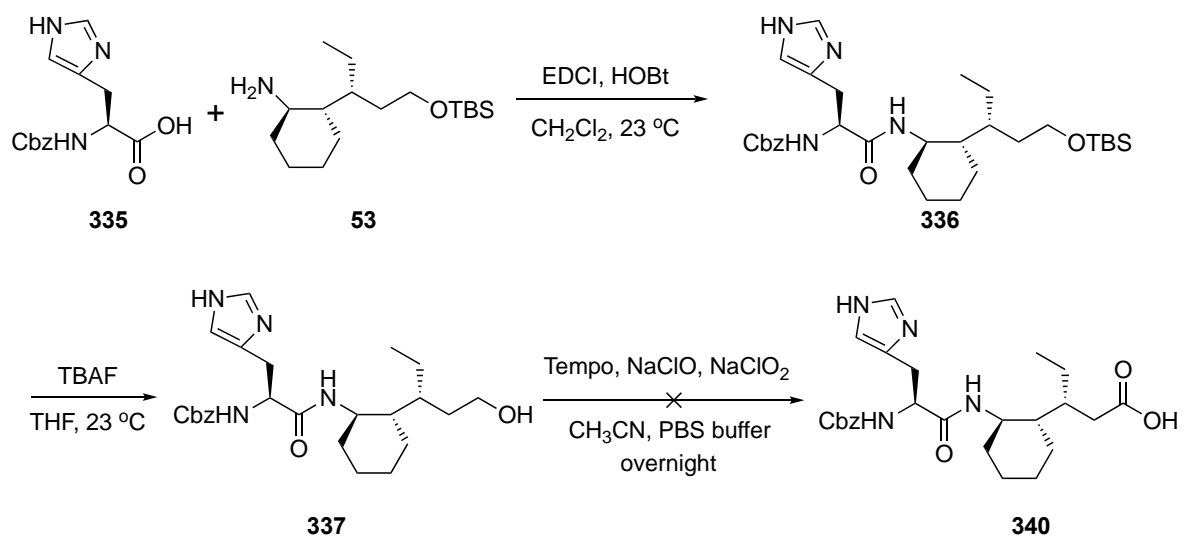
4.2.2 Synthesis of Histidine-Containing Foldamer

The synthesis of histidine-containing peptide **350** is slightly different from the synthetic procedure mentioned above because of the different polarity and solubility of histidine. The synthesis of foldamer **350** could make use of the two building blocks (**97** and **285**) (Scheme 4-5), whose syntheses were described in Chapter 3. Due to the activity of the imidazole residue, some issues and problems were encountered during the synthesis of building block **340**.

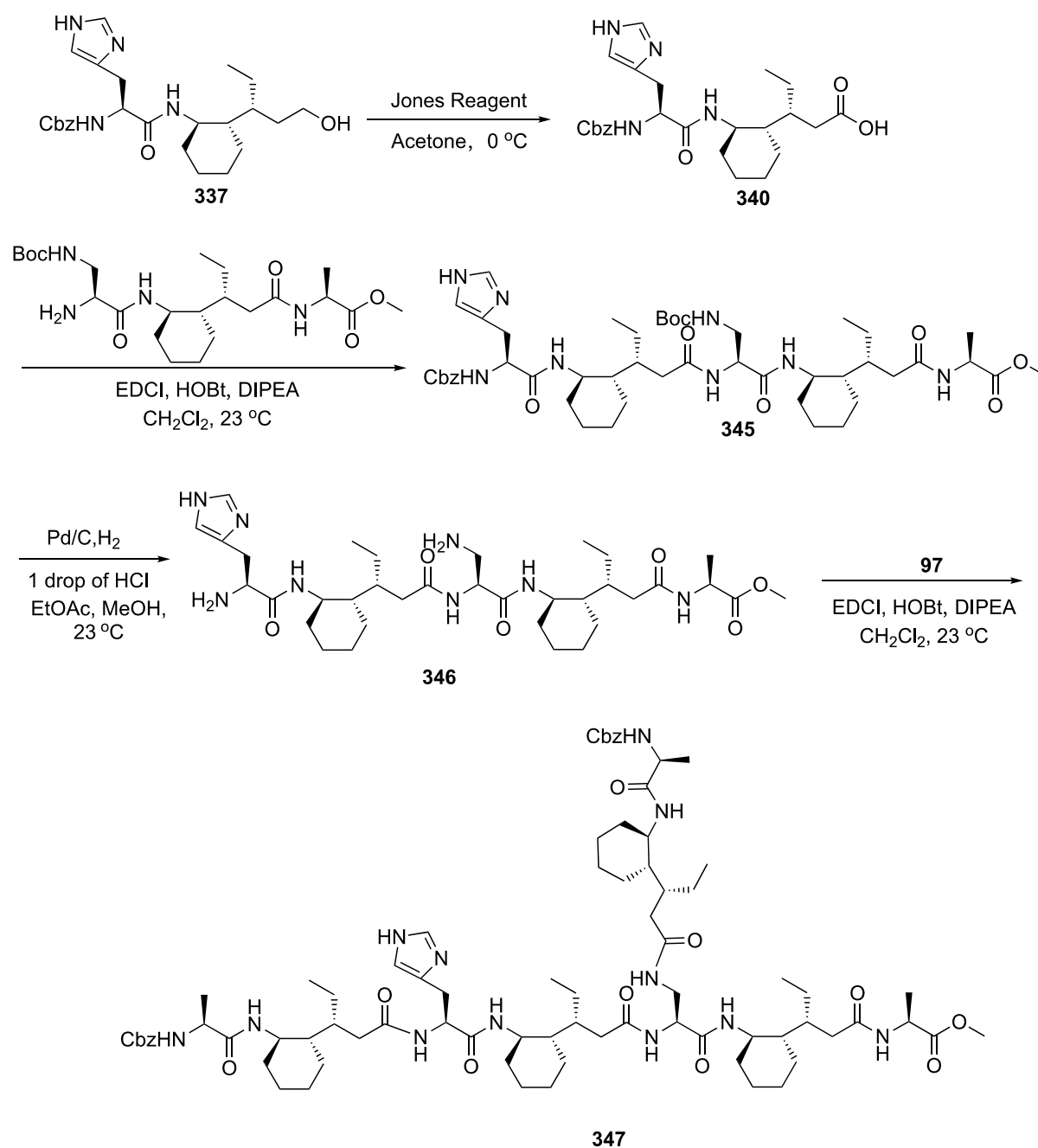


Scheme 4-5 Retrosynthesis of foldamer **350**

Following the general peptide coupling reaction, histidine-containing dipeptide **336** was successfully synthesized with a reasonable yield, and compound **336** was carried out to the next step without further purification. After the TBS deprotection procedure, the crude was purified via reverse-phase chromatography due to the high polarity and water-soluble property of compound **337**. Compound **337** was successfully synthesized, which was confirmed by HPLC and LC-MS. However, the oxidation of **337** to **340** did not work. Using the general oxidation procedure, the reaction did not happen after 2 h—a general oxidation time using this method. More equivalent of bleach were added to promote oxidation, and the reaction was left overnight for the reaction to be completed. Under these conditions, the dipeptide **337** was over-oxidized and produced a mixture of different over-oxidized compounds (Scheme 4-6). To avoid overoxidation and improve oxidation efficiency, Jones oxidation was applied, and compound **340** was successfully synthesized. However, the general procedure of hydrogenation of **345** was unsuccessful. The initial hypothesis is that the coordination of the histidine with the palladium catalyst might prevent the hydrogenation from happening, so a fresh new portion of palladium on carbon was added to the reaction mixture with one drop of 1M HCl to break the possible coordination. The reaction occurred; however, the acidic conditions also removed the Boc-protection on the side chain amine, and the further coupling with **97** generated the compound **347** (Scheme 4-7).

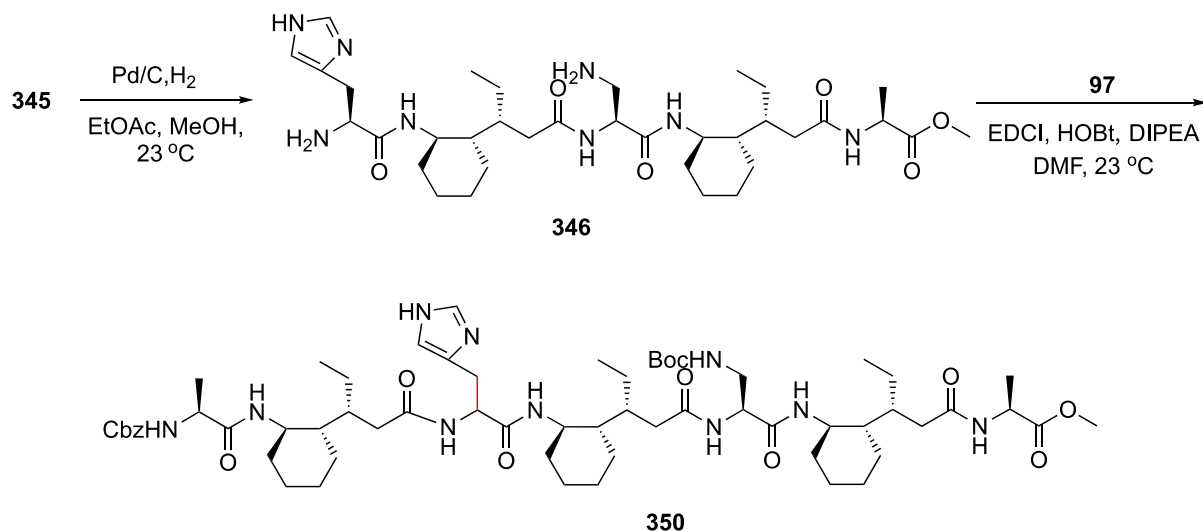


Scheme 4-6 Unsuccessful procedure of synthesizing building block 340

**Scheme 4-7** Unexpected product formation of **347**

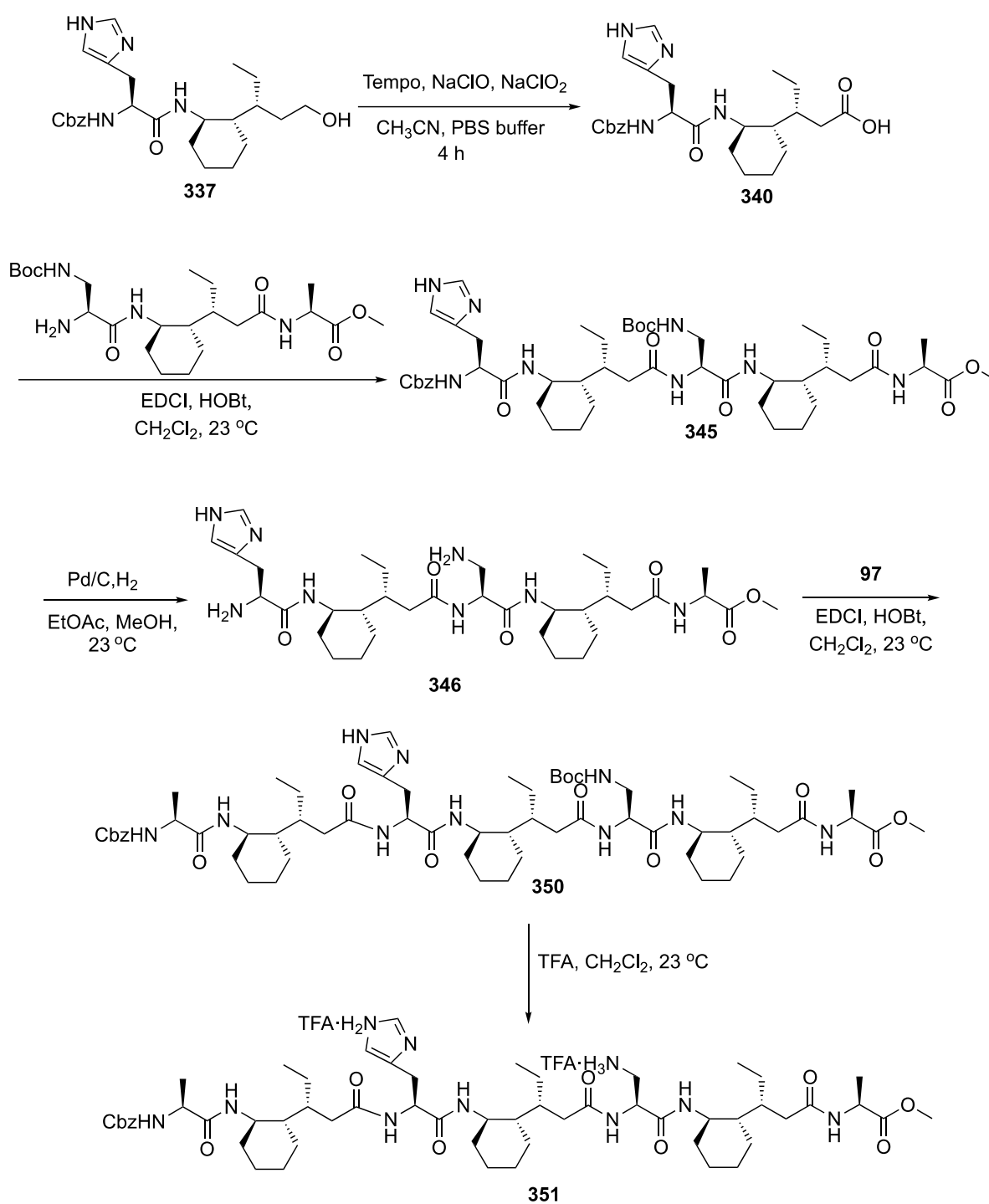
A further repeat of the procedure discovered that the unsuccessful hydrogenation was not because of the coordination of the histidine with the palladium. The residual amount of chromium ion from the Jones oxidation poisoned the palladium. When the chromium ion was entirely removed from the crude, the product **346** was synthesized via a general hydrogenation procedure. However, the epimerization happened during the synthesis, and the product was the

mixture of two diastereomers of compound **350**, which was detected by HPLC and HRMS (Scheme 4-8). The epimerization is most likely to occur on the histidine residue. To avoid epimerization, which is usually caused by harsh conditions, a new procedure needs to be introduced to synthesize the histidine-containing heptamer (Scheme 4-9).

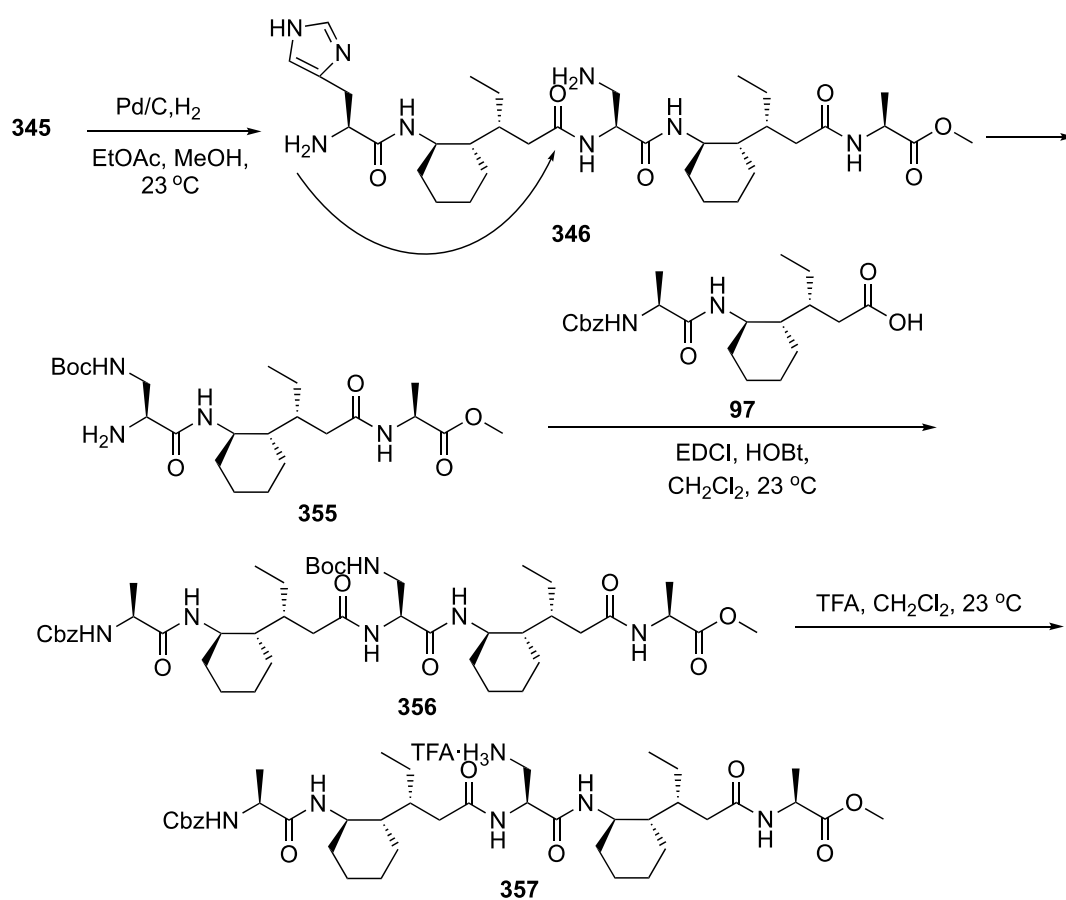


Scheme 4-8 The procedure of synthesizing epimerized histidine-containing heptamer.

The Jones reaction is a strong acidic condition that might cause the epimerization, and the addition of DIPEA in the coupling reaction might also induce epimerization. The TEMPO-catalyzed bleach oxidation of **337** to **340** was investigated again, which are milder conditions to avoid epimerization. The new procedure was developed to add two more equivalents of bleach into the reaction and monitor the reaction every half an hour via LC-MS. The target product **340** was successfully synthesized after 4h, and once the reaction was completed, it was quenched with NaS_2O_3 and freeze-dried to remove the solvent. Acetone was added to dissolve the product **340** and then the mixture was filtered to remove the insoluble salt, the crude was purified via a reverse-phase column to collect the pure compound. Following the general procedure of peptide coupling without DIPEA, the product was successfully synthesized without epimerization (Scheme 4-9). However, due to the high activity of histidine residue, we observed self-cleavage of the peptide, which appeared to generate foldamer **351** and **357** according to MS (Scheme 4-10).



Scheme 4-9 The procedure of synthesizing histidine-containing foldamer **351**.

**Scheme 4-10** The proposed procedure of peptide self-cleavage.

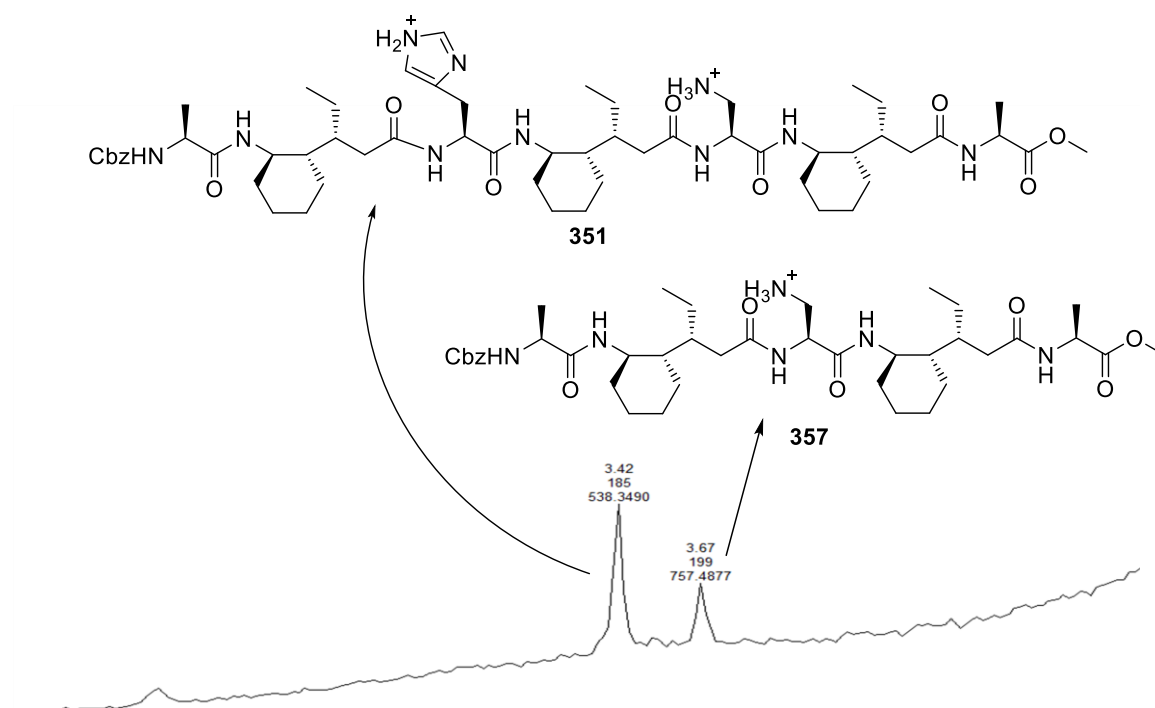


Figure 4.12 The HPLC and HRMS of the mixture of foldamer **351** and **357**.

Given the limited amount of crude being synthesized, the mixture of foldamer **351** and **357** was used as a crude catalyst to test the efficiency of the catalysis to check if the histidine-containing foldamer **351** could significantly improve the catalytic efficiency of the retro-aldol cleavage/elimination reaction. Under the same condition of the catalytic reaction described in chloroform, the crude of foldamer **351** and **357** did not show an improvement in the catalysis of the reaction. Moreover, this catalyst was less efficient than foldamer **300** and **310**. The possibility might be that the crude catalyst of foldamer **351** and **357** are both presented as a TFA-salt version, limiting the catalytic efficiency.

4.2.3 Optimizing the Catalytic Condition of Foldamer **300**

The other ways of improving the rate of reaction are to improve the substrate concentration or change the condition of the reaction, such as the solvent system or the temperature. The foldamer **300** catalysis was chosen as a standard catalyst to investigate the impact of changing concentration on the catalytic efficiency of the reaction. The standard method of using 15 mM substrate concentration, and 1.5 mM foldamer was taken as a reference, as shown in Figure

4.13, at the concentration of substrate is 15 mM, the yield is 18%, and the ee is -7.6% after 8 days, when the concentration was increased to 150 mM, the yield is 34%, and the ee is -11% which after 2 days, this indicates that the improve the concentration of the substrate could improve the yield and ee accordingly. The kinetic resolution of foldamer **300** under 200 mM substrate was monitored and analyzed (Figure 4.14). The reaction rate of 200 mM substrate is improved 7-fold compared to the rate of 15 mM substrate.

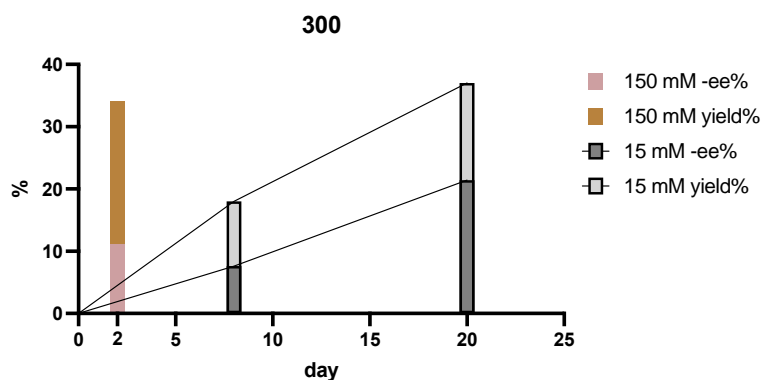


Figure 4.13 Time-based product formation at 20 °C in CDCl_3 , yield is monitored by ^1H NMR, ee is monitored by chiral HPLC. The comparison between foldamer **300** (1.5 mM) on [methodol] (15 mM) and foldamer **300** (15 mM) on [methodol] (150 mM)

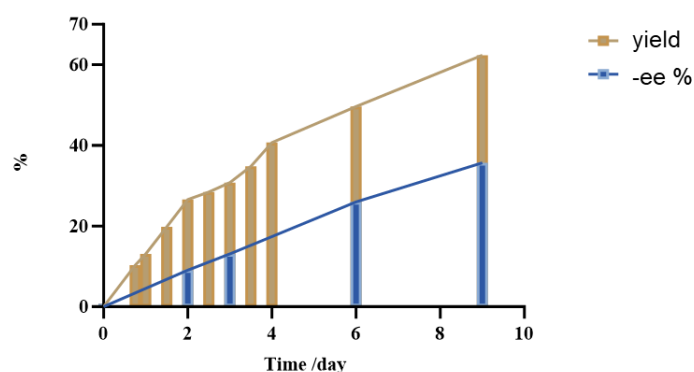


Figure 4.14 Time-based product formation under foldamer **300** (20 mM) on [methodol] (200 mM) at 20 °C in CDCl_3 , yield is monitored by ^1H NMR, ee is monitored by chiral HPLC.

The ee at different solvents after 2 days of reaction was also tested at a standard substrate concentration of 15 mM (Figure 4.15). Due to the injection issue on the HPLC, the yield was

not detected. In polar protic solvents like methanol and IPA, the ee is relatively lower than the polar aprotic solvent. This might be because of the H-bond interactions between solvent and foldamer catalyst that interfered the folding propensity of the foldamer catalyst. Hence the non-polar solvent like toluene and diethyl ether shows a -10% ee after 2 days, the high ee in the diethyl ether might cause by the increased substrate concentration by the solvent evaporation, and the toluene is the best solvent among the tested solvents for foldamer **300** to catalyze the aldol retro-aldol cleavage/condensation.

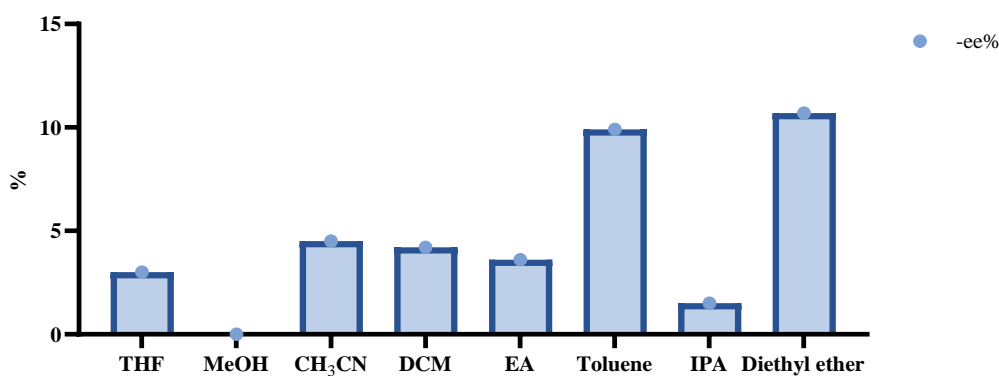


Figure 4.15 ee of foldamer **300** (2 mM) on [methodol] (20 mM) at 20 °C in different solvents, monitored by chiral HPLC.

The catalysis of foldamer **288** and foldamer **300** in aqueous solution were also monitored. In PBS buffer, foldamer **288** only generates the retro-aldol cleavage product, and the aldehyde yield is higher than foldamer **244** (Figure 4.16). foldamer **300**, which only produces aldol condensation in chloroform, produced both retro-aldol products and eliminated product in PBS.

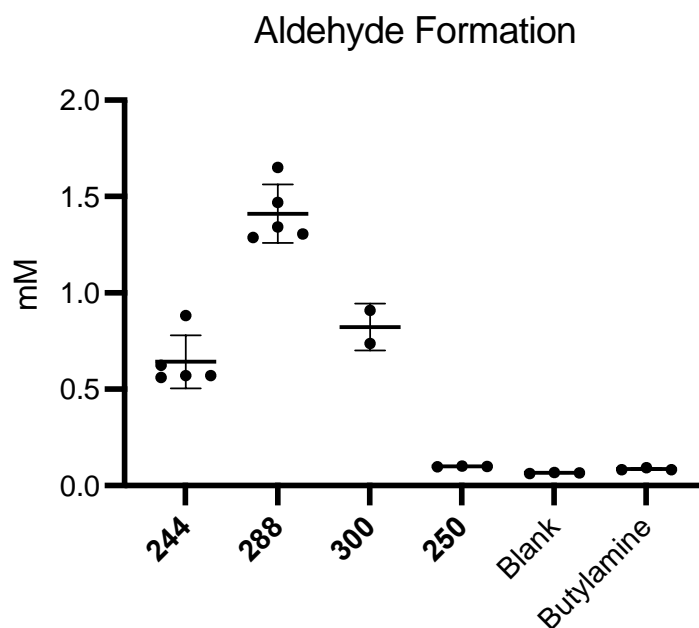


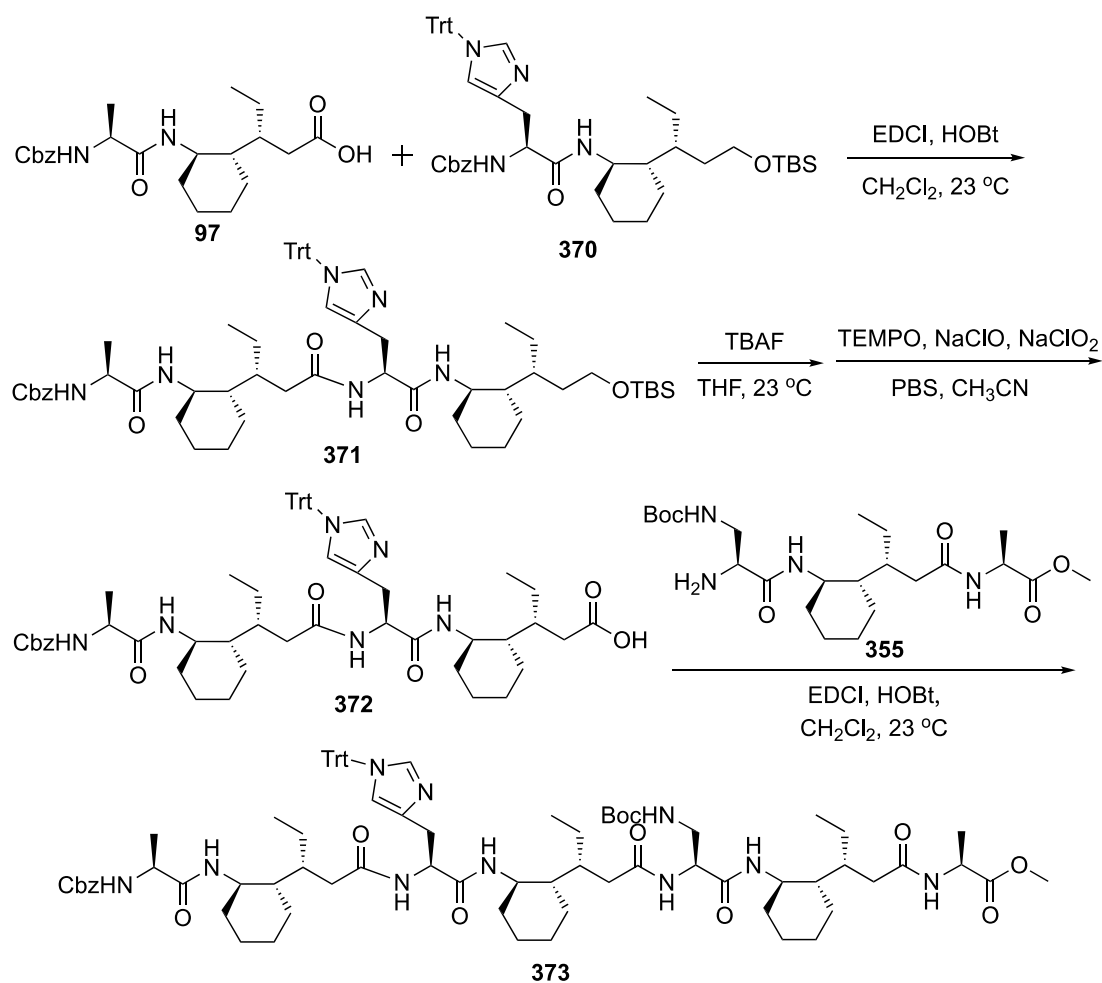
Figure 4.16 Aldehyde formation of: 15 mM substrate and 1 mM foldamers **244**/1 mM foldamers **288**/2mM foldamer **300**/2mM unstructured amine were stirred in 100 μ L of 5% CH_3CN -PBS buffer at room reacted for 24 h. The reaction was diluted with 200 μ L of H_2O and 200 μ L of CH_3CN , and the aldehyde product was monitored by HPLC.

4.3 Conclusion

In this chapter, based on the structural information concluded from Chapter 2 and the model reaction confirmed in Chapter 3, we designed a Dap-containing foldamer and realized the enantioselectivity of the foldamer catalyst. Moreover, the reversible ee could be modulated by changing the position of the active site on the foldamer. It is worth comparing the CD of the Dap-containing foldamers to see if the chirality of the foldamer changes upon altering the position of the catalytic site, thereby leading to the reversible ee. Although the mechanism of the reaction is not yet confirmed, the results observed so far are promising and inspiring.

Plenty of future work is proposed based on the results in this chapter. During the catalysis monitoring, some kinetic processes took up to several weeks. In the follow-up work, the HPLC and mass spectrometry of the foldamer catalysts need to be tested to check for potential foldamer degradation. For the catalytic condition, using a higher concentration in toluene might

give a satisfied yield and enantioselectivity. The kinetics of the histidine-containing peptide (as a free amine version instead of TFA salted ammonium) have yet to be confirmed because of the limited product being synthesized. To avoid the self-cleavage of the histidine-containing peptide, the coupling order could be altered without increasing the steps of the whole procedure (Scheme 4-11).



Scheme 4-11 Proposed procedure for synthesizing histidine-containing peptide

Chapter 5 Other Experiments

5.1 A Flavin Conjugated Foldamer for Decarboxylative Cyanation

5.1.1 Aims and Plans

In nature, riboflavin, also known as vitamin B12, is an essential compound for forming coenzyme FAD and FMN that help with the metabolism of carbohydrates, protein, and fats. Conjugating the flavin residue onto the foldamer structure might introduce a photoactive peptide catalyst that could be an alternative to the widely used metal-based photocatalysts, and the helicity of foldamer structure could make it an asymmetric photoactive catalyst.

As we have discussed in previous chapters, within our α,δ -systems, the α -residue is embedded into the helix circle, and more readily modified compared to the δ -residue. There are different ways of stitching a flavin residue onto the foldamer, one of which is by synthesizing a flavin-conjugated amino acid monomer and using this amino acid in the peptide synthesis (Figure 5.1a). The other way is to use the idea of post-synthetic modification, by preparing the foldamer with a reactive site on the side chain, and then stitching the flavin residue onto the foldamer backbone through it (Figure 5.1b). As the goal of conjugating flavin on the foldamer is to utilize the helix structure to realize the enantioselectivity of photocatalysis, a shorter distance between the flavin residue and peptide backbone is preferred. The method of post-synthetic modification makes it relatively easier to synthesize the foldamer catalyst, but the distance between the flavin and peptide backbone is likely to be critical for any potential control.

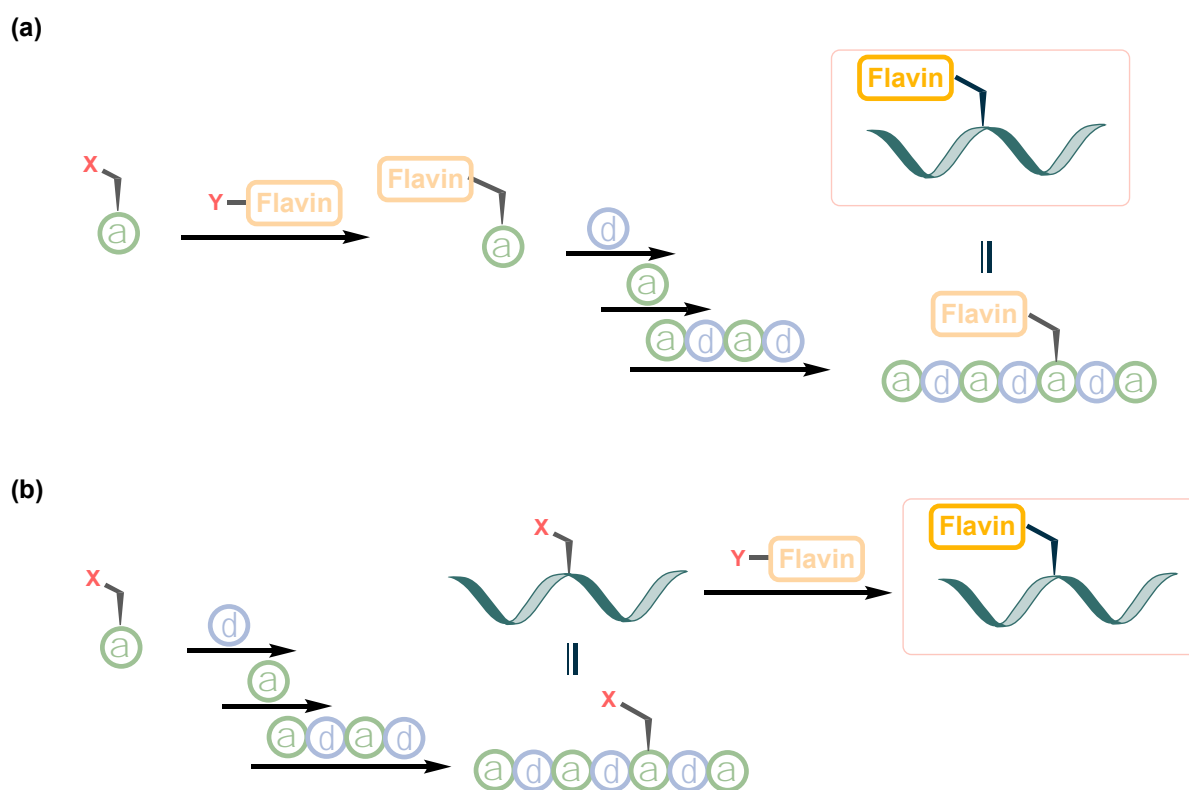
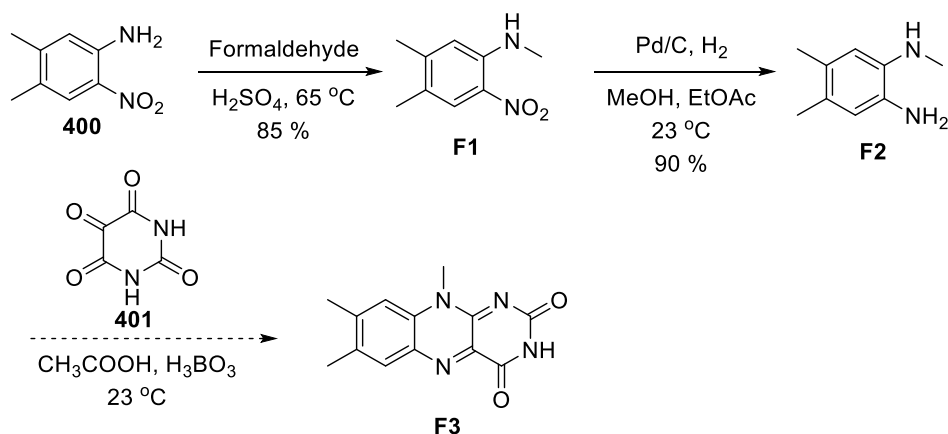


Figure 5.1 Two approaches to synthesize flavin conjugated foldamer. (a) Synthesize the flavin-conjugated α -amino acid, then build this amino acid into a foldamer. (b) Build a foldamer with a reactive site reserved on the side chain, then bond the flavin onto the foldamer.

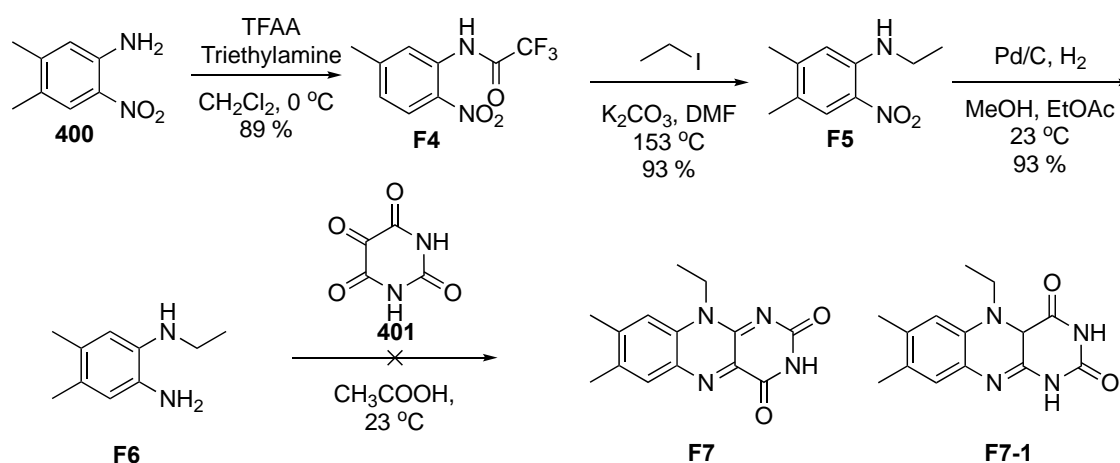
The first target molecule is the lumiflavin-conjugated α -amino acid, which contains only one methylene between flavin and the amino acid backbone. The synthesis of this lumiflavin-conjugated α -amino acid can be broken down into lumiflavin compound **F3** (Scheme 5-1) and the halogen-substituted alanine. Following reported methods, the synthesis of compound **F3** started from 4,5-dimethyl-2-nitroaniline **400**, the starting material was treated with formaldehyde and sulfuric acid to yield secondary amine **F1** in high yield without producing dimethylated compounds.⁹⁷ The nitro alanine compound **F1** was reduced with metal-catalyzed hydrogenation to get the diamine **F2** in 90% yield, no further purification needed after these two steps, the crude was carried to the next step of the reaction. The diamine **F2** was then reacted with alloxan **401** to get lumiflavin **F3**, however, the crude product is sparingly soluble in CHCl_3 and CH_2Cl_2 which are the general solvent used for the further peptide synthesis and characterization, and the characterization of the crude product was not performed due to the low solubility, it is uncertain whether the target product was obtained. To increase the solubility

of the flavin-derivatives, the compound **F7** was proposed which contains an ethyl-side chain on flavin residue and might increase its solubility in organic solvent.

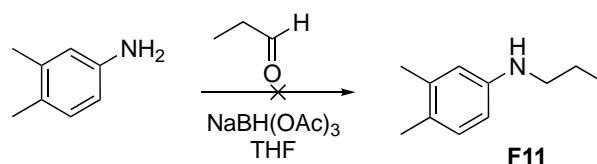


Scheme 5-1 Unsuccessful synthesis of lumiflavin **F3**

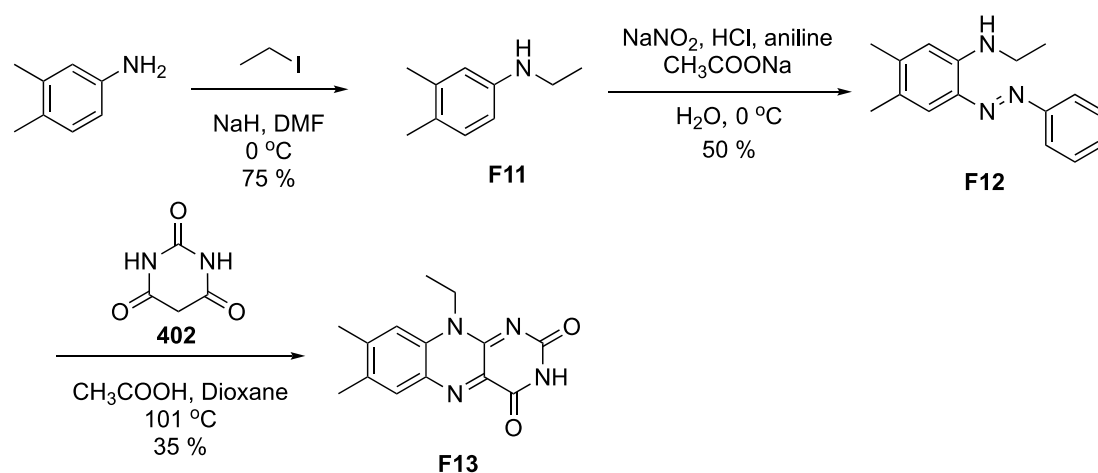
Monoethylation of 4,5-dimethyl-2-nitroaniline **400** was then attempted (Scheme 5-2). Substrate **400** was treated with trifluoroacetic anhydride to obtain trifluoroacetamide compound **F4**, and iodoethane was used to synthesize the secondary amine **F5**. This compound was subsequently reduced to diamine **F6** through hydrogenation, achieving a 74% yield over three steps. The reaction of **F6** with alloxan **401** was then attempted to obtain the flavin derivative **F7**.⁹⁸ According to the ^1H NMR, there is a 1:1 ratio of two compounds which was not easily separated through column chromatography, we suspect these might represent the two configurations of the flavin derivative **F7**, although we cannot confirm this with certainty. An alternative method for synthesizing flavin was explored to circumvent the formation of two isomers.

Scheme 5-2 Unsuccessful synthesis of lumiflavin **F7**

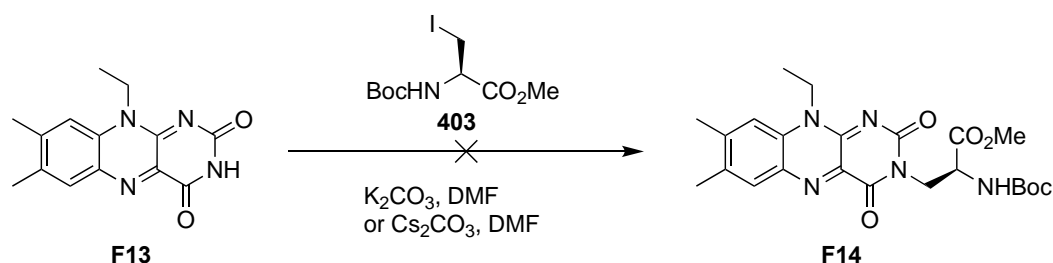
To simplify the ethylation reaction of 3,4-dimethylaniline which takes two steps as discussed above (if going through trifluoroacetamide intermediate), a reductive amination was conducted using sodium triacetoxyborohydride as the reduction reagent, however, the reaction was unsuccessful (Scheme 5-3). We then attempted a straightforward alkylation using ethyl iodide. To avoid di-substitution happening, the amount of iodoethane was controlled below 1 equivalent relative to the 3,4-dimethylaniline. Although the di-substitution reaction did happen, leading to the formation of *N,N*-diethyl-3,4-dimethylaniline with a yield of 20%, the product **F11** was collected with a satisfactory yield of 75%.⁹⁹ The *N*-ethyl-3,4-dimethylaniline (**F11**) was then reacted with aniline in the presence of sodium nitrite to get the **F12**, the **F12** was then reacted with barbituric acid **402** to get flavin-derivative **F13** (Scheme 5-4),¹⁰⁰ the **F13** was successfully synthesized without the formation of the other isomer, the next step was to conjugate the **F13** on the α -amino acid.



Scheme 5-3 unsuccessful reductive amination of 3,4-dimethylaniline

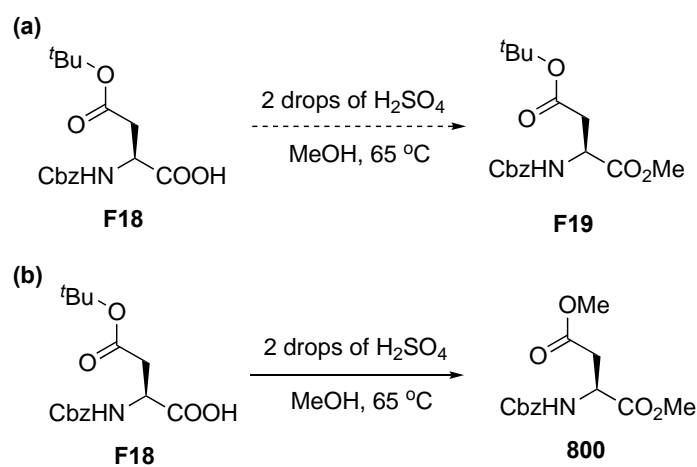
Scheme 5-4 Procedure of synthesizing **F13**

The diacetamide amine on flavin is relatively acidic and could be deprotonated under basic conditions. The approach for conjugating the flavin onto the α -amino acid involves reacting the flavin derivative, **F13**, with iodo-L-Ala **403** through a nucleophilic substitution reaction. Initially, the flavin compound **F13** was treated with either K_2CO_3 or Cs_2CO_3 in DMF for a short time, followed by the addition of iodo-alanine. Unfortunately, instead of forming **F14** (Scheme 5-5), the iodo-alanine underwent elimination to form dehydro-alanine. The structural composition of the halide-substituted alanine renders the α -CH of the α -amino acid notably acidic, with the halide positioned at the beta position, significantly increases the susceptibility of iodo-alanine to elimination when exposed to a base. To avoid this elimination reaction, the strategy employed was to increase the distance between the flavin and peptide backbone by extending it to two methylene units.

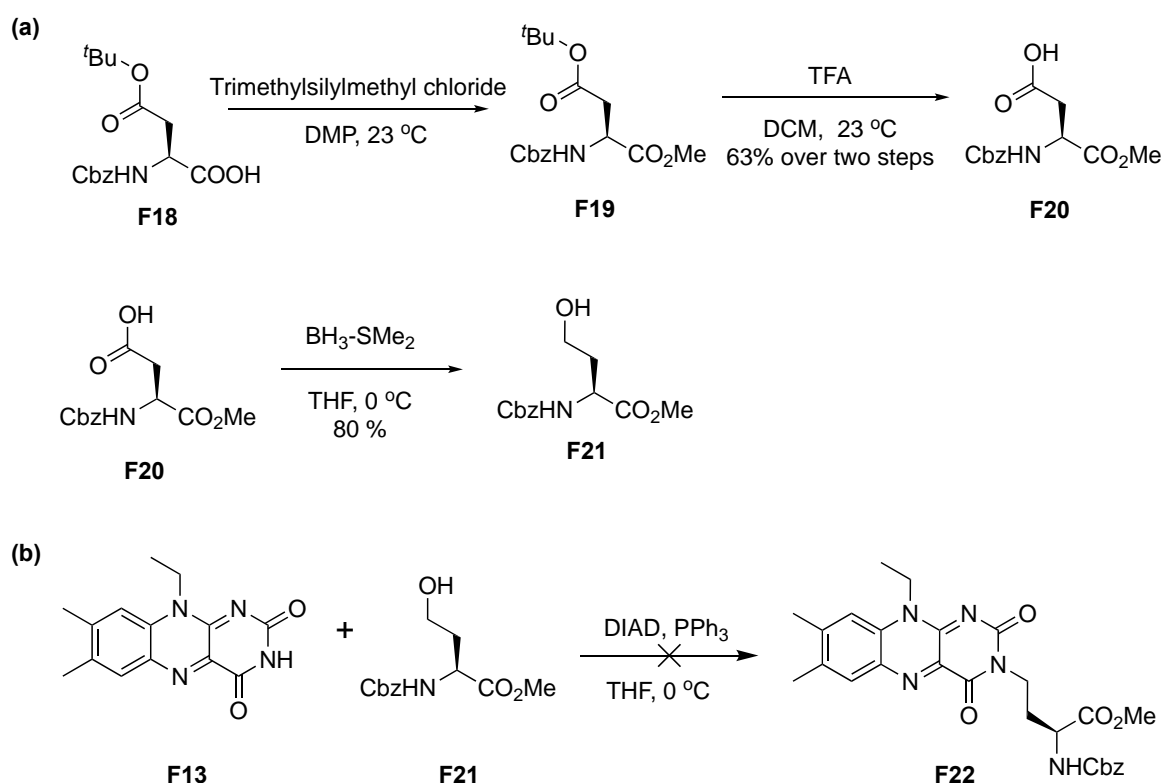
Scheme 5-5 Unsuccessful synthesis of **F14**

The new procedure required the synthesis of the flavin-conjugated α -amino acid **F22** through Mitsunobu reaction using the flavin residue-**F13**, which are already successfully synthesized.

The synthesis of α -residue **F21** started from commercially available aspartic acid. To selectively reduce the side-chain carboxylic acid, we first protect the C-terminus carboxylic acid with methyl ester (Scheme 5-6a). However, the refluxing of carboxylic acid **F18** in methanol with two drops of H_2SO_4 did not work as expected. In this condition, the Boc-ester on the side chain was removed first, then both carboxylic acids on the substrate were protected with methyl ester (Scheme 5-6b). Therefore, the other method of methylation using trimethylsilylmethyl chloride was applied and compound **F19** was collected with a good yield, then the side chain Boc-protection was removed by treating with TFA. To selectively reduce carboxylic acid to alcohol while keeping the methyl-ester unaffected, the borane dimethylsulfide (BMS) reduction was applied and **F21** was collected with high yield (Scheme 5-7a).¹⁰¹ We then reacted **F21** with flavin **F13** using the Mitsunobu reaction, unfortunately, the reaction did not occur (Scheme 5-7b),¹⁰² which might be caused by the low solubility of the flavin derivative **F13** in THF.

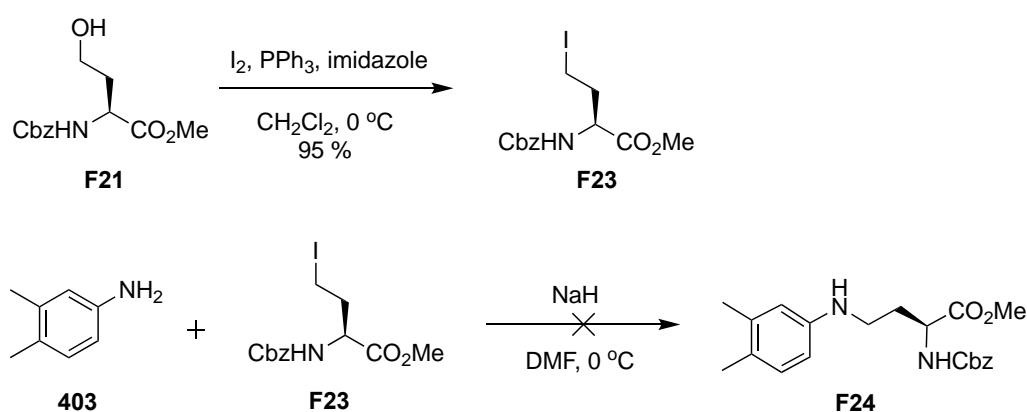


Scheme 5-6 (a) Expected *tert*-butyl esterification. (b) The actual product.

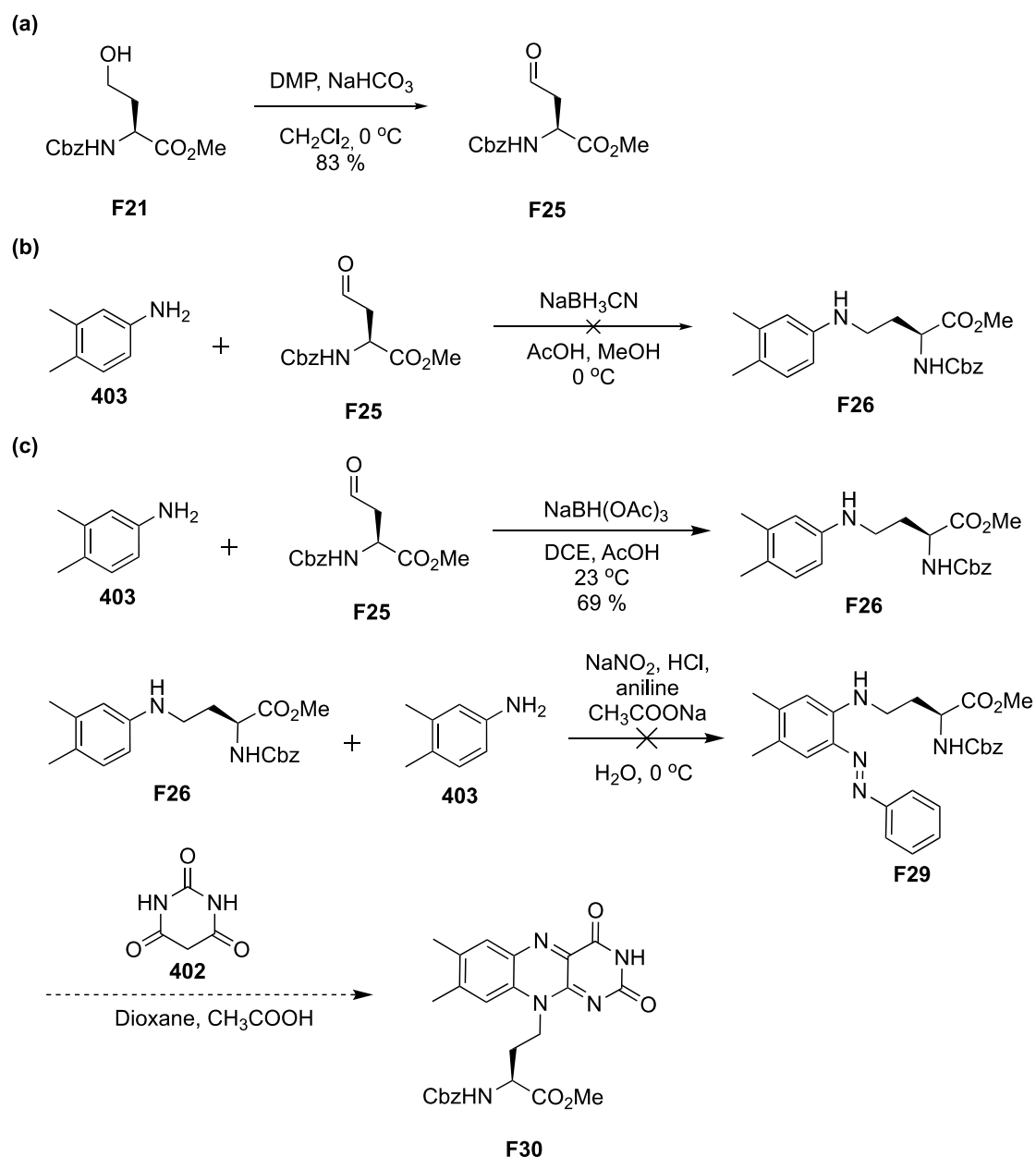


Scheme 5-7 (a) Synthesis of **F21**. (b) Unsuccessful synthesis of **F22**

Although the flavin derivative **F13** is only slightly soluble in organic solvent, we believe that once conjugated with α -amino acid to form compound **F22**, the **F22** should be more soluble in organic solvent. To avoid the solubility issue of the substrate during the synthesis, we decided to synthesize flavin conjugated α -amino acid through a different procedure, instead of combining flavin with α -amino acid, the new procedure was to synthesize the tricyclic heterocycle isoalloxazine on the side chain of α -amino acid (Scheme 5-8).

Scheme 5-8 Unsuccessful synthesis of **F24**

To add the 3,4-dimethylaniline **403** to the α -amino acid, the iodination on **F21** was conducted to get compound **F23** which was used in the next step for the nucleophilic substitution with 3,4-dimethylaniline to get **F24**. The compound **F23** was collected with over 90% yield, however, the next step did not work (Scheme 5-8). The substituent method was reductive amination (Scheme 5-9), alcohol **F21** was oxidized to aldehyde using DMP (Scheme 5-9a), and the product **F25** was reacted with 3,4-dimethylaniline using sodium cyanoborohydride as the reduction reagent, which did not work as well (Scheme 5-9b). We then tried different reductive amination methods, and the reductive amination through sodium triacetoxyborohydride gave a good yield, then compound **F26** was reacted with 3,4-dimethylaniline to prepare an azo-compound **F29**, however, the product **F29** was not collected (Scheme 5-9c).

Scheme 5-9 Unsuccessful synthesis of **F30**

5.1.2 Post-synthetic Modification Method for the Synthesis of Flavin-Foldamer.

After a variety of trials on synthesizing flavin-conjugated α -amino acids, the target compound was not successfully synthesized, more discovery and synthetic efforts are needed to get this compound. On the other hand, carrying the flavin residue during the peptide synthesis is risky

given the active property of the flavin compound, for instance, the decarboxylative activity of flavin when exposed to light might cause a low yield during the peptide coupling. Therefore, the other plan was applied, to prepare the foldamer with a reactive site on the side chain and bond it with flavin residue through a one-step reaction. With the methylamine foldamer **300** successfully synthesized in Chapter 4, reductive amination was chosen to connect side-chain amine with the flavin residue.

The flavin aldehyde was prepared via oxidative cleavage of the riboflavin. Riboflavin was treated with NaIO_4 in water, and the product was purified via refluxing crude product in toluene to remove the soluble impurity, **F31** was collected in a 50% yield over 2 steps (Figure 5.2).¹⁰³

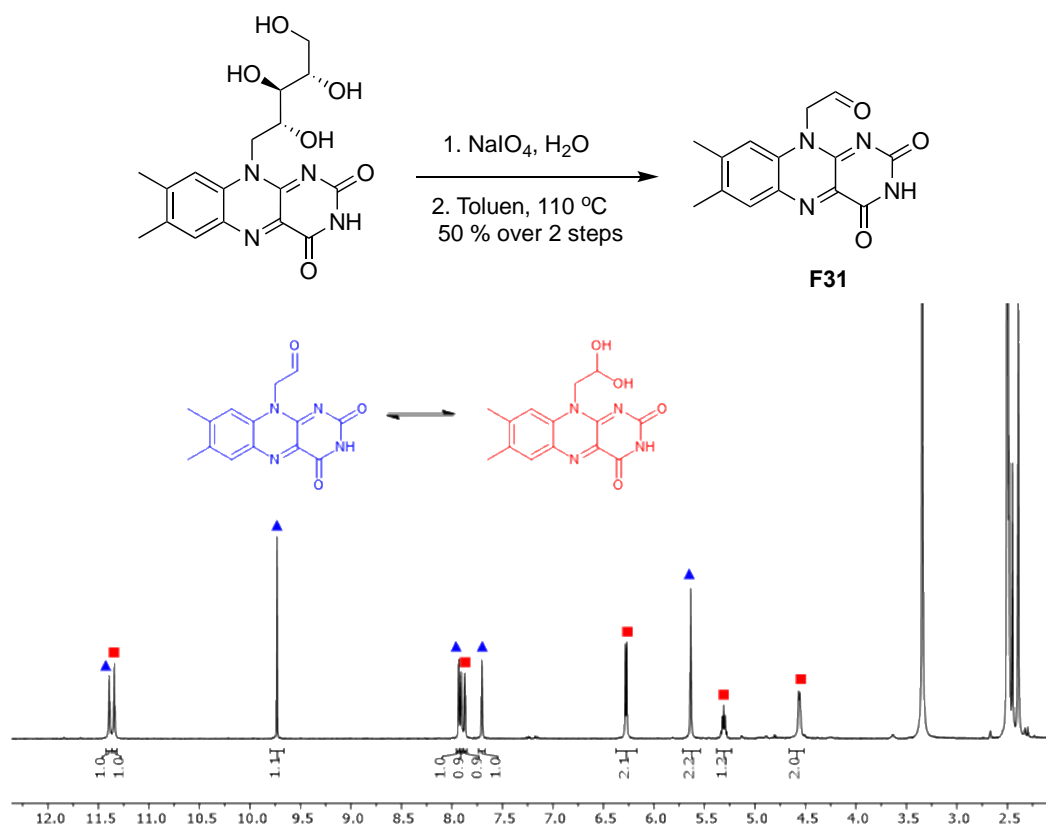
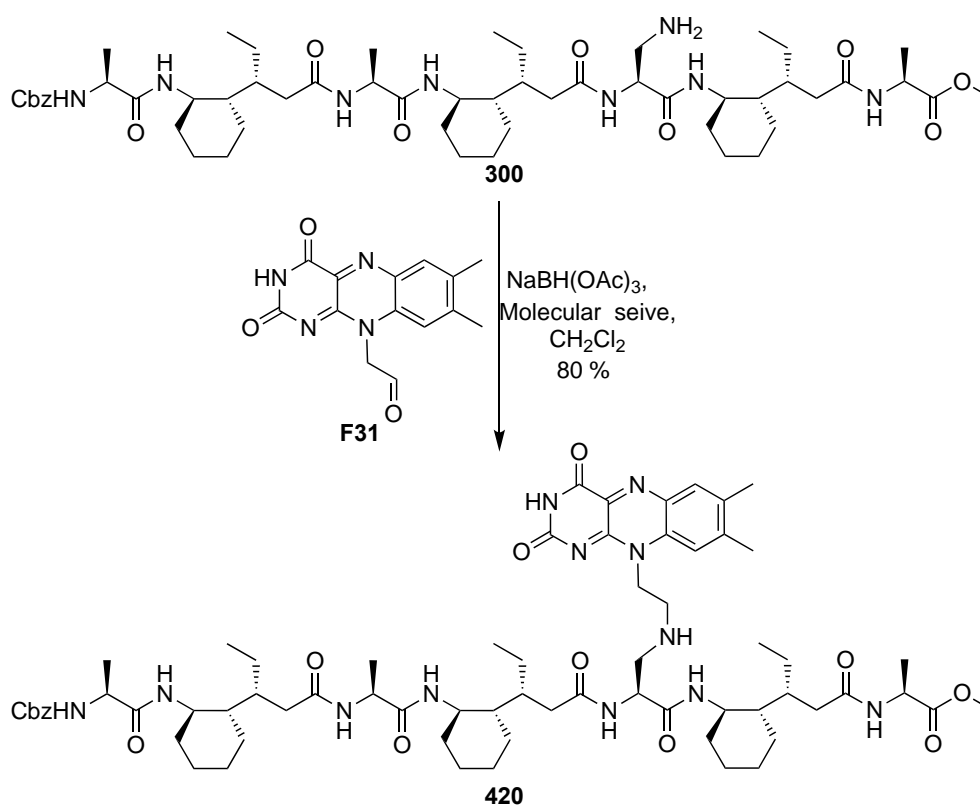


Figure 5.2 Synthesis of **F31** and its ^1H NMR in chloroform.

In the NMR spectrum, two sets of peaks were observed which might be the aldehyde product **F31** and its hydrate product, the mixture was brought to the next step without further purification. The crude product of **F31** was attached to foldamer **300** via reductive amination (Scheme 5-10), although an excess amount of **F31** was added to the reaction because of its

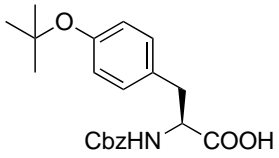
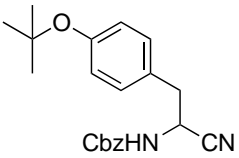
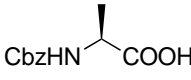
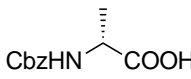
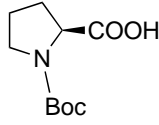
poor solubility in dichloromethane. Flavin foldamer **420**, however, was soluble in CH_2Cl_2 , and so was easy to separate *via* filtration. After several trials, the best yield achieved was 80%, containing 20% of unreacted foldamer **300**. The reaction was kept under dark conditions to avoid side reactions, and the crude product was purified via prep-HPLC to get photocatalyst **420**.



Scheme 5-10 Synthesis of flavin-foldamer **420** through reductive amination.

The catalyst was then applied to a decarboxylative cyanation reaction devised by Jose C. Gonzalez-Gomez and co-workers.¹⁰⁴ Amino acids are readily available compounds with a carboxylic acid end and heteroatom at its β -position. Four amino acid substrates were chosen to check the activity of **420** (Table 5-1). Under low-strength blue light, no product was observed, whereas, under the strong blue light, the tyrosine substrate gave a decarboxylative cyanation product, which was confirmed by LC-MS (Figure 5.3).

Table 5-1 The result of **420** catalyzed decarboxylative reduction on four substrates.

Substrate	Condition	Result
	CH ₃ CN, 5 mol% 420 , 12 h	
	CH ₃ CN, 5 mol% 420 , 12 h	No product detected
	CH ₃ CN, 5 mol% 420 , 12 h	No product detected
	CH ₃ CN, 5 mol% 420 , 12 h	No product detected

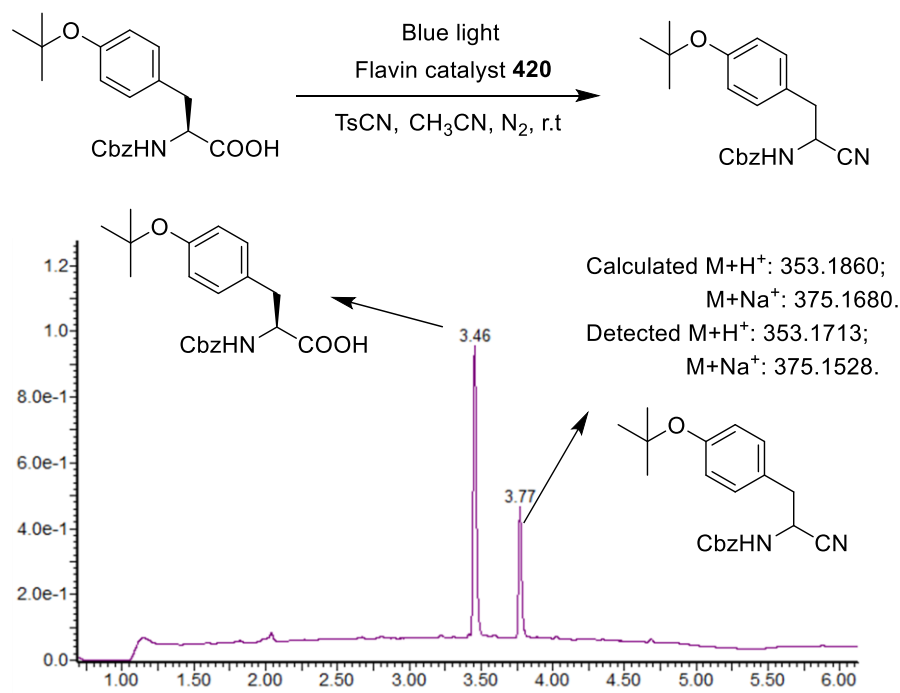


Figure 5.3 The catalytic decarboxylative cyanation and the LC-MS result.

In conclusion, the flavin residue was successfully bound on the foldamer via the idea of post-synthetic modification, and the photoactive foldamer was proved effective for the decarboxylative cyanation of D-tyrosine, due to the unsuccessful synthesis of the mirror imaged tyrosine substrate, the enantioselectivity of the foldamer is not yet known.

5.2 Synthesis of Piperidine-Based δ -amino acid

5.2.1 Aims and Plans

In Chapter 2, the crystal structure of L-alanine constructed foldamers illustrated that the ethyl side chain on δ -residue ($i+2$ position) points towards the cyclohexane of the δ -residue (i position). As illustrated in Figure 5.4, the pink-coloured atom represents these two positions, and the two sites are aligned at the same side of the helix, which is an ideal position to realize high bifunctionality. Inspired by Gellman's work of bifunctional amine foldamer catalyst, we decided to synthesize a catalytic foldamer with a secondary amine inserted in the cyclohexane of the δ -residue and a primary amine attached on the ethyl side chain of the next δ -residue. The

new building blocks of the catalytic foldamer would be monomer **500** and monomer **501**, using the asymmetric catalytic Michael addition methods described in Chapter 2, the synthesis of monomer could be broken down to compound **503** and compound **504** (Figure 5.5).

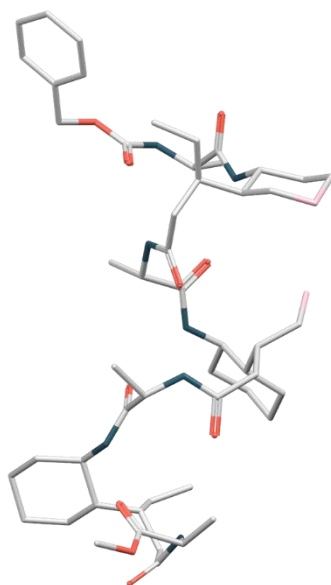


Figure 5.4 The crystal structure of foldamer **103**, the pink colour marked the two proximal positions.

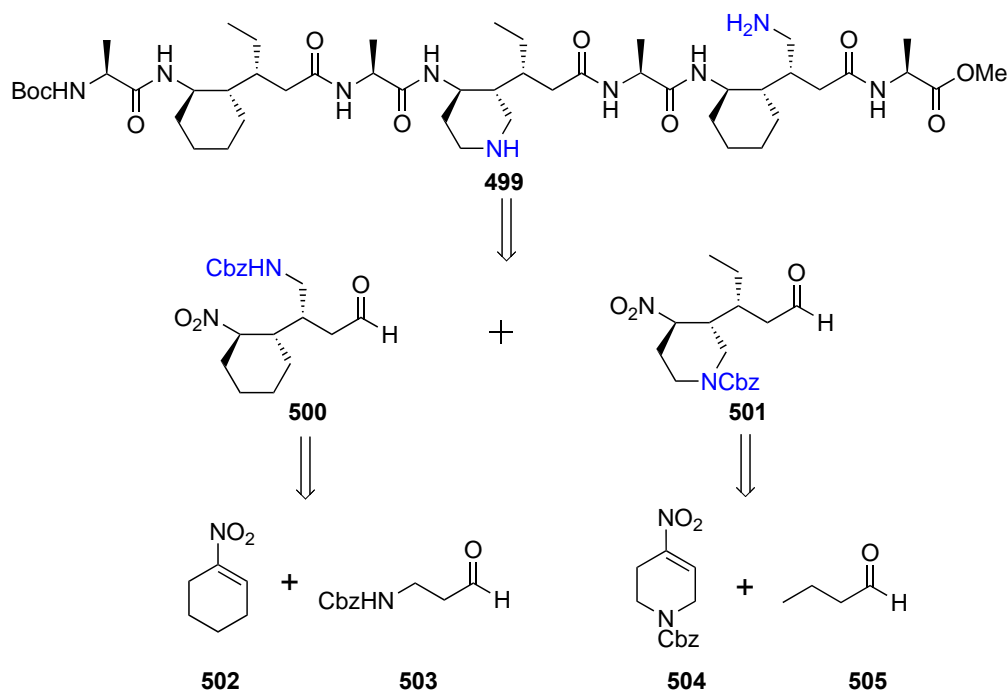
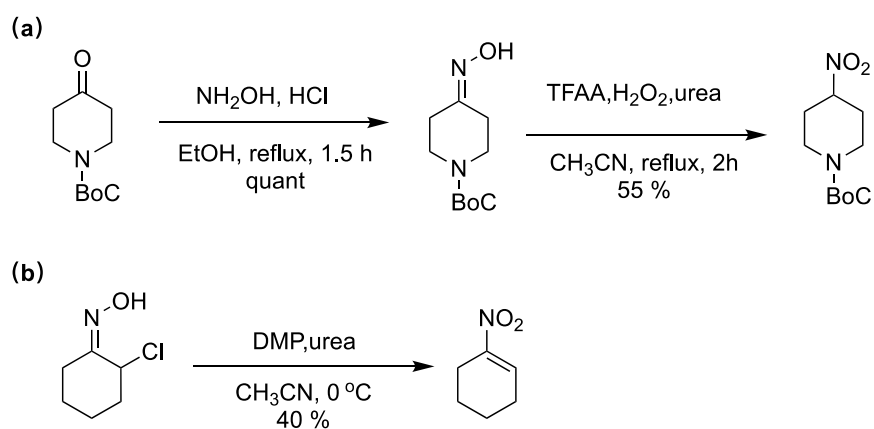


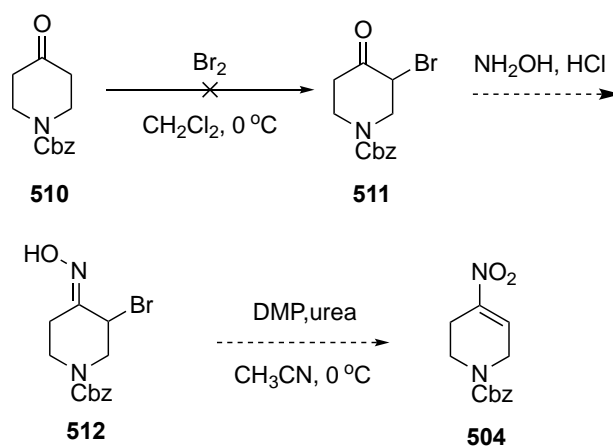
Figure 5.5 Retrosynthesis of piperidine-based foldamer and the structure of the building block **500**, **501**, **503**, **504**.

5.2.2 Synthesis of Building Blocks

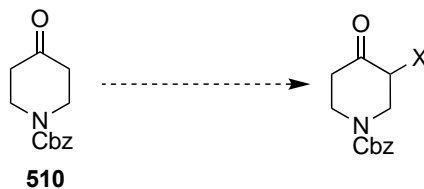
Referring to the method developed by McKerverey *et al.* and Carlos Jiménez *et al.* of replacing the ketone to nitro group on the cyclohexane ring^{105, 106} (Scheme 5-11), the synthesis of compound **504** started from the commercially available compound **510** (Scheme 5-12), the plan was to brominate the α -position of the ketone to get the compound **511**, and then **511** was reacted with hydroxylamine to form the oxime, the oxidation of oxime used DMP, urea would generate the target compound **504**. However, the bromination or chlorination on **510** did not work under a variety of conditions as concluded in Table 5-2.



Scheme 5-11 (a) The method developed by M. Anthony McKervery's group. (b) The method was developed by Carlos Jiménez's group.

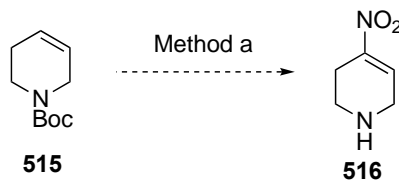


Scheme 5-12 Proposed procedure for the synthesis of compound **504**

Table 5-2 Methods of bromination/chlorination reactions.

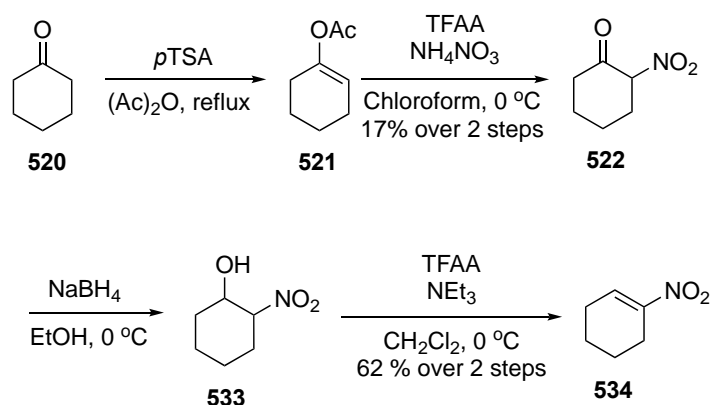
Product	Method	Result
X=Cl	NCS, DMSO, r.t ¹⁰⁷	Not reacted
X=Br	NBS, <i>p</i> -TsOH, CH ₂ Cl ₂ , 0 °C~Reflux ¹⁰⁸	Messy ¹ H NMR
X=Br	NBS, NH ₄ OAc, Et ₂ O, r.t ¹⁰⁹	Not reacted
X=Br	Br ₂ , CH ₂ Cl ₂ , r.t ¹¹⁰	Messy ¹ H NMR
X=Cl	NCS, <i>S</i> -proline, 2-Nitro-PhCO ₂ H, CH ₃ CN, r.t ¹¹¹	Not reacted
X=Cl	Oxone, NH ₄ Cl, MeOH, r.t ¹¹²	Acetal product
X=Cl	4,5-DPI, 2-Nitro-PhCO ₂ H, NCS, CH ₃ CN, r.t ¹¹¹	Messy ¹ H NMR

The new proposed procedure was to synthesize the 4-nitro-1,2,3,6-tetrahydropyridine **516** through one-step nitration on the commercially available substrate **515**, unfortunately, none of the methods used worked as concluded in Table 5-3.

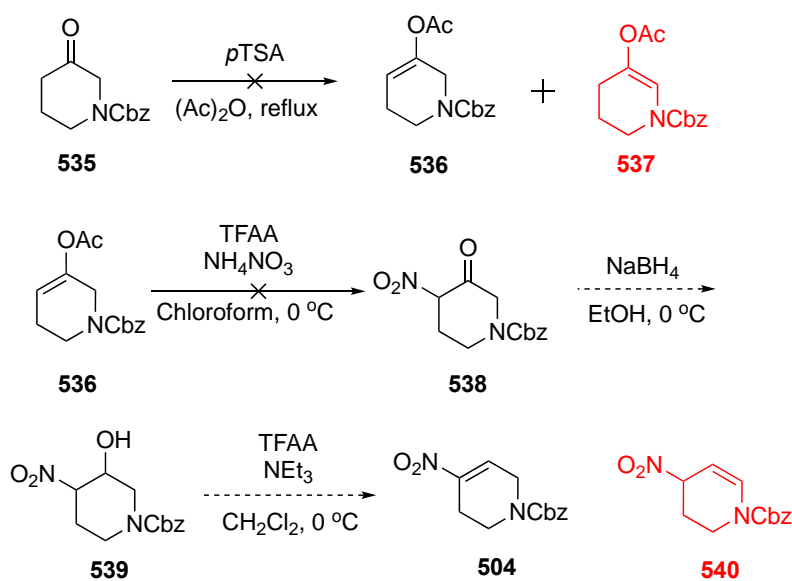
Table 5-3 Methods of nitration reaction

Method a	Result
NaNO_2 , CH_3COOH , CAN ¹¹³	Not reacted
$\text{K}_2\text{S}_2\text{O}_8$, <i>tert</i> -butyl nitrite, Quinoline ¹¹⁴	Not reacted
Tempo, AgNO_2 ¹¹⁵	Not reacted
$\text{Bu}_4\text{N}^+\text{NO}_3^-$, Tf_2O , $\text{Bu}_4\text{N}^+\text{OTf}$ ¹¹⁵	Not reacted

The other way of synthesizing compound **504** is to follow the procedure of synthesizing the nitro-cyclohexane from cyclohexanone¹¹⁶ (Scheme 5-13). The acetylation of the ketone under catalysis of *p*TSA produced **521** in a 50% yield, and the nitration of this via ammonium nitrate in the presence of trifluoroacetic anhydride gave α -nitroketone **522** in a 57% yield after purification. Subsequent reduction of ketone by sodium borohydride produced alcohol compound **533** which underwent elimination to give nitro-cyclohexene in 62% yield over 2 steps. The compound **504** might be obtained through the same procedure, the issue with this procedure is that the side reaction of forming the isomer might comprise the yield of the reaction, and the generated isomer should be able to be separated via chromatography. The acylation of **535** produced **536** as the major isomer, and **537** was the minor side-product (Scheme 5-14). The crude was purified via chromatography, which gave a crude product with 70% purity. Unfortunately, the nitration of **536** the next step did not work as expected.



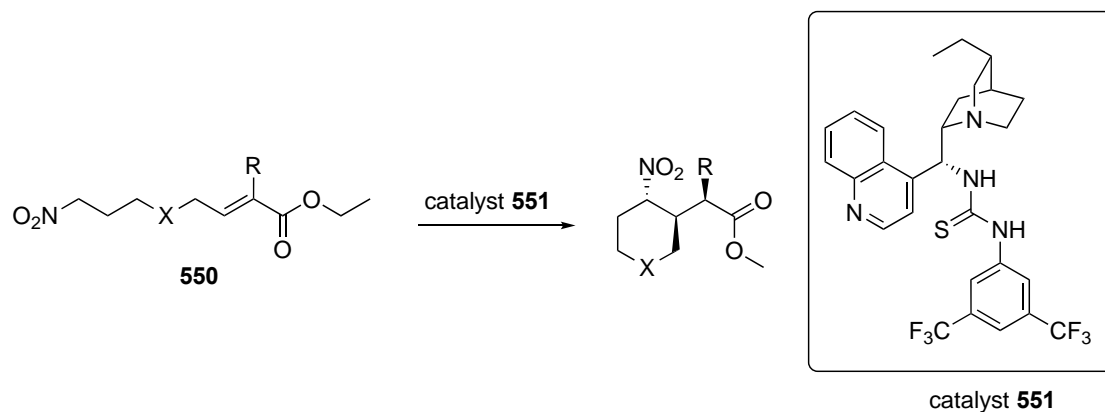
Scheme 5-13 Synthesis of nitro-cyclohexene from cyclohexanone.



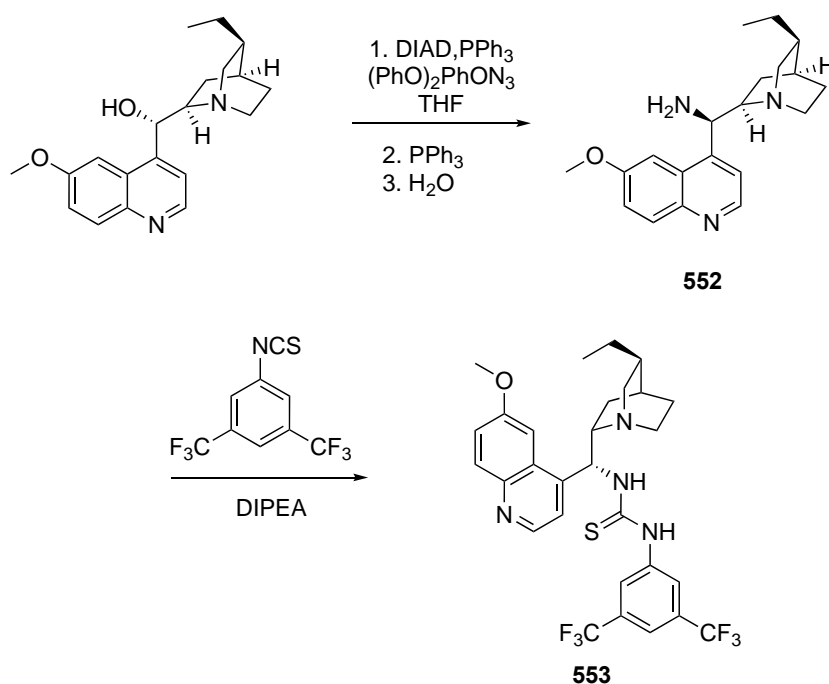
Scheme 5-14 Proposed procedure of synthesizing compound 504 and the side reaction that might happen.

Another approach to getting the piperidine-based δ -amino acid is by using the procedure developed by our group (Scheme 5-15).⁶⁷ Hydroquinidine derivative **551** could catalyze the intramolecular Michael addition, forming a γ -amino acid precursor with good yield and high enantioselectivity. The challenge of this method is to synthesize the substrate **550**. The synthesis of catalyst **551** followed the general method published by Paolo Melchiorre's group,¹¹⁷ using commercially available hydroquinidine as a starting material, the hydroquinidine was first formed an azide via the Mitsunobu reaction, and the azide was reduced to an amine via

Staudinger azide reduction to get the compound **552**, then the amine on **552** reacted with 3,5-bis(trifluoromethyl)phenyl isothiocyanate to form the target catalyst **553** (Scheme 5-16).¹¹⁸

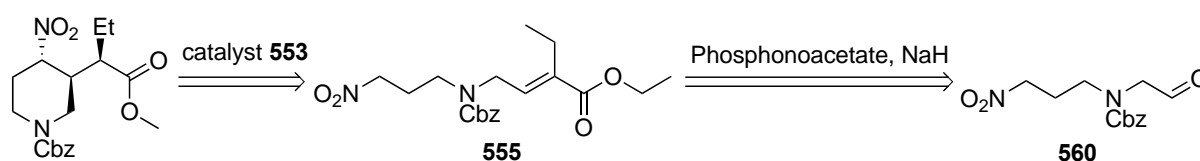


Scheme 5-15 Approach of synthesizing the piperidine-based γ -amino acid precursor.



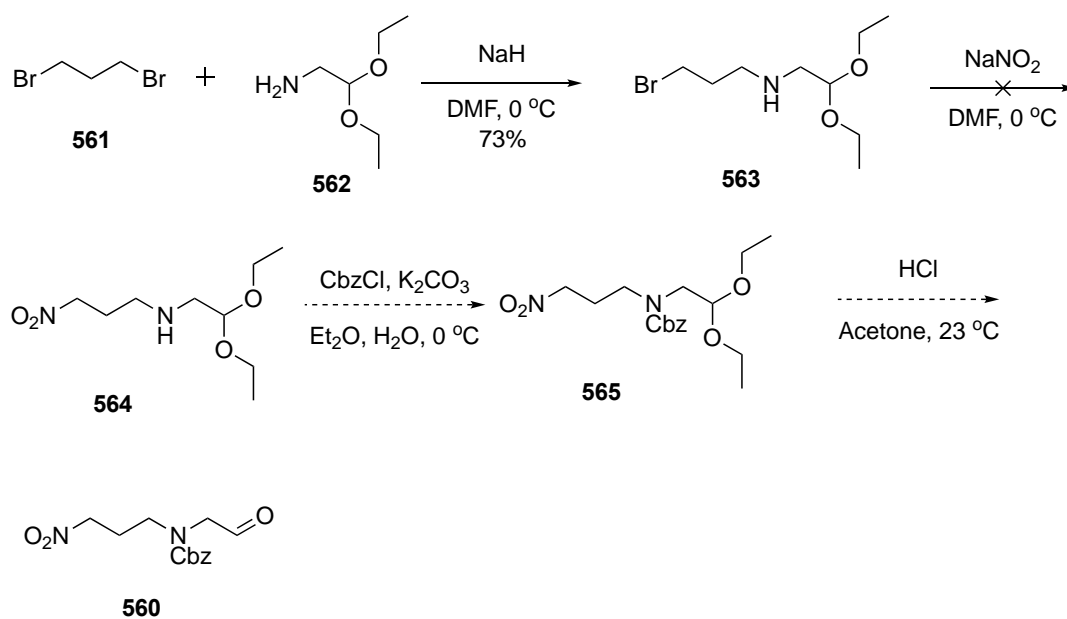
Scheme 5-16 Proposed procedure of synthesizing catalyst **553**.

The synthesis of the substrate **555** could be realized by the Wittig reaction between aldehyde compound **560** and phosphonoacetate (Scheme 5-17). Compound **560** was obtained after trying different procedures.

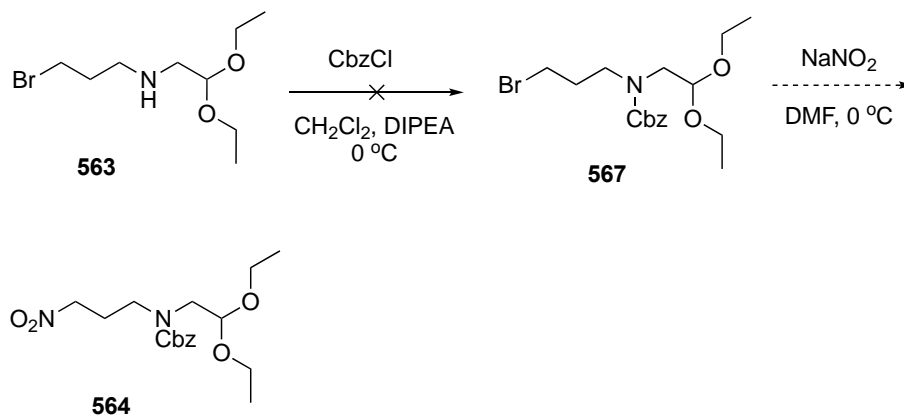


Scheme 5-17 Retrosynthesis of γ -amino acid precursor

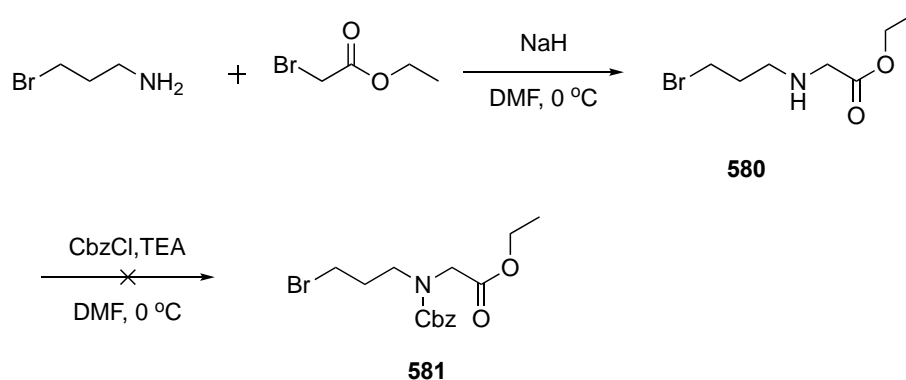
As shown in Scheme 5-18, the first proposed method started from the nucleophilic addition of 2,2-diethoxyethan-1-amine **562** onto 1,3-dibromopropane **561**. Using them in a 1:1 stoichiometry, compound **563** could be obtained in a good yield. Then the substitution of bromo to the nitro group would generate compound **564**, the amine **564** needs to be protected by the Cbz group to get the compound **565**, and the acetal deprotection of **565** at an acidic condition would generate the target compound **560**. However, the nitrate substitution of **563** did not work, and the crude product was a mixture of several side products. The explanation might be the unprotected amine could be an issue that caused the side reactions. The next approach protected the amine with the Cbz-group *before* the nitration step, as shown in Scheme 5-19. However, the Cbz-group cannot be added onto the secondary amine under general Cbz-protection conditions. In an alternative approach, ester **580** was synthesized, but unfortunately, Cbz-protection still did not work (Scheme 5-20). This result indicated that the reactivity of the secondary amine with CbzCl might be problematic, and so we then investigated other procedures to avoid the Cbz-protection reaction on the secondary amine.



Scheme 5-18 The unsuccessful procedure of synthesizing compound 560

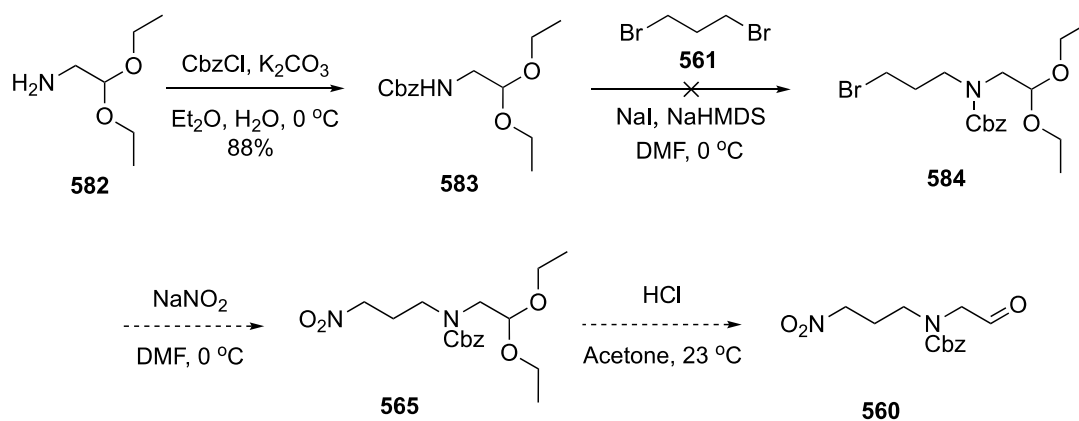


Scheme 5-19 The unsuccessful procedure of synthesizing compound 564

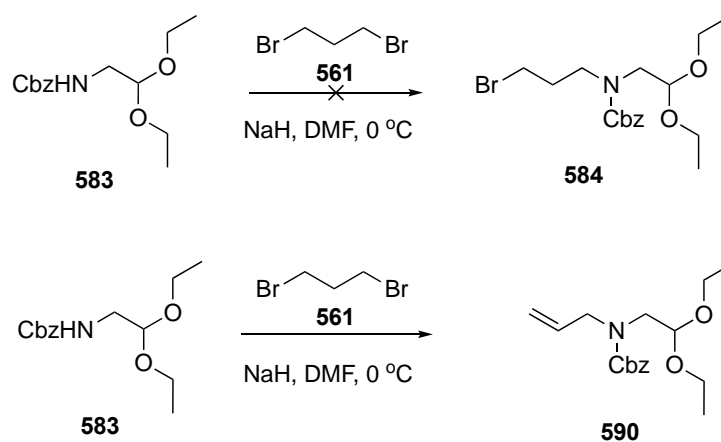


Scheme 5-20 Unsuccessful procedure of synthesizing compound **581**

Our next approach was to add the Cbz-group on the primary amine to gain compound **583**, whereby nucleophilic addition to 1,3-dibromopropane would generate the compound **584**. Nitration and deprotection of the acetal would generate compound **560** (Scheme 5-21). **583** was successfully synthesised in high yield, however, the nucleophilic addition to 1,3-dibromopropane **561** using NaHMDS failed. We then changed the base to NaH, and whilst C-N bond formation reaction happened, the other bromine was eliminated under these conditions to give alkene product **590** - although in good yield (Scheme 5-22).

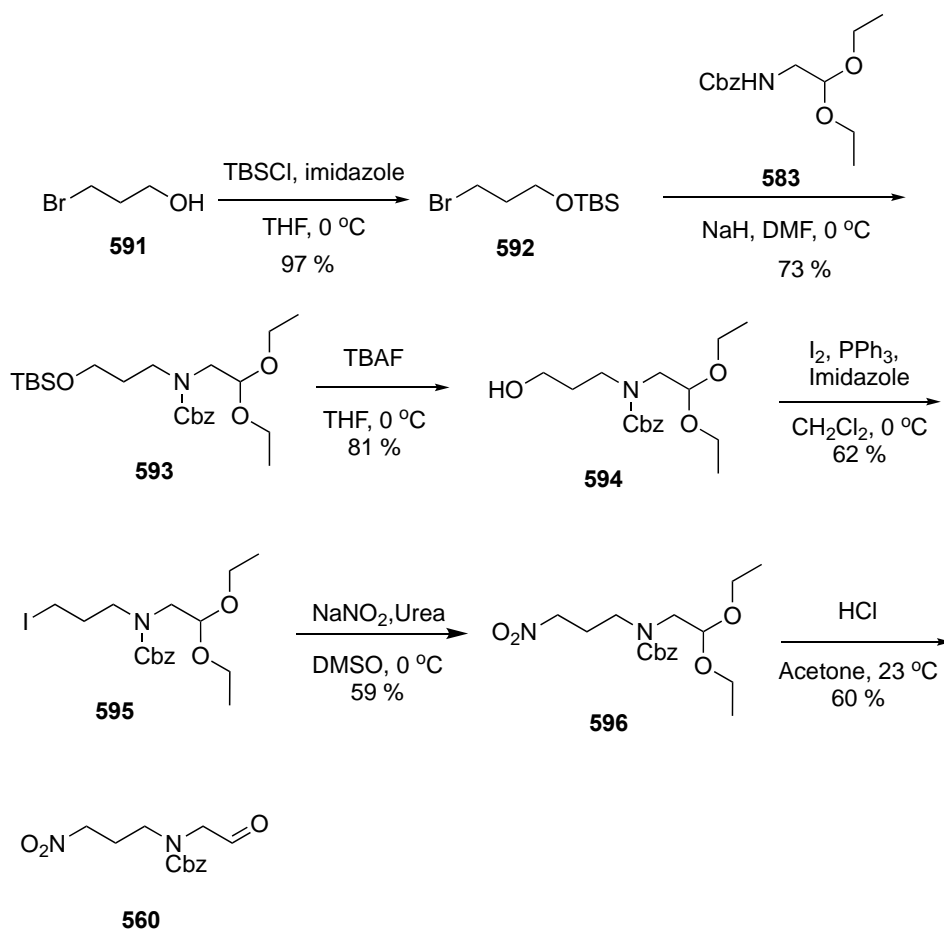
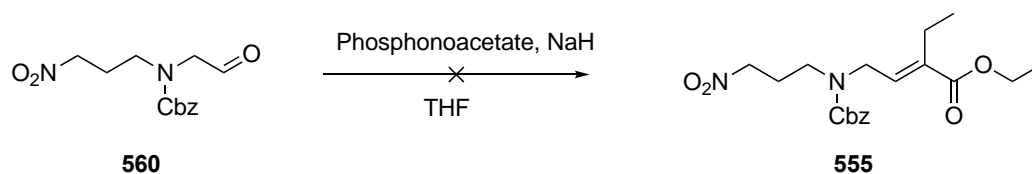


Scheme 5-21 Proposed procedure of synthesizing compound **560**.



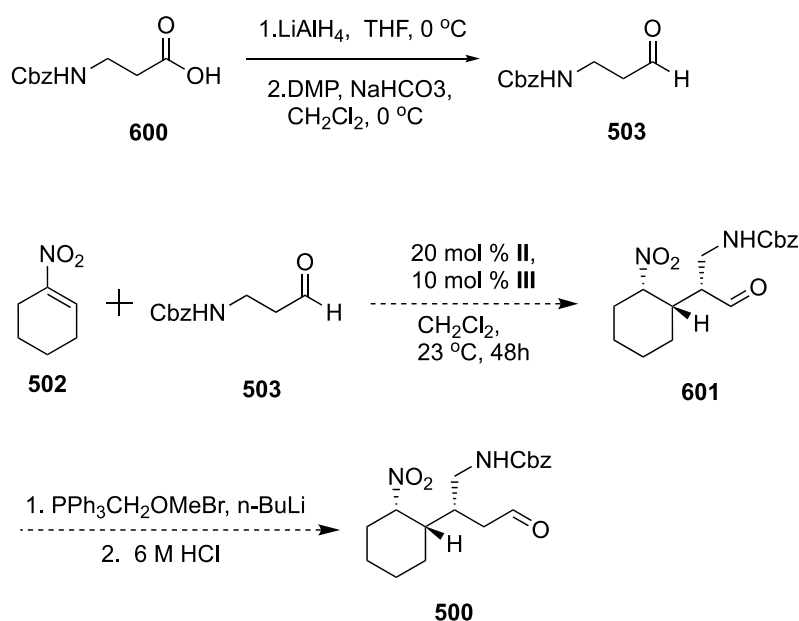
Scheme 5-22 The unexpected elimination of compound **583**

A new procedure was proposed to avoid the elimination of bromine using a terminal TBS-protected alcohol instead of bromine. The required alkylation agent **592** was obtained by the TBS protection on the 3-bromopropan-1-ol, and then reacted with **583** using the method described above to give amine **593** in a good yield. The TBS protection was removed by treating with TBAF to form alcohol **594**, which was then substituted with iodo to form the compound **595** in a good yield. The iodide **595** was nitrated to generate compound **596** in a 50% yield, and the acetal deprotection of compound **596** produced the target molecule **560** in 60% yield (Scheme 5-23). Unfortunately, the Horner-Wadsworth Emmons reaction on compound **560** was unsuccessful (Scheme 5-24). There are some other homologation reactions that might be worth trying if more amount of compound **560** was obtained by repeating the synthesis.

Scheme 5-23 Procedure of synthesizing compound **560**Scheme 5-24 Unsuccessful reaction from compound **560** to compound **555**.

Unfortunately, in terms of synthesizing the δ -amino acid monomer with a heteroatom on the ethyl side chain, the synthesis was also unsuccessful. The plan is to use the Jorgensen catalyst as the asymmetric catalyst to synthesize compound **500** using aldehyde **503**. The synthesis of compound **503** was successful via a two-step reaction from a commercially available Z-protected β -alanine **600** (Scheme 5-25). In this method, the carboxylic acid was reduced to

alcohol by LiAlH_4 reduction and then re-oxidized by DMP to aldehyde **503** in a good yield. Compound **503** was then reacted with nitro-cyclohexene to get the γ -amino acid precursor **601** (Scheme 5-25). The product was characterized by ^1H NMR, however, two sets of peaks were observed on the ^1H NMR, it was unclear whether the splitting of the ^1H NMR was caused by the different conformation adopted by compound **601** or two diastereomers existing in the crude.



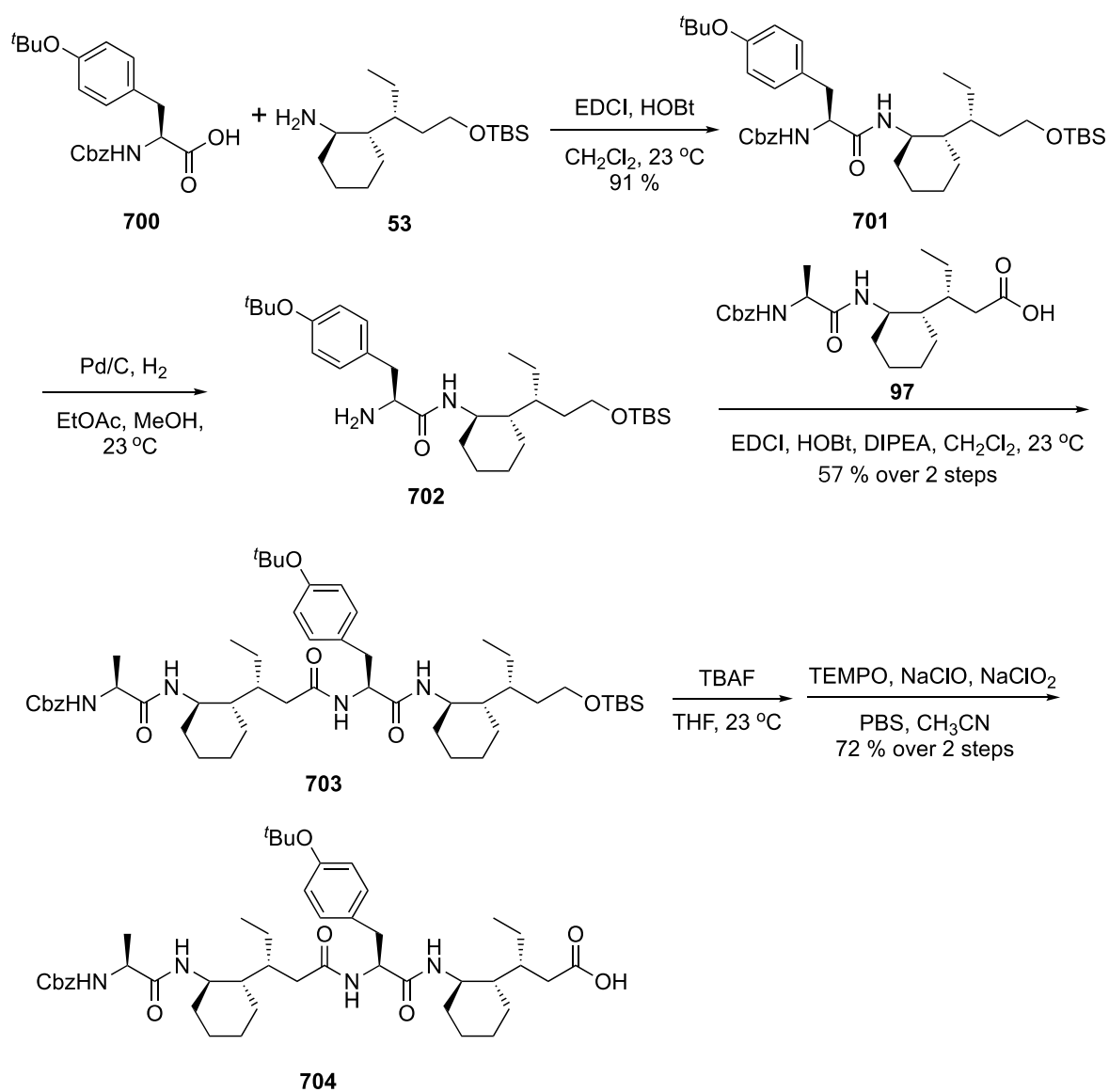
Scheme 5-25 Proposed method of synthesizing compound **500**

In conclusion, the synthesis of the N-hetero δ -amino acid monomer is unsuccessful, the method of using hydroquinidine derivative to catalyse the intramolecular Michael addition might produce the target γ -amino acid precursor **601**.

5.3 Synthesis of Tyrosine Containing Foldamer

As described in Chapter 3, the key residues in that proposed catalytic cycle are lysine and tyrosine. The tyrosine helps with the proton transfer and regenerates the lysine residue from the iminium intermediate. As concluded in Chapter 3, the kinetics of our bis-ornithine foldamer

involve a burst state and a steady-state, the slowing down of reaction rate might be caused by the slow hydrolysis of the acetone-lysine iminium intermediate. We therefore modified the foldamer catalyst with both amine and phenol groups on the side chain to see if the tyrosine could help with the proton transfer process, and consequently, accelerate the rate of the retroaldol cleavage. The synthesis of the tyrosine-ornithine foldamer followed the general procedure of foldamer synthesis (Scheme 5-26), the foldamer **707** was successfully synthesized and characterized by NMR and MS.



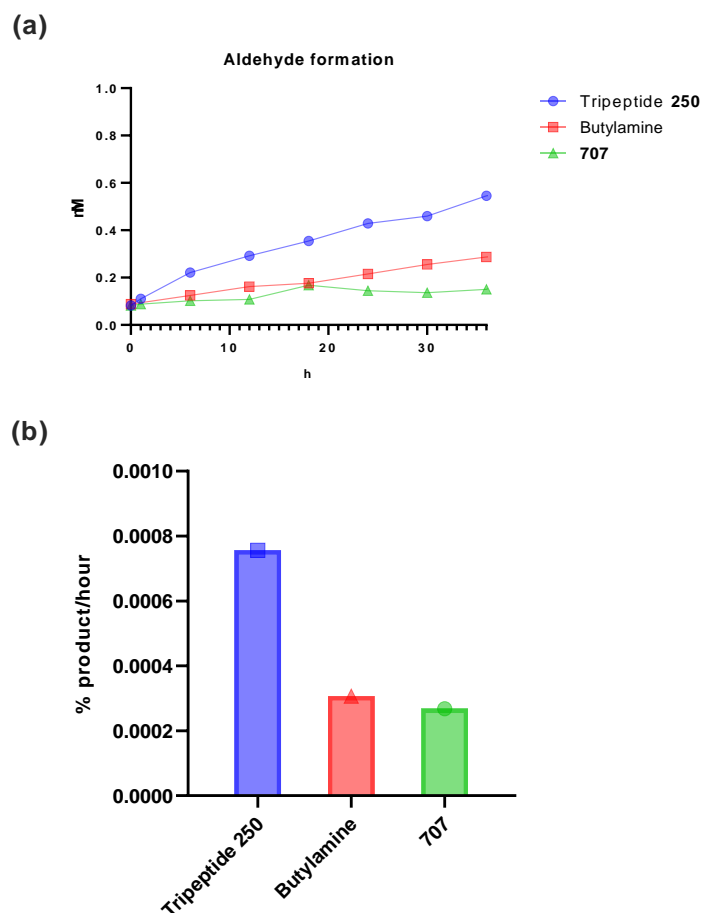


Figure 5.6 The aldehyde formation of (a) In CDCl_3 , foldamer **707** (1.5 mM) on [methodol] (15 mM) at 20 °C, monitored with ^1H NMR every 6 h. (b) In 5% CH_3CN -PBS buffer, 15 mM substrate and 1 mM foldamer **707** at room temperature, were monitored by HPLC after 48 hours of reaction time.

5.4 Conclusion

In conclusion, the content in this chapter is the combination of three unfinished projects. The first part of this chapter is about the synthesis of flavin-conjugated foldamer and decarboxylative catalysis. By utilizing the idea of post-synthetic modification, the flavin-conjugated foldamer was successfully synthesized and was demonstrated as an effective catalyst for the tyrosine substrate. Although the other approach of synthesizing flavin conjugated foldamer was unsuccessful, it presented different ways of synthesizing the flavin

molecules. The second project is about synthesizing a functional δ -amino acid monomer, the synthesis did not lead to the target molecule but has screened out the feasible methods for future synthesis, if the suitable method of homologation could be discovered, using the compound successfully synthesized in Chapter 5.2, the γ -amino acid precursor could be obtained as proposed. The last project is the synthesis of the tyrosine-conjugated foldamer, the result shows that with only one amine and one tyrosine on the catalyst, instead of being a bifunctional catalysis, the interaction between the two active sites might decrease the catalytic efficiency of the foldamer. The either positive or negative result presented in this chapter could be a useful reference for future study on the catalytic α,δ -foldamers.

Chapter 6 Experimental Section

6.1 Methods and Materials

Substrates: All starting materials were received from commercial suppliers unless otherwise stated. Anhydrous THF were supplied as Sureseal® bottles by Sigma Aldrich.

NMR data: Nuclear Magnetic Resonance (NMR) spectra were recorded using a Bruker Ascend 400 (400 MHz) spectrometer. The ^1H NMR and ^{13}C NMR spectra were analysed with Mestrenova.

MS data: High-resolution mass spectra were recorded on Waters Xevo G2-XS QToF Quadrupole Time-of-Flight Mass Spectrometer

Optical Rotation: Optical rotation readings were recorded using an Anton Parr 100 mm Polarimeter. Specific rotations are reported as ($[\alpha]^{25}_{\text{D}}$), and solution concentrations (c) are given in units of g/100 mL, temperatures are 25 °C.

HPLC: HPLC analysis was determined on Agilent Technologies with G7161BR 1290 Infinity II Sampler, G7112BR 1260 Infinity II Binary pump - up to 600 bar, G7116AR 1260 Infinity II MCT, G7115A 1260 Infinity II DAD.

Chromatography: Reactions were monitored by thin layer chromatography on silica gel precoated aluminium sheets (TLC Silica Gel 60, Merck). Visualisation was accomplished by potassium permanganate stain. Column chromatography was performed on Merck silica gel (60 °A, 230 - 400 mesh, 40 - 63 μm) or on a Teledyne CombiflashRF+ system.

Single Crystal X-ray: X-ray data was collected on an Oxford Gemini S-ultra diffractometer using $\text{K}\alpha$ radiation. Data were diffracted at the $\text{CuK}\alpha$ wavelength, and data-collection

strategies were based on Omega scans at 100(2) K. The Rigaku CrystalClear suite version 2.0 were used to index, integrate and scale the data with a multi-scan absorption correction.

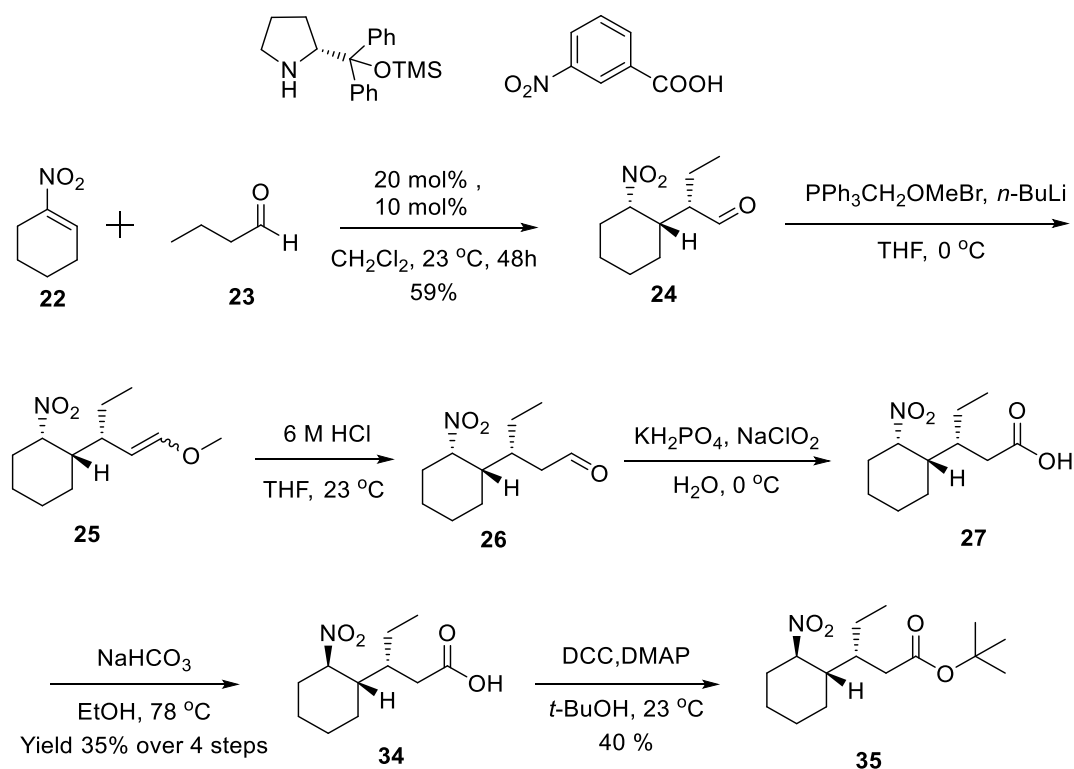
Circular Dichroism: All CD spectra were measured in an Applied Photophysics Circular Dichroism Spectrophotometer, Chirascan V100. cells of pathlength 1 cm (Hellma).

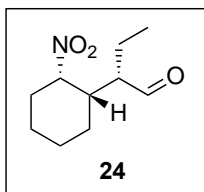
Microplate Reader: Kinetic measurement was monitored by Hidex Sense Microplate Reader. The appearance of 6-methoxy-2-naphthaldehyde was monitored with excitation at 320/40 nm and emission at 460/20 nm, flash=5, at 25 °C. The sample was placed in a black, bottom cleared, 96 Well Advanced TC™ treated plate. Reaction was recorded every 10 minutes over 120 cycles.

6.2 Synthesis and Characterization for Chapter 2

6.2.1 Preparation of δ -amino Acid Precursor

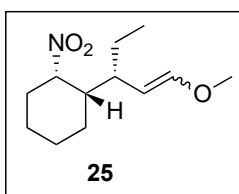
6.2.1.1 Synthesis of Building Blocks





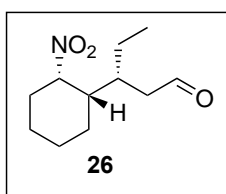
(S)-2-((1S,2S)-2-nitrocyclohexyl)butanal 24⁶⁸ To a 100mL round bottomed flask was added catalyst **II** (1.276 g, 4.12 mmol), catalyst **III** (0.328 g, 1.96 mmol), 20 mL CH₂Cl₂, *n*-butanal (8.82 mL, 98.16 mmol), and 1-nitro-1-cyclohexene (2.22 mL, 19.66 mmol). The resulting mixture

was stirred at room temperature for 2 days. After this time, solvent was removed under reduced pressure and the crude reaction mixture was purified via column chromatography eluting with EtOAc/hexane to give the desired product as a pale-yellow oil in 59% yield. Data are in agreement with the literature. ¹H NMR (400 MHz, CDCl₃) δ 9.66 (d, J = 1.8 Hz, 1H), 4.86 (q, J = 3.6 Hz, 1H), 2.49 (dddd, J = 9.9, 8.0, 3.6, 1.8 Hz, 1H), 2.27 (dtd, J = 10.9, 2.9, 1.9 Hz, 1H), 2.12 (m, J = 10.0, 6.0, 4.0 Hz, 1H), 1.90 – 1.81 (m, 1H), 1.80 – 1.70 (m, 3H), 1.69 – 1.52 (m, 4H), 1.32 (m, 1H), 0.83 (t, J = 7.5 Hz, 3H). ¹³C NMR (101 MHz, CDCl₃) δ 203.70, 83.61, 53.20, 37.34, 29.70, 25.01, 23.33, 20.25, 19.39, 9.98. HRMS of this compound could not be obtained using Waters Xevo G2-XS QToF Quadrupole Time-of-Flight Mass Spectrometer.



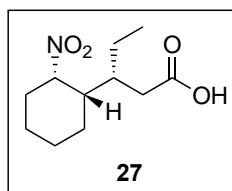
(1S,2S)-1-((S,E)-1-methoxypent-1-en-3-yl)-2-nitrocyclohexane 25

Under a nitrogen atmosphere, (Methoxymethyl)triphenylphosphonium chloride (8.92 g, 26.02 mmol) was dissolved in anhydrous THF (40 mL) and the mixture was cooled to 0 °C. *n*-BuLi (2.0 M in hexane, 9.50 mL, 23.12 mmol) was added dropwise to the solution. The resulting mixture was stirred for 45 minutes at 0 °C. **24** (2.30 g, 11.56 mmol) was then added to the mixture, and the solution allowed to warm to room temperature and stirred for 4 hours. After this time, the reaction was quenched with saturated aqueous NH₄Cl solution and extracted with CH₂Cl₂. The combined organic layers were washed with aqueous NaHCO₃ and brine, before being dried over MgSO₄, filtered and concentrated. The crude product was carried on without further purification.



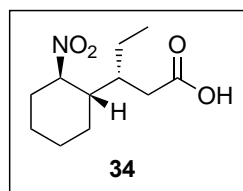
(R)-3-((1S,2S)-2-nitrocyclohexyl)pentanal 26 HCl (6M, 5.5 mL) was added to a solution of **25** (1.78 g, 7.82 mmol) in THF (40 mL). The resulting solution was stirred at room temperature overnight, EtOAc was added, the organic layer was washed with brine three times, the combined

organic layers were dried over MgSO_4 , filtered and concentrated to give a yellow oil. The crude product was carried on without further purification.



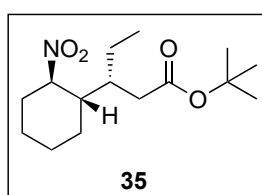
(R)-3-((1S,2S)-2-nitrocyclohexyl)pentanoic acid 27 To a solution of **26** (1.03 g, 4.83 mmol) in acetonitrile (25 mL) at 0 °C, was added a solution of KH_2PO_4 (500mg, 3.67 mmol) in H_2O (12.5 mL), followed by addition of hydrogen peroxide (30%, 650 μL).

After subsequent addition of a solution of NaClO_2 (1.25 g, 13.82 mmol) in water (25 mL), the resulting mixture was allowed to stir at room temperature for 4 hours. After this time, the solution was quenched with $\text{Na}_2\text{S}_2\text{O}_3$, acidified with HCl (pH 2~4), extracted with dichloromethane, and the combined organic layer was dried with MgSO_4 , filtered and concentrated under reduced pressure to give the compound as an oil. The crude product was carried on without further purification.



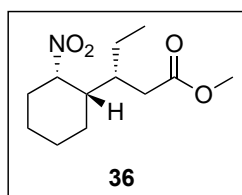
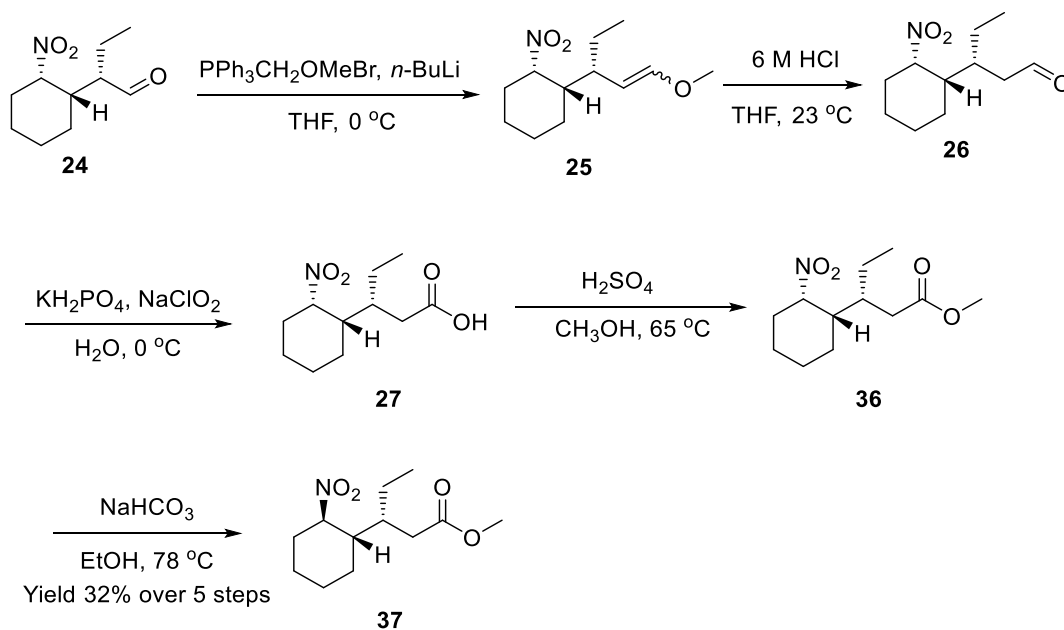
(R)-3-((1S,2R)-2-nitrocyclohexyl)pentanoic acid 34 To a solution of **27** (0.50 g, 2.18 mmol) in absolute ethanol (30 mL) was added NaHCO_3 (1.8 g, 21.83 mmol) in one portion and the resulting mixture heated at reflux for 3 hours. The mixture was allowed to cool to room temperature,

filtered through filter paper and concentrated to give the desired product in 35% yield over 4 steps. ^1H NMR (400 MHz, CDCl_3) δ 4.48 (tt, $J = 11.4, 3.9$ Hz, 1H), 2.43 (ddd, $J = 15.3, 10.4, 5.3$ Hz, 1H), 2.21 (m, 2H), 1.94 – 1.64 (m, 6H), 1.58 – 1.44 (m, 1H), 1.35 – 1.26 (m, 2H), 1.14 – 0.99 (m, 2H), 0.93 – 0.83 (m, 3H). ^{13}C NMR (101 MHz, CDCl_3) δ 178.48, 88.79, 51.82, 44.16, 37.50, 36.18, 32.49, 25.19, 24.52, 22.07, 12.58. Compound **34** was tentatively assigned using HRMS.

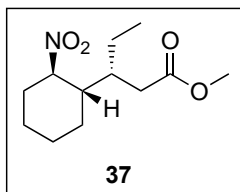


tert-butyl (R)-3-((1S,2R)-2-nitrocyclohexyl)pentanoate 35 To a solution of **34** (0.52 g, 2.27 mmol) in dichloromethane (10 mL), was added DCC (0.71g, 3.41 mmol), DMAP (0.04 g, 0.34 mmol), tert-butyl alcohol (0.44 mL), the resulting mixture was reacted overnight at room

temperature. CH_2Cl_2 was added into the reaction, the organic layer was washed with water, and the combined organic layer was dried with MgSO_4 , filtered and concentrated. The residue was purified via column chromatography eluting with EtOAc/Hexane to give a colourless oil in 40% yield. ^1H NMR (400 MHz, CDCl_3) δ 4.47 (td, $J = 11.3, 4.0$ Hz, 1H), 2.35 (dd, $J = 14.4, 5.3$ Hz, 1H), 2.21 (ddt, $J = 11.0, 4.1, 2.0$ Hz, 1H), 2.08 – 1.97 (m, 2H), 1.92 – 1.72 (m, 4H), 1.64 (tdd, $J = 11.3, 4.8, 2.2$ Hz, 1H), 1.50 (dtd, $J = 13.4, 7.4, 3.4$ Hz, 1H), 1.44 (s, 9H), 1.26 (ddt, $J = 11.0, 9.3, 2.6$ Hz, 2H), 1.11 – 0.96 (m, 2H), 0.88 (t, $J = 7.3$ Hz, 3H). ^{13}C NMR (101 MHz, CDCl_3) δ 172.27, 88.62, 80.84, 44.21, 38.16, 37.93, 32.53, 28.27, 25.33, 24.74, 24.37, 22.22, 12.74. Compound **35** was tentatively assigned using HRMS.



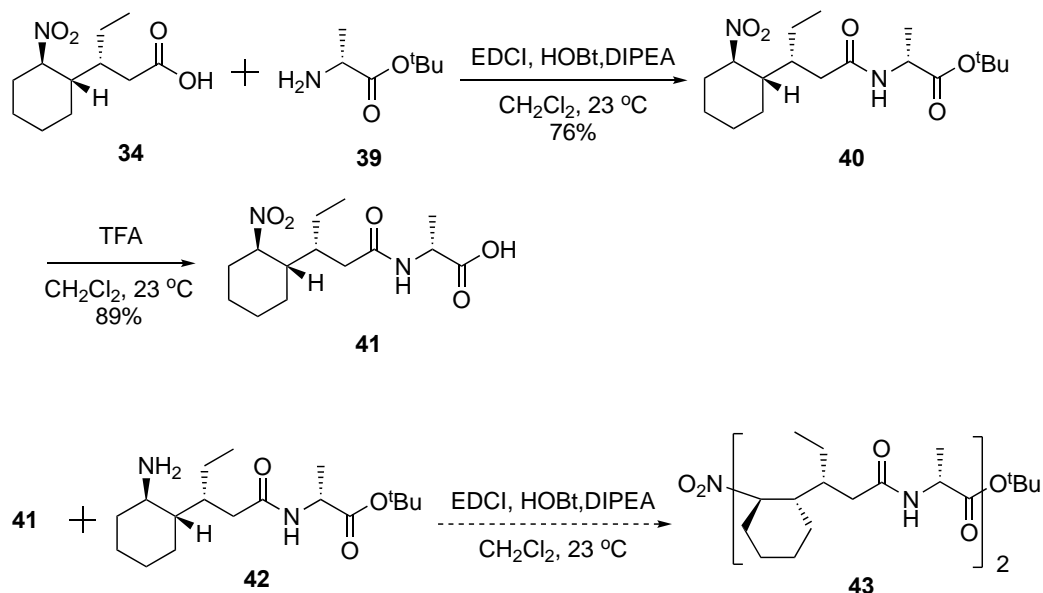
Methyl (R) -3-(($1S,2S$)-2-nitrocyclohexyl)pentanoate **36** To a solution of **27** (0.10 g, 0.44 mmol) in MeOH (50 mL) was added 2 drops of H_2SO_4 , the mixture was refluxed for 1.5 hours. Then the mixture was neutralized with aqueous NaHCO_3 , methanol was evaporated and the residue was washed with brine and extracted with EtOAc, dried over MgSO_4 , filtered and concentrated. The crude product was carried on without further purification.



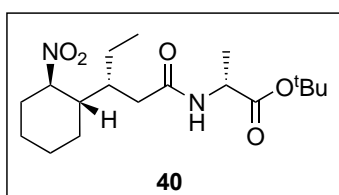
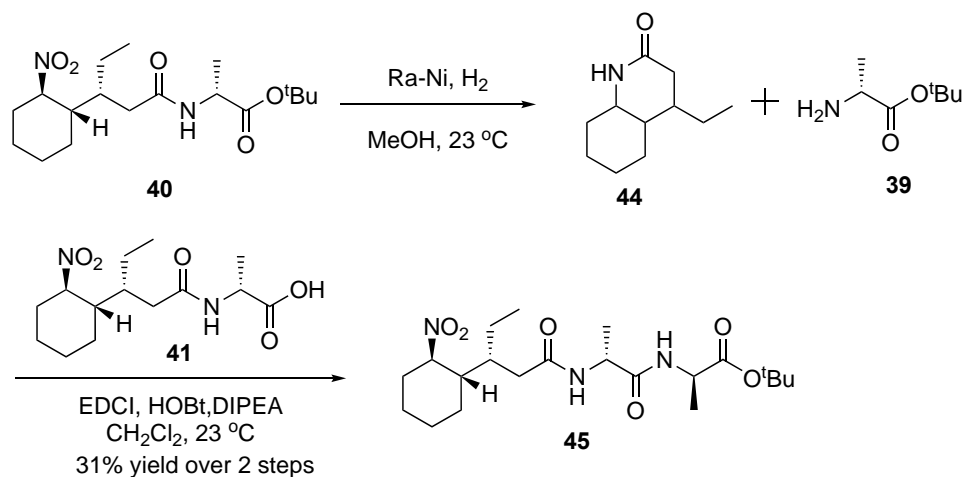
Methyl (*R*)-3-((1*S*,2*R*)-2-nitrocyclohexyl)pentanoate **37** To **36** (0.50 g, 2.06 mmol) and NaHCO₃ (1.72 g, 20.58 mmol) was added 30 mL absolute ethanol, and the mixture was refluxed for 5 hours. Then the mixture was filtered through filter paper and the filtrate was concentrated to give the desired product in 32% yield over five steps. ¹H NMR (400 MHz, CDCl₃) δ 4.47 (td, *J* = 11.3, 4.1 Hz, 1H), 3.66 (s, 3H), 2.41 (dd, *J* = 14.8, 5.3 Hz, 1H), 2.26 – 2.17 (m, 1H), 2.00 (dddd, *J* = 12.8, 11.0, 3.4, 2.2 Hz, 1H), 1.93 – 1.81 (m, 2H), 1.77 (tdd, *J* = 8.0, 4.0, 2.0 Hz, 2H), 1.67 (dddd, *J* = 12.6, 9.0, 3.3, 1.8 Hz, 1H), 1.49 (dq, *J* = 13.4, 7.4, 3.6 Hz, 1H), 1.33 – 1.20 (m, 3H), 1.12 – 0.98 (m, 2H), 0.88 (t, *J* = 7.3 Hz, 3H). Compound **37** was tentatively assigned using ¹³C NMR, HRMS.

6.2.1.2 Study on Lactam Formation

Proposed scheme of synthesizing *dada* tetramer



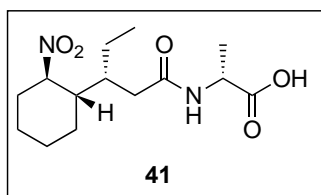
Actual products because of lactam formation



tert-butyl ((*R*)-3-((*1S,2R*)-2-nitrocyclohexyl)pentanoyl)-*D*-alaninate **40** **34** (0.47 g, 2.06 mmol) was added to the solution of HCl·NH₂-*D*-Ala-OtBu (0.41 g, 2.27 mmol), EDCI (0.43 mL, 2.47 mmol), HOBT (0.38 g, 2.47 mmol), DIPEA (0.51 mL, 3.09 mmol)

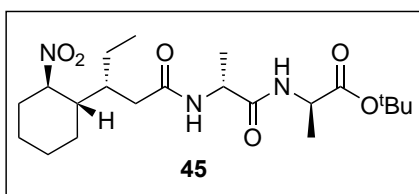
in 20 mL CH₂Cl₂. The resulting solution was stirred at room temperature overnight. EtOAc

was added to the solution, then washed with aqueous citric acid, aqueous saturated NaHCO_3 and brine, the organic layer was dried over MgSO_4 , filtered and concentrated. The residue was purified via column chromatography eluting with EtOAc /hexane to give the desired product as a white solid in 76% yield. ^1H NMR (400 MHz, CDCl_3) δ 5.98 (d, $J = 7.5$ Hz, 1H), 4.62 – 4.38 (m, 2H), 2.35 (dd, $J = 14.3, 5.4$ Hz, 1H), 2.27 – 2.18 (m, 1H), 2.15 – 2.02 (m, 2H), 1.92 – 1.81 (m, 2H), 1.80 – 1.68 (m, 2H), 1.63 – 1.53 (m, 1H), 1.53 – 1.42 (m, 1H), 1.46 (s, 9H), 1.38 (d, $J = 7.1$ Hz, 3H), 1.34 – 1.21 (m, 2H), 1.13 – 0.98 (m, 2H), 0.90 (t, $J = 7.3$ Hz, 3H). ^{13}C NMR (101 MHz, CDCl_3) δ 172.58, 171.12, 88.47, 81.99, 48.56, 43.36, 38.46, 38.26, 32.36, 28.02, 24.94, 24.51, 22.34, 18.57, 12.64. Compound **40** was tentatively assigned using HRMS.



((R)-3-((1S,2R)-2-nitrocyclohexyl)pentanoyl)-D-alanine 41

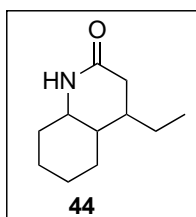
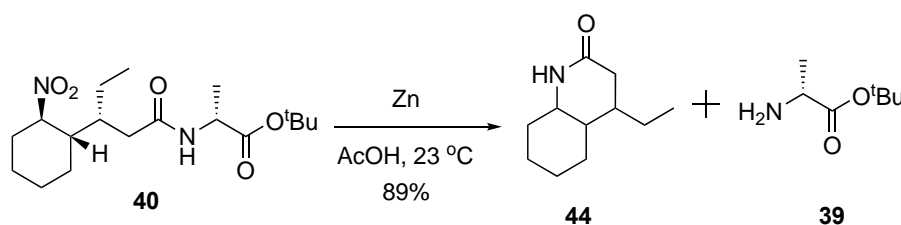
To a solution of **40** (0.15 g, 0.42 mmol) in CH_2Cl_2 (3 mL) was slowly added 3 mL TFA under nitrogen protection, the solution was stirred at room temperature for 1 hour. TFA and CH_2Cl_2 was removed under reduced pressure, then hexane was added to recrystallize the product to get a white solid with 89% yield. ^1H NMR (400 MHz, CDCl_3) δ 6.76 (d, $J = 7.3$ Hz, 1H), 4.64 (p, $J = 7.4$ Hz, 1H), 4.47 (td, $J = 11.3, 3.9$ Hz, 1H), 2.46 (dd, $J = 14.4, 5.5$ Hz, 1H), 2.30 – 2.10 (m, 2H), 2.03 (t, $J = 11.8$ Hz, 1H), 1.92 – 1.67 (m, 4H), 1.66 – 1.53 (m, 1H), 1.47 (d, $J = 7.2$ Hz, 3H), 1.36 – 1.18 (m, 3H), 1.14 – 0.97 (m, 2H), 0.88 (t, $J = 7.4$ Hz, 3H). ^{13}C NMR (101 MHz, CDCl_3) δ 176.16, 173.68, 88.52, 48.43, 43.44, 38.57, 37.92, 32.37, 24.85, 24.49, 24.37, 22.27, 17.86, 12.55. Compound **41** was tentatively assigned using HRMS.



$\text{NO}_2\text{-AChPA-D-Ala-D-Ala}\cdot(\text{CH}_2\text{OTBS})$ 45

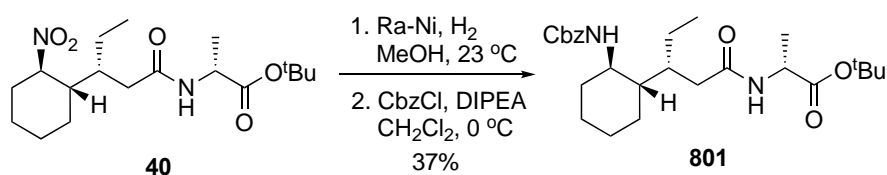
45 (0.62 g, 2.06 mmol) was added to the solution of the crude hydrogenated product from **40**, EDCI (0.43 mL, 2.47 mmol), HOBT (0.38 g, 2.47 mmol), DIEA (0.51 mL, 3.09 mmol) in 20 mL CH_2Cl_2 . The resulting solution was stirred at room temperature overnight. EtOAc was added to the solution, then washed with aqueous citric acid, aqueous saturated NaHCO_3 and brine, the organic layer was dried over MgSO_4 , filtered and concentrated. The

residue was purified via column chromatography eluting with EtOAc/hexane to give the desired product in 31% yield over two steps. ^1H NMR (400 MHz, CDCl_3) δ 6.59 (d, $J = 7.3$ Hz, 1H), 6.15 (d, $J = 7.5$ Hz, 1H), 4.62 – 4.32 (m, 3H), 2.35 (dd, $J = 14.4, 5.4$ Hz, 1H), 2.26 – 2.19 (m, 1H), 2.11 – 2.05 (m, 2H), 1.92 – 1.82 (m, 2H), 1.61 (dtq, $J = 9.5, 7.5, 2.5$ Hz, 1H), 1.46 (s, 10H), 1.39 (dd, $J = 7.1, 6.3$ Hz, 6H), 1.26 (d, $J = 5.4$ Hz, 4H), 1.14 – 0.99 (m, 2H), 0.90 (t, $J = 7.3$ Hz, 3H). ^{13}C NMR (101 MHz, CDCl_3) δ 171.77, 171.65, 171.48, 88.39, 82.04, 48.83, 48.69, 43.42, 38.30, 38.21, 32.30, 27.96, 24.89, 24.45, 24.42, 22.25, 18.40, 12.57. Compound **45** was tentatively assigned using HRMS.



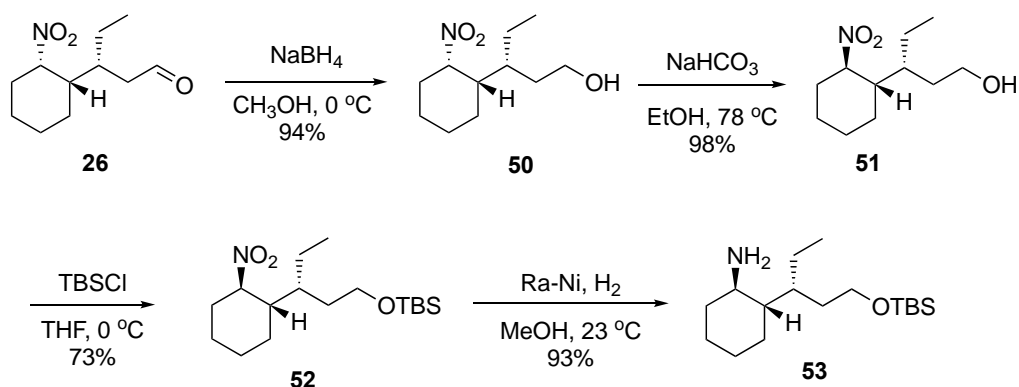
4-ethyloctahydroquinolin-2(1H)-one 44 **40** (0.21 g, 0.59 mmol) was dissolved in 8 mL AcOH at N_2 atmosphere, then Zn powder (0.66 g) was added in several portions over 1.5h, the mixture was stirred under an N_2 atmosphere for two hours at room temperature. The reaction mixture was filtered through a pad of celite and concentrated. The residue was purified

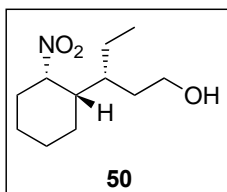
via column chromatography eluting with EtOAc/Dichloromethane to give the desired product in 89% yield. ^1H NMR (400 MHz, CDCl_3) δ 6.90 (s, 1H), 2.88 (td, $J = 10.3, 3.9$ Hz, 1H), 2.47 (dd, $J = 17.8, 5.7$ Hz, 1H), 2.03 – 1.88 (m, 2H), 1.86 – 1.79 (m, 1H), 1.78 – 1.70 (m, 2H), 1.60 (m, 1H), 1.47 (m, 1H), 1.34 – 1.14 (m, 3H), 1.14 – 0.97 (m, 2H), 0.94 – 0.85 (m, 1H), 0.85 – 0.79 (t, $J = 7.44$, 3H). ^{13}C NMR (101 MHz, CDCl_3) δ 172.69, 57.46, 44.10, 38.35, 36.81, 33.43, 27.66, 25.84, 24.44, 24.42, 9.93. Compound **44** was tentatively assigned using HRMS.



40 (0.21 g, 0.59 mmol) was dissolved in 8 mL MeOH, then the Raney Nickel (1 g) was added, and the flask was flushed with H₂, the mixture was stirred under a hydrogen balloon for 2 hours at room temperature. After quickly filtration, the solvent was removed immediately under reduced pressure to afford a residue, the residue was dissolved in anhydrous CH₂Cl₂ under N₂ atmosphere, the solvent was cooled to 0 °C, DIPEA (0.10 mL, 0.70 mmol) was added, then benzyl chloroformate was added dropwise. The mixture was reacted at room temperature overnight. Methanol was added, and the solution was concentrated under reduced pressure and purified via column chromatography eluting with EtOAc/hexane to give the desired product as a yellow oil in 37% yield. ¹H NMR (400 MHz, CDCl₃) δ 7.34 – 7.20 (m, 5H), 6.00 (d, J = 7.5 Hz, 1H), 5.13 – 4.92 (m, 3H), 4.37 (p, J = 7.2 Hz, 1H), 3.38 (tdd, J = 11.0, 8.8, 4.1 Hz, 1H), 2.23 (dd, J = 14.2, 3.6 Hz, 1H), 2.07 – 1.97 (m, 2H), 1.93 (dd, J = 14.2, 10.4 Hz, 1H), 1.57 (dt, J = 14.8, 3.0 Hz, 2H), 1.44 (ddd, J = 13.4, 7.4, 3.3 Hz, 1H), 1.38 (s, 9H), 1.27 (d, J = 7.1 Hz, 3H), 1.20 (dt, J = 6.8, 2.5 Hz, 5H), 1.10 – 0.98 (m, 2H), 0.78 (t, J = 6.2 Hz, 3H). ¹³C NMR (101 MHz, CDCl₃) δ 172.58, 172.57, 156.16, 137.14, 128.45, 127.96, 127.87, 82.00, 66.32, 51.74, 48.63, 45.56, 38.12, 36.48, 34.79, 31.66, 28.03, 25.92, 25.60, 25.37, 22.73, 22.29, 18.60, 14.19, 12.83. Compound **801** was tentatively assigned using HRMS.

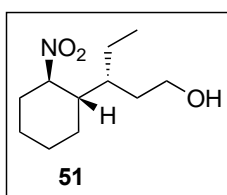
6.2.1.3 Synthesis of δ-Building Block 53





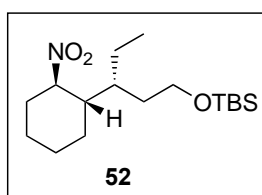
(R)-3-((1S,2S)-2-nitrocyclohexyl)pentan-1-ol 50 To a stirred solution of **26** (0.5 g, 2.34 mmol) in MeOH (30 mL) at 0 °C was added NaBH₄ (0.24 g, 7.03 mmol). The mixture was stirred for a few minutes. The mixture was slowly poured into a 200 mL beaker containing 50 mL 1M NH₄Cl at

0 °C, and the resulting mixture was extracted with EtOAc, the organic layers were collected, washed with brine, dried over MgSO₄ filtered and concentrated. The residue was purified via column chromatography eluting with EtOAc/hexane to give a colourless oil in 94% yield. ¹H NMR (400 MHz, CDCl₃) δ 4.89 (q, J = 3.5 Hz, 1H), 3.77 – 3.40 (m, 2H), 2.27 – 2.16 (m, 1H), 1.82 (dddd, J = 13.3, 8.0, 6.7, 4.0 Hz, 1H), 1.75 – 1.59 (m, 5H), 1.57 – 1.49 (m, 2H), 1.48 – 1.15 (m, 5H), 0.76 (t, J = 7.4 Hz, 3H). ¹³C NMR (101 MHz, CDCl₃) δ 84.23, 60.82, 42.11, 37.13, 32.31, 30.84, 25.47, 23.56, 21.78, 20.18, 9.63. Optical rotation [α]²⁵_D +1.00 (c 1.00, CHCl₃). Compound **50** was tentatively assigned using HRMS.



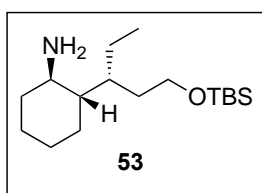
(R)-3-((1S,2R)-2-nitrocyclohexyl)pentan-1-ol 51 To **50** (0.51 g, 2.37 mmol) and NaHCO₃ (1.9 g, 23.70 mmol) was added 30 mL absolute ethanol, the mixture was refluxed for 3 hours. Then the mixture was filtered through filter paper and the filtrate was concentrated to give the

desired product in 98% yield. ¹H NMR (400 MHz, CDCl₃) δ 4.50 (td, J = 11.4, 4.1 Hz, 1H), 3.64 (t, J = 6.9 Hz, 2H), 2.25 (dddd, J = 12.0, 6.3, 3.0, 1.4 Hz, 1H), 2.04 (dddd, J = 13.0, 11.3, 3.5, 2.1 Hz, 1H), 1.93 – 1.83 (m, 2H), 1.82 – 1.74 (m, 2H), 1.67 (dtd, J = 13.9, 7.5, 4.2 Hz, 1H), 1.48 – 1.37 (m, 2H), 1.32 – 1.23 (m, 2H), 1.15 (dddd, J = 12.5, 9.4, 5.1, 2.6 Hz, 1H), 1.10 – 0.99 (m, 2H), 0.89 (t, J = 7.2 Hz, 3H). ¹³C NMR (101 MHz, CDCl₃) δ 88.91, 61.29, 43.59, 37.01, 33.65, 32.63, 25.19, 24.71, 24.16, 22.59, 12.93. Optical rotation [α]²⁵_D -58.00 (c 1.00, CHCl₃). HRMS of this compound was unable to be obtained on Waters Xevo G2-XS QToF Quadrupole Time-of-Flight Mass Spectrometer.



tert*-butyldimethyl(((*R*)-3-((1*S*,2*R*)-2-nitrocyclohexyl)pentyl)oxy) silane **52* To a solution of **51** (0.51 g, 2.37 mmol) and imidazole (0.32 g, 4.74 mmol) in THF (20 mL) was added *tert*-butylchlorodimethylsilane (0.71g, 4.74 mmol) in THF (4 mL) at 0 °C.

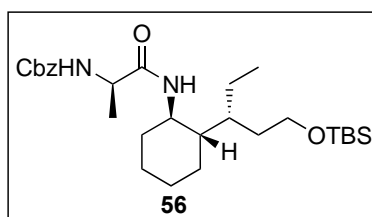
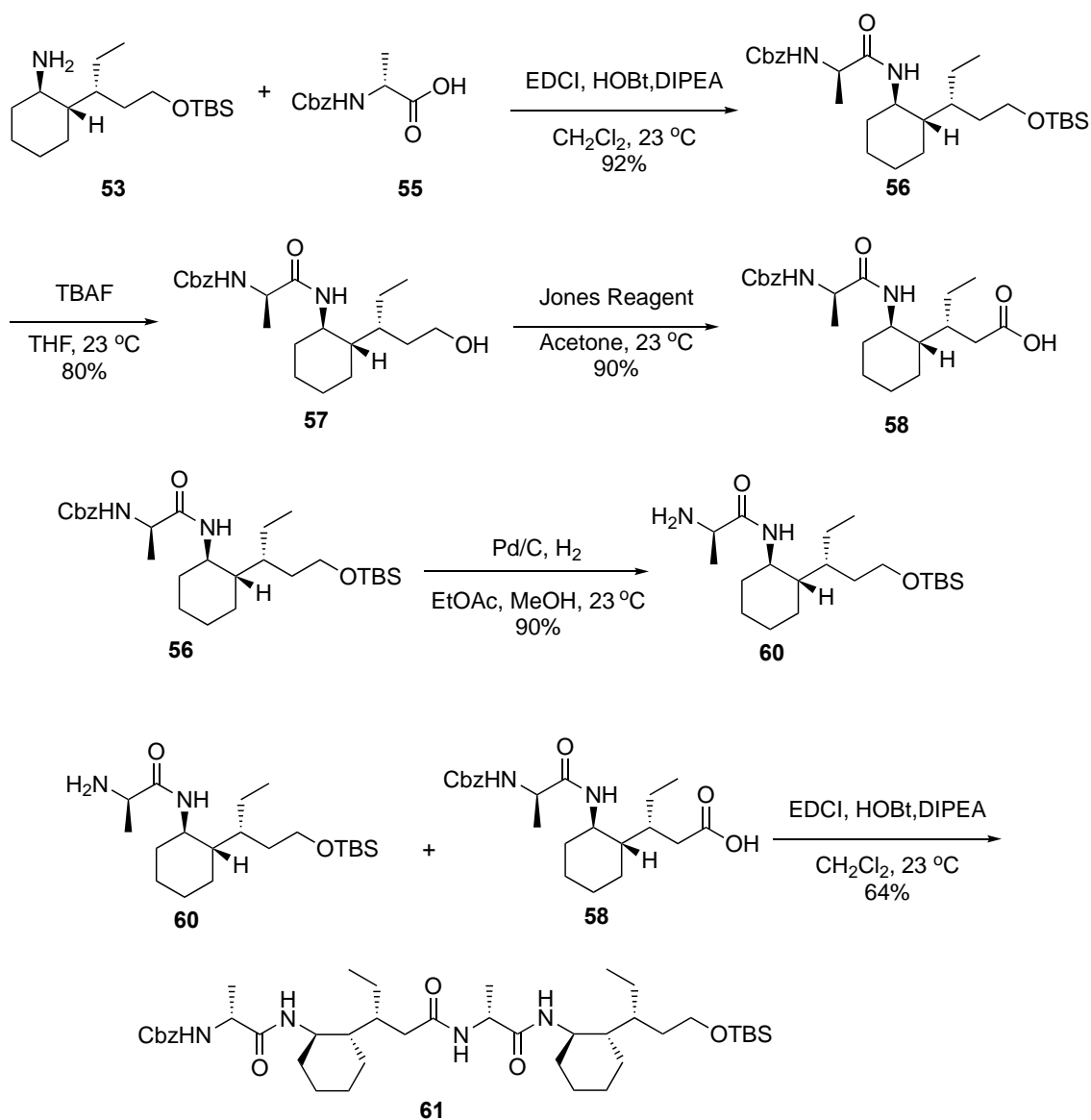
Cooling was removed after 30 min, after stirring overnight at rt, the saturated aqueous NH₄Cl (15 mL) was added, and the mixture was extracted with CH₂Cl₂, dried with MgSO₄ and concentrated, the crude product was purified via column chromatography eluting with EtOAc/hexane to give the desired product in 73% yield. ¹H NMR (400 MHz, CDCl₃) δ 4.49 (td, J = 11.3, 4.0 Hz, 1H), 3.57 (ddt, J = 10.2, 7.4, 3.6 Hz, 2H), 2.29 – 2.17 (m, 1H), 2.11 – 2.01 (m, 1H), 1.93 – 1.71 (m, 4H), 1.68 – 1.54 (m, 1H), 1.49 – 1.36 (m, 2H), 1.27 (tq, J = 9.0, 2.8 Hz, 2H), 1.14 (dddd, J = 14.5, 12.2, 6.1, 3.4 Hz, 1H), 1.09 – 0.96 (m, 2H), 0.89 (d, J = 2.4 Hz, 12H), 0.05 (s, 6H). ¹³C NMR (101 MHz, CDCl₃) δ 88.83, 61.92, 43.99, 37.48, 34.05, 32.49, 26.08, 25.25, 24.72, 24.41, 22.54, 18.40, 12.95, -5.23. Optical rotation [α]²⁵_D -31.00 (c 1.00, CHCl₃). HRMS of this compound was unable to be obtained on Waters Xevo G2-XS QToF Quadrupole Time-of-Flight Mass Spectrometer.



(1*R*,2*S*)-2-((*R*)-1-((*tert*-butyldimethylsilyl)oxy)pentan-3-yl)cyclohexan-1-amine **R17 52** (0.55 g, 1.67 mmol) was dissolved in 25 mL MeOH, then Raney Nickel (1 g) was added and the flask was sparged with H₂, the mixture was stirred under two H₂ balloons for two

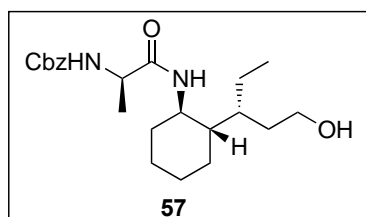
hours at room temperature. The reaction mixture was filtered through a pad of celite and concentrated to give a crude product in 93% yield. ¹H NMR (400 MHz, CDCl₃) δ 3.74 – 3.51 (m, 2H), 2.58 – 2.50 (m, 1H), 1.90 – 1.81 (m, 1H), 1.75 – 1.54 (m, 5H), 1.50 – 1.39 (m, 2H), 1.23 – 1.01 (m, 4H), 1.01 – 0.85 (m, 14H), 0.04 (s, 6H). ¹³C NMR (101 MHz, CDCl₃) δ 62.29, 51.59, 48.68, 37.39, 35.72, 34.47, 26.58, 26.12, 25.89, 25.08, 22.14, 18.45, 13.30, -5.10. HRMS-ESI (m/z) calc'd for C₁₇H₃₇NOSi [M+H]⁺, 300.2717; found, 300.2732. Optical rotation [α]²⁵_D -30.00 (c 1.00, CHCl₃).

6.2.1.4 Synthesis of D-alanine Constructed Hexamer with TBS-Protected Alcohol at C-terminus



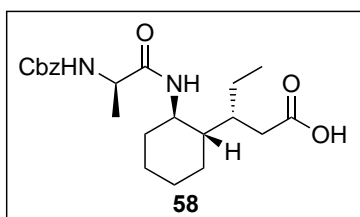
Cbz-D-Ala-AChPA•(CH₂OTBS) 56 Cbz-Ala-OH (0.36 g, 1.60 mmol) was added to the solution of **53** (0.43 g, 1.45 mmol), EDCI (0.31 mL, 1.3 mmol), HOBt (0.27 g, 1.3 mmol) in 10 mL CH₂Cl₂. The resulting solution was stirred at room temperature overnight. EtOAc was added to the solution, then

washed with aqueous citric acid, aqueous saturated NaHCO_3 and brine, the organic layer was dried over MgSO_4 , filtered and concentrated. The residue was purified via column chromatography eluting with EtOAc /hexane to give the desired product as a white solid in 92% yield. ^1H NMR (400 MHz, CDCl_3) δ 7.35 (d, $J = 3.7$ Hz, 5H), 5.57 (d, $J = 9.3$ Hz, 1H), 5.47 (d, $J = 7.3$ Hz, 1H), 5.10 (s, 2H), 4.14 (t, $J = 7.3$ Hz, 1H), 3.88 – 3.69 (m, 1H), 3.61 (t, $J = 6.6$ Hz, 2H), 1.95 (t, $J = 7.4$ Hz, 1H), 1.69 (d, $J = 9.1$ Hz, 2H), 1.59 (dp, $J = 11.0, 4.0$ Hz, 1H), 1.47 (qd, $J = 7.1, 4.3$ Hz, 2H), 1.37 (d, $J = 7.0$ Hz, 4H), 1.32 – 1.21 (m, 4H), 1.14 – 1.01 (m, 2H), 0.90 (m, 10H), 0.82 (t, $J = 7.1$ Hz, 3H), 0.06 (d, $J = 0.9$ Hz, 6H). ^{13}C NMR (101 MHz, CDCl_3) δ 171.12, 155.79, 136.32, 128.54, 128.16, 128.02, 66.86, 62.13, 53.44, 50.69, 49.76, 45.65, 36.20, 34.44, 33.92, 26.00, 25.40, 25.18, 22.37, 19.43, 18.35, 13.06, -5.18. HRMS-ESI (m/z) calc'd for $\text{C}_{28}\text{H}_{48}\text{N}_2\text{O}_4\text{Na}$ $[\text{M}+\text{Na}]^+$, 527.3276; found, 527.3295.



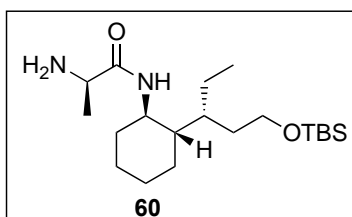
Cbz-D-Ala-AChPA-(CH₂OH) 57 TBAF (1.20 mL, 1 M in THF, 1.30 mmol) and acetic acid (0.09 mL, 1.62 mmol) was added to a stirred solution of **56** (0.41 g, 0.81 mmol) in THF (20 mL) at 0 °C under nitrogen atmosphere. After addition, the reaction mixture was brought to room temperature and stirred

for 1 h. The reaction mixture was quenched with brine and extracted with EtOAc , the organic layer was dried over MgSO_4 , filtered and concentrated. The residue was purified via column chromatography eluting with EtOAc /hexane to give the desired product in 80% yield. ^1H NMR (400 MHz, CDCl_3) δ 7.40 – 7.29 (m, 5H), 6.08 (d, $J = 9.2$ Hz, 1H), 5.43 (d, $J = 7.2$ Hz, 1H), 5.10 (s, 2H), 4.21 – 4.12 (m, 1H), 3.74 (qd, $J = 10.8, 10.0, 3.1$ Hz, 1H), 3.67 – 3.56 (m, 2H), 1.99 – 1.92 (m, 1H), 1.76 – 1.59 (m, 3H), 1.59 – 1.45 (m, 2H), 1.38 (d, $J = 7.1$ Hz, 3H), 1.36 – 1.23 (m, 5H), 1.10 (dq, $J = 14.9, 12.5, 2.9$ Hz, 2H), 0.99 – 0.90 (m, 1H), 0.85 (q, $J = 7.2, 5.9$ Hz, 3H). ^{13}C NMR (101 MHz, CDCl_3) δ 171.34 (d, $J = 6.9$ Hz), 156.19, 136.27, 128.69, 128.37, 128.18, 67.21, 61.05, 60.53, 51.06, 49.89, 45.34, 35.42, 34.37, 33.73, 26.10, 25.53, 25.15, 22.64, 19.12, 13.12. HRMS-ESI (m/z) calc'd for $\text{C}_{22}\text{H}_{35}\text{N}_2\text{O}_4$ $[\text{M}+\text{H}]^+$, 391.2592; found, 391.2608.



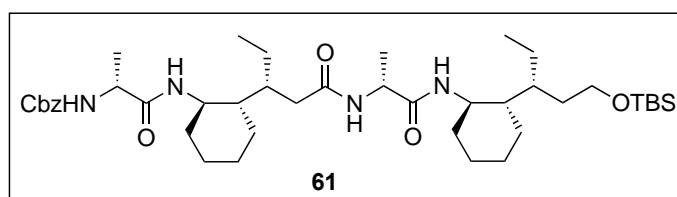
Cbz-D-Ala-AChPA•(COOH) 58 A solution of **57** (0.20 g, 0.51 mmol) and acetone (5 mL) was placed in a round-bottle flask under nitrogen and cooled to 0 °C. To the stirred solution was added dropwise a solution consisting of Jones reagent (0.5 mL, 2 M) and 2 mL of acetone. The solution was reacted at 0 °C for

10 min. Isopropyl alcohol was added dropwise to destroy excess Jones reagent, the green precipitate was filtered. The filtrate was evaporated and 60 mL EtOAc was added, the solution was washed with brine for 2 times, dried over MgSO₄, filtered and concentrated to give a desired product in 90% yield. ¹H NMR (400 MHz, CDCl₃) δ 7.35 (d, J = 4.7 Hz, 5H), 6.46 (d, J = 9.1 Hz, 1H), 6.28 (s, 1H), 5.86 (d, J = 7.8 Hz, 1H), 5.18 – 5.05 (m, 2H), 4.35 (t, J = 7.3 Hz, 1H), 3.77 (d, J = 11.6 Hz, 1H), 2.55 – 2.41 (m, 1H), 2.30 – 2.15 (m, 1H), 1.96 (d, J = 13.0 Hz, 2H), 1.71 (d, J = 16.3 Hz, 3H), 1.43 (d, J = 7.0 Hz, 3H), 1.31 – 1.27 (m, 3H), 1.08 (d, J = 11.2 Hz, 2H), 0.92 – 0.87 (m, 4H). ¹³C NMR (101 MHz, CDCl₃) δ 178.02, 172.30, 156.15, 136.22, 128.54, 128.17, 127.92, 66.99, 50.72, 49.66, 45.86, 36.00, 35.29, 33.86, 29.70, 25.80, 25.23, 21.51, 19.35, 12.77. HRMS-ESI (m/z) calc'd for C₂₂H₃₃N₂O₅ [M+H]⁺, 405.2384; found, 405.2400.



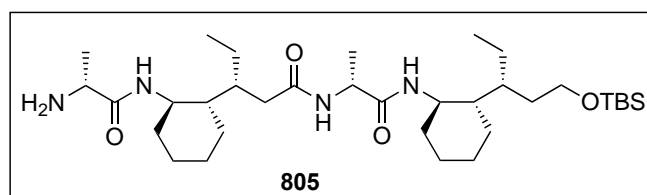
NH₂-D-Ala-AChPA•(CH₂OTBS) 60 Pd/C (24 mg) was added to a solution of **56** (0.24 g, 0.46 mmol) in EtOAc (5 mL), then MeOH (10 mL) was added, the solution was sparged with H₂. The mixture was stirred under hydrogen atmosphere at room temperature for 1.5 h. The reaction mixture was filtered through

a pad of celite and concentrated to give a desired product in 90% yield. ¹H NMR: (400 MHz, CDCl₃) δ 6.85 (d, J = 9.6 Hz, 1H), 3.80 – 3.69 (m, 1H), 3.61 (ddd, J = 7.4, 6.0, 1.6 Hz, 2H), 3.45 (q, J = 6.9 Hz, 1H), 2.01 – 1.93 (m, 1H), 1.76 – 1.63 (m, 2H), 1.59 (ddt, J = 13.5, 7.2, 3.6 Hz, 1H), 1.48 (tdd, J = 13.2, 7.0, 4.0 Hz, 2H), 1.41 – 1.33 (m, 1H), 1.31 (d, J = 6.9 Hz, 3H), 1.27 – 1.24 (m, 3H), 1.19 – 1.01 (m, 3H), 0.99 – 0.91 (m, 1H), 0.89 (s, 9H), 0.88 – 0.86 (m, 1H), 0.83 (t, J = 7.2 Hz, 4H), 0.05 (s, 6H). ¹³C NMR: (101 MHz, CDCl₃) δ 174.66, 61.98, 50.81, 49.08, 45.68, 36.08, 34.59, 34.04, 26.13, 26.00, 25.49, 25.36, 22.40, 21.97, 18.32, 13.11, -5.19. Compound **60** was tentatively assigned using HRMS.



Cbz-D-Ala-AChPA-D-Ala-AChPA•
(CH₂OTBS) 61 58 (0.12 g, 0.30 mmol) was added to the solution of **60** (0.11 g, 0.30 mmol), EDCI (0.06 mL,

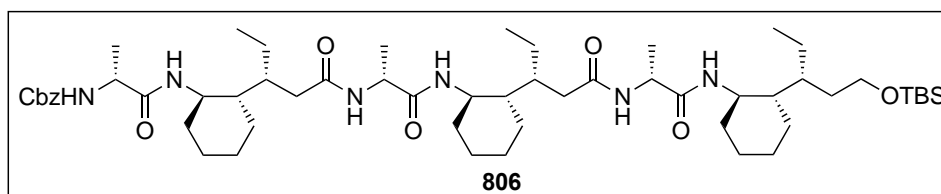
0.36 mmol), HOBt (0.06 g, 1.3 mmol) in 5 mL CH₂Cl₂. The resulting solution was stirred at room temperature overnight. EtOAc was added to the solution, then washed with aqueous citric acid, aqueous saturated NaHCO₃ and brine, the organic layer was dried over MgSO₄, filtered and concentrated. The residue was purified via column to give the desired product as a white solid in 64% yield. ¹H NMR: (400 MHz, CDCl₃) δ 7.30 – 7.22 (m, 5H), 6.60 (d, J = 8.4 Hz, 1H), 6.50 (d, J = 7.4 Hz, 1H), 5.91 (d, J = 9.5 Hz, 1H), 5.79 – 5.66 (m, 1H), 5.03 (s, 2H), 4.35 (p, J = 7.0 Hz, 1H), 4.20 (q, J = 7.2 Hz, 1H), 3.72 (qd, J = 10.8, 3.9 Hz, 1H), 3.58 – 3.53 (m, 3H), 2.27 – 2.17 (m, 1H), 1.97 – 1.82 (m, 4H), 1.71 – 1.45 (m, 7H), 1.43 – 1.35 (m, 6H), 1.29 (d, J = 6.9 Hz, 3H), 1.20 (t, J = 7.1 Hz, 4H), 1.03 (qd, J = 12.0, 6.5 Hz, 6H), 0.84 (s, 12H), 0.78 (m, J = 7.1, 2.9 Hz, 6H), -0.00 (s, J = 1.0 Hz, 6H). ¹³C NMR: (101 MHz, CDCl₃) δ 172.84, 171.77, 171.42, 155.77, 136.59, 128.54, 128.08, 127.97, 66.71, 62.16, 60.47, 50.22, 49.76, 49.03, 45.89, 45.77, 38.12, 36.33, 36.27, 34.58, 34.21, 34.06, 26.07, 25.94, 25.47, 25.34, 25.23, 22.47, 22.17, 21.12, 19.76, 19.43, 18.41, 14.27, 13.20, 13.04, -5.09. Compound **61** was tentatively assigned using HRMS.



NH₂-D-Ala-AChPA-D-Ala-AChPA•
(CH₂OTBS) 805 Pd/C (15 mg) was added to a solution of **61** (0.15 g, 0.20 mmol) in EtOAc (2 mL), then MeOH (4

mL) was added, the solution was sparged with H₂. The mixture was stirred under hydrogen atmosphere at room temperature for 1.5 h. The reaction mixture was filtered through a pad of celite and concentrated to give a desired product in 87% yield. ¹H NMR (400 MHz, Chloroform-d) δ 7.04 (d, J = 9.3 Hz, 1H), 6.35 (dd, J = 7.6, 2.9 Hz, 1H), 5.79 (d, J = 8.6 Hz, 1H), 4.38 (p, J = 7.0 Hz, 1H), 3.83 – 3.65 (m, 2H), 3.61 (dd, J = 7.0, 5.9 Hz, 2H), 3.51 (q, J = 6.9 Hz, 1H), 2.31 (dd, J = 14.4, 3.6 Hz, 1H), 2.26 – 2.10 (m, 2H), 2.01 – 1.88 (m, 3H), 1.77 – 1.64 (m, 5H), 1.64 – 1.37 (m, 7H), 1.37 (s, 3H), 1.31 (d, J = 6.9 Hz, 4H), 1.29 – 1.01 (m, 11H),

1.01 – 0.89 (m, 9H), 0.83 (q, $J = 7.5$ Hz, 6H), 0.05 (s, 6H). ^{13}C NMR: (101 MHz, CDCl_3) δ 175.28, 172.76, 171.39, 62.08, 51.01, 49.88, 49.11, 49.02, 46.08, 45.70, 38.32, 36.74, 36.19, 34.73, 34.38, 34.06, 26.12, 26.09, 26.04, 25.52, 25.46, 25.42, 25.27, 22.47, 22.27, 21.92, 19.32, 18.47, 13.24, 13.01, -5.04. Compound **805** was tentatively assigned using HRMS.

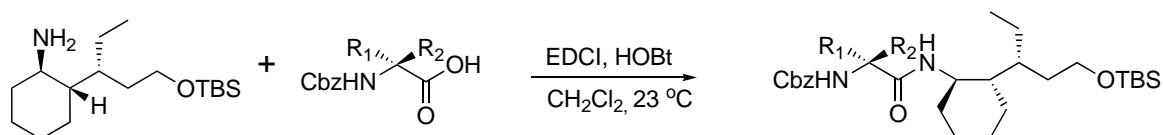


NH₂-D-Ala-
AChPA-D-Ala-
AChPA-D-Ala-
AChPA

•(**CH₂OTBS**) **806 58** (87 mg, 0.14 mmol) was added to the solution of **805** (68 mg, 0.17 mmol), EDCI (0.03 mL, 0.17 mmol), HOBt (26 mg, 0.17 mmol) in 3 mL CH_2Cl_2 . The resulting solution was stirred at room temperature overnight. EtOAc was added to the solution, then washed with aqueous citric acid, aqueous saturated NaHCO_3 and brine, the organic layer was dried over MgSO_4 , filtered and concentrated. The residue was purified via column to give the desired product as a white solid in 49% yield. ^1H NMR: (400 MHz, CDCl_3) δ 7.44 – 7.17 (m, 5H), 7.12 (d, $J = 8.5$ Hz, 1H), 6.76 (d, $J = 7.3$ Hz, 1H), 6.71 (d, $J = 8.1$ Hz, 1H), 6.53 (m, $J = 9.6$ Hz, 2H), 5.96 (d, $J = 7.4$ Hz, 1H), 5.05 (s, $J = 3.4$ Hz, 2H), 4.56 – 4.46 (m, 2H), 4.32 (t, $J = 7.0$ Hz, 1H), 3.82 – 3.49 (m, 5H), 2.28 (m, 3H), 2.01– 1.93 (m, 6H), 1.65– 1.54 (m, 10H), 1.46– 1.32 (m, 16H), 1.27– 1.18 (m, 7H), 1.11– 0.97 (m, 8H), 0.87– 0.77 (m, 19H), 0.00 (s, 6H). ^{13}C NMR: (101 MHz, CDCl_3) δ 172.79, 172.63, 171.78, 171.63, 171.43, 155.74, 136.39, 128.47, 127.96, 127.59, 66.52, 62.21, 60.38, 50.63, 50.31, 49.75, 49.45, 48.90, 48.80, 46.26, 46.14, 45.66, 38.68, 37.83, 36.22, 34.44, 34.32, 34.12, 34.07, 29.66, 25.95, 25.47, 25.18, 25.13, 22.41, 22.08, 21.85, 20.03, 19.97, 18.52, 18.29, 14.18, 13.13, 12.96, 12.91, -5.19. Compound **806** was tentatively assigned using HRMS.

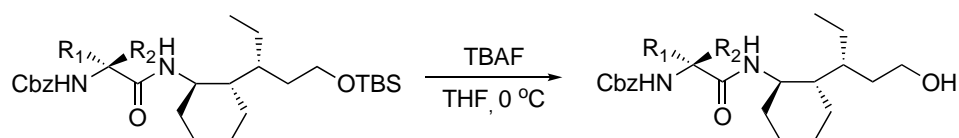
6.2.2 General Procedure for Foldamer Synthesis

6.2.2.1 General Procedure A: Peptide Coupling



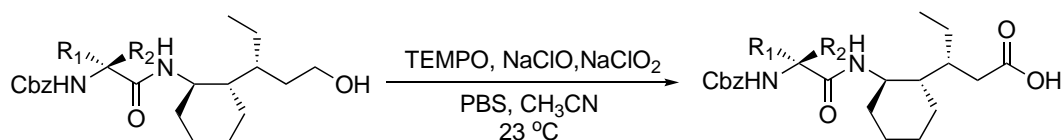
Carboxylic acid (1.60 mmol) was added to the solution of amine (1.45 mmol), EDCI (1.3 mmol), HOBT (1.3 mmol) in 10 mL CH₂Cl₂. The resulting solution was stirred at room temperature overnight. EtOAc was added to the solution, the mixture was washed with aqueous citric acid, aqueous saturated NaHCO₃ and brine, organic layer was dried over MgSO₄, filtered and concentrated. The residue was purified via column chromatography eluting with EtOAc/hexane to give the desired product. Yield (dimer: 80%~95%; tetramer: 65%~75%; hexamer: 50%~60%; octamer: 40%~65%).

6.2.2.2 General Procedure B: TBS-Deprotecting



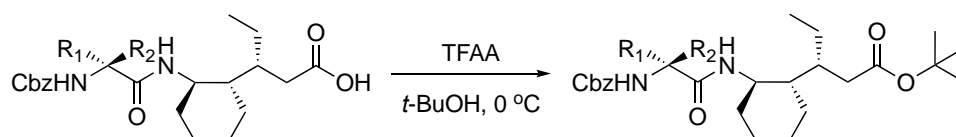
TBAF (1.30 mmol) and acetic acid (1.3 mmol) was added to a stirred solution of tert-butyldimethylsilane (0.81 mmol) in THF (20 mL) at 0 °C under nitrogen atmosphere. After addition, the reaction mixture was brought to room temperature and stirred overnight. The reaction mixture was quenched with brine and extracted with EtOAc, the organic layer was dried over MgSO₄, filtered and concentrated. The residue was purified via column chromatography eluting with EtOAc/hexane to give the desired product. Yield (85%~95%)

6.2.2.3 General Procedure C: Oxidizing Alcohol to Carboxylic Acid



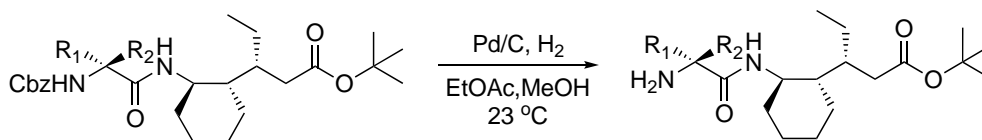
The alcohol compound (4 mmol) and Tempo (0.28 mmol) were dissolved in 20 mL of acetonitrile and 15 mL of 0.67M of sodium phosphate buffer (pH 6.7). 4 mL of sodium chlorite (2M in water) and 2 mL of sodium hypochlorite (0.3 % in water) were added simultaneously over 30 minutes, and the mixture was stirred at room temperature for another 30 minutes. The reaction mixture was quenched with sodium sulfite solution and extracted with ethyl acetate, the organic layer was dried over MgSO₄, filtered and concentrated. The crude product was carried on without further purification. Yield (92%~97%)

6.2.2.4 General Procedure D: Protecting Carboxylic Acid with *tert*-Butyl Ester



TFA anhydride (10 mmol) was added dropwise to a solution of carboxylic acid (2 mmol) in *tert*-butyl alcohol (20 mL) at 0 °C under nitrogen atmosphere. The mixture was brought to room temperature and reacted overnight, the mixture was quenched with saturated aqueous sodium bicarbonate, extracted with ethyl acetate, organic layer was dried over MgSO₄, filtered and concentrated. The residue was purified via column chromatography eluting with EtOAc/hexane to give the desired product. Yield (50%~56%)

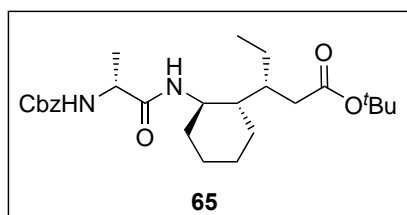
6.2.2.5 General Procedure E: Cbz-Deprotection



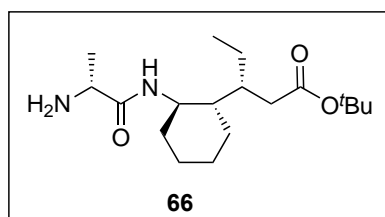
Benzyl ester compound (0.5 g) and Pd/C (50 mg) were dissolved in 10 mL of ethyl acetate and 10 mL of methanol, the reaction atmosphere was exchanged with hydrogen three times, and reacted under hydrogen over 2h at room temperature. The reaction mixture was filtered through a pad of celite, washed with ethyl acetate, and the organic layer was dried over MgSO₄, filtered

and concentrated. The crude product was carried on without further purification. Yield (90%~95%)

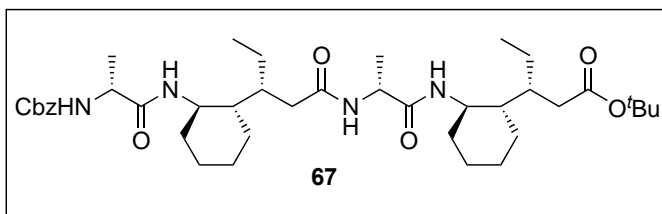
6.2.3 Synthesis of Foldamer 72



Cbz-D-Ala-AChPA-O'Bu 65 Following general procedure D, **65** was collected as a white solid in 55% yield. ^1H NMR (400 MHz, CDCl_3) δ 7.39 – 7.27 (m, 5H), 6.12 (d, $J = 8.9$ Hz, 1H), 5.64 (d, $J = 7.7$ Hz, 1H), 5.08 (d, $J = 3.2$ Hz, 2H), 4.22 (p, $J = 7.1$ Hz, 1H), 3.69 (tdd, $J = 11.0, 8.6, 4.1$ Hz, 1H), 2.29 (dd, $J = 16.0, 4.1$ Hz, 1H), 2.12 – 1.96 (m, 2H), 1.94 – 1.84 (m, 1H), 1.75 – 1.61 (m, 3H), 1.53 – 1.37 (m, 13H), 1.35 – 1.17 (m, 3H), 1.06 (q, $J = 12.5, 11.9$ Hz, 3H), 0.98 – 0.87 (m, 1H), 0.82 (t, $J = 7.2$ Hz, 3H). ^{13}C NMR (101 MHz, CDCl_3) δ 173.56, 171.59, 155.81, 136.54, 128.56, 128.40, 128.14, 128.08, 80.46, 66.83, 50.78, 50.00, 46.09, 37.43, 36.23, 34.28, 28.25, 26.04, 25.27, 25.11, 21.82, 19.71, 12.90. HRMS-ESI (m/z) calc'd for $\text{C}_{26}\text{H}_{40}\text{N}_2\text{O}_5\text{Na}$ $[\text{M}+\text{Na}]^+$, 483.2830; found, 483.2869.



NH_2 -D-Ala-AChPA-OtBu 66 Following general procedure E, NH_2 -D-Ala-AChPA-OtBu was collected as a white solid in 95% yield. ^1H NMR: (400 MHz, CDCl_3) δ 7.00 – 6.84 (m, 1H), 3.71 (tdd, $J = 11.0, 9.4, 4.1$ Hz, 1H), 3.52 – 3.43 (m, 1H), 2.29 (dd, $J = 15.4, 4.5$ Hz, 1H), 2.06 (d, $J = 10.1$ Hz, 1H), 2.02 – 1.93 (m, 1H), 1.88 (dddt, $J = 10.5, 7.1, 4.2, 2.4$ Hz, 1H), 1.77 – 1.61 (m, 4H), 1.51 – 1.42 (dq, $J = 12.7, 7.2, 3.1$ Hz, 3H), 1.43 (s, 9H), 1.31 (d, $J = 6.9$ Hz, 3H), 1.20 – 0.98 (m, 4H), 0.99 – 0.86 (m, 1H), 0.82 (t, $J = 7.2$ Hz, 3H). ^{13}C NMR: (101 MHz, CDCl_3) δ 174.96, 173.42, 80.13, 50.86, 48.96, 46.29, 37.54, 36.56, 34.41, 28.16, 26.03, 25.34, 25.10, 21.86, 21.81, 12.77. Compound **66** was tentatively assigned using HRMS.

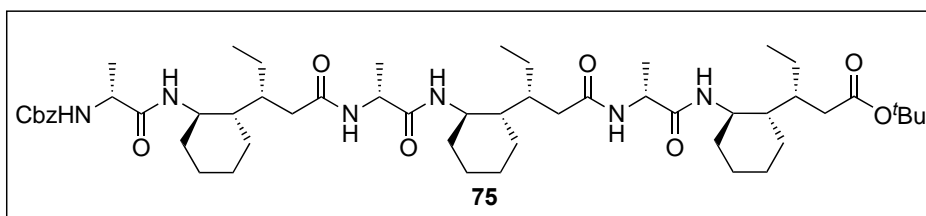


Cbz-D-Ala-AChPA-D-Ala-AChPA-

O^tBu 67 Following general procedure

A, **67** was collected as a white solid in 67% yield. ¹H NMR (400 MHz, CDCl₃) δ 7.30 – 7.15 (m, 5H), 6.90 (d, J = 8.2 Hz, 1H), 6.76 (d, J = 7.4 Hz, 1H), 6.53 (d, J = 8.8 Hz, 1H), 5.88 (d, J = 7.6 Hz, 1H), 5.13 – 4.88 (m, 2H), 4.41 (p, J = 7.0 Hz, 1H), 4.19 (p, J = 7.0 Hz, 1H), 3.60 (dddd, J = 23.4, 15.2, 13.2, 7.6 Hz, 2H), 2.23 (dd, J = 15.8, 4.5 Hz, 2H), 2.05 – 1.79 (m, 6H), 1.70 – 1.48 (m, 6H), 1.46 – 1.28 (m, 17H), 1.25 – 1.12 (m, 4H), 1.10 – 0.93 (m, 6H), 0.93 – 0.80 (m, 2H), 0.76 (td, J = 7.2, 3.2 Hz, 6H). ¹³C NMR (101 MHz, CDCl₃) δ 173.52, 172.82, 171.83, 171.65, 155.71, 136.54, 128.40, 127.92, 127.85, 80.41, 66.54, 50.65, 50.01, 49.82, 48.94, 46.08, 45.54, 38.03, 37.52, 36.24, 36.15, 34.19, 33.96, 28.12, 25.90, 25.85, 25.21, 25.17, 24.97, 21.96, 21.74, 19.71, 19.32, 12.92, 12.81. HRMS-ESI (m/z) calc'd for C₄₀H₆₄N₄O₇Na [M+Na]⁺, 713.4848; found, 713.4838.

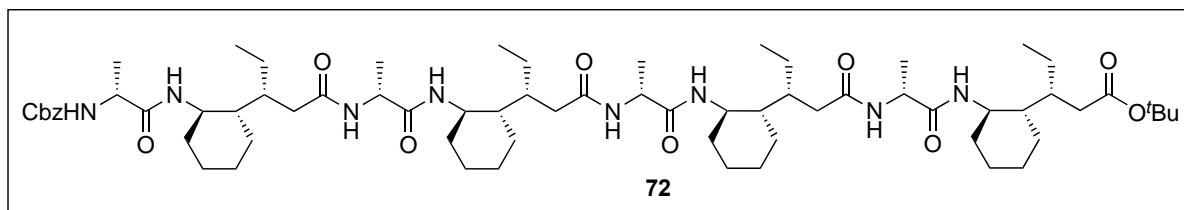
¹H NMR (400 MHz, CDCl₃) δ 7.30 – 7.15 (m, 5H), 6.90 (d, J = 8.2 Hz, 1H), 6.76 (d, J = 7.4 Hz, 1H), 6.53 (d, J = 8.8 Hz, 1H), 5.88 (d, J = 7.6 Hz, 1H), 5.13 – 4.88 (m, 2H), 4.41 (p, J = 7.0 Hz, 1H), 4.19 (p, J = 7.0 Hz, 1H), 3.60 (dddd, J = 23.4, 15.2, 13.2, 7.6 Hz, 2H), 2.23 (dd, J = 15.8, 4.5 Hz, 2H), 2.05 – 1.79 (m, 6H), 1.70 – 1.48 (m, 6H), 1.46 – 1.28 (m, 17H), 1.25 – 1.12 (m, 4H), 1.10 – 0.93 (m, 6H), 0.93 – 0.80 (m, 2H), 0.76 (td, J = 7.2, 3.2 Hz, 6H). ¹³C NMR (101 MHz, CDCl₃) δ 173.52, 172.82, 171.83, 171.65, 155.71, 136.54, 128.40, 127.92, 127.85, 80.41, 66.54, 50.65, 50.01, 49.82, 48.94, 46.08, 45.54, 38.03, 37.52, 36.24, 36.15, 34.19, 33.96, 28.12, 25.90, 25.85, 25.21, 25.17, 24.97, 21.96, 21.74, 19.71, 19.32, 12.92, 12.81. HRMS-ESI (m/z) calc'd for C₄₀H₆₄N₄O₇Na [M+Na]⁺, 713.4848; found, 713.4838.



Cbz-D-Ala-
AChPA-D-Ala-
AChPA-D-Ala-
AChPA-O^tBu 75

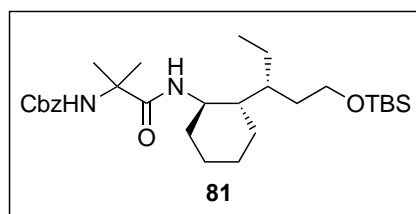
Following general procedure A, **75** was collected as a white solid in 65% yield. ¹H NMR (400 MHz, CDCl₃) δ 7.36 – 7.27 (m, 5H), 6.88 (d, J = 8.5 Hz, 1H), 6.68 (d, J = 8.2 Hz, 1H), 6.51 (d, J = 7.1 Hz, 1H), 6.45 (d, J = 8.8 Hz, 1H), 6.30 (d, J = 7.4 Hz, 1H), 5.81 (d, J = 7.6 Hz, 1H), 5.09 (s, 2H), 4.48 (td, J = 7.1, 4.0 Hz, 2H), 4.30 (t, J = 7.2 Hz, 1H), 3.70 (dq, J = 37.1, 10.1, 9.2 Hz, 3H), 2.38 – 2.23 (m, 6H), 2.11 – 1.94 (m, 8H), 1.92 (d, J = 10.6 Hz, 1H), 1.78 – 1.55 (m, 10H), 1.54 – 1.37 (m, 21H), 1.27 (dd, J = 13.3, 6.7 Hz, 7H), 1.18 – 1.01 (m, 9H), 1.01 – 0.89 (m, 4H), 0.89 – 0.79 (m, 9H). ¹³C NMR (101 MHz, CDCl₃) δ 173.47, 172.74, 172.60, 171.78, 171.63, 171.58, 155.70, 136.51, 128.48, 127.99, 127.81, 80.47, 66.61, 50.65, 50.46, 49.97, 49.09, 48.96, 46.22, 45.83, 45.52, 38.34, 37.83, 37.55, 36.25, 36.07, 34.22, 34.14, 34.08, 28.17, 25.94, 25.24,

25.20, 25.14, 25.01, 21.96, 21.82, 19.97, 19.75, 18.79, 13.00, 12.92, 12.87. HRMS-ESI (m/z) calc'd for $C^{54}H^{89}N^6O^9$ $[M+H]^+$, 987.6505; found, 987.6491.

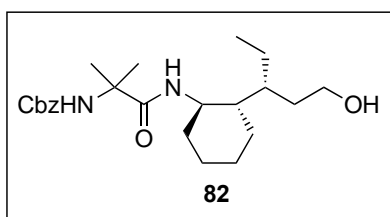


Cbz-D-Ala-AChPA-D-Ala-AChPA-D-Ala-AChPA-D-Ala-AChPA-O'Bu 72 Following general procedure A, octamer **72** was collected as a white solid in 57% yield. 1H NMR (400 MHz, $CDCl_3$) δ 7.42 – 7.27 (m, 5H), 7.01 (d, $J = 8.5$ Hz, 1H), 6.96 (d, $J = 8.0$ Hz, 1H), 6.87 (d, $J = 8.3$ Hz, 1H), 6.60 (d, $J = 7.8$ Hz, 2H), 6.46 (d, $J = 7.4$ Hz, 1H), 6.37 (d, $J = 7.2$ Hz, 1H), 5.92 (d, $J = 7.6$ Hz, 1H), 5.09 (d, $J = 2.9$ Hz, 2H), 4.49 (dt, $J = 13.2, 6.9$ Hz, 3H), 4.33 – 4.18 (m, 1H), 3.87 – 3.54 (m, 4H), 2.49 – 2.23 (m, 4H), 2.18 – 1.86 (m, 12H), 1.80 – 1.55 (m, 12H), 1.53 – 1.36 (m, 25H), 1.34 – 1.21 (m, 9H), 1.22 – 0.92 (m, 16H), 0.91 – 0.74 (m, 12H). ^{13}C NMR (101 MHz, $CDCl_3$) δ 173.59, 173.06, 172.89, 172.77, 172.04, 171.96, 171.88, 155.83, 136.75, 128.58, 128.07, 127.96, 80.53, 77.48, 66.67, 50.79, 50.54, 50.46, 50.06, 49.29, 49.11, 46.37, 45.71, 45.61, 38.25, 38.19, 38.08, 38.08, 37.73, 36.49, 36.44, 36.23, 36.14, 34.30, 34.17, 31.73, 28.29, 26.06, 25.39, 25.27, 25.20, 25.14, 22.79, 22.06, 21.95, 20.11, 19.90, 19.18, 18.98, 14.26, 13.10, 12.98. HRMS-ESI (m/z) calc'd for $C_{68}H_{112}N_8O_{11}Na$ $[M+Na]^+$, 1239.8343; found, 1239.8347.

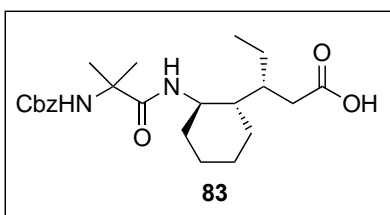
6.2.4 Synthesis of Foldamer **86**



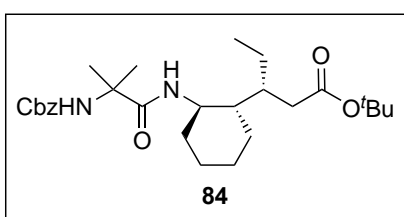
Cbz-Aib-AChPA•(CH₂OTBS) 81 Following general procedure A, **81** was collected as a colourless oil. The crude product was carried on without further purification.



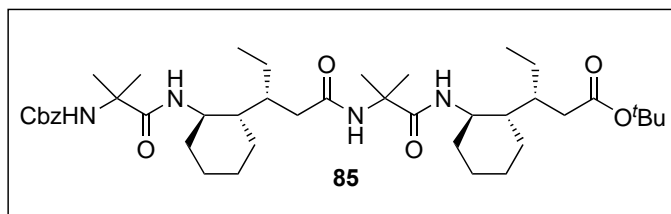
Cbz-Aib-AChPA• (CH₂OH) 82 Following general procedure B, **82** was collected as a colourless oil. The crude product was carried on without further purification.



Cbz-Aib-AChPA-OH 83 Following general procedure C, **83** was collected as a colourless oil in 61% yield over 3 steps. ¹H NMR (400 MHz, CDCl₃) δ 7.39 – 7.26 (m, 5H), 6.26 (b, 1H), 5.80 (b, 1H), 5.09 (d, J = 11.5 Hz, 2H), 3.69 (tdd, J = 11.0, 8.7, 4.1 Hz, 1H), 2.50 – 2.35 (m, 1H), 2.28 – 2.13 (m, 1H), 2.08 – 1.89 (m, 2H), 1.79 – 1.60 (m, 3H), 1.59 – 1.45 (m, 7H), 1.25 (m, J = 7.1 Hz, 2H), 1.15 – 1.03 (m, 2H), 1.03 – 0.89 (m, 2H), 0.84 (t, J = 7.1 Hz, 3H). ¹³C NMR (101 MHz, CDCl₃) δ 178.23, 173.86, 128.64, 128.28, 128.19, 66.56, 50.08, 46.05, 35.88, 35.81, 33.94, 31.07, 29.83, 25.97, 25.28, 25.05, 21.80, 12.93. HRMS-ESI (m/z) calc'd for C₂₃H₃₅N₂O₅ [M+H]⁺, 419.2541; found, 419.2550.

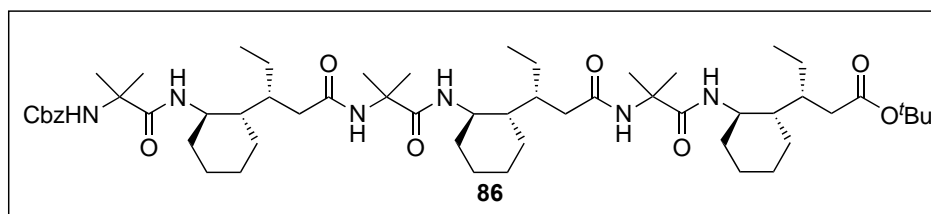


Cbz-Aib-ACPA-O'Bu 84 Following general procedure D, **84** was collected as a white solid in 50% yield. ¹H NMR (400 MHz, CDCl₃) δ 7.41 – 7.27 (m, 5H), 6.33 (d, J = 8.3 Hz, 1H), 5.68 (s, 1H), 5.16 – 5.03 (m, 2H), 3.66 (tdd, J = 11.3, 8.2, 4.2 Hz, 1H), 2.30 (dd, J = 16.3, 3.8 Hz, 1H), 2.13 – 2.02 (m, 2H), 1.97 – 1.85 (m, 1H), 1.70 (m, 3H), 1.57 (m, 6H), 1.44 (m, 10H), 1.32 – 1.22 (m, 2H), 1.16 – 1.04 (m, 2H), 1.02 – 0.87 (m, 2H), 0.83 (t, J = 7.2 Hz, 3H). ¹³C NMR (101 MHz, CDCl₃) δ 173.82, 154.94, 136.72, 128.61, 128.19, 128.16, 80.54, 77.48, 77.16, 76.84, 66.55, 56.90, 50.28, 46.10, 37.41, 36.09, 34.14, 28.31, 26.18, 25.25, 25.22, 21.90, 12.97. HRMS-ESI (m/z) calc'd for C₂₇H₄₃N₂O₅ [M+H]⁺, 475.3167; found, 475.3163.

**Cbz-Aib-AChPA-Aib-AChPA-O^tBu**

85 Following general procedure A, **85** was collected as a white solid in 69% yield over 2 steps. ¹H NMR (400 MHz, CDCl₃) δ 7.30 – 7.16 (m, 5H), 6.78 (d, J = 8.3 Hz, 1H), 6.60 (s, 1H), 6.49 (d, J = 8.0 Hz, 1H), 6.08 (s, 1H), 5.06 – 4.92 (m, 2H), 3.58 (dt, J = 11.4, 7.8, 4.1 Hz, 2H), 2.30 – 2.18 (m, 2H), 2.05 – 1.96 (m, 2H), 1.95 – 1.81 (m, 4H), 1.67 – 1.47 (m, 18H), 1.44 – 1.32 (m, 11H), 1.30 – 1.18 (m, 4H), 1.07 – 0.81 (m, 8H), 0.76 (t, J = 7.2 Hz, 6H). ¹³C NMR (101 MHz, CDCl₃) δ 174.20, 174.10, 173.83, 172.85, 154.78, 136.76, 128.40, 127.88, 127.87, 80.49, 66.15, 56.98, 56.63, 50.45, 50.15, 45.74, 45.02, 38.76, 37.22, 36.51, 35.79, 34.03, 33.96, 28.13, 25.98, 25.22, 25.16, 25.03, 24.63, 22.10, 21.79, 12.92, 12.90. HRMS-ESI (m/z) calc'd for C₄₂H₆₉N₄O₇ [M+H]⁺, 741.5161; found, 741.5180.

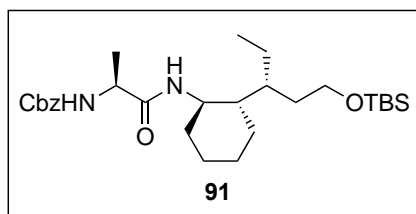
85 Following general procedure A, **85** was collected as a white solid in 69% yield over 2 steps. ¹H NMR (400 MHz, CDCl₃) δ 7.30 – 7.16 (m, 5H), 6.78 (d, J = 8.3 Hz, 1H), 6.60 (s, 1H), 6.49 (d, J = 8.0 Hz, 1H), 6.08 (s, 1H), 5.06 – 4.92 (m, 2H), 3.58 (dt, J = 11.4, 7.8, 4.1 Hz, 2H), 2.30 – 2.18 (m, 2H), 2.05 – 1.96 (m, 2H), 1.95 – 1.81 (m, 4H), 1.67 – 1.47 (m, 18H), 1.44 – 1.32 (m, 11H), 1.30 – 1.18 (m, 4H), 1.07 – 0.81 (m, 8H), 0.76 (t, J = 7.2 Hz, 6H). ¹³C NMR (101 MHz, CDCl₃) δ 174.20, 174.10, 173.83, 172.85, 154.78, 136.76, 128.40, 127.88, 127.87, 80.49, 66.15, 56.98, 56.63, 50.45, 50.15, 45.74, 45.02, 38.76, 37.22, 36.51, 35.79, 34.03, 33.96, 28.13, 25.98, 25.22, 25.16, 25.03, 24.63, 22.10, 21.79, 12.92, 12.90. HRMS-ESI (m/z) calc'd for C₄₂H₆₉N₄O₇ [M+H]⁺, 741.5161; found, 741.5180.

**Cbz-Aib-AChPA-Aib-AChPA-Aib-AChPA-O^tBu**

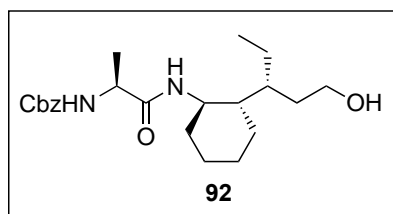
Following

general procedure A, foldamer **86** was collected as a white solid in 52% yield over 2 steps. ¹H NMR (400 MHz, CDCl₃) δ 7.41 – 7.23 (m, 5H), 6.98 (d, J = 7.8 Hz, 1H), 6.84 (d, J = 9.7 Hz, 2H), 6.65 (s, 1H), 6.50 (d, J = 7.9 Hz, 1H), 6.16 (s, 1H), 5.14 – 4.96 (m, 2H), 3.77 – 3.53 (m, 3H), 2.31 (dq, J = 16.7, 3.7, 3.2 Hz, 3H), 2.13 – 1.86 (m, 9H), 1.83 – 1.48 (m, 27H), 1.43 (s, 12H), 1.26 (m, 6H), 1.18 – 0.89 (m, 12H), 0.84 (t, J = 8.2 Hz, 9H). ¹³C NMR (101 MHz, CDCl₃) δ 174.62, 174.24, 174.17, 173.94, 173.01, 172.77, 154.83, 136.91, 128.51, 127.96, 80.65, 66.09, 57.12, 57.04, 56.70, 50.88, 50.64, 50.25, 45.84, 45.14, 44.73, 38.95, 38.59, 37.28, 36.76, 36.58, 35.83, 34.14, 34.10, 28.25, 26.13, 26.08, 25.61, 25.27, 25.25, 25.20, 25.13, 25.11, 25.02, 24.80, 24.40, 22.40, 22.10, 21.92, 13.14, 13.06, 13.05. HRMS-ESI (m/z) calc'd for C₅₇H₉₄N₆O₉Na [M+Na]⁺, 1029.6975; found, 1029.6995.

6.2.5 Synthesis of Foldamer 97

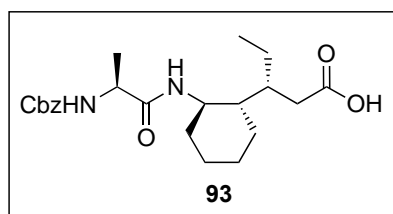


Cbz-L-Ala-AChPA•(CH₂OTBS) 91 Following general procedure A, **91** was collected as a colourless oil. The crude product was carried on without further purification.

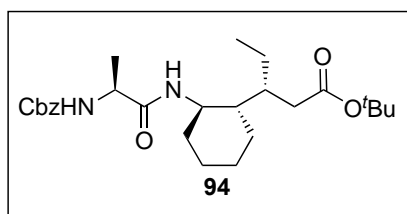


Cbz-L-Ala-AChPA•(CH₂OH) 92 Following general procedure B, **92** was collected as a colourless oil in 72% yield over 2 steps. ¹H NMR (400 MHz, CDCl₃) δ 7.41 – 7.27 (m, 5H), 6.32 (d, J = 9.3 Hz, 1H), 5.62 (d, J = 7.8 Hz, 1H), 5.22 – 4.91 (m, 2H), 4.11 (m, J = 7.1 Hz, 1H), 3.76 (h, J = 9.3, 8.4

Hz, 1H), 3.69 – 3.54 (m, 2H), 1.95 (d, J = 12.3 Hz, 1H), 1.83 – 1.58 (m, 4H), 1.58 – 1.42 (m, 2H), 1.41 – 1.20 (m, 6H), 1.20 – 0.98 (m, 3H), 0.98 – 0.84 (m, 1H), 0.79 (t, J = 7.1 Hz, 3H). ¹³C NMR (101 MHz, CDCl₃) δ 171.78, 156.42, 136.13, 128.67, 128.36, 128.19, 67.25, 60.76, 51.04, 49.88, 45.30, 34.79, 34.35, 33.74, 26.09, 25.52, 24.99, 22.60, 18.15, 13.06. HRMS-ESI (m/z) calc'd for C₂₂H₃₅N₂O₄ [M+H]⁺, 391.2591; found, 391.2608.

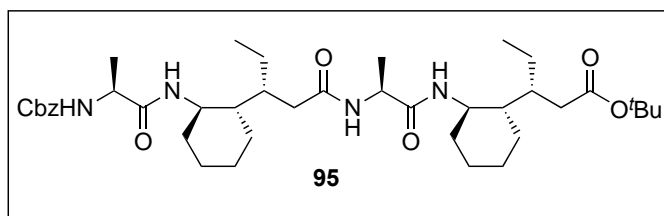


Cbz-L-Ala-AChPA-OH 93 Following general procedure C, **93** was collected as a colourless oil. The crude product was carried on without further purification.



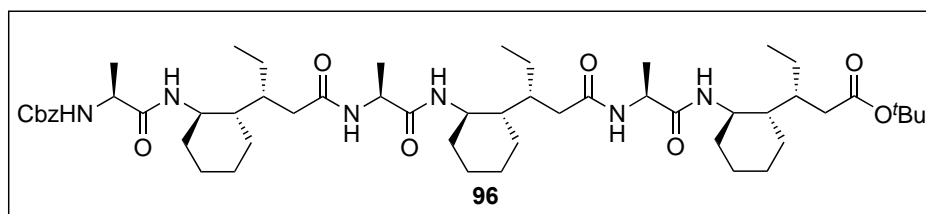
Cbz-L-Ala-AChPA-O'Bu 94 Following general procedure D, **94** was collected as a white solid in 45% yield over 2 steps. ¹H NMR (400 MHz, CDCl₃) δ 7.54 – 7.22 (m, 5H), 6.34 (d, J = 8.7 Hz, 1H), 5.78 (d, J = 8.0 Hz, 1H), 5.20 –

5.06 (m, 2H), 4.29 (p, $J = 7.3$ Hz, 1H), 3.67 (tdd, $J = 10.7, 8.7, 4.1$ Hz, 1H), 2.27 (dd, $J = 16.3, 3.8$ Hz, 1H), 2.11 – 1.97 (m, 2H), 1.86 (td, $J = 10.6, 4.9$ Hz, 1H), 1.77 – 1.57 (m, 3H), 1.52 – 1.32 (m, 13H), 1.23 (t, $J = 7.1$ Hz, 1H), 1.08 (tdd, $J = 24.0, 12.0, 9.7$ Hz, 4), 0.97 – 0.86 (m, 1H), 0.81 (t, $J = 7.2$ Hz, 3H). ^{13}C NMR (101 MHz, CDCl_3) δ 173.78, 171.51, 155.91, 136.38, 128.43, 128.11, 128.05, 80.54, 66.85, 50.77, 49.76, 46.19, 37.27, 35.84, 33.99, 28.08, 25.93, 25.12, 25.04, 21.75, 19.15, 12.78. HRMS-ESI (m/z) calc'd for $\text{C}_{26}\text{H}_{40}\text{N}_2\text{O}_5\text{Na}$ $[\text{M}+\text{Na}]^+$, 483.2830; found, 483.2824.



Cbz-L-Ala-AChPA-L-Ala-ACPA-O^tBu 95 Following general procedure A, **95** was collected as a white solid in 70% yield over 2 steps. ^1H NMR (400 MHz, CDCl_3) δ 7.67 (d, $J = 9.5$

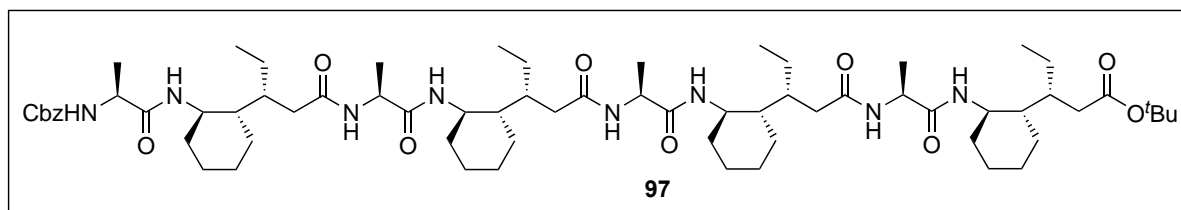
Hz, 1H), 7.33 (d, $J = 3.7$ Hz, 5H), 7.21 (d, $J = 7.8$ Hz, 1H), 6.22 (d, $J = 7.8$ Hz, 1H), 5.49 (d, $J = 7.8$ Hz, 1H), 5.16 – 4.94 (m, 2H), 4.50 (p, $J = 7.2$ Hz, 1H), 4.20 (p, $J = 7.1$ Hz, 1H), 3.74 (qd, $J = 10.7, 3.9$ Hz, 1H), 3.64 (tdd, $J = 11.2, 7.7, 4.1$ Hz, 1H), 2.58 – 2.32 (m, 2H), 2.14 – 1.99 (m, 3H), 1.98 – 1.84 (m, 3H), 1.79 – 1.59 (m, 6H), 1.46 (m, 11H), 1.32 (d, $J = 7.2$ Hz, 3H), 1.35–1.27 (m, 6H), 1.18 – 0.94 (m, 8H), 0.91 – 0.88 (m, 4H), 0.80 (t, $J = 6.9$ Hz, 3H). ^{13}C NMR (101 MHz, CDCl_3) δ 173.85, 173.43, 173.15, 172.75, 156.12, 136.45, 128.59, 128.24, 80.65, 67.01, 51.03, 50.54, 49.23, 48.82, 45.29, 44.69, 38.65, 37.27, 36.91, 35.48, 34.15, 34.07, 28.33, 26.08, 25.79, 25.51, 25.20, 25.14, 24.72, 22.23, 22.02, 18.53, 13.02, 12.88. HRMS-ESI (m/z) calc'd for $\text{C}_{40}\text{H}_{64}\text{N}_4\text{O}_7\text{Na}$ $[\text{M}+\text{Na}]^+$, 735.4668; found, 735.4672.



Cbz-L-Ala-AChPA-L-Ala-ACPA-L-Ala-AChPA-O^tBu 96

Following general procedure A, **96** was collected as a white solid in 58% over 2 steps. ^1H NMR (400 MHz, CDCl_3)

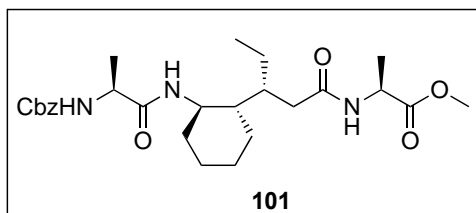
δ 7.98 (d, $J = 9.6$ Hz, 1H), 7.79 (d, $J = 9.7$ Hz, 1H), 7.49 (d, $J = 6.2$ Hz, 1H), 7.44 (d, $J = 7.3$ Hz, 1H), 7.24 – 7.13 (m, 5H), 6.14 (d, $J = 7.7$ Hz, 1H), 5.15 (d, $J = 7.0$ Hz, 1H), 5.04 – 4.78 (m, 2H), 4.33 (p, $J = 7.3$ Hz, 1H), 4.22 (p, $J = 7.0$ Hz, 1H), 3.98 (p, $J = 6.9$ Hz, 1H), 3.71 – 3.47 (m, 3H), 2.41 (ddd, $J = 23.7, 13.6, 3.1$ Hz, 2H), 2.29 – 2.20 (m, 1H), 2.01 – 1.71 (m, 9H), 1.67 – 1.44 (m, 9H), 1.32 (m, 12H), 1.25 (d, $J = 6.9$ Hz, 3H), 1.21 – 1.12 (m, 12H), 1.04 – 0.88 (m, 9H), 0.80 – 0.68 (m, 12H). ^{13}C NMR (101 MHz, CDCl_3) δ 174.38, 173.89, 173.86, 173.77, 173.72, 172.84, 156.14, 136.33, 128.60, 128.25, 128.11, 80.65, 66.99, 51.27, 50.45, 49.96, 49.31, 49.26, 45.21, 44.61, 44.21, 39.44, 38.81, 37.38, 37.34, 36.62, 35.40, 34.36, 34.14, 33.74, 28.34, 26.10, 25.72, 25.49, 25.43, 25.30, 25.20, 25.01, 24.80, 23.01, 22.38, 22.07, 18.43, 18.06, 17.68, 13.97, 13.00, 12.85. HRMS-ESI (m/z) calc'd for $\text{C}_{54}\text{H}_{88}\text{N}_6\text{O}_9\text{Na}$ $[\text{M}+\text{Na}]^+$, 987.6505; found, 987.6491.



Cbz-L-Ala-AChPA-L-Ala-AChPA-L-Ala-AChPA-L-Ala-AChPA-O'Bu 97 Following general procedure A, foldamer **97** was collected as a white solid in 49% yield over 2 steps. ^1H NMR (400 MHz, CDCl_3) δ 8.15 (d, $J = 4.4$ Hz, 1H), 8.12 (d, $J = 4.3$ Hz, 1H), 7.98 (d, $J = 6.0$ Hz, 1H), 7.88 (d, $J = 9.7$ Hz, 1H), 7.71 (d, $J = 7.4$ Hz, 1H), 7.66 (d, $J = 5.8$ Hz, 1H), 7.38 – 7.27 (m, 5H), 6.23 (d, $J = 7.8$ Hz, 1H), 5.24 (d, $J = 7.0$ Hz, 1H), 5.13 (d, $J = 12.3$ Hz, 1H), 4.96 (d, $J = 12.3$ Hz, 1H), 4.47 (p, $J = 7.3$ Hz, 1H), 4.34 (dt, $J = 11.3, 6.6$ Hz, 2H), 4.09 (p, $J = 6.9$ Hz, 1H), 3.85 – 3.58 (m, 4H), 2.63 – 2.49 (m, 3H), 2.37 (d, $J = 12.9$ Hz, 1H), 2.09 (dd, $J = 22.8, 9.3$ Hz, 6H), 2.00 – 1.82 (m, 9H), 1.69 (d, $J = 10.6$ Hz, 12H), 1.46 (m, 13H), 1.38 (d, $J = 6.9$ Hz, 3H), 1.28 (m, 15H), 1.20 – 1.03 (m, 12H), 1.01 – 0.94 (m, 8H), 0.93 – 0.79 (m, 7H). ^{13}C NMR (101 MHz, CDCl_3) δ 174.46, 174.20, 174.12, 173.79, 173.67, 172.73, 156.12, 136.31, 128.60, 128.25, 128.08, 80.58, 66.97, 60.53, 53.56, 51.35, 50.39, 50.20, 49.17, 49.13, 49.01, 45.18, 44.72, 44.38, 44.03, 39.61, 39.51, 38.91, 37.47, 37.32, 36.77, 36.47, 35.38, 34.36, 34.14, 34.07, 33.80, 31.71, 28.34, 26.09, 25.73, 25.51, 25.41, 25.15, 25.04, 24.97, 24.78, 23.03, 22.78,

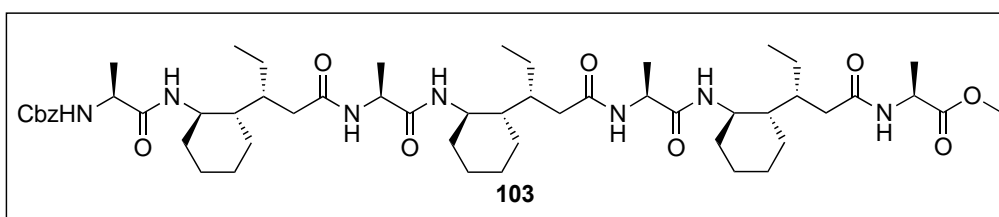
22.44, 22.08, 21.20, 18.43, 17.86, 17.70, 17.47, 14.32, 14.26, 14.02, 13.99, 12.96, 12.83. HRMS-ESI (m/z) calc'd for $C_{68}H_{112}N_8O_{11}Na$ $[M+Na]^+$, 1239.8343; found, 1239.8347.

6.2.6 Synthesis of Foldamer 103



Cbz-L-Ala-ACHPA-L-Ala-OMe 101 Following general procedure A, **101** was collected as a white solid in 82% yield. 1H NMR (400 MHz, $CDCl_3$) δ 7.39 – 7.28 (m, 6H), 7.06 (d, $J = 9.8$ Hz, 1H), 5.38 (d, $J = 7.8$ Hz, 1H), 5.09 (d, $J = 12.2$ Hz, 1H), 4.97 (d, $J =$

12.2 Hz, 1H), 4.79 – 4.68 (m, 1H), 3.98 (p, $J = 7.1$ Hz, 1H), 3.75 (m, 4H), 2.47 (dd, $J = 13.2$, 3.2 Hz, 1H), 1.94 – 1.75 (m, 3H), 1.70 (d, $J = 12.8$ Hz, 3H), 1.51 (ddt, $J = 13.1$, 7.9, 6.6 Hz, 1H), 1.36 (dd, $J = 7.3$, 6.3 Hz, 6H), 1.20 – 1.08 (m, 4H), 1.01 (td, $J = 12.3$, 3.0 Hz, 1H), 0.85 (ddt, $J = 12.4$, 9.4, 6.3 Hz, 1H), 0.76 (t, $J = 7.1$ Hz, 3H). ^{13}C NMR (101 MHz, $CDCl_3$) δ 175.84, 173.68, 172.47, 156.26, 136.21, 128.63, 128.36, 128.21, 67.19, 52.64, 51.26, 49.14, 47.40, 44.68, 38.67, 37.15, 34.15, 25.74, 25.55, 24.58, 22.20, 18.15, 17.56, 12.79. HRMS-ESI (m/z) calc'd for $C_{26}H_{39}N_3O_6Na$ $[M+Na]^+$, 512.2732; found, 512.2770.



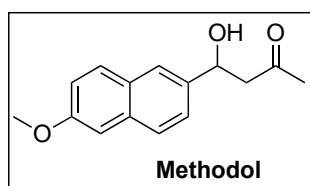
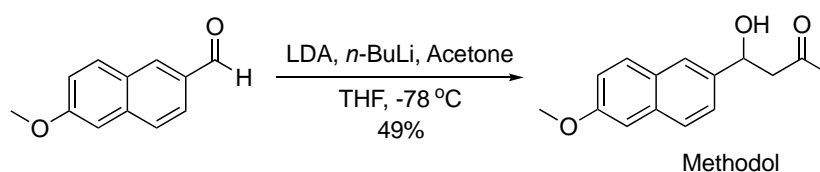
**Cbz-L-Ala-
ACHPA-L-
Ala-
ACHPA-L-
Ala-**

ACHPA-L-Ala-OMe 103 Following general procedure A, the non-catalytic foldamer **103** was collected as a white solid in 41% yield over 4 steps. 1H NMR (400 MHz, $CDCl_3$) δ 8.05 (d, $J = 5.6$ Hz, 1H), 7.99 (d, $J = 9.5$ Hz, 1H), 7.86 (d, $J = 7.4$ Hz, 2H), 7.67 (d, $J = 5.6$ Hz, 1H), 7.38 – 7.25 (m, 6H), 5.37 – 5.20 (m, 1H), 5.12 (d, $J = 12.2$ Hz, 1H), 4.95 (d, $J = 12.3$ Hz, 1H), 4.65 (p, $J = 7.5$ Hz, 1H), 4.30 (q, $J = 6.7$ Hz, 1H), 4.09 (m, 2H), 3.75 (m, 6H), 2.66 – 2.47 (m, 3H), 2.15 – 1.83 (m, 9H), 1.67 (m, 9H), 1.48 (m, 3H), 1.43 – 1.06 (m, 27H), 1.04 – 0.76 (m, 12H). ^{13}C NMR (101 MHz, $CDCl_3$) δ 176.58, 174.51, 174.34, 173.91, 173.74, 156.12, 136.29,

128.59, 128.24, 128.06, 66.98, 52.66, 50.48, 50.41, 49.12, 49.03, 47.93, 44.91, 44.46, 44.10, 39.57, 39.39, 38.90, 37.46, 36.74, 36.65, 34.40, 34.05, 33.88, 25.68, 25.51, 25.47, 25.38, 25.30, 25.23, 25.02, 24.85, 24.77, 23.01, 18.38, 17.67, 17.34, 16.76, 14.04, 13.96, 12.84. HRMS-ESI (m/z) calc'd for C₅₄H₈₈N₇O₁₀ [M+H]⁺, 994.6588; found, 994.6590.

6.3 Synthesis and Characterization for Chapter 3

6.3.1 Synthesis of Methodol

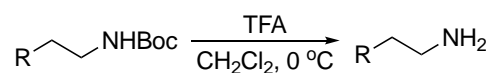


4-hydroxy-4-(6-methoxynaphthalen-2-yl)butan-2-one ¹¹⁹

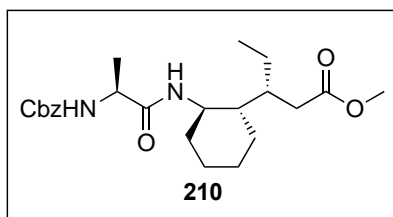
(Methodol) Diiodopropylamine (1.40 mL, 10 mmol) was dissolved in to anhydrous THF (20 mL) at 0 °C, then *n*-BuLi (4 mL of 2.5 M solution in THF, 10 mmol) was added into the solution dropwise and reacted at 0 °C for 20 min to make the LDA solution. Then the LDA solution was cooled to -78 °C, then anhydrous acetone(0.70 mL, 9.5 mmol) was added dropwise into the LDA solution, and after 30 min, the 6-methoxy-2-naphthaldehyde (0.93 g, 5 mmol) in 10 mL of dry THF was added dropwise, the mixture was stirred for another 15 mins, 2mL of saturated NH₄Cl solution was added dropwise, then the reaction was warmed up to room temperature, and diethyl ether was added, the organic layer was washed with water, dried over MgSO₄, filtered and concentrated. The residue was purified via column to give the desired product as a pale-yellow solid in 49% yield. ¹H NMR (400 MHz, CDCl₃) δ 7.80 – 7.66 (m, 3H), 7.43 (dd, J = 8.5, 1.8 Hz, 1H), 7.19 – 7.09 (m, 2H), 5.29 (dd, J = 8.9, 3.5 Hz, 1H), 3.92 (s, 3H), 3.03 – 2.84 (m, 2H), 2.29 – 2.06 (s, 3H). ¹³C NMR (101 MHz, CDCl₃) δ 209.23, 157.75, 137.79, 134.12, 129.47, 128.74, 127.23, 124.30, 119.08, 105.64, 69.99, 55.33, 51.95, 30.86.

6.3.2 Synthesis of Catalytic Foldamer 233

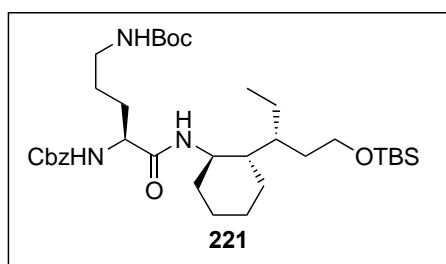
6.3.2.1 General Procedure F: Boc-Deprotection



To the *tert*-butyl carbamate-foldamer (50 mg) in dichloromethane (2 mL) was added TFA (2 mL) at 0 °C under nitrogen atmosphere, the mixture was stirred at room temperature for 2 h. NaHCO₃ solution was slowly added at 0 °C and the solution was extracted with ethyl acetate, the organic layer was dried over MgSO₄, filtered and concentrated to give the amine catalyst.



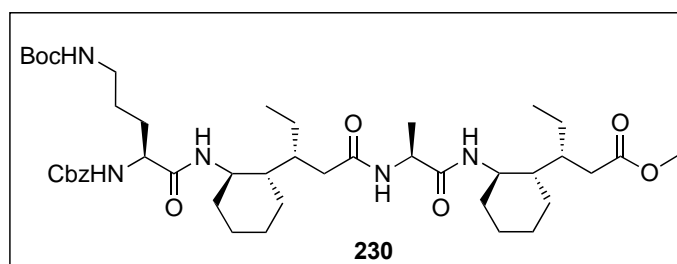
Cbz-L-Ala-AChPA-OMe 210 To a solution of **93** (0.61 g, 1.5 mmol) in dimethoxypropane (2.4 mL) and MeOH (0.6 mL) was added trimethylsilylchloride (19 μL, 0.15 mmol), the mixture was stirred at rt for 16 h, and the solvent was removed in vacuo, the residue was diluted with Et₂O, washed with H₂O and brine, dried over MgSO₄, filtered and concentrated. The residue was purified via column chromatography to give the desired product **210** as a white solid in 86% yield. ¹H NMR (400 MHz, CDCl₃) δ 7.35 (m, 5H), 6.12 (d, J = 8.9 Hz, 1H), 5.50 (s, 1H), 5.14 (s, 2H), 4.27 (t, J = 7.5 Hz, 1H), 3.75 – 3.66 (m, 1H), 3.65 (s, 3H), 2.37 (dd, J = 16.8, 3.5 Hz, 1H), 2.16 (dd, J = 16.8, 10.9 Hz, 1H), 2.10 – 2.00 (m, 1H), 1.90 (t, J = 10.8 Hz, 1H), 1.77 – 1.60 (m, 3H), 1.54 – 1.43 (m, 1H), 1.41 (d, J = 7.0 Hz, 3H), 1.25 (m, 1H), 1.19 – 0.99 (m, 4H), 0.99 – 0.89 (m, 1H), 0.83 (t, J = 7.2 Hz, 3H). ¹³C NMR (101 MHz, CDCl₃) δ 174.87, 171.58, 156.00, 136.55, 128.64, 128.27, 128.19, 67.07, 51.74, 50.94, 49.92, 46.30, 35.92, 35.79, 34.12, 26.00, 25.26, 25.15, 21.89, 19.28, 12.95. HRMS-ESI (m/z) calc'd for C₂₃H₃₃N₂O₅ [M+H]⁺, 419.2540; found, 419.2550.



Cbz-L-Orn•Boc-AChPA•(CH₂OTBS) 221 Following general procedure A, **221** was collected as a white solid in 90% yield.

¹H NMR (400 MHz, CDCl₃) δ 7.29 (m, 5H), 6.05 (d, J = 9.3 Hz, 1H), 5.52 (d, J = 8.1 Hz, 1H), 5.10 – 4.95 (m, 2H), 4.66 (m, 1H), 4.28 – 4.07 (m, 1H),

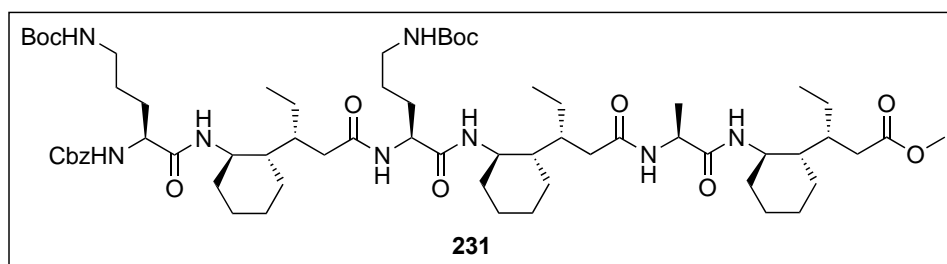
3.72 (qd, J = 10.9, 3.9 Hz, 1H), 3.56 (m, 2H), 3.25 (m, 1H), 2.99 (q, J = 6.2 Hz, 1H), 1.87 (m, 1H), 1.80 – 1.70 (m, 1H), 1.68 – 1.60 (m, 3H), 1.56 – 1.48 (m, 3H), 1.38 (m, 12H), 1.28 – 1.17 (m, 3H), 1.07 – 0.96 (m, 3H), 0.84 (m, 10H), 0.75 (t, J = 7.2 Hz, 3H), 0.00 (s, 6H).



Cbz-L-Orn•Boc-AChPA-L-Ala-AChPA-OMe 230 Following general procedure A, **230** was collected as a white solid in 60% yield.

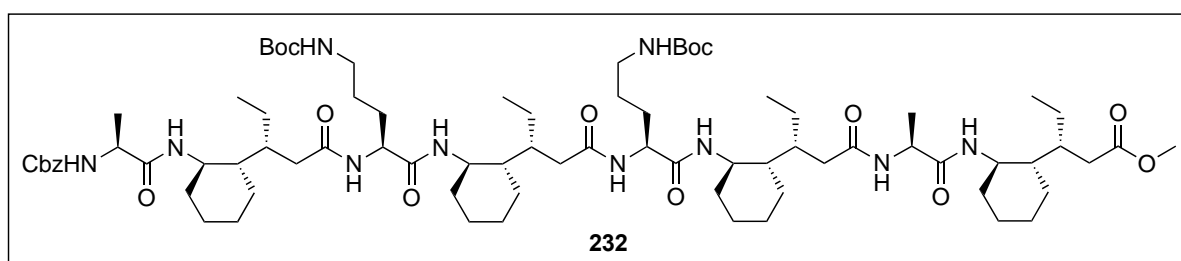
¹H NMR (400 MHz, CDCl₃) δ 7.78 (d, J = 9.5

Hz, 1H), 7.41 – 7.27 (m, 6H), 6.23 (d, J = 8.1 Hz, 1H), 5.42 (d, J = 8.3 Hz, 1H), 5.22 – 4.94 (m, 2H), 4.88 (s, 1H), 4.48 (t, J = 7.3 Hz, 1H), 4.17 (d, J = 7.6 Hz, 1H), 3.69 (m, 5H), 3.19 (dd, J = 13.2, 6.5 Hz, 1H), 3.14 – 2.99 (m, 1H), 2.66 – 2.34 (m, 2H), 2.26 – 2.07 (m, 2H), 2.05 – 1.87 (m, 4H), 1.76 – 1.46 (m, 12H), 1.42 (s, 9H), 1.32 (d, J = 7.2 Hz, 3H), 1.30 – 1.22 (m, 3H), 1.08 (m, 8H), 0.90 (m, J = 7.2 Hz, 4H), 0.80 (t, J = 6.9 Hz, 3H). ¹³C NMR (101 MHz, CDCl₃) δ 174.93, 173.72, 173.46, 171.81, 156.49, 156.10, 136.41, 128.62, 128.28, 128.25, 79.19, 67.13, 54.72, 51.77, 50.51, 49.09, 45.37, 44.69, 39.65, 38.80, 37.03, 35.84, 35.54, 34.32, 34.28, 29.50, 28.58, 26.01, 25.80, 25.49, 25.25, 25.16, 24.76, 22.34, 22.16, 18.53, 13.14, 12.90. HRMS-ESI (m/z) calc'd for C₄₄H₇₂N₅O₉ [M+H]⁺, 814.5325; found, 814.5335.



**Cbz-L-
Orn•Boc-
AChPA-L-
Orn•Boc-
AChPA-L-Ala-**

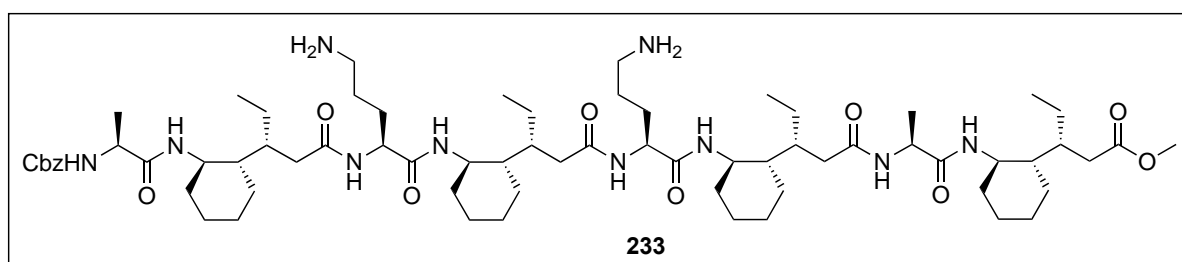
AChPA-OMe 231 Following general procedure A, **231** was collected as a white solid in 54% yield over 2 steps. ^1H NMR (400 MHz, CDCl_3) δ 8.13 (d, $J = 9.7$ Hz, 1H), 7.97 (d, $J = 9.5$ Hz, 1H), 7.50 (d, $J = 6.8$ Hz, 1H), 7.44 (d, $J = 6.4$ Hz, 1H), 7.38 – 7.28 (m, 5H), 6.27 (d, $J = 8.2$ Hz, 1H), 5.27 (m, 3H), 5.03 (q, $J = 12.4$ Hz, 2H), 4.39 (m, 2H), 4.09 (m, 1H), 3.68 (m, 6H), 3.30 – 3.05 (m, 2H), 2.99 – 2.83 (m, 2H), 2.60 – 2.42 (m, 3H), 2.19 (m, 2H), 2.02 – 1.86 (m, 7H), 1.83 – 1.58 (m, 15H), 1.56 – 1.36 (m, 24H), 1.35 – 1.29 (m, 5H), 1.22 – 1.02 (m, 12H), 1.01 – 0.76 (m, 12H). ^{13}C NMR (101 MHz, CDCl_3) δ 174.86, 174.78, 174.60, 173.66, 172.10, 156.87, 156.24, 139.43, 136.21, 128.64, 128.30, 128.08, 114.21, 78.97, 67.16, 54.30, 53.45, 51.74, 50.41, 49.85, 49.22, 49.09, 45.37, 44.49, 44.33, 39.35, 39.04, 37.71, 37.00, 35.91, 35.35, 34.56, 34.44, 33.86, 32.07, 30.45, 29.84, 28.62, 25.99, 25.67, 25.43, 25.28, 25.19, 25.02, 24.83, 23.02, 22.83, 22.48, 22.27, 18.02, 14.26, 14.13, 13.24, 12.93. HRMS-ESI (m/z) calc'd for $\text{C}_{65}\text{H}_{109}\text{N}_8\text{O}_{13}$ [$\text{M}+\text{H}$] $^+$, 1209.8109; found, 1209.8149.



Cbz-L-Ala-AChPA-L-Orn•Boc-AChPA-L-Orn•Boc-AChPA-L-Ala-AChPA-Ome 232

Following general procedure A, foldamer **232** was collected as a white solid in 43% yield over 2 steps. ^1H NMR (400 MHz, CDCl_3) δ 8.23 (d, $J = 9.8$ Hz, 1H), 8.07 (d, $J = 9.7$ Hz, 1H), 7.98 (d, $J = 9.6$ Hz, 1H), 7.82 (d, $J = 6.7$ Hz, 1H), 7.63 (m, 2H), 7.43 – 7.29 (m, 5H), 6.31 (d, $J = 8.4$ Hz, 1H), 5.70 (s, 1H), 5.31 (s, 0H), 5.27 (d, $J = 7.0$ Hz, 1H), 5.16 – 5.00 (m, 2H), 4.43 (p, $J = 7.3$ Hz, 2H), 4.31 (m, 1H), 4.08 (p, $J = 7.2$ Hz, 1H), 3.71 (m, 7H), 3.18 (m, $J = 14.8$ Hz,

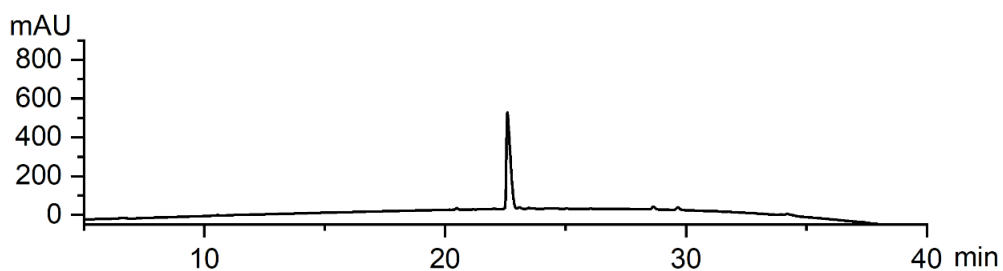
2H), 2.93 (m, $J = 22.1$ Hz, 1H), 2.72 (m, 1H), 2.59 (td, $J = 13.5, 2.9$ Hz, 3H), 2.47 (dd, $J = 14.0, 8.0$ Hz, 1H), 2.29 – 2.12 (m, 3H), 2.09 – 1.84 (m, 12H), 1.81 – 1.63 (m, 18H), 1.50 (m, 1H), 1.46 (s, 9H), 1.44 (s, 9H), 1.39 (d, $J = 6.8$ Hz, 3H), 1.35 – 1.25 (m, 11H), 1.21 – 1.06 (m, 13H), 1.01 (m, 7H), 0.95 (t, $J = 7.2$ Hz, 3H), 0.90 – 0.84 (m, 4H). ^{13}C NMR (101 MHz, CDCl_3) δ 175.21, 174.88, 174.69, 174.21, 173.72, 173.48, 172.72, 156.29, 128.64, 128.28, 128.03, 79.02, 78.76, 67.15, 53.94, 52.96, 51.75, 51.39, 50.45, 49.82, 49.21, 49.16, 48.99, 45.34, 44.57, 44.06, 39.75, 39.40, 39.25, 38.96, 38.16, 37.54, 37.10, 36.95, 35.93, 35.39, 34.56, 34.45, 34.10, 33.87, 28.71, 28.65, 25.99, 25.65, 25.56, 25.46, 25.36, 25.25, 25.03, 24.90, 24.80, 23.10, 22.98, 22.49, 22.29, 18.42, 17.92, 14.22, 14.02, 13.25, 12.86. HRMS-ESI (m/z) calc'd for $\text{C}_{79}\text{H}_{132}\text{N}_{10}\text{O}_{15}\text{Na}$ $[\text{M}+\text{Na}]^+$, 1483.9766; found, 1483.9779.



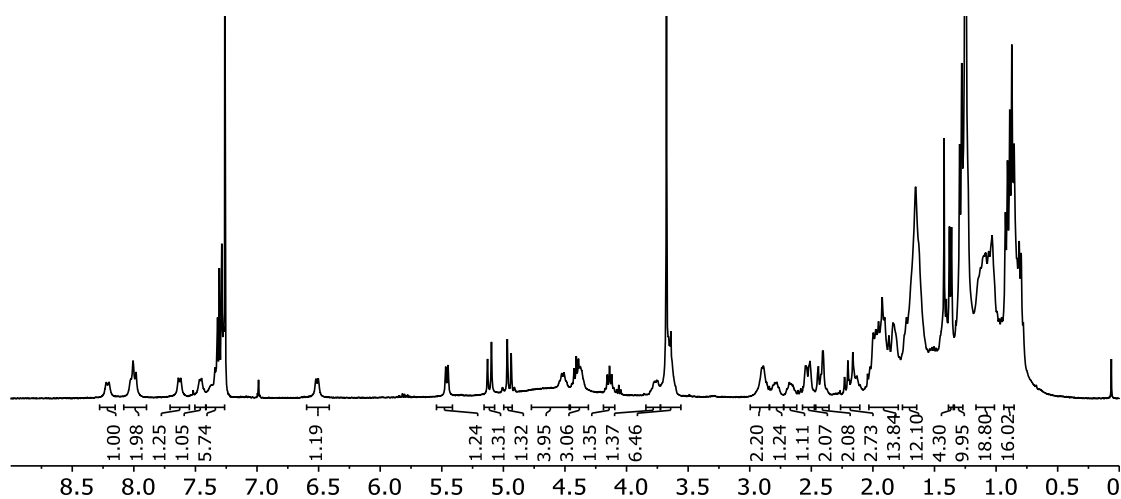
Cbz-L-Ala-AChPA-L-Orn•NH₂-AChPA-L-Orn•NH₂-AChPA-L-Ala-AChPA-OMe 233

Following general procedure F, foldamer **233** was collected as a white solid in 33% yield. ^1H NMR (400 MHz, CDCl_3) δ 8.21 (d, $J = 9.2$ Hz, 1H), 8.01 (t, $J = 9.3$ Hz, 2H), 7.63 (d, $J = 7.9$ Hz, 1H), 7.46 (d, $J = 6.5$ Hz, 1H), 7.41 – 7.26 (m, 6H), 6.51 (d, $J = 8.0$ Hz, 1H), 5.46 (d, $J = 7.7$ Hz, 1H), 5.11 (d, $J = 12.7$ Hz, 1H), 4.95 (d, $J = 12.6$ Hz, 1H), 4.52 (m, 4H), 4.40 (m, 3H), 4.13 (q, $J = 6.8$ Hz, 1H), 3.76 (m, 1H), 3.74 – 3.54 (m, 6H), 2.87 (m, 2H), 2.79 (m, 1H), 2.67 (m, 1H), 2.58 – 2.47 (m, 2H), 2.43 (m, 2H), 2.26 – 2.11 (m, 3H), 2.04 – 1.79 (m, 14H), 1.65 (m, 12H), 1.39 – 1.35 (m, 4H), 1.29 (m, 10H), 1.18 – 1.02 (m, 19H), 0.93 – 0.86 (m, 16H). HRMS-ESI (m/z) calc'd for $\text{C}_{69}\text{H}_{117}\text{N}_{10}\text{O}_{11}$ $[\text{M}+\text{H}]^+$, 1261.8898; found, 1261.8895.

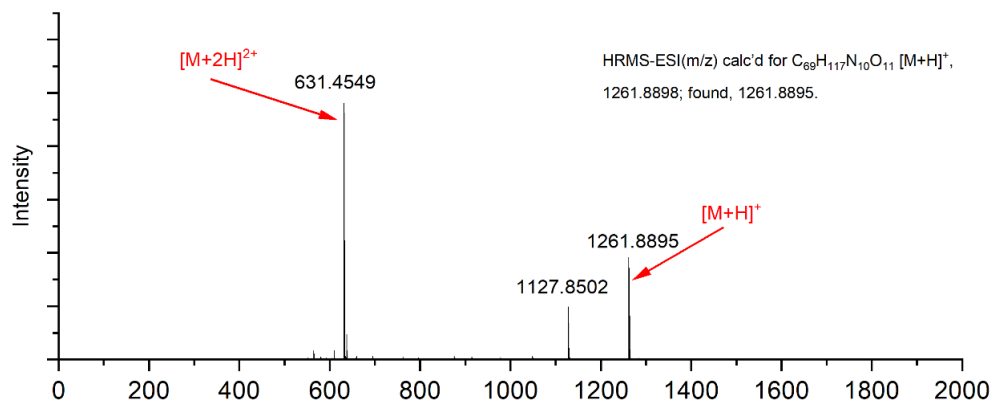
HPLC analysis: Acetonitrile+0.1% TFA/Water+0.1% TFA, 1.0 mL/min, 25 °C, detection at 210 nm, retention time (min): 22.6.



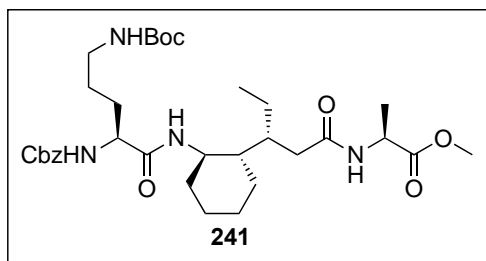
^1H NMR spectrum of foldamer **233** (400 MHz, CDCl_3).



HRMS spectrum of foldamer **233**.

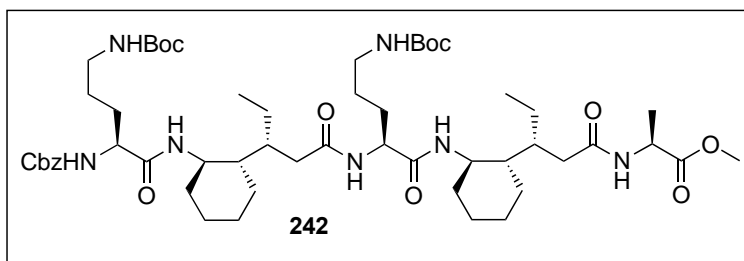


6.3.3 Synthesis of Foldamer 244



Cbz-L-Orn•Boc-AChPA-L-Ala-OMe **241**

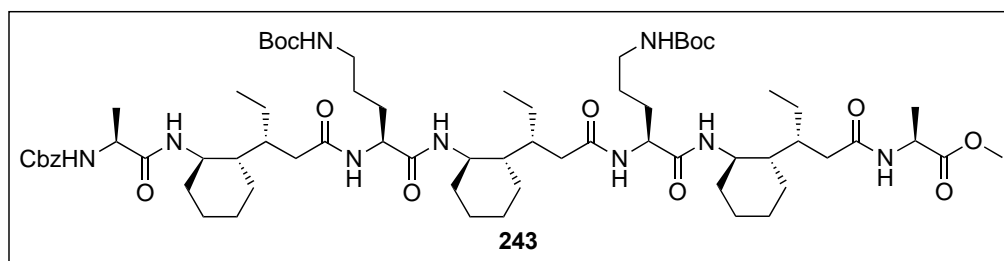
Following general procedure A, **241** was collected as a white solid in 89% yield. ^1H NMR (400 MHz, CDCl_3) δ 7.39 – 7.28 (m, 5H), 7.18 (d, J = 9.7 Hz, 1H), 5.34 (d, J = 8.3 Hz, 1H), 5.09 (d, J = 12.2 Hz, 1H), 4.97 (d, J = 12.2 Hz, 1H), 4.77 (p, J = 7.6 Hz, 1H), 4.59 (s, 1H), 3.90 (q, J = 7.5 Hz, 1H), 3.75 (s, 4H), 3.13 (p, J = 6.9 Hz, 2H), 2.47 (dd, J = 13.4, 3.4 Hz, 1H), 2.00 – 1.51 (m, 6H), 1.50 – 1.32 (m, 12H), 1.25 – 1.07 (m, 4H), 1.06 – 0.93 (m, 1H), 0.92 – 0.81 (m, 1H), 0.76 (t, J = 7.1 Hz, 3H). ^{13}C NMR (101 MHz, CDCl_3) δ 176.03, 173.58, 171.42, 156.42, 156.05, 136.10, 128.66, 128.42, 128.27, 79.40, 67.31, 55.38, 52.74, 49.18, 47.37, 44.57, 40.00, 38.72, 37.25, 34.30, 29.28, 28.52, 26.55, 25.71, 25.50, 24.58, 22.21, 17.63, 12.87. HRMS-ESI (m/z) calc'd for $\text{C}_{33}\text{H}_{53}\text{N}_4\text{O}_8$ [$\text{M}+\text{H}$] $^+$, 633.3858; found, 633.3845.



Cbz-L-Orn•Boc-AChPA-L-Orn•Boc-AChPA-L-Ala-OMe **242**

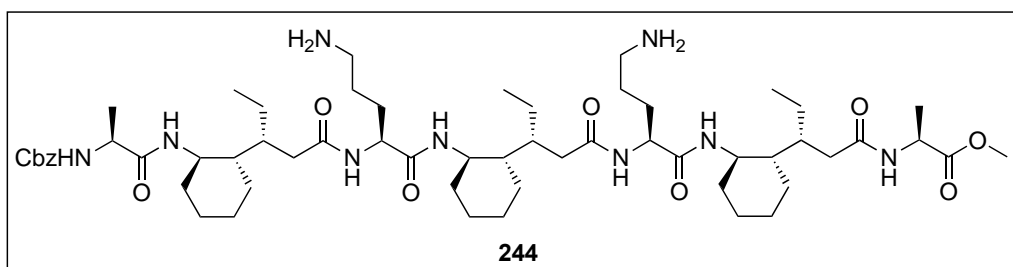
Following general procedure A, **242** was collected as a white solid in 66% yield over 2 steps. ^1H NMR (400 MHz, CDCl_3) δ 7.88 (d, J = 9.5 Hz, 1H), 7.61 (d, J = 7.5 Hz, 1H), 7.46 (d, J = 6.4 Hz, 1H), 7.40 (d, J = 9.7 Hz, 1H), 7.32 (m, 5H), 5.29 (d, J = 8.0 Hz, 1H), 5.08 (m, 2H), 4.99 (d, J = 12.3 Hz, 1H), 4.76 (b, 1H), 4.67 (p, J = 7.8 Hz, 1H), 4.07 (m, 2H), 3.77 (m, 5H), 3.28 – 3.11 (m, 1H), 3.01 (m, 3H), 2.53 (dd, J = 24.3, 10.6 Hz, 2H), 2.00 (d, J = 8.2 Hz, 2H), 1.90 (m, 4H), 1.84 – 1.59 (m, 13H), 1.59 – 1.48 (m, 3H), 1.43 (s, 9H), 1.40 (s, 9H), 1.36 (d, J = 7.5 Hz, 3H), 1.24 – 1.01 (m, 11H), 0.98 (t, J = 7.1 Hz, 3H), 0.94 – 0.87 (m, 1H), 0.87 – 0.78 (m, 3H). ^{13}C NMR (101 MHz, CDCl_3) δ 174.70, 173.92, 173.05, 171.97, 156.87, 156.15, 156.03, 136.21, 128.66, 128.32, 127.97, 79.21, 67.11, 54.49, 52.85, 49.44, 49.09, 47.99, 44.53, 44.37, 39.97, 39.28, 39.10, 38.94, 37.72, 37.11, 34.47, 33.87, 29.12, 28.88, 28.60,

28.55, 26.81, 25.64, 25.46, 25.39, 25.28, 25.07, 24.80, 23.08, 22.44, 16.99, 14.08, 12.95.
HRMS-ESI (m/z) calc'd for C₅₄H₉₀N₇O₁₂ [M+H]⁺, 1028.6642; found, 1028.6621.



Cbz-L-Ala-
AChPA-L-
Orn•Boc-
AChPA-L-
Orn•Boc-

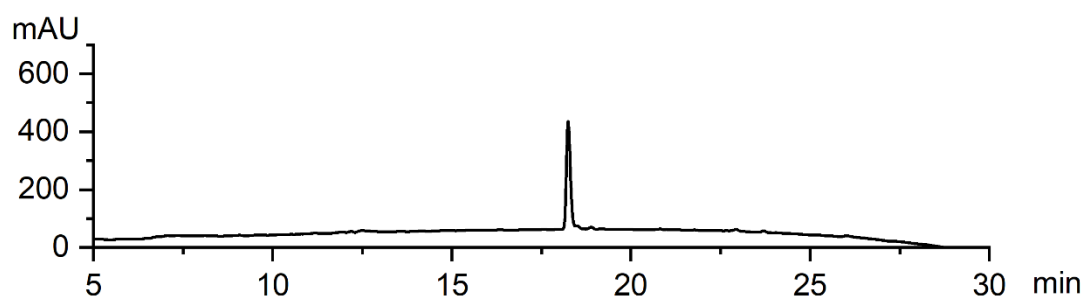
AChPA-L-Ala-OMe 243 Following general procedure A, foldamer **243** was collected as a white solid in 49% yield over 2 steps. ¹H NMR (400 MHz, CDCl₃) δ 7.95 (t, J = 8.9 Hz, 2H), 7.79 (d, J = 6.2 Hz, 1H), 7.70 (d, J = 7.6 Hz, 1H), 7.62 (d, J = 6.3 Hz, 1H), 7.43 (d, J = 9.8 Hz, 1H), 7.39 – 7.27 (m, 5H), 5.47 (b, 1H), 5.26 (d, J = 7.3 Hz, 1H), 5.07 (d, J = 12.5 Hz, 1H), 5.00 (d, J = 12.3 Hz, 1H), 4.83 (b, 1H), 4.68 (p, J = 7.5 Hz, 1H), 4.27 (b, 1H), 4.05 (tq, J = 6.1, 2.9, 2.4 Hz, 2H), 3.76 (m, 6H), 3.17 (m, 1H), 3.06 (m, 2H), 2.72 (m, 1H), 2.64 – 2.49 (m, 3H), 2.06 – 1.83 (m, 9H), 1.76 – 1.60 (m, 14H), 1.42 (m, 12H), 1.41 (s, 9H), 1.37 (d, J = 6.9 Hz, 3H), 1.34 (d, J = 7.5 Hz, 3H), 1.25 – 0.96 (m, 21H), 0.90 – 0.81 (m, 9H). ¹³C NMR (101 MHz, CDCl₃) δ 176.93, 175.23, 174.63, 173.93, 173.61, 173.37, 172.73, 156.30, 156.24, 156.07, 136.15, 128.64, 128.28, 127.97, 79.27, 78.88, 77.48, 77.16, 76.84, 67.10, 54.96, 53.07, 52.82, 51.34, 49.42, 49.11, 48.99, 47.96, 44.65, 44.60, 44.09, 40.07, 39.65, 39.32, 38.91, 38.42, 37.53, 37.11, 37.04, 34.44, 34.07, 33.85, 31.72, 29.83, 28.77, 28.67, 28.57, 27.67, 27.13, 25.80, 25.61, 25.52, 25.43, 25.31, 25.24, 25.01, 24.88, 24.77, 23.06, 23.01, 22.78, 22.46, 18.40, 16.93, 14.25, 14.19, 14.03, 12.86, -3.43. HRMS-ESI (m/z) calc'd for C₆₈H₁₁₄N₉O₁₄ [M+H]⁺, 1280.8480; found, 1280.8710



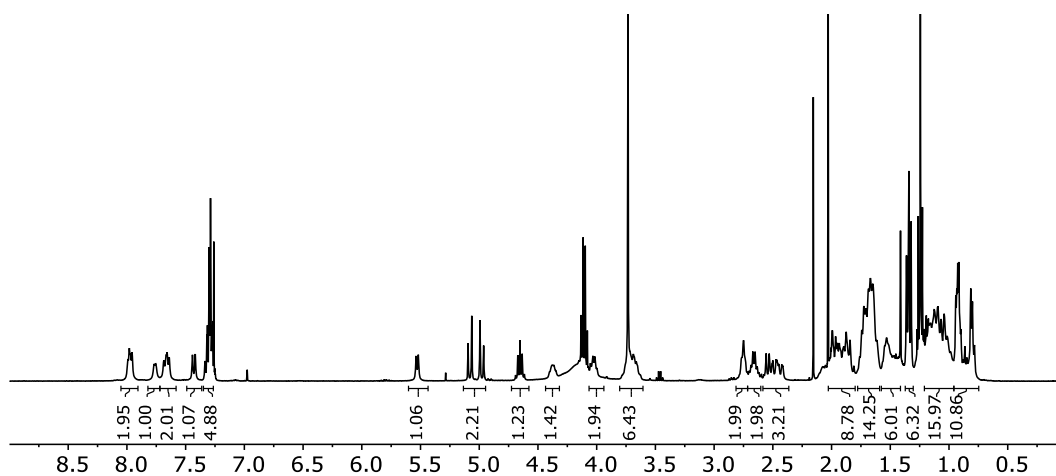
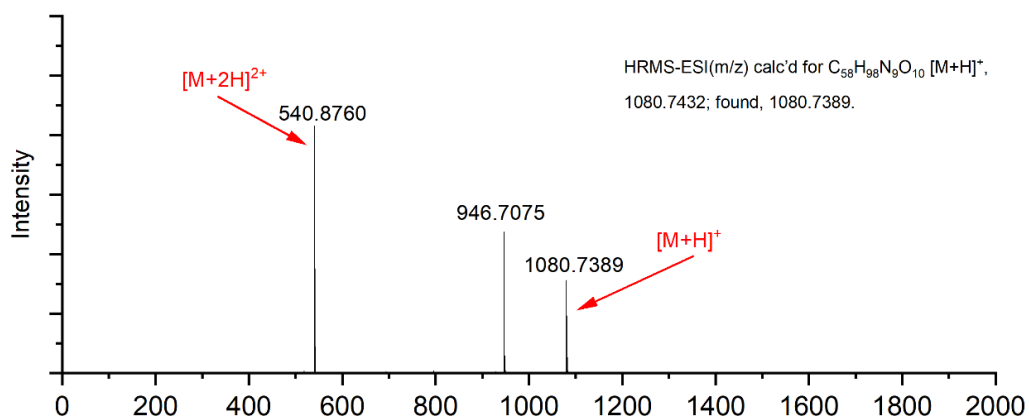
**Cbz-L-
Ala-
AChPA-
L-
Orn•NH₂-
AChPA-**

L-Orn•NH₂-AChPA-L-Ala-OMe 244 Following general procedure F, foldamer **244** was collected as a white solid in 31% yield. ¹H NMR (400 MHz, CDCl₃) δ 7.97 (m, 2H), 7.76 (d, J = 6.2 Hz, 1H), 7.66 (m, 2H), 7.43 (d, J = 9.7 Hz, 1H), 7.35 – 7.27 (m, 5H), 5.53 (d, J = 7.5 Hz, 1H), 5.14 – 4.93 (m, 2H), 4.65 (p, J = 7.5 Hz, 1H), 4.37 (m, 1H), 4.30 – 4.11 (b, 4H), 4.03 (m, 2H), 3.73 (m, 6H), 2.76 (m, 2H), 2.66 (m, 2H), 2.59 – 2.36 (m, 3H), 2.01 – 1.80 (m, 9H), 1.78 – 1.59 (m, 14H), 1.57 – 1.41 (m, 6H), 1.34 (t, J = 8.6, 7.2 Hz, 6H), 1.21 – 0.96 (m, 16H), 0.96 – 0.75 (m, 11H). HRMS-ESI (m/z) calc'd for C₅₈H₉₈N₉O₁₀ [M+H]⁺, 1080.7432; found, 1080.7389. Compound **244** was tentatively assigned using ¹³C NMR.

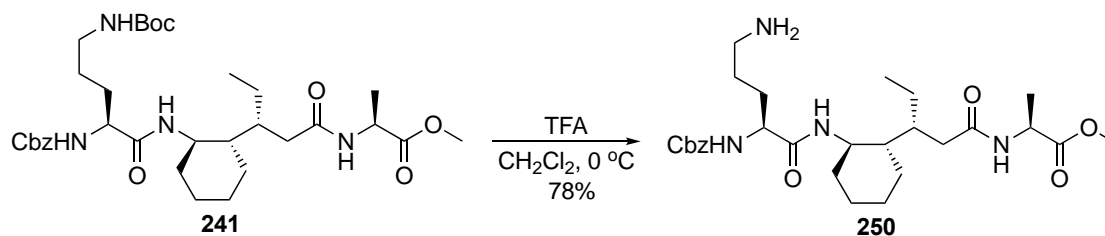
HPLC analysis: Acetonitrile+0.1% TFA/Water+0.1% TFA, 1.0 mL/min, 25 °C, detection at 210 nm, retention time (min): 18.2.

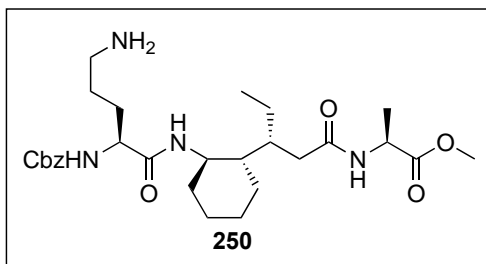


¹H NMR spectrum of foldamer **244** (400 MHz, CDCl₃)

HRMS spectrum of foldamer **244**.

6.3.4 Synthesis of Tripeptide **250**

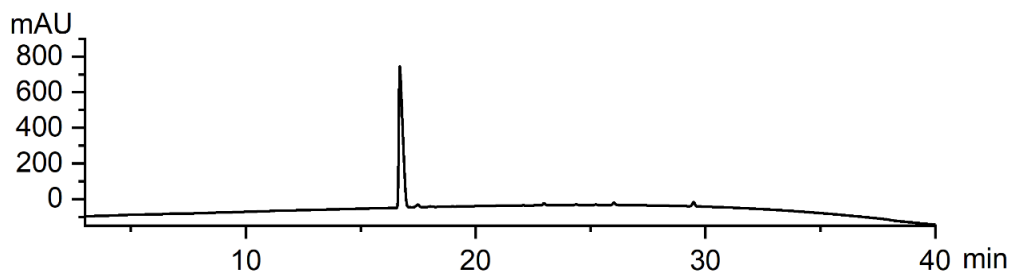




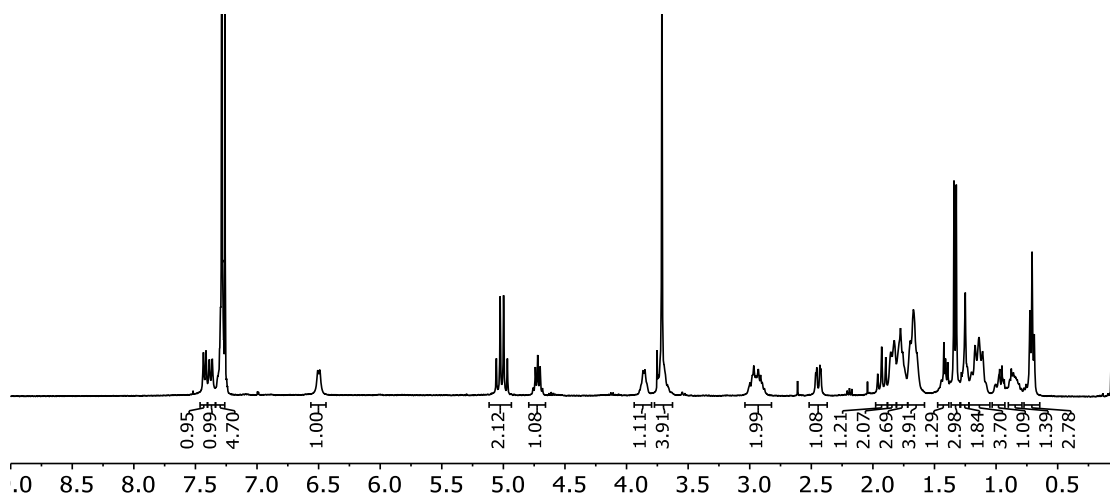
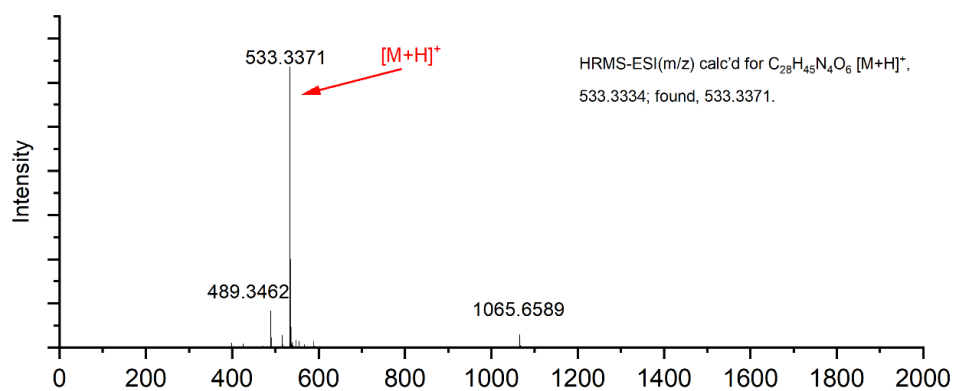
Cbz-L-Boc•NH₂-ACPA-L-Ala-OMe 250 Following general procedure F, Tripeptide **250** was collected as a white solid in 78% yield. ¹H NMR (400 MHz, CDCl₃) δ 7.43 (d, J = 8.4 Hz, 1H), 7.38 (d, J = 9.7 Hz, 1H), 7.34 – 7.27 (m, 5H), 6.50 (d, J = 7.2 Hz, 1H),

5.01 (q, J = 12.4 Hz, 2H), 4.72 (p, J = 7.5 Hz, 1H), 3.86 (d, J = 6.7 Hz, 1H), 3.71 (m, 4H), 2.94 (dp, J = 20.2, 7.4 Hz, 2H), 2.44 (dd, J = 13.4, 3.6 Hz, 1H), 1.93 (t, J = 13.0 Hz, 1H), 1.84 (m, 2H), 1.77 (m, 3H), 1.69 (m, 4H), 1.47 – 1.39 (m, 1H), 1.33 (d, J = 7.4 Hz, 3H), 1.29 – 1.22 (m, 2H), 1.15 (q, J = 11.9 Hz, 4H), 1.04 – 0.91 (m, 1H), 0.90 – 0.80 (m, 1H), 0.71 (t, J = 7.1 Hz, 3H). HRMS-ESI (m/z) calc'd for C₂₈H₄₅N₄O₆ [M+H]⁺, 533.3334; found, 533.3371. Compound **250** was tentatively assigned using ¹³C NMR.

HPLC analysis: Acetonitrile+0.1% TFA/Water+0.1% TFA, 1.0 mL/min, 25 °C, detection at 210 nm, retention time (min): 16.7.

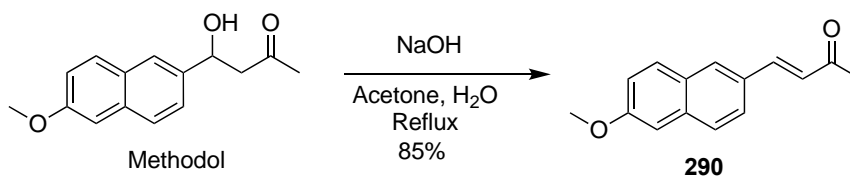


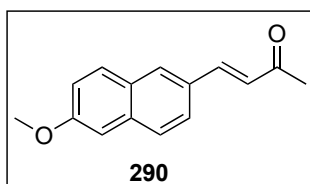
¹H NMR spectrum of Tripeptide **250** (400 MHz, CDCl₃).

HRMS spectrum of Tripeptide **250**

6.4 Synthesis and Characterization for Chapter 4

6.4.1 Synthesis of **290**

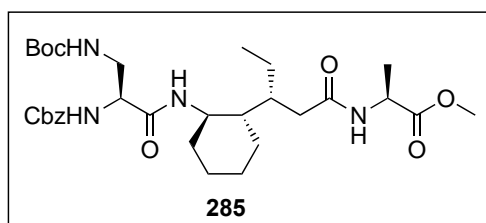




(E)-4-(6-methoxynaphthalen-2-yl)but-3-en-2-one¹²⁰

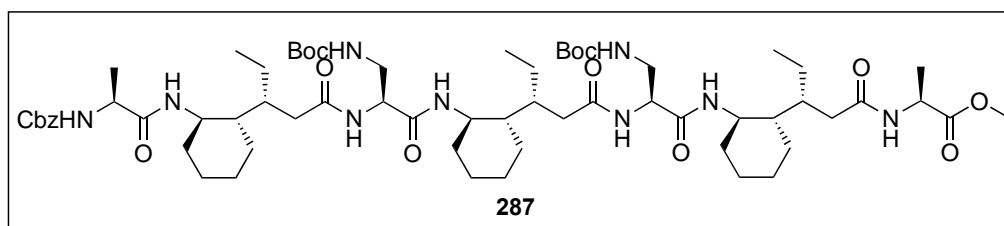
Methodol (0.5 g) was dissolved in 2.5 mL of acetone, and 0.125 g of NaOH was dissolved in 4.5 mL of H₂O, the reaction was refluxed for 1h, then the reaction was cooled, and acetone was evaporated, CH₂Cl₂ was added, the organic layer was washed with water, dried over MgSO₄, filtered and concentrated. The residue was purified via column to give the desired product as a pale-yellow solid in 85% yield. Data are in agreement with the literature. ¹H NMR (400 MHz, CDCl₃) δ 7.86 (s, 1H), 7.73 (t, J = 9.2 Hz, 2H), 7.64 (dd, J = 12.0, 4.0 Hz, 2H), 7.22 – 7.08 (m, 2H), 6.78 (d, J = 16.2 Hz, 1H), 3.93 (s, 3H), 2.40 (s, 3H). ¹³C NMR (101 MHz, CDCl₃) δ 198.46, 158.95, 143.82, 135.86, 130.21, 130.16, 129.77, 128.69, 127.61, 126.29, 124.20, 119.58, 106.00, 55.41, 27.55.

6.4.2 Synthesis of Foldamer 288



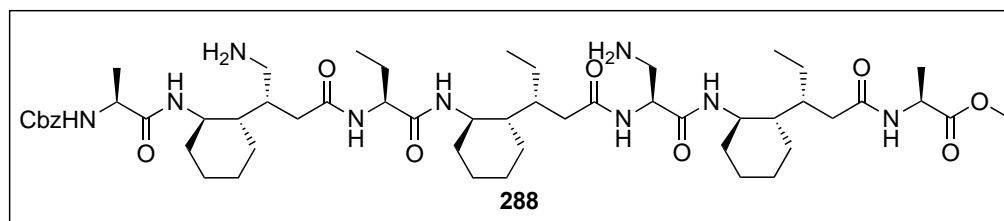
Cbz-L-Dap•Boc-AChPA-L-Ala-Ome **285**

Following general procedure A, **285** was collected as a white solid in 57% yield over 4 steps. ¹H NMR (400 MHz, CDCl₃) δ 7.39 – 7.28 (m, 5H), 7.25 – 7.12 (m, 2H), 5.79 (d, J = 7.7 Hz, 1H), 5.17 (t, J = 6.1 Hz, 1H), 5.09 (d, J = 12.2 Hz, 1H), 5.00 (d, J = 12.3 Hz, 1H), 4.82 – 4.65 (m, 1H), 4.07 (d, J = 7.9 Hz, 1H), 3.74 (m, 4H), 3.49 (m, 1H), 3.41 (m, 2H), 2.46 (d, J = 13.4 Hz, 1H), 1.91 (m, 3H), 1.70 (m, 3H), 1.49 (m, 1H), 1.42 (s, 9H), 1.37 (d, J = 7.5 Hz, 3H), 1.26 – 1.08 (m, 4H), 1.00 (m, 1H), 0.92 – 0.82 (m, 1H), 0.78 (t, J = 7.1 Hz, 3H). ¹³C NMR (101 MHz, CDCl₃) δ 173.50, 170.23, 156.49, 136.09, 128.69, 128.46, 128.26, 79.98, 67.41, 54.98, 52.79, 49.35, 47.39, 44.55, 42.13, 38.66, 37.32, 34.19, 28.45, 25.69, 25.54, 24.59, 22.25, 17.62, 12.90. HRMS-ESI (m/z) calc'd for C₃₁H₄₉N₄O₈ [M+H]⁺, 605.3545; found, 605.3535.



**Cbz-L-Ala-
AChPA-L-
Dap•Boc-
AChPA-L-
Dap•Boc-**

AChPA-L-Ala-OMe 287 Following general procedure A, foldamer **287** was collected as a white solid in 37% yield over 4 steps. ^1H NMR (400 MHz, CDCl_3) δ 8.24 (d, $J = 9.6$ Hz, 1H), 7.67 (m, 5H), 7.31 (m, 5H), 5.58 (d, $J = 7.7$ Hz, 1H), 5.45 (m, , 2H), 5.11 – 4.96 (m, 2H), 4.63 (p, $J = 7.5$ Hz, 1H), 4.44 (q, $J = 7.0$ Hz, 1H), 4.21 (dt, $J = 10.6, 5.6$ Hz, 1H), 4.12 (p, $J = 7.3$ Hz, 1H), 3.82 (s, 3H), 3.80 – 3.65 (m, 3H), 3.56 (ddt, $J = 23.8, 10.7, 5.4$ Hz, 1H), 3.21 (m, 1H), 3.10 (m, 1H), 2.65 – 2.48 (m, 3H), 1.95 (m, 9H), 1.77 – 1.58 (m, 9H), 1.39 (m, 24H), 1.31 (d, $J = 7.6$ Hz, 3H), 1.28 – 1.00 (m, 17H), 0.99 – 0.91 (m, 6H), 0.86 (m, 1H), 0.81 (q, $J = 8.6, 7.1$ Hz, 3H). ^{13}C NMR (101 MHz, CDCl_3) δ 175.81, 175.44, 174.64, 174.02, 172.67, 170.81, 170.43, 156.72, 156.23, 155.64, 135.96, 128.67, 128.34, 127.97, 79.60, 79.32, 67.18, 55.30, 54.89, 52.93, 51.26, 49.48, 49.44, 49.16, 47.84, 44.53, 44.41, 44.27, 41.54, 41.04, 39.56, 39.19, 38.79, 37.83, 37.30, 37.05, 34.19, 33.92, 33.63, 28.50, 28.47, 25.65, 25.46, 25.43, 25.31, 25.24, 24.88, 24.70, 22.97, 22.87, 22.23, 18.58, 16.72, 13.96, 12.84. HRMS-ESI (m/z) calc'd for $\text{C}_{64}\text{H}_{106}\text{N}_9\text{O}_{14}$ $[\text{M}+\text{H}]^+$, 1224.7854; found, 1224.8386.

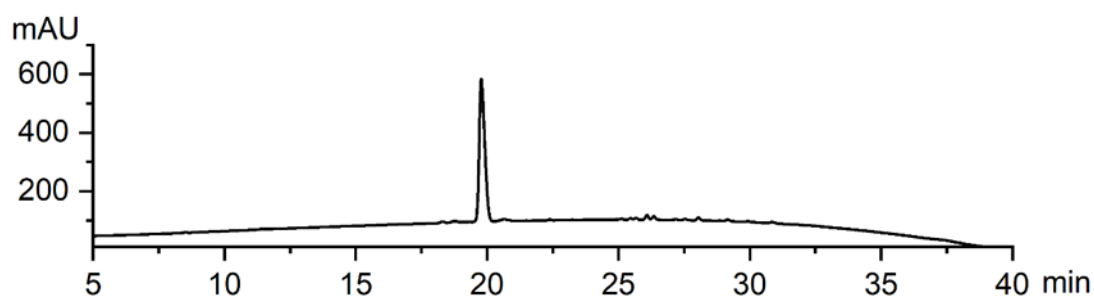


**Cbz-L-Ala-
AChPA-L-
Dap•NH₂-
AChPA-L-
Dap•NH₂-**

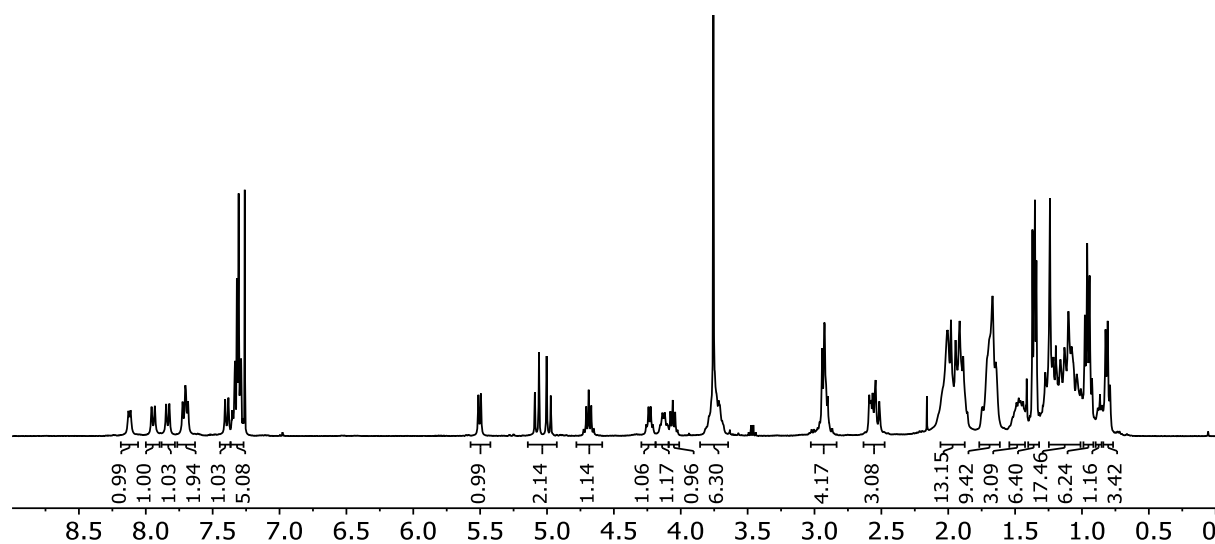
AChPA-L-Ala-OMe 288 Following general procedure F, foldamer **288** was collected as a white solid in 59% yield. ^1H NMR (400 MHz, CDCl_3) δ 8.12 (d, $J = 6.4$ Hz, 1H), 7.94 (d, $J = 9.7$ Hz, 1H), 7.84 (d, $J = 9.6$ Hz, 1H), 7.75 – 7.64 (m, 2H), 7.39 (d, $J = 9.8$ Hz, 1H), 7.31 (m, 5H), 5.50 (d, $J = 7.4$ Hz, 1H), 5.14 – 4.93 (m, 2H), 4.69 (p, $J = 7.5$ Hz, 1H), 4.23 (q, $J = 6.7$ Hz, 1H), 4.13 (q, $J = 6.9$ Hz, 1H), 4.05 (q, $J = 7.1$ Hz, 1H), 3.84 – 3.65 (m, 6H), 3.03 – 2.84 (m, 4H), 2.63 – 2.48 (m, 3H), 2.10 – 1.84 (m, 13H), 1.68 (m, 9H), 1.55 – 1.38 (m, 3H), 1.36

(m, 6H), 1.27 – 1.01 (m, 17H), 0.95 (m, 6H), 0.87 (m, 1H), 0.81 (m, 3H). HRMS-ESI (m/z) calc'd for $C_{54}H_{90}N_9O_{10}$ $[M+H]^+$, 1024.6806; found, 1024.6821.

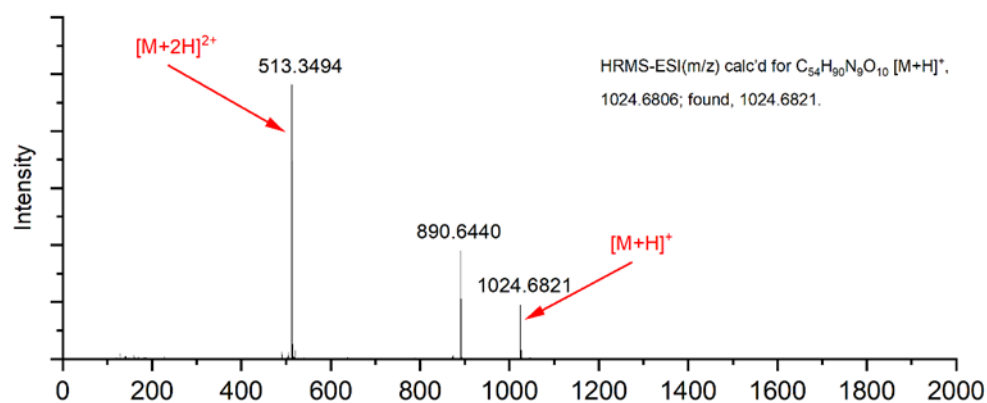
HPLC analysis: Acetonitrile+0.1% TFA/Water+0.1% TFA, 1.0 mL/min, 25 °C, detection at 210 nm, retention time (min): 19.8.



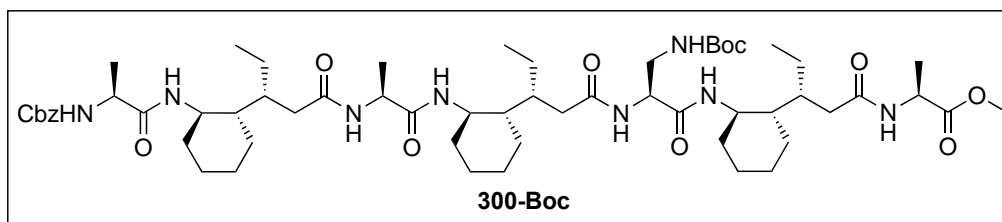
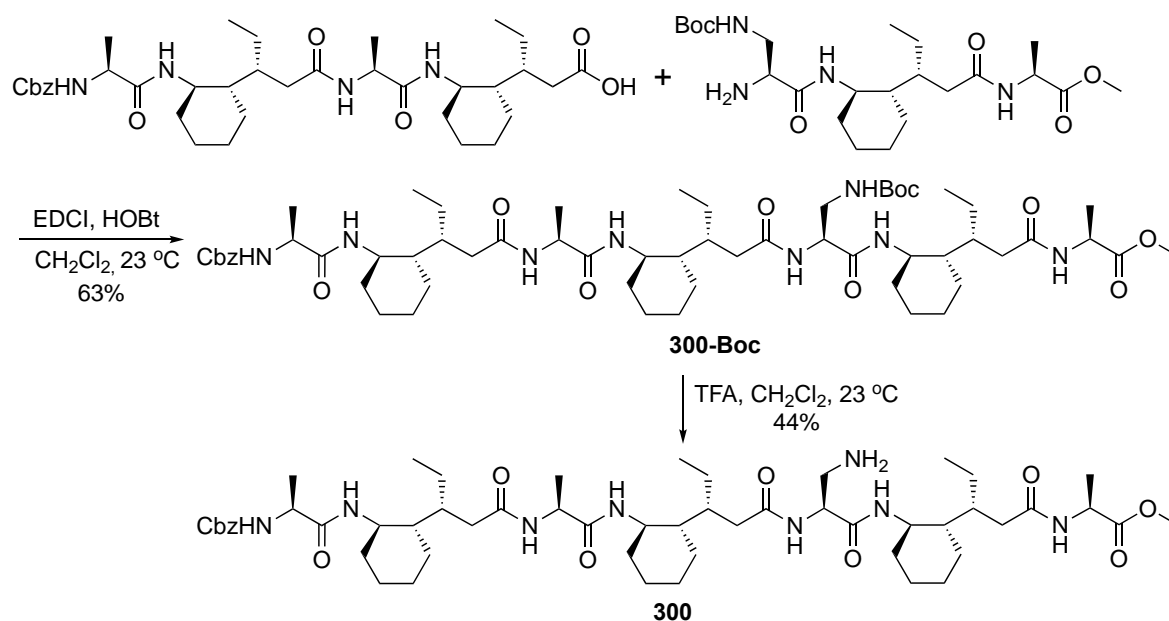
1H NMR spectrum of foldamer **288** (400 MHz, $CDCl_3$).



HRMS spectrum of foldamer **288**



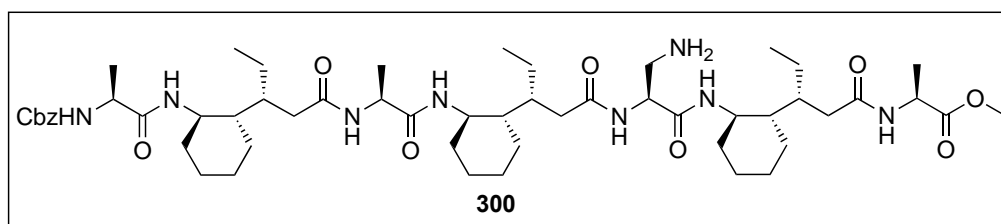
6.4.3 Synthesis of Foldamer 300



Cbz-L-Ala-
AChPA-L-
Ala-
AChPA-L-
Dap•Boc-

AChPA-L-Ala-OMe 300-Boc Following general coupling procedure, foldamer **300-Boc** was collected as a white solid in 63% yield. $^1\text{H NMR}$ (400 MHz, CDCl_3) δ 7.89 – 7.78 (m, 3H),

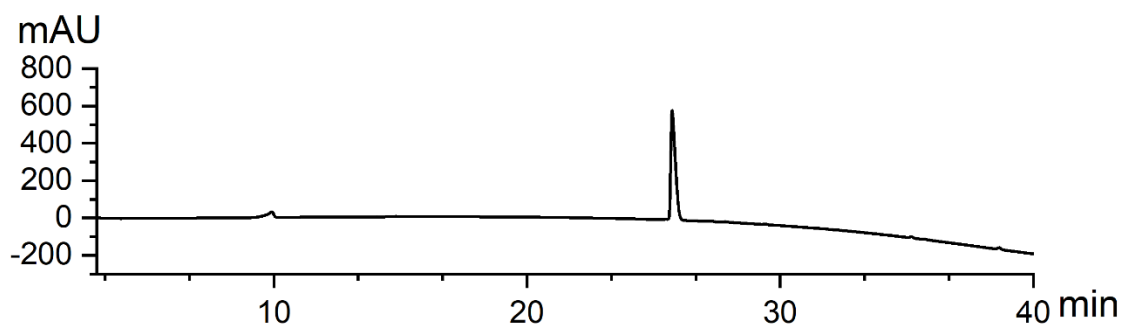
7.70 (dd, $J = 14.8, 8.6$ Hz, 2H), 7.62 (d, $J = 9.7$ Hz, 1H), 7.25 (m, 5H), 5.38 – 5.32 (m, 1H), 5.29 (d, $J = 6.9$ Hz, 1H), 5.05 (d, $J = 12.3$ Hz, 1H), 4.88 (d, $J = 12.3$ Hz, 1H), 4.57 (p, $J = 7.5$ Hz, 1H), 4.15 (m, 2H), 4.01 (h, $J = 6.9$ Hz, 1H), 3.78 (s, 3H), 3.67 (m, 4H), 3.56 – 3.47 (m, 1H), 3.01 (ddd, $J = 14.8, 10.5, 5.0$ Hz, 1H), 2.57 – 2.41 (m, 4H), 1.94 (m, 5H), 1.86 – 1.80 (m, 3H), 1.68 – 1.55 (m, 8H), 1.34 (s, 9H), 1.31 (m, 4H), 1.25 – 1.14 (m, 17H), 1.02 (m, 5H), 0.92 (m, 7H), 0.83 – 0.75 (m, 6H). ^{13}C NMR (101 MHz, CDCl_3) δ 174.64, 174.13, 173.60, 172.90, 172.47, 171.64, 169.60, 155.06, 154.49, 135.12, 127.47, 127.12, 126.85, 78.12, 65.84, 54.38, 51.82, 50.22, 49.37, 48.30, 48.00, 47.94, 46.72, 43.47, 43.28, 43.17, 40.05, 38.57, 38.20, 37.74, 36.17, 35.88, 35.77, 33.12, 32.96, 32.54, 30.57, 28.66 (d, $J = 3.5$ Hz), 27.31, 24.52, 24.33, 24.25, 24.12, 23.76, 23.68, 21.98, 21.82, 21.64, 21.25, 17.19, 16.63, 15.47, 13.12 (d, $J = 1.8$ Hz), 12.82, 11.63. Compound was tentatively assigned using HRMS.



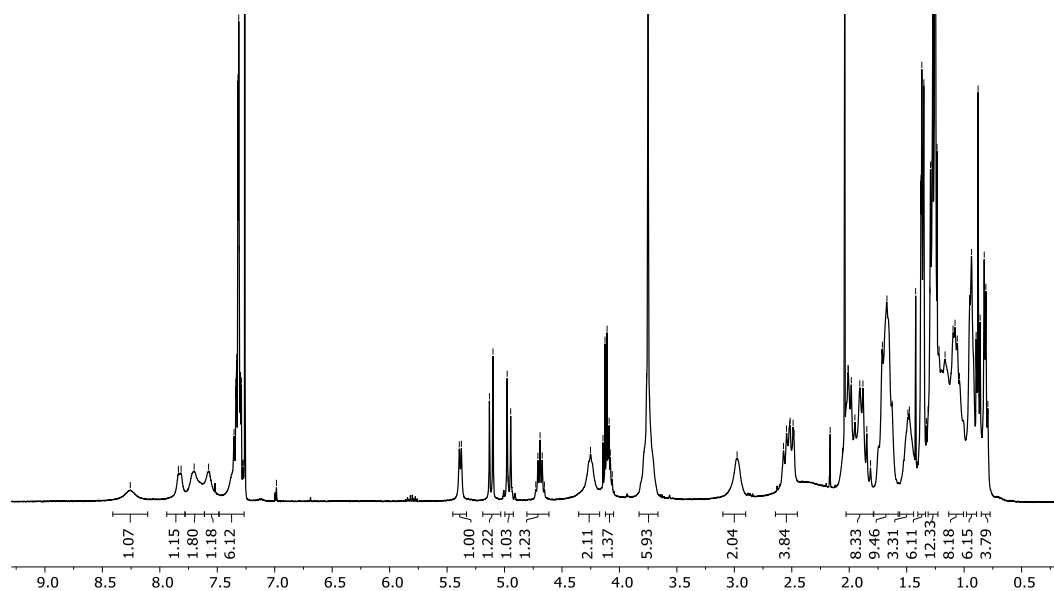
Cbz-L-Ala-
AChPA-L-
Ala-
AChPA-L-
Dap•NH₂

AChPA-L-Ala-OMe 300 Following general procedure F, foldamer **300** was collected as a white solid in 44% yield. ^1H NMR (400 MHz, CDCl_3) δ 8.26 (s, 1H), 7.83 (d, $J = 9.6$ Hz, 1H), 7.70 (m, 2H), 7.58 (s, 1H), 7.45 – 7.29 (m, 6H), 5.38 (d, $J = 7.2$ Hz, 1H), 5.12 (d, $J = 12.3$ Hz, 1H), 4.96 (d, $J = 12.3$ Hz, 1H), 4.69 (p, $J = 7.4$ Hz, 1H), 4.25 (m, 2H), 4.10 (m, 1H), 3.75 (m, 6H), 2.98 (m, 2H), 2.61 – 2.46 (m, 4H), 2.05 – 1.80 (m, 8H), 1.69 (m, 9H), 1.48 (m, 3H), 1.36 (m, 6H), 1.26 (m, 12H), 1.07 (m, 8H), 0.98 – 0.89 (m, 6H), 0.85 – 0.77 (m, 4H). HRMS-ESI (m/z) calc'd for $\text{C}_{54}\text{H}_{89}\text{N}_8\text{O}_{10}$ $[\text{M}+\text{H}]^+$, 1009.6696; found, 1009.6811. Compound **300** was tentatively assigned using ^{13}C NMR.

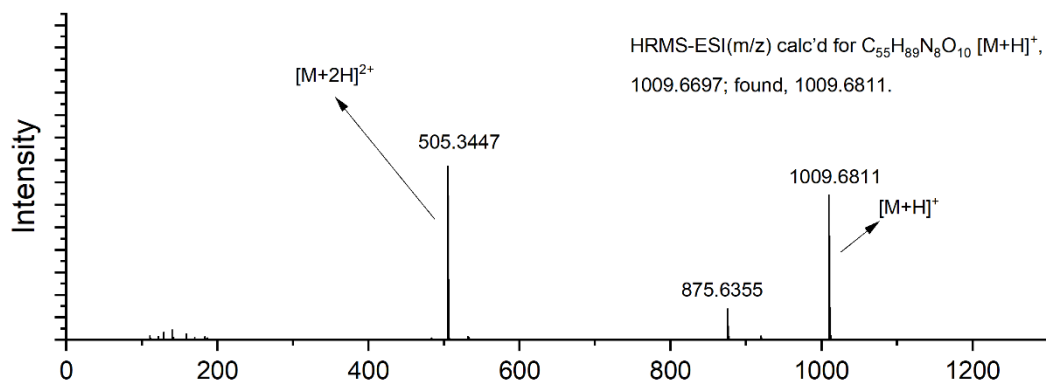
HPLC analysis: Acetonitrile+0.1% TFA/Water+0.1% TFA, 1.0 mL/min, 25 °C, detection at 210 nm, retention time (min): 25.7



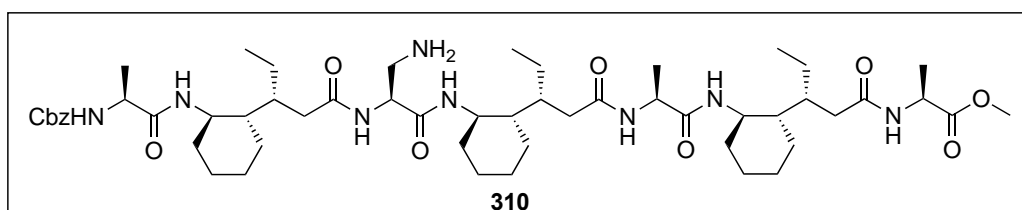
^1H NMR spectrum of foldamer **300** (400 MHz, CDCl_3).



HRMS spectrum of foldamer **300**



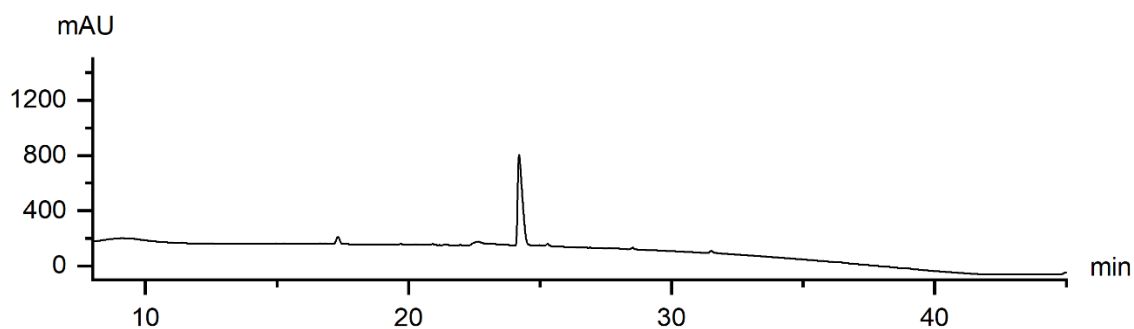
Dap•Boc-AChPA-L-Ala-AChPA-L-Ala-OMe 310-Boc Following general coupling procedure, foldamer **13-Boc** was collected as a white solid in 24% yield over 3 steps. ^1H NMR (400 MHz, CDCl_3) δ 8.17 (d, $J = 9.6$ Hz, 1H), 7.74 (d, $J = 6.0$ Hz, 1H), 7.71 – 7.56 (m, 3H), 7.34 – 7.23 (m, 5H), 7.17 (d, $J = 10.0$ Hz, 1H), 5.47 (d, $J = 7.5$ Hz, 1H), 5.38 (m, 1H), 5.03 (d, $J = 12.2$ Hz, 1H), 4.94 (d, $J = 12.3$ Hz, 1H), 4.60 (p, $J = 7.5$ Hz, 1H), 4.41 (q, $J = 6.8$ Hz, 1H), 4.13 – 4.07 (m, 1H), 3.69 (m, 6H), 3.59 (dt, $J = 14.1, 7.2$ Hz, 2H), 3.15 (ddd, $J = 13.2, 7.4, 4.4$ Hz, 1H), 2.58 – 2.39 (m, 3H), 1.92 – 1.82 (m, 46H), 1.60 (m, 10H), 1.49 – 1.42 (m, 2H), 1.33 (m, 11H), 1.26 (d, $J = 7.5$ Hz, 4H), 1.21 – 1.15 (m, 14H), 1.11 – 1.00 (m, 8H), 0.91 (m, 8H), 0.77 – 0.73 (m, 3H). ^{13}C NMR (101 MHz, CDCl_3) δ 176.39, 174.63, 174.15, 173.92, 173.76, 172.52, 170.45, 156.51, 155.94, 135.91, 128.51, 128.17, 127.90, 79.19, 67.00, 54.83, 52.50, 51.17, 50.24, 49.27, 49.06, 48.92, 47.78, 44.78, 44.30, 43.93, 41.45, 39.33, 39.04, 38.70, 37.82, 37.00, 36.75, 34.07, 33.77 (d, $J = 4.6$ Hz), 33.60, 31.56, 28.36, 26.89, 25.55, 25.35 (d, $J = 3.9$ Hz), 25.17, 25.06, 24.89, 24.71, 24.56, 22.77 (d, $J = 6.2$ Hz), 22.63, 22.17, 18.50, 17.13, 16.69, 14.10, 13.99, 13.67, 12.72. Compound was tentatively assigned using HRMS.



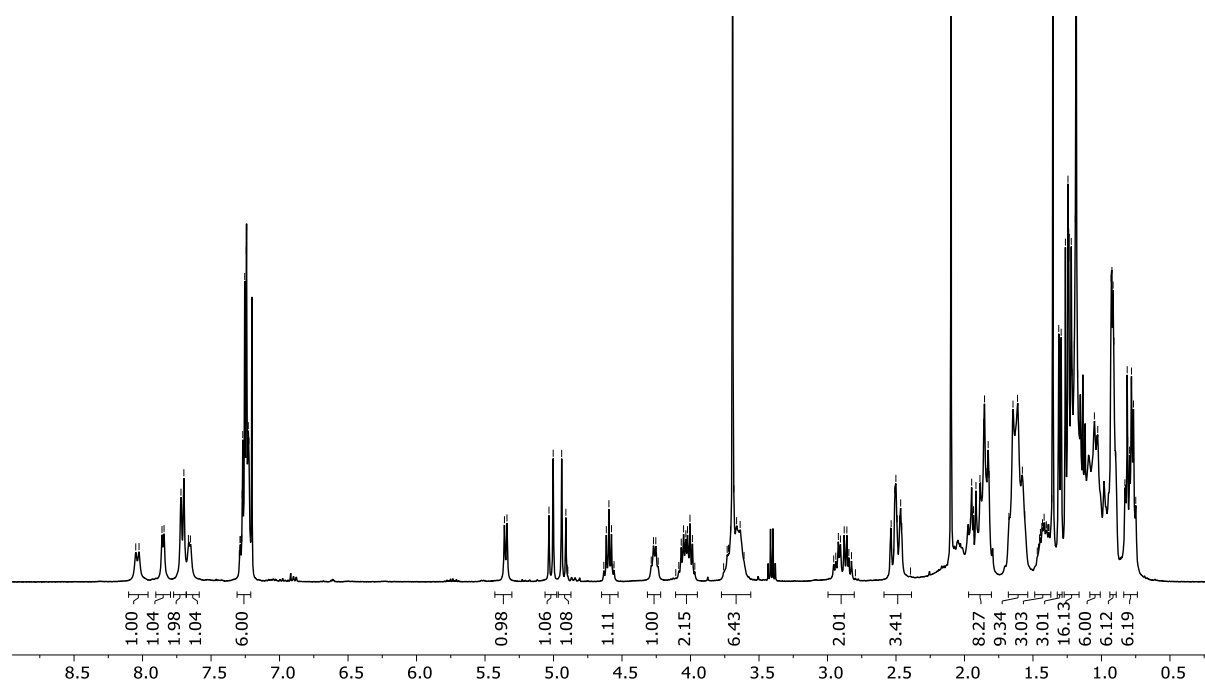
**Cbz-L-
Ala-
AChPA-
L-**

Dap•NH₂-AChPA-L-Ala-AChPA-L-Ala-OMe 310 Following general procedure F, foldamer **13** was collected as a white solid in 39% yield. ^1H NMR (400 MHz, CDCl_3) δ 8.04 (d, $J = 9.6$ Hz, 1H), 7.85 (d, $J = 6.0$ Hz, 1H), 7.71 (m, 2H), 7.66 (d, $J = 5.9$ Hz, 1H), 7.31 – 7.21 (m, 6H), 5.35 (d, $J = 7.4$ Hz, 1H), 5.02 (d, $J = 12.3$ Hz, 1H), 4.93 (d, $J = 12.3$ Hz, 1H), 4.60 (p, $J = 7.5$ Hz, 1H), 4.26 (q, $J = 6.8$ Hz, 1H), 4.03 (dp, $J = 18.2, 7.0$ Hz, 2H), 3.69 (m, 6H), 2.88 (qt, $J = 19.2, 8.8$ Hz, 2H), 2.50 (tt, $J = 13.7, 2.7$ Hz, 3H), 1.97 – 1.81 (m, 8H), 1.60 (m, 9H), 1.48 – 1.37 (m, 3H), 1.30 (d, $J = 6.9$ Hz, 3H), 1.27 – 1.17 (m, 16H), 1.04 (m, 6H), 0.92 (m, 6H), 0.79 (m, 6H). HRMS-ESI (m/z) calc'd for $\text{C}_{54}\text{H}_{89}\text{N}_8\text{O}_{10}$ $[\text{M}+\text{H}]^+$, 1009.6696; found, 1009.6716. Compound **310** was tentatively assigned using ^{13}C NMR.

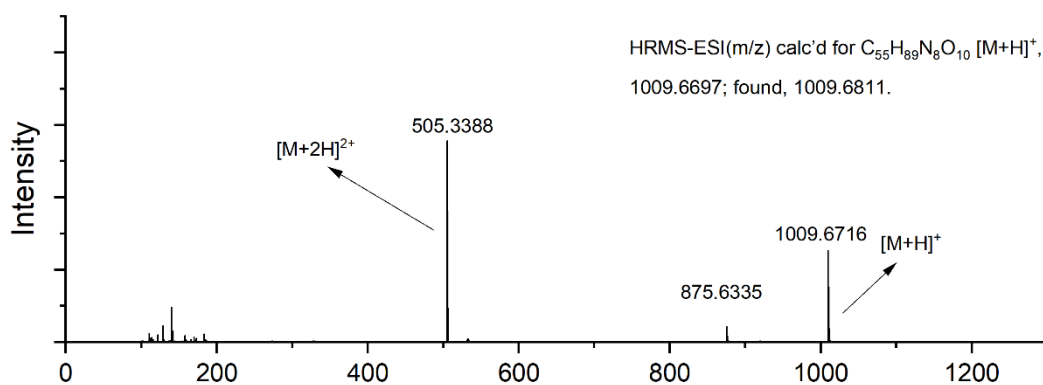
HPLC analysis: Acetonitrile+0.1% TFA/Water+0.1% TFA, 1.0 mL/min, 25 °C, detection at 210 nm, retention time (min): 24.2



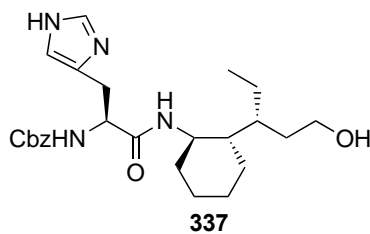
^1H NMR spectrum of foldamer **310** (400 MHz, CDCl_3).



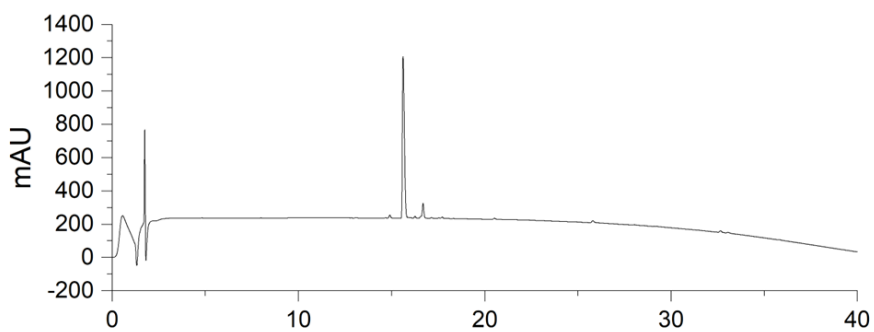
HRMS spectrum of foldamer **310**



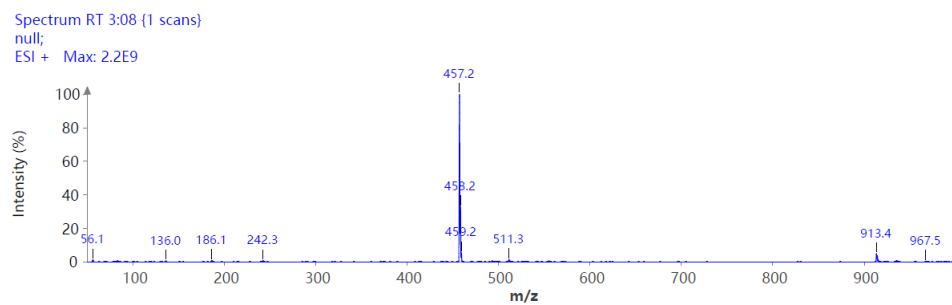
6.4.5 Characterization of Foldamer 337

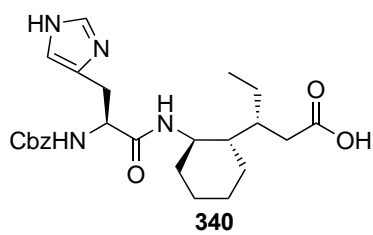


HPLC Result of **337**:

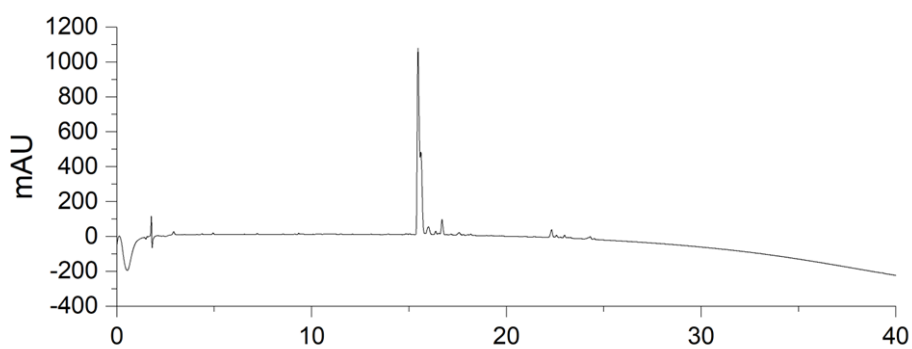


MS result of **337**:

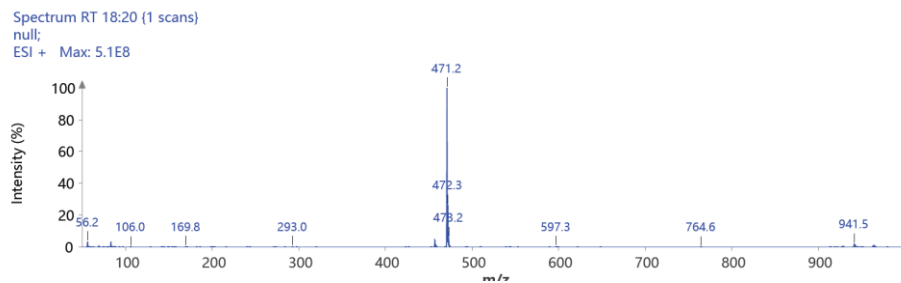


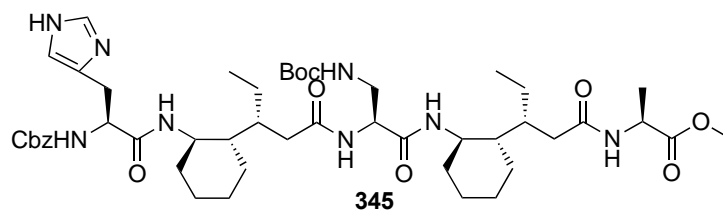


HPLC Result of **340**:

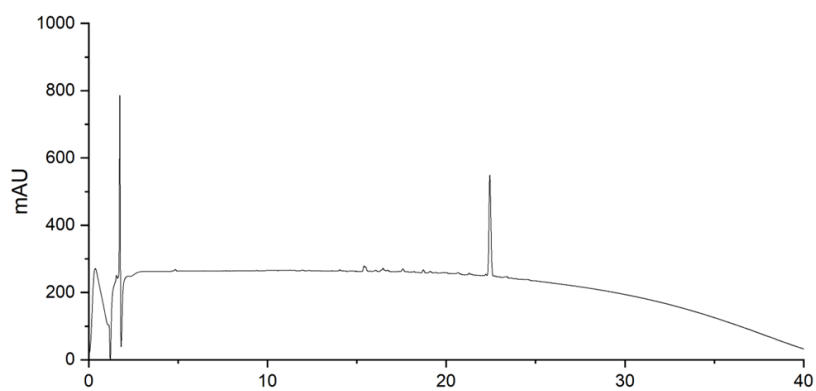


MS result of **340**:

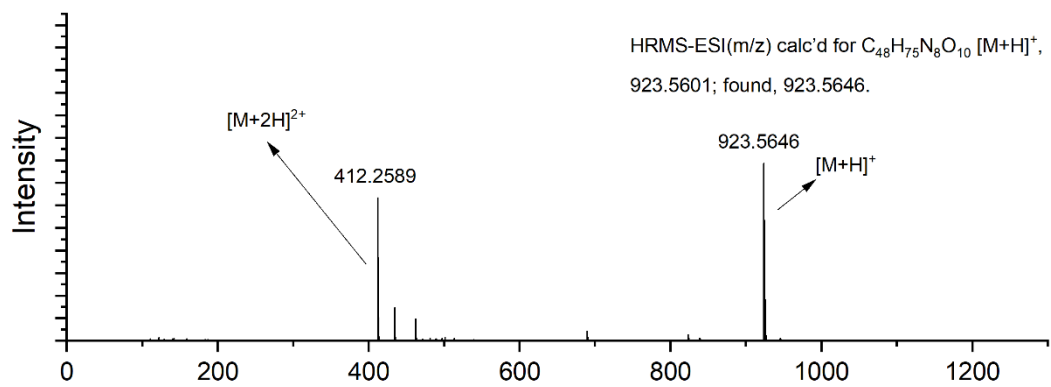


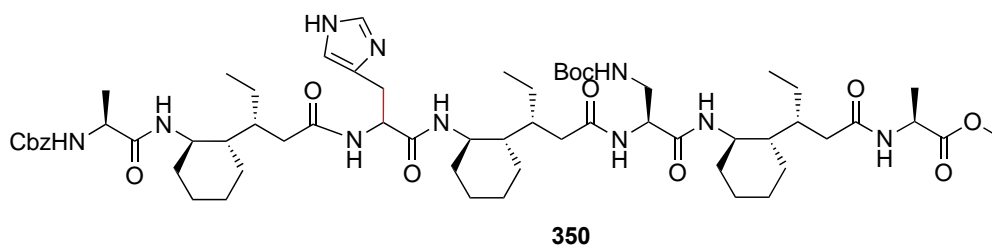


HPLC Result of **345**:

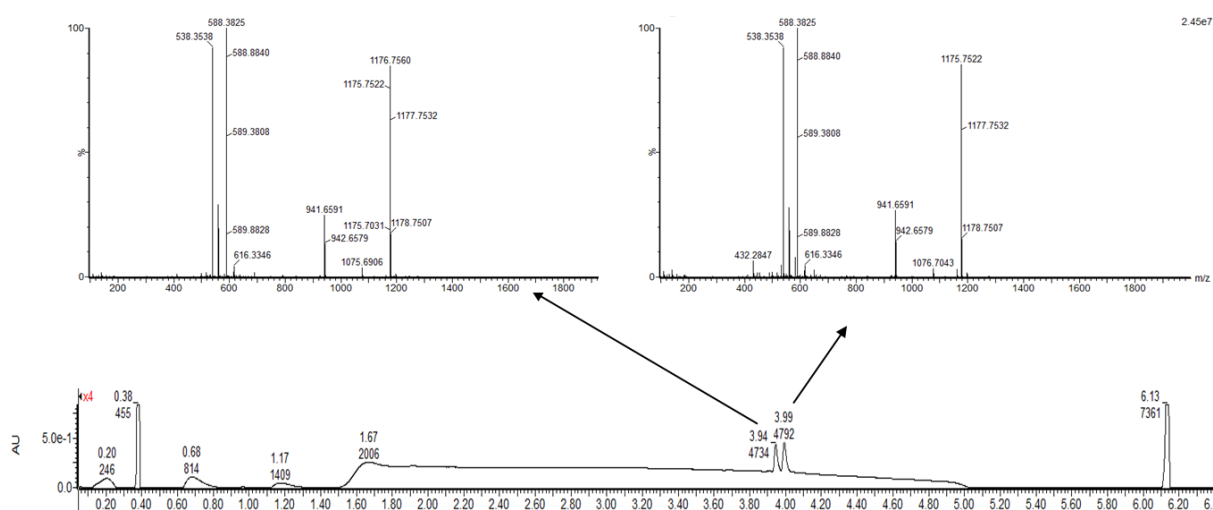


HRMS result of **345**:



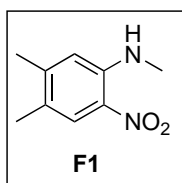


HPLC and HRMS result of epimerized **350**:



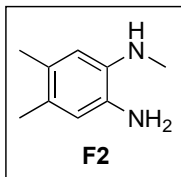
6.5 Synthesis and Characterization for Chapter 5

6.5.1 Synthesis of Flavin-Conjugated Foldamer F34

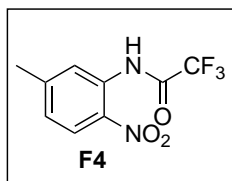


N,4,5-trimethyl-2-nitroaniline **F1**⁹⁷ 4,5-dimethyl-2-nitroaniline (1g, 6.02 mmol) was mixed and stirred with H₂SO₄ (Conc., 10 mL) in a 100 mL flask, then aqueous formaldehyde (37%, 10 mL) was added dropwise to the solution over 3h, after addition, the mixture was reacted at 65 °C for 3h. Then the reaction was cooled down and slowly poured into 200 mL of ice water, then filtered to collect the solid, the solid was dissolved in EtOAc and washes with saturated NaHCO₃, the organic layer was dried over MgSO₄, filtered and concentrated to give an orange solid in 85 % yield. ¹H NMR (400 MHz, CDCl₃) δ 7.92 (s, 1H), 6.61 (s, 1H), 3.00 (s, 3H), 2.28 (s, 3H), 2.18 (s,

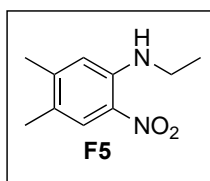
3H). ^{13}C NMR (101 MHz, CDCl_3) δ 147.48, 145.16, 129.99, 126.57, 124.46, 113.87, 29.89, 20.87, 18.67. Compound was tentatively assigned using HRMS.



***N*¹,4,5-trimethylbenzene-1,2-diamine F2⁹⁷ F1** (0.8 g, 4.44 mmol) was dissolved in 10 mL of Methanol and 10 mL of ethyl acetate, 10 w% Pd/C was added, the solution was sparged with H_2 and reacted under H_2 for 4 h, then the mixture was filtered through a pad of celite and concentrated to give the product in 90% yield. ^1H NMR (400 MHz, CDCl_3) δ 6.53 (s, 1H), 6.48 (s, 1H), 2.85 (s, 3H), 2.22 (s, 3H), 2.16 (s, 3H). ^{13}C NMR (101 MHz, CDCl_3) δ 136.92, 131.92, 128.20, 125.99, 118.37, 113.21, 31.37, 19.38, 18.85. Compound was tentatively assigned using HRMS.

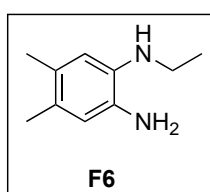


***N*-(4,5-dimethyl-2-nitrophenyl)-2,2,2-trifluoroacetamide F4⁹⁸** 4,5-dimethyl-2-nitroaniline (2.0 g, 12.0 mmol) was dissolved in CH_2Cl_2 (25 mL) and stirred at 0 °C, Trifluoroacetic anhydride (3.3 mL, 24.1 mmol) was added to the solution dropwise, and the triethylamine (3 mL) was added to the vigorously stirred solution dropwise, after the addition, the reaction was brought to room temperature and reacted for 1 h. The mixture was washed with 2 M HCl, aqueous NaHCO_3 and brine. The organic layer was dried over MgSO_4 , concentrated, and dried over vacuum to get the product in 89% yield. ^1H NMR (400 MHz, CDCl_3) δ 11.34 (s, 1H), 8.50 (s, 1H), 8.07 (s, 1H), 2.39 (s, 3H), 2.34 (s, 3H). ^{13}C NMR (101 MHz, CDCl_3) δ 155.56, 155.18, 147.50, 135.06, 129.99, 126.58, 122.91, 117.03, 114.16, 20.68, 19.46. Compound was tentatively assigned using HRMS.

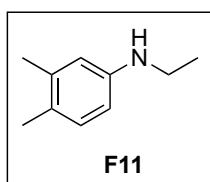


***N*-ethyl-4,5-dimethyl-2-nitroaniline F5⁹⁸ F4** (1.8 g, 4.96 mmol) and K_2CO_3 (3.42 g, 24.80 mmol) were dissolved in DMF (25 mL) and reacted for 30 min, then iodoethane (1.16 g, 7.44 mmol) was added dropwise, the mixture was refluxed overnight, then DMF was evaporated, and the residue was dissolved in water and extracted with chloroform and washed with aqueous LiCl, the organic

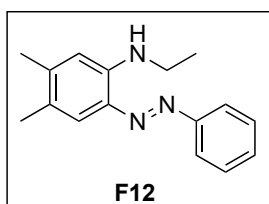
layer was dried over MgSO₄ and concentrated to give the product in 93% yield. ¹H NMR (400 MHz, CDCl₃) δ 7.92 (d, J = 1.0 Hz, 1H), 6.62 (s, 1H), 3.33 (q, J = 7.2 Hz, 2H), 2.29 – 2.24 (m, 3H), 2.17 (d, J = 0.8 Hz, 3H), 1.36 (t, J = 7.2 Hz, 3H). ¹³C NMR (101 MHz, CDCl₃) δ 147.38, 144.31, 129.82, 126.59, 124.39, 114.23, 37.82, 20.87, 18.68, 14.61. Compound was tentatively assigned using HRMS.



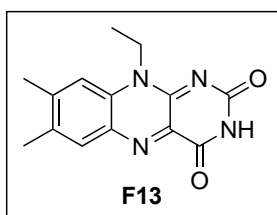
***N*¹-ethyl-4,5-dimethylbenzene-1,2-diamine F6⁹⁸ F5** (1.0 g, 3.82 mmol) was dissolved in 10 mL of Methanol and 10 mL of ethyl acetate, 10 w% Pd/C was added, the solution was sparged with H₂ and reacted under H₂ for 4 h, then the mixture was filtered through a pad of celite and concentrated to give the product in 93% yield. ¹H NMR (400 MHz, CDCl₃) δ 6.54 (s, 1H), 6.49 (d, J = 2.3 Hz, 1H), 3.41 – 2.95 (m, 4H), 2.20 (s, 3H), 2.15 (s, 3H), 1.30 (td, J = 7.1, 2.2 Hz, 3H). ¹³C NMR (101 MHz, CDCl₃) δ 135.99, 131.98, 128.16, 126.14, 118.51, 114.12, 39.21, 19.40, 18.90, 15.24. Compound was tentatively assigned using HRMS.



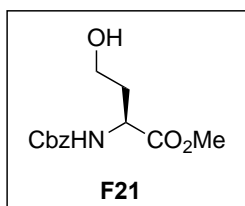
***N*-ethyl-3,4-dimethylaniline F11¹²¹** 3,5-Dimethyl aniline (3.0 g, 24.8 mmol) was dissolved in DMF (25 mL), the solution was cooled to 0 °C, to this solution was added NaH (1.19 g, 49.5 mmol) in several portions, the resulting mixture was stirred at 0 °C for 15 min, then iodoethane (3.9 g, 24.8 mmol) was added dropwise, and the mixture was stirred at room temperature for 12 h. The reaction was quenched with ice water, and most of DMF was evaporated under reduced pressure, the residue was extracted with ethyl acetate washed with water, aqueous LiCl, brine and dried over MgSO₄, concentrated, and purified via column chromatography to collect the compound in 75% yield. ¹H NMR (400 MHz, CDCl₃) δ 7.01 (d, J = 8.0 Hz, 1H), 6.51 (d, J = 2.6 Hz, 1H), 6.45 (dd, J = 8.0, 2.6 Hz, 1H), 3.19 (q, J = 7.1 Hz, 2H), 2.27 (s, 3H), 2.23 (s, 3H), 1.30 (t, J = 7.1 Hz, 3H). ¹³C NMR (101 MHz, CDCl₃) δ 146.77, 137.28, 130.34, 125.29, 114.82, 110.40, 38.91, 20.11, 18.76, 15.07. Compound was tentatively assigned using HRMS.



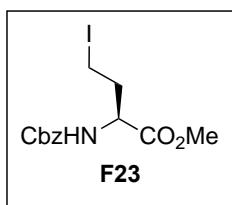
(E)-N-ethyl-4,5-dimethyl-2-(phenyldiazenyl)aniline F12 In a 50 ml round bottle flask, aniline (1.26 g, 13.5 mmol), 12 N HCl (3.77 mL), H₂O (8.86 mL) was stirred at 0 °C for 10 min. Then NaNO₂ (0.93 g, 13.5 mmol) was added in several small portions, the mixture was stirred at 0 °C for 30 min to make the diazotized aniline solution. To another 50 mL round bottle flask was added (1.66 g, 11.13 mmol), 23 mL H₂O, then 12 N HCl (4 mL) and 3.77 g of sodium acetate were added, the mixture was cooled to –6 °C, diazotized aniline solution was added, and the mixture was reacted at –6 °C for 1 h and 0 °C for 2 h. The reaction was warmed up to room temperature, and the aqueous sodium acetate solution (1.89 g in 14.3 mL) was slowly added to maintain the pH≈3, the mixture was stirred at room temperature for 12 h. The solid was removed by filtration and the solution was concentrated and the residue was purified by flash chromatography to give an orange solid with a 50% yield. ¹H NMR (400 MHz, CDCl₃) δ 7.82 – 7.75 (m, 2H), 7.61 (s, 1H), 7.47 (dd, J = 8.4, 7.0 Hz, 2H), 7.39 – 7.32 (m, 1H), 6.60 (s, 1H), 3.33 (q, J = 7.2 Hz, 2H), 2.29 (s, 3H), 2.24 (s, 3H), 1.36 (t, J = 7.2 Hz, 3H). ¹³C NMR (101 MHz, CDCl₃) δ 153.24, 142.83, 141.88, 134.93, 131.30, 129.16 (d, J = 3.1 Hz), 124.14, 121.87, 112.91, 37.58, 20.77, 18.70, 14.77. The compound was tentatively assigned using HRMS.



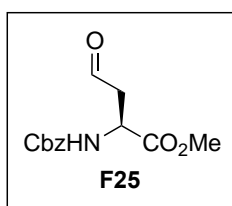
10-ethyl-7,8-dimethylbenzo[γ]pteridine-2,4(3H,10H)-dione F13⁹⁸ **F12** (0.29 g, 1.15 mmol), barbituric acid (0.29 g, 2.30 mmol), and 0.6 mL acetic acid were dissolved in 5 mL dioxane and refluxed for 5 h, the mixture was cooled down, the produced was filtered off and washes with diethyl ether, the crude material was purified via column chromatography to give a yellow solid in a 35% yield. ¹H NMR (400 MHz, DMSO-*d*⁶) δ 11.27 (s, 1H), 7.91 (s, 1H), 7.82 (s, 1H), 4.64 (q, J = 7.0 Hz, 2H), 2.52 (s, 3H), 2.40 (s, 3H), 1.33 (t, J = 7.0 Hz, 3H). ¹³C NMR (101 MHz, DMSO-*d*⁶) δ 159.94, 155.67, 149.79, 146.61, 137.17, 135.70, 133.84, 131.05, 130.47, 115.93, 40.15, 20.55, 18.75, 11.95. Compound was tentatively assigned using HRMS.



Benzyl (S)-(1-hydroxy-4-oxopentan-3-yl)carbamate F21¹²² F20 (4.0 g, 14.22 mmol) was dissolved in 30 mL of THF, then $\text{BH}_3 \cdot \text{SMe}_2$ (9.24 mL, 2M in THF) was added at 0 °C, the solution was stirred at room temperature overnight, then slowly quenched with H_2O and K_2CO_3 , the solution was filtered through celite and concentrated, the residue was dissolved into ethyl acetate and washes with aqueous NaHCO_3 , the organic layer was dried over MgSO_4 , filtered and concentrated to give the desired product in 80% yield. ^1H NMR (400 MHz, CDCl_3) δ 7.38 – 7.24 (m, 5H), 5.91 (d, $J = 8.1$ Hz, 1H), 5.08 (s, $J = 2.3$ Hz, 2H), 4.50 (td, $J = 8.5, 4.3$ Hz, 1H), 3.80 – 3.54 (m, 5H), 3.19 (s, 1H), 2.09 (ddt, $J = 13.9, 9.2, 5.0$ Hz, 1H), 1.76 (ddt, $J = 13.5, 8.7, 4.3$ Hz, 1H). ^{13}C NMR (101 MHz, CDCl_3) δ 173.05, 156.68, 136.12, 128.51, 128.21, 128.08, 67.15, 58.39, 52.51, 51.46, 35.12. Compound was tentatively assigned using HRMS.

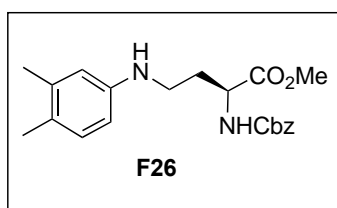


Benzyl (S)-(1-iodo-4-oxopentan-3-yl)carbamate F23¹²³ Iodine (1.14 g, 4.49 mmol) was added in several portions to a solution of 1*H*-imidazole (0.31 g, 4.49 mmol) and PPh_3 (1.18 g, 4.49 mmol) in 22 mL of CH_2Cl_2 at 0 °C, the resulting mixture was warmed to room temperature, then a solution of **F21** (1 g, 3.74 mmol) in 4 mL of CH_2Cl_2 was added, the mixture was stirred at room temperature for another 2 h. The solution was concentrated and purified via column chromatography to collect the desired product in a 95% yield. ^1H NMR (400 MHz, CDCl_3) δ 7.41 – 7.29 (m, 5H), 5.40 (d, $J = 8.3$ Hz, 1H), 5.12 (s, 2H), 4.43 (td, $J = 8.0, 4.8$ Hz, 1H), 3.76 (s, 3H), 3.16 (t, $J = 7.5$ Hz, 2H), 2.44 (dq, $J = 13.8, 7.1$ Hz, 1H), 2.21 (dq, $J = 14.5, 7.4$ Hz, 1H). ^{13}C NMR (101 MHz, CDCl_3) δ 171.82, 156.01, 136.13, 128.69, 128.42, 128.28, 67.36, 54.79, 52.85, 36.98, -0.77. Compound was tentatively assigned using HRMS.



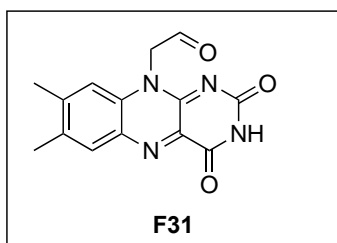
Benzyl (S)-(1,4-dioxopentan-3-yl)carbamate F25¹²⁴ F21 (1.4 g, 5.24 mmol) was dissolved in 10 mL of CH_2Cl_2 , NaHCO_3 (1.89 g, 31.45 mmol) was added at 0 °C, then DMP (3.30 g, 7.78 mmol) was added, the mixture was brought to room temperature and reacted for 4 h. The solution was concentrated and purified via column chromatography to collect the desired product in an 83%

yield. ^1H NMR (400 MHz, CDCl_3) δ 9.69 (s, 1H), 7.39 – 7.27 (m, 5H), 5.74 (d, J = 8.4 Hz, 1H), 5.10 (s, 2H), 4.65 (dt, J = 9.0, 4.8 Hz, 1H), 3.73 (s, 3H), 3.07 (qd, J = 18.5, 4.9 Hz, 2H). ^{13}C NMR (101 MHz, CDCl_3) δ 199.27, 171.22, 156.01, 136.14, 128.62, 128.33, 128.17, 67.24, 52.93, 49.09, 45.85. Compound was tentatively assigned using HRMS.



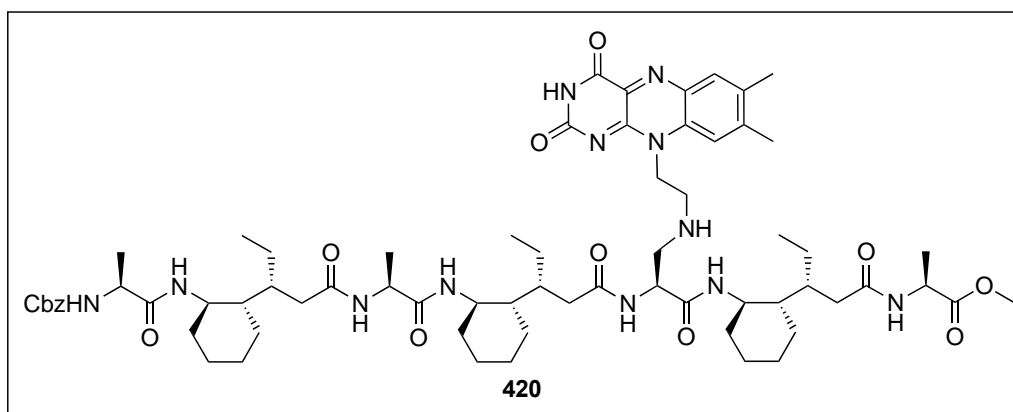
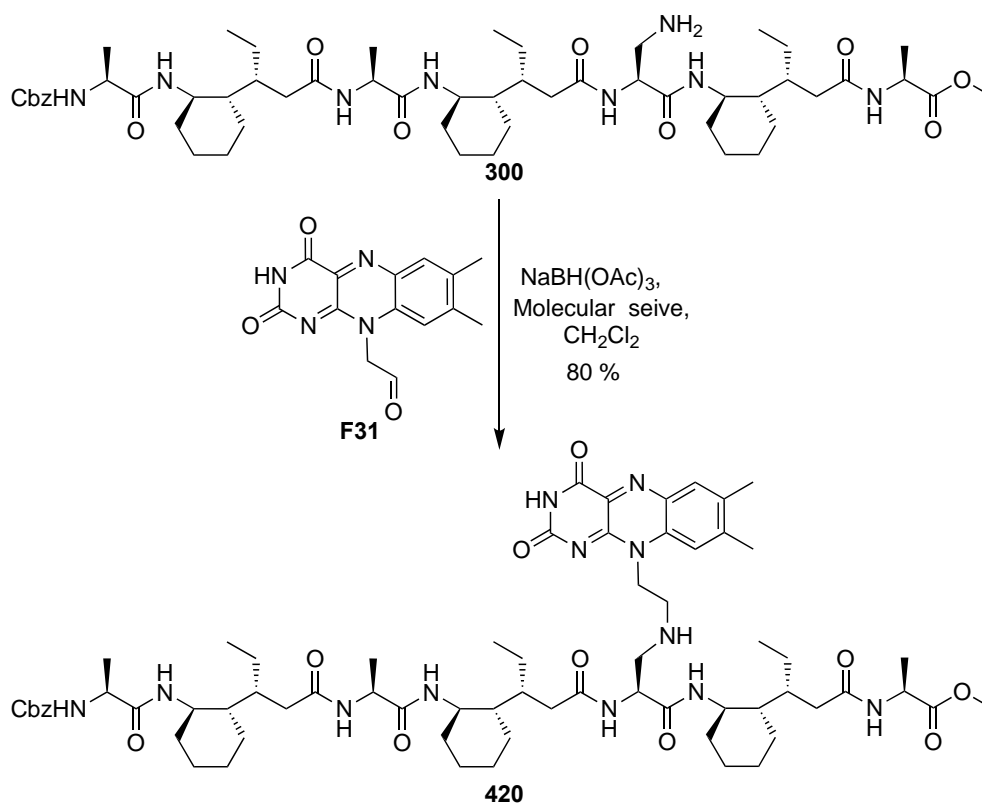
methyl (S)-2-(((benzyloxy)carbonyl)amino)-4-((3,4-dimethylphenyl)amino) butanoate F26 $\text{NaBH}(\text{OAc})_3$ (0.36 g, 1.70 mmol) was added into a solution of **F25** (0.30 g, 1.14 mmol) and aniline (0.15 g, 1.25 mmol) in 20 mL of anhydrous

dichloroethane, then 2 drops of glacial acetic acid was added, the mixture was stirred at room temperature for 2 h. The solution was concentrated and purified via column chromatography to collect the desired product in an 69% yield. ^1H NMR (400 MHz, CDCl_3) δ 7.44 – 7.29 (m, 5H), 6.93 (d, J = 8.0 Hz, 1H), 6.46 – 6.42 (s, 1H), 6.38 (d, J = 8.3 Hz, 1H), 5.52 (d, J = 8.1 Hz, 1H), 5.13 (d, J = 1.6 Hz, 2H), 4.51 (td, J = 7.9, 4.6 Hz, 1H), 3.71 (s, 3H), 3.36 – 3.20 (m, 2H), 2.19 (s, 3H), 2.15 (m, 4H), 1.90 (ddt, J = 13.9, 7.9, 6.0 Hz, 1H). ^{13}C NMR (101 MHz, CDCl_3) δ 173.02, 156.23, 145.87, 137.49, 136.28, 130.44, 128.71, 128.39, 128.27, 125.82, 115.04, 110.54, 67.26, 52.64, 52.21, 40.33, 32.37, 20.16, 18.81. The compound was tentatively assigned using HRMS.



2-(7,8-dimethyl-2,4-dioxo-3,4-dihydrobenzo[g]pteridin-10(2H)-yl) acetaldehyde F31¹⁰³ To a tin foil wrapped 250 mL round bottle flask, was added riboflavin (2.5 g) and 100 mL of H_2O , followed by NaIO_4 (4.0 g), the mixture was stirred at room temperature overnight. The precipitate was filtered and washes

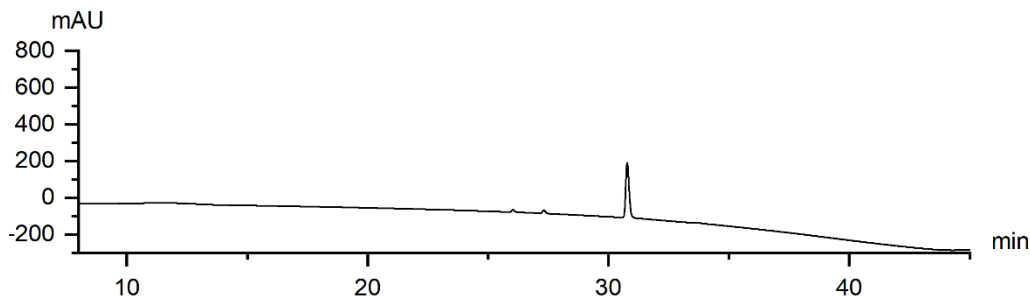
with water, methanol, and ether, dried over vacuum. The residue was suspended in 50 mL of toluene and refluxed for 4 h, the precipitate was filtered and washed with ether to give a yellow solid. The crude product was used in the next step without further purification.



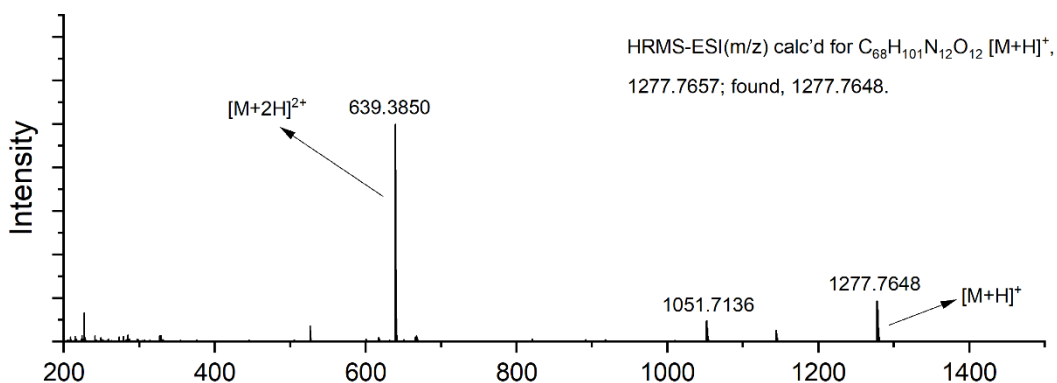
15 mg of foldamer **300**, 40 mg of **F31**, and molecular sieve were dissolved in 5 mL of

anhydrous DMF, the mixture was stirred at room temperature under dark condition for 2 days, 5 mL of DCM was added and filtered off the insoluble solid, the organic layer was washed with LiCl aqueous solution, concentrated and purified via reverse phase column to collect the **420** as a bright yellow solid in 80% yield. (avoid light during the whole procedure). Purity was conformed using HPLC. HRMS-ESI (m/z) calc'd for C₆₈H₁₀₁N₁₂O₁₂ [M+H]⁺, 1277.7657; found, 1277.7648. The compound was tentatively assigned using NMR.

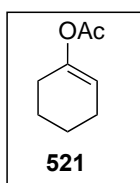
HPLC result of **420**:



HRMS result of **420**:

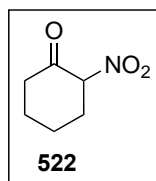


6.5.2 Synthesis of Piperidine-Based δ -Amino Acid



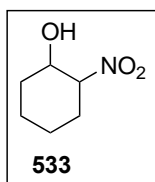
cyclohex-1-en-1-yl acetate 510 Compound **510** was prepared according to literature¹¹⁶. 25 mL of cyclohexanone, 45 mL of acetic anhydride, and 250 mg of *para*-toluenesulfonic acid monohydrate were refluxed overnight, the reaction mixture was concentrated and purified via column chromatograph to get a crude.

And the product was distilled under decreased pressure to get a colourless product. This compound was used in the next step without further purification.

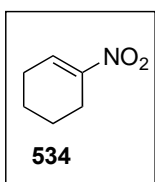


2-nitrocyclohexan-1-one 522 Compound **510** was prepared according to literature¹¹⁶. R87 (6.0 g, 42.8 mmol) was dissolved in 50 mL of chloroform, the solution was cooled down to 0 °C, then trifluoroacetic anhydride (43 mL) was added dropwise, then the mixture was bring up to room temperature to react for

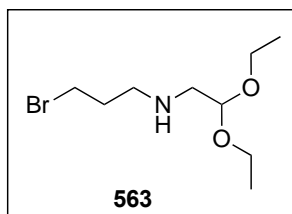
1h, then the reaction was slowly and added into ice water in several portions, extracted with dichloromethane, the organic layer was dried over MgSO_4 , filtered and concentrated. The residue was purified via column to give the desired product as an oil in 17% yield over 2 steps. ^1H NMR (400 MHz, CDCl_3) δ 5.23 (ddd, $J = 12.0, 5.9, 1.0$ Hz, 1H), 2.69 – 2.60 (m, 1H), 2.57 – 2.38 (m, 3H), 2.12 (m, 1H), 2.06 – 1.99 (m, 1H), 1.82 – 1.72 (m, 2H). ^{13}C NMR (101 MHz, CDCl_3) δ 198.56, 91.89, 40.78, 31.64, 26.45, 22.59. Data are in agreement with the literature.



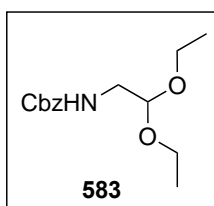
2-nitrocyclohexan-1-ol 533¹¹⁶ To a solution of **522** (3 g, 21 mmol) in 50 mL of Methanol at 0 °C was added NaBH_4 (0.87 g, 23 mmol) slowly in several portions, the reaction was stirred at 0 °C and TLC every 10 minutes until most of the starting material was consumed, then the reaction mixture was poured into cooled NH_4Cl aqueous solution, extracted with ethyl acetate, washed with water and brine, dried over MgSO_4 , filtered and concentrated, the crude was bring forward to next step without further purification.



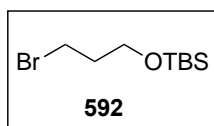
1-nitrocyclohex-1-ene 534¹¹⁶ Compound **534** was prepared according to literature¹¹⁶. To a solution of **533** (2.3 g, 15.8 mmol) in 75 mL of dichloromethane at -40 °C was dropwise added trifluoroacetic anhydride (2.2 mL, 15.8 mmol) and then triethylamine (4.42mL, 31.7 mmol) over 1 h, the reaction was brought to room temperature and reacted for 5 h, then quenched with saturated NH_4Cl aqueous solution, extracted with dichloromethane, washed with water and brine, the organic layer was dried over MgSO_4 , filtered and concentrated. The residue was purified via column to give the desired product as a pale-yellow liquid in a 62% yield over two steps. ^1H NMR (400 MHz, CDCl_3) δ 7.30 (tt, $J = 4.8, 1.8$ Hz, 1H), 2.55 (ttd, $J = 6.3, 2.7, 1.6$ Hz, 2H), 2.37 – 2.26 (m, 2H), 1.81 – 1.70 (m, 2H), 1.67 – 1.56 (m, 2H). ^{13}C NMR (101 MHz, CDCl_3) δ 149.70, 134.33, 24.78, 23.90, 21.78, 20.66. Data are in agreement with the literature.



3-bromo-*N*-(2,2-diethoxyethyl)propan-1-amine 563 To a stirred solution of 1,3-dibromopropane (1.08 mL, 7.5 mmol) and 2,2-diethoxyethan-1-amine (0.5 mL, 5.0 mmol) in dry DMF was added NaH (0.12 g, 5.0 mmol) in several portions at 0 °C, the reaction mixture was reacted at 0 °C for 2 h, and was poured into iced water, extracted with hexane, the organic layer was dried over MgSO₄, filtered and concentrated. The residue was purified via column to give the desired product as a liquid in 73% yield. ¹H NMR (400 MHz, CDCl₃) δ 4.58 (t, J = 5.5 Hz, 1H), 3.70 (m, 2H), 3.60 – 3.53 (m, 2H), 3.47 (t, J = 6.6 Hz, 2H), 2.77 (t, J = 6.8 Hz, 2H), 2.72 (d, J = 5.6 Hz, 2H), 2.02 (p, J = 6.7 Hz, 2H), 1.21 (t, J = 7.1 Hz, 6H). The compound was tentatively assigned using HRMS.

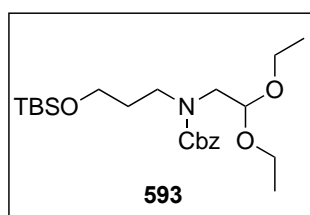


Benzyl (2,2-diethoxyethyl)carbamate 583¹²⁵ To a solution of aminoacetaldehyde diethyl acetal (2.18 mL, 15 mmol) in Et₂O (75 mL) was added potassium carbonate (6.20 g, 44.9 mmol) and water (75 mL). The reaction mixture was then cooled to 0 °C, and benzyl chloroformate (2.1 mL, 15.0 mmol) was added. The reaction mixture was warmed up to room temperature and stirred for 18 h. Et₂O was added, and the organic layer was washed with 5% aqueous citric acid and brine. The organic layer was dried over MgSO₄, filtered and concentrated to get a colourless oil in 88% yield. ¹H NMR (400 MHz, CDCl₃) δ 7.41 – 7.31 (m, 5H), 5.12 (s, 2H), 5.05 (t, J = 6.2 Hz, 1H), 4.52 (t, J = 5.3 Hz, 1H), 3.72 (dq, J = 9.3, 7.0 Hz, 2H), 3.55 (dq, J = 9.4, 7.0 Hz, 2H), 3.35 (t, J = 5.7 Hz, 2H), 1.22 (t, J = 7.1 Hz, 6H). ¹³C NMR (101 MHz, CDCl₃) δ 156.45, 136.50, 128.54, 128.16, 100.98, 66.81, 62.85, 43.53, 15.31. Data are in agreement with the literature.



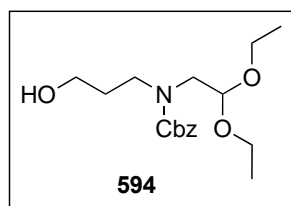
(3-bromopropoxy)(*tert*-butyl)dimethylsilane 592¹²⁶ To a solution of 3-bromopropan-1-ol (1 g, 7.19 mmol) and imidazole (0.74 g, 10.8 mmol) in THF (30 mL) was added *tert*-butylchlorodimethylsilane (1.63g, 10.8 mmol) in THF (4 mL) at 0 °C. Cooling was removed after 30 min, after stirring overnight at room temperature, the saturated aqueous NH₄Cl (15 mL) was added, and the mixture was extracted with CH₂Cl₂, dried with MgSO₄ and concentrated, the crude product was purified via

column chromatography eluting with EtOAc/hexane to give the desired product in 97% yield. ^1H NMR (400 MHz, CDCl_3) δ 3.73 (t, $J = 5.7$ Hz, 1H), 3.51 (t, $J = 6.5$ Hz, 1H), 2.03 (ddd, $J = 12.2, 6.4, 5.7$ Hz, 1H), 0.89 (s, 5H), 0.06 (s, 3H). ^{13}C NMR (101 MHz, CDCl_3) δ 60.41, 35.55, 30.67, 25.91, 18.30, -5.37. Data are in agreement with the literature.



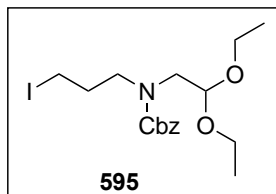
Benzyl (3-((*tert*-butyldimethylsilyl)oxy)propyl)(2,2-diethoxyethyl)carbamate 593 To a stirred solution of **583** (1.04 g, 3.89 mmol) and **592** (0.99 g, 3.89 mmol) in dry DMF was added NaH (0.10 g, 4.28 mmol) in several portions at 0 °C, the reaction mixture was reacted at 0 °C for 2 h, and was poured into iced water,

extracted with ethylacetate, the organic layer was dried over MgSO_4 , filtered and concentrated. The residue was purified via column to give the desired product as a liquid in 73% yield. ^1H NMR (400 MHz, CDCl_3) δ 7.39 – 7.27 (m, 10H), 5.12 (s, 4H), 4.64 (t, $J = 5.4$ Hz, 1H), 4.54 – 4.47 (m, 1H), 3.76 – 3.65 (m, 2H), 3.65 – 3.55 (m, 6H), 3.51 (dtd, $J = 9.4, 7.1, 4.3$ Hz, 2H), 3.41 (q, $J = 9.2, 8.3$ Hz, 6H), 3.32 (dd, $J = 6.9, 5.3$ Hz, 4H), 1.74 (tt, $J = 14.6, 6.3$ Hz, 4H), 1.15 (dt, $J = 20.6, 7.1$ Hz, 12H), 0.86 (d, $J = 6.9$ Hz, 18H). 0.01 (d, $J = 10.0$ Hz, 12H). The compound was tentatively assigned using ^{13}C NMR and HRMS.

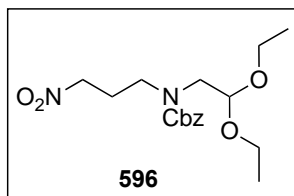


benzyl (2,2-diethoxyethyl)(3-hydroxypropyl)carbamate 594 TBAF (5.6 mL of 1M solution, 5.6 mmol) and acetic acid (5.6 mmol) was added to a stirred solution of **593** (1.65 g, 3.8 mmol) in THF (30 mL) at 0 °C under nitrogen atmosphere. After addition, the reaction

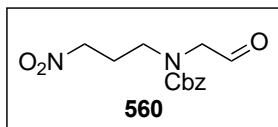
mixture was brought to room temperature and stirred overnight. The reaction mixture was quenched with brine and extracted with EtOAc, the organic layer was dried over MgSO_4 , filtered and concentrated. The residue was purified via column chromatography eluting with EtOAc/hexane to give the desired product in an 81% yield. ^1H NMR (400 MHz, CDCl_3) δ 7.27 (m, 5H), 5.07 (s, 2H), 4.47 – 4.39 (m, 1H), 3.66 – 3.59 (m, 1H), 3.54 (m, 2H), 3.45 (m, 4H), 3.33 (m, 1H), 3.18 (d, $J = 5.3$ Hz, 2H), 1.67 – 1.59 (m, 2H), 1.05 (t, $J = 7.0$ Hz, 6H). The compound was tentatively assigned using ^{13}C NMR and HRMS.



Benzyl (2,2-diethoxyethyl)(3-iodopropyl)carbamate 595 I₂ (0.94 g, 3.7 mmol) was added in portions to a solution of imidazole (0.25 g, 3.7 mmol) and PPh₃ (0.97 g, 3.7 mmol) in CH₂Cl₂ (20 mL) at 0 °C, the resulting dark-yellow suspension was warmed to room temperature, and a solution of **594** (1 g, 3.1 mmol) in CH₂Cl₂ was added, the mixture was stirred at room temperature for 2 h. The reaction was washed with water and brine, extracted with CH₂Cl₂, the organic layer was dried over MgSO₄, filtered and concentrated. The residue was purified via column chromatography eluting with EtOAc/hexane to give the desired product in an 62% yield. ¹H NMR (400 MHz, CDCl₃) δ 7.41 – 7.36 (m, 10H), 5.16 (d, J = 2.6 Hz, 4H), 4.67 (t, J = 5.3 Hz, 1H), 4.52 (t, J = 5.3 Hz, 1H), 3.75 (dq, J = 9.4, 7.1 Hz, 2H), 3.65 (dq, J = 9.4, 7.1 Hz, 2H), 3.60 – 3.51 (m, 2H), 3.49 – 3.41 (m, 6H), 3.38 – 3.32 (m, 4H), 3.14 (dt, J = 22.7, 6.9 Hz, 4H), 2.20 – 2.07 (m, 4H), 1.20 (dt, J = 19.7, 7.0 Hz, 12H). The compound was tentatively assigned using ¹³C NMR and HRMS.

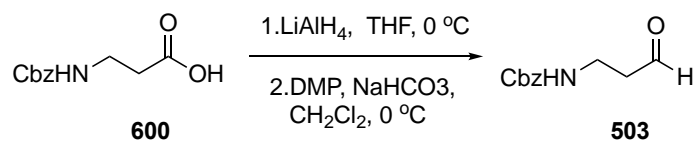


Benzyl (2,2-diethoxyethyl)(3-nitropropyl)carbamate 596 Sodium nitrite (0.25 g, 3.7 mmol) and urea (0.24 g, 4.1 mmol) were dissolved in DMSO (3 mL), then **595** (0.84 g, 1.9 mmol) in DMSO was added, the reaction mixture was stirred at 0 °C for 45 min and room temperature for another 45 min. CH₂Cl₂ was added, the organic layer was washed with water and brine, dried over MgSO₄, filtered and concentrated. The residue was purified via column chromatography eluting with EtOAc/hexane to give the desired product in an 59% yield. ¹H NMR (400 MHz, CDCl₃) δ 7.40 – 7.29 (m, 10H), 5.13 (s, 4H), 4.65 (t, J = 5.3 Hz, 1H), 4.49 (t, J = 5.3 Hz, 1H), 4.40 (t, J = 7.1 Hz, 2H), 4.33 (t, J = 6.8 Hz, 2H), 3.72 (dq, J = 9.4, 7.1 Hz, 2H), 3.61 (dq, J = 9.3, 7.1 Hz, 2H), 3.56 – 3.45 (m, 6H), 3.40 (dq, J = 9.3, 7.0 Hz, 2H), 3.30 (t, J = 5.8 Hz, 4H), 2.24 (dq, J = 20.4, 6.8 Hz, 4H), 1.16 (dt, J = 20.2, 7.0 Hz, 12H). ¹³C NMR (101 MHz, CDCl₃) δ 156.18 (d, J = 5.2 Hz), 136.32, 128.55 (d, J = 2.6 Hz), 128.22, 128.10, 101.75, 101.25, 73.18, 72.78, 67.48, 67.43, 63.57, 63.30, 51.23, 50.71, 46.23, 45.69, 31.57, 26.13, 25.96, 22.64, 15.30, 15.22, 14.10. The compound was tentatively assigned using HRMS.



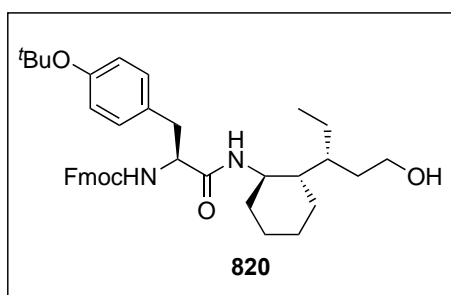
Benzyl (3-nitropropyl)(2-oxoethyl)carbamate 560 596(0.4 g, 1.1 mmol) was dissolved in 10 mL of 2M HCl and 10 mL of acetone, the solution was stirred at room temperature overnight. The mixture was

basified to pH~6, CH₂Cl₂ was added, the organic layer was washed with water and brine, dried over MgSO₄, filtered and concentrated. The residue was purified via column chromatography eluting with EtOAc/hexane to give the desired product in an 60% yield. ¹H NMR (400 MHz, CDCl₃) δ 9.49 (d, J = 13.5 Hz, 1H), 7.40 – 7.12 (m, 5H), 5.04 (d, J = 21.5 Hz, 2H), 4.36 (dt, J = 29.0, 6.8 Hz, 2H), 4.02 (d, J = 8.5 Hz, 2H), 3.36 (q, J = 6.7 Hz, 2H), 2.11 (dt, J = 20.0, 6.6 Hz, 2H). The compound was tentatively assigned using ¹³C NMR and HRMS.



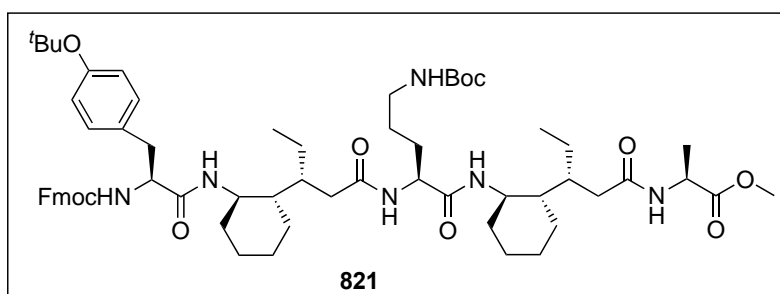
LiAlH₄ (1.7 mL of 4M in THF) was dissolved in 30 mL of anhydrous THF, **600** (1 g, 4.4 mmol) in 20 mL of anhydrous THF was added dropwise to the LiAlH₄ solution at 0 °C, after the addition, the reaction was brought to room temperature to react for 45 min, then cooled to 0 °C and iced water was added slowly, then CH₂Cl₂ was added, the organic layer was washed with water, brine, dried over MgSO₄, filtered and concentrated. The crude was dissolved in CH₂Cl₂ (12 mL), and NaHCO₃ (2.2 g, 26.4 mmol) was added, DMP (2.8 g, 6.6 mmol) was added at 0 °C, then the reaction was brought to room temperature to react for 1h, water was added, extracted with CH₂Cl₂, the organic layer was washed with water and brine, dried over MgSO₄, filtered and concentrated. The residue was purified via column chromatography eluting with EtOAc/hexane to give the desired product in 61% yield over 2 steps. ¹H NMR (400 MHz, CDCl₃) δ 9.90 – 9.63 (m, 1H), 7.41 – 7.31 (m, 5H), 5.27 (p, J = 8.6, 7.1 Hz, 1H), 5.09 (s, 2H), 3.49 (q, J = 6.1, 4.9 Hz, 2H), 2.73 (t, J = 5.9 Hz, 2H). ¹³C NMR (101 MHz, CDCl₃) δ 201.28, 156.35, 136.42, 128.55, 128.18, 128.11, 66.76, 44.08, 34.49. The compound was tentatively assigned using HRMS.

6.5.3 Synthesis of Foldamer 707



Following the general procedure B, Compound **820** was obtained as a white solid. ^1H NMR (400 MHz, CDCl_3) δ 7.76 (d, $J = 7.5$ Hz, 2H), 7.57 (d, $J = 7.5$ Hz, 2H), 7.40 (t, $J = 7.5$ Hz, 2H), 7.31 (td, $J = 7.4, 1.2$ Hz, 2H), 7.10 (d, $J = 8.0$ Hz, 2H), 6.90 (d, $J = 8.2$ Hz, 2H), 5.61 (d, $J = 7.8$ Hz, 1H), 5.56 (d, $J = 9.2$ Hz, 1H), 4.38 (td, $J =$

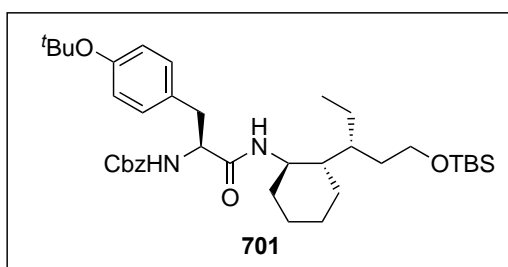
10.4, 7.0 Hz, 2H), 4.18 (t, $J = 6.7$ Hz, 1H), 4.12 (q, $J = 7.1$ Hz, 1H), 3.69 (m, 1H), 3.54 (m, 2H), 3.04 – 2.93 (m, 2H), 1.67 (m, 3H), 1.61 – 1.48 (m, 3H), 1.44 (m, 2H), 1.31 (s, 9H), 1.23 – 1.14 (m, 1H), 1.14 – 0.96 (m, 3H), 0.85 (m, 2H), 0.77 (t, $J = 6.9$ Hz, 3H). The compound was tentatively assigned using ^{13}C NMR and HRMS.



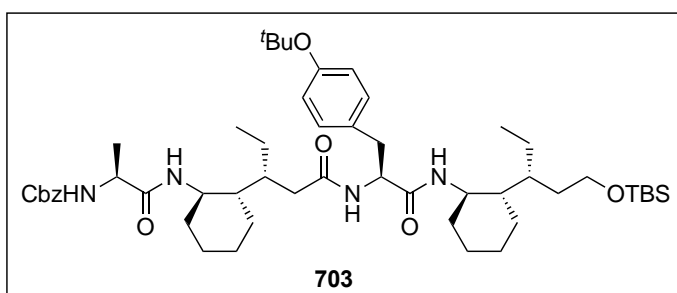
Following the general procedure B, Compound **821** was obtained as a white solid. ^1H NMR (400 MHz, CDCl_3) δ 8.03 (d, $J = 9.6$ Hz, 1H), 7.75 (d, $J = 7.5$ Hz, 2H), 7.59

(d, $J = 7.5$ Hz, 1H), 7.52 (t, $J = 6.8$ Hz, 2H), 7.45 – 7.34 (m, 4H), 7.33 – 7.27 (m, 2H), 7.17 – 7.11 (m, 2H), 6.92 – 6.85 (m, 2H), 5.52 – 5.41 (m, 1H), 4.70 – 4.56 (m, 2H), 4.39 (q, $J = 7.9$ Hz, 1H), 4.26 – 4.20 (m, 2H), 4.19 – 4.13 (m, 1H), 4.07 – 3.96 (m, 1H), 3.78 (d, $J = 6.8$ Hz, 1H), 3.75 (s, 3H), 3.65 (m, 1H), 3.04 (dd, $J = 13.6, 6.8$ Hz, 1H), 2.90 (dd, $J = 13.6, 8.5$ Hz, 1H), 2.77 (q, $J = 6.7$ Hz, 2H), 2.58 – 2.40 (m, 2H), 2.01 – 1.89 (m, 6H), 1.80 – 1.65 (m, 5H), 1.59 (m, 3H), 1.54 – 1.48 (m, 2H), 1.47 – 1.40 (m, 3H), 1.36 (s, 9H), 1.33 (s, 12H), 1.24 – 1.13 (m, 5H), 1.11 – 1.00 (m, 4H), 0.94 (t, $J = 7.1$ Hz, 4H), 0.88 – 0.81 (m, 1H), 0.75 (t, $J = 7.0$ Hz, 3H). ^{13}C NMR (101 MHz, CDCl_3) δ 176.51, 174.58, 173.85, 172.54, 171.20, 156.49, 155.83, 154.07, 143.85, 143.56, 141.21, 141.18, 131.81, 129.84, 127.82, 127.23, 127.14, 125.10,

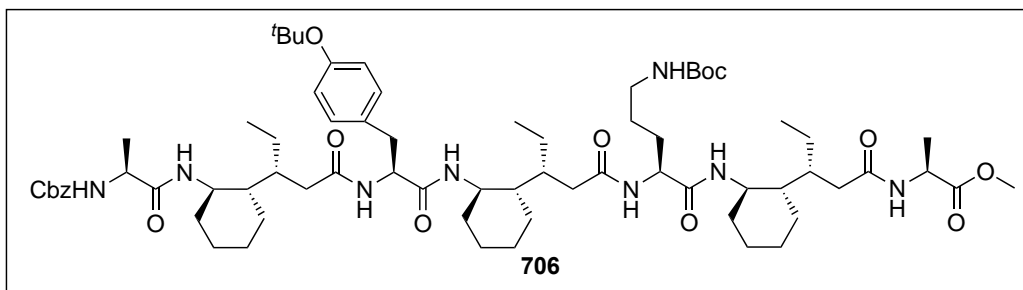
125.03, 124.08, 120.06, 78.38, 67.41, 56.95, 54.07, 52.74, 49.22, 48.89, 47.86, 46.93, 44.38, 44.18, 39.80, 38.97, 38.75, 37.86, 37.54, 37.11, 34.47, 33.63, 28.80, 28.52, 28.36, 26.66, 25.56, 25.45, 25.14, 24.61, 22.88, 22.25, 16.85, 13.84, 12.74. The compound was tentatively assigned using HRMS.



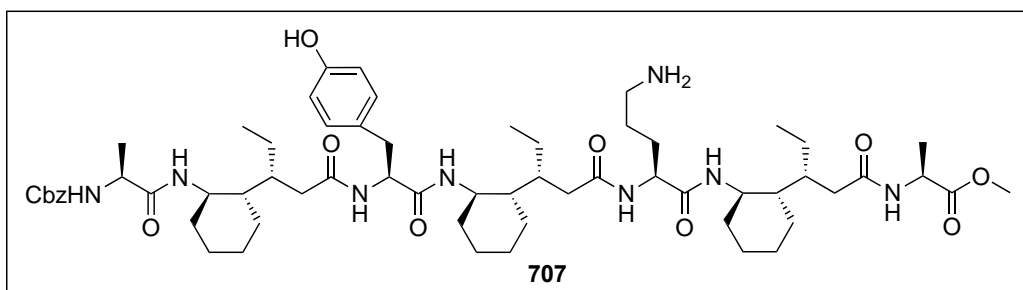
Following the general procedure A, Compound **701** was obtained as a white solid in 91% yield. ^1H NMR (400 MHz, CDCl_3) δ 7.36 – 7.25 (m, 5H), 7.06 (d, $J = 7.9$ Hz, 2H), 6.90 – 6.82 (m, 2H), 5.49 (d, $J = 7.9$ Hz, 1H), 5.15 (d, $J = 9.4$ Hz, 1H), 5.05 (m, 2H), 4.22 – 4.12 (m, 1H), 3.67 (qd, $J = 10.7, 3.9$ Hz, 1H), 3.51 (t, $J = 6.5$ Hz, 2H), 3.00 (dd, $J = 13.6, 5.5$ Hz, 1H), 2.90 (dd, $J = 13.5, 8.9$ Hz, 1H), 1.71 – 1.46 (m, 6H), 1.44 – 1.31 (m, 3H), 1.28 (s, 9H), 1.15 – 0.90 (m, 4H), 0.84 (s, 9H), 0.75 (t, $J = 7.1$ Hz, 3H), 0.68 (m, 1H). ^{13}C NMR (101 MHz, CDCl_3) δ 169.61, 155.73, 154.30, 136.25, 131.53, 129.82, 128.54, 128.18, 128.04, 124.41, 78.40, 66.91, 62.21, 56.94, 49.64, 45.39, 38.44, 36.17, 34.26, 33.97, 28.81, 25.99, 25.84, 25.31, 25.18, 22.38, 18.30, 13.00. The compound was tentatively assigned using HRMS.



Following the general procedure A, Compound **703** was obtained as a white solid in 57% yield over 2 steps. ^1H NMR (400 MHz, CDCl_3) δ 7.56 (d, $J = 9.7$ Hz, 1H), 7.40 (d, $J = 7.5$ Hz, 1H), 7.26 (m, 5H), 7.06 (d, $J = 8.4$ Hz, 2H), 6.86 (d, $J = 8.4$ Hz, 2H), 5.50 (d, $J = 7.6$ Hz, 1H), 5.15 (d, $J = 8.7$ Hz, 1H), 5.06 (d, $J = 12.3$ Hz, 1H), 4.95 (d, $J = 12.3$ Hz, 1H), 4.38 (dt, $J = 9.1, 6.8$ Hz, 1H), 4.27 (p, $J = 7.1$ Hz, 1H), 3.81 – 3.66 (m, 1H), 3.65 – 3.50 (m, 3H), 2.84 (qd, $J = 13.7, 8.0$ Hz, 2H), 2.51 – 2.38 (m, 1H), 1.94 – 1.79 (m, 3H), 1.70 (dd, $J = 12.8, 3.9$ Hz, 1H), 1.64 – 1.55 (m, 5H), 1.53 – 1.43 (m, 4H), 1.38 (d, $J = 7.0$ Hz, 2H), 1.35 – 1.30 (m, 2H), 1.28 (s, 9H), 1.22 – 1.18 (m, 1H), 1.13 – 1.05 (m, 3H), 1.01 – 0.91 (m, 5H), 0.85 (s, 9H), 0.81 – 0.74 (m, 8H), 0.69 – 0.54 (m, 1H), 0.00 (d,

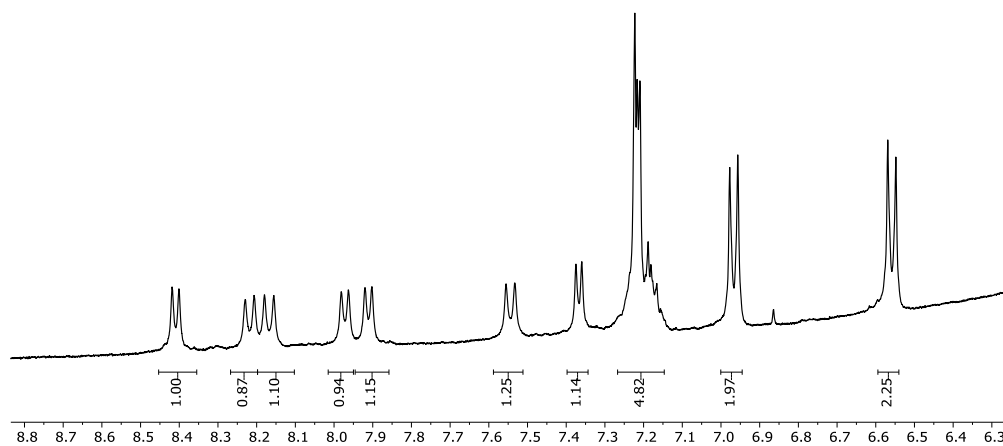


Following the general procedure A, Compound **706** was obtained as a white solid in 48% yield. ^1H NMR (400 MHz, CDCl_3) δ 8.31 (d, $J = 9.5$ Hz, 1H), 8.10 (d, $J = 9.6$ Hz, 1H), 7.81 (d, $J = 6.4$ Hz, 1H), 7.74 (d, $J = 7.5$ Hz, 1H), 7.66 (d, $J = 6.5$ Hz, 1H), 7.40 (d, $J = 9.7$ Hz, 1H), 7.33 (m, 5H), 7.19 (d, $J = 8.1$ Hz, 2H), 6.81 (d, $J = 8.1$ Hz, 2H), 5.35 (d, $J = 7.4$ Hz, 1H), 5.21 (d, $J = 12.4$ Hz, 1H), 5.06 (d, $J = 12.4$ Hz, 1H), 4.99 (m, 1H), 4.66 (p, $J = 7.5$ Hz, 1H), 4.50 (q, $J = 7.1$ Hz, 1H), 4.27 (p, $J = 7.0$ Hz, 1H), 4.04 – 3.95 (m, 1H), 3.78 (m, 5H), 3.65 (m, 1H), 3.01 – 2.82 (m, 3H), 2.68 – 2.44 (m, 5H), 2.23 – 2.07 (m, 3H), 1.84 – 1.74 (m, 5H), 1.66 (m, 7H), 1.57 – 1.48 (m, 3H), 1.43 (m, 14H), 1.33 (s, 9H), 1.27 (m, 9H), 1.11 (m, 9H), 0.98 (m, 7H), 0.88 (m, 10H). ^{13}C NMR (101 MHz, CDCl_3) δ 176.61, 174.78, 174.49, 173.96, 172.64, 172.19, 156.30, 155.96, 153.70, 78.39, 56.77, 54.70, 52.75, 51.34, 49.13, 49.01, 48.96, 47.88, 44.57, 44.28, 43.92, 41.35, 40.06, 39.44, 39.06, 38.74, 37.46, 36.90, 36.85, 34.54, 33.93, 33.78, 31.60, 28.78, 28.42, 28.12, 26.96, 25.55, 25.52, 25.40, 25.29, 25.10, 24.95, 24.83, 24.61, 22.92, 22.86, 22.67, 22.64, 22.34, 18.25, 16.71, 14.14, 12.74. The compound was tentatively assigned using HRMS.

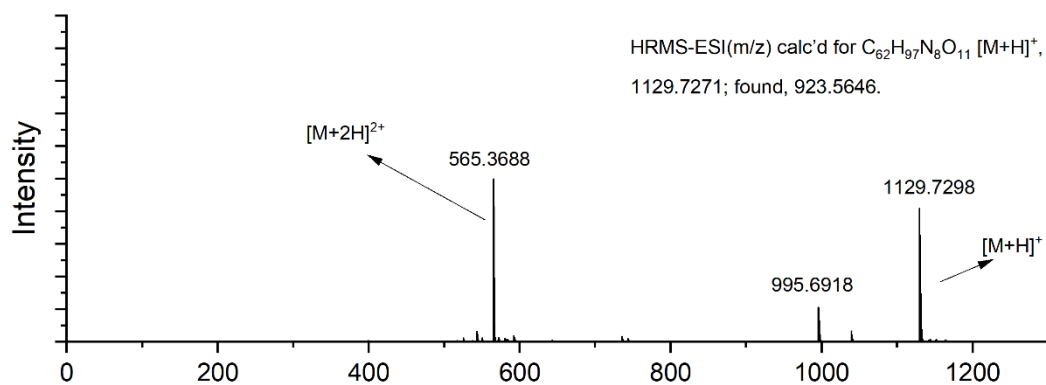
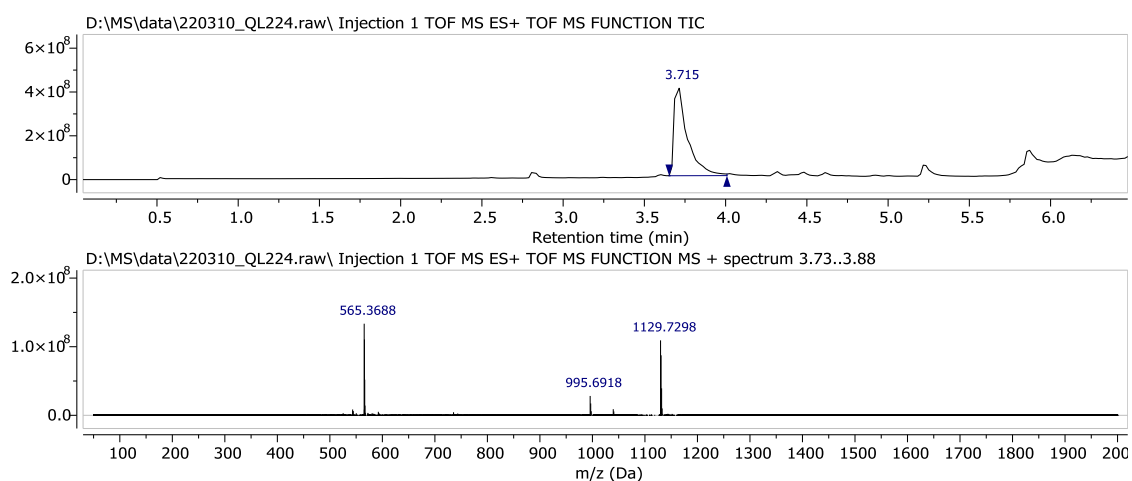


Following the general procedure F, foldamer **707** was obtained as a white solid. HRMS-ESI (m/z) calc'd for $\text{C}_{62}\text{H}_{97}\text{N}_8\text{O}_{11}$ $[\text{M}+\text{H}]^+$, 1129.7271; found, 1129.7298. The compound was tentatively assigned using NMR.

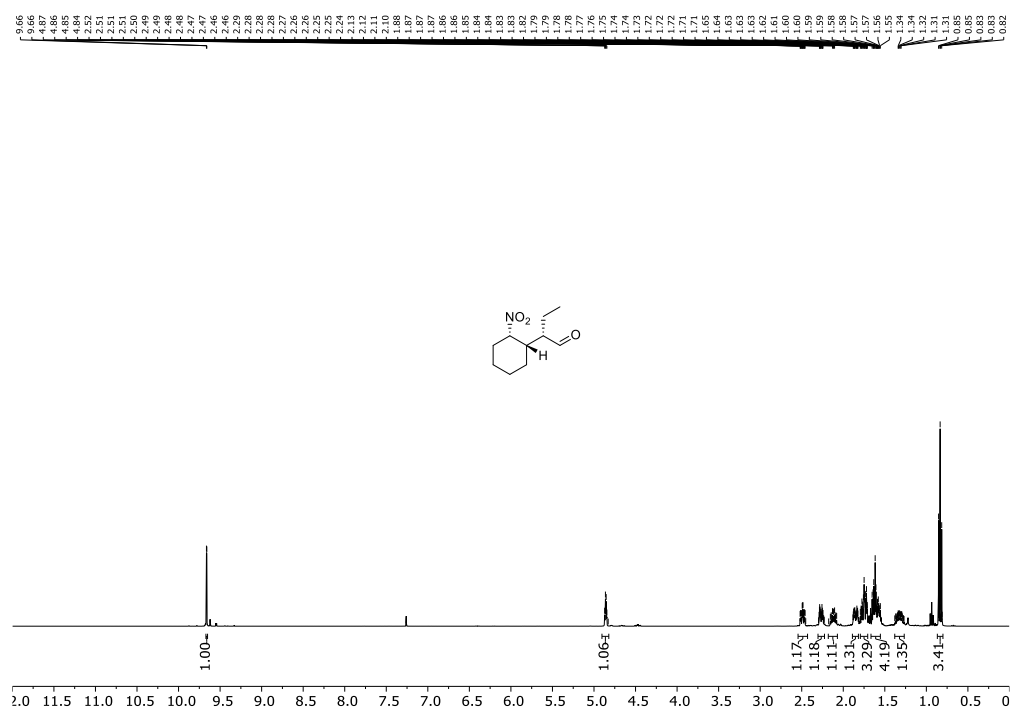
The ^1H NMR of **707** was taken in CD_3OH :



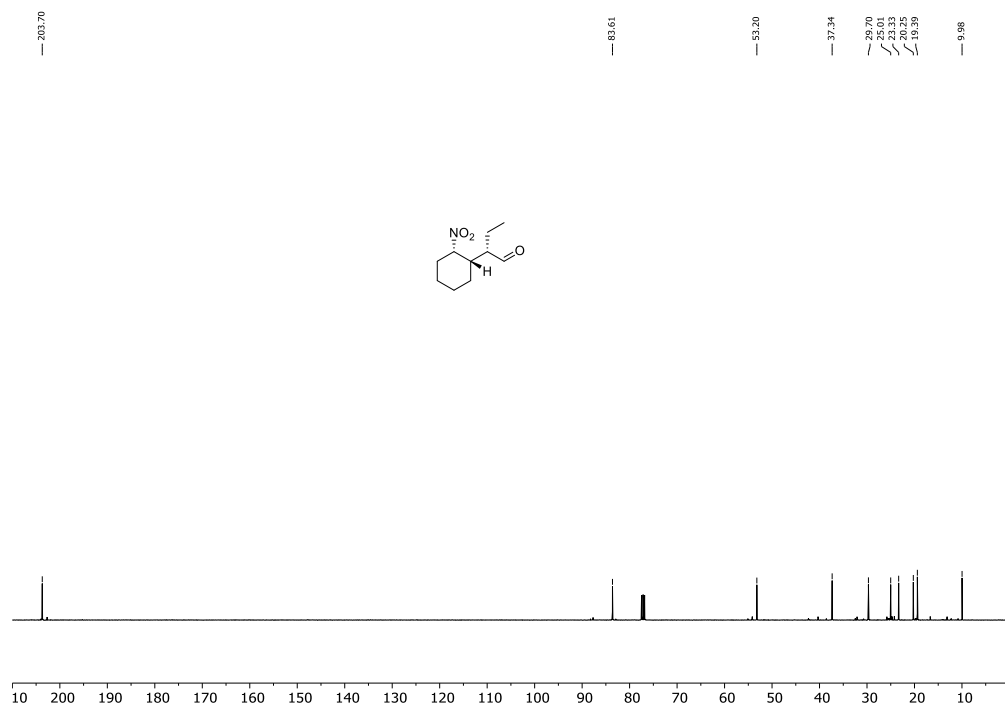
HRMS result of **707**:

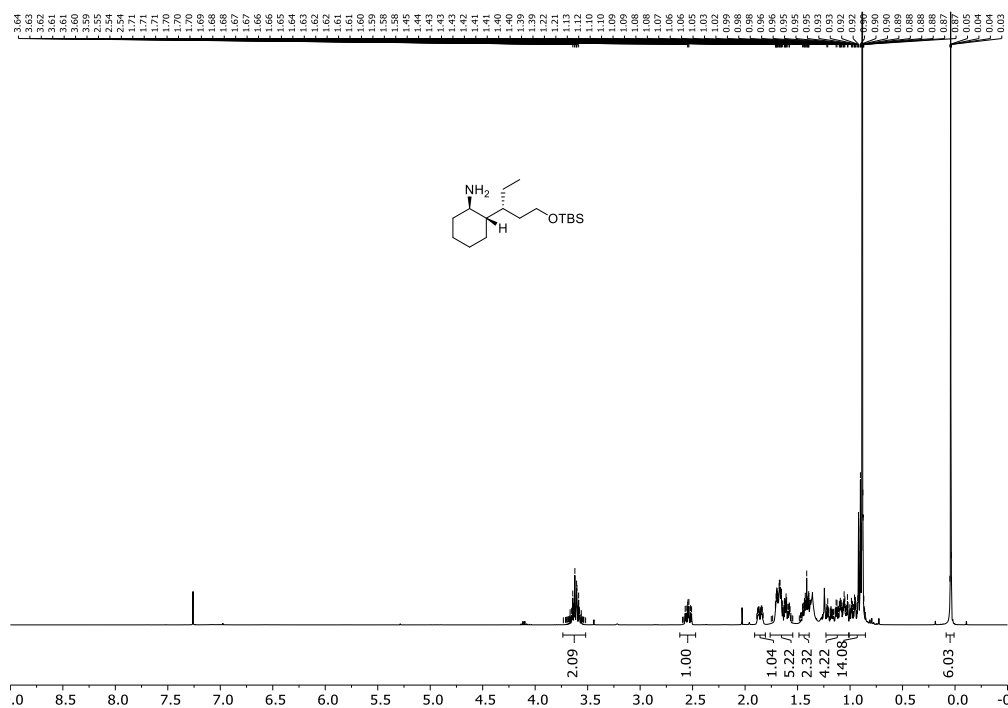
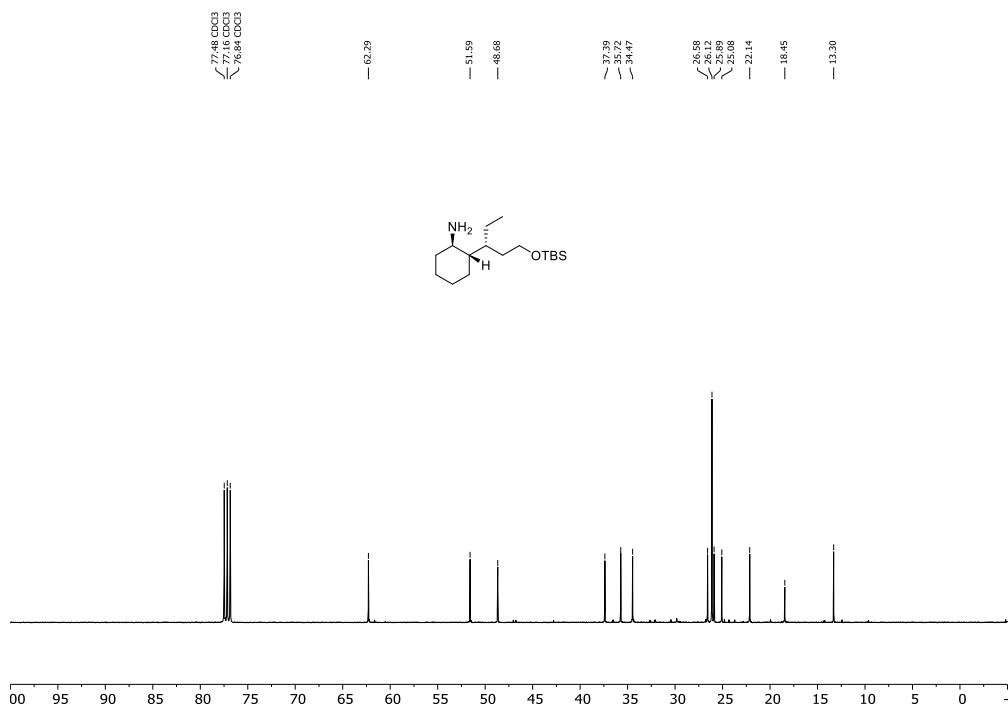


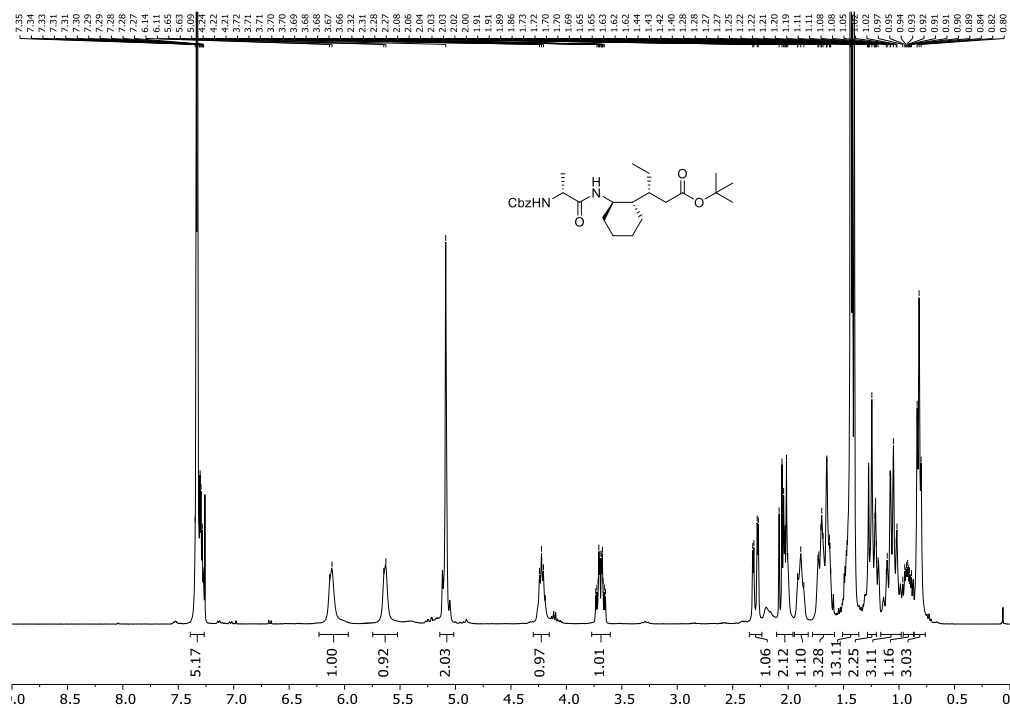
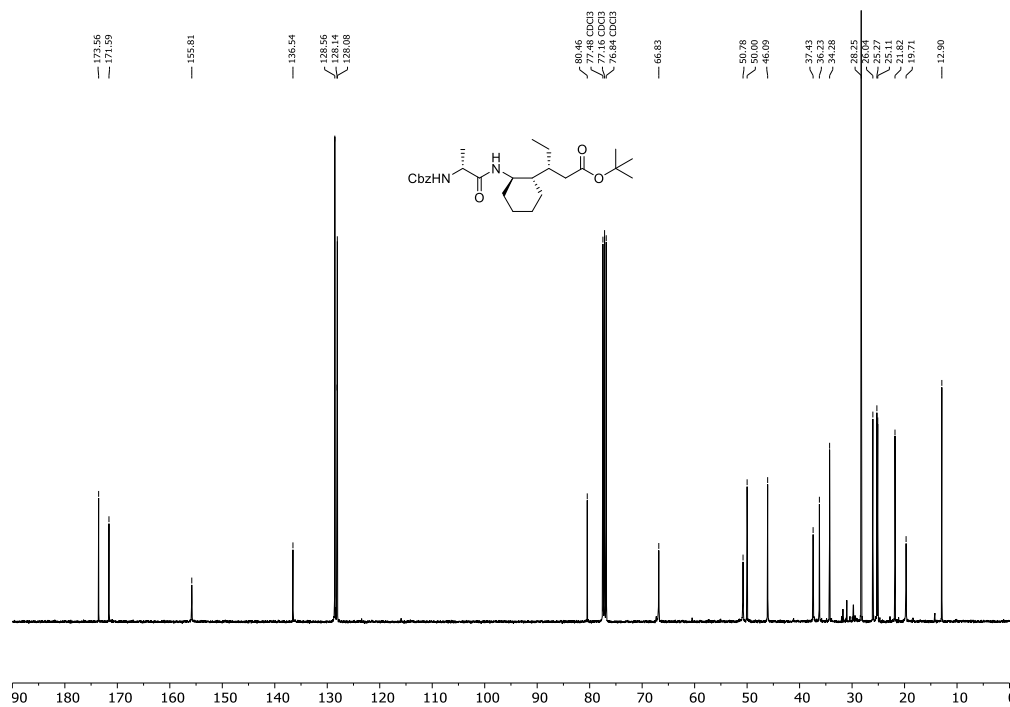
6.6 Spectrum of Key Compounds

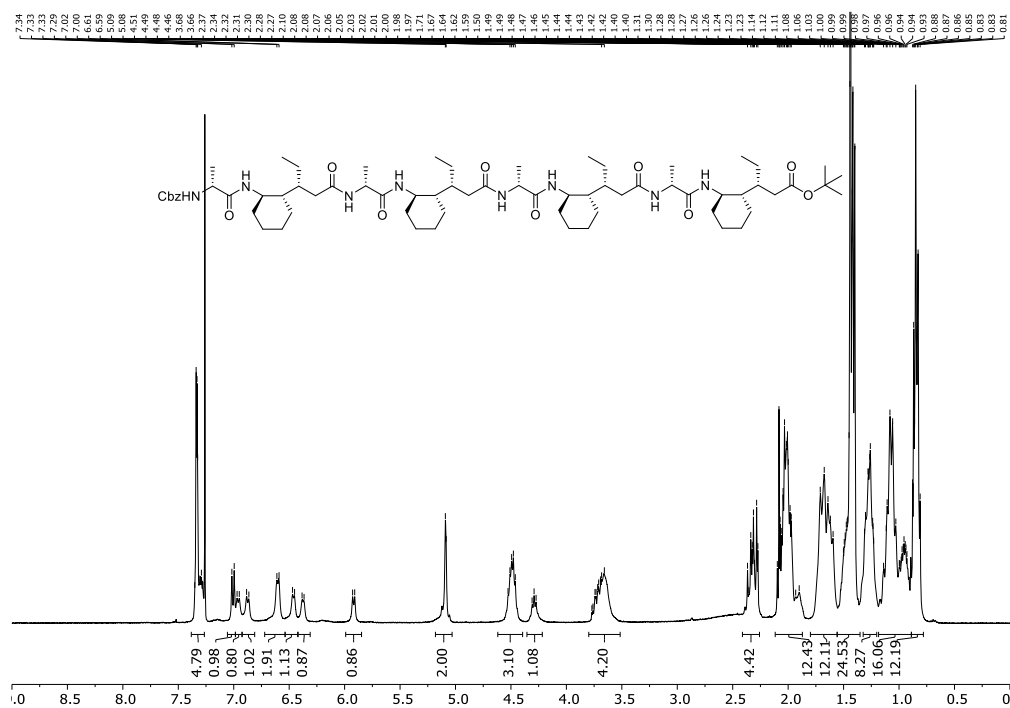


Spectrum 1: ^1H NMR: (400 MHz, CDCl_3) of **24**

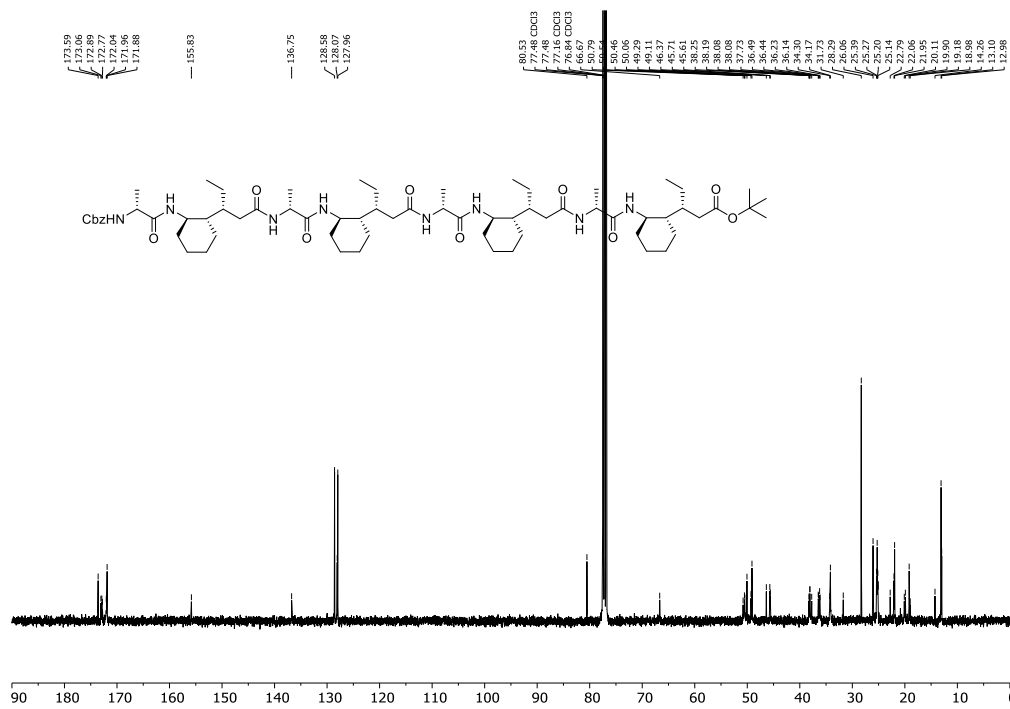
Spectrum 2: ^{13}C NMR: (101 MHz, CDCl_3) of **24**

Spectrum 3: $^1\text{H NMR}$: (400 MHz, CDCl_3) of 53Spectrum 4: $^{13}\text{C NMR}$: (101 MHz, CDCl_3) of 53

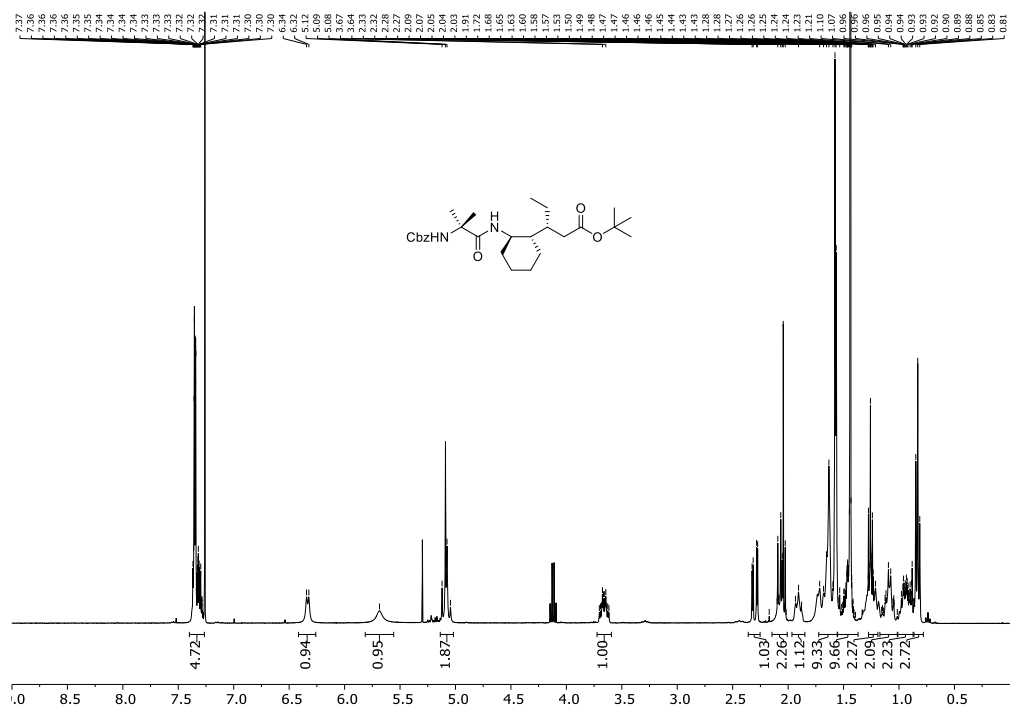
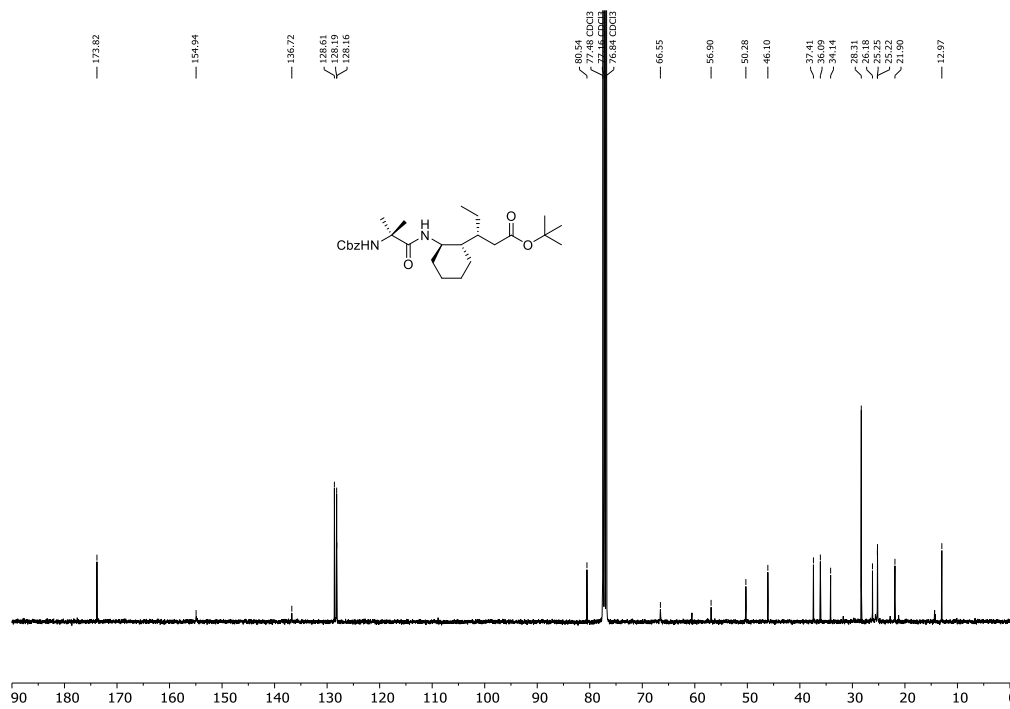
Spectrum 5: $^1\text{H NMR}$: (400 MHz, CDCl_3) of 65Spectrum 6: $^{13}\text{C NMR}$: (101 MHz, CDCl_3) of 65

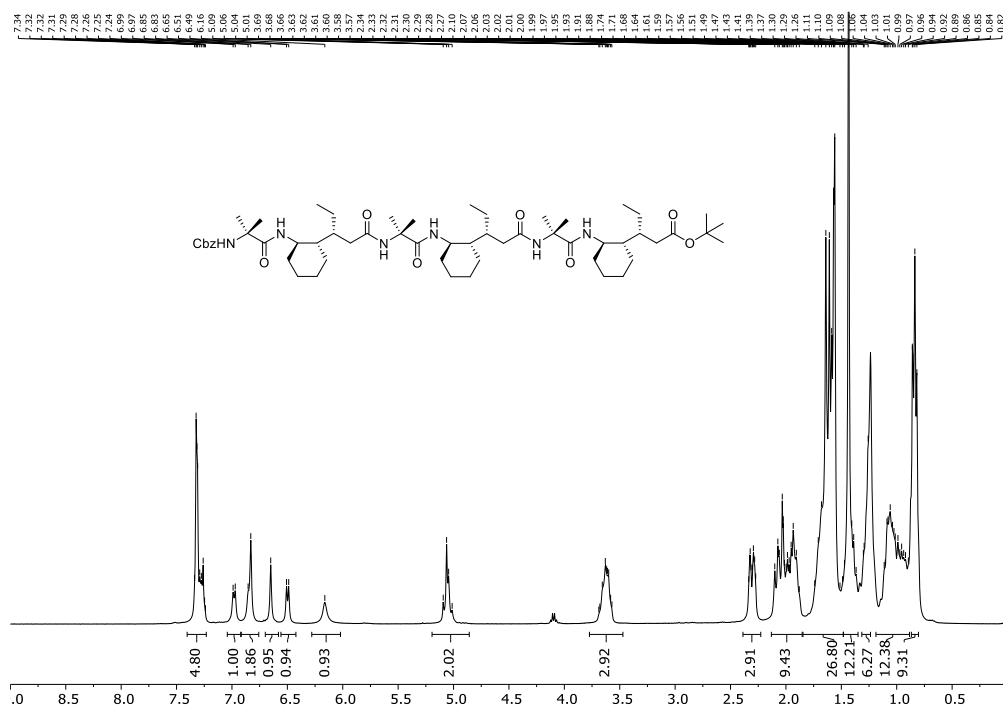
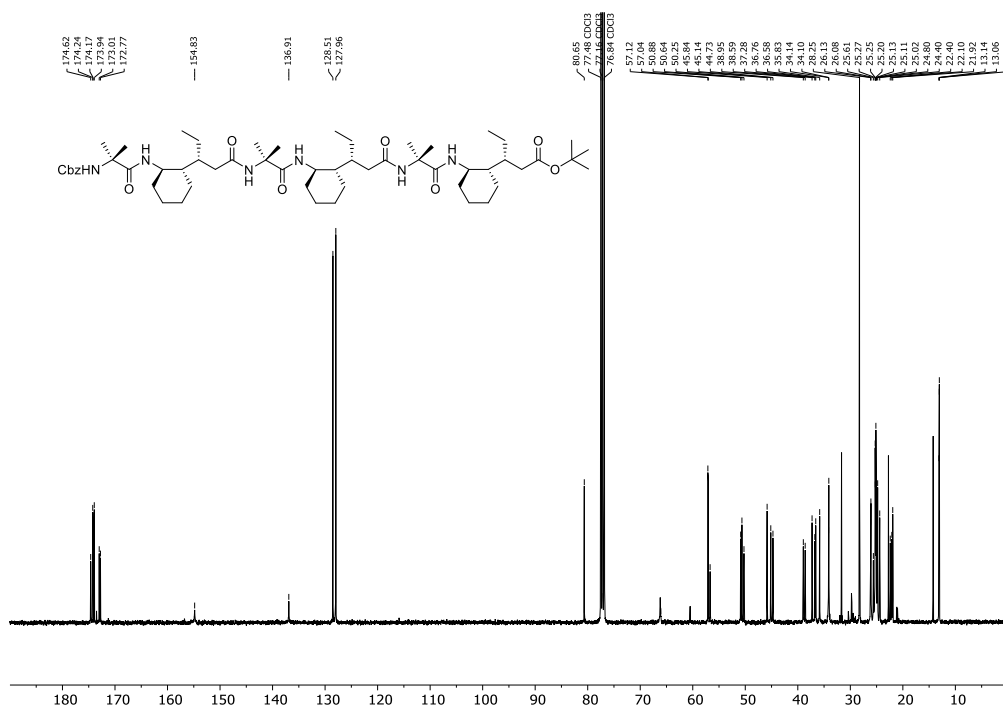


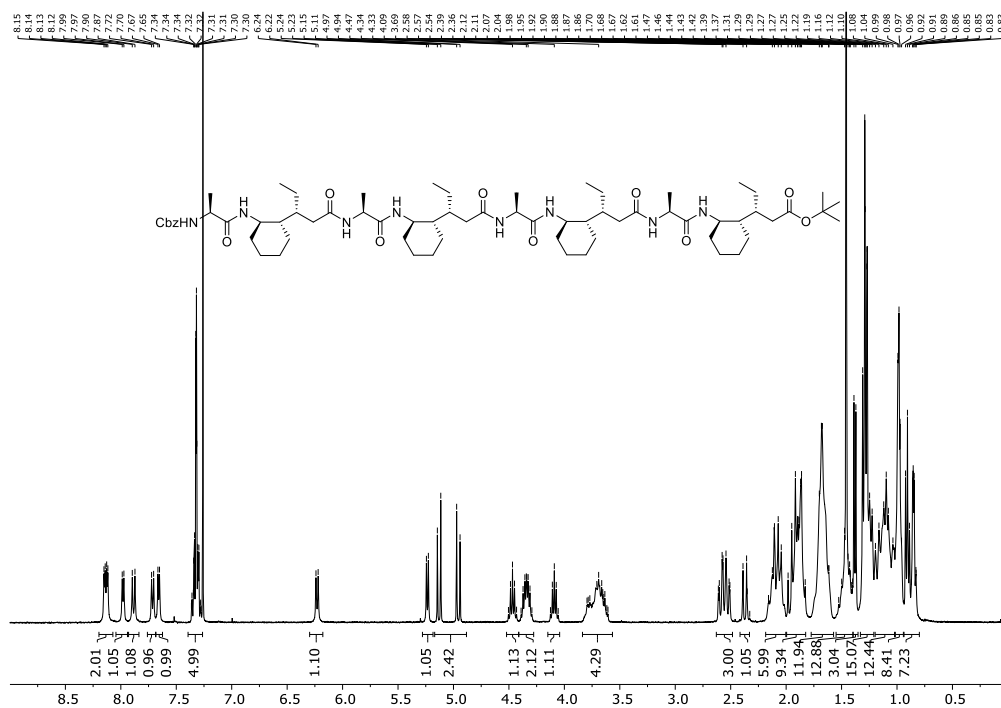
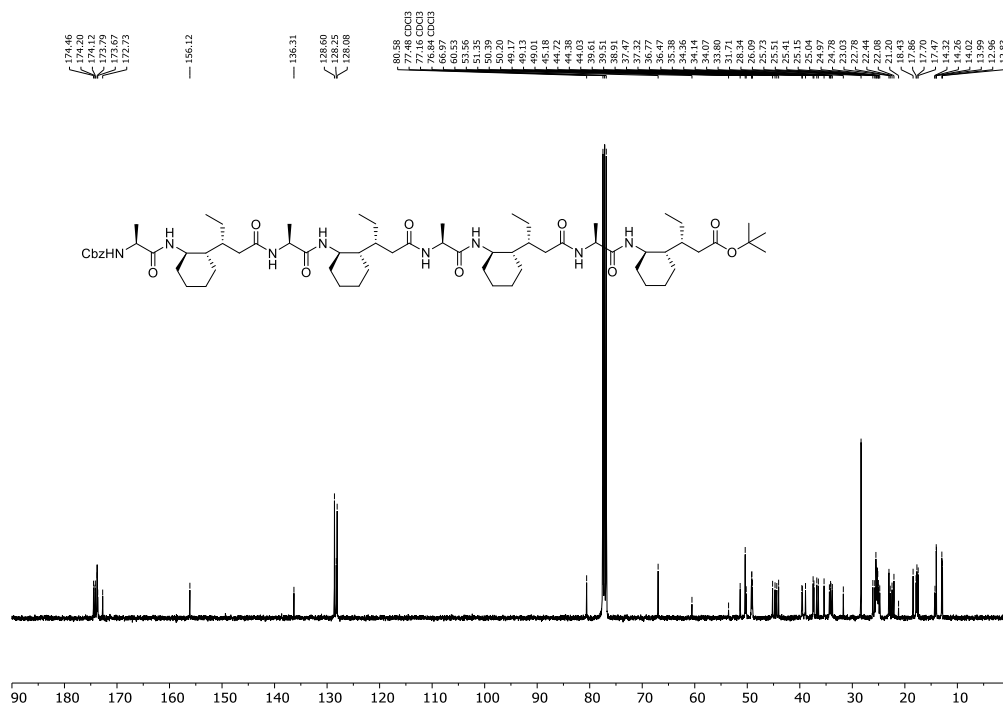
Spectrum 7: ^1H NMR: (400 MHz, CDCl_3) of foldamer 72

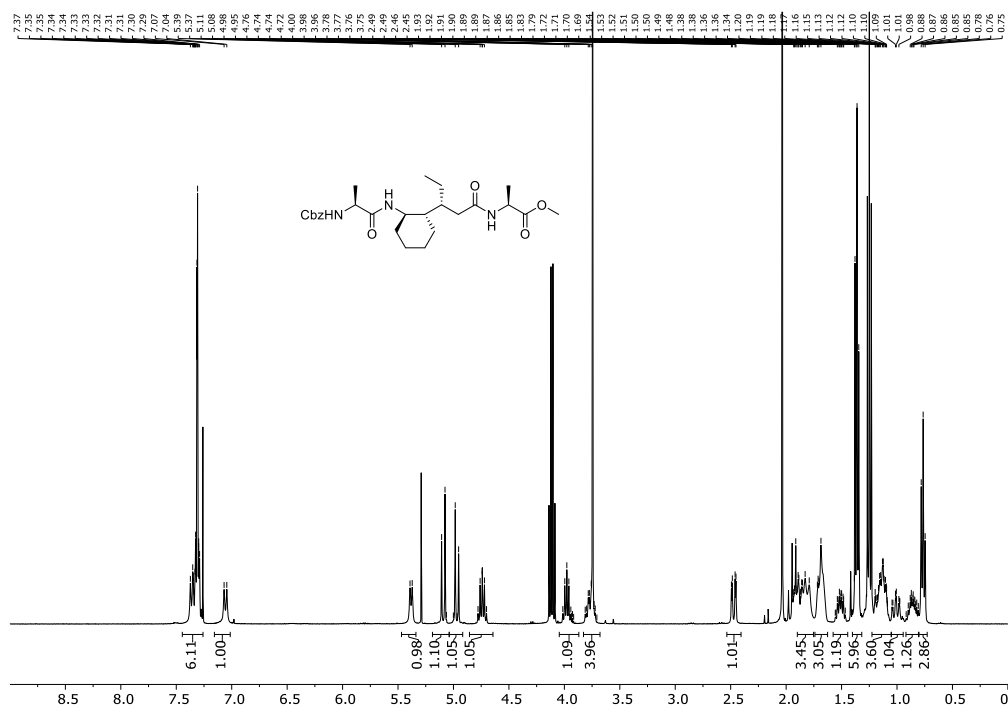
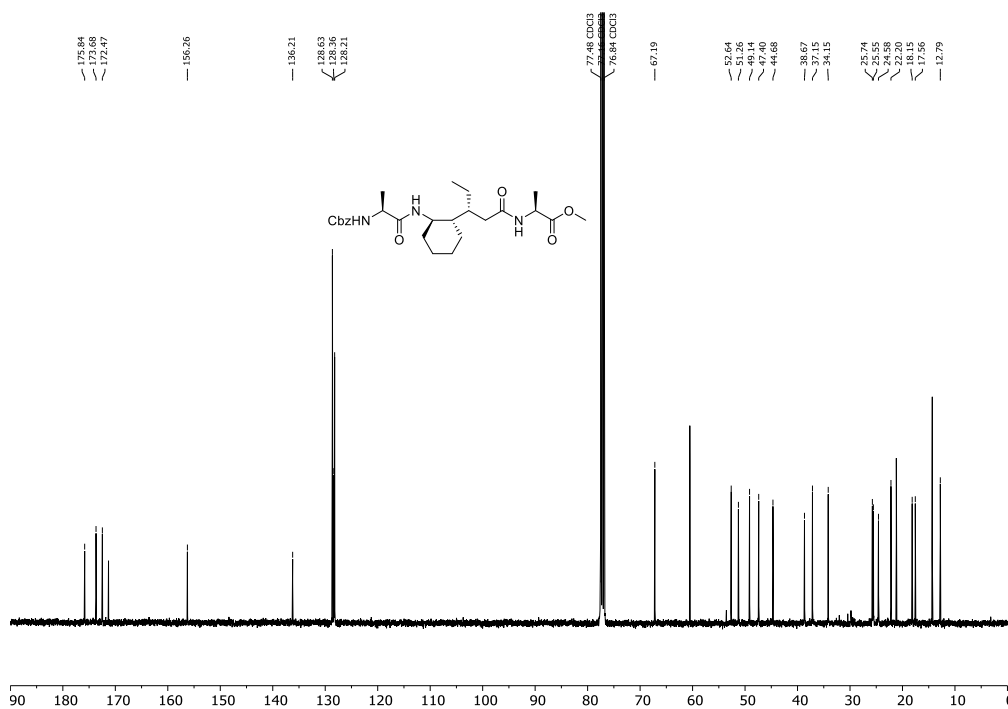


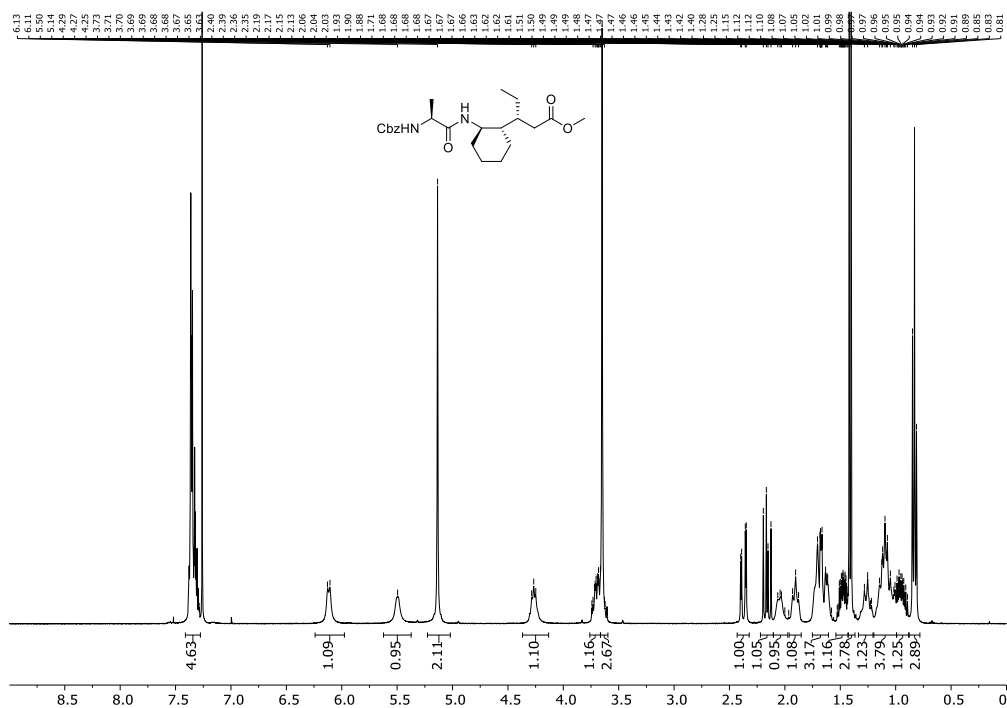
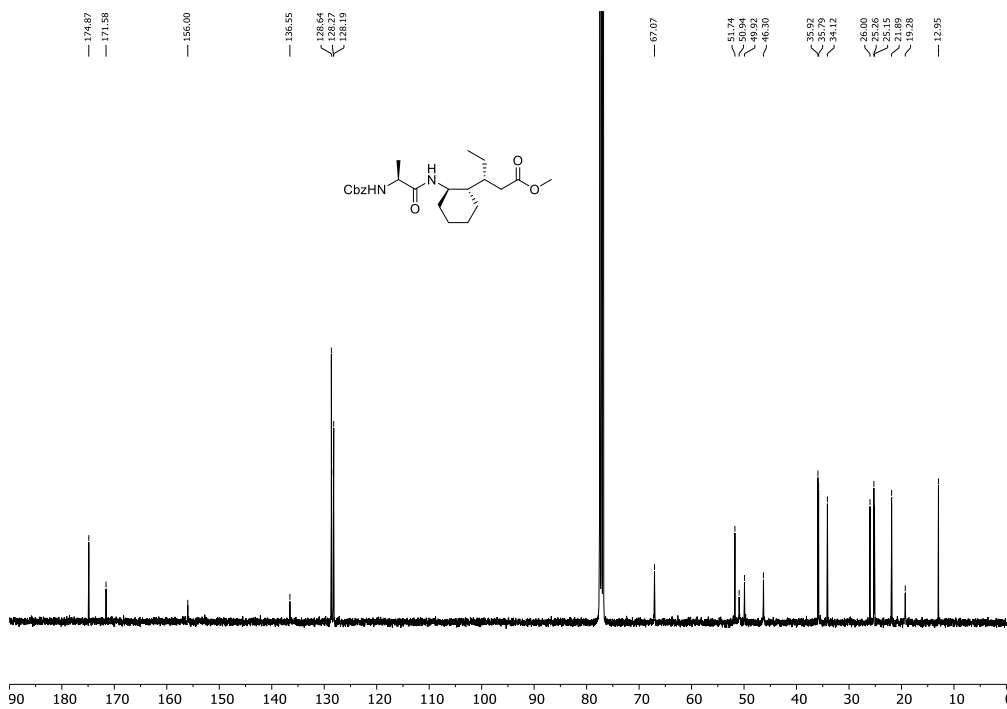
Spectrum 8: ^{13}C NMR: (101 MHz, CDCl_3) of foldamer 72

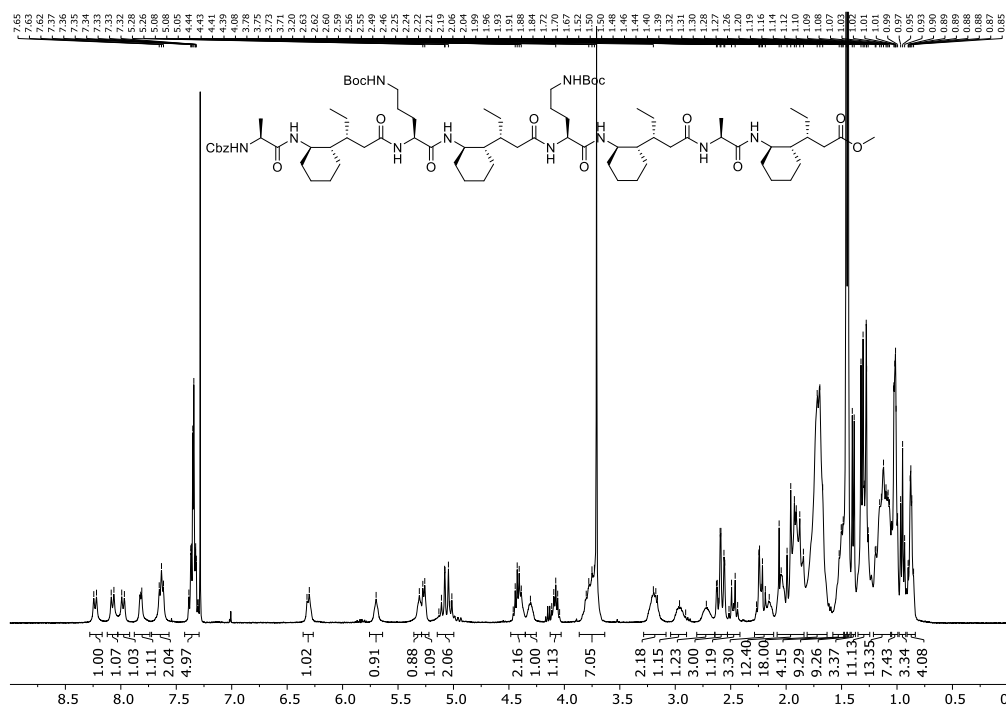
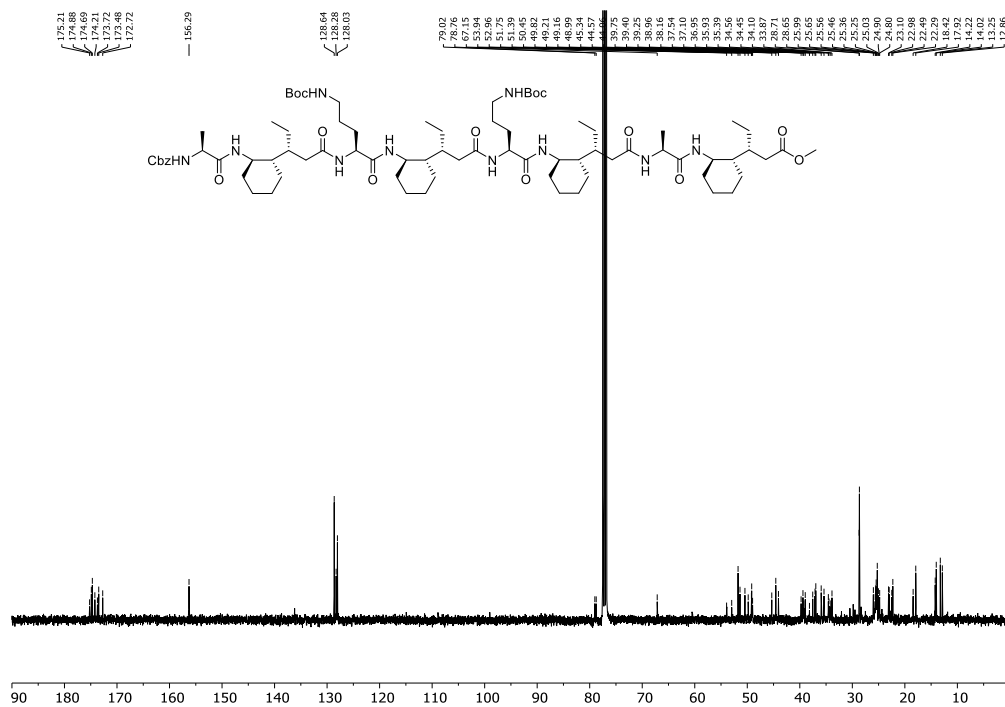
Spectrum 9: ¹H NMR: (400 MHz, CDCl₃) of **84**Spectrum 10: ¹³C NMR: (101 MHz, CDCl₃) of **84**

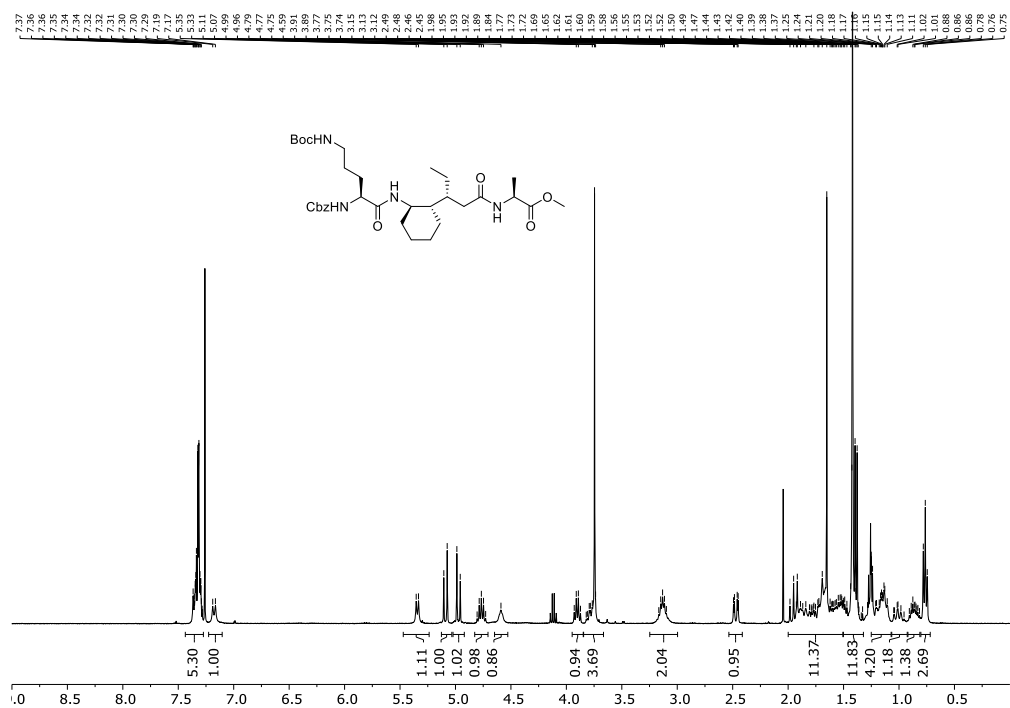
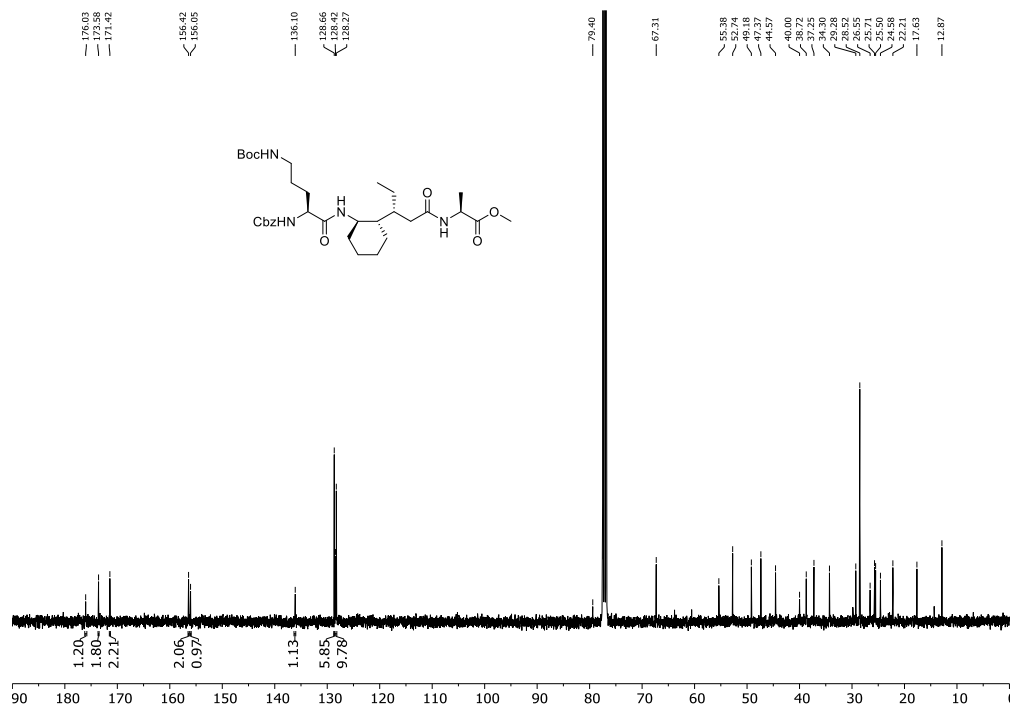
Spectrum 11: $^1\text{H NMR}$: (400 MHz, CDCl_3) of foldamer **86**Spectrum 12: $^{13}\text{C NMR}$: (101 MHz, CDCl_3) of foldamer **86**

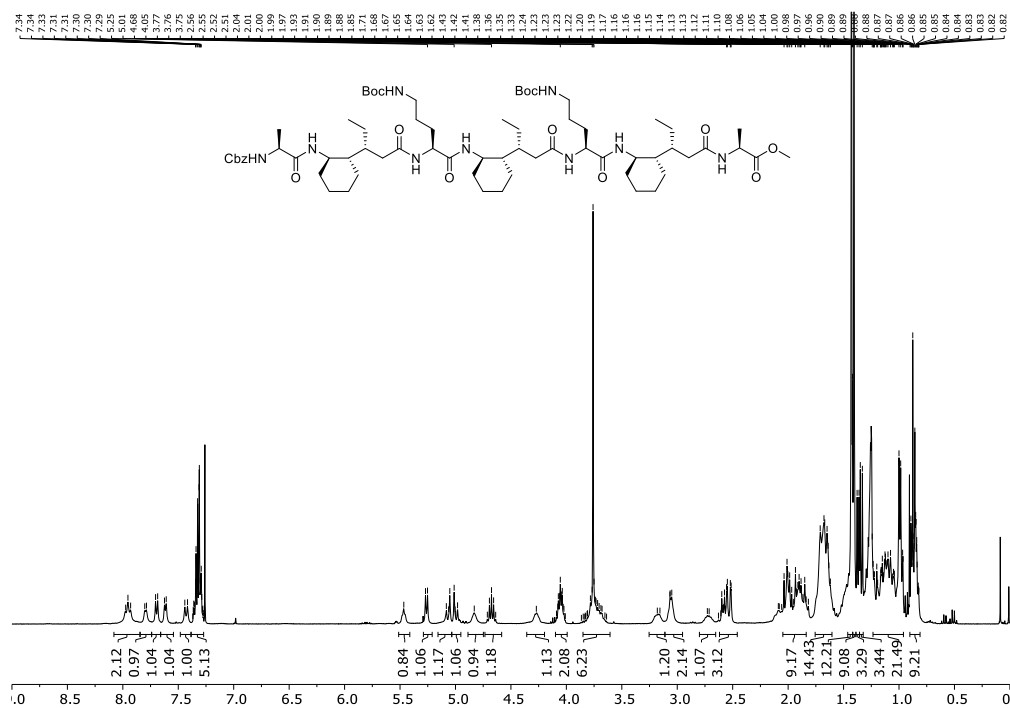
Spectrum 15: ^1H NMR: (400 MHz, CDCl_3) of foldamer **97**Spectrum 16: ^{13}C NMR: (101 MHz, CDCl_3) of foldamer **97**

Spectrum 17: $^1\text{H NMR}$: (400 MHz, CDCl_3) of 101Spectrum 18: $^{13}\text{C NMR}$: (101 MHz, CDCl_3) of 101

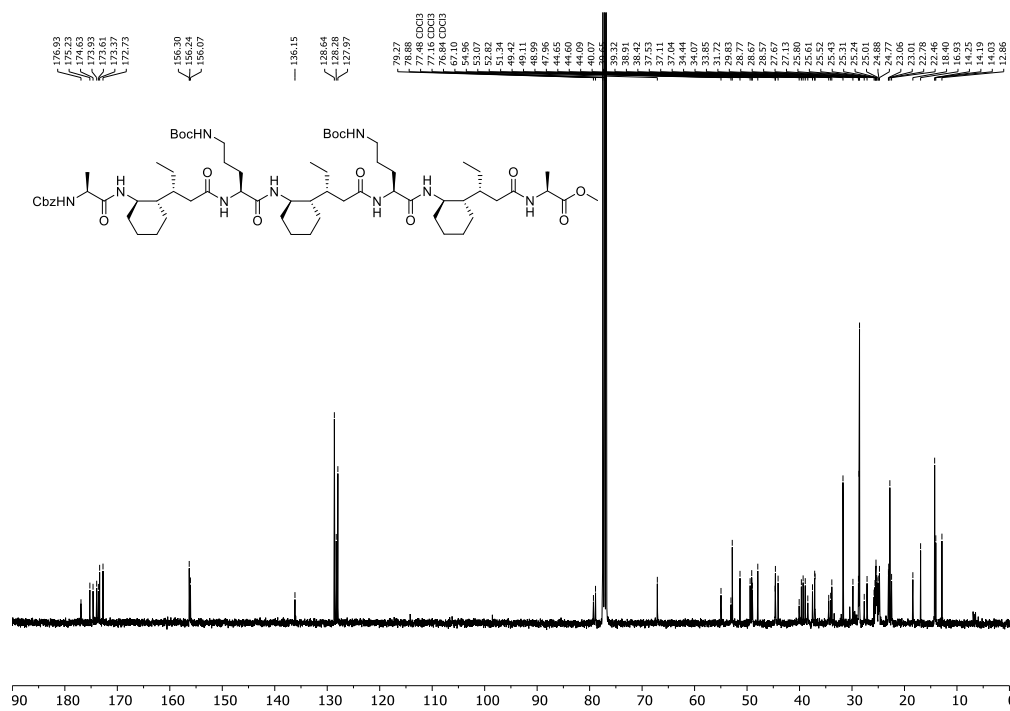
Spectrum 21: $^1\text{H NMR}$: (400 MHz, CDCl_3) of 210Spectrum 22: $^{13}\text{C NMR}$: (101 MHz, CDCl_3) of 210

Spectrum 23: ¹H NMR: (400 MHz, CDCl₃) of foldamer **232**Spectrum 24: ¹³C NMR: (101 MHz, CDCl₃) of foldamer **232**

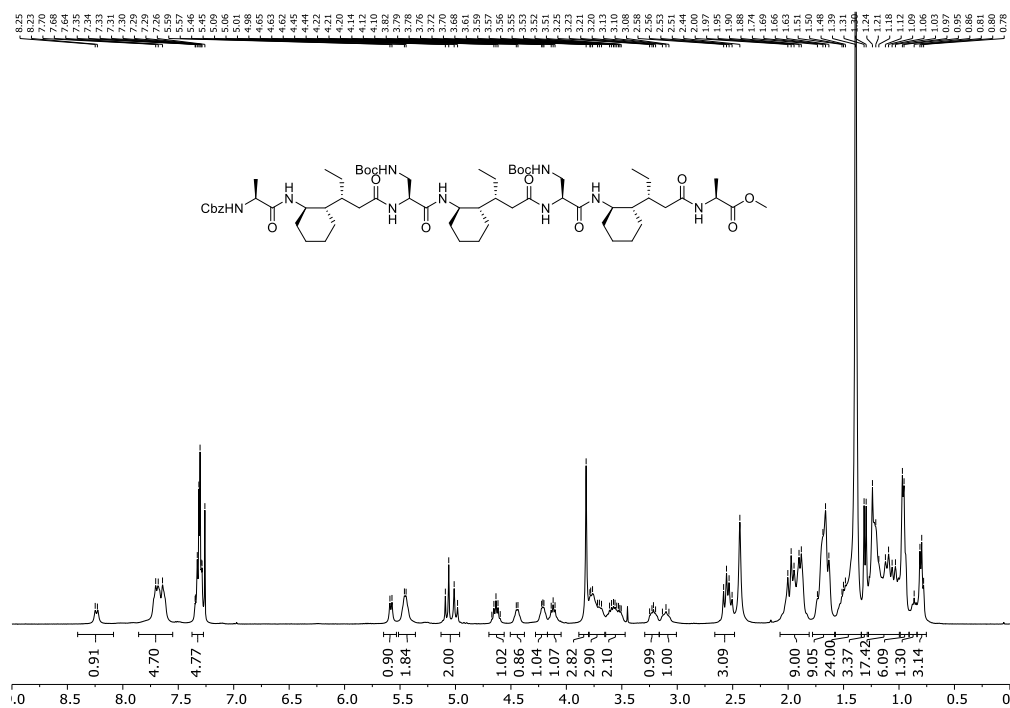
Spectrum 25: $^1\text{H NMR}$: (400 MHz, CDCl_3) of 241Spectrum 26: $^{13}\text{C NMR}$: (101 MHz, CDCl_3) of 241



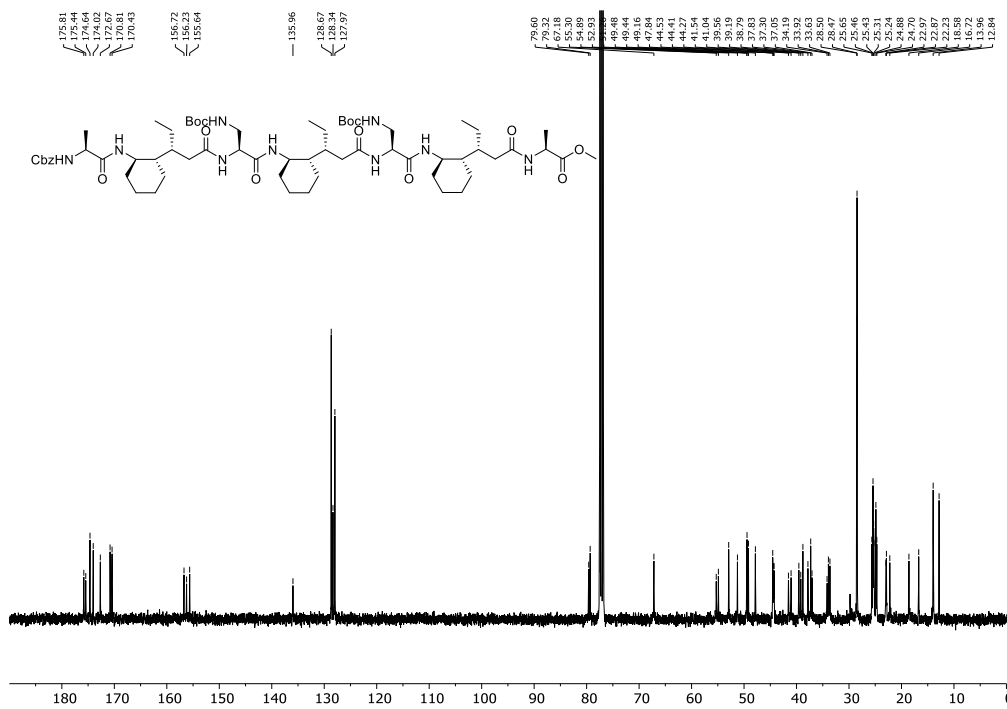
Spectrum 27: ^1H NMR: (400 MHz, CDCl_3) of foldamer **243**



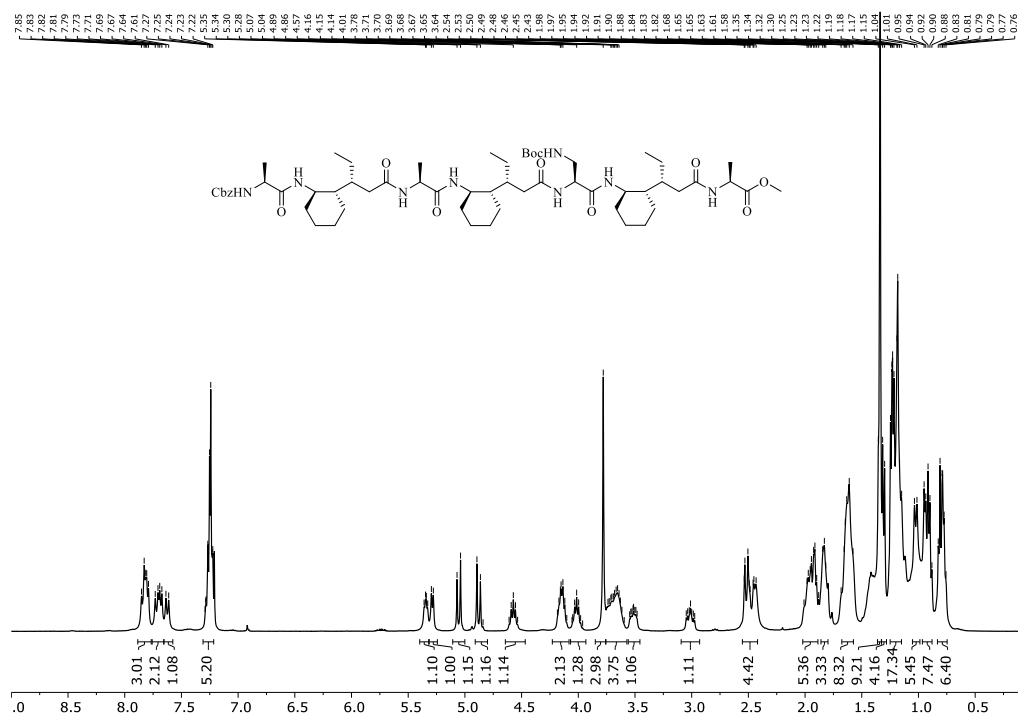
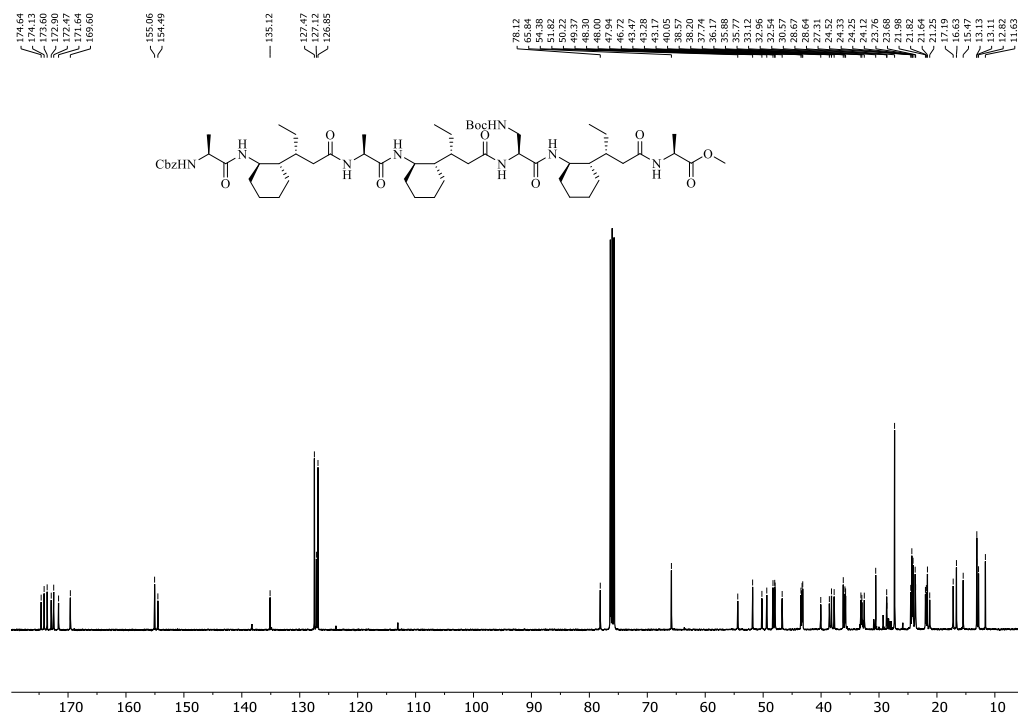
Spectrum 28: ^{13}C NMR: (101 MHz, CDCl_3) of foldamer **243**

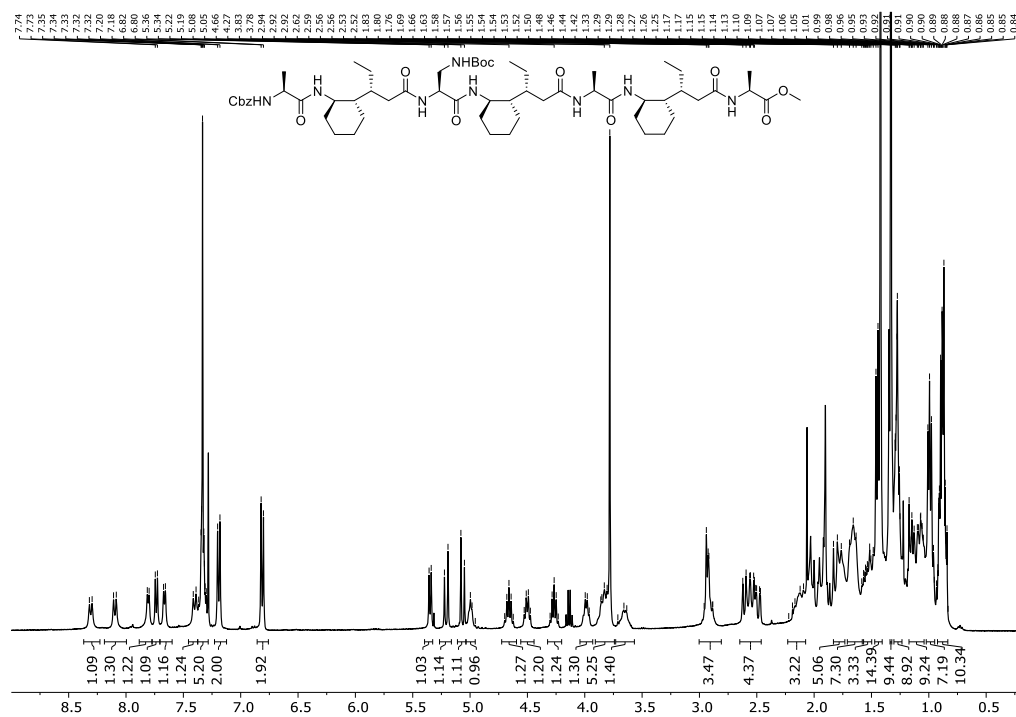


Spectrum 31: ^1H NMR: (400 MHz, CDCl_3) of foldamer **287**

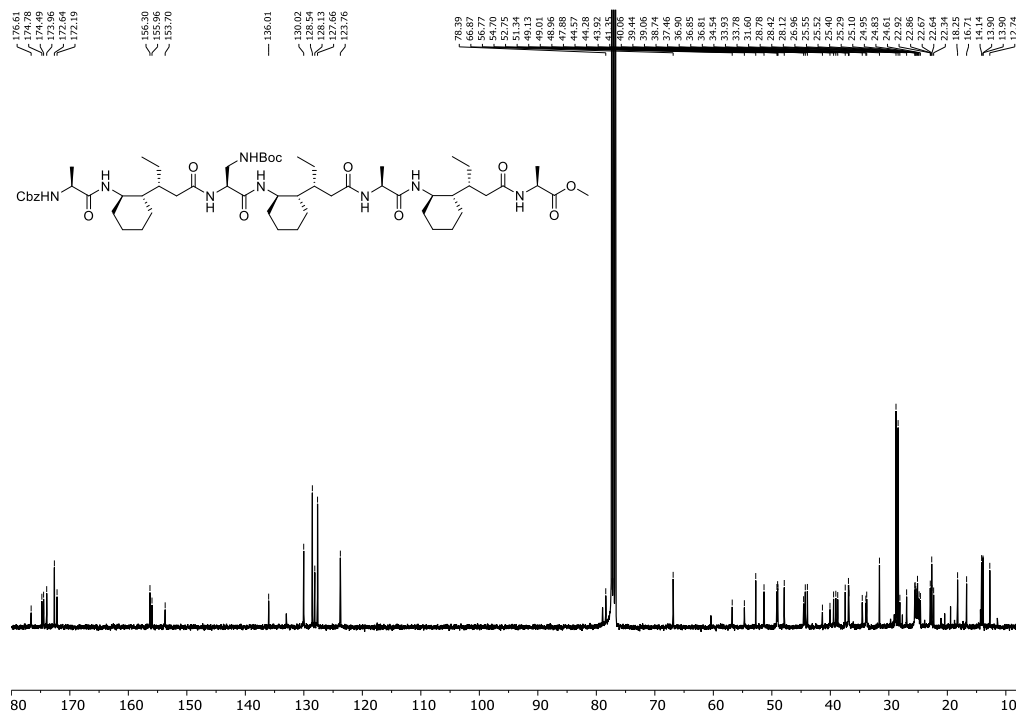


Spectrum 32: ^{13}C NMR: (101 MHz, CDCl_3) of foldamer **287**

Spectrum 33: $^1\text{H NMR}$: (400 MHz, CDCl_3) of foldamer 300-BocSpectrum 34: $^{13}\text{C NMR}$: (101 MHz, CDCl_3) of foldamer 300-Boc



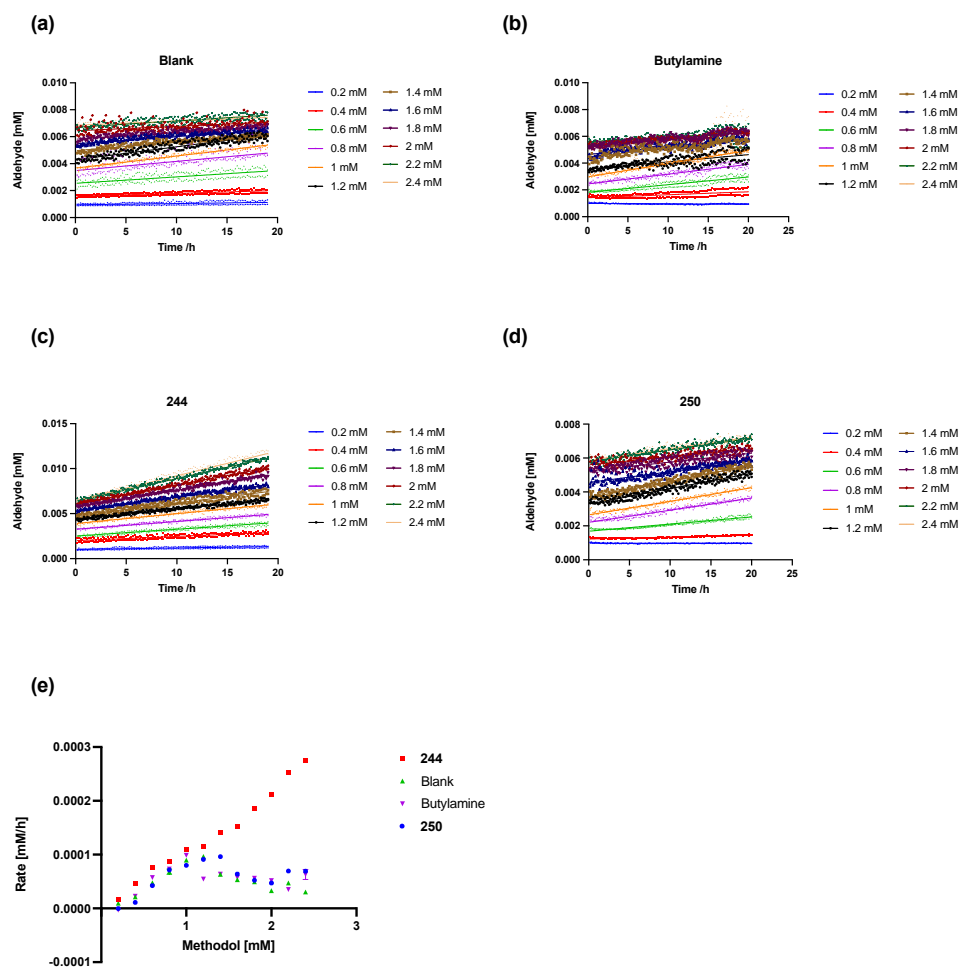
Spectrum 35: ^1H NMR: (400 MHz, CDCl_3) of foldamer **310-Boc**



Spectrum 36: ^{13}C NMR: (101 MHz, CDCl_3) of foldamer **310-Boc**

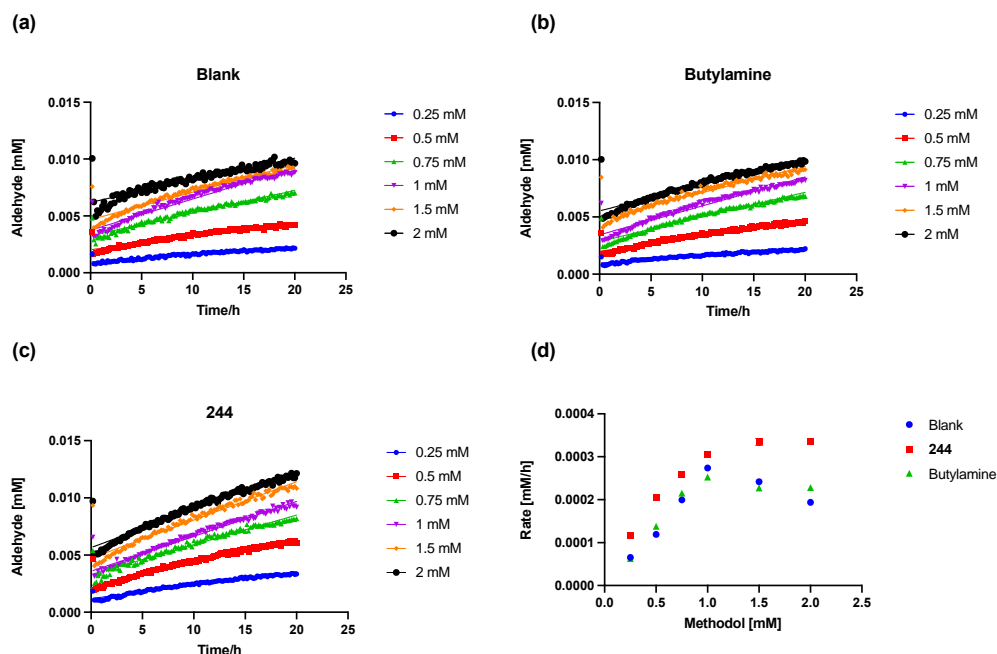
6.7 Kinetic Data of Plate Reader Reading

- 5% CH₃CN in PBS Buffer



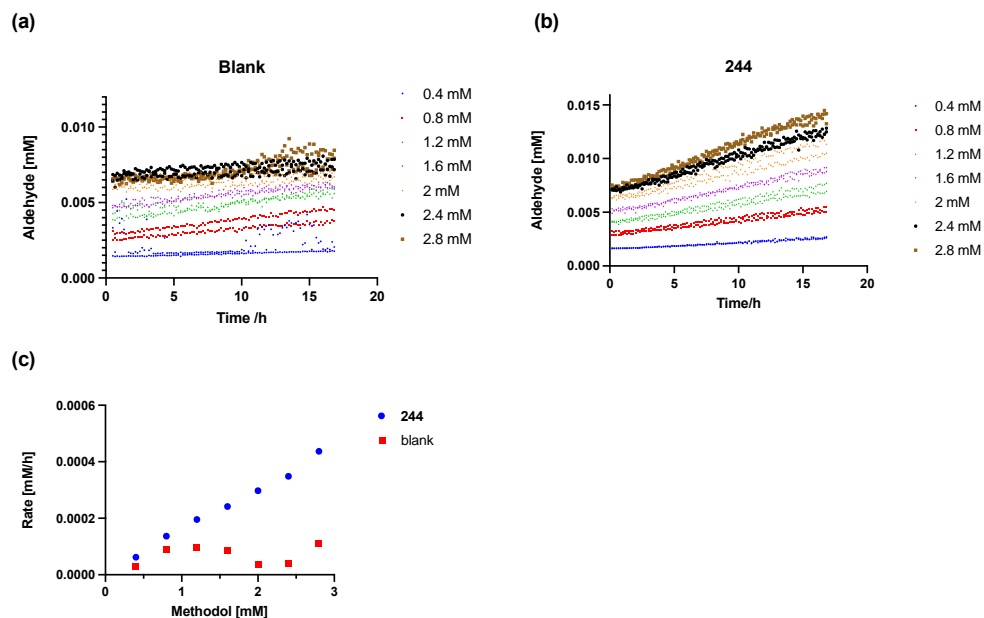
Method: At 25 °C, in 5% CH₃CN in PBS buffer (42.5 mM, pH=7.5), monitored by plater reader, (a) The proceeded product formation with varying substrate concentration (0.2-2.4 mM) (b) The proceeded product formation with 200 μM of butylamine and varying substrate concentration (0.2-2.4 mM). (c) The proceeded product formation with 100 μM of foldamer **244** and varying substrate concentration (0.2-2.4 mM). (d) The proceeded product formation with 200 μM of Tripeptide **250** and varying substrate concentration (0.2-2.4 mM) (e) Rate comparison between blank contrast, butylamine, foldamer **8** and tripeptide **9** catalysed reaction at different methodol concentration (0.2-2.4 mM).

- 5% CH₃CN in Tris Buffer



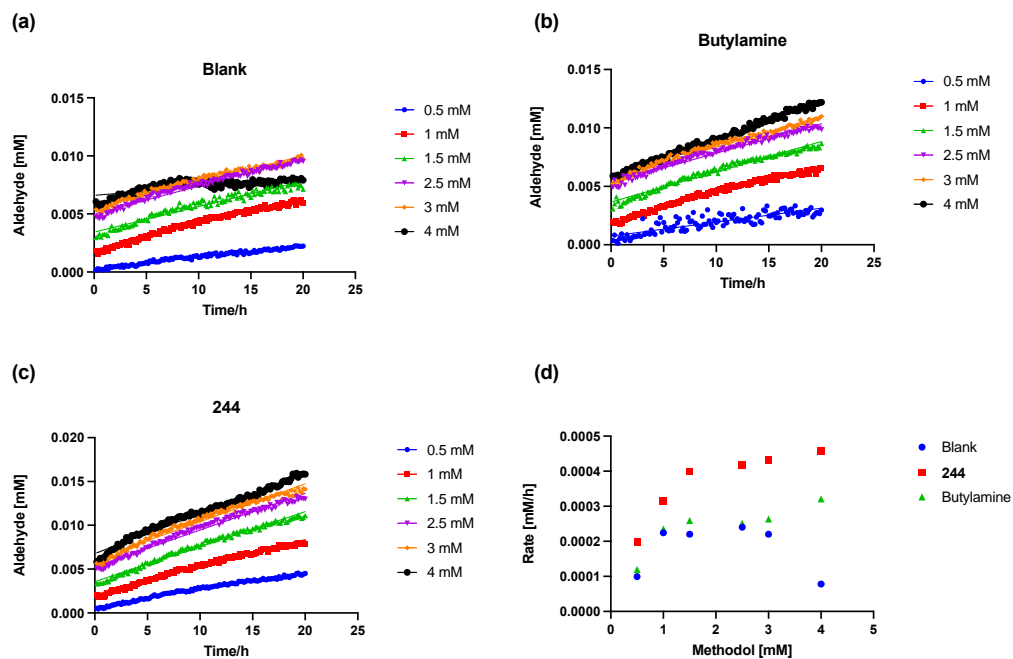
Method: At 25 °C, in 5% CH₃CN in Tris buffer (50 mM Tris, pH=8, 150 mM NaCl), monitored by plater reader, (a) The proceeded product formation with varying substrate concentration (0.25-2 mM) (b) The proceeded product formation with 200 μM of butylamine and varying substrate concentration (0.25-2 mM). (c) The proceeded product formation with 100 μM of foldamer **244** and varying substrate concentrations (0.25-2 mM). (d) Rate comparison between blank contrast, 200 μM butylamine and 100 μM foldamer **244** catalysed reactions at different methodol concentrations (0.25-2 mM).

- 10% CH₃CN in PBS Buffer



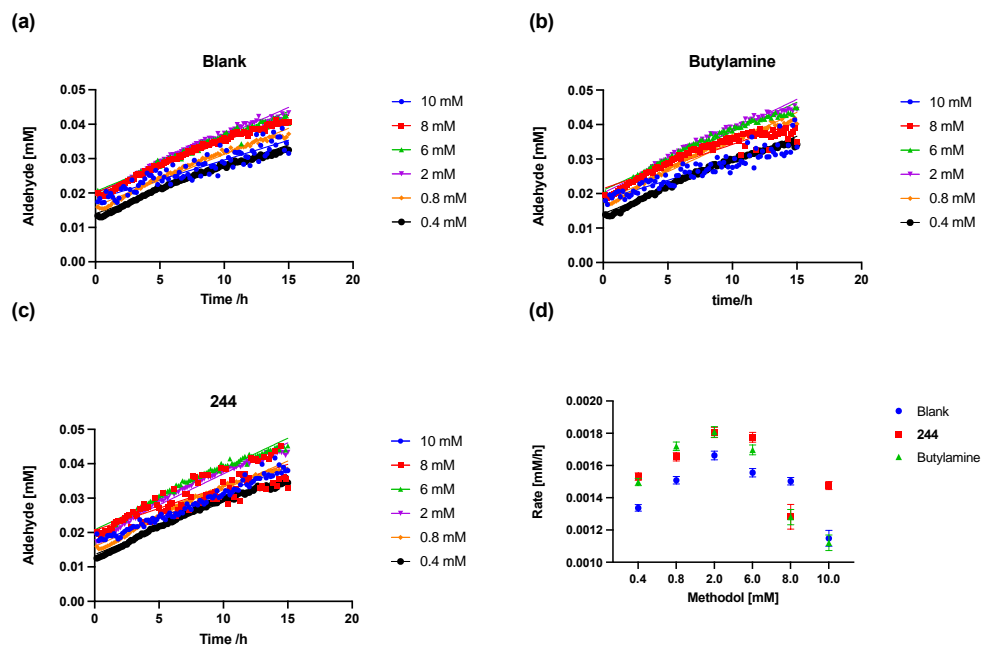
Method: At 25 °C, in 10% CH₃CN in PBS buffer (42.5 mM, pH=7.5), monitored by plater reader, (a) The proceeded product formation with varying substrate concentration (0.4-2.8 mM) (b) The proceeded product formation with 100 μM of foldamer **244** and varying substrate concentration (0.4-2.8 mM). (c) Rate comparison between blank contrast and foldamer **244** catalysed reaction at different methodol concentration (0.4-2.8 mM).

- 10% CH₃CN in Tris Buffer



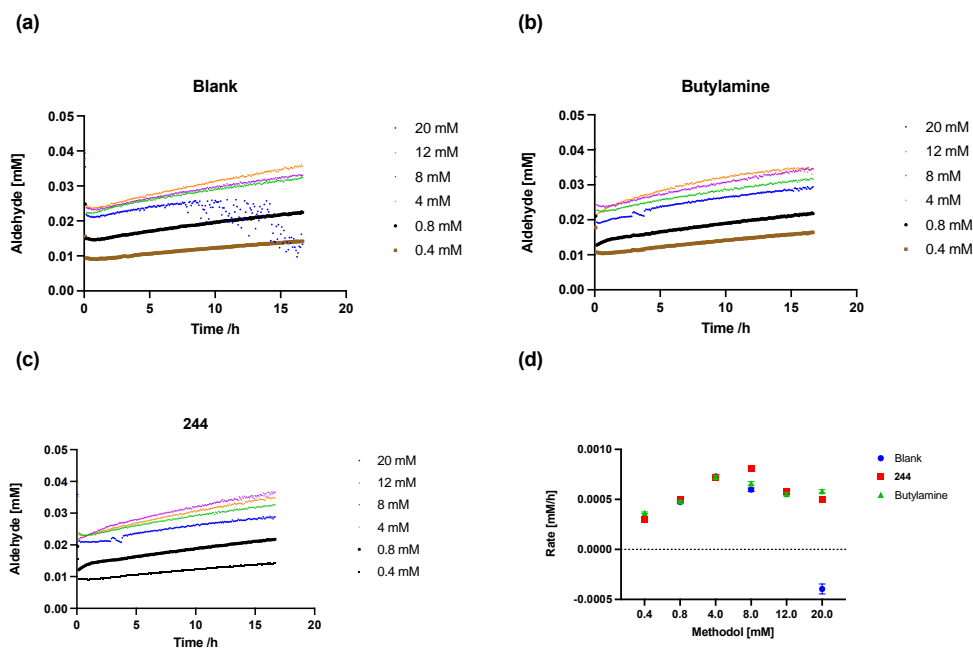
Method: At 25 °C, in 10% CH₃CN in Tris buffer (50 mM Tris, pH=8, 150 mM NaCl), monitored by plater reader, (a) The proceeded product formation with varying substrate concentration (0.5-4 mM) (b) The proceeded product formation with 200 μM of butylamine and varying substrate concentration (0.5-4 mM). (c) The proceeded product formation with 100 μM of foldamer **244** and varying substrate concentrations (0.5-4 mM). (d) Rate comparison between blank contrast, 200 uM butylamine and 100 μM foldamer **244** catalysed reactions at different methodol concentrations (0.5-4 mM).

- 20% CH₃CN in HEPES Buffer



Method: At 40 °C, in 20% CH₃CN in HEPES (25 mM HEPES, pH=7.5, 100 mM NaCl), monitored by plater reader, (a) The proceeded product formation with varying substrate concentration (0.4-10 mM) (b) The proceeded product formation with 200 μM of butylamine and varying substrate concentration (0.4-10 mM). (c) The proceeded product formation with 100 μM of foldamer **244** and varying substrate concentrations (0.4-10 mM). (d) Rate comparison between blank contrast, 200 μM butylamine and 100 uM foldamer **244** catalysed reactions at different methodol concentrations (0.4-10 mM).

- 30% CH₃CN in Tris Buffer



Method: At 30 °C, in 30% CH₃CN in Tris buffer (50 mM Tris, pH=8, 150 mM NaCl), monitored by plater reader, (a) The proceeded product formation with varying substrate concentration (0.4-20 mM) (b) The proceeded product formation with 200 μM of butylamine and varying substrate concentration (0.4-20 mM). (c) The proceeded product formation with 100 μM of foldamer **244** and varying substrate concentrations (0.4-20 mM). (d) Rate comparison between blank contrast, 200 μM butylamine and 100 uM foldamer **244** catalysed reactions at different methodol concentrations (0.4-20 mM).

6.8 Fershtp 147 Equation

For systems exhibiting burst-phase kinetics, time courses were fit to equation 1.

$$[P] = [E]_0 \left(\frac{k'_1}{k'_1 + k_2} \right) \left(\frac{k'_1}{k'_1 + k_2} \{1 - e^{-(k'_1 + k_2)t}\} + k_2 t \right) \quad \text{Eq 1,}$$

where $k'_1 = k_1[Aldol]_0$ and $[E]_0 = 0.75 \text{ mM}$. For control amines, a linear equation (Eq 2) was used:

$$[P] = k'_1[E]_0 t \quad \text{Eq 2,}$$

Where $k'_1 = k_1[Aldol]_0$ and $[E]_0 = 1.5 \text{ mM}$.

6.9 X-Ray Crystallography

The crystal of foldamer **97** was obtained from the diffusion of $\text{CHCl}_3/\text{CH}_3\text{CN}$. The crystal of foldamer **103** was obtained from the diffusion of EtOAc/Heptane. The crystal of foldamer **243** was obtained from slow evaporation of EtOAc, CH_3CN , dichloroethane, methanol, heptane, diethyl ether, Diisopropyl ether. The structures were solved by direct methods using SHELXT¹²⁷ and refined against F2 on all data by full-matrix least squares with SHELXL¹²⁸ following established refinement strategies.¹²⁹ Most of the non-H atoms were refined with anisotropic temperature parameters, and the disordered ones were refined with isotropic temperature parameters. All hydrogen atoms were included in the model at geometrically calculated positions and refined using a riding model. SHELX ISOR, DELU, and SIMU restraints were used in the refinement strategy to reduce the anisotropic displacement parameters of the side chains. DFIX instructions were used to geometrically restrain most of the side chains. FLAT instructions were used to geometrically restrain benzene rings. The contribution of the electron density associated with disordered solvent molecules, which could not be modeled with discrete atomic positions was handled using the SQUEEZE¹³⁰ routine in PLATON.^{131, 132} Crystallographic data have been deposited with the CCDC.

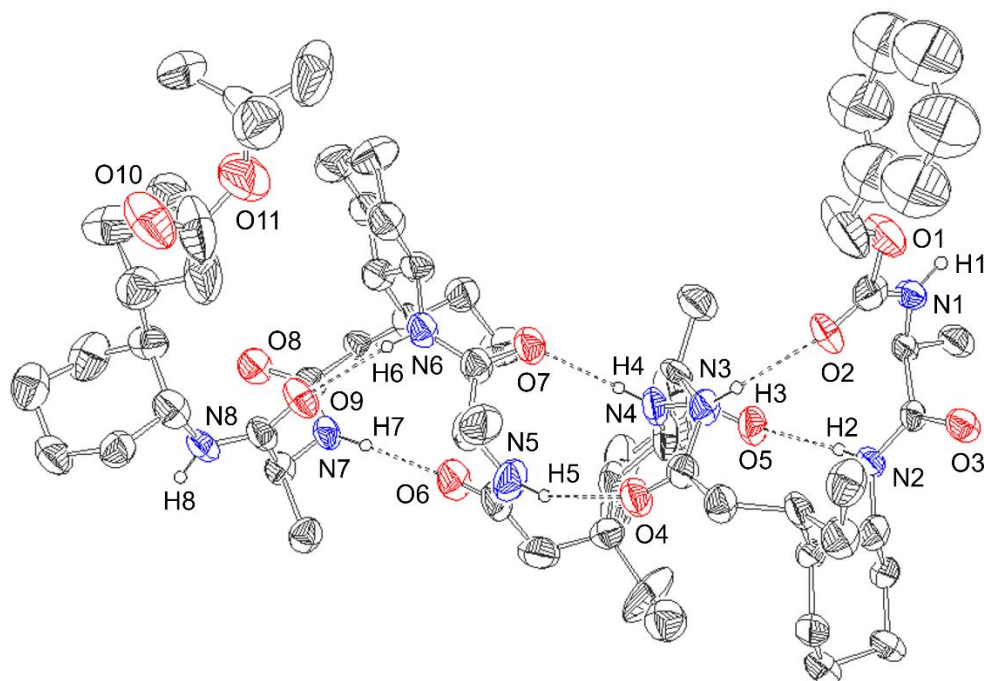


Figure 6.1 The molecular structure of foldamer **97** (CCDC 2252028). Thermal ellipsoids displayed at the 50% probability level. Hydrogen atoms are pictured as spheres of arbitrary radii (and most have been omitted for clarity).

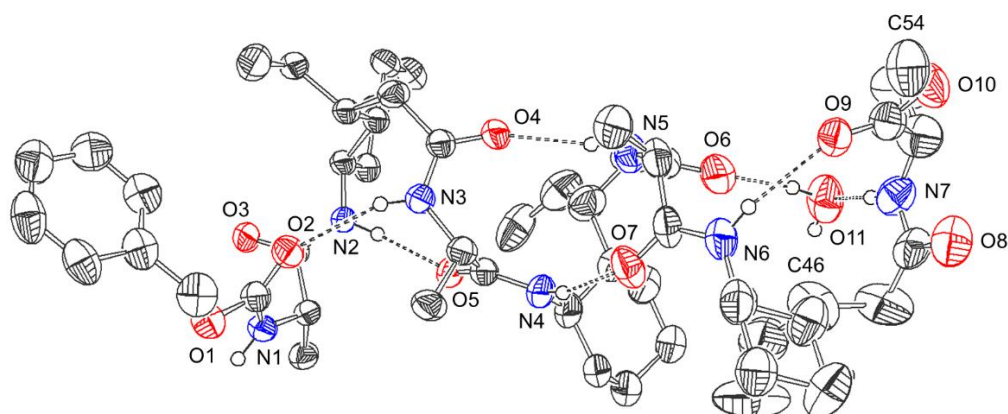


Figure 6.2 The molecular structure of foldamer **103** (CCDC : 2251914). Thermal ellipsoids displayed at the 50% probability level. Hydrogen atoms are pictured as spheres of arbitrary radii (and most have been omitted for clarity). The terminal $-(\text{CH}_2\text{CH}_3)\text{CH}_2\text{CONHC}(\text{CH}_3)\text{COOCH}_3$ group (C46, C47, C48, C49, C50, O8, N7, C51, C52, C53, O9, O10, C54) is disordered across two positions, and the position of highest relative occupancy

(57%) is displayed. The water molecule (O11) is also disordered across three positions, and the position of highest relative occupancy (57%) is displayed.

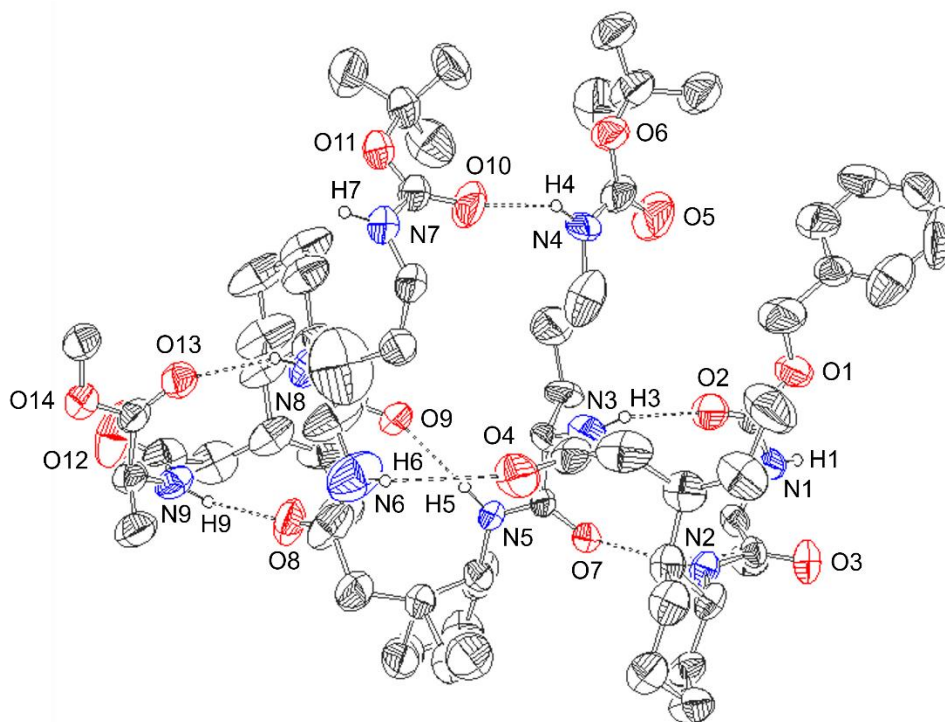


Figure 6.3 The molecular structure of bis-Boc-ornithine heptamer **243** (CCDC : 2252029). Thermal ellipsoids displayed at the 50% probability level. Hydrogen atoms are pictured as spheres of arbitrary radii (and most have been omitted for clarity). The terminal $-\text{OCH}_2\text{C}_6\text{H}_5$ group (O14, C62, C63, C64, C65, C66, C67, C68) is disordered across two positions, and the position of highest relative occupancy (85%) is displayed).

6.9.1 XRD Methodology

Foldamer 97: All data were processed with the CrysAlisPro software package from Rigaku Oxford Diffraction. The crystal structure was solved and refined by least-squares within the Olex2 program suite¹²⁷ using the ShelXT structure-solution program¹²⁸ and the ShelXL 2014 refinement program.¹²⁹ Positions of hydrogen atoms were identified as the strongest peaks in Fourier difference maps and constrained with AFIX commands within SHELX. Crystallographic details are provided in **Table 6-1**.

Foldamer 103 : A single crystal of the heptamer (0.20×0.06×0.03 mm) was held in a MiTeGen loop, and measurements were made at 100 K using a Rigaku 007 HF four-circle diffractometer

and monochromated CuK α radiation ($\lambda = 1.54178 \text{ \AA}$) with a hybrid pixel array HyPix-6000HE detector.¹³⁰ The sample temperature was controlled with an Oxford Cryosystems 800 Series CryoStream. Crystallographic details are provided in Table 6-1.

Foldamer 243: A single crystal (0.02 x 0.05 x 0.07 mm) was mounted on a nylon loop and data measurements were made at 100 K using a Rigaku Synergy diffractometer equipped with a Cu microsource tube (CuK $\alpha = 1.54184 \text{ \AA}$), a Hypix6000HE photon counting detector and an Oxford Cryosystems Cryostream. The crystal structure was solved and refined with the Olex2 program suite, using ShelXT for structure solution and ShelXL for structure refinement. The structure was additionally validated by periodic dispersion-corrected DFT calculations using Quantum Espresso,¹²² following the approach of van de Streek.¹²³ Crystallographic details are provided in Table 6-1.

Table 6-1 Crystallographic data for foldamer **97**, foldamer **103**, foldamer **243**

und	ZAXAXAXAOMe	Octamer 97	Heptamer 243
Empirical formula	C ₅₄ H ₈₉ N ₇ O ₁₁	C ₆₈ H ₁₁₂ N ₈ O ₁₁	C ₆₈ H ₁₁₃ N ₉ O ₁₄
Formula weight	1012.32	1217.65	1280.67
Temperature/K	100(2)	100.00(10)	100.15
Crystal system	orthorhombic	monoclinic	monoclinic
Space group	P2 ₁ 2 ₁ 2 ₁	P2 ₁	P2 ₁
a/Å	8.91084(12)	8.9665(5)	9.7832(2)
b/Å	12.2957(2)	32.2159(17)	55.6208(12)
c/Å	53.1813(7)	25.6602(15)	14.0694(2)
α/°	90	90	90
β/°	90	91.943(6)	90.3234(18)
γ/°	90	90	90
Volume/Å ³	5826.78(15)	7408.0(7)	7655.7(3)
Z	4	4	4
ρ _{calc} /cm ³	1.154	1.092	1.111
μ/mm ⁻¹	0.650	0.589	0.627
F(000)	2200.0	2656.0	2784.0
Crystal size/mm ³	0.20 × 0.06 × 0.025	0.03 × 0.06 × 0.28	0.02 × 0.05 × 0.07
Radiation	Cu Kα (λ = 1.54178)	Cu Kα (λ = 1.54184)	CuKα (λ = 1.54184)
2θ range for data collection/°	6.648 to 140.128	5.486 to 157.134	6.282 to 152.85
Index ranges	-10 ≤ h ≤ 10, -14 ≤ k ≤ 14, -60 ≤ l ≤ 64	-11 ≤ h ≤ 11, -40 ≤ k ≤ 40, -20 ≤ l ≤ 32	-12 ≤ h ≤ 11, -69 ≤ k ≤ 70, -17 ≤ l ≤ 16
Reflections collected	86919 11024	62172 26732	122167 29275
Independent reflections	[R _{int} = 0.0631, R _{sigma} = 0.0271]	[R _{int} = 0.1053, R _{sigma} = 0.1060]	[R _{int} = 0.1290, R _{sigma} = 0.1098]
Data/restraints/parameters	11024/1411/795	26732/181/1591	29275/1/1663
Goodness-of-fit on F ²	1.070	1.023	1.040
Final R indexes [I ≥ 2σ (I)]	R ₁ = 0.0649, wR ₂ = 0.1731	R ₁ = 0.1135, wR ₂ = 0.3023	R ₁ = 0.0908, wR ₂ = 0.2340
Final R indexes [all data]	R ₁ = 0.0730, wR ₂ = 0.1792	R ₁ = 0.1386, wR ₂ = 0.3254	R ₁ = 0.1375, wR ₂ = 0.2624
Largest diff. peak/hole/e Å ⁻³	0.56/-0.22	0.81/-0.51	0.35/-0.27
Flack parameter	0.22(7)	0.48(18)	0.46(15)

Chapter 7 Conclusion and Outlook

This thesis focused on the research of foldamer structure and catalysis. Based on computational analysis, a novel unnatural δ -amino acid was proposed and synthesized. By combining it with natural α -amino acids, three peptidic sequences with alternating α - and δ -amino acids ($\alpha\delta\alpha\delta\alpha\delta$) were successfully synthesized. Characterizations of these sequences indicated that only the L-alanine was structurally compatible with the proposed δ -amino acid in terms of forming a helix. Full structural characterization using NMR, MS, and XRD confirmed the formation of a 13/11 helix, and additional structural insights were also obtained from computational simulations.

Based on structural results drawn from XRD and NMR simulations, a catalyst was designed with amine side chains appended to the foldamer, resulting in catalytic foldamer, which were then applied to catalyze the retro-aldol cleavage reaction as a minimized mimic of the aldolase. Although not as efficient as natural enzymes, the foldamer catalyst proved to be an effective bifunctional catalyst compared to the background and butylamine catalyst.

By modifying the distance between the catalytic site and the foldamer's helicity center, a new foldamer catalyst was designed and synthesized. As detailed in Chapter 4, this catalyst achieved kinetic resolution and, more surprisingly, the enantioselectivity of the substrate could be reversed solely by changing the position of the catalytic site without altering the point chirality of the foldamer's structure. The work presented in this chapter is unfinished, future work should include collecting the crystal structure of the foldamer catalyst to confirm its secondary structure, specifically, the interaction of the catalytic site with the foldamer's backbone. Circular Dichroism (CD) analysis of the foldamer catalysts should also be performed to confirm if the helicity of the foldamer changes while changing position of the catalytic site. Additionally, computational simulations might also provide insights into the secondary structure of the foldamer catalyst.

The follow-up project in Chapter 5 on flavin-conjugated foldamer catalysis is also promising. The catalytic decarboxylative cyanation of L-tyrosine has already been realized. Future work should explore the catalysis on D-tyrosine to determine if kinetic resolution is also achievable within the photocatalytic mechanism.

References

- (1) Gellman, S. H. Foldamers: a manifesto. *Accounts of Chemical Research* **1998**, *31* (4), 173-180.
- (2) Corvaglia, V.; Ait Mohamed Amar, I.; Garambois, V.; Letast, S.; Garcin, A.; Gongora, C.; Del Rio, M.; Denevault-Sabourin, C.; Joubert, N.; Huc, I.; Pourquier, P. Internalization of foldamer-based DNA mimics through a site-specific antibody conjugate to target HER2-positive cancer cells. *Pharmaceuticals (Basel)* **2021**, *14* (7), 624.
- (3) Oba, M. Cell-penetrating peptide foldamers: drug-delivery yools. *Chembiochem* **2019**, *20* (16), 2041-2045.
- (4) Girvin, Z. C.; Gellman, S. H. Foldamer catalysis. *Journal of the American Chemical Society* **2020**, *142* (41), 17211-17223.
- (5) Mateus, P.; Chandramouli, N.; Mackereth, C. D.; Kauffmann, B.; Ferrand, Y.; Huc, I. Allosteric recognition of homomeric and heteromeric pairs of monosaccharides by a foldamer capsule. *Angewandte Chemie International Edition* **2020**, *59* (14), 5797-5805.
- (6) Koch, O.; Bocola, M.; Klebe, G. Cooperative effects in hydrogen-bonding of protein secondary structure elements: a systematic analysis of crystal data using scabase. *Proteins: Structure, Function, and Bioinformatics* **2005**, *61* (2), 310-317.
- (7) Fujiwara, K.; Ebisawa, S.; Watanabe, Y.; Fujiwara, H.; Ikeguchi, M. The origin of β -strand bending in globular proteins. *BMC Structural Biology* **2015**, *15* (1), 21.
- (8) Sinatra, L.; Kolano, L.; Icker, M.; Fritzsche, S. R.; Volke, D.; Gockel, I.; Thieme, R.; Hoffmann, R.; Hansen, F. K. Hybrid peptides based on α -aminoxy acids as antimicrobial and anticancer foldamers. *ChemPlusChem* **2021**, *86* (6), 827-835.
- (9) Seebach, D.; Overhand, M.; Kühnle, F. N. M.; Martinoni, B.; Oberer, L.; Hommel, U.; Widmer, H. β -Peptides: synthesis by Arndt-Eistert homologation with concomitant peptide coupling. Structure determination by NMR and CD spectroscopy and by X-ray crystallography. Helical secondary structure of a β -hexapeptide in solution and its stability towards pepsin. *Helvetica Chimica Acta* **1996**, *79* (4), 913-941.
- (10) Appella, D. H.; Christianson, L. A.; Karle, I. L.; Powell, D. R.; Gellman, S. H. β -Peptide foldamers: robust helix formation in a new family of β -amino acid oligomers. *Journal of the American Chemical Society* **1996**, *118* (51), 13071-13072.
- (11) Appella, D. H.; Christianson, L. A.; Klein, D. A.; Powell, D. R.; Huang, X.; Barchi, J. J.; Gellman, S. H. Residue-based control of helix shape in β -peptide oligomers. *Nature* **1997**, *387* (6631), 381-384.
- (12) Fernandes, C.; Faure, S.; Pereira, E.; Théry, V.; Declerck, V.; Guillot, R.; Aitken, D. J. 12-Helix folding of cyclobutane β -amino acid oligomers. *Organic Letters* **2010**, *12* (16), 3606-3609.

- (13) Altmayer-Henzien, A.; Declerck, V.; Farjon, J.; Merlet, D.; Guillot, R.; Aitken, D. J. Fine tuning of β -peptide foldamers: a single atom replacement holds back the switch from an 8-helix to a 12-helix. *Angewandte Chemie International Edition* **2015**, *54* (37), 10807-10810.
- (14) Hintermann, T.; Gademann, K.; Jaun, B.; Seebach, D. γ -Peptides forming more stable secondary structures than α -peptides: synthesis and helical NMR-solution structure of the γ -hexapeptide analog of H-(Val-Ala-Leu)₂-OH. *Helvetica Chimica Acta* **1998**, *81* (5-8), 983-1002.
- (15) Hanessian, S.; Luo, X.; Schaum, R.; Michnick, S. Design of secondary structures in unnatural peptides: stable helical γ -tetra-, hexa-, and octapeptides and consequences of α -substitution. *Journal of the American Chemical Society* **1998**, *120* (33), 8569-8570.
- (16) Bonnel, C.; Legrand, B.; Bantignies, J. L.; Petitjean, H.; Martinez, J.; Masurier, N.; Maillard, L. T. FT-IR and NMR structural markers for thiazole-based γ -peptide foldamers. *Organic & Biomolecular Chemistry* **2016**, *14* (37), 8664-8669.
- (17) Farrera-Sinfreu, J.; Zaccaro, L.; Vidal, D.; Salvatella, X.; Giralt, E.; Pons, M.; Albericio, F.; Royo, M. A new class of foldamers based on cis- γ -amino-l-proline_{1,2}. *Journal of the American Chemical Society* **2004**, *126* (19), 6048-6057.
- (18) Szabo, L.; Smith, B. L.; McReynolds, K. D.; Parrill, A. L.; Morris, E. R.; Gervay, J. Solid Phase synthesis and secondary structural studies of (1 \rightarrow 5) amide-linked sialooligomers₁. *The Journal of Organic Chemistry* **1998**, *63* (4), 1074-1078.
- (19) Smith, M. D.; Fleet, G. W. J. Designing secondary structures: 5-azidomethyl tetrahydrofuran-2-carboxylates as carbohydrate-derived dipeptide isosteres. *Journal of Peptide Science* **1999**, *5* (10), 425-441.
- (20) Chakraborty, T. K.; Roy, S.; Kumar, S. K.; Kunwar, A. C. Synthesis and structural studies of peptides containing a glucose-derived furanoid sugar amino acid. *Tetrahedron Letters* **2005**, *46* (17), 3065-3070.
- (21) Siriwardena, A.; Pulukuri, K. K.; Kandiyal, P. S.; Roy, S.; Bande, O.; Ghosh, S.; Garcia Fernández, J. M.; Ariel Martin, F.; Ghigo, J.-M.; Beloin, C.; et al. Sugar-modified foldamers as conformationally defined and biologically distinct glycopeptide mimics. *Angewandte Chemie International Edition* **2013**, *52* (39), 10221-10226.
- (22) Hayen, A.; Schmitt, M. A.; Ngassa, F. N.; Thomasson, K. A.; Gellman, S. H. Two helical conformations from a single foldamer backbone: "split personality" in short α/β -peptides. *Angewandte Chemie International Edition* **2004**, *43* (4), 505-510.
- (23) Schmitt, M. A.; Weisblum, B.; Gellman, S. H. Unexpected relationships between structure and function in α,β -peptides: antimicrobial foldamers with heterogeneous backbones. *Journal of the American Chemical Society* **2004**, *126* (22), 6848-6849.
- (24) Choi, S. H.; Guzei, I. A.; Spencer, L. C.; Gellman, S. H. Crystallographic characterization of helical secondary structures in α/β -peptides with 1:1 residue alternation. *Journal of the American Chemical Society* **2008**, *130* (20), 6544-6550.
- (25) De Pol, S.; Zorn, C.; Klein, C. D.; Zerbe, O.; Reiser, O. Surprisingly stable helical conformations in α/β -peptides by incorporation of cis- β -aminocyclopropane carboxylic acids. *Angewandte Chemie International Edition* **2004**, *43* (4), 511-514.

- (26) Lee, M.; Shim, J.; Kang, P.; Choi, M.-G.; Choi, S. H. Stabilization of 11/9-helical α/β -peptide foldamers in protic solvents. *Chemical Communications* **2016**, 52 (35), 5950-5952.
- (27) Cheloha, R. W.; Woodham, A. W.; Bousbaine, D.; Wang, T.; Liu, S.; Sidney, J.; Sette, A.; Gellman, S. H.; Ploegh, H. L. Recognition of class II MHC peptide ligands that contain β -amino acids. *The Journal of Immunology* **2019**, ji1900536.
- (28) Fisher, B. F.; Hong, S. H.; Gellman, S. H. Thermodynamic scale of β -amino acid residue propensities for an α -helix-like conformation. *Journal of the American Chemical Society* **2018**, 140 (30), 9396-9399.
- (29) Sharma, G. V. M.; Nagendar, P.; Jayaprakash, P.; Radha Krishna, P.; Ramakrishna, K. V. S.; Kunwar, A. C. 9/11 mixed helices in α/β peptides derived from C-linked carbo- β -amino Acid and L-ala repeats. *Angewandte Chemie International Edition* **2005**, 44 (36), 5878-5882.
- (30) Marafon, G.; Crisma, M.; Moretto, A. Tunable E-Z photoisomerization in α,β -peptide foldamers featuring multiple (E/Z)-3-aminoprop-2-enoic acid units. *Organic Letters* **2019**, 21 (11), 4182-4186.
- (31) Sonti, R.; Dinesh, B.; Basuroy, K.; Raghothama, S.; Shamala, N.; Balam, P. C12 helices in long hybrid ($\alpha\gamma$)_n peptides composed entirely of unconstrained residues with proteinogenic side chains. *Organic Letters* **2014**, 16 (6), 1656-1659.
- (32) Chatterjee, S.; Vasudev, P. G.; Raghothama, S.; Ramakrishnan, C.; Shamala, N.; Balam, P. Expanding the peptide β -turn in $\alpha\gamma$ hybrid sequences: 12 atom hydrogen bonded helical and hairpin turns. *Journal of the American Chemical Society* **2009**, 131 (16), 5956-5965.
- (33) Fisher, B. F.; Guo, L.; Dolinar, B. S.; Guzei, I. A.; Gellman, S. H. Heterogeneous H-bonding in a foldamer helix. *Journal of the American Chemical Society* **2015**, 137 (20), 6484-6487.
- (34) Guo, L.; Zhang, W.; Guzei, I. A.; Spencer, L. C.; Gellman, S. H. Helical secondary structures in 2:1 and 1:2 α/γ -peptide foldamers. *Tetrahedron* **2012**, 68 (23), 4413-4417.
- (35) Sharma, G. V. M.; Babu, B. S.; Ramakrishna, K. V. S.; Nagendar, P.; Kunwar, A. C.; Schramm, P.; Baldauf, C.; Hofmann, H.-J. Synthesis and structure of α/δ -hybrid peptides-access to novel helix patterns in foldamers. *Chemistry – A European Journal* **2009**, 15 (22), 5552-5566.
- (36) Reja, R. M.; Kumar, V.; George, G.; Patel, R.; Puneeth Kumar, D. R.; Raghothama, S.; Gopi, H. N. Structural investigation of hybrid peptide foldamers composed of α -dipeptide equivalent β -Oxy- δ^5 -amino acids. *Chemistry – A European Journal* **2020**, 26 (19), 4304-4309.
- (37) Violette, A.; Lancelot, N.; Poschalko, A.; Piotto, M.; Briand, J.-P.; Raya, J.; Elbayed, K.; Bianco, A.; Guichard, G. Exploring helical folding of oligoureas during chain elongation by high-resolution magic-angle-spinning (HRMAS) NMR spectroscopy. *Chemistry – A European Journal* **2008**, 14 (13), 3874-3882.
- (38) Fischer, L.; Didierjean, C.; Jolibois, F.; Semetey, V.; Manuel Lozano, J.; Briand, J.-P.; Marraud, M.; Poteau, R.; Guichard, G. Propensity for local folding induced by the urea fragment in short-chain oligomers. *Organic & Biomolecular Chemistry* **2008**, 6 (14), 2596-2610.

- (39) Fischer, L.; Claudon, P.; Pendem, N.; Miclet, E.; Didierjean, C.; Ennifar, E.; Guichard, G. The canonical helix of urea oligomers at atomic resolution: insights into folding-induced axial organization. *Angewandte Chemie International Edition* **2010**, *49* (6), 1067-1070.
- (40) Pendem, N.; Nelli, Y. R.; Douat, C.; Fischer, L.; Laguerre, M.; Ennifar, E.; Kauffmann, B.; Guichard, G. Controlling helix formation in the γ -peptide superfamily: heterogeneous foldamers with urea/amide and urea/carbamate backbones. *Angewandte Chemie International Edition* **2013**, *52* (15), 4147-4151.
- (41) Maurizot, V.; Léger, J. M.; Guionneau, P.; Huc, I. Diversity of interstrand π - π stacking motifs in the double helices of pyridinedicarboxamide oligomers. *Russian Chemical Bulletin* **2004**, *53* (7), 1572-1576.
- (42) Jiang, H.; Léger, J.-M.; Huc, I. Aromatic δ -peptides. *Journal of the American Chemical Society* **2003**, *125* (12), 3448-3449.
- (43) Bao, C.; Kauffmann, B.; Gan, Q.; Srinivas, K.; Jiang, H.; Huc, I. Converting sequences of aromatic amino acid monomers into functional three-dimensional structures: second-generation helical capsules. *Angewandte Chemie International Edition* **2008**, *47* (22), 4153-4156.
- (44) Dodson, G.; Wlodawer, A. Catalytic triads and their relatives. *Trends in Biochemical Sciences* **1998**, *23* (9), 347-352.
- (45) Blow, D. M.; Birktoft, J. J.; Hartley, B. S. Role of a buried acid group in the mechanism of action of chymotrypsin. *Nature* **1969**, *221* (5178), 337-340.
- (46) Nicholson, W. I.; Howard, J. L.; Magri, G.; Seastram, A. C.; Khan, A.; Bolt, R. R. A.; Morrill, L. C.; Richards, E.; Browne, D. L. Ball-milling-enabled reactivity of manganese metal**. *Angewandte Chemie International Edition* **2021**, *60* (43), 23128-23133.
- (47) Read de Alaniz, J.; Rovis, T. A highly enantio- and diastereoselective catalytic intramolecular stetter reaction. *Journal of the American Chemical Society* **2005**, *127* (17), 6284-6289.
- (48) Karlsson, S.; Högberg, H.-E. Catalytic enantioselective 1,3-dipolar cycloaddition of nitrones to cyclopent-1-enecarbaldehyde. *Tetrahedron: Asymmetry* **2002**, *13* (9), 923-926.
- (49) List, B.; Hoang, L.; Martin, H. J. New mechanistic studies on the proline-catalyzed aldol reaction. *Proceedings of the National Academy of Sciences* **2004**, *101* (16), 5839-5842.
- (50) Kumaragurubaran, N.; Juhl, K.; Zhuang, W.; Bøgevig, A.; Jørgensen, K. A. Direct l-proline-catalyzed asymmetric α -amination of ketones. *Journal of the American Chemical Society* **2002**, *124* (22), 6254-6255.
- (51) Ahrendt, K. A.; Borths, C. J.; MacMillan, D. W. C. New strategies for organic catalysis: the first highly enantioselective organocatalytic Diels–Alder reaction. *Journal of the American Chemical Society* **2000**, *122* (17), 4243-4244.
- (52) Jen, W. S.; Wiener, J. J. M.; MacMillan, D. W. C. New strategies for organic catalysis: The first enantioselective organocatalytic 1,3-dipolar cycloaddition. *Journal of the American Chemical Society* **2000**, *122* (40), 9874-9875.
- (53) Akiyama, T. Stronger brønsted acids. *Chemical Reviews* **2007**, *107* (12), 5744-5758.

- (54) Dove, A. P.; Pratt, R. C.; Lohmeijer, B. G. G.; Waymouth, R. M.; Hedrick, J. L. Thiourea-based bifunctional organocatalysis: supramolecular recognition for living polymerization. *Journal of the American Chemical Society* **2005**, *127* (40), 13798-13799.
- (55) Zhu, J.-L.; Zhang, Y.; Liu, C.; Zheng, A.-M.; Wang, W. Insights into the dual activation mechanism involving bifunctional cinchona alkaloid thiourea organocatalysts: an NMR and DFT Study. *The Journal of Organic Chemistry* **2012**, *77* (21), 9813-9825.
- (56) Girvin, Z. C.; Gellman, S. H. Exploration of diverse reactive diad geometries for bifunctional catalysis via foldamer backbone variation. *Journal of the American Chemical Society* **2018**, *140* (39), 12476-12483.
- (57) Girvin, Z. C.; Andrews, M. K.; Liu, X.; Gellman, S. H. Foldamer-templated catalysis of macrocycle formation. *Science* **2019**, *366* (6472), 1528-1531.
- (58) Kinghorn, M. J.; Valdivia-Berroeta, G. A.; Chantry, D. R.; Smith, M. S.; Ence, C. C.; Draper, S. R. E.; Duval, J. S.; Masino, B. M.; Cahoon, S. B.; Flansburg, R. R.; et al. Proximity-induced reactivity and product selectivity with a rationally designed bifunctional peptide catalyst. *ACS Catalysis* **2017**, *7* (11), 7704-7708.
- (59) Byrne, L.; Solà, J.; Boddaert, T.; Marcelli, T.; Adams, R. W.; Morris, G. A.; Clayden, J. Foldamer-mediated remote stereocontrol: >1,60 asymmetric induction. *Angewandte Chemie International Edition* **2014**, *53* (1), 151-155.
- (60) Maayan, G.; Ward, M. D.; Kirshenbaum, K. Folded biomimetic oligomers for enantioselective catalysis. *Proceedings of the National Academy of Sciences* **2009**, *106* (33), 13679-13684.
- (61) Aguesseau-Kondrotas, J.; Simon, M.; Legrand, B.; Bantignières, J.-L.; Kang, Y. K.; Dumitrescu, D.; Van der Lee, A.; Campagne, J.-M.; de Figueiredo, R. M.; Maillard, L. T. Prospect of thiazole-based γ -peptide foldamers in enamine catalysis: exploration of the nitro-michael addition. *Chemistry – A European Journal* **2019**, *25* (30), 7396-7401.
- (62) Bécart, D.; Diemer, V.; Salaün, A.; Oiarbide, M.; Nelli, Y. R.; Kauffmann, B.; Fischer, L.; Palomo, C.; Guichard, G. Helical oligourea foldamers as powerful hydrogen bonding catalysts for enantioselective C–C bond-forming reactions. *Journal of the American Chemical Society* **2017**, *139* (36), 12524-12532.
- (63) Nestl, B. M.; Geinitz, C.; Popa, S.; Rizek, S.; Haselbeck, R. J.; Stephen, R.; Noble, M. A.; Fischer, M.-P.; Ralph, E. C.; Hau, H. T.; et al. Structural and functional insights into asymmetric enzymatic dehydration of alkenols. *Nature Chemical Biology* **2017**, *13* (3), 275-281.
- (64) Müller, M. M.; Windsor, M. A.; Pomerantz, W. C.; Gellman, S. H.; Hilvert, D. A Rationally designed aldolase foldamer. *Angewandte Chemie International Edition* **2009**, *48* (5), 922-925.
- (65) Wang, P. S. P.; Nguyen, J. B.; Schepartz, A. Design and high-resolution structure of a β^3 -peptide bundle catalyst. *Journal of the American Chemical Society* **2014**, *136* (19), 6810-6813.
- (66) Nagata, M.; Watanabe, M.; Doi, R.; Uemura, M.; Ochiai, N.; Ichinose, W.; Fujiwara, K.; Sato, Y.; Kameda, T.; Takeuchi, K.; Shuto, S. Helix-forming aliphatic homo- δ -peptide foldamers based on the conformational restriction effects of cyclopropane. *Organic & Biomolecular Chemistry* **2023**, *21* (5), 970-980.

- (67) Nodes, W. J.; Nutt, D. R.; Chippindale, A. M.; Cobb, A. J. A. Enantioselective intramolecular Michael Addition of nitronates onto conjugated esters: access to cyclic γ -amino acids with up to three stereocenters. *Journal of the American Chemical Society* **2009**, *131* (44), 16016-16017.
- (68) Guo, L.; Chi, Y.; Almeida, A. M.; Guzei, I. A.; Parker, B. K.; Gellman, S. H. Stereospecific synthesis of conformationally constrained γ -amino acids: new foldamer building blocks that support helical secondary structure. *Journal of the American Chemical Society* **2009**, *131* (44), 16018-16020.
- (69) Hunsen, M. Carboxylic acids from primary alcohols and aldehydes by a pyridinium chlorochromate catalyzed oxidation. *Synthesis* **2005**, *2005* (15), 2487-2490.
- (70) Travis, B. R.; Sivakumar, M.; Hollist, G. O.; Borhan, B. Facile oxidation of aldehydes to acids and esters with oxone. *Organic Letters* **2003**, *5* (7), 1031-1034.
- (71) Schmidt, A.-K. C.; Stark, C. B. W. TPAP-Catalyzed direct oxidation of primary alcohols to carboxylic acids through stabilized aldehyde hydrates. *Organic Letters* **2011**, *13* (16), 4164-4167.
- (72) Harding, K. E.; May, L. M.; Dick, K. F. Selective oxidation of allylic alcohols with chromic acid. *The Journal of Organic Chemistry* **1975**, *40* (11), 1664-1665.
- (73) Lin, Q.; Lan, H.; Ma, C.; Stendall, R. T.; Shankland, K.; Musgrave, R. A.; Horton, P. N.; Baldauf, C.; Hofmann, H.-J.; Butts, C. P.; et al. Crystal structure and NMR of an α,δ -peptide foldamer helix shows side-chains are well placed for bifunctional catalysis: application as a minimalist aldolase mimic. *Angewandte Chemie International Edition* **2023**, *62* (36), e202305326.
- (74) Du, S.; Guan, Z.; Hao, L.; Song, Y.; Wang, L.; Gong, L.; Liu, L.; Qi, X.; Hou, Z.; Shao, S. Fructose-bisphosphate aldolase a is a potential metastasis-associated marker of lung squamous cell carcinoma and promotes lung cell tumorigenesis and migration. *PLoS One* **2014**, *9* (1), e85804.
- (75) Yao, D. C.; Tolan, D. R.; Murray, M. F.; Harris, D. J.; Darras, B. T.; Geva, A.; Neufeld, E. J. Hemolytic anemia and severe rhabdomyolysis caused by compound heterozygous mutations of the gene for erythrocyte/muscle isozyme of aldolase, ALDOA(Arg303X/Cys338Tyr). *Blood* **2004**, *103* (6), 2401-2403.
- (76) Henry, I.; Gallano, P.; Besmond, C.; Weil, D.; Mattei, M. G.; Turleau, C.; BouÉ, J.; Kahn, A.; Junien, C. The structural gene for aldolase B (ALDB) maps to 9q13→32. *Annals of Human Genetics* **1985**, *49* (3), 173-180.
- (77) Reginald H. Garrett, C. M. G. *Biochemistry*; Brooks/Cole Pub Co; 4th edition (19 Dec. 2008).
- (78) Choi, K. H.; Shi, J.; Hopkins, C. E.; Tolan, D. R.; Allen, K. N. Snapshots of catalysis: the structure of fructose-1,6-(bis)phosphate aldolase covalently bound to the substrate dihydroxyacetone phosphate. *Biochemistry* **2001**, *40* (46), 13868-13875.
- (79) Obexer, R.; Godina, A.; Garrabou, X.; Mittl, P. R. E.; Baker, D.; Griffiths, A. D.; Hilvert, D. Emergence of a catalytic tetrad during evolution of a highly active artificial aldolase. *Nature Chemistry* **2017**, *9* (1), 50-56.

-
- (80) Neises, B.; Steglich, W. Simple method for the esterification of carboxylic acids. *Angewandte Chemie International Edition in English* **1978**, *17* (7), 522-524.
- (81) Leggio, A.; Liguori, A.; Perri, F.; Siciliano, C.; Viscomi, M. C. Methylation of α -amino acids and derivatives using trimethylsilyldiazomethane. *Chemical Biology & Drug Design* **2009**, *73* (3), 287-291.
- (82) Horneff, T.; Herdtweck, E.; Randoll, S.; Bach, T. Stereoselective allyl transfer to chiral α -methoxycarbaldehydes: A model study related to the C-9/C-15 fragment of geldanamycin. *Bioorganic & Medicinal Chemistry* **2006**, *14* (18), 6223-6234.
- (83) Matthew M. Zhao, J. L., Eiichi Mano, Zhiguo J. Song, and David M. Tschaen. Oxidation of primary alcohols to carboxylic acids with sodium chlorite catalyzed by TEMPO and bleach: 4-Methoxyphenylacetic acid. *Org. Synth.* **2005**, *81*.
- (84) Fersht. *Structure and Mechanism in Protein Science*.
- (85) Schmidt, J.; Ehasz, C.; Epperson, M.; Klas, K.; Wyatt, J.; Hennig, M.; Forconi, M. The effect of the hydrophobic environment on the retro-aldol reaction: comparison to a computationally-designed enzyme. *Organic & Biomolecular Chemistry* **2013**, *11* (48), 8419-8425.
- (86) Tanaka, F.; Fuller, R.; Barbas, C. F. Development of small designer aldolase enzymes: catalytic activity, folding, and substrate specificity. *Biochemistry* **2005**, *44* (20), 7583-7592.
- (87) Shen, Z.; Sang, Y.; Wang, T.; Jiang, J.; Meng, Y.; Jiang, Y.; Okuro, K.; Aida, T.; Liu, M. Asymmetric catalysis mediated by a mirror symmetry-broken helical nanoribbon. *Nature Communications* **2019**, *10* (1), 3976.
- (88) Megens, R. P.; Roelfes, G. Asymmetric catalysis with helical polymers. *Chemistry – A European Journal* **2011**, *17* (31), 8514-8523.
- (89) List, B.; Lerner, R. A.; Barbas, C. F. Proline-catalyzed direct asymmetric aldol reactions. *Journal of the American Chemical Society* **2000**, *122* (10), 2395-2396.
- (90) Zimmerman, H. E.; Traxler, M. D. The stereochemistry of the ivanov and reformatsky reactions I. *Journal of the American Chemical Society* **1957**, *79* (8), 1920-1923.
- (91) Wiesner, M.; Revell, J. D.; Tonazzi, S.; Wennemers, H. Peptide catalyzed asymmetric conjugate addition reactions of aldehydes to nitroethylene-a convenient entry into γ^2 -amino acids. *Journal of the American Chemical Society* **2008**, *130* (17), 5610-5611.
- (92) Miller, S. J. In Search of peptide-based catalysts for asymmetric organic synthesis. *Accounts of Chemical Research* **2004**, *37* (8), 601-610.
- (93) Copeland, G. T.; Jarvo, E. R.; Miller, S. J. Minimal acylase-like peptides. Conformational control of absolute stereospecificity. *J Org Chem* **1998**, *63* (20), 6784-6785.
- (94) Miller, S. J.; Copeland, G. T.; Papaioannou, N.; Horstmann, A.; Ruel, E. M. Kinetic resolution of alcohols catalyzed by tripeptides containing the N-alkylimidazole substructure. *Journal of the American Chemical Society* **1998**, *120*, 1629-1630.
- (95) Rao Raghothama, S.; Kumar Awasthi, S.; Balaram, P. β -Hairpin nucleation by Pro-Gly β -turns. Comparison of D-Pro-Gly and L-Pro-Gly sequences in an apolar octapeptide. *Journal of the Chemical Society, Perkin Transactions 2* **1998**, (1), 137-144.

- (96) Metrano, A. J.; Chinn, A. J.; Shugrue, C. R.; Stone, E. A.; Kim, B.; Miller, S. J. Asymmetric catalysis mediated by synthetic peptides, version 2.0: expansion of scope and mechanisms. *Chemical Reviews* **2020**, *120* (20), 11479-11615.
- (97) Jhulki, I.; Chanani, P. K.; Abdelwahed, S. H.; Begley, T. P. A Remarkable oxidative cascade that replaces the riboflavin C⁸ methyl with an amino group during roseoflavin biosynthesis. *Journal of the American Chemical Society* **2016**, *138* (27), 8324-8327.
- (98) Sichula, V.; Hu, Y.; Mirzakulova, E.; Manzer, S. F.; Vyas, S.; Hadad, C. M.; Glusac, K. D. Mechanism of N(5)-ethyl-flavinium cation formation upon electrochemical oxidation of N(5)-ethyl-4^a-hydroxyflavin pseudobase. *The Journal of Physical Chemistry B* **2010**, *114* (29), 9452-9461.
- (99) Kale, A. P.; Kumar, G. S.; Mangadan, A. R. K.; Kapur, M. Palladium-catalyzed α -arylation of enones in the synthesis of 2-alkenylindoles and carbazoles. *Organic Letters* **2015**, *17* (5), 1324-1327.
- (100) Neti, S. S.; Poulter, C. D. Site-selective synthesis of ¹⁵N- and ¹³C-enriched flavin mononucleotide coenzyme isotopologues. *The Journal of Organic Chemistry* **2016**, *81* (12), 5087-5092.
- (101) Yang, W.; Gao, L.; Lu, J.; Song, Z. Chemoselective deoxygenation of ether-substituted alcohols and carbonyl compounds by B(C₆F₅)₃-catalyzed reduction with (HMe₂SiCH₂)₂. *Chemical Communications* **2018**, *54* (38), 4834-4837.
- (102) Sen, S. E.; Roach, S. L. A Convenient two-step procedure for the synthesis of substituted allylic amines from allylic alcohols. *Synthesis* **1995**, *1995* (07), 756-758.
- (103) Murahashi, S.-I.; Zhang, D.; Iida, H.; Miyawaki, T.; Uenaka, M.; Murano, K.; Meguro, K. Flavin-catalyzed aerobic oxidation of sulfides and thiols with formic acid/triethylamine. *Chemical Communications* **2014**, *50* (71), 10295-10298.
- (104) Ramirez, N. P.; König, B.; Gonzalez-Gomez, J. C. Decarboxylative cyanation of aliphatic carboxylic acids via visible-light flavin photocatalysis. *Organic Letters* **2019**, *21* (5), 1368-1373.
- (105) Mullen, P.; Miel, H.; Anthony McKerverey, M. N-Boc-4-nitropiperidine: preparation and conversion into a spiropiperidine analogue of the eastern part of maraviroc. *Tetrahedron Letters* **2010**, *51* (24), 3216-3217.
- (106) Souto, A.; Rodríguez, J.; Jiménez, C. A mild oxidative method for the preparation of γ -hydroxy- α -nitroolefins from α,β -epoxyketoximes using IBX. *Tetrahedron Letters* **2009**, *50* (52), 7395-7398.
- (107) Sreedhar, B.; Surendra Reddy, P.; Madhavi, M. Rapid and catalyst-free α -halogenation of ketones using N-halosuccinamides in DMSO. *Synthetic Communications* **2007**, *37* (23), 4149-4156.
- (108) Zhang, G. B.; Wang, F. X.; Du, J. Y.; Qu, H.; Ma, X. Y.; Wei, M. X.; Wang, C. T.; Li, Q.; Fan, C. A. Toward the total synthesis of pahlanine A: expedient assembly of multifunctionalized isotwistane ring system with contiguous quaternary stereocenters. *Organic Letters* **2012**, *14* (14), 3696-3699.

- (109) Tanemura, K.; Suzuki, T.; Nishida, Y.; Satsumabayashi, K.; Horaguchi, T. A mild and efficient procedure for α -bromination of ketones using N-bromosuccinimide catalysed by ammonium acetate. *Chemical Communications* **2004**, (4), 470-471.
- (110) Xing, J.; Yang, L.; Zhou, J.; Zhang, H. Design, synthesis and biological evaluation of anthranilamide derivatives as potential factor Xa (fXa) inhibitors. *Bioorganic & Medicinal Chemistry* **2018**, 26 (23), 5987-5999.
- (111) Marigo, M.; Bachmann, S.; Halland, N.; Braunton, A.; Jørgensen, K. A. Highly enantioselective direct organocatalytic α -chlorination of ketones. *Angewandte Chemie International Edition* **2004**, 43 (41), 5507-5510.
- (112) Zhou, Z. S.; Li, L.; He, X. H. A simple and convenient method for direct α -chlorination of ketones with ammonium chloride and Oxone®. *Chinese Chemical Letters* **2012**, 23 (11), 1213-1216.
- (113) Hwu, J. R.; Chen, K.-L.; Ananthan, S. A new method for nitration of alkenes to α,β -unsaturated nitroalkenes. *Journal of the Chemical Society, Chemical Communications* **1994**, (12), 1425-1426.
- (114) Mir, B. A.; Singh, S. J.; Kumar, R.; Patel, B. K. *tert*-Butyl nitrite mediated different functionalizations of internal alkenes: paths to furoxans and nitroalkenes. *Advanced Synthesis & Catalysis* **2018**, 360 (19), 3801-3809.
- (115) Jana, S.; Chakraborty, A.; Shirinian, V. Z.; Hajra, A. Synthesis of benzo[4,5]imidazo[2,1-b]thiazole by copper(II)-catalyzed thioamination of nitroalkene with ¹H-benzo[δ]imidazole-2-thiol. *Advanced Synthesis & Catalysis* **2018**, 360 (12), 2402-2408.
- (116) Murphy, J. J.; Bastida, D.; Paria, S.; Fagnoni, M.; Melchiorre, P. Asymmetric catalytic formation of quaternary carbons by iminium ion trapping of radicals. *Nature* **2016**, 532 (7598), 218-222.
- (117) Cassani, C.; Martín-Rapún, R.; Arceo, E.; Bravo, F.; Melchiorre, P. Synthesis of 9-amino(9-deoxy)epi cinchona alkaloids, general chiral organocatalysts for the stereoselective functionalization of carbonyl compounds. *Nature Protocols* **2013**, 8 (2), 325-344.
- (118) Tripathi, C. B.; Mukherjee, S. Catalytic enantioselective iodoetherification of oximes. *Angewandte Chemie International Edition* **2013**, 52 (32), 8450-8453.
- (119) Reja, A.; Afrose, S. P.; Das, D. Aldolase Cascade Facilitated by self-assembled nanotubes from short peptide amphiphiles. *Angewandte Chemie International Edition* **2020**, 59 (11), 4329-4334.
- (120) Viviano, M.; Glasnov, T. N.; Reichart, B.; Tekautz, G.; Kappe, C. O. A scalable two-step continuous flow synthesis of nabumetone and related 4-aryl-2-butanones. *Organic Process Research & Development* **2011**, 15 (4), 858-870.
- (121) Pan, Y.; Luo, Z.; Xu, X.; Zhao, H.; Han, J.; Xu, L.; Fan, Q.; Xiao, J. Ru-catalyzed deoxygenative transfer hydrogenation of amides to amines with formic acid/triethylamine. *Advanced Synthesis & Catalysis* **2019**, 361 (16), 3800-3806.
- (122) Lang, C.-S.; Wong, S.-H.; Chow, S.; Challinor, V. L.; Yong, K. W. L.; Fletcher, M. T.; Arthur, D. M.; Ng, J. C.; De Voss, J. J. Synthesis of l-indospicine, [5,5,6-2H₃]-l-indospicine and l-norindospicine. *Organic & Biomolecular Chemistry* **2016**, 14 (28), 6826-6832.

- (123) O'Donnell, J. S.; Singh, S. P.; Metcalf, T. A.; Schwan, A. L. Cesium (*Z*)-2-carbomethoxyethenethiolate: a reagent for the preparation of (*Z*)-2-carbomethoxyethenyl thioethers including selected cysteine and homocysteine derivatives. *European Journal of Organic Chemistry* **2009**, 2009 (4), 547-553.
- (124) Garrard, E. A.; Borman, E. C.; Cook, B. N.; Pike, E. J.; Alberg, D. G. Inhibition of trypanothione reductase by substrate analogues. *Organic Letters* **2000**, 2 (23), 3639-3642.
- (125) Isoda, S.; Yamaguchi, H.; Satoh, Y.; Hirata, M. Medicinal chemical studies on antiplasmin drugs. VII. Oxa analogs of 4-aminomethylcyclohexanecarboxylic acid. *Chemical and Pharmaceutical Bulletin* **1980**, 28 (8), 2329-2336.
- (126) Targel, T.; Ramesh, P.; Portnoy, M. Domino Two-step oxidation of β -alkoxy alcohols to hemiacetal esters: linking a stoichiometric step to an organocatalytic step with a common organic oxidant. *European Journal of Organic Chemistry* **2018**, 2018 (23), 3017-3021.
- (127) I. O. V. Dolomanov, L. J. Bourhis, R. J. Gildea, J. A. K. Howard, H. Puschmann, J. Appl. Crystallogr. 2009, 42, 339-341.
- (128) Sheldrick, G. M. *Acta Crystallogr*; 2015.
- (129) Sheldrick, G. M. *Acta Crystallogr.* **2015**, (C71), 3-8.
- (130) Coles, S.; Allan, D.; Beavers, C.; Teat, S.; Holgate, S.; Tovee, C. Leading edge chemical crystallography service provision and its impact on crystallographic data science in the twenty-first century. 2020.
- (131) P. Giannozzi, S. B., N. Bonini, M. Calandra, R. Car, C. Cavazzoni, D. Ceresoli, G.L. Chiarotti, M. Cococcioni, I. Dabo et al. *J. Phys. Condes. Matter.* **2009**, 21.
- (132) J. van de Streek and M. A. Neumann. *Acta Crystallogr., Sect. B: Struct. Sci.* **2010**, 66, 544-558.